Complexity

Complex Optimization and Simulation in Power Systems

Lead Guest Editor: João Soares
Guest Editors: Fernando Lezama, Hugo Morais, and Tiago Pinto

Complex Optimization and Simulation in Power Systems

Complexity

Complex Optimization and Simulation in Power Systems

Lead Guest Editor: João Soares
Guest Editors: Fernando Lezama, Hugo Morais, and Tiago Pinto

Editorial Board

Contents

Hindawi
Complexity
Volume 2018, Article ID 6562876, 3 pages
https://doi.org/10.1155/2018/6562876

Editorial

Complex Optimization and Simulation in Power Systems

João Soares,[1] **Fernando Lezama**,[2] **Tiago Pinto**,[3] **and Hugo Morais**[4]

[1]*GECAD, Research Group on Intelligent Engineering and Computing for Advanced Innovation and Development, Polytechnic of Porto (IPP), R. Dr. António Bernardino de Almeida, 431, 4200-072 Porto, Portugal*
[2]*National Institute of Astrophysics, Optics and Electronics (INAOE), Puebla, Mexico*
[3]*BiSITE, University of Salamanca, Calle Espejo, 2, 37007 Salamanca, Spain*
[4]*Électricité de France R&D, Paris, France*

Correspondence should be addressed to João Soares; jan@isep.ipp.pt

Received 6 September 2018; Accepted 6 September 2018; Published 14 October 2018

Deregulation of energy markets has changed the way of delivering power to electricity customers while introducing serious competition [1]. Meanwhile, electricity demand has been increasing steadily, and the limited earth resources require more sustainability, which is critical to keep up the world at the current pace [2, 3]. In this context, not only is energy efficiency crucial to contribute to sustainability, but also adequate methods of energy production and consumption are highly relevant (e.g., energy resource management) [4]. Optimization and simulation approaches are a key part of the planning, operation, and control of energy systems [5]. In addition to the ever-increasing penetration of renewables, the expected massive penetration of electric vehicles is challenging the power system and transportation industry as never before. Dealing with these new challenges while being able to create innovative and prosperous business ideas is essential for survival in the advent of smartening power systems. The complexity of optimization and simulation problems in this domain is increasing. Optimization is usually highly constrained and faces issues related to high-dimensionality, lack of information, and noisy and corrupted data as well as real-time requirements, while simulation requires multidomain knowledge (communications, market mechanisms, etc.) to capture the essence of the new paradigm of power systems.

This special issue (SI) entitled "Complex Optimization and Simulation in Power Systems" (COSPS) attracted several contributions in related topics with novel ideas to tackle complex problems in optimization and simulation in power systems. More precisely, COSPS SI attracted 33 submissions from researchers all over the world. From those submissions, 14 papers have been accepted, including a survey paper from the guest editors.

We accepted 13 out of the 33 received papers. Besides, our accepted survey paper reviews last decade work on the special issue topics entitled "Survey on Complex Optimization and Simulation for the New Paradigm of Power Systems". This survey paper was handled by external editors and reviewers. Presented papers in this special issue deal with complexity at different levels of the power system field. This special issue covers papers that deal with energy management algorithms at the bottom levels of the power system grid. Those papers explore the flexibility properties of demand, which has been considered crucial for the stability and sustained growth of future power systems (renewables and EVs integration [6]). In addition, this special issue provides an interesting discussion on the research of the most challenging problems in power systems, namely, economic dispatch and planning with advanced optimization algorithms such as Quantum Particle Swarm Optimization.

The paper "A Cosimulation Architecture for Power System, Communication, and Market in the Smart Grid" presents a cosimulation architecture for the complex representation of the new paradigm of power systems, namely, the smart grid. The multidomain simulation environment of power system, communication, and market mechanism is considered. Different requirements and use cases are identified and a comprehensive data model is proposed. A case study of virtual power plant is presented in the cosimulation framework and a communication network.

The paper "Dealing with Demand in Electric Grids with an Adaptive Consumption Management Platform" explores flexibility in both homes and workplaces. A multiagent system with advanced reasoning and learning capabilities is proposed to tackle the problem and adjust consumption to the current demand situation automatically. The system seems to provide promising results.

The paper "An Evaluation of a Metaheuristic Artificial Immune System for Household Energy Optimization" proposes the use of artificial immune systems, which use special bioinspired algorithms, in the home energy management system. The work aims to present the application of an artificial immune system in the context of different energy optimization problems. Likewise, a case study is performed in which an artificial immune system is incorporated to solve an energy management problem in a domestic environment. A thorough analysis of the different strategies is carried out to demonstrate the ability of an artificial immune system to find a successful optimum which satisfies the problem constraints.

The paper "An Ising Spin-Based Model to Explore Efficient Flexibility in Distributed Power Systems" analyzes consumers' demand flexibility at distribution system level using an Ising spin-based model. A local exchange scheme is considered to enable energy trade. A modified Metropolis-Hasting algorithm is proposed to analyze the system on large scale, considering total aggregation. Results suggest that profit increases with the number of aggregators in a maximum flexibility scenario.

The paper "Optimal Scheduling of a Microgrid Including Pump Scheduling and Network Constraints" proposes an energy management system for industrial microgrids. The considered energy resources include diesel generators, battery energy storage systems, renewable energy sources, flexible loads, and interruptible loads. The network constraints are evaluated with an optimal power flow in a second-stage optimization. The results indicate that electricity costs are reduced thanks to adequate pump scheduling and load management strategies.

The paper "Analysis of Constraint-Handling in Metaheuristic Approaches for the Generation and Transmission Expansion Planning Problem with Renewable Energy" presents a multiperiod generation and transmission expansion planning problem. Using a stochastic approach, the authors can find expansion plans that satisfy the uncertainty conditions regarding demand and renewable generation.

The paper "An Elitist Transposon Quantum-Based Particle Swarm Optimization Algorithm for Economic Dispatch Problems" uses an advanced PSO to solve a highly nonlinear constrained economic dispatch problem. The authors compared their double elitist breeding quantum-based particle swarm optimization (DEB-QPSO) against state-of-the-art algorithms, showing its superiority in different testbeds.

The paper "Minimizing Harmonic Distortion Impact at Distribution System with Considering Large-Scale EV Load Behaviour Using Modified Lightning Search Algorithm and Pareto-Fuzzy Approach" proposes a multiobjective lightning search algorithm for optimal placement sizing of variable passive filters to mitigate harmonic distortion due to charging stations of a large-scale EV fleet. The analysis carried out is modelled in MATLAB/m-file platform, using High Performance Computing (HPC) to make simulation efficient. Authors concluded that their approach is suitable to mitigate harmonic and minimize the impact of large-scale charging station installations.

The paper "Techno-Economic Distribution Networks Planning Using Smart Grid Techniques with Evolutionary Self-Healing Network States" proposes a new model tool for distribution network planning called scenario investment planning. The tool uses advanced computational resources to help network operators to visualize and design operational planning investments in the short and long terms.

The paper "Simulation Study on Clustering Approaches for Short-Term Electricity Forecasting" addresses the topics of load profiling and forecasting. A comprehensive study of clustering methods to identify residential electricity demand profiles and forecast energy consumption is provided. The paper explores the most relevant time series similarity measures, including measures based on the shape of time series, measures based on editing the time series, and measures based on the time series features. The paper also provides a discussion on measures for determining the relevant number of clusters, which comprehends fourteen alternative indexes. A case study using data from forty-six households in Austin, Texas, is performed, in which the similarity measures from different time series are analyzed. The experiments are conducted using nine different segmentation-enhanced forecasting algorithms. The paper concludes that of all the developed methods, neural network models, are the ones that can achieve the best results for aggregating the entire population for hourly data and that the forecasting error decreases when the number of clusters increases. Finally, the paper discusses the implications of the results from the operator's perspective.

The paper "A Novel Control Strategy on Multiple-Mode Application of Electric Vehicle in Distributed Photovoltaic Systems" addresses the integration of electric vehicles in the system. The authors propose a novel control scheme for electric vehicles with vehicle-to-grid capabilities. The proposed control structure enables the customer to achieve the lowest expense on electricity through the storage battery system control and electric vehicle optimal scheduling. The authors propose two day-ahead optimal control strategies with different objective functions, namely, minimizing the daily electricity expense of individual distributed PV system and minimizing the daily total expense of distributed PV systems to which vehicles can be connected to. The model is assessed using an entire year of historical data from 300 households with PV users, provided by a utility in Australia. The meteorological correlation parameters and electricity prices are also based on real data from Australia. Results show that the integration of electric vehicles with vehicle-to-grid capabilities as distributed storage can significantly increase the advantages for the system.

The paper "Investigation and Optimization of Grounding Grid Based on Lightning Response by Using ATP-EMTP and Genetic Algorithm" addresses an innovative method to determine the optimal grounding grid. In the paper,

the transient methodology is introduced to investigate the lightning effect on grounding body at each point of grounding grid in normal and optimized conditions. Genetic algorithm is applied for regular and irregular grounding grid to obtain best values of mesh size with the lower ground potential rise (GPR) as compared with the normal condition for more safety. Several voltages on different positions of grounding grid are described in this paper using ATP-EMTP and genetic algorithm. The computer simulation presented in the paper allows concluding that the proposed scheme is highly feasible and technically attractive.

The paper "Bidirectional Tracking Robust Controls for a DC/DC Buck Converter-DC Motor System" proposes two new designs of differential flatness-based bidirectional tracking robust controls for a DC/DC Buck converter-DC motor system. The first design considers the complete dynamics of the system; i.e., it considers the DC/DC Buck converter-inverter-DC motor connection as a whole. The second separates the dynamics of the Buck converter from the one of the inverter-DC motor, so that a hierarchical controller is generated. The experimental implementation of both controls was performed via MATLAB-Simulink and a DS1104 board in a built prototype of the DC/DC Buck converter-inverter-DC motor connection. Controls show a good performance even when system parameters are subjected to abrupt uncertainties. The paper concludes that the robustness of such controls is verified.

Having said this, we invite the reader to continue with us in this special issue throughout one or more of the 14 articles we briefly described above. The research proposals covered by this special issue indicate several directions which future work may tackle in order to deal with increasing levels of complexity in this field, namely, at optimization and simulation. Many times both coexist together and cannot be conceived, developed, and implemented separately.

Conflicts of Interest

The authors declare that there are no conflicts of interests regarding the publication of this paper.

Acknowledgments

We want to thank coauthors that contributed to our special issue COSPS by submitting their valuable works. We also thank the reviewers that worked voluntarily to produce high quality feedback of the submitted manuscripts. Thanks are also due to the remaining staff of Complexity who help us to reach this result. The present special issue has been possible to funding in part under the EUREKA-ITEA2 Project M2MGrids (ITEA-13011) and Project SIMOCE (ANI|P2020 17690) and FEDER funds through COMPETE program and from national funds through Fundação para a Ciência e a Tecnologia under the project UID/EEA/00760/2013. In addition, it was supported in part by Grant agreement no. 703689 (project ADAPT). Additionally, this work was partially supported by 02/SAICT/2017, POCI-01-0145-FEDER-028983 (project CENEGERTIC).

João Soares
Fernando Lezama
Tiago Pinto
Hugo Morais

References

[1] F. Lezama, J. Soares, P. Hernandez-Leal, M. Kaisers, T. Pinto, and Z. M. Almeida do Vale, "Local energy markets: paving the path towards fully transactive energy systems," *IEEE Transactions on Power Systems*, pp. 1-1, 2018.

[2] P. Siano, "Demand response and smart grids—a survey," *Renewable & Sustainable Energy Reviews*, vol. 30, pp. 461–478, 2014.

[3] S. D. Ramchurn, P. Vytelingum, A. Rogers, and N. R. Jennings, "Putting the 'smarts' into the smart grid: A grand challenge for artificial intelligence," *Communications of the ACM*, vol. 55, no. 4, pp. 86–97, 2012.

[4] J. Soares, B. Canizes, M. A. Fotouhi Gazvhini, Z. Vale, and G. K. Venayagamoorthy, "Two-stage Stochastic Model using Benders' Decomposition for Large-scale Energy Resources Management in Smart grids," *IEEE Transactions on Industry Applications*, pp. 1-1, 2017.

[5] J. L. Bernal-Agustín and R. Dufo-López, "Simulation and optimization of stand-alone hybrid renewable energy systems," *Renewable & Sustainable Energy Reviews*, vol. 13, no. 8, pp. 2111–2118, 2009.

[6] P. Sterchele, A. Palzer, and H.-M. Henning, "Electrify everything?" *IEEE Power and Energy Magazine*, vol. 16, no. 4, pp. 24–33, 2018.

Hindawi
Complexity
Volume 2018, Article ID 1543179, 18 pages
https://doi.org/10.1155/2018/1543179

Research Article

Technoeconomic Distribution Network Planning Using Smart Grid Techniques with Evolutionary Self-Healing Network States

Jesus Nieto-Martin,[1] **Timoleon Kipouros**,[1,2] **Mark Savill**,[1] **Jennifer Woodruff**,[3] **and Jevgenijs Butans**[4]

[1]*Power and Propulsion Sciences Group, Cranfield University, Cranfield MK43 0AL, UK*
[2]*Engineering Design Centre, Cambridge University, Trumpington Street, Cambridge CB2 1PZ, UK*
[3]*Western Power Distribution Innovation, Pegasus Business Park, Derby DE74 2TU, UK*
[4]*Complex System Research Centre, Cranfield School of Management, Cranfield MK43 0AL, UK*

Correspondence should be addressed to Jesus Nieto-Martin; j.nietomartin@cranfield.ac.uk

Received 26 January 2018; Revised 4 July 2018; Accepted 25 July 2018; Published 10 October 2018

Academic Editor: Fernando Lezama

The transition to a secure low-carbon system is raising a set of uncertainties when planning the path to a reliable decarbonised supply. The electricity sector is committing large investments in the transmission and distribution sector upon 2050 in order to ensure grid resilience. The cost and limited flexibility of traditional approaches to 11 kV network reinforcement threaten to constrain the uptake of low-carbon technologies. This paper investigates the suitability and cost-effectiveness of smart grid techniques along with traditional reinforcements for the 11 kV electricity distribution network, in order to analyse expected investments up to 2050 under different DECC demand scenarios. The evaluation of asset planning is based on an area of study in Milton Keynes (East Midlands, United Kingdom), being composed of six 11 kV primaries. To undertake this, the analysis used a revolutionary new model tool for electricity distribution network planning, called scenario investment model (SIM). Comprehensive comparisons of short- and long-term evolutionary investment planning strategies are presented. The work helps electricity network operators to visualise and design operational planning investments providing bottom-up decision support.

1. Introduction

Distribution networks are a key enabler for a low-carbon future. In the UK, distribution network operators (DNOs) are entering a period of significant changes due to UK energy targets up to 2050 [1]. By 2020, it is expected that 15% of its total demand will be from renewable energy sources with a 20% reduction in greenhouse gas emissions and, moreover, 80% reduction in greenhouse gas emissions by 2050. The challenges presented by the transition to a low-carbon economy will directly impact the electricity distribution network.

As for an increasing connection of distributed generators and electrification of heat and transport, new approaches to design, construct, and operate networks will be required [2]. A more active management of local distribution networks, interconnections, storage, or flexibility services are some of the strategic propositions that will maximise the full potential of the digital network revolution. In that sense, the UK National Infrastructure Commission, the UK regulator, OFGEM, and the Department of Business, Energy and Industrial Strategy (BEIS) are contributing to the smart, flexible energy system debate [3].

In 2010, OFGEM introduced RIIO, namely, setting revenue using incentives to deliver innovation and outputs [4]. This new performance-based pricing framework sought to make network operators more consumer-centric encouraging longer-term thinking, greater innovation, and more efficient delivery.

The RIIO framework has been applied to both gas and electricity transmission and distribution networks. The current price control (called "RIIO-1") is the first generation

(2015–2023) of controls under this new framework. As we look forward towards the discussion of defining the price control for RIIO-2 (2023–2031), we have to take account of the dramatic changes and the increased complexity that are underway in the energy sector, as well as the experience and lessons learned, from RIIO-ED1 by DNOs.

In response to these challenges, DNOs are evaluating the performance of novel intervention techniques along with traditional reinforcements for future network planning [5–7]. Furthermore, the deployment of these novel techniques is expected to improve the quality of service [8]. The rising number of stakeholders in the electricity value chain increases the complexity for asset planning. Besides the number of decision makers, the energy sector is facing a data revolution, and therefore, utilities of the future must include in their planning capabilities the implementation of information and communication technologies (ICTs).

Most network modelling tools, such as IPSA Power, ETAP, or DINIS [9–11], perform power flow analysis and look after overloads and stress points of the network. Their approach can be considered static, in the sense that they evaluate an instantaneous view of the network at a certain given time. However, dynamic modelling like the ones implemented within the SIM [12] extends those static approaches making a series of evaluation runs, adjusting future network states (configuration of the network) to previous fixed states where the grid needed an intervention across its topology.

The novel techniques under study in this research are classified as engineering techniques: automatic load transfer (ALT), dynamic asset rating (DAR) for cables and transformers, meshed networks, and energy storage, and commercial techniques: distributed generation (DG) and demand side management (DSM). Traditional reinforcements (TRAD) are modelled as follows: transformer replacement or addition; cable or overhead line (OHL) replacement; transfer load to adjacent feeder; and installation of new feeder [13]. In addition, the assets considered to be fixed during this assessment are the cables and transformers of the local 11 kV network.

This study is populated with the data from the FALCON (Flexible Approaches to Low Carbon Optimised Networks) project trials, using a section of Western Power Distribution (WPD) in Milton Keynes area, composed of six 11 kV primaries. In contrast with the parametric top-down representation embedded in the transform model [14], the SIM aims at creating long-term strategic investment plans. This study will deliver insights and scalability of these novel interventions for asset planning of the UK distribution power networks.

There are a number of previous notable projects that address the uncertainty around the integration of low carbon and low-carbon technologies into the distribution grid [15–18]. The smart distribution network operation for maximising the integration of renewable generation project [19] performs the optimisation of network operation modes and reinforcement planning in the presence of renewable generation. The OFGEM smart grid forum work stream 3, which later became the EA technology transform model [14], is a parametric representation of the electricity distribution network that aimed at creating long-term strategic investment plans [20]. It is important to note that there are certain limitations in transform that are characteristic to all parametric models. The operating characteristics of devices and their relationship to other technologies require extensive calibration to produce a qualified answer. To some extent, the limitations of transform were addressed by smart grid forum work stream 7 [21], which took four of transform's parametric representations of typical distribution networks and converted them into nodal network models. Other examples include the energy system catapult energy path model, which targets local energy systems [22], and the Comillas University reference network model (RNM) [23], which is a large-scale distribution network planning tools that can create optimal networks.

Despite the differences in their respective approaches, the aforementioned models and software tools share some common limitations [24]. They have limited ability to capture emerging behaviour arising from the simultaneous application of multiple low-carbon and smart technologies to the electricity distribution network. Likewise, it is complex to add new technologies into the mix, due to either the lack of automatic application of smart techniques or, as in the case with transform, the parametric approach which needs information about the way different technologies compete with each other, which is difficult to obtain. And finally, no decision support for a particular piece of distribution network can be provided because of either lack of automation or the parametric nature of the model. The following sections introduce and describe the smart techniques and the novel technoeconomic approach for performing dynamic network modelling in distribution networks and analysis in the presence of multiple smart grid techniques. It uses nodal network modelling to capture the emerging behaviour and create localised network development plans.

2. Overview of Techniques

2.1. Technique 1: Dynamic Asset Rating. The heating effect of current passing through a metal restricts the capacity of all transformers, overhead conductors, and cables on a distribution network represented in Figure 1. This restriction is based on the maximum temperature on a critical component within the asset. Therefore, each asset will have a finite current-carrying capacity rating based on assumed values of external conditions which affect thermal buildup, i.e., wind speed, ambient temperature, soil, and humidity. As the assets in general do not have temperature monitoring, the assumed values of the external conditions used in these calculations have as a basis a statistically low level of the risk of the asset exceeding its critical temperature. By more accurately monitoring metrological conditions and modelling asset ratings in real time, the capacity of the asset can be increased while keeping the risk of exceeding the critical temperature to a minimum. Further models and algorithms will be developed as part of this second implementation to cater for the increased information available.

In addition, many assets have a thermal capacity, such that it takes time for the asset to raise its temperature

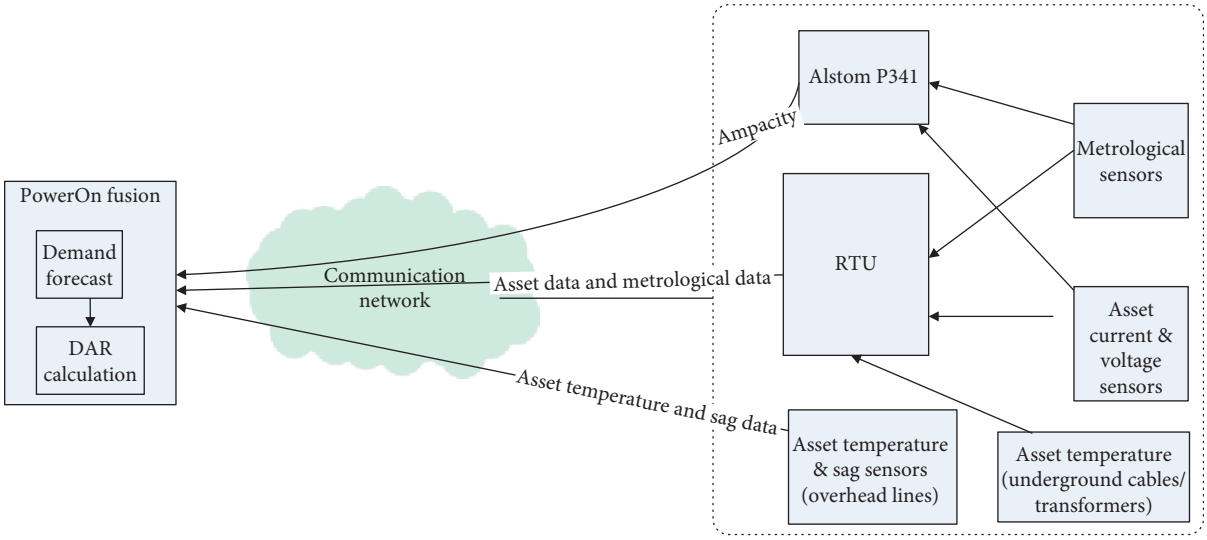

Figure 1: DAR trial schematic.

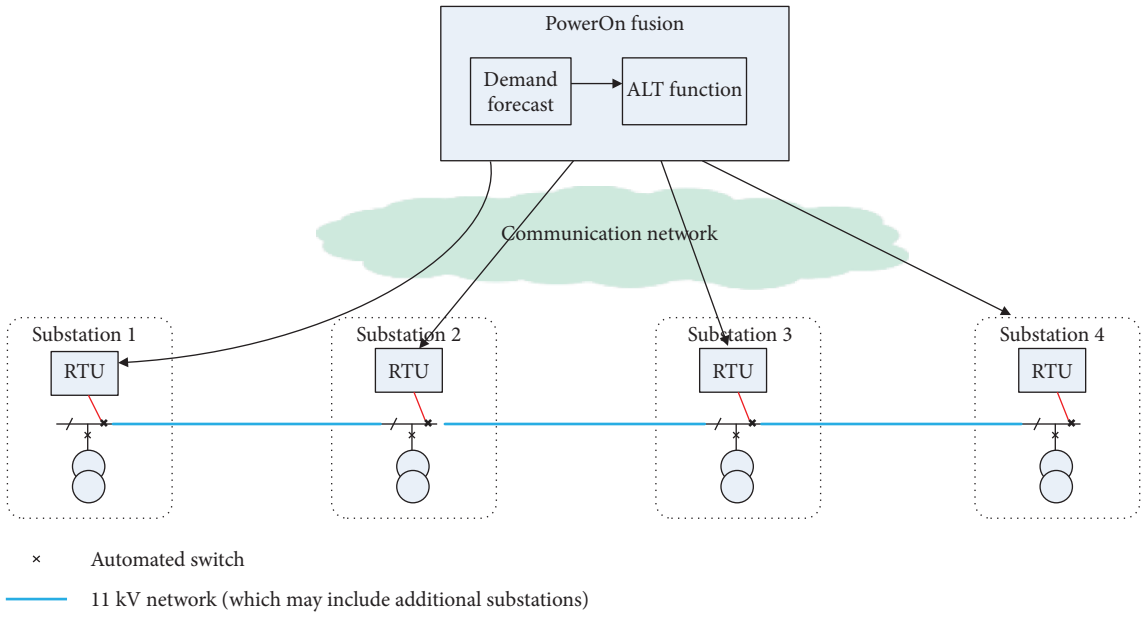

Figure 2: ALT trial schematic.

(i.e., an increase in the current passing through the asset will not cause a step change in the temperature of the asset). Such assets typically have short-term current ratings which are significantly greater than their continuous current rating. These short-term ratings are based on specific current-carrying curves. By being able to forecast the actual current-carrying curves, the asset ratings can be further refined such that an even greater short-term current can be supported. Transformers and underground cables have significant thermal capacity that can utilise this method whereas overhead line circuits do not have significant thermal capacity.

2.2. Technique 2: Automated Load Transfer. Consumers of electricity on the network use energy at different rates at different times of the day, and by actively managing the network connectivity, the loads across connected feeders can be evenly balanced. Rather than the position of normal switching open points being determined for average network conditions, the positions can be changed automatically by the network management system to a more optimum location based on a number of factors such as security, voltage drop, capacity utilisation, and load forecasts as displayed in Figure 2.

2.3. Technique 3: Meshed Networks. This technique represents the process by which circuit breakers on the network are switched in order to feed loads from multiple locations. This approach fundamentally allows the load on each feeder

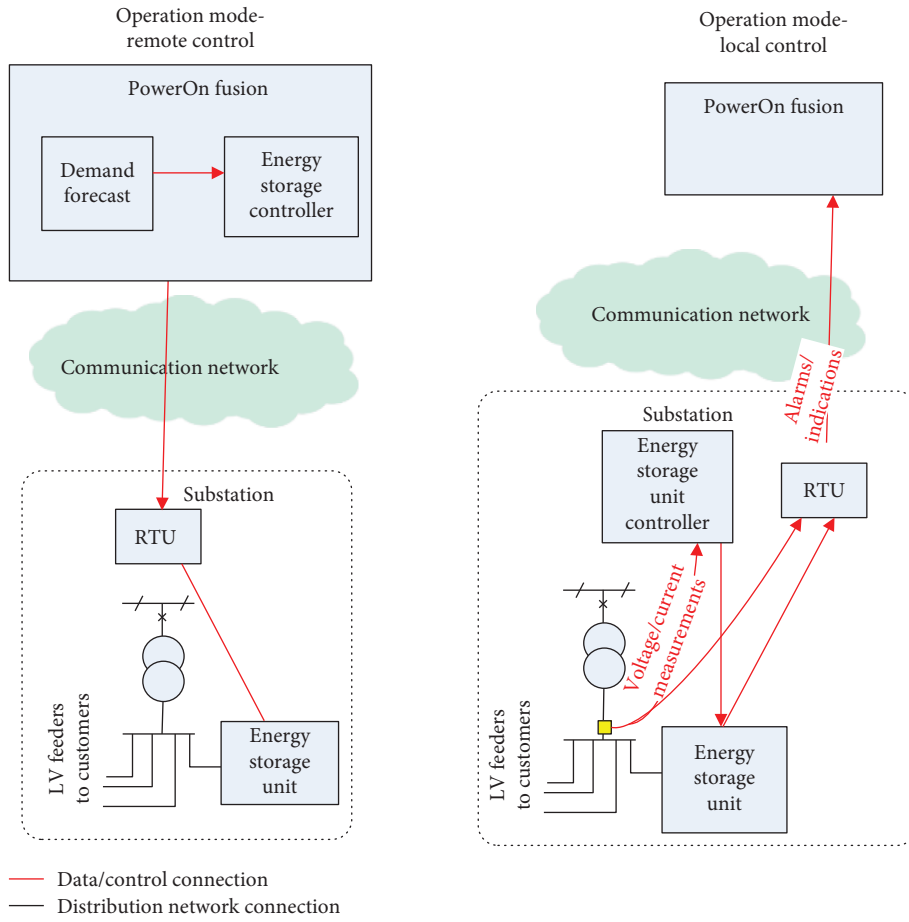

Figure 3: Storage trial representation.

in a meshed circuit to deviate according to the routine variations in the connected load, without the need for pre-existing analysis and changes to switch states.

However, simply closing normal open points (NOPs) exposes more connected customers to supply interruption following a network fault. Therefore, any planned closure of open points for long-term operation is routinely accompanied by the installation of along-the-feeder fault sensing and interruption equipment (protection relays and circuit breakers). The installation of along-the-feeder protection devices restores and potentially reduces the probability of customer interruption under fault conditions with mesh operations.

The aim of trialing this technique was to operate the designated 11 kV networks with parallel feeding arrangements, protective device-driven autosectioning zones, while exploring: potential impacts, both benefits and trade-offs, that could be derived from parallel feeder configurations; and potential impact, both benefits and constraints of operation with autosectioning zones balanced against time/effort and cost.

2.4. Technique 4: Storage. Energy demand in an 11 kV feeder tends to occur in peaks and troughs throughout a 24-hour cycle. The current supplying capacity of a feeder is limited to the current-carrying capability of the smallest cable or conductor in the circuit, and these usually decrease in cross-sectional area size further away from the primary they are located. This is acceptable when the load is spread evenly across a circuit, but when the load occurs unevenly, then the utilisation factor of the assets will also be uneven. By introducing energy storage devices on the network (Figure 3), they can feed out onto the system at peak demands and recharge during times of low demand, thus deferring the need to replace existing assets.

2.5. Technique 5: Distributed Generation Control. A number of industrial and commercial customers have their own on-site generation, and this number is likely to increase with the transition to a low-carbon economy. In some cases, this may be uncontrollable renewable generation (wind or solar) but the majority is in the form of either standby generators or controllable plants such as biomass, refuse incinerators, or combined heat and power (CHP) plants. If customers with controllable distributed generation can be incentivised to accept instruction from a DNO to increase or decrease generation, this can be used to reduce or increase site demand and/or provide or remove supply from the grid as a means of rectifying network problems.

2.6. Technique 6: Demand Side Management. Similar to distributed generation, DSM involves putting in place

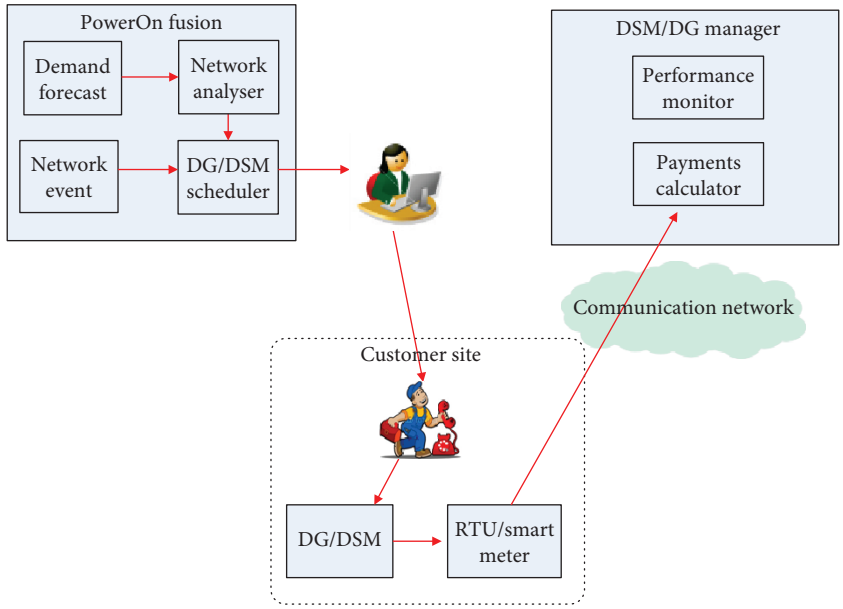

Figure 4: Commercial trials representation: DG/DSM.

commercial agreements between the DNO and industrial and commercial customers who have the ability to control appreciable amounts of load in a relatively short period of time. We expect demand side response to be in two forms using the representation in Figure 4:

(i) To reduce the impact of predicted peak loads

(ii) To respond to an unplanned event, such as a fault

Demand side response actions can be used by the DNO to enable a change in behaviour by a customer site in response to an explicit signal triggering a preagreed action. The action should be the interruption of a customer's internal electricity-consuming processes, either to avoid or, more likely, to defer these to a later time. Its metrics: capacity/delta reduction, duration/frequency, and OPEX, are detailed in [13].

3. Methodology

To undertake the analysis of the aforementioned techniques, a revolutionary new software tool for electricity distribution network planning, called the scenario investment model (SIM), is used. Results from evaluations using the SIM are obtained through a series of experiments that modelled the network evolution under different demand scenarios, presented in Table 1, at short- (2015–2023) and long-term lookahead (2015–2050) to assist decision-makers in future power network planning.

Currently, electricity distribution networks have been planned with typically linear load growths of up to 1% per annum. The expected increase in low-carbon technologies will have a significant effect on the electricity demands on the network which may have significant rapid sporadic increases in the electricity demand on the 11 kV networks

Table 1: Demand scenarios.

Demand scenarios	Fuel efficiency	Low-carbon heat	Wall insulation
DECC1	Medium	High	High
DECC2	High	Medium	High
DECC3	High	High	Low
DECC4	Low	Low	Medium

[25]. In addition, the daily electricity load shapes may be also altered significantly. The networks will need to be upgraded, and systems are being able to evolve and cope with new demand profiles.

There had been identified two main streams of work to consider the use of the innovative techniques, namely, strategic and tactical planning and Design, Build, and Operation. The strategic and tactical planning stream will consider the network planning roles while the design and operation stream will consider design, build, and operation roles. In Figure 5, the smart grid planning framework diagram presents the key elements of each stream which are displayed with their main interactions.

In order to leverage the capability of existing network analysis tools which are already extensively used by electricity network operators, the SIM is separated into two main packages: a network modelling tool which primarily performs the technical assessment of the application of the techniques and the SIM harness which manages the overall process and perform the economic assessment and reporting functions.

Demand data modelling has been based on a bottom-up approach. The methods used provide an estimate of demand for each half-hour at each secondary substation for 18 different season-day types [12].

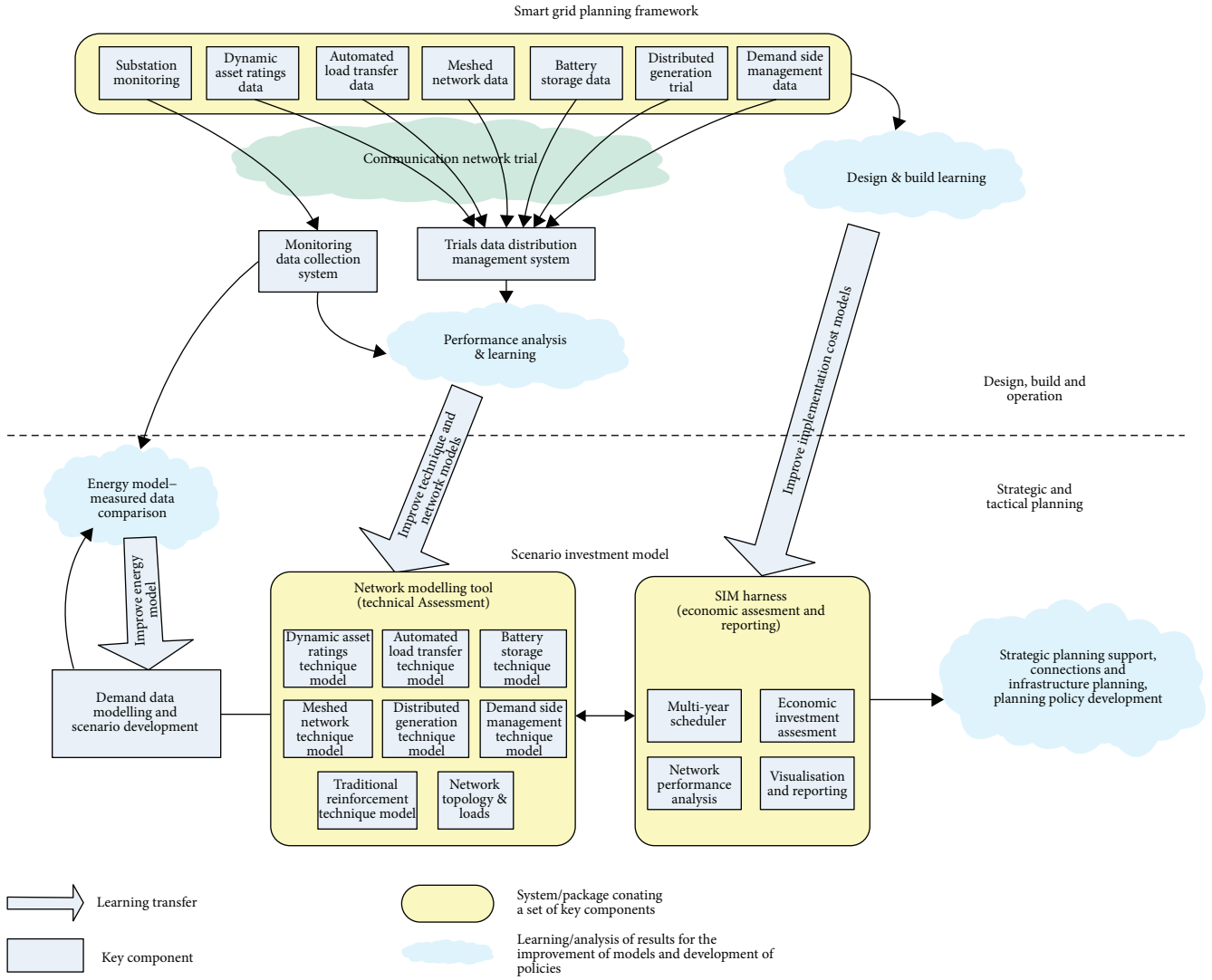

Figure 5: Smart grid planning framework diagram.

The research objective is settled to prove the suitability of the six novel smart interventions presented in Section 2 and, along with the traditional reinforcements, provide an evolutionary planning insight for future power networks. To undertake this study, specific experiments were selected for a certain power trial network under different demand scenarios and evaluation periods, assessing smart techniques along with traditional reinforcements. The approach involved running a set of experiments using the SIM for the six 11 kV primaries in the FALCON trial area.

3.1. SIM Support Algorithms. The essence of the SIM approach is its ability to take a network configuration and corresponding load profiles in a particular year (termed as initial network state), perform power flow and reliability analysis, and create derivative network states in a process known as "network state expansion." The expansion happens either by transitioning to the following year for network states without any failures or by applying intervention techniques to resolve network issues. With each new network state created, the SIM, therefore, is faced with a decision as to which network state from the execution history to expand next. The expansion can be guided by simple depth first or breadth first algorithms, which are implemented in the SIM for verification purposes. The depth-first algorithm always selects the newest, i.e., the most recently created network state that is not fully expanded for expansion, while the breadth-first algorithm always selects the oldest network state. However, those simple heuristics are inadequate for any practical use beyond simple test cases due to the size of the search space obtained by permuting all possible interventions over a number of years. To perform intelligent exploration of the search space, the SIM uses a heuristic approach that is based on an A* algorithm [26, 27].

The baseline A* algorithm aims at finding the least-cost path through the search space. As A* traverses the search space, it builds a tree of partial paths. The leaf nodes of this

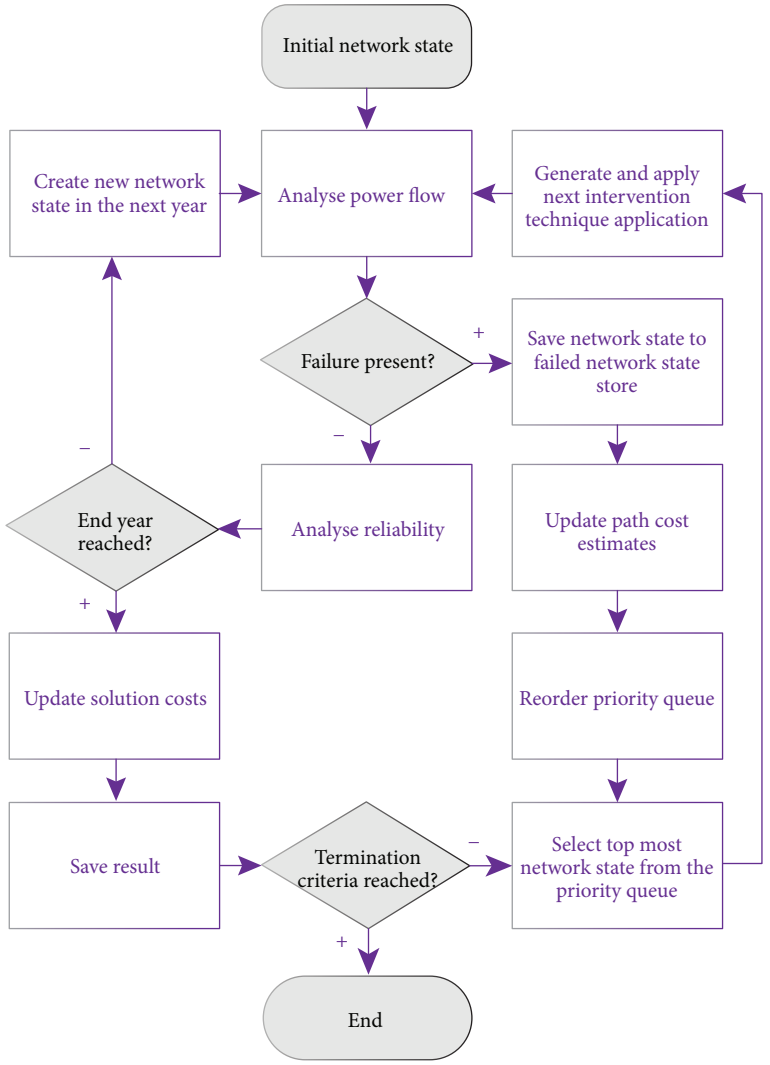

Figure 6: SIM evaluation flowchart.

tree (failed network states) are stored in a priority queue that is ordered using a cost function:

$$f(x) = g(x) + h(x), \tag{1}$$

where $h(x)$ is a heuristic estimate of the path cost to reach the goal and $g(x)$ is the distance travelled from the initial node.

The SIM selects network states from the priority queue to apply intervention techniques, one application at a time. Deployment of a technique produces a new network state, for which a power flow analysis is performed in intact and all $n-1$ (contingency) network operation modes. If all the failures are resolved, a reliability analysis comprising customer minutes lost (CML), customer interruptions (CI), losses, and fault level studies is performed. A new network state is subsequently created in the next year of evaluation, or if it is already the last year of evaluation, the costs of interventions are calculated and the network state together with all its expansion history is saved to the result store as a new result. The evaluation is terminated (Figure 6) when criteria such as the number of results, number of network state evaluations, or run time are reached. As noted, previously, A* uses a combination of distance travelled so far and a heuristic estimate of the distance to reach the endpoint.

In SIM case, this corresponds to $g(x)$ being the total expenditures (TOTEX) incurred so far and $h(x)$ being a heuristic estimate of TOTEX to reach the end year of the experiment. TOTEX, also referred to as the total expenditure, comprises implementation costs (CAPEX) that occur only once when an intervention is applied to the network, operation costs (OPEX) that refer to an ongoing expense of operating an asset or a scheme along with asset life degradation, and metric costs that include incentive payments for losses, fault levels, and network reliability. Referring to (2), the $g(x)$ for a network state x_i in year i is defined as

$$g(x_i) = (c_i + o_i) + \sum_{j=1}^{j-1} (c_j + o_j + m_j), \tag{2}$$

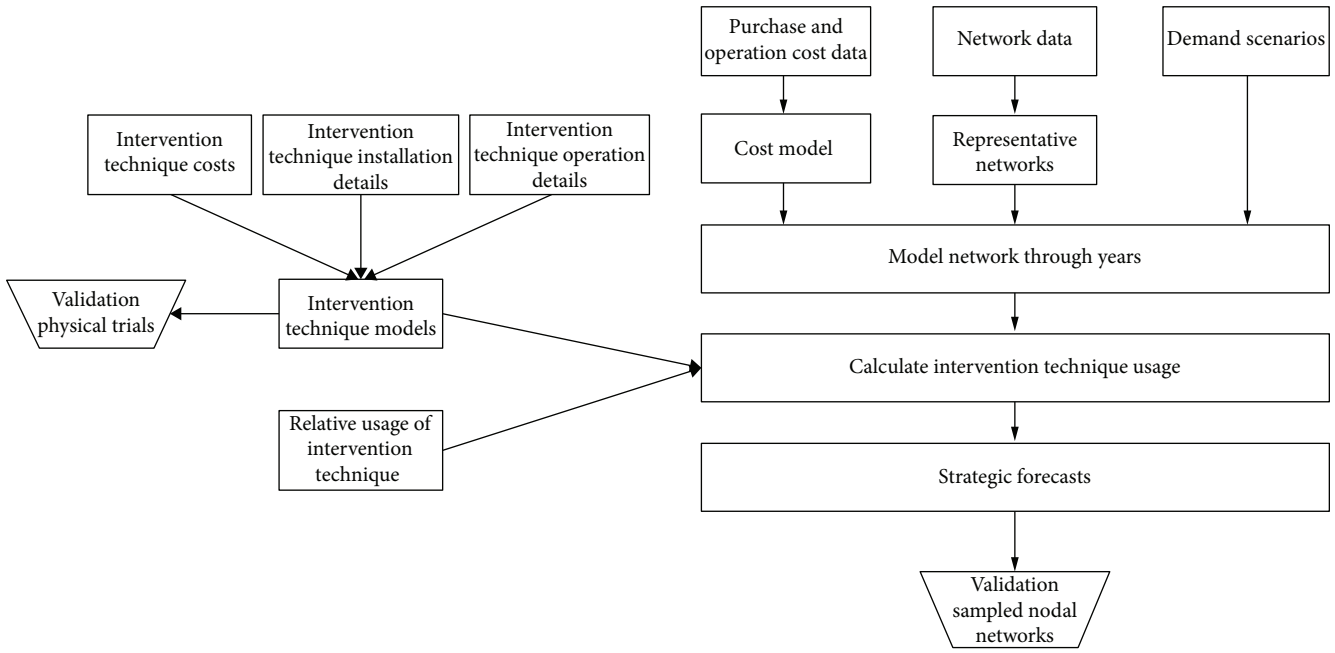

Figure 7: Top-down conceptualisation of evolutionary power networks planning.

where c_i is CAPEX in the current year; o_i is OPEX in the current year; and c_j, o_j, and m_j are CAPEX, OPEX, and metrics costs, respectively, of the ancestor network state with no issues in year j. The heuristic estimate $h(x)$ of the cost to reach the end year is given by

$$h(x_i) = (\bar{c}_{\mathrm{REM}i} + \bar{m}_i) + \sum_{k=i+1}^{n} (\bar{c}_k + \bar{o}_k + \bar{m}_k), \tag{3}$$

where $\bar{c}_{\mathrm{REM}i}$ is the average remaining CAPEX in the current year i; $\bar{m}_i$ is the average metric cost in this year; $\bar{c}_k$, $\bar{o}_k$, and $\bar{m}_k$ are the average CAPEX, OPEX, and metric costs, respectively, of the descendant network state in year k with no issues; and n is the end year of evaluation. Preseeded to a constant value, $\bar{c}_0$, the average CAPEX is updated each time a network state is expanded in a particular year; thus, the estimated costs of fixing all issues in a particular year progressively approach true average. Setting $\bar{c}_0$ to a value greater than 0 speeds up the expansion process; i.e., all interventions that cost less than $\bar{c}_0$ will result in new network states that are at the top of the priority queue. The business rationale is that DNOs are not that interested in optimizing interventions costing less than a certain threshold. The learned averages are propagated back to network states in the priority queue, thus updating their estimated effort and leading to the reordering of the queue, unlike the average CAPEX, average OPEX, and metrics costs which are assumed to be 0 for years with no network states. The average OPEX value for a year is obtained using

$$\bar{o} = j^T o_c \left(j^T j\right)^{-1}, \tag{4}$$

where j is a column vector of ones and $\bar{o}_c$ is an OPEX vector of compliant network states in that year. Likewise, the average metric cost is obtained according to

$$\bar{m} = j^T m_c \left(j^T j\right)^{-1}, \tag{5}$$

where j is a column vector of ones and $\bar{m}_c$ is a vector of the metric costs of compliant network states in that year.

3.2. Conceptualising Bottom-Up Evolutionary Planning. Model-driven engineering (MDE) uses analysis, construction, and development of frameworks to formulate metamodels. Those models are usually characterised using domain-specific modelling approaches [28], containing appropriate detail abstraction of particular domain through a specific metamodel. The use of metamodels requires therefore inputs from domain experts which can be used to generate aggregated or disaggregated models. Top-down and bottom-up are the conceptual definition of aggregated and disaggregated models [29]. These two modelling paradigms are frequently used to epitomise domain interactions among the operation of the energy system, the econometrics related, and the technical performance indicators [30].

From a bottom-up modelling approach [31, 32], the top-down perspective is a simplistic characterisation of how electrical power networks combine locational events and individual asset performance with high-level objectives like improving the CML of a certain congested area [33, 34]. From an engineering point of view, both are still valid since outputs and strategic forecast are produced in both. How those outcomes are calculated, validated, and transformed to strategy is presented in Figure 7 (top-down) and Figure 8 (bottom-up).

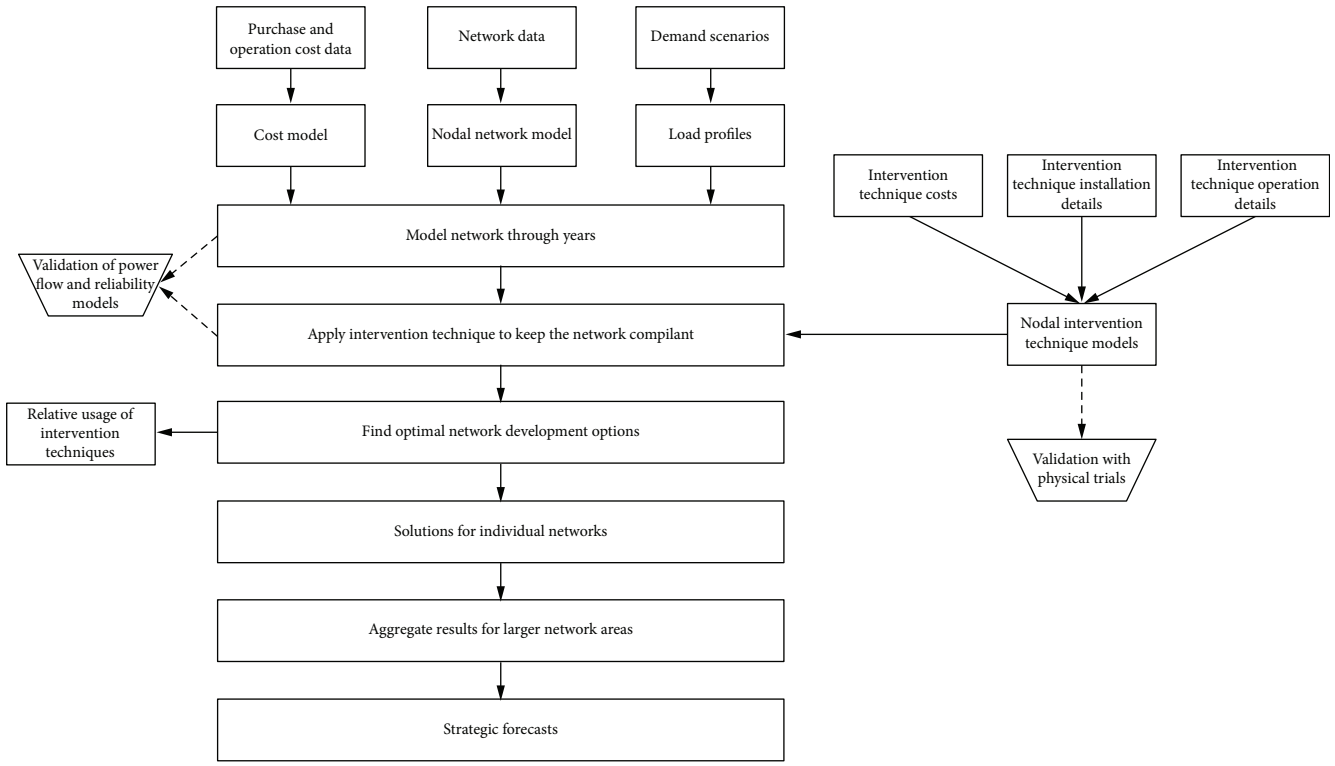

Figure 8: Bottom-up conceptualisation of evolutionary power networks planning.

The ability of bottom-up to capture discrete locational impacts of technologies on the system and their disaggregated costs is triggering the following subsections. Trade-off methodologies are needed for planning evolutionary power systems where observing disaggregated result strategic forecasts are to be produced. These methodologies need to be interactive in the sense that starting from an initial state and after a testing or learning phase, the network is able to accommodate techniques that have improved the system, providing an exploratory set of solutions that can be expanded or discarded as the model evolves through time.

3.3. Experiment Characterisation. To illustrate the processing of the methodology adopted, we consider a typical network scenario tree created by the tool that consists of failed (red) and compliant (green) network states in different years of evaluation. The SIM starts with a single network state in the first year of evaluation. Every year, the network is evaluated for compliance in intact and $n-1$ contingency operation modes. If failures are detected, the SIM applies intervention techniques described in Section 2 to create network patches that resolve the failures. Each application of an intervention technique creates a new network state. The tool has to resolve all issues in the network before transitioning into the next year. DNO planners usually run power flow studies with a single fixed load pattern. In contrast, the SIM checks each network state for compliance under 18 characteristic day load scenarios each comprising of 48 half-hour settlement periods. All studies are performed under intact and $n-1$ contingency network operation modes. The SIM calculates patch costs using cost drivers returned by the network modelling tool. The cost driver describes a network intervention and consists of two parts, namely, the patch key and the scaling. The patch key identifies the nature of the modification of the network performed (removal or addition of an asset and the type of the asset). Scaling data is relevant only to patches that can be installed in multiples of one, such as cable upgrades and additional transformer installation. Scaling data structure provides a list of multipliers to the base cost data available in the SIM database. In case of cable upgrade or replacement, it enables the SIM to correctly estimate full installation costs from per unit of length values. Finally, for postprocessing analysis, the SIM also returns a list of failures by asset. It was identified by DNO planners as indispensable features to help validate the system and correlate the expansion trees to the actual assets on the network diagram. The failure detail table contains asset ID and description alongside information about the number of failures in intact and $n-1$ operating modes as well as absolute and per unit thermal and voltage failure magnitude.

3.4. Case Characterisation. Two set of experiments were performed for this study, one for comparing short-term evaluation period for RIIO-ED1 (2015–2023) where the RIIO-ED1 investment planning has been stylised and a longer planning period for RIIO-ED1 to RIIO-ED4, from 2015 up to 2047. The other set aimed at evaluating different DECC demand scenarios. Experiments evaluated two demand scenarios: DECC2 and DECC4. DECC4 represents, as displayed in Table 1, the slow-progression scenario, and

DECC2 is with DECC3 the most challenging scenario in terms of electrification and low-carbon technology integration. The procedure to run the experiments in the SIM is shown in Figure 6. The inputs to be sent to the SIM are detailed in Figure 5, the selected network, techniques, evaluation period, demand scenario, and cost model, whereas the outputs of the SIM we obtain are techniques used, failures solved, assets fixed, and electrical performance indicators. The SIM address mentioned outputs for long-term planning reinforcements, to optimise investment asset planning resolving network constraints. The performance criteria evaluated were capital expenditures (CAPEX), operating expenditures (OPEX), utilisation of assets, CMLs, CIs, and losses. These parameter values are delivered by the SIM after each simulation. In order to look for the optimal solution among the feasible solution pathways, the SIM allows a granularity study of each network state.

4. Results

This section presents the assessment of the six smart grid interventions along with traditional reinforcements in the trial area, compounded by six 11 kV primaries in Milton Keynes, UK, for two different evaluation periods, DECC2 and DECC4. Subsection 4.1 introduces the results for the 2015–2023 period as short-term planning, and Subsection 4.2 presents the results for a long-term evaluation period, 2015–2047.

4.1. Short-Term Planning. This section presents the assessment of the six smart grid interventions along with traditional reinforcements in the trial area, compounded by six 11 kV primaries in Milton Keynes, UK, for two different demand scenarios, DECC2 and DECC4.

4.1.1. DECC4, 2015–2023. Figure 9 shows the trends of CAPEX and OPEX. Note that in the year 2015, there is a CAPEX's peak due to the application of more techniques and OPEX increments over time from 2017 to 2023.

Despite the investment, the increase is compensated by a benefit in the electricity distribution network, with a reduction in CML and CI as shown in Figure 10.

The summary of the proportion of installations required during this evaluation period and by capital expenditures per technique is presented in Table 2 for both DECC scenarios.

The average yearly price of each technique implemented to fix a network state is key for future decision-making considerations.

Figure 11 displays the average price of each technique disaggregated by CAPEX and OPEX.

Performance indicators are key parameters for future decision-making within electricity distribution planning as quantifiers due to their influence on the quality of service.

Therefore, as shown in Figure 12, the only smart technique used in combination with traditional reinforcements in this scenario and evaluation period that slightly influence slightly CML and CI is meshed networks.

4.1.2. DECC2, 2015–2023. Figure 13 plots the trend of CAPEX and OPEX over the evaluation period. It is important to highlight that there is a CAPEX peak in 2015, due to an increase of techniques applied in this period.

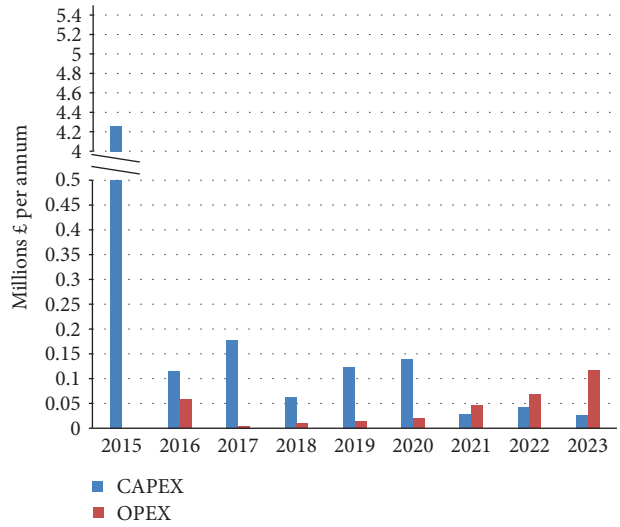

Figure 9: CAPEX and OPEX; DECC4, 2015–2023.

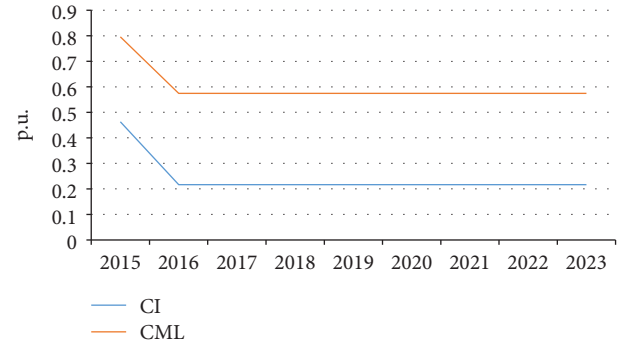

Figure 10: CML and CI; DECC4, 2015–2023.

This CAPEX increment produces a benefit in terms of CML and CI, as observed in Figure 14.

The distribution of techniques applied and capital expenditures per technique are shown in Table 2. The average price of each technique implementation in this demand scenario for this evaluation period is shown in Figure 15.

As displayed in Figure 12 for DECC4's simulation, the only smart grid technique that improves the quality of service is the meshed network. In Figure 16, the contribution of smart techniques on CML and CI for DECC2 demand evaluation is captured.

4.1.3. Comparison between DECC2 and DECC4 for 2015–2023. The results presented may facilitate improvements in electricity distribution network operations and planning resulting in better-informed decision-making when upgrading current electricity distribution networks. The assessment of the six smart grid techniques discovered that only three of them were selected as part of optimal

Table 2: Number of interventions and CAPEX involved; DECC4 and DECC2, 2015–2023.

Technique	DECC4		DECC2	
	Proportion of interventions (%)	CAPEX (%)	Proportion of interventions (%)	CAPEX (%)
DAR-cable	15%	2%	14%	2%
DAR-transformer	7%	1%	5%	1%
ALT	0%	0%	0%	0%
Mesh	3%	1%	4%	1%
Batteries	0%	0%	0%	0%
DSM	0%	0%	0%	0%
DG	0%	0%	0%	0%
TRAD-transformer	8%	3%	7%	2%
TRAD-cable	60%	89%	65%	91%
TRAD-transfer load	6%	2%	4%	1%
TRAD-new feeder	1%	2%	1%	2%

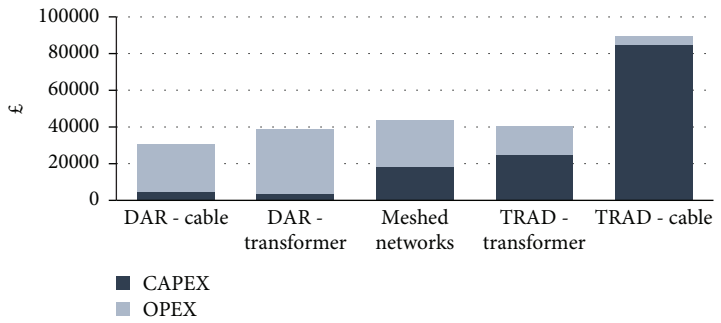

Figure 11: Average cost disaggregation per technique; DECC4, 2015–2023.

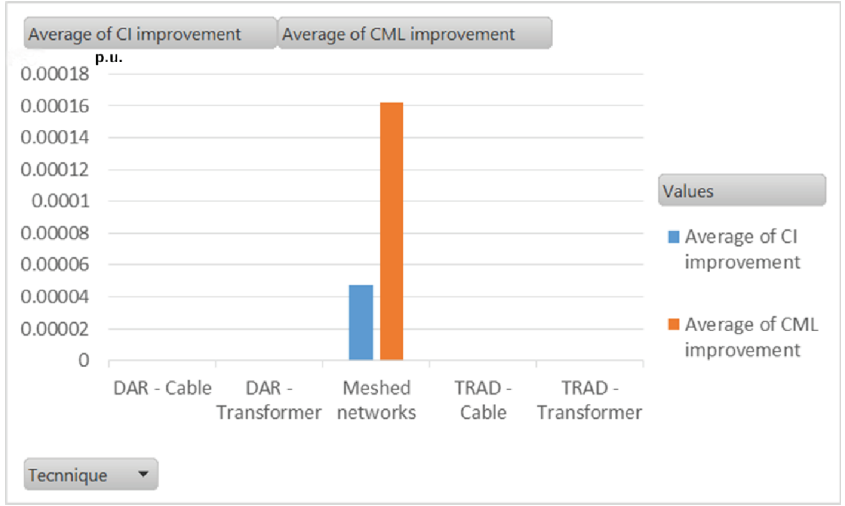

Figure 12: Average CML and CI improvement per technique; DECC4, 2015–2023.

solutions for DECC4 and DECC2, as described in Table 2. These three techniques applied are DAR for cables and transformers and meshed networks.

Comparing the cost trends of the two assessed scenarios, it is notable that in both demand scenarios, DECC4 and DECC2, the CAPEX peak occurs in 2015 (Figures 9 and 13), reflecting the more difficult nature of network states to be feasible in a demanding scenario, whereas DECC2 shows a higher improvement of CI and CML performance indicators as can be seen in Figures 10 and 14.

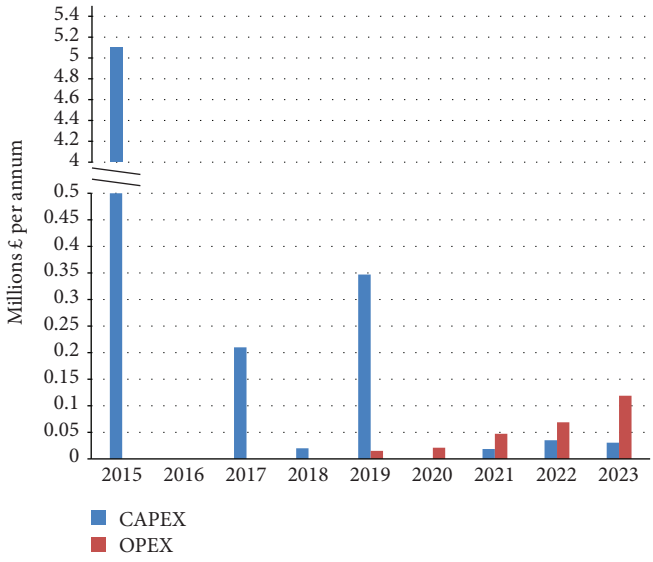

Figure 13: CAPEX and OPEX; DECC2, 2015–2023.

The techniques applied are the key consideration to be assessed. It is necessary to analyse the number of interventions applied by type, the effect of these techniques in the electric grid solving failures and fixing assets. Figures 11 and 15 show average prices of techniques used in each demand scenario. Smart techniques have a lower TOTEX than traditional reinforcements. These novel techniques above are not frequently able to fix failures and therefore produce feasible network states. In terms of CML and CI, the only technique able to moderately contribute to their improvement is meshed networks as shown in Figures 12 and 16. Results attribute the majority of fixes to traditional reinforcements with a comparatively smaller number of failures being solved by smart techniques (Table 2). The results obtained in terms of traditional reinforcement share for 2015–2023 show a 60% proportion of intervention for DECC4 and a 65% proportion of intervention for DECC2, which is close to the 59% forecasted by the transform model for this evaluation period.

For DECC4, the three mentioned techniques along with traditional cable and transformer replacement are applied (Table 2), whereas for DECC2, two of them are applied, DAR for cables and meshed networks (Table 2). Comparing the cost trends of the two assessed scenarios, it is notable that in DECC4, the CAPEX peak occurs in 2015 (Figure 7), whereas in DECC2, besides the peak in 2015, there is also one in 2019 (Figure 11), reflecting the more difficult nature of network states to be feasible in a demanding scenario. However, DECC2 shows a higher improvement of electrical performance indicators as can be seen in Figure 12.

In addition, traditional cable replacement, DAR for cables, and meshed networks are able to fix the cable, whereas traditional transformer replacement and DAR for transformers are able to fix transformer issues (Figure 16). The results obtained in terms of traditional reinforcement share for 2015–2023 show a 60% proportion of intervention for DECC4 and a 65% proportion of intervention for DECC2, which is close to the 59% forecasted by the transform model for this evaluation period.

4.2. Long-Term Planning. This section evaluates two experiments, namely, characterising the DECC2 and DECC4 scenarios for 2015–2047 evaluation period. For each demand scenario, expected investments disaggregating CAPEX and OPEX are presented, the evolution of electrical performance indicators and the number of techniques applied.

4.2.1. DECC4, 2015–2047. In this experiment, the most significant results to analyse the suitability of each technique are presented.

Figure 17 shows the trend of CAPEX and OPEX from 2015 to 2047.

There are CAPEX peaks in the year 2018 and during the beginning of RIIO-ED2 in the years 2025 to 2026, due to the application of more techniques to fulfill low-carbon targets.

Figure 18 indicates that upgrades on the network are directly related to technical performance indicators, CML and CI.

In Table 3, the techniques applied and their contribution to CAPEX during the evaluation period from 2015 to 2047 by a demand scenario are shown.

4.2.2. DECC2, 2015–2047. Within this experiment, the most relevant results to analyse the evolutionary network states are presented.

In Figure 19, the trend of CAPEX and OPEX from 2015 to 2047 is shown. There is a significant increase of CAPEX in the years 2024 to 2026 at the beginning of RIIO-ED2, due to the necessary implementation of new techniques to reach low-carbon targets. The evolution of CML and CI is presented in Figure 20, linking larger investment years when major reductions are found. The contribution of each solution technique is presented in Table 3.

4.2.3. Comparison between DECC2 and DECC4 for 2015–2047. Figure 21 presents a multidimensional parallel coordinate representation of the feasible network state's combinations that produced a 2015–2047 investment pathway for the evaluated area. It bundles economic indicators, i.e., CAPEX and OPEX, with technical performance indicators providing valuable insights on the number of traditional reinforcements utilised to heal falling network states. Results are also clustered by the two demand scenarios assessed during the experiments.

Solutions of DECC2 (represented in orange and green) and DECC4 (in black and blue) are clustered by the percentage of traditional reinforcements utilised as well as the utilisation factor.

Solutions in green and in black represent those where smart grids were more used, whereas orange and blue represent the cheapest (CAPEX and OPEX), less utilised, and the worst responding to the decrease of CML, CI, and losses, and the ones using more traditional reinforcement to fix network states.

Besides the fact that DECC2 smart solutions are between 16% and 28% more expensive than DECC4 traditional

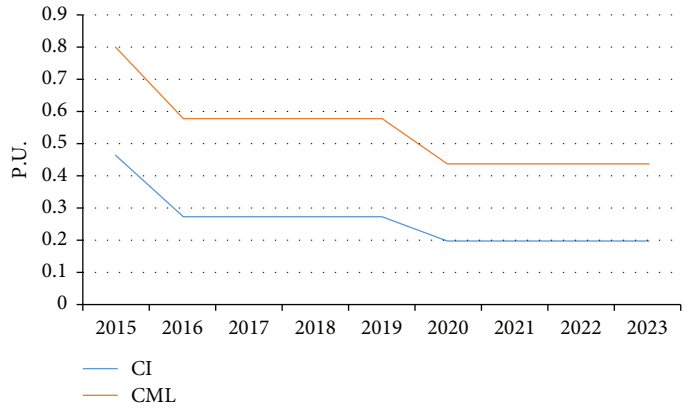

Figure 14: CML and CI; DECC2, 2015–2023.

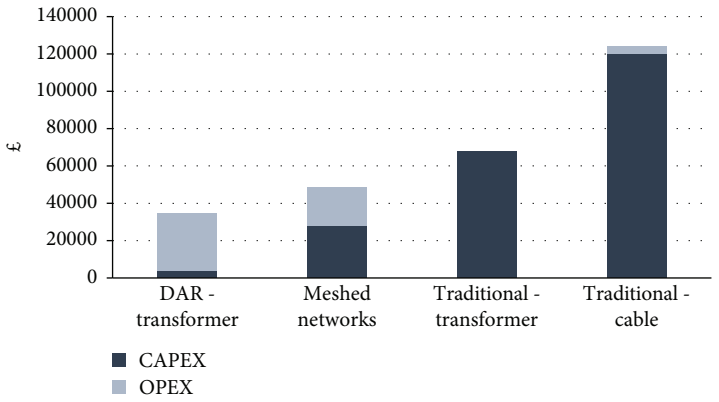

Figure 15: Average cost disaggregation per technique; DECC2, 2015–2023.

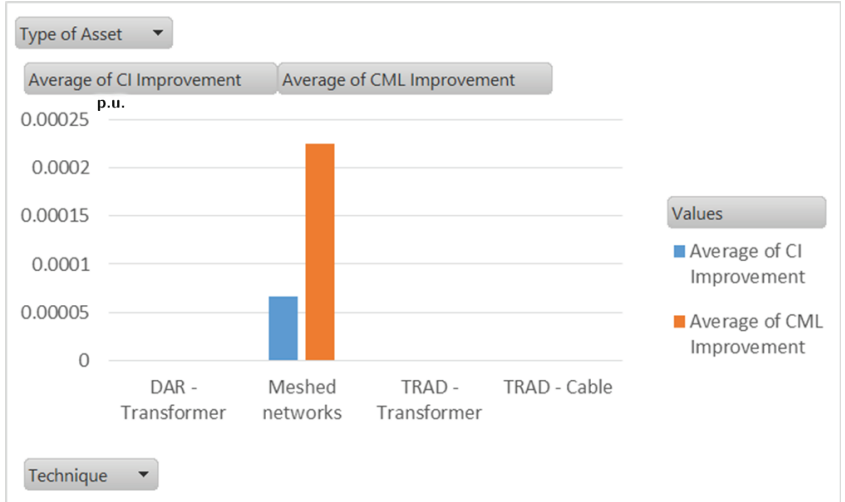

Figure 16: Average CML and CI improvement per technique; DECC2, 2015–2023.

reinforcement solutions (green solutions versus blue solutions in Figure 21), DECC2 traditional solutions are in the range of costs of smart solutions of DECC4 (orange and black solutions in Figure 21). It can also be concluded that investment pathways using less smart techniques provide a cheaper response to technical performance evaluators such as utilisation, CML, CI, and losses.

4.3. Summary. Experiment evaluation runs from the 2015–2047 period present lower investment rates for the

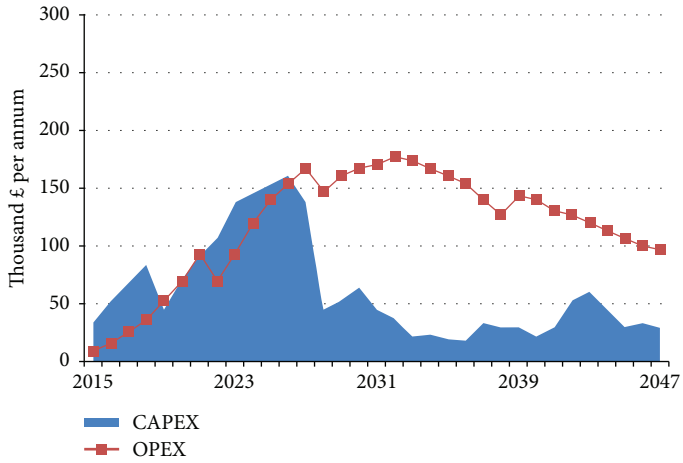

Figure 17: CAPEX and OPEX; DECC4, 2015–2047.

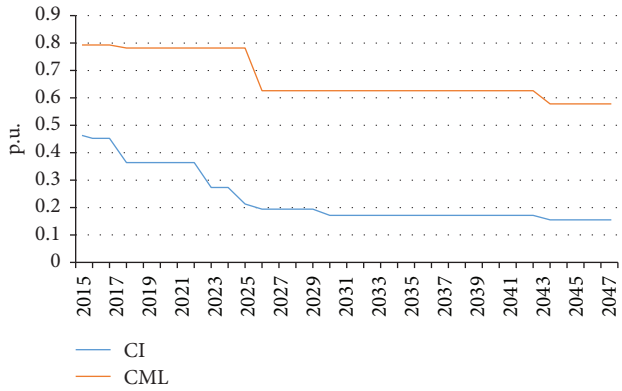

Figure 18: CML and CI; DECC4, 2015–2047.

2015–2023 period than if the evaluation is just performed with a 2015–2023 time frame. This occurs as a result of the challenging low-carbon targets up to 2047 and a myopic planning with short-term lookahead. For an evaluation period four times larger, the CAPEX and TOTEX increased just 18% compared to 2015–2023, concluding that between £5.2M and £6.8M, the evaluation area regardless of the time horizon for the investment or the demand scenario considered is required.

Furthermore, it can be inferred comparing Tables 2 and 3 that for less smart interventions, the short-term planning is used compared to the long-term horizon planning. DAR-cable and DAR-transformer experienced a significant implementation variation between the two evaluation periods for both demand scenarios, as well as CAPEX allocated in cable upgrades falling from 89–91% (2015–2023) to 29–66% in the long term 2015–2047 run. Both technical performance evaluators, CML and CI, respond to their respective CAPEX curve shape. Due to a more incentivised smart grid technique during RIIO-ED2 and ED3, the percentages of smart techniques implemented varied notably. For DECC4 in 2023's outlook, the share of techniques is 25% for smart grid interventions whereas for 2050's outlook, the share is increased up to 58%. In the same way for DECC2 in 2023's outlook, the share of smart interventions is 23% whereas in 2050's outlook, the share increases up to 69%.

Feasible solutions characterising the solution space (Figure 21) differ in the degree of investment required and technical performance evaluators. Each of the solution path represented in the multidimensional solution space in Figure 21 represents the intersection of that dimension with each axis. Parallel coordinates [35] are low complexity working for any N-dimension. In the case of Figure 21, it has 8 dimensions, treating every variable uniformly. Each intersection of one solution path with each axis is the value of that solution for that axis. As for axis DECC2 and DECC4, it represents the feasible solutions for each demand scenario. Making a query by the percentage of traditional reinforcement used in that solution, we have the partition between orange and green for DECC2 and blue and black, being the first solutions that use more traditional reinforcement compared with the ones that use more smart techniques represented in green (DECC2) and black (DECC4). From Figure 21, we can argue that solutions that use more smart techniques (green and blacks) are more expensive in terms of CAPEX and OPEX than their peers (orange and blues) when compared by a demand scenario. It can also be stated that solutions with a higher use of traditional reinforcements are the ones that decrease the most, CML, CI, and losses.

Disaggregating results by network state of the six 11 kV primaries and by the feeder, if necessary for further granular debugging, can discern locational capacity. Under both demand scenarios, Secklow Gate was seen to be the one with greater capacity, being necessary to apply fewer techniques over the evaluation period, 2015–2047. On the other hand, Newport Pagnell exceeds the capacity as soon as 2015, requiring a high number of network state evaluation to be fixed that happens for each subsequent year; hence, the large number of network states is presented in Table 4.

Table 3: Number of interventions and CAPEX involved; DECC4 and DECC2, 2015–2047.

Technique	DECC4		DECC2	
	Proportion of interventions (%)	CAPEX (%)	Proportion of interventions (%)	CAPEX (%)
DAR-cable	18%	5%	31%	6%
DAR-transformer	32%	16%	32%	6%
ALT	0%	0%	0%	0%
Mesh	8%	3%	6%	3%
Batteries	0%	0%	0%	0%
DSM	0%	0%	0%	0%
DG	0%	0%	0%	0%
TRAD-transformer	25%	44%	9%	16%
TRAD-cable	15%	29%	20%	66%
TRAD-transfer load	1%	1%	1%	1%
TRAD-new feeder	1%	2%	1%	2%

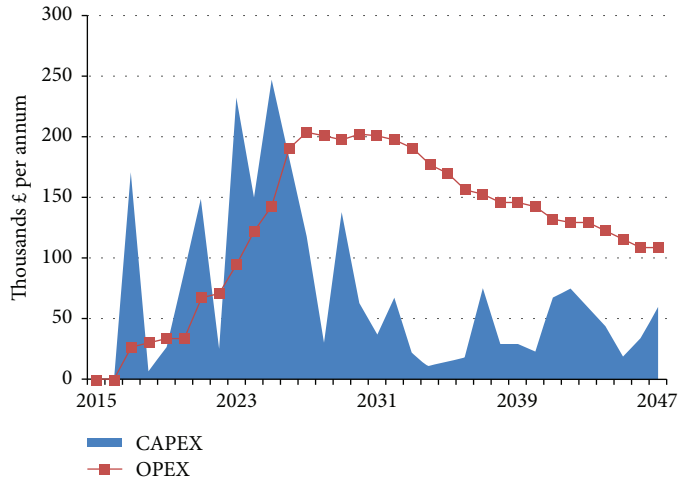

Figure 19: CAPEX and OPEX; DECC2, 2015–2047.

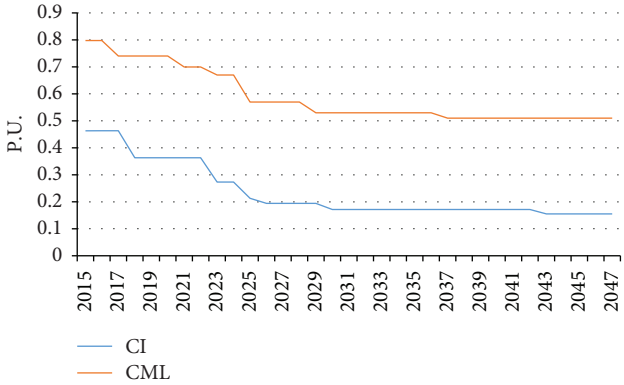

Figure 20: CML and CI; DECC2, 2015–2047.

5. Conclusions

Power flow analysis using a nodal network model is essential when determining the benefits of trailed smart interventions because the interactions and implications are highly specific to a particular location and scenario.

This suggests that while the bottom-up approach is onerous in terms of data handling and manipulation, this is worthwhile for strategic planning and policy evaluation. Comparing both investment strategies, investment strategy adjustments will be necessary in future regulation periods if an over-invested network behaves as displayed in the short-term section of this study.

Traditional reinforcement will continue to be the main method by which network issues are mostly resolved, followed by dynamic asset rating and meshed networks.

The assessment of the six novel smart interventions in the FALCON 11 kV primary test area in Milton Keynes has proved the suitability of three techniques able to fix failures, improving the quality of service, and their readiness to be deployed in the near future. These techniques are DAR for cables and transformers and meshed networks. Meshed networks have been repeatedly selected as a feasible technique because using it will reduce CML, CI, and power losses,

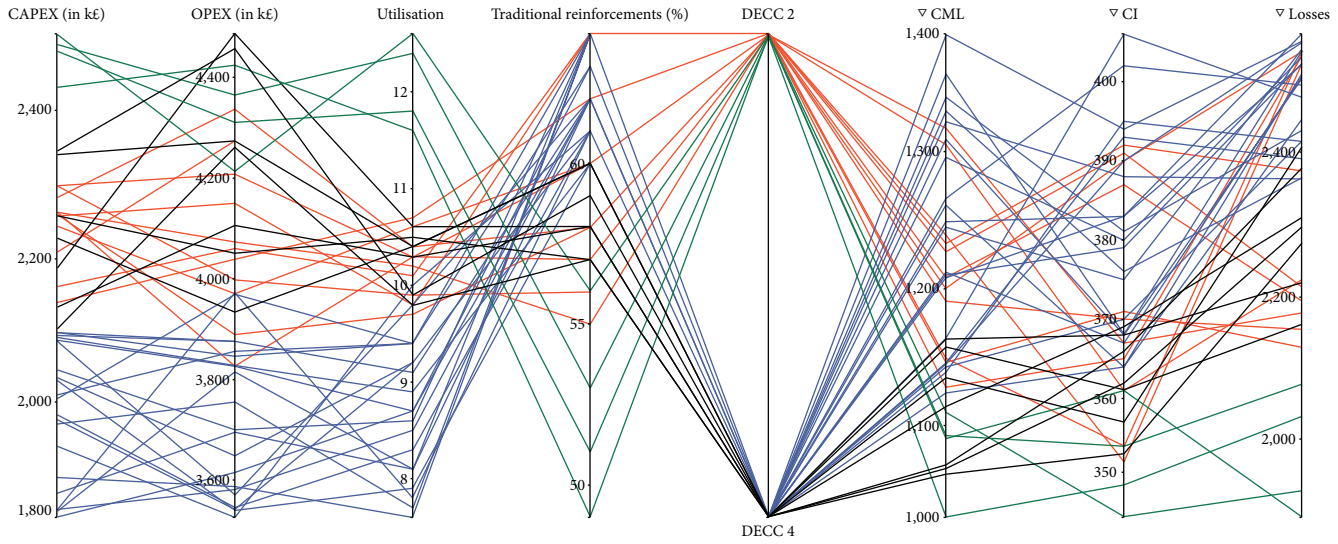

Figure 21: Parallel coordinate visualisation of technoeconomic performance indicators under DECC4 and DECC2.

Table 4: Summary of network states and results for demand scenario; DECC4 and DECC2.

Primary 11 kV substation	Feeders	Year	Techniques	Results DECC4	NS DECC4	Results DECC2	NS DECC2
Fox Milne	13	2047	Smart and traditional	54	276	47	259
Newport Pagnell	9	2047	Smart and traditional	48	317	31	318
Secklow Gate	9	2047	Smart and traditional	27	29	15	16
Bletchley	19	2047	Smart and traditional	32	40	21	48
Marlborough Street	11	2047	Smart and traditional	31	52	19	37
Childs Way	17	2047	Smart and traditional	67	398	54	181

improving the quality of service and the efficiency, while being a cost-effective solution.

The initial capacity at primary substations differed significantly, and this affected the number and complexity of interventions required by the SIM. Due to the load scenarios showing significant peak load increases, DAR was often a temporary measure that would delay but not remove the eventual need for traditional reinforcement.

Implementing DAR for cables and transformers, the monitoring of assets when their peak capacity is increased was analysed. On the other hand, it was observed that traditional reinforcements still play a key role in keeping the electricity distribution networks free of constraints. TRAD techniques such as transformer and cable replacements are able to fix the majority of failures and will be essential also in the future.

The comparison between traditional reinforcements and novel smart techniques has provided a new knowledge about the suitability of each technique to be applied, in terms of costs, electrical performance, failures fixed, and asset replaced. Cable replacement is the most costly technique; however, its use is unavoidable in a number of cases. Furthermore, the applicability of each technique regarding costs involved, improvements on power quality and efficiency, and failures solved lead to new questions to be analysed, such as the lack of these techniques to provide flexible capacity within the trailed area.

To sum up, this study has performed a comparative analysis of novel smart intervention techniques, providing insights for future investments in electricity distribution planning. Further work can focus on scaling up the analysis to include a larger section of the network or a constrained area to evaluate national applicability of the current findings.

Data Availability

Some of the data relevant to this submission is proprietary from Western Power Distribution. It can be accessed for research purposes under a signed collaboration agreement.

Conflicts of Interest

The authors declare that they have no conflicts of interest.

Acknowledgments

The authors would like to thank the rest of the Western Power Distribution Innovation team, particularly the other

members of the FALCON project, as well as Paul Charleton, Stuart Fowler, Ilja Orlovs, Dan Taylor, and Steve Ingram. Also, the authors want to acknowledge OFGEM and the Low Carbon Network Fund for funding this piece of research.

References

[1] European Commission, "Communication from the Commission to the European Parliament, the Council, the European Economic and Social Committee and the Committee of the Regions," 2011, December 2016, https://eur-lex.europa.eu/legal-content/EN/TXT/?qid=1537473508968&uri=CELEX:52016PC076721.

[2] F. G. N. Li and E. Trutnevyte, "Investment appraisal of cost-optimal and near-optimal pathways for the UK electricity sector transition to 2050," *Applied Energy*, vol. 189, pp. 89–109, 2017.

[3] G. Strbac, I. Konstantelos, M. Pollitt, and R. Green, *Delivering Future-Proof Energy Infrastructure*, National Infrastructure Commission, 2016.

[4] Ofgem, "GB Network regulation - the RIIO model," 2010, December 2014, https://www.ofgem.gov.uk/network-regulation-riio-model.

[5] R. Poudineh and T. Jamasb, "Distributed generation, storage, demand response and energy efficiency as alternatives to grid capacity enhancement," *Energy Policy*, vol. 67, pp. 222–231, 2014.

[6] J. Yang, X. Bai, D. Strickland, L. Jenkins, and A. M. Cross, "Dynamic network rating for low carbon distribution network operation—A U.K. application," *IEEE Transactions on Smart Grid*, vol. 6, no. 2, pp. 988–998, 2015.

[7] M. Behnke, W. Erdman, S. Horgan et al., "Secondary network distribution systems background and issues related to the interconnection of distributed resources," National Renewable Energy Laboratory (NREL), Tech. Rep. NREL/TP-560-38079, 2005.

[8] J. Crispim, J. Braz, R. Castro, and J. Esteves, "Smart grids in the EU with smart regulation: experiences from the UK, Italy and Portugal," *Utilities Policy*, vol. 31, pp. 85–93, 2014.

[9] Tnei, "IPSA Power software for power systems," March 2016, http://www.ipsa-power.com/.

[10] ETAP, "ETAP PS," 2018, April 2016, https://etap.com/software/product-overview-main.

[11] DINIS, "DINIS: distribution network information systems," 2002, March 2016, https://etap.com/software/product-overview-main.

[12] Western Power Distribution, "SIM final report," 2015, November 2016, http://www.westernpowerinnovation.co.uk/Projects/Falcon.aspx.

[13] Western Power Distribution, "Project FALCON," 2015, November 2017, http://www.dinis.com.

[14] EA Technology, "Transform model," March 2016, http://www.eatechnology.com/products-and-services/create-smarter-grids/transform-model.

[15] L. Sigrist, E. Lobato, L. Rouco, M. Gazzino, and M. Cantu, "Economic assessment of smart grid initiatives for island power systems," *Applied Energy*, vol. 189, pp. 403–415, 2017.

[16] J. A. Momoh, "Smart grid design for efficient and flexible power networks operation and control," in *2009 IEEE/PES Power Systems Conference and Exposition*, pp. 1–8, Seattle, WA, USA, 2009.

[17] N. Good, K. A. Ellis, and P. Mancarella, "Review and classification of barriers and enablers of demand response in the smart grid," *Renewable and Sustainable Energy Reviews*, vol. 72, pp. 57–72, 2017.

[18] Z. Yang, J. Xiang, and Y. Li, "Distributed consensus based supply–demand balance algorithm for economic dispatch problem in a smart grid with switching graph," *IEEE Transactions on Industrial Electronics*, vol. 64, no. 2, pp. 1600–1610, 2017.

[19] SuSTAINABLE, "Smart distribution network operation for maximising the integration of renewable generation," 2015, March 2016, http://www.sustainableproject.eu/Home.aspx.

[20] S. Mohtashami, D. Pudjianto, and G. Strbac, "Strategic distribution network planning with smart grid technologies," *IEEE Transactions on Smart Grid*, vol. 8, no. 6, pp. 2656–2664, 2017.

[21] Smart Grid Forum, "Smart grid forum work stream 7," 2015, March 2016, http://www.smarternetworks.org/project/nia_nget015425.

[22] ETI, "EnergyPath networks," March 2016, http://www.eti.co.uk/project/energypath/.

[23] C. Mateo Domingo, T. Gomez San Roman, Á. Sanchez-Miralles, J. P. Peco Gonzalez, and A. Candela Martinez, "A reference network model for large-scale distribution planning with automatic street map generation," *IEEE Transactions on Power Systems*, vol. 26, no. 1, pp. 190–197, 2011.

[24] R. Bolton and T. J. Foxon, "Infrastructure transformation as a socio-technical process — implications for the governance of energy distribution networks in the UK," *Technological Forecasting and Social Change*, vol. 90, pp. 538–550, 2015.

[25] UK Power Networks, "DNO guide to future. Smart management of distribution networks. Summary report," 2014, https://innovation.ukpowernetworks.co.uk/innovation/en/Projects/tier-2-projects/Low-Carbon-London-(LCL)/Project-Documents/LCL%20Learning%20Report%20-%20SR%20-%20Summary%20Report%20-%20DNO%20Guide%20to%20Future%20Smart%20Management%20of%20Distribution%20Networks.pdf.

[26] A. Botea, J. Rintanen, and D. Banerjee, "Optimal reconfiguration for supply restoration with informed A*Search," *IEEE Transactions on Smart Grid*, vol. 3, no. 2, pp. 583–593, 2012.

[27] T. Logenthiran, D. Srinivasan, and T. Z. Shun, "Demand side management in smart grid using heuristic optimization," *IEEE Transactions on Smart Grid*, vol. 3, no. 3, pp. 1244–1252, 2012.

[28] J. Sánchez-Cuadrado, J. de Lara, and E. Guerra, "Bottom-up meta-modelling: an interactive approach," in *Model Driven Engineering Languages and Systems*, pp. 3–19, Springer, 2012.

[29] Y. H. Kim, F. J. Sting, and C. H. Loch, "Top-down, bottom-up, or both? Toward an integrative perspective on operations strategy formation," *Journal of Operations Management*, vol. 32, no. 7-8, pp. 462–474, 2014.

[30] C. Bohringer, "The synthesis of bottom-up and top-down in energy policy modeling," *Energy Economics*, vol. 20, no. 3, pp. 233–248, 1998.

[31] T. G. R. Bower, "Repetition in human development," *Merrill-Palmer Quarterly of Behavior and Development*, vol. 20, no. 4, pp. 303–318, 1974.

[32] H. Mintzberg and J. A. Waters, "Of strategies, deliberate and emergent," *Strategic Management Journal*, vol. 6, no. 3, pp. 257–272, 1985.

[33] K. Moslehi and R. Kumar, "A reliability perspective of the smart grid," *IEEE Transactions on Smart Grid*, vol. 1, no. 1, pp. 57–64, 2010.

[34] F. Rahimi and A. Ipakchi, "Demand response as a market resource under the smart grid paradigm," *IEEE Transactions on Smart Grid*, vol. 1, no. 1, pp. 82–88, 2010.

[35] A. Inselberg, *Parallel Coordinates: Visual Multidimensional Geometry and Its Applications*, Springer, 2009.

Hindawi
Complexity
Volume 2018, Article ID 1438196, 22 pages
https://doi.org/10.1155/2018/1438196

Research Article

Analysis of Constraint-Handling in Metaheuristic Approaches for the Generation and Transmission Expansion Planning Problem with Renewable Energy

Lourdes Martínez-Villaseñor,[1] **Hiram Ponce**,[1] **José Antonio Marmolejo-Saucedo**,[1] **Juan Manuel Ramírez**,[2] **and Agustina Hernández**[2]

[1]*Facultad de Ingeniería, Universidad Panamericana, Augusto Rodin 498, 03920 Ciudad de México, Mexico*
[2]*Centro de Investigación y de Estudios Avanzados, Instituto Politécnico Nacional, Zapopan, JAL, Mexico*

Correspondence should be addressed to José Antonio Marmolejo-Saucedo; jmarmolejo@up.edu.mx

Received 23 February 2018; Revised 2 May 2018; Accepted 26 June 2018; Published 2 October 2018

Academic Editor: João Soares

A multiperiod generation and transmission expansion planning (G&TEP) problem is considered. This model integrates conventional generation with renewable energy sources, assuming a stochastic approach. The proposed approach is based on a centralized planned transmission expansion. Due to the worldwide recent energy guidelines, it is necessary to generate expansion plans adequate to the forecast demand over the next years. Nowadays, in most energy systems, a public entity develops both the short and long of electricity-grid expansion planning. Due to the complexity of the problem, there are different strategies to find expansion plans that satisfy the uncertainty conditions addressed. We proposed to address the G&TEP problem with a pure genetic algorithm approach. Different constraint-handling techniques were applied to deal with two complex case studies presented. Numerical results are shown to compare the strategies used in the test systems, and key factors such as a prior initialization of population and the estimated minimum number of generations are discussed.

1. Introduction

Reasons for conducting a planning process are numerous. Some reasons that can potentially lead to a planning process are the following: (i) high costs for transport and storage equipment; (ii) high rate of accidents, failures, and breakdowns; (iii) bottlenecks, damage, or rejections in your production; (iv) out-of-date technical or infrastructural equipment, and so on. Two fundamental types of planning should be distinguished. The first one is a complete replanning, and the second one is a planning that aims at modernizing your planning objective. The second one is the approach in this paper. The modernization planning is characterized by a high number of planning constraints, a lower amount of possible solutions, and a high rate of by-the-way-planning. This may lead to unsatisfactory results.

Planning for power systems is essentially a projection of how the system should grow over a specific period of time, given certain assumptions and judgment about the future loads and the size of investment in generating capacity additions and transmission facility expansion and reinforcements. Power system planning faces enormous challenges and problems as, for example, future load growth in the face of uncertainties, the constraints imposed on investment, the type and availability of fuel for the generating units, and the need for consolidating the dispersed electric utilities in the isolated regions as a prerequisite for future interconnecting these regions via local national grids and with other neighboring countries. Also, an optimal reliability level should be achieved that will guarantee a continuous power flow with a reasonable cost. All these obstacles made power system planners and concerned agencies face

tremendous difficulties in planning electric power facilities and making sound and appropriate decisions in constructing new power plants or adding new generating units or reinforcing the transmission and distribution networks [1–5].

A typical power system consists of enormous number of elements. The elements may vary from a small lamp switch to a giant generator. However, in this paper, the main elements of concern become the following: (i) generating facilities; (ii) transmission facilities. As a matter of fact, in power system planning, the details of each element design are not of main interest. For instance, for a generating facility, the type (steam turbine, gas turbine, etc.), the capacity, and its location are only determined [6]. Regarding the transmission lines, the periods when they should be installed are determined.

Power system expansion has been widely investigated as a generation and transmission expansion planning (G&TEP) optimization problem. Real-world G&TEP problems are nonlinear and complex, given that it entails handling high number of constraints, high dimensionality, and uncertainty related to the demand, fuel price, market price, interest rate, among other factors. In the technical literature, generation (GEP), transmission (TEP), and G&TEP problems have been solved using different methods of mathematical programming. The application of linear programming (LP) in the planning of electrical networks started with [7]. Later, in [8], a comprehensive review of the models applied to GEP was made in the 1970s. Another widely used approach for modeling expansion of a transmission system is mixed integer programming (MIP), which was introduced in [9, 10]. In the MIP context, a decision variable for system expansion is represented by an integer or binary variable.

One of the first integral approaches for generation and transmission expansion planning was reported in [11], which solution technique is based on the Benders decomposition. In [12], a methodology for planning the expansion of energy systems is described assuming several factors with uncertainty: (i) growth in demand; (ii) fuel cost; (iii) delay in the completion of the project; (iv) financial constraints, and so on, by using stochastic programming. A recent study [13] includes the costs of reducing CO_2 emissions; the demand and the wind potential are modeled as two correlated random variables; subsequently, scenarios are generated by means of Monte Carlo techniques, and GEP is formulated as a problem of stochastic optimization of two stages that is solved using Benders decomposition. More complex models have been reported as in [14] where a multistage stochastic integer programming formulation for the problem expansion of capacity in an uncertain environment is presented. A scenario tree approach was used to model the evolution of demand uncertainty, parameters, and fixed cost functions.

Aiming to reduce greenhouse gas emissions, power systems worldwide are utilizing more energy from renewable sources. To this end, setting renewable targets is one of the mechanisms largely adopted to guide this process with tight levels of renewable penetration. Many countries have established policy targets related to renewable energy. The European Union (EU), for example, established a target to meet 20% of its energy consumption by means of renewable sources by 2020. Some EU member countries have stricter targets, for example, Germany with 30% by 2020 and 60% by 2050.

Currently, due to the high penetration of renewable energy, energy storage elements are extensively used, whose main function is to support the electrical network especially during frequency and voltage transients [15]. Energy storage also helps smoothing wind uncertainty. In recent work [16], Hemmati presented a unified planning for battery energy systems in electric power systems. However, in the problem raised in this paper, dynamic conditions are not assumed, so the inclusion of such elements has been omitted.

In [17, 18], different models and solution methods in order to solve a generation and transmission expansion planning problem are presented; authors propose mathematical programming by either approach direct or decomposition for solving the problem.

In mathematical problems with a high number of constraints, the search for a feasible solution can be almost as difficult as finding the optimal solution. The stochastic G&TEP considers the generation of uncertainty scenarios related to demand, fuel prices, equipment failures, and other conditions. These considerations increase exponentially the number of constraints, so obtaining feasible solutions complicates the direct solution by commercial optimizers or heuristic strategies. In [19], we can observe the development of valid inequalities for multistage stochastic integer programs.

Metaheuristic approaches have proven to be well suited to solve large real-world problems. Genetic algorithms, artificial bee colony algorithm, harmony search method, big bang-big algorithm, cuckoo search algorithm, firefly algorithm, group search algorithm, bat-inspired algorithm, and hunting search algorithm are some examples of metaheuristic techniques. However, it is difficult to use these methods successfully for complex optimization problems with high number of constraints. Researchers have developed constraint-handling techniques to deal with specific features of these problems [20]. It is difficult to estimate good penalty factors or even generate a single feasible solution [20]. Many of these so-called pure metaheuristic techniques have been used to solve the power system expansion as a GEP [21], TEP [22], or distribution (DEP) problem. Recently, the combined G&TEP have been addressed mainly with hybrid metaheuristic approaches [23].

In this paper, we propose to address the combined G&TEP problem with a genetic algorithm dealing with this nonlinear complexity and high number of constraints with several techniques reported in literature [20]. We compare several constraint-handling techniques in order to determine if a pure metaheuristic like genetic algorithm is enough to handle the complexity of G&TEP problem avoiding more complex processes. We propose a multiperiod stochastic model applied to G&TEP considering the insertion of renewable energies, which objective is to achieve a generation and transmission expansion plan that minimizes the total cost of investment. The solution to the problem is approached from two perspectives: (i) using a heuristic method and (ii) a conventional full-scale mixed integer

method. The stochastic framework allows to represent, through scenarios, a wide range of demand-operating conditions throughout the planning horizon. In this work, we employed two case studies for our experiments: a three-year period time with eight different scenarios and a ten-year period time with 1024 scenarios. This allows to include uncertainty in the costs of future investments. Due to environmental considerations, a minimum amount of clean energies (30%) of the total installed generation is assumed, which must meet the demand in each instance.

The remainder of this paper is organized as follows. A review of previous contributions to G&TEP in the literature is formally presented in Section 2. Then, in Section 3, the mathematical model is provided. Section 4 describes the design of our solution method and constraint-handling strategies used for G&TEP. Case studies for three- and ten-year period times are presented in Section 5. Description of experiments and computational results are presented in Section 6. Lastly, conclusions are provided.

2. Metaheuristic Approaches for G&TEP Problem

Real-world problems like G&TEP are high-dimensional optimization tasks that cannot always be solved with deterministic methods. Metaheuristic approaches are well suited to solve this complex optimization problem. An introduction to metaheuristics and their evolution is presented below. Next, the most representative solutions in literature using metaheuristic algorithms or framework for GEP, TEP, and G&TEP optimization problems are discussed.

2.1. Metaheuristics. Stochastic optimization methods have proven to solve large problems finding a good solution. Stochastic algorithms are relatively easy to implement on complex problems [24]. Besides probabilistic methods, there are two types of stochastic approaches, heuristic and metaheuristic. In heuristic methods, a search is performed step by step and a heuristic technique aims to select the best option for expansion in order to exploit and explore the search space. Methods of local search are adequate when looking for a satisfactory solution. Heuristic methods usually obtain good quality solutions in a reasonable time although optimal solution cannot be guaranteed. Metaheuristic procedures consist in "applying at each step a subordinate heuristic which has to be designed for each particular problem type" [25]. According to [26], the term "metaheuristic" has been used with two different meanings. The first meaning conceives metaheuristic as a framework, a set of concept and strategies that guides the development of optimization algorithms. The second meaning refers to a specific implementation or algorithm based on certain strategies. This difference can be understood analyzing the evolution of metaheuristics in the last four decades [26].

An important shift of paradigm occurred in 2000 from method-centric to framework-centric. Metaheuristic concepts and strategies imitate nature, social culture, biology, or laws of physics to guide the search in an optimization problem [27]. The implementations of metaheuristic algorithms have the ability to conduct global searches avoiding local optimal solutions [28]. There is always a trade-off between two characteristics in metaheuristic algorithms balanced in order to obtain better results: intensification and diversification [24]. Metaheuristic algorithms generally perform better than simple heuristics; they are robust and efficient [29].

From the 1970s, early metaheuristic methods were used to solve different optimization problems. References [26, 29–31] reviewed the history and development of metaheuristics. Genetic algorithms, simulated annealing, immune algorithm, and tabu search [30] are some examples of early metaheuristic techniques. Ant colony optimization, differential evolution, and swarm optimization appeared in the nineties. As these so-called pure metaheuristic techniques prove to be valuable in finding good solutions in reasonable time, new techniques were developed in the nineties and the first years from 2000. Artificial bee colony algorithm, harmony search method, big bang-big algorithm, cuckoo search algorithm, firefly algorithm, group search algorithm, bat-inspired algorithm, and hunting search algorithm are some examples among many nature-inspired techniques.

Many of the above-mentioned methods became successful for solving many optimization techniques. Hence, in recent decades, it became clear that pure metaheuristic algorithms had reached their limits, and the research community shifted towards combining several techniques [31]. Memetic algorithm, for example, uses a local search to improve solutions obtained with an evolutionary algorithm. As we stated above, in the early 2000s, the paradigm of metaheuristics changed so they are described as high-level frameworks, and hybridization began to be more commonly used. Hybrid metaheuristic approaches try to use complementary strategies even from different frameworks in order to achieve better results. A combination of metaheuristics with exact methods, for example, was done creating "metaheuristics" [32]. For more details in hybrid metaheuristics, see [31].

In summary, for real-world problem with high dimensionality, deterministic methods do not reach optimal or good solutions in reasonable computing time. Stochastic and in particular metaheuristic approaches have proven to be robust and efficient for complex problems delivering near to optimal solutions, with no guarantee to be optimal, in reasonable amount of time. When human and computational time is critical, hybrid metaheuristics are not recommended; if a pure metaheuristic works well, there is no need to use more complex processes [31].

2.2. Related Work. Power system expansion has been widely investigated as a GEP, TEP, or DEP optimization problems [33]. In recent years, research works also address the combined G&TEP problem. Real-world G&TEP problems are nonlinear and complex, given that it entails handling high number of constraints, high dimensionality, and uncertainty related to the demand, fuel price, market price, interest rate, among other factors. For two decades, GEP, TEP, and G&TEP problems have been solved with deterministic and stochastic approaches. Models can be linear or nonlinear

and single- or multiobjective. In this section, we present an overview of literature that tackles these three problems focusing in those using metaheuristic strategies.

2.2.1. Metaheuristics for GEP Problem. "Regardless of being linear/nonlinear and multi-/single-objective, a multitude of methods were applied successfully to solve the GEP problem during the past few decades. These methods are very diverse, from conventional techniques to modern metaheuristic algorithms" [21].

According to [21] review, genetic algorithms [34, 35] and particle swarm optimization [36, 37] are the most frequently used metaheuristic techniques to address GEP problem. The authors also enumerated related works using evolutionary programming algorithm [38], differential evolution algorithm [39], ant colony optimization, tabu search [40], simulated annealing, modified honey bee mating optimization algorithm [41], artificial immune systems [42], modified shuffled frog leaping algorithm [43], NSGA [44, 45], and gravity search algorithm [46].

In [47], they presented one of the early hybrid approaches to solve GEP long-term problem. The authors combined a genetic algorithm with tunnel-based dynamic programming. The genetic algorithm aimed to find the global optimum while the tunnel-based dynamic programming gets a local optimum. In [48], the GEP problem is analyzed with three test systems with 6-year, 14-year, and 24-year horizons. They compare the performance of nine metaheuristic techniques applied to solve GEP problem, namely, genetic algorithms, differential evolution, evolutionary programming, evolutionary strategy, ant colony optimization, particle swarm optimization, tabu search, simulated annealing, and a hybrid approach. Optimal or near-optimal solutions were obtained in a reasonable time. This work showed that metaheuristic techniques could be adaptable and more efficient in comparison with other optimization approaches.

2.2.2. Metaheuristics for TEP Problem. TEP problem is solved with many metaheuristic optimization methods [22], such as genetic algorithms [49–51], simulated annealing [52, 53], tabu search [54, 55], ant colony optimization [56], artificial immune system [57], harmony search [58], particle swarm optimization [59, 60], and hybrid metaheuristic methods [61, 62].

In [61], they presented an approach based in a genetic algorithm and tabu search that presented the ability of avoiding local optimum and compared their results with other methods. They conclude that tabu search needed longer computational time and the genetic algorithm could present good solutions without tabu search.

One of the most recent works is [63]. In this paper, they proposed to solve TEP problem using an imperialist competitive algorithm comparing the results with other evolutionary methods. Given that optimality is not guaranteed, comparisons between different heuristic performances are frequently found in last decade's literature. Comparison in terms of time of performance and the quality of the solutions found is necessary in order to evaluate the suitability of certain proposed method [63].

2.2.3. Metaheuristics for G&TEP Problem. Recently, the coordinated problem G&TEP has gained more attention [23]. Given that the problem should be associated with uncertainty, market concepts, congestion management, reliability, distributed generation, and reactive power planning [23], metaheuristics are well suited to address this coordinated problem.

In [64], they present a novel idea on the model in the expansion and transmission planning problem: a multiobjective framework to evaluate the integration of distant wind farm. The first objective considers annual operation and investment cost while the second objective deals with minimizing the expected energy not served. In [65], they proposed a multiperiod-integrated framework based in genetic algorithms for GEP, TEP, and natural gas grid expansion planning for large-scale systems. It was applied to the Iranian power proving that the proposed framework can be applicable for large-scale real-world problems. In [66], they proposed a framework for transmission planning considering also generation expansion. In order to solve this interrelated multilevel optimization problem, the authors present an iterative solution linking agent-based and search-based algorithms. Murugan et al. and Kannan et al. published several works using sorting genetic algorithm version II (NSGA-II) to solve G&TEP problem [44, 45]. Lastly, the authors applied elitist nondominated NSGA-II to the combined G&TEP problem [67]. The addressed problem is multiobjective.

A combination of genetic algorithm and fuzzy technique was developed to solve the multiperiod G&TEP problem [68]. The framework optimizes multiple goals in a deregulated environment. The authors performed a comparison with genetic algorithms, NSGA-II, and others to evaluate the optimization method.

From the foregoing, we recap the following:

(1) The evolution of metaheuristics described above is also valid when reviewing, in literature, the solutions presented for G&TEP with metaheuristics. Early works use pure metaheuristics; comparisons are made from 2000 to validate the method; hybridization is more commonly used in recent years. Nevertheless, hybridization is not recommended if a pure metaheuristic works well for a given scenario.

(2) Metaheuristic approaches have proven to find high-quality solutions at relatively low computational costs when addressing G&TEP problem, hence optimality cannot be guaranteed. Heuristic methods generally perform better than classical ones for large problems where classical optimization methods become unmanageable [63].

(3) In [69], they mentioned two difficulties when implementing evolutionary optimization methods for G&TEP problem: handling the highly constraints in large and medium G&TEP problems and large computational time-consuming algorithms that do not permit online applications. A drawback of heuristic and metaheuristic methods applied to

G&TEP problem is that they highly rely in the setting of control parameters and operation mechanisms [50]. The search for the best settings is also a big challenge.

3. Mathematical Model

To solve the problem, in the following, a linearized stochastic mixed integer multiperiod problem is proposed, assuming the insertion of renewable energies. The power and location of wind units were chosen to take into account a generation and transmission reinforcement, as well as a totally new transmission case. The capacities of such elements were estimated to provide the expected demand in all periods of study. Thus, the problem minimizes an objective function of costs, subject to a set of constraints, which include the following: (i) investment constraints and (ii) operating constraints. The latter refer to both conventional and renewable generation costs, nonsupplied demand, and costs for failing with a percentage of clean energies; such costs are multiplied by a weighting factor associated with the number of hours of operation. For each scenario, the investment and operation costs are added along the entire planning horizon, and the resulting value in turn is multiplied by the probability of each scenario. The final investment integrates the sum of all the scenarios.

The economic assessment method used in this paper is the annual equivalent method [70], which converts the cost during the operational lifetime to an equivalent annual cost. The annual amortization rate α multiplied by the capital cost of the proposed scheme (generating units and transmission lines) expresses the annual amortization cost. The amortization rate α is expressed as (1), where i is the interest rate or discount rate and j stands for the project's lifetime. The discount rate assumed in the studies becomes 10% [71]. The lifetime for generating units and transmission lines has been considered as 35 and 40 years, respectively.

$$\alpha = \frac{i(1+i)^j}{(1+i)^j - 1}. \tag{1}$$

The set of constraints corresponding to investment (4), (5), (6), (7), (8), (9), and (10) takes into account the physical limitations of the generating units and the budget limit. Within the group of operating constraints (11), (12), (13), (14), (15), (16), (17), (18), (19), (20), (21), (22), (23), (24), (25), (26), (27), (28), (29), and (30), (11), (12), (13), (14), and (15) state that if there are operating points with the same demand, they will have the same expansion plan in generation and transmission. Power balance constraints, thermal capacity limits in existing lines and those proposed by the model, constraints of direct current (DC) power flows for existing lines and candidates are represented in (17), (18), (19), (20), and (21), respectively. The maximum generation capacity for existing and proposed units (conventional and clean) is guaranteed by (22), (23), (24), and (25). The limits on nonsupplied demand and the phase angle are described in (26), (27), and (28). The clean energy deficit for each operating point corresponding to each period and scenario is represented by (29) and (30); such a constraint implies that a fixed percentage of the loads must be supplied from renewable energies.

The objective function (2) and constraints (4), (5), (6), (7), (8), (9), (10), (11), (12), (13), (14), (15), (16), (17), (18), (19), (20), (21), (22), (23), (24), (25), (26), (27), (28), (29), and (30) are the following [13, 14, 17]:

$$\begin{aligned}\min_{\Delta} \quad \mathrm{SD} = \sum_{\omega} \varphi_{\omega} \Bigg\{ \sum_{t} \Bigg[\sum_{o} \rho_o \Bigg(\sum_{g} C_g^E P_{got\omega}^E + \sum_{c} C_c^C P_{cot\omega}^C + \sum_{d} C_d^{LS} P_{dot\omega}^{LS} \\ + \sum_{\mathrm{gw}} C_{\mathrm{gw}}^{\mathrm{EW}} P_{\mathrm{gwot}\omega}^{\mathrm{EW}} + \sum_{\mathrm{cw}} C_{\mathrm{cw}}^{\mathrm{CW}} P_{\mathrm{cwot}\omega}^{\mathrm{CW}} + \gamma_o \mathrm{TT}_{ot\omega} \Bigg) \\ + \alpha_t \Bigg(\sum_{c} \tilde{I}_c P_{ct\omega}^{C^{\max}} + \sum_{\mathrm{cw}} \tilde{I}_{\mathrm{cw}} P_{ct\omega}^{\mathrm{CW}^{\max}} + \sum_{l \in \Omega^{L^+}} \tilde{I}_l x_{lt\omega}^L \Bigg) \Bigg] \Bigg\},\end{aligned} \tag{2}$$

where

$$\Delta = \left\{ P_{got\omega}^E, P_{cot\omega}^C, P_{\mathrm{gwot}\omega}^{\mathrm{EW}}, P_{\mathrm{cwot}\omega}^{\mathrm{CW}}, P_{dot\omega}^{LS}, P_{lot\omega}^L, \theta_{not\omega}, P_{ct\omega}^{\mathrm{CW}^{\max}}, P_{ct\omega}^{C^{\max}}, x_{lt\omega}^L, \mathrm{TT}_{ot\omega} \right\} \tag{3}$$

subject to constraints:

$$0 \le \sum_{t} P_{\mathrm{cw}t\omega}^{\mathrm{CW}^{\max}} \le \bar{P}_{\mathrm{cw}}^{\mathrm{CW}^{\max}}, \quad \forall \mathrm{cw}, \omega, \tag{4}$$

$$0 \le \sum_{t} P_{ct\omega}^{C^{\max}} \le \bar{P}_{c}^{C^{\max}}, \quad \forall c, \omega, \tag{5}$$

$$x_{lt\omega}^L \in \{0, 1\}, \quad \forall l \in \Omega^{L^+}, t, \omega, \tag{6}$$

$$\sum_{t} x_{lt\omega}^L \le 1, \quad \forall l \in \Omega^{L^+}, \omega, \tag{7}$$

$$\sum_{\mathrm{cw}} \tilde{I}_{\mathrm{cw}} P_{ct\omega}^{\mathrm{CW}^{\max}} \le I_t^{\mathrm{CW,max}}, \quad \forall t, \omega, \tag{8}$$

$$\sum_{c} \tilde{I}_c P_{ct\omega}^{C^{\max}} \le I_t^{C,\max}, \quad \forall t, \omega, \tag{9}$$

$$\sum_{l \in \Omega^{L^+}} \tilde{I}_l x_{lt\omega}^L \le I_t^{L,\max}, \quad \forall t, \omega, \tag{10}$$

$$P_{ct\omega}^{C^{\max}} = P_{ct\tilde{\omega}}^{C^{\max}}, \quad \forall c, t, \omega, \tilde{\omega}, \tag{11}$$

$$P_{do\tau\omega}^{D^{\max}} = P_{do\tau\tilde{\omega}}^{D^{\max}}, \quad \forall d, o, \tau < t, \tag{12}$$

$$P_{\mathrm{cw}t\omega}^{\mathrm{CW}^{\max}} = P_{\mathrm{cw}t\tilde{\omega}}^{\mathrm{CW}^{\max}}, \quad \forall \mathrm{cw}, t, \omega, \tilde{\omega}, \tag{13}$$

$$P_{do\tau\omega}^{D^{\max}} = P_{do\tau\tilde{\omega}}^{D^{\max}}, \quad \forall d, o, \tau < t, \tag{14}$$

$$x_{lt\omega}^L = x_{lt\tilde{\omega}}^L, \quad \forall l, t, \omega, \tilde{\omega}, \tag{15}$$

$$P_{do\tau\omega}^{D^{\max}} = P_{do\tau\tilde{\omega}}^{D^{\max}}, \quad \forall d, o, \tau < t, \tag{16}$$

$$\sum_{g\in\Omega_n^E} P^E_{got\omega} + \sum_{c\in\Omega_n^C} P^C_{cot\omega} + \sum_{\mathrm{gw}\in\Omega_n^{\mathrm{EW}}} P^{\mathrm{EW}}_{\mathrm{gw}ot\omega} + \sum_{\mathrm{cw}\in\Omega_n^{\mathrm{CW}}} P^{\mathrm{CW}}_{\mathrm{cw}ot\omega} - \sum_{l|s(l)=n} P^L_{lot\omega} + \sum_{l|r(l)=n} P^L_{lot\omega} = \sum_{d\in\Omega_n^D} \left(P^{D^{\max}}_{dot\omega} - P^{LS}_{dot\omega}\right), \quad \forall n, o, t, \omega, \tag{17}$$

$$P^L_{lot\omega} = B_l\left(\theta_{s(l)ot\omega} - \theta_{r(l)ot\omega}\right), \quad \forall l \in \Omega^{L^+}, o, t, \omega, \tag{18}$$

$$-\sum_{\tau\le t} x^L_{l\tau\omega} F^{\max}_l \le P^L_{lot\omega} \le \sum_{\tau\le t} x^L_{l\tau\omega} F^{\max}_l, \quad \forall l \in \Omega^{L^+}, o, t, \omega, \tag{19}$$

$$-\left(1 - \sum_{\tau\le t} x^L_{l\tau\omega}\right) M \le P^L_{lot\omega} - B_l\left(\theta_{s(l)ot\omega} - \theta_{r(l)ot\omega}\right) \le \left(1 - \sum_{\tau\le t} x^L_{l\tau\omega}\right) M, \quad \forall l \in \Omega^{L^+}, o, t, \omega, \tag{20}$$

$$-F^{\max}_l \le P^L_{lot\omega} \le F^{\max}_l, \quad \forall l, o, t, \omega, \tag{21}$$

$$0 \le P^E_{got\omega} \le P^{E^{\max}}_g, \quad \forall g, o, t, \omega, \tag{22}$$

$$0 \le P^{\mathrm{EW}}_{\mathrm{gw}ot\omega} \le P^{\mathrm{EW}^{\max}}_{\mathrm{gw}}, \quad \forall \mathrm{gw}, o, t, \omega, \tag{23}$$

$$0 \le P^{\mathrm{CW}}_{\mathrm{cw}ot\omega} \le \sum_{\tau\le t} P^{\mathrm{CW}^{\max}}_{\mathrm{cw}\tau\omega}, \quad \forall \mathrm{cw}, o, t, \omega, \tag{24}$$

$$0 \le P^C_{cot\omega} \le \sum_{\tau\le t} P^{C^{\max}}_{c\tau\omega}, \quad \forall c, o, t, \omega, \tag{25}$$

$$0 \le P^{\mathrm{LS}}_{dot\omega} \le P^{D^{\max}}_{dot\omega}, \quad \forall d, o, t, \omega, \tag{26}$$

$$-\pi \le \theta_{not\omega} \le \pi, \quad \forall n, o, t, \omega, \tag{27}$$

$$\theta_{not\omega} = 0, \quad n : \mathrm{ref}, \forall o, t, \omega, \tag{28}$$

$$\sum_{\mathrm{gw}\in\Omega_n^{\mathrm{EW}}} P^{\mathrm{EW}}_{\mathrm{gw}ot\omega} + \sum_{\mathrm{cw}\in\Omega_n^C} P^{\mathrm{CW}}_{\mathrm{cw}ot\omega} + \mathrm{TT}_{ot\omega} \ge k_t \left\{ \sum_{g\in\Omega_n^E} P^E_{got\omega} + \sum_{\mathrm{gw}\in\Omega_n^{\mathrm{EW}}} P^{\mathrm{EW}}_{\mathrm{gw}ot\omega} + \sum_{c\in\Omega_n^C} P^C_{cot\omega} + \sum_{\mathrm{cw}\in\Omega_n^{\mathrm{CW}}} P^{\mathrm{CW}}_{\mathrm{cw}ot\omega} \right\}, \quad \forall \mathrm{gw}, c, \mathrm{cw}, g, o, t, \omega, \tag{29}$$

$$\mathrm{TT}_{ot\omega} \ge 0, \quad \forall o, t, \omega. \tag{30}$$

The mixed integer nonlinear problem model preview is nonlinear, due to the products of binary x^L_l and continuous θ_n variables in constraints (see (31)). These nonlinear constraints are replaced by the following sets of exact equivalent mixed integer linear constraints (32) and (33), where M is a large enough positive constant.

$$p^L_l = x^L_l B_l\left(\theta_{s(l)} - \theta_{r(l)}\right), \tag{31}$$

$$-x^L_l F^{\max}_l \le p^L_l \le x^L_l F^{\max}_l, \quad \forall l, \tag{32}$$

$$-\left(1 - x^L_l\right) M \le p^L_l - B_l\left(\theta_{s(l)} - \theta_{r(l)}\right) \le \left(1 - x^L_l\right) M, \quad \forall l. \tag{33}$$

Let us consider that prospective transmission line l is built, that is, binary variable x^L_l is equal to 1. In such a case, (32) and (33) impose that $-F^{\max}_l \le p^L_l \le F^{\max}_l$ and $p^L_l - B_l(\theta_{s(l)} - \theta_{r(l)}) = 0$. On the other hand, let us consider that prospective transmission line l is not built, that is, binary variable x^L_l is equal to 0. In such a case, (32) and (33) impose that $p^L_l = 0$ and $-(1 - x^L_l)M \le p^L_l - B_l(\theta_{s(l)} - \theta_{r(l)}) \le (1 - x^L_l)M$. First, we impose that the power flow through this transmission line is null. Second, we consider large enough bounds on the difference between the voltage angles at two nodes that are not connected through the disjunctive parameter M [17].

In this paper, criterion $N-1$ was not included. To take it into account, it is necessary to consider the following aspects. The present work solves the G&TEP of the electric system under normal operating requirements since the objective is to forecast the capacity, location, and start date of operation of the generation units and transmission lines that will be installed in a given planning horizon. However, a safety study of the system can be included using security-constrained optimal power flow, where a contingency analysis is combined with an optimal power flow that seeks to make changes to the optimal dispatch of generation, as well as other adjustments, so that when a security analysis is run, no contingencies result in violations [72]. One of the easiest ways to provide a quick calculation of possible overloads is to use linear sensitivity factors. These factors show the approximate change in line flows for changes in generation on the network configuration and are derived from the DC load flow. Power transfer distribution factors (PTDF) and line outage distribution factors (LODF) are used to model the pre- and postcontingency constraints. A strategy is proposed in [73] where the authors use the nodal admittance matrix in order to transform the DC-network balance constraints to a global power balance equation, and the transmission limit constraints are modeled using the PTDF matrix. The proposed methodology solves the optimization problem taking into account only the power units to be built and the active power generation of each unit as decision variables. In [74], the PTDF and LODF are used to model the pre- and postcontingency constraints simultaneously in a stochastic model. In our work, we choose to make a good approximation of the $N-1$ contingencies in transmission using distribution factors based on [75]. We show its use applied to the 3-year period G&TEP case scenario (see Section 5.1).

Given the complexity of the problem, the authors decided not to include transmission losses in the formulation. Likewise, it was assumed that the degree of uncertainty handled in the proposal may be of the level of such losses; this, coupled with the fact of managing a sufficiently long term, results in a favorable aspect of the proposal in a stochastic environment.

Similarly to the transmission losses, the uncertainty that the wind energy systems have will fall within the ranges of randomness of the problem posed, especially as regard the load refers. For this reason, the authors consider that the results found may well be considered appropriate by the assumptions made, which gives additional value to the stochastic approach.

4. Design of Genetic Algorithm for G&TEP Problem

As we described in Section 2, genetic algorithms are among the most used metaheuristic techniques when addressing GET, TEP, or combined G&TEP problems. Hybrid metaheuristic approaches are recently used to solve complex real-world optimization problems, but it is important to avoid high computational costs if possible. Therefore, if a pure metaheuristic works well for a given scenario, it is not necessary to use a hybrid approach. In this section, we describe an attempt to solve the G&TEP problem with a genetic algorithm using this unconstrained optimization procedure and several constraint-handling techniques.

The well-known procedure of genetic algorithms considers an initial population of individuals, each representing a solution to the problem at stake. The set of individuals is evaluated with a fitness function to select those which represent the best solutions. The application of crossover and mutation operation to selected individuals generates new offspring at each epoch. The generations evolve as in natural selection, creating more fitted individuals delivering eventually a good solution to the problem. Algorithm 1 describes a simple genetic algorithm.

4.1. Individual Representation. The genetic algorithm begins by defining the solution representation, for example, chromosome or the array of variables to be optimized. The chromosome that defines and individual solution for the G&TEP proposed problem consists in an array of real variables that represent the decision variables (see Section 3) to be optimized in the case studies of G&TEP described in Section 5. A detailed description of a chromosome is presented in Table 1 for the 3-year period case study. The chromosome was encoded in a similar way for the 10-year period case study. Due to space restrictions and since the latter has 552,960 variables, we are not able to provide a detailed description of the values.

4.2. Evaluation Function. The evaluation function $\mathrm{ff}(\mathrm{individual})$ is based on the objective function (SD) shown in (2) of the mathematical model. The feasibility of each G&TEP solution is subject to constraints corresponding to those described in the mathematical models (4), (5), (6), (7), (8), (9), (10), (11), (12), (13), (14), (15), (16), (17), (18), (19), (20), (21), (22), (23), (24), (25), (26), (27), (28), (29), and (30). In order to handle these complex constraints in the genetic algorithm, first, we transformed the constrained problem to an unconstrained problem. Next, we use seven different constraint-handling techniques to deal with the infeasibility, presented below.

1: initialize population
2: **while** termination criterion is not reached **do**
3: evaluate population using fitness function
4: select individuals
5: perform crossover and mutation
6: update population
7: **end while**

Algorithm 1: Simple genetic algorithm.

Table 1: Description of a chromosome.

Variable	Number of genes	Positions in chromosome	Lower value	Upper value
$P^{L}_{lot\omega}$	288	0–47	−40	40
		48–95	−100	100
		96–143	−140	140
		144–191	−105	105
		192–239	−200	200
		240–287	−40	40
$\theta_{not\omega}$	192	288–479	−3.141592	3.141592
$P^{E}_{got\omega}$	96	480–575	0	400 (for 480–527) 150 (for 528–575)
$P^{\mathrm{EW}}_{gwot\omega}$	48	576–623	0	100
$P^{\mathrm{CW}}_{cwot\omega}$	48	624–671	0	150
$P^{C}_{cot\omega}$	48	672–719	0	50
$P^{\mathrm{CW}^{\max}}_{ct\omega}$	24	720–743	0	150
$P^{C^{\max}}_{ct\omega}$	24	744–767	0	50
$P^{LS}_{dot\omega}$	192	768–959	0	According to the demand for each operating condition and period along the planning horizon (Table 3)
$\mathrm{TT}_{ot\omega}$	48	960–1007		100
$x^{L}_{lt\omega}$	144	1008–1152	0	1

4.3. Strategies of Constraint-Handling for G&TEP Problem. Several constraint-handling techniques have been adopted in order to handle high constraint problems. In this paper, we used different approaches inspired in the most popular constraint-handling techniques reported in [20]: static penalty functions.

(1) Number of violated constraints: the first strategy consists in considering only counting the number of violated constraints (N) so that

$$\mathrm{ff}(\mathrm{individual}) = N. \tag{34}$$

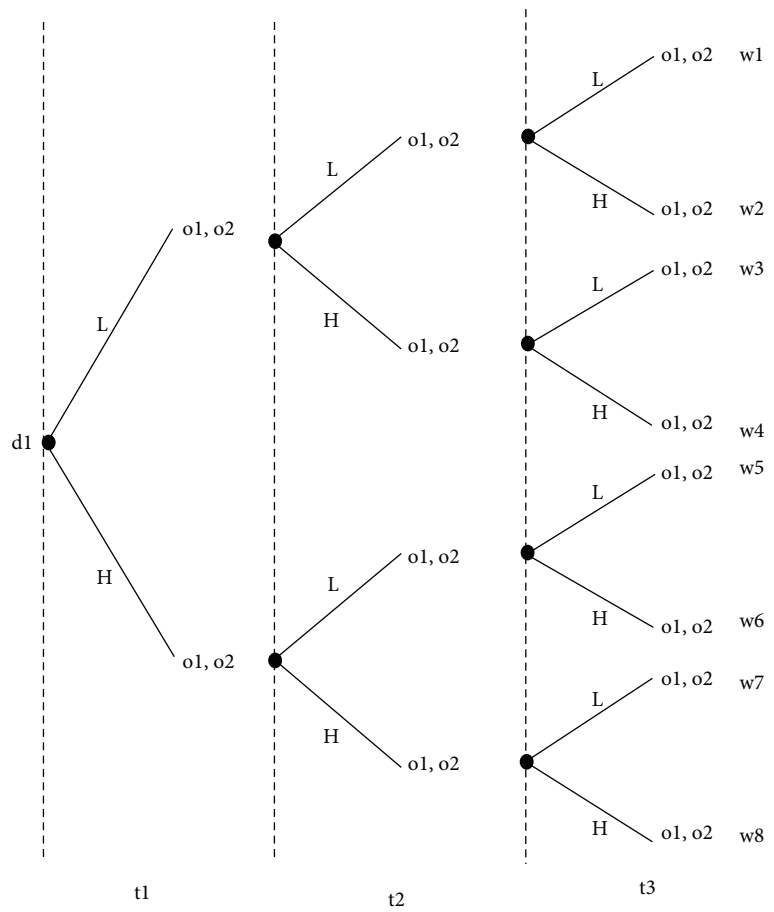

Figure 1: Scenario tree for the stochastic load demand in bus 1.

Table 2: Maximum and minimum demand by bus [MWh/h].

Demand	t_1		t_2		t_3	
	Low	High	Low	High	Low	High
d_1	40–46	46–52	50–57.5	57.5–65	60–69	69–78
d_2	136–150	150–176.8	170–195.5	195.5–221	204–234.6	234.6–265.2
d_3	160–184	184–208	200–230	230–260	240–276	276–312
d_4	64–70	70–83.2	80–92	92–104	96–110.4	110.4–124.8

(2) Objective function incorporating the number of constraints: this strategy follows a common penalty function incorporating the objective function plus a static penalty to the fitness function. When applying a penalization in the fitness function, we decrease the aptitude of those individuals that violate one or more constraints.

$$\mathrm{ff}(\text{individual}) = \mathrm{SD} + \mathrm{kk}N, \tag{35}$$

where N are the constraints not fulfilled by the individual and kk is a large constant.

(3) Harmonic mean: this strategy, inspired in [76], formulates the fitness function as a harmonic mean of the two objectives: SD and N. It tries to get a trade-off of SD and N.

$$\mathrm{ff}(\text{individual}) = \frac{\mathrm{SD} * N}{\mathrm{SD} + N}. \tag{36}$$

(4) Feasibility differentiation: following [77], this approach defines a different fitness function to infeasible individuals. In this case, SD is not computed for all infeasible individuals.

$$\mathrm{ff}(\text{individual}) = \begin{cases} \mathrm{SD}, & \text{if the solution is feasible,} \\ \mathrm{kk} - \sum_{i=1}^{S} \left(\frac{\mathrm{kk}}{m}\right), \end{cases} \tag{37}$$

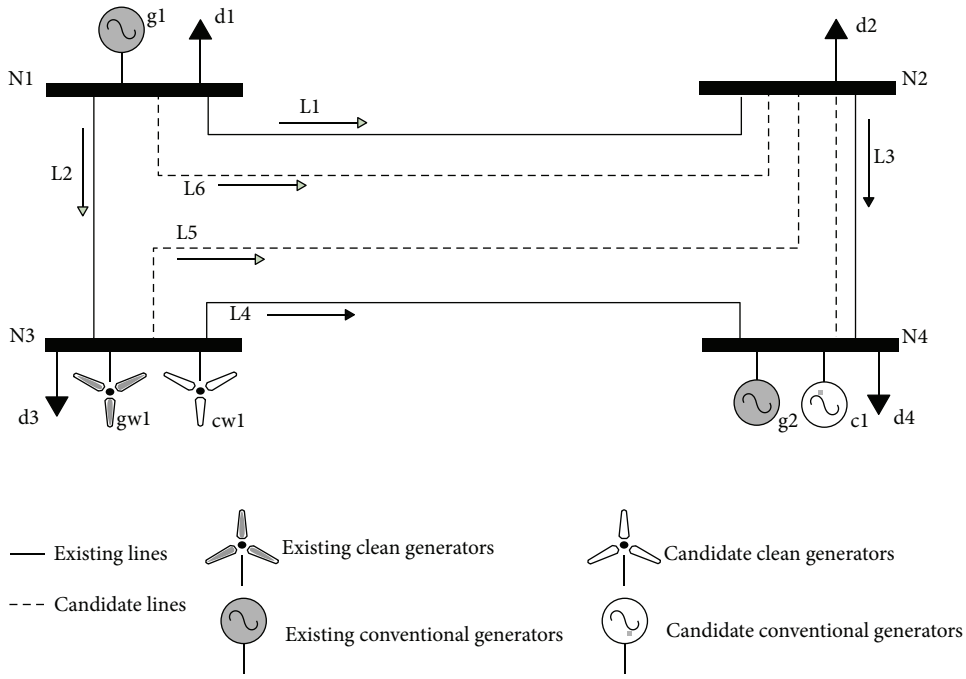

Figure 2: Four-buses test power system.

Table 3: Demand d_1, for each operating condition and period along the planning horizon.

Scenario	t_1	t_2	t_3	Probability
Scenario 1	$P = 45.43$	$P = 50.64$	$P = 64.45$	$0.5^*0.5^*0.5 = 0.125$
	$P = 45.88$	$P = 51.97$	$P = 67.01$	$0.5^*0.5^*0.5 = 0.125$
Scenario 2	$P = 45.43$	$P = 50.64$	$P = 60.27$	$0.5^*0.5^*0.5 = 0.125$
	$P = 45.88$	$P = 50.27$	$P = 66.70$	$0.5^*0.5^*0.5 = 0.125$
Scenario 3	$P = 45.43$	$P = 51.77$	$P = 67.25$	$0.5^*0.5^*0.5 = 0.125$
	$P = 45.88$	$P = 53.44$	$P = 65.19$	$0.5^*0.5^*0.5 = 0.125$
Scenario 4	$P = 45.43$	$P = 51.77$	$P = 68.61$	$0.5^*0.5^*0.5 = 0.125$
	$P = 45.88$	$P = 53.44$	$P = 66.41$	$0.5^*0.5^*0.5 = 0.125$
Scenario 5	$P = 49.61$	$P = 62.59$	$P = 73.70$	$0.5^*0.5^*0.5 = 0.125$
	$P = 50.27$	$P = 60.46$	$P = 69.90$	$0.5^*0.5^*0.5 = 0.125$
Scenario 6	$P = 49.61$	$P = 62.59$	$P = 77.76$	$0.5^*0.5^*0.5 = 0.125$
	$P = 50.27$	$P = 60.46$	$P = 74.84$	$0.5^*0.5^*0.5 = 0.125$
Scenario 7	$P = 49.61$	$P = 58.24$	$P = 70.56$	$0.5^*0.5^*0.5 = 0.125$
	$P = 50.27$	$P = 59.46$	$P = 72.52$	$0.5^*0.5^*0.5 = 0.125$
Scenario 8	$P = 49.61$	$P = 58.24$	$P = 74.91$	$0.5^*0.5^*0.5 = 0.125$
	$P = 50.27$	$P = 59.46$	$P = 74.65$	$0.5^*0.5^*0.5 = 0.125$

where S = number of satisfied constraints and m = total number of constraints.

(5) Weighted: in this approach, the penalty is not the same for all the violated constraints. Based on the knowledge of an expert in the domain, weights are set for each constraint.

$$\mathrm{ff}(\text{individual}) = \mathrm{SD} + \sum_{i=1}^{m} \mathrm{kk} w_i, \tag{38}$$

where w_i is the weight of i constraint and $w_i \in (0, 1]$.

(6) Distance-based: the aim of this strategy is to measure the amount of the individual infeasibility. Fitness function is determined assessing the individual distance from the feasibility in each constraint.

$$\mathrm{ff}(\text{individual}) = \sum_{i=1}^{m} |c_i(\text{individual}) - b_i|, \tag{39}$$

where $c_i(\text{individual})$ is the evaluation of the individual in constraint i and b_i is the bound of constraint i.

(7) Squares of distance: this strategy seeks to achieve a greater sensitivity to the infeasibility of individuals.

$$\mathrm{ff}(\text{individual}) = \sum_{i=1}^{m} (c_i(\text{individual}) - b_i)^2. \tag{40}$$

Table 4: Installed capacity for the candidate clean energy [MW].

Scenarios / Unit	Period	ω_1	ω_2	ω_3	ω_4	ω_5	ω_6	ω_7	ω_8
cw_1	t_1	150	150	150	150	150	150	150	150

Table 5: Installed capacity for the candidate conventional energy [MW].

Unit	Scenarios / Period	ω_1	ω_2	ω_3	ω_4	ω_5	ω_6	ω_7	ω_8
c_1	t_1	0	0	0	0	0	0	0	0
c_1	t_2	0	0	0	0	100.83	100.83	47.080	47.080
c_1	t_3	124.96	115.94	101.48	100.96	89.16	85.80	142.91	140.67
Total installed power [MW]		124.96	115.94	101.48	100.96	190	186.63	190	187.76

4.4. Selection, Crossover, and Mutation Operators. The parents of each generation are selected by the tournament selection method, which randomly picks a small subset of mating pool and the lowest cost chromosome becomes a parent. This method avoids sorting as in elitisms providing a good choice of selection for large population sizes [78]. Crossover is done using a single-point crossover operator that picks two selected individuals with probability pc and randomly determines a crossover point so that the segments of the chromosomes beyond this point are exchanged to form two new individuals. Finally, each new individual is subjected to uniform random mutation operator that selects each gene of the individual and changes its value with probability pm.

5. Case Studies

In this work, two case studies were employed for testing a pure genetic algorithm in G&TEP problems. The first case study considers a three-year period time and eight scenarios that helped to configure the parameters of the genetic algorithm. Then, the second case study with a ten-year period and 1024 scenarios was considered for testing purposes.

5.1. Case Study 1: G&TEP for 3-Year Periods. Regarding the generating scenarios, in this paper, two demand levels are taken into account, Figure 1, where L means low demand and H means high demand. Likewise, it is assumed that subsequent periods exhibit L and H scenarios. Data for combinations in the tree diagram are obtained by using a uniform distribution with the intervals in Table 2. The second and third columns provide the lower and higher demand for the first period by each demand bus. Each period represents a year, which in turn has been divided into two operating conditions o_1 and o_2, which weights (for all periods) become 6000 and 2760 hours, respectively. For this case study, it was assumed that $M = 3 \times 105$ and equal probability for each scenario 0.125. Notice that the test system has 4 load buses as shown in Figure 2. Then, for every load bus, there is a tree diagram similar to that in Figure 1. Tables 2 and 3 summarize demand d_1 for each operating condition and period during the planning horizon.

Figure 2 includes all elements described in the proposed formulation: (i) candidate transmission lines (dotted lines, l_5 and l_6); (ii) candidate conventional and wind generators (c_1 and cw_1). For each bus, low (L) and high (H) load demands are taken into account (see Tables 2 and 3). This gives rise to eight scenarios per bus (see Figure 1).

Table 6: Transmission lines installed during the planning horizon.

Lines	Scenarios / Period	ω_1	ω_2	ω_3	ω_4	ω_5	ω_6	ω_7	ω_8
L_5	t_1	1	1	1	1	1	1	1	1
L_6	t_2	1	1			1	1	1	1
L_6	t_3			1	1				

A linear stochastic mixed integer programming strategy was used for solving the problem from (2), (4), (5), (6), (7), (8), (9), (10), (11), (12), (13), (14), (15), (16), (17), (18), (19), (20), (21), (22), (23), (24), (25), (26), (27), (28), (29), and (30) using the above information for the 3-year period time. In this regard, the best expansion plan obtained is objective function = \$468.85M USD.

Table 4 shows that the clean energy candidate unit cw_1 with rating equal to 150 MW must be installed during the first period for all scenarios ω_1–ω_8. Table 5 indicates that the conventional candidate unit c_1 is installed during period t_2 for scenarios ω_5–ω_8. In the period t_3, it is proposed to install an initial capacity for the scenarios ω_1–ω_4 and an additional capacity for the scenarios ω_5–ω_8.

According to the information in Table 6, transmission line l_5 must be installed during period t_1 for the 8 demand scenarios, while line l_6 is installed during period t_2 for scenarios ω_1, ω_2, and ω_5–ω_8. If scenarios ω_3 and ω_4 arise, it is installed during period t_3.

Tables 7–13 summarize the installed capacity of clean and conventional power, as well as the number of lines installed along the planning horizon, Figure 3. The next step is related to the generators' dispatch for each operating condition, period, and particular scenario. For this case study, there are two demand conditions o_1 and o_2; three periods t_1, t_2, and t_3; and eight scenarios ω_1–ω_8. Therefore, the present model generates 48 different ways of dispatching the generating units ($2 \times 3 \times 8 = 48$). It is impossible to describe each case here, so the following analysis corresponds to the condition o_2, t_3, and ω_8. Figure 3 displays the magnitude of the power flow through the transmission lines l_1–l_6, the generation of units g_1, g_2, gw_1, cw_1, and c_1, and the demand level at buses d_1–d_4.

An approximate analysis of the problem of $N-1$ contingencies by distribution factors [75] can corroborate that it is

Table 7: Data for transmission lines.

Number	B (susceptance)	$F_l^{\max}$ [MW] (maximum power flow)
l_1	500	40
l_2	500	100
l_3	500	140
l_4	500	105
l_5	500	200
l_6	500	40

Table 8: Data for existing and candidate generators.

Number	$P_g^{E^{\max}}$;$P_{gw}^{E^{\max}}$ [MW]	C_c^C;$C_{\text{cw}}^{\text{CW}}$ [\$/MWh]
g_1	400	35
g_2	150	35
tc_1	190	35
gw_4	100	35
c_1	150	35

Table 9: Costs of nonsupplied demand.

Number	C_d^{LS}[\$/MWh]
d_1	80
d_2	80
d_3	80
d_4	80

difficult to be able to operate satisfactorily in the face of out-of-service elements (either generation or transmission). For the system studied, Table 14 illustrates the case of $N-1$ contingencies in transmission. In that sense, the problem can be seen as a financial one, since to support the outage of elements, the others have to be oversized. Although there are direct ways of dealing with the problem of contingencies [79], the mentioned approach seems a good approximation in this case. That is, it is reiterated that in this case, one way to solve such problems is by oversizing the generation and transmission elements.

5.2. Case Study 2: G&TEP for 10-Year Periods. This case study considers the same model presented from (2), (4), (5), (6), (7), (8), (9), (10), (11), (12), (13), (14), (15), (16), (17), (18), (19), (20), (21), (22), (23), (24), (25), (26), (27), (28), (29), and (30). In this particular case, the demand for each operating condition and period was defined in correspondence of each one of 1024 scenarios. Data for combinations in the scenario tree are obtained by using a uniform distribution with the intervals summarized in Table 15 (only shown for t_1, t_5, and t_{10}). In the second and third columns of the same table, the lower and higher demands are provided for the first period by each demand bus. Similar to the previous case study, each period represents a year, which in turn has been divided into two operating conditions o_1 and o_2, with weights (for all periods) becoming 6000 and 2760 hours. This case study assumes $M = 3 \times 105$ and equal probability for each scenario of 0.00097. Notice that test system has 4 load buses, as shown in Figure 4. Then, for every load bus, there is a tree diagram similar to that in Figure 5. The demand for each operating condition and period was defined in correspondence of each one of 1024 scenarios. The installed capacity for clean energy for all ten periods and 1024 scenarios was set to 60 MW.

Figure 4 includes all elements described in the proposed formulation: (i) candidate transmission lines (dotted lines, l_5 and l_8); (ii) candidate conventional and wind generators (c_1 and cw_1). For each bus, low (L) and high (H) load demands are taken into account (see Tables 15–20. This gives rise to one thousand twenty-four scenarios per bus (see, e.g., Figure 5). The strategy to solve the problem is the linear mixed integer programming. After solving problems (2), (4), (5), (6), (7), (8), (9), (10), (11), (12), (13), (14), (15), (16), (17), (18), (19), (20), (21), (22), (23), (24), (25), (26), (27), (28), (29), and (30), the optimal expansion plan considers an objective function value of \$3375.6M USD.

Table 10: Time for each operating condition and weighting factor for each operating condition not satisfying clean energy's goal.

Operating condition	Hours	Cost [\$/MWh]
o_1	6000	100
o_2	2760	100

Table 11: Amortization rate per period and clean energy's goal per period.

Period	Amortization rate α_t[%]	Clean energy's goal k_t[%]
t_1	0.3	0.1
t_2	0.2	0.2
t_3	0.1	0.3

Table 12: Investment costs.

Type of generator	[\$/MWh]
Candidate wind generator $\tilde{I}_{\text{cw}}$	700,000
Candidate conventional generator $\tilde{I}_c$	700,000

Table 13: Investment costs.

Item	[\$]
Transmission line $\tilde{I}_l$	1,000,000
Budget for installing candidate wind generators $I_t^{\text{CW,max}}$	105,000,000
Budget for installing candidate conventional generators $I_t^{C,\max}$	133,000,000
Budget for installing candidate transmission lines $I_t^{L,\max}$	2,000,000

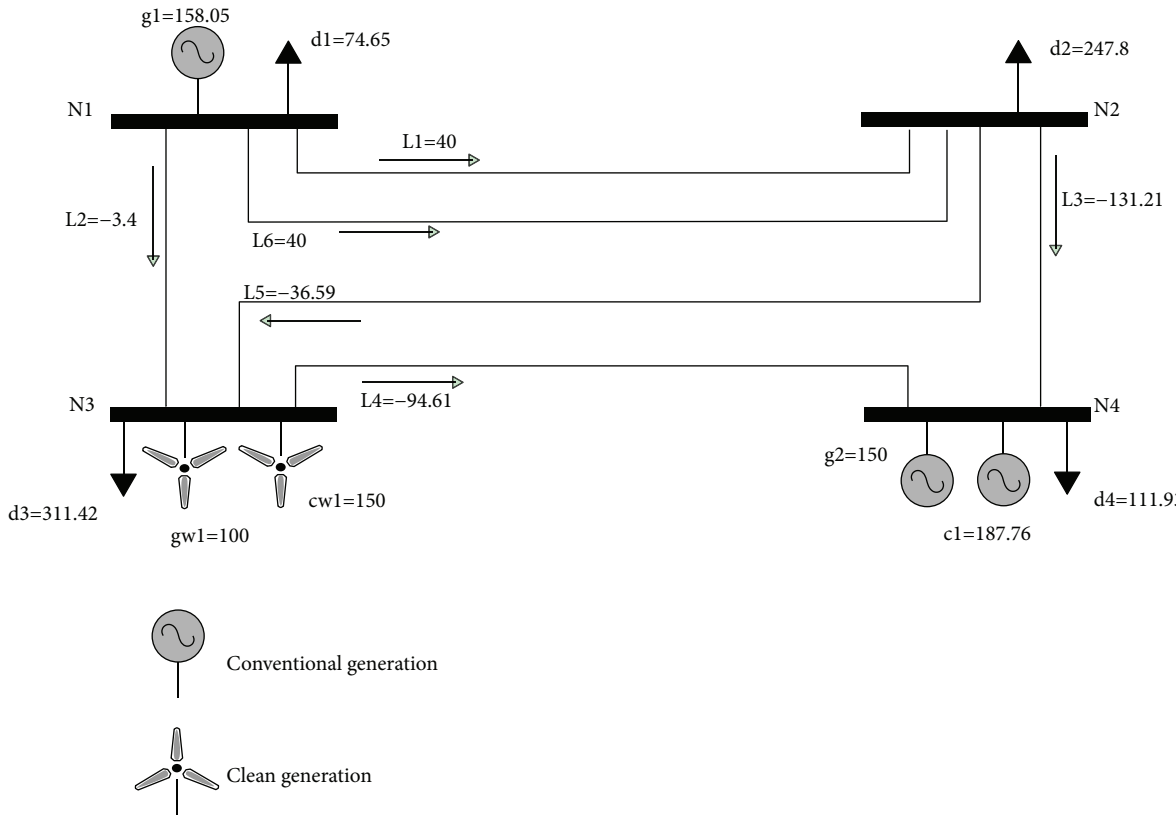

Figure 3: Results attained by the linear mixed integer programming method (condition $o_2t_3\omega_8$).

Table 14: Power flow after line outage using distribution factors [75].

Lines	Base case P_l [MW]	Power flow outage [MW]						$F_{l_{max}}$ [MW]
		L_1(1-2)	L_2(1–3)	L_3(2–4)	L_4(3-4)	L_5(2-3)	L_6(1-2)	
L_1(1-2)	40.00	—	−30.47	58.17	33.51	56.88	65.00	40.00
L_2(1–3)	−19.07	−4.07	—	−55.56	−6.09	−52.82	−4.07	100.00
L_3(2–3)	−91.52	−96.52	−97.88	—	−123.96	−116.84	−96.52	140.00
L_4(3-4)	−32.44	−27.44	−26.08	−123.96	—	−7.12	−27.44	105.00
L_5(2-3)	−59.07	−69.07	−71.78	−113.98	−39.61	—	−69.07	200.00
L_6(1-2)	40.00	65.00	30.47	58.17	33.51	56.88	—	−40.00

Table 15: Maximum and minimum demand by bus [MWh/h].

Demand	Period t_1		Period t_5		Period t_{10}	
	Low	High	Low	High	Low	High
d_1	40–43.2	43.2–46.4	82.94–89.58	89.58–96.22	206.39–222.9	222.9–239.41
d_2	136–146.88	146.88–157.76	282.01–304.57	304.57–327.13	701.73–757.87	757.87–814.01
d_3	160–172.8	172.8–185.6	331.78–358.32	358.32–384.86	825.56–891.61	891.61–957.66
d_4	64–69.12	69.12–74.24	132.71–143.33	143.33–153.95	330.23–356.64	356.64–383.06

Table 16 indicates that the conventional candidate unit c_1 is installed from the period t_3. Table 17 provides information about transmission lines. Tables 18–20 summarize the installed capacity of clean and conventional power, as well as the number of lines installed along the planning horizon, as shown in Figure 6. The next step is related to the generators' dispatch for each operating condition, period, and particular scenario. For this case study, there are two

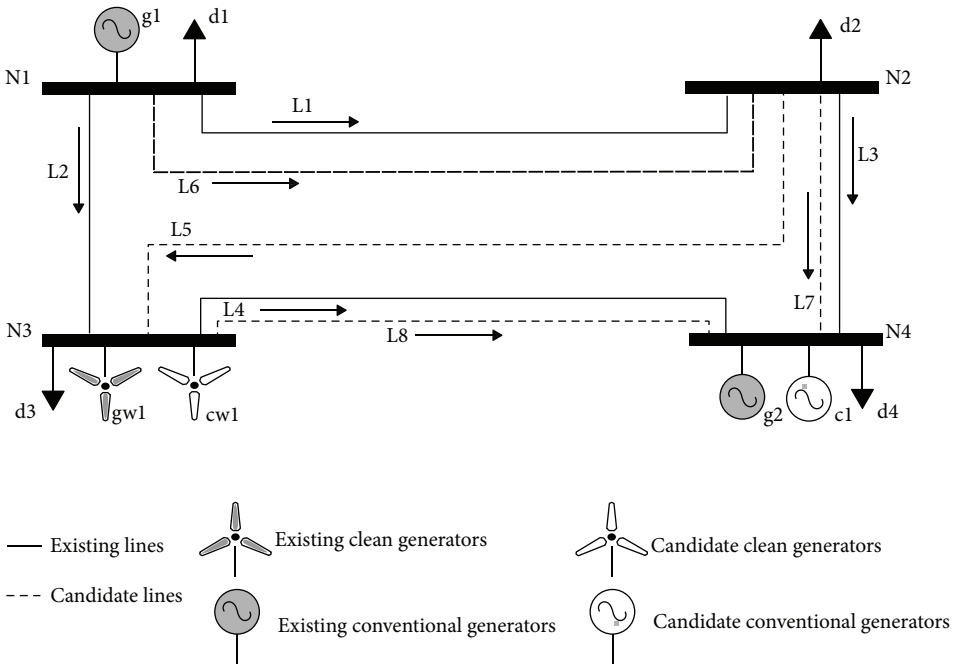

Figure 4: Four-buses test power system.

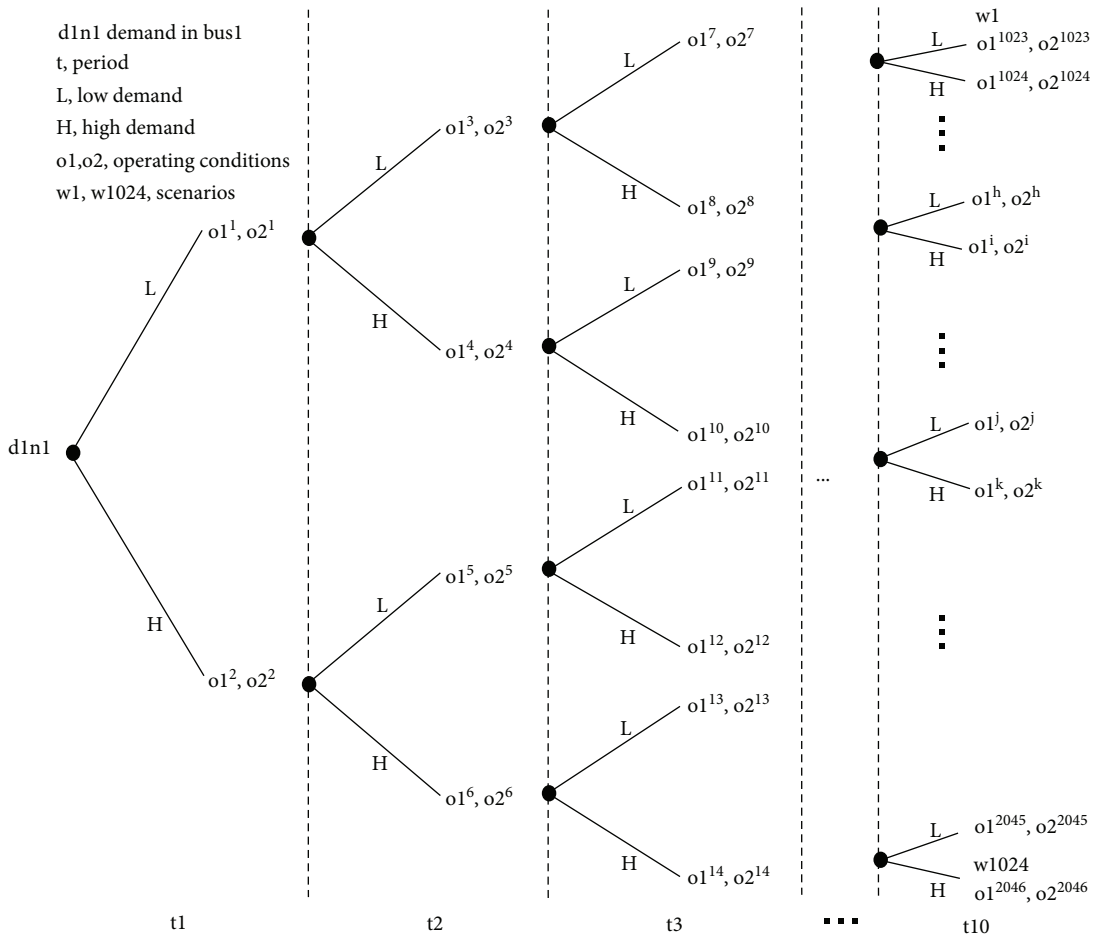

Figure 5: Scenario tree for the stochastic load demand in bus 1.

Table 16: Expected value of the installed capacity for the conventional candidate energy [MW].

Scenarios / Unit	Period	ω_1–ω_{128}	ω_{129}–ω_{256}	ω_{257}–ω_{384}	ω_{385}–ω_{512}	ω_{513}–ω_{640}	ω_{641}–ω_{768}	ω_{769}–ω_{896}	ω_{897}–ω_{1024}
c_1	t_3	0	0	0	0	0	16.68	0	20.16
c_1	t_4	14.44	0	0	13.91	20.79	17.47	30	30
c_1	t_5	30	15.95	15.24	30	30	30	28.11	23.94
c_1	t_6	27.86	30	30	29.96	30	30	30	30
c_1	t_7	30	30	30	30	30	30	30	30
c_1	t_8	30	30	30	30	30	30	30	30
c_1	t_9	30	30	30	30	30	30	30	30
c_1	t_{10}	30	30	30	30	30	30	30	30
Expected value of total installed power [MW]		192.3	165.95	165.24	193.87	200.79	214.15	208.11	224.1

Table 17: Data for transmission lines.

Number	B (susceptance)	$F_l^{\max}$ [MW] (maximum power flow)
l_1	500	40
l_2	500	100
l_3	500	140
l_4	500	105
l_5	500	200
l_6	500	40
l_7	500	100
l_8	500	105

Table 18: Data for existing and candidate generators.

Number	$P_g^{E^{\max}}$;$P_{\text{gw}}^{E^{\max}}$ [MW]	C_c^C;$C_{\text{cw}}^{\text{CW}}$ [\$/MWh]
g_1	800	35
g_2	300	35
c_1	300	35
gw_1	400	25
cw_1	600	25

demand conditions o_1 and o_2; ten periods t_1–t_{10}; and one thousand twenty-four scenarios ω_1–ω_{1024}. Therefore, the present model generates 20,480 different ways of dispatching the generating units ($2 \times 10 \times 1024 = 20,480$). It is impossible to describe each case here, so the following analysis corresponds to the condition o_2, t_{10}, and ω_{571}. Figure 6 displays the magnitude of the power flow through the transmission lines l_1–l_7, the generation of units g_1, g_2, gw_1, cw_1, and c_1, and the demand level at buses d_1–d_4. Data for costs of nonsupplied demand and operating conditions were used from Tables 9 and 10.

Table 19: Amortization rate per period and clean energy's goal per period.

Period	Amortization rate α_t[%]	Clean energy's goal k_t[%]
t_1	1.0	0.05
t_2	0.9	0.10
t_3	0.8	0.15
t_4	0.7	0.20
t_5	0.6	0.25
t_6	0.5	0.30
t_7	0.4	0.35
t_8	0.3	0.40
t_9	0.2	0.41
t_{10}	0.1	0.42

Table 20: Investment costs.

Type of generator	[\$/MWh]
Candidate wind generator $\tilde{I}_{\text{cw}}$	300,000
Candidate conventional generator $\tilde{I}_c$	700,000

6. Experiments and Results

In this section, we describe the computational experiments designed to assess the performance of the proposed genetic algorithm, and we present the corresponding results. We make a comparative analysis of constraint-handling techniques applied in the pure genetic algorithm for three- and ten-year period time case studies of G&TEP problem. In these complex optimization problems with high number of constraints, it is very difficult even to find feasible solutions. The aim of the experiments is to determine which of these techniques is able to reduce the number of constraints that are not fulfilled and is better suited for complex problems.

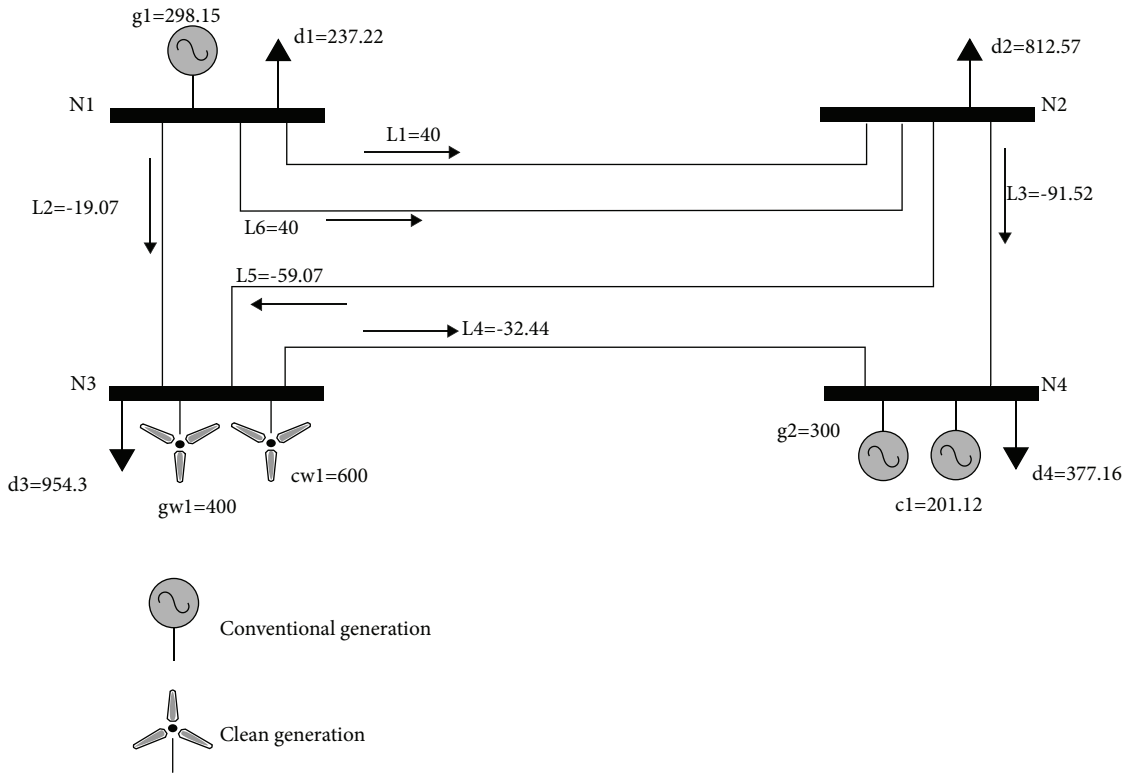

Figure 6: Results attained by the linear mixed integer programming method (condition $o_2t_{10}\omega_{571}$).

Table 21: Genetic algorithm parameters for all experiments.

Parameter	Value
Population size	200
Crossover probability (pc)	0.8
Mutation probability (pm)	0.1
Number of generations	1500
kk (for experiments with strategies 2 and 4)	1,000,000

Therefore, even if infeasible solutions are reported, the purpose of identifying the best strategy was achieved.

6.1. Experiments. We designed eight experiments for each of the three- and ten-year period time case studies. The first experiment was done for comparison purposes just taking into account the unconstraint problem. The fitness function is equal to the computation of the objective function SD of the case study. No penalty was incorporated to the fitness function $ff(\text{individual}) = \text{SD}$. Seven computational experiments were performed to test the effectiveness of the constraint-handling strategies presented in Section 4. The parameters of the pure genetic algorithm were set as shown in Table 21 for all experiments.

6.2. Results. For comparison purposes, we used the results of the best solution found of each experiment. We report the best result in the objective function of each experiment. The fitness function cannot be compared given that each constraint-handling strategy is computed in different ways. We also calculate the distance of the best SD with the aim of determining the completion cost, that is, the distance to feasibility. The number of constraints violated by the best solution in the generation is also considered.

First, we conducted the experiments over case study 1 (3-year period G&TEP problem). For the analysis, we also considered comparing the effectiveness of the pure genetic algorithm when the initial population is created randomly, but bounded; and also in the case when the initial set of individuals is populated with an initial guess trying to fulfill with all constraints, as many as possible. Table 22 summarizes the results for all experiments, including the following information: best SD, the distance to feasibility of the best SD presented as the sum of the absolute error calculated with (39) and the relative error of the distance to feasibility, and the number of violated constraints of the best SD. In addition, the evolution of the fitness function through generations is presented in Figures 7–14 for both initialization procedures (black lines for random and red lines for prior) and using all handling-constraint strategies.

In terms of the random initialization, the results of the first experiment (Figure 7), considering the unconstrained problem, show that although it seems to achieve the best SD, the distance to feasibility of the best solution is huge in relation to a great number of constraints violated. The next experiments were compared with this result in order to determine the quantity of improvement obtained with each of the different proposed strategies. Then, in the

Table 22: Summary of results for all experiments over case study 1: 3-year period G&TEP problem.

Strategy	Random initialization			Customized initialization		
	Best SD [M$]	Distance of the best SD [M$]	N of the best SD	Best SD [M$]	Distance of the best SD [M$]	N of the best SD
Unconstrained	58.6	20.3	664	61.4	13.0	629
Strategy 1	772.1	0.5	436	740.1	0.6	419
Strategy 2	77.8	0.6	436	98.9	0.5	421
Strategy 3	214.3	0.6	446	209.4	0.6	410
Strategy 4	746.7	0.5	427	773.1	0.8	422
Strategy 5	83.4	2.0	452	73.1	1.9	419
Strategy 6	712.8	0.02	386	708.1	0.02	367
Strategy 7	725.8	0.03	408	721.1	0.02	379

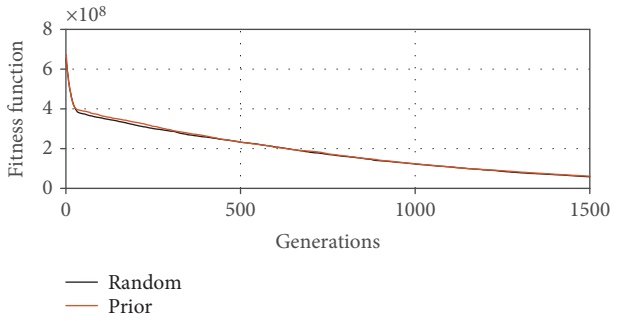

Figure 7: Evolution of the unconstrained fitness function through generations.

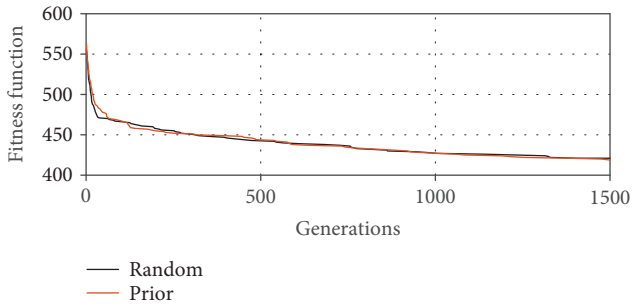

Figure 8: Evolution of the fitness function of strategy 1 through generations.

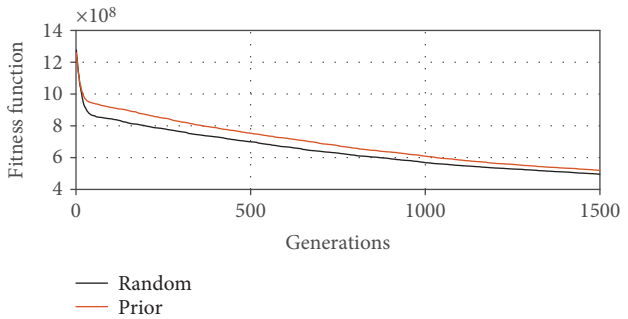

Figure 9: Evolution of the fitness function of strategy 2 through generations.

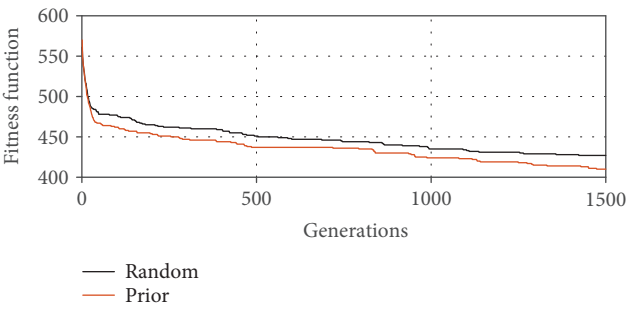

Figure 10: ff harmonic evolution of the fitness function of strategy 3 through generations.

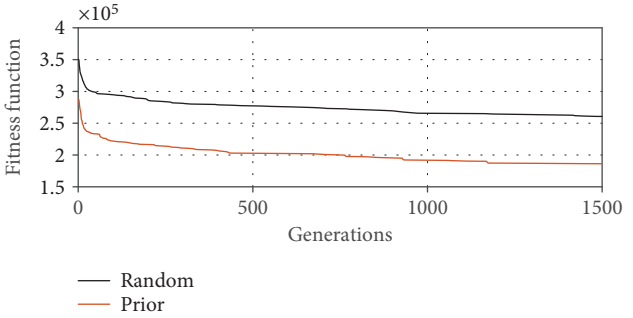

Figure 11: Evolution of the fitness function of strategy 4 through generations.

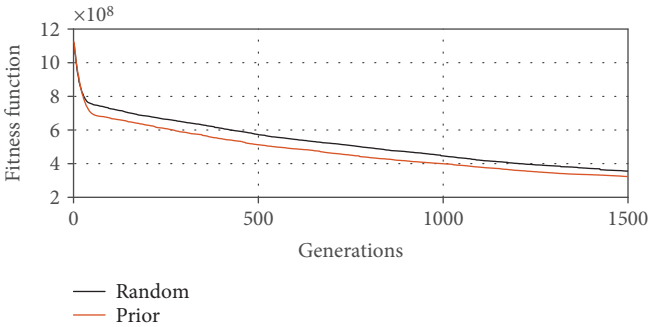

Figure 12: Evolution of the fitness function of strategy 5 through generations.

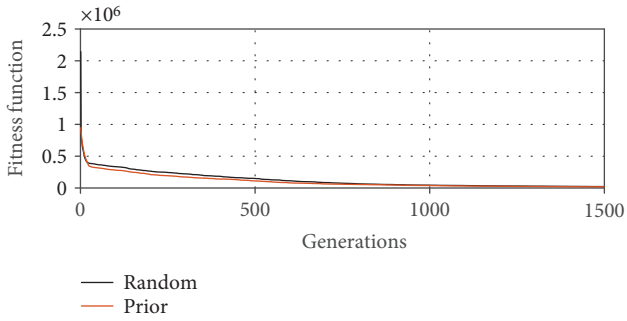

Figure 13: Evolution of the fitness function of strategy 6 through generations.

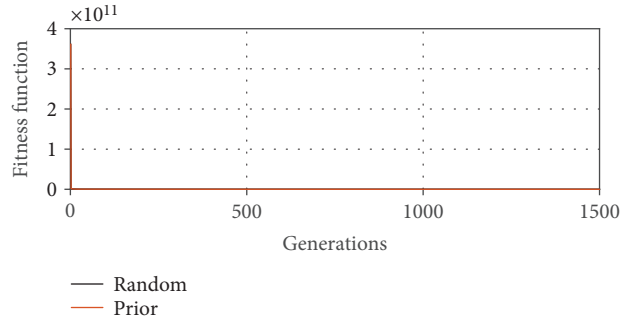

Figure 14: Evolution of the fitness function of strategy 7 through generations.

Table 23: Summary of results for all experiments over case study 2: 10-year period G&TEP problem.

Strategy	Best SD [billion $]	Distance of the best SD [billion $]	N of the best SD
Unconstrained	16.1	2777.9	459,346
Strategy 1	16.3	2826.5	456,958
Strategy 2	16.3	2805.9	457,757
Strategy 3	16.3	2803.3	457,587
Strategy 4	16.2	2797.4	455,969
Strategy 5	16.3	2831.2	456,888
Strategy 6	16.2	2699.1	459,419
Strategy 7	16.2	2698.8	459,374

second experiment, we applied the number of violated constraints strategy (strategy 1). The results show a considerable improvement in the distance to feasibility. Nevertheless, the best SD increased significantly (Figure 8). The third experiment uses strategy 2 (Figure 9) which incorporates the number of violated constraints to the objective function. Although the distance to feasibility and the number of violated constraints remained similar to the previous experiment, the best SD is below from the best solution presented in Section 5. The harmonic mean strategy (strategy 3, Figure 10) was applied in the fourth experiment. Even if this strategy balanced both objectives, the distance of feasibility and number of constraints violated, the best SD remained below the best solution. The feasibility differentiation strategy (strategy 4, Figure 11) did not provide a significant improvement in comparison with previous strategies. The performance of weighted strategy (strategy 5, Figure 12) is similar to the results obtained in strategy 2, hence the infeasibility of the best solution shown with the distance increased. The performance of the distance-based strategies 6 (Figure 13) and 7 (Figure 14) proved to obtain a solution closer to feasibility region. They achieved the best improvement in comparison with the first experiment. However, the SD is still not close to the best solution of the case study.

In contrast to the random initialization process, results from deliberative initialization showed a significant improvement in terms of the number of constraints violated. It is evident that fulfilling more constraints, the objective function SD increases more than when many constraints are violated. Moreover, the distance of the best SD also decreases, as expected. To this end and considering the above results, strategies 4, 6, and 7 are the better alternatives for using in a pure genetic algorithm for solving the G&TEP problem. Prior initialization avoiding constraint failure is an improvement for the algorithm, too. Also, it can be observed that an abrupt change in the evolution of the minimization of the fitness function occurs in less than 150 generations.

Later on, we conducted the experiments over case study 2 (10-year period G&TEP problem). Notice that this problem is challenging in the way that there are 552,960 variables for optimizing, in contrast to the 1152 variables from the 3-year period G&TEP problem. Thus, we ran the experiments using the observations from the previous case study: prior initialization of the population was done trying to fulfill the constraints as many as possible, and a maximum of 200 generations was fixed. Table 23 summarizes the results of all the experiments over case study 2, and Figures 15–22 show the evolution of the fitness function over generations.

As shown in the results, strategy 4 (Figure 19) obtained the least number of violated constraints among the other strategies. However, it can be seen that all strategies had difficulties to minimize the fitness functions, in comparison to the unconstrained strategy. However, in terms of the distance of the best SD, strategies 6 and 7 were the best ones comparing to the unconstrained strategy. It is remarkable to say that these experiments had issues in terms of the implementation. For this case study, all experiments were run in a flexible cloud-service in order to achieve the results because they could not run under a standard quadcore computer, as done for case study 1.

To this end, the present analysis highlights that using a pure genetic algorithm for G&TEP problems can achieve a first approximation to a suitable solution. However, it is worth noting that other optimization approaches should be selected in order to handle this complex problem. Furthermore, it can be shown that strategies 4, 6, and 7 consistently achieve better results than the other strategies, and a prior initialization of the population is a key insight for further research when dealing with G&TEP problems.

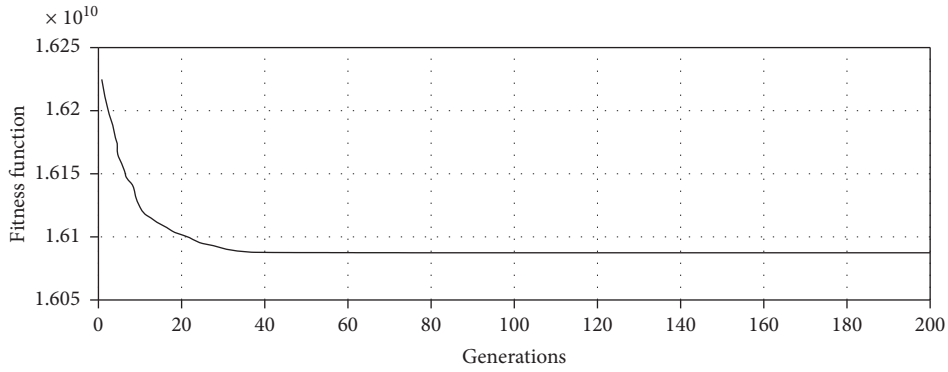

Figure 15: Evolution of the unconstrained fitness function through generations.

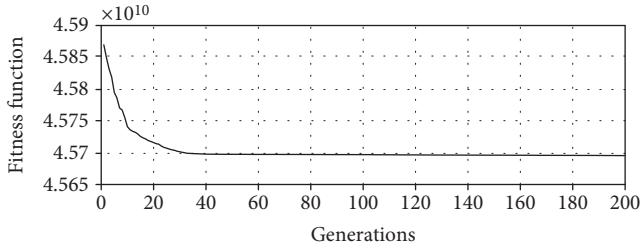

Figure 16: Evolution of the fitness function of strategy 1 through generations.

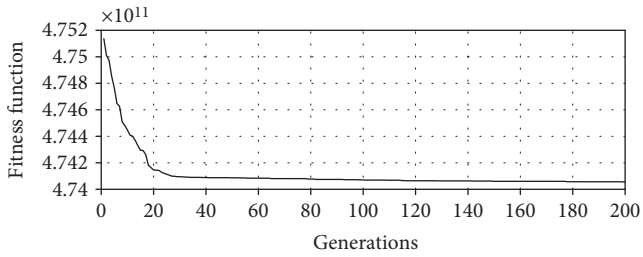

Figure 17: Evolution of the fitness function of strategy 2 through generations.

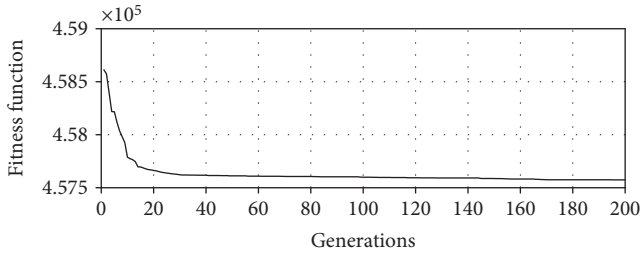

Figure 18: f f harmonic evolution of the fitness function of strategy 3 through generations.

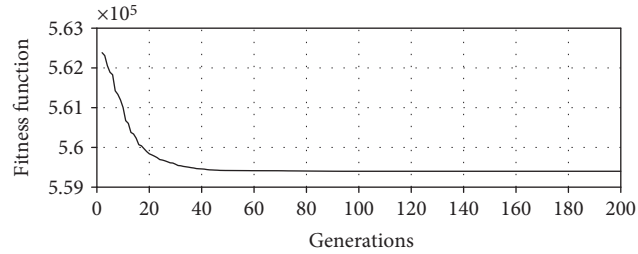

Figure 19: Evolution of the fitness function of strategy 4 through generations.

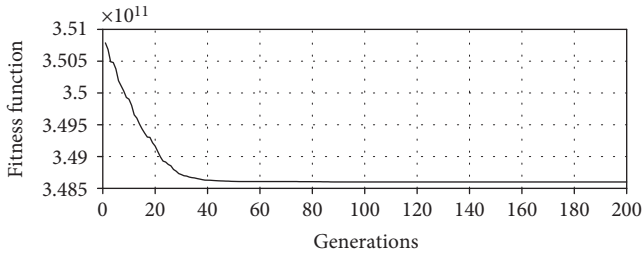

Figure 20: Evolution of the fitness function of strategy 5 through generations.

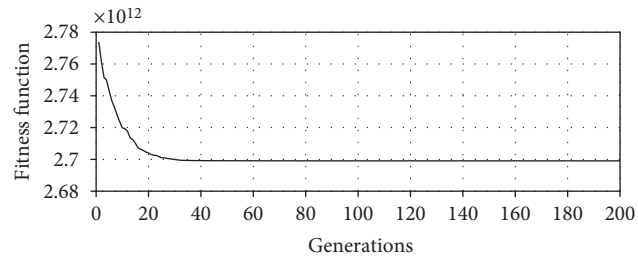

Figure 21: Evolution of the fitness function of strategy 6 through generations.

7. Conclusions and Future Work

In this paper, we proposed a multiperiod stochastic model applied to the G&TEP problem considering the insertion of renewable energies, which objective is to achieve a generation and transmission expansion plan that minimizes the total cost of investment. In addition, we proposed to address the G&TEP problem with a pure genetic algorithm approach.

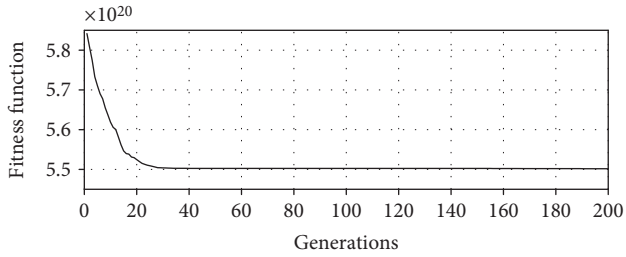

Figure 22: Evolution of the fitness function of strategy 7 through generations.

Different constraint-handling techniques were applied to deal with the complex case studies.

The comparative analysis conducted in this work shows that although we applied many of the most commonly used constraint-handling techniques reported in literature, our proposed genetic algorithm did not performed efficiently as required. The best solutions reported did not provide a feasible solution. From these results, we can state that a pure metaheuristic approach like genetic algorithm is not fitted for this particular G&TEP case study with clean energies, which is a nonlinear complexity problem with a high number of constraints (e.g., the 10-year period G&TEP problem). However, our analysis showed that the techniques to handle constraints with penalty functions based on the feasibility differentiation, the absolute-distance, and the squares-of-distance performed better than the other implemented strategies. Ultimately, a pure genetic algorithm implementing those strategies, as well as a prior initialization of the population, promotes a first approximation to a suitable solution if other optimization approaches are then conducted.

Unless these results with a metaheuristic method apparently show worst performance than the linear stochastic mixed integer programming method, a large-scale real-world problem cannot be solved without using metaheuristic optimization approaches as stated in [18]. Therefore, for future work, we will explore hybrid metaheuristic approaches for this G&TEP problem. With regard to the mathematical model, we will search for possible valid inequalities to ensure a bigger feasibility region. We will also explore an analysis including $N - K$ contingencies.

Notations

Indices

n: Buses
g: Existing conventional generators
gw: Existing clean energy generators
c: Candidate conventional generators
cw: Candidate clean energy generators
d: Demand
l: Transmission lines
o: Operating conditions
t: Time periods
ω: Scenarios.

Sets

Ω^{L^+}: Candidate transmission lines
Ω_n^E: Conventional existing generators located at bus n
Ω_n^{EW}: Existing wind generators located at bus n
Ω_n^C: Candidate conventional generators located at bus n
Ω_n^{CW}: Candidate clean energy generators located at bus n
Ω_n^D: Demand at bus n
$s(l)$: Sending bus for transmission line l
$r(l)$: Ending bus for transmission line l.

Parameters

B_l: Susceptance of transmission line l
C_c^C: Production cost of the conventional candidate generating unit[\$/MWh]
$C_{\mathrm{cw}}^{\mathrm{CW}}$: Production cost of the clean candidate generating unit [\$/MWh]
C_d^{LS}: Cost of the not supplied demand not supplied [\$/MWh]
C_n^E: Production cost for the existing conventional generating unit [\$/MWh]
C_n^{EW}: Production cost of the existing clean generating unit [\$/MWh]
$F_l^{\max}$: Rating of the transmission line l [MW]
$I_t^{\mathrm{CW,max}}$: Investment budget to build the clean generation candidate unit [\$]
$I_t^{C,\max}$: Investment budget to build the conventional generating candidate unit [\$]
$I_t^{L,\max}$: Investment budget to build the candidate transmission line l [\$]
$\tilde{I}_{\mathrm{cw}}$: Investment cost for the candidate clean generation unit cw [\$/MW]
$\tilde{I}_c$: Investment cost for the candidate conventional generating unit c [\$/MW]
$\tilde{I}_l$: Investment cost for the candidate transmission line l [\$]
$\bar{P}_c^{\mathrm{CW}^{\max}}$: Maximum generation capacity of the candidate clean generation unit cw [MW]
$\bar{P}_c^{\mathrm{C}^{\max}}$: Maximum generation capacity of the candidate conventional generation unit c [MW]
$P_d^{D^{\max}}$: Maximum demand d [MW]
$P_g^{E^{\max}}$: Maximum production capacity of the existing conventional generation unit g [MW]
$P_{\mathrm{gw}}^{E^{\max}}$: Maximum production capacity of the existing clean energy generation unit gw [MW]
ρ_o: Weight of the operating condition o [h]
γ_o: Penalization cost for breaching the renewable portfolio requirement [\$/MWh]
α_t: Amortization rate [%]
k_t: Clean energy's goal [%]
φ_ω: Probability of the scenario ω [$p.u.$].

Binary Variables

X_l^L: Binary variable: equal to 1 if the candidate transmission line is constructed, and 0 otherwise.

Continuous Variables

P_g^E: Power supplied by the existing conventional generating unit [MW]
$P_{\text{gw}}^{\text{EW}}$: Power supplied by the existing wind generating unit [MW]
$P_{\text{cw}}^{\text{CW}}$: Power supplied by the candidate wind generator unit [MW]
P_c^C: Power supplied by the conventional candidate generating unit [MW]
P_d^{LS}: Not supplied demand [MW]
P_l^L: Power flow through the transmission line l [MW]
θ_n: Angle of voltage at bus n [rad]
$P_c^{\text{CW}^{\max}}$: Rating of the candidate clean generation unit [MW]
$P_c^{C^{\max}}$: Rating of the candidate conventional generating unit [MW]
$\text{TT}_{ot\omega}$: Deficiency of the renewable goal [MW]
SD: Objective function, total investment [$].

Genetic Algorithms

ff: Fitness function
N: Number of violated constraints
kk: Large penalty constant
S: Number of satisfied constraints
m: Total number of constraints
w_i: Penalty weights
b_i: Bounds of constraints.

Data Availability

The data used to support the findings of this study are available from the corresponding author upon request.

Conflicts of Interest

The authors declare that they have no conflict of interest.

References

[1] A. M. Al-Shaalan, "Essential aspects of power system planning in developing countries," *Journal of King Saud University-Engineering Sciences*, vol. 23, no. 1, pp. 27–32, 2011.

[2] P. C. M. Munasinghe, *The Economics of Power System Reliability and Planning*, vol. 1, The World Bank Publications, 1979.

[3] G. Schramm, "Electric power in developing countries: status, problems, prospects," *Annual Review of Energy*, vol. 15, no. 1, pp. 307–333, 1990.

[4] H. Stoll, *Least-Cost Utility Planning*, John Wiley and Sons, Inc., 1st edition, 1989.

[5] R. Sullivan, *Power System Planning*, McGraw-Hill Inc., 1st edition, 1977.

[6] H. Seifi and M. S. Sepasian, *Electric Power System Planning*, Springer, Berlin, Heidelberg, 1st edition, 2011.

[7] P. Masse and R. Gibrat, "Application of linear programming to investments in the electric power industry," *Management Science*, vol. 3, no. 2, pp. 149–166, 1957.

[8] D. Anderson, "Models for determining least-cost investments in electricity supply," *The Bell Journal of Economics and Management Science*, vol. 3, no. 1, p. 267, 1972.

[9] N. Alguacil, A. L. Motto, and A. J. Conejo, "Transmission expansion planning: a mixed-integer LP approach," *IEEE Transactions on Power Systems*, vol. 18, no. 3, pp. 1070–1077, 2003.

[10] R. Romero, A. Monticelli, A. Garcia, and S. Haffner, "Test systems and mathematical models for transmission network expansion planning," *IEE Proceedings - Generation, Transmission and Distribution*, vol. 149, no. 1, pp. 27–36, 2002.

[11] M. F. Pereira, L. V. G. Pinto, S. F. Cunha, and G. Oliveira, "A decomposition approach to automated generation/transmission expansion planning," *IEEE Transactions on Power Apparatus and Systems*, vol. PAS-104, no. 11, pp. 3074–3083, 1985.

[12] B. G. Gorenstin, N. M. Campodonico, J. P. Costa, and M. V. F. Pereira, "Power system expansion planning under uncertainty," *IEEE Transactions on Power Systems*, vol. 8, no. 1, pp. 129–136, 1993.

[13] H. Park and R. Baldick, "Stochastic generation capacity expansion planning reducing greenhouse gas emissions," *IEEE Transactions on Power Systems*, vol. 30, no. 2, pp. 1026–1034, 2015.

[14] S. Ahmed, A. J. King, and G. Parija, "A multi-stage stochastic integer programming approach for capacity expansion under uncertainty," *Journal of Global Optimization*, vol. 26, no. 1, pp. 3–24, 2003.

[15] Q.-C. Zhong, "Power-electronics-enabled autonomous power systems: architecture and technical routes," *IEEE Transactions on Industrial Electronics*, vol. 64, no. 7, pp. 5907–5918, 2017.

[16] R. Hemmati, "Optimal design and operation of energy storage systems and generators in the network installed with wind turbines considering practical characteristics of storage units as design variable," *Journal of Cleaner Production*, vol. 185, pp. 680–693, 2018.

[17] A. Conejo, L. Baringo, S. Kazempour, and A. Siddiqui, *Investment in Electricity Generation and Transmission: Decision Making under Uncertainty*, Springer, Berlin, Heidelberg, 1st edition, 2016.

[18] Y. Liu, R. Sioshansi, and A. J. Conejo, "Multistage stochastic investment planning with multiscale representation of uncertainties and decisions," *IEEE Transactions on Power Systems*, vol. 33, no. 1, pp. 781–791, 2018.

[19] Y. Guan, S. Ahmed, and G. L. Nemhauser, "Cutting planes for multistage stochastic integer programs," *Operations Research*, vol. 57, no. 2, pp. 287–298, 2009.

[20] C. A. Coello Coello, "Theoretical and numerical constraint-handling techniques used with evolutionary algorithms: a survey of the state of the art," *Computer Methods in Applied Mechanics and Engineering*, vol. 191, no. 11-12, pp. 1245–1287, 2002.

[21] H. Sadeghi, M. Rashidinejad, and A. Abdollahi, "A comprehensive sequential review study through the generation expansion planning," *Renewable and Sustainable Energy Reviews*, vol. 67, pp. 1369–1394, 2017.

[22] R. Hemmati, R.-A. Hooshmand, and A. Khodabakhshian, "State-of-the-art of transmission expansion planning: comprehensive review," *Renewable and Sustainable Energy Reviews*, vol. 23, pp. 312–319, 2013.

[23] R. Hemmati, R.-A. Hooshmand, and A. Khodabakhshian, "Comprehensive review of generation and transmission expansion planning," *IET Generation, Transmission & Distribution*, vol. 7, no. 9, pp. 955–964, 2013.

[24] P. Kunche and K. Reddy, "Heuristic and meta-heuristic optimization," in *Metaheuristic Applications to Speech Enhancement*, pp. 17–24, Springer, 2016.

[25] A. Hertz and D. de Werra, "The tabu search metaheuristic: how we used it," *Annals of Mathematics and Artificial Intelligence*, vol. 1, no. 1–4, pp. 111–121, 1990.

[26] K. Sorensen, M. Sevaux, and F. Glover, "A history of Metaheuristics," 2017, https://arxiv.org/abs/1704.00853.

[27] M. P. Saka, O. Hasançebi, and Z. W. Geem, "Metaheuristics in structural optimization and discussions on harmony search algorithm," *Swarm and Evolutionary Computation*, vol. 28, pp. 88–97, 2016.

[28] A. M. Leite da Silva, M. R. Freire, and L. M. Honório, "Transmission expansion planning optimization by adaptive multi-operator evolutionary algorithms," *Electric Power Systems Research*, vol. 133, pp. 173–181, 2016.

[29] M. P. Saka and E. Dogan, "Recent developments in metaheuristic algorithms: a review," *Computer Technology Review*, vol. 5, pp. 31–78, 2012.

[30] F. W. Glover and G. A. Kochenberger, *Handbook of Metaheuristics*, vol. 57, Springer Science & Business Media, 2006.

[31] C. Blum, J. Puchinger, G. R. Raidl, and A. Roli, "Hybrid metaheuristics in combinatorial optimization: a survey," *Applied Soft Computing*, vol. 11, no. 6, pp. 4135–4151, 2011.

[32] M. A. Boschetti, V. Maniezzo, M. Roffilli, and A. B. Röhler, "Matheuristics: optimization, simulation and control," in *International Workshop on Hybrid Metaheuristics*, pp. 171–177, Springer, 2009.

[33] J. Soares, Z. Vale, N. Borges, F. Lezama, and N. Kagan, "Multi-objective robust optimization to solve energy scheduling in buildings under uncertainty," in *2017 19th International Conference on Intelligent System Application to Power Systems (ISAP)*, pp. 1–6, San Antonio, TX, USA, 2017.

[34] J.-B. Park, J.-H. Kim, and K. Y. Lee, "Generation expansion planning in a competitive environment using a genetic algorithm," in *IEEE Power Engineering Society Summer Meeting*, pp. 1169–1172, Chicago, IL, USA, 2002.

[35] A. J. C. Pereira and J. T. Saraiva, "Generation expansion planning (GEP)–a long-term approach using system dynamics and genetic algorithms (GAs)," *Energy*, vol. 36, no. 8, pp. 5180–5199, 2011.

[36] S. Kannan, S. M. R. Slochanal, P. Subbaraj, and N. P. Padhy, "Application of particle swarm optimization technique and its variants to generation expansion planning problem," *Electric Power Systems Research*, vol. 70, no. 3, pp. 203–210, 2004.

[37] N. Neshat and M. R. Amin-Naseri, "Cleaner power generation through market-driven generation expansion planning: an agent-based hybrid framework of game theory and particle swarm optimization," *Journal of Cleaner Production*, vol. 105, pp. 206–217, 2015.

[38] J. L. C. Meza, M. B. Yildirim, and A. S. M. Masud, "A multiobjective evolutionary programming algorithm and its applications to power generation expansion planning," *IEEE Transactions on Systems, Man, and Cybernetics - Part A: Systems and Humans*, vol. 39, no. 5, pp. 1086–1096, 2009.

[39] K. Rajesh, A. Bhuvanesh, S. Kannan, and C. Thangaraj, "Least cost generation expansion planning with solar power plant using differential evolution algorithm," *Renewable Energy*, vol. 85, pp. 677–686, 2016.

[40] A. Yoza, A. Yona, T. Senjyu, and T. Funabashi, "Optimal capacity and expansion planning methodology of PV and battery in smart house," *Renewable Energy*, vol. 69, pp. 25–33, 2014.

[41] A. R. Abbasi and A. R. Seifi, "Energy expansion planning by considering electrical and thermal expansion simultaneously," *Energy Conversion and Management*, vol. 83, pp. 9–18, 2014.

[42] S.-L. Chen, T.-S. Zhan, and M.-T. Tsay, "Generation expansion planning of the utility with refined immune algorithm," *Electric Power Systems Research*, vol. 76, no. 4, pp. 251–258, 2006.

[43] M. Jadidoleslam and A. Ebrahimi, "Reliability constrained generation expansion planning by a modified shuffled frog leaping algorithm," *International Journal of Electrical Power & Energy Systems*, vol. 64, pp. 743–751, 2015.

[44] P. Murugan, S. Kannan, and S. Baskar, "NSGA-II algorithm for multi-objective generation expansion planning problem," *Electric Power Systems Research*, vol. 79, no. 4, pp. 622–628, 2009.

[45] S. Kannan, S. Baskar, J. D. McCalley, and P. Murugan, "Application of NSGA-II algorithm to generation expansion planning," *IEEE Transactions on Power Systems*, vol. 24, no. 1, pp. 454–461, 2009.

[46] H. Sadeghi, A. Abdollahi, and M. Rashidinejad, "Evaluating the impact of fit financial burden on social welfare in renewable expansion planning," *Renewable Energy*, vol. 75, pp. 199–209, 2015.

[47] Y. M. Park, J. B. Park, and J. R. Won, "A hybrid genetic algorithm/dynamic programming approach to optimal long-term generation expansion planning," *International Journal of Electrical Power & Energy Systems*, vol. 20, no. 4, pp. 295–303, 1998.

[48] S. Kannan, S. M. R. Slochanal, and N. P. Padhy, "Application and comparison of metaheuristic techniques to generation expansion planning problem," *IEEE Transactions on Power Systems*, vol. 20, no. 1, pp. 466–475, 2005.

[49] F. Cadini, E. Zio, and C.-A. Petrescu, "Optimal expansion of an existing electrical power transmission network by multi-objective genetic algorithms," *Reliability Engineering & System Safety*, vol. 95, no. 3, pp. 173–181, 2010.

[50] S. Jalilzadeh, A. Shabani, and A. Azadru, "Multi-period generation expansion planning using genetic algorithm," in *International Congress on Ultra Modern Telecommunications and Control Systems*, pp. 358–363, Moscow, Russia, October 2010.

[51] H. Rudnick, R. Palma, E. L. da Silva, H. A. Gil, and J. M. Areiza, "Transmission network expansion planning under an improved genetic algorithm [discussion and closure]," *IEEE Transactions on Power Systems*, vol. 16, no. 4, pp. 930-931, 2001.

[52] M. Cortes-Carmona, R. Palma-Behnke, and O. Moya, "Transmission network expansion planning by a hybrid simulated annealing algorithm," in *2009 15th International Conference on Intelligent System Applications to Power Systems*, pp. 1–7, Curitiba, Brazil, November 2009.

[53] R. Romero, R. A. Gallego, and A. Monticelli, "Transmission system expansion planning by simulated annealing," *IEEE Transactions on Power Systems*, vol. 11, no. 1, pp. 364–369, 1996.

[54] R. A. Gallego, A. Monticelli, and R. Romero, "Transmision system expansion planning by an extended genetic algorithm," *IEE Proceedings - Generation, Transmission and Distribution*, vol. 145, no. 3, p. 329, 1998.

[55] R. A. Gallego, R. Romero, and A. J. Monticelli, "Tabu search algorithm for network synthesis," *IEEE Transactions on Power Systems*, vol. 15, no. 2, pp. 490–495, 2000.

[56] A. M. Leite da Silva, L. S. Rezende, L. A. da Fonseca Manso, and L. C. de Resende, "Reliability worth applied to transmission expansion planning based on ant colony system," *International Journal of Electrical Power & Energy Systems*, vol. 32, no. 10, pp. 1077–1084, 2010.

[57] L. S. Rezende, A. M. Leite da Silva, and L. de Mello Honório, "Artificial immune system applied to the multi-stage transmission expansion planning," *Lecture Notes in Computer Science*, vol. 5666, pp. 178–191, 2009.

[58] A. Verma, B. K. Panigrahi, and P. R. Bijwe, "Harmony search algorithm for transmission network expansion planning," *IET Generation, Transmission & Distribution*, vol. 4, no. 6, p. 663, 2010.

[59] H. Shayeghi, M. Mahdavi, and A. Bagheri, "Discrete PSO algorithm based optimization of transmission lines loading in TNEP problem," *Energy Conversion and Management*, vol. 51, no. 1, pp. 112–121, 2010.

[60] Y.-X. Jin, H.-Z. Cheng, J.-y. Yan, and L. Zhang, "New discrete method for particle swarm optimization and its application in transmission network expansion planning," *Electric Power Systems Research*, vol. 77, no. 3-4, pp. 227–233, 2007.

[61] A. Sadegheih and P. R. Drake, "System network planning expansion using mathematical programming, genetic algorithms and tabu search," *Energy Conversion and Management*, vol. 49, no. 6, pp. 1557–1566, 2008.

[62] H. Faria Jr., S. Binato, M. G. C. Resende, and D. M. Falcao, "Power transmission network design by greedy randomized adaptive path relinking," *IEEE Transactions on Power Systems*, vol. 20, no. 1, pp. 43–49, 2005.

[63] M. Moradi, H. Abdi, S. Lumbreras, A. Ramos, and S. Karimi, "Transmission expansion planning in the presence of wind farms with a mixed ac and dc power flow model using an imperialist competitive algorithm," *Electric Power Systems Research*, vol. 140, pp. 493–506, 2016.

[64] M. S. Javadi, H. R. Mashhadi, M. Saniei, and G. Gutiérrez-Alcaraz, "Multi-objective expansion planning approach: distant wind farms and limited energy resources integration," *IET Renewable Power Generation*, vol. 7, no. 6, pp. 652–668, 2013.

[65] F. Barati, H. Seifi, M. S. Sepasian, A. Nateghi, M. Shafie-khah, and J. P. S. Catalao, "Multi-period integrated framework of generation, transmission, and natural gas grid expansion planning for large-scale systems," *IEEE Transactions on Power Systems*, vol. 30, no. 5, pp. 2527–2537, 2015.

[66] A. Motamedi, H. Zareipour, M. O. Buygi, and W. D. Rosehart, "A transmission planning framework considering future generation expansions in electricity markets," *IEEE Transactions on Power Systems*, vol. 25, no. 4, pp. 1987–1995, 2010.

[67] P. Murugan, S. Kannan, and S. Baskar, "Application of NSGA-II algorithm to single-objective transmission constrained generation expansion planning," *IEEE Transactions on Power Systems*, vol. 24, no. 4, pp. 1790–1797, 2009.

[68] M. Khakpoor, M. Jafari-Nokandi, and A. Akbar Abdoos, "A new hybrid GA-fuzzy optimization algorithm for security-constrained based generation and transmission expansion planning in the deregulated environment," *Journal of Intelligent & Fuzzy Systems*, vol. 33, no. 6, pp. 3789–3803, 2017.

[69] B. Alizadeh and S. Jadid, "Reliability constrained coordination of generation and transmission expansion planning in power systems using mixed integer programming," *IET Generation, Transmission & Distribution*, vol. 5, no. 9, pp. 948–960, 2011.

[70] X. Wang and J. R. McDonald, *Modern Power System Planning*, McGrawHill Companies, 1994.

[71] Secretaría de Energía (SENER), "Program of development of the national electrical system (in Spanish)," 2017, https://www.gob.mx/sener/acciones-y-programas/programa-de-desarrollo-del-sistema-electrico-nacional-33462.

[72] A. J. Wood and B. F. Wollenberg, *Power Generation, Operation, and Control*, John Wiley & Sons, 2012.

[73] V. H. Hinojosa and J. Velásquez, "Improving the mathematical formulation of security-constrained generation capacity expansion planning using power transmission distribution factors and line outage distribution factors," *Electric Power Systems Research*, vol. 140, pp. 391–400, 2016.

[74] V. H. Hinojosa and J. Velásquez, "Stochastic security-constrained generation expansion planning based on linear distribution factors," *Electric Power Systems Research*, vol. 140, pp. 139–146, 2016.

[75] F. Gonzalez-Longatt and J. L. E. Rueda, *Power Factory Applications for Power System Analysis*, Springer, 1st edition, 2016.

[76] G. K. Awal and K. Bharadwaj, "Mining set of influencers in signed social networks with maximal collective influential power: a genetic algorithm approach," in *International Conference on Information and Communication Technology for Intelligent Systems*, pp. 263–274, Springer, 2017.

[77] A. K. Morales and C. V. Quezada, "A universal eclectic genetic algorithm for constrained optimization," in *Proceedings of the 6th European Congress on Intelligent Techniques and Soft Computing*, vol. 1, pp. 518–522, Aachen, Germany, 1998.

[78] R. L. Haupt, S. E. Haupt, and S. E. Haupt, *Practical Genetic Algorithms*, vol. 2, Wiley, New York, 1998.

[79] S. Hong, H. Cheng, and P. Zeng, "N-K constrained composite generation and transmission expansion planning with interval load," *IEEE Access*, vol. 5, pp. 2779–2789, 2017.

Hindawi
Complexity
Volume 2018, Article ID 1260743, 10 pages
https://doi.org/10.1155/2018/1260743

Research Article

Bidirectional Tracking Robust Controls for a DC/DC Buck Converter-DC Motor System

Eduardo Hernández-Márquez,[1] **José Rafael García-Sánchez**,[1] **Ramón Silva-Ortigoza**,[1] **Mayra Antonio-Cruz**,[1] **Victor Manuel Hernández-Guzmán**,[2] **Hind Taud**,[1] **and Mariana Marcelino-Aranda**[3]

[1]*Área de Mecatrónica, CIDETEC, Instituto Politécnico Nacional, 07700 Mexico City, Mexico*
[2]*Facultad de Ingeniería, Universidad Autónoma de Querétaro, 76150 Querétaro, QRO, Mexico*
[3]*SEPI, UPIICSA, Instituto Politécnico Nacional, 08400 Mexico City, Mexico*

Correspondence should be addressed to Ramón Silva-Ortigoza; rsilvao@ipn.mx

Received 25 January 2018; Revised 17 April 2018; Accepted 10 May 2018; Published 23 August 2018

Academic Editor: Hugo Morais

Two differential flatness-based bidirectional tracking robust controls for a DC/DC Buck converter-DC motor system are designed. To achieve such a bidirectional tracking, an inverter is used in the system. First control considers the complete dynamics of the system, that is, it considers the DC/DC Buck converter-inverter-DC motor connection as a whole. Whereas the second separates the dynamics of the Buck converter from the one of the inverter-DC motor, so that a hierarchical controller is generated. The experimental implementation of both controls is performed via MATLAB-Simulink and a DS1104 board in a built prototype of the DC/DC Buck converter-inverter-DC motor connection. Controls show a good performance even when system parameters are subjected to abrupt uncertainties. Thus, robustness of such controls is verified.

1. Introduction

The electrical energy control with power electronic devices has been an important research topic during the last years [1]. Where the driving of new classes of motors has been possible thanks to the power electronics [2]. Likewise, the use of the control engineering and power electronics [3], among other areas, glimpses the possibility of achieving a driving more efficient of the new forms of electrical energy generation [4]. In that direction, the different forms of electrical conversion result very important in the energy processing. Thus, the appropriate supply of multiple applications of the new energy forms is achieved [5–10]. In such applications, some involving motion generations are found whose operation is reduced to the design of drivers for motors (see [11, 12]). Among others, the DC motors have been benefited by the design of drivers based on DC/DC power electronic converters. Thus, according to the rotation of the motor shaft, works related to the control of DC/DC power converters-driven DC motors can be divided in two fashions: (a) with unidirectional rotation and (b) with bidirectional rotation. Thus, the state-of-the-art review is as follows.

1.1. Unidirectional Rotation. Lyshevski [11] proposed mathematical models for DC/DC power converters connected to DC motors. The topologies there considered were the Buck, Boost, and Cuk. Also, Lyshevski designed a nonlinear PI control for regulating the angular velocity of the DC/DC Buck converter-DC motor system. On the other hand, Boldea and Nasar [12] presented position, velocity, and torque controls to solve the regulation problem of DC/DC power converter-DC motor systems. Later, for the first time, Linares-Flores in [13] proposed a differential flatness-based control, an average GPI control, and a passivity-based control. These three controls solve the trajectory tracking

task in the DC/DC Buck converter-DC motor system. Also, for the same system, Ahmad et al. in [14] presented a performance assessment of the PI, fuzzy PI, and LQR controls for the angular velocity tracking problem. While Bingöl and Paçaci [15] reported a virtual laboratory based on neural networks to control angular velocity of such system. Recent works dealing with the angular velocity trajectory tracking for the DC/DC Buck converter-DC motor system have been reported in [16–21]. Sira-Ramírez and Oliver-Salazar [16] proposed a robust control based on the active disturbance rejection and differential flatness for two configurations of the DC/DC Buck converter-DC motor system. Silva-Ortigoza et al. introduced robust hierarchical controls based on differential flatness [17, 18] and sliding mode-PI with flatness in [19]. Likewise, Hernández-Guzmán et al. [20] proposed a sliding mode control and PI for controlling the converter voltage, the armature current, and the angular velocity of the motor. On the other hand, via a sensorless load torque estimation, a control based on the exact tracking error dynamics passive output feedback methodology was proposed by Kumar and Thilagar in [21]. More recently, Khubalkar et al. in [22] presented a stand-alone digital fractional order PID tracking control for the DC/DC Buck converter-DC motor system. Rigatos et al. in [23] designed a flatness-based control to solve the trajectory tracking problem. Another solution was proposed by Nizami et al. in [24], where a neuro-adaptive backstepping control for the angular velocity tracking was developed for the aforementioned system. Other interesting works reported in the last months, on tracking control design for the DC/DC Buck-DC motor system, are [25–29]. Additional works where other topologies of DC/DC power converters driven DC motors are [30–32] for the Boost converter, [33] for the Buck-Boost converter, and [34] for the Sepic and Cuk converters.

1.2. Bidirectional Rotation. Due to the principle of operation of the DC/DC power converters, the bidirectional velocity tracking control in DC/DC converters-DC motor systems is not possible using only DC/DC converters. Thus, to overcome this restriction, which has been a topic of interest in the last years, an inverter circuit has been introduced in such systems, leading to DC/DC converter-inverter-DC motor systems. In this direction, Ortigoza et al. presented in [35] the modeling and experimental validation of the DC/DC Buck converter-inverter-DC motor system. While in [36], Ortigoza et al. designed and tested a passivity-based tracking control for a built prototype of the same system. Furthermore, the model and a passivity-based tracking control for the DC/DC Boost converter-inverter-DC motor system were reported in [37] by García-Rodríguez et al. and [38] by Ortigoza et al., respectively. On the other hand, Márquez et al. reported the modeling and experimental validation of the DC/DC Buck-Boost converter-inverter-DC motor system in [39]. Also, for the same system, Hernández-Márquez et al. in [40] solved the regulation problem via a sensorless passivity-based control. Lastly, for the DC/DC Sepic converter-inverter-DC motor system Linares-Flores et al. in [41] solved the regulation problem through a passive control.

After reviewing the literature of the DC motors driven by DC/DC power converters, it was found that different controls have executed the angular velocity regulation and trajectory tracking tasks in two fashions: (i) for unidirectional rotation of the motor shaft [11–34] and (ii) for bidirectional rotation of the motor shaft [35–41]. From the point of view of the practical and industrial applications, [11–34] are limited when compared with [35–41]. Regarding the latter, to the authors' knowledge, for the DC/DC converter-inverter-DC motor systems, robust solution for the trajectory tracking has not been proposed. Thus, the main contribution of this paper is to propose two robust controls based on flatness for the tracking task in the DC/DC Buck converter-inverter-DC motor system. The first control considers the system complete dynamics; whereas the second takes into account the dynamics conforming the system separately (i.e., Buck converter and inverter-DC motor), producing a hierarchical controller. The designed controls are experimentally verified on a prototype, showing robustness under parametric uncertainty.

The remainder of the paper is organized as follows. In Section 2, the design of the robust controllers is developed. The experimental results are shown in Section 3. Finally, conclusions are presented in Section 4.

2. Tracking Controls Based on Differential Flatness

In this section, two controls are designed with the purpose of carrying out the bidirectional angular velocity trajectory tracking task of a DC/DC Buck converter-DC motor system.

2.1. System Model. The electronic circuit of the system under study is shown in Figure 1. This system, in general, is composed of three stages, namely, a DC/DC Buck converter, a complete bridge inverter, and a DC motor. Unlike the arrangements presented in [11–29], such configuration allows the bidirectional driving of the motor shaft.

The system average model presented in Figure 1, which was deduced and experimentally validated in [35], is given by

$$L\frac{di}{dt} = Eu_{1\mathrm{av}} - v, \tag{1}$$

$$C\frac{dv}{dt} = i - \frac{v}{R} - i_{\mathrm{a}}u_{2\mathrm{av}}, \tag{2}$$

$$L_{\mathrm{a}}\frac{di_{\mathrm{a}}}{dt} = vu_{2\mathrm{av}} - R_{\mathrm{a}}i_{\mathrm{a}} - k_{\mathrm{e}}\omega, \tag{3}$$

$$J\frac{d\omega}{dt} = k_{\mathrm{m}}i_{\mathrm{a}} - b\omega, \tag{4}$$

where i represents the inductor current, v is the capacitor output voltage, i_{a} is the armature current, ω is the angular velocity, the voltage source has the constant value E, L is the inductance of the input circuit, C is the capacitance of the output filter, R is the output load, L_{a} is the armature inductance, R_{a} is the armature resistance, J is the moment of inertia of the rotor and motor load, k_{e} is the

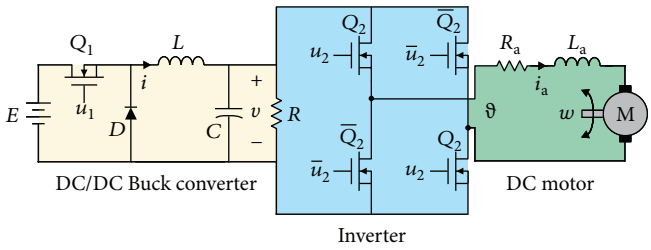

Figure 1: DC/DC Buck converter-inverter-DC motor system.

counterelectromotive force constant, k_m is the motor torque constant, and b is the viscous friction coefficient of the motor. Whereas u_{1av} and u_{2av} represent the system average controls, under the restrictions $u_{1av} \in [0, 1]$ and $u_{2av} \in [-1, 1]$, also known as duty cycles.

2.2. Flatness Control: Complete Dynamics. Here, the first flatness control that solves the bidirectional velocity tracking for the DC/DC Buck converter-inverter-DC motor system is designed. This first control considers all the system dynamics, that is, it is based on the fourth-order nonlinear model (1), (2), (3), and (4).

Departing from the work experience related to the DC/DC Buck converter-DC motor, particularly [17, 18], and [19], and from the control objectives, the flat outputs of the system (1), (2), (3), and (4) are proposed as $F_1 = v$ and $F_2 = \omega$. Thus, the system differential parametrization is determined by

$$v = F_1, \tag{5}$$

$$\omega = F_2, \tag{6}$$

$$i = C\dot{F}_1 + \frac{1}{R}F_1 + i_a u_{2av}, \tag{7}$$

$$i_a = \frac{1}{k_m}\left(J\dot{F}_2 + bF_2\right), \tag{8}$$

$$u_{1av} = \frac{L}{E}\left[C\ddot{F}_1 + \frac{1}{R}\dot{F}_1 + \frac{d(i_a u_{2av})}{dt} + \frac{1}{L}F_1\right], \tag{9}$$

$$u_{2av} = \frac{1}{F_1}\left[\frac{JL_a}{k_m}\ddot{F}_2 + \frac{1}{k_m}(bL_a + JR_a)\dot{F}_2 + \left(\frac{bR_a}{k_m} + k_e\right)F_2\right]. \tag{10}$$

From the parametrization of u_{1av} (9) and u_{2av} (10), the following controls are proposed:

$$u_{1av} = \frac{L}{E}\left[C\eta + \frac{1}{R}\dot{F}_1 + \frac{d(i_a u_{2av})}{dt} + \frac{1}{L}F_1\right], \tag{11}$$

$$u_{2av} = \frac{1}{F_1}\left[\frac{JL_a}{k_m}\mu + \frac{1}{k_m}(bL_a + JR_a)\dot{F}_2 + \left(\frac{bR_a}{k_m} + k_e\right)F_2\right]. \tag{12}$$

After replacing (11) and (12) in (9) and (10), respectively, the trajectory tracking problem, related to F_1 and F_2, is reduced to control the following:

$$\eta = \ddot{F}_1, \tag{13}$$

$$\mu = \ddot{F}_2. \tag{14}$$

With the intention of achieving $F_1 \to F_1^*$ and $F_2 \to F_2^*$, with F_1^* being a desired voltage and F_2^* a desired angular velocity. Proposals for the auxiliary controls, η and μ, that achieve such objectives are the following:

$$\eta = \ddot{F}_1^* - \beta_2\left(\dot{F}_1 - \dot{F}_1^*\right) - \beta_1(F_1 - F_1^*) - \beta_0\int_0^t (F_1 - F_1^*)d\tau, \tag{15}$$

$$\mu = \ddot{F}_2^* - \gamma_2\left(\dot{F}_2 - \dot{F}_2^*\right) - \gamma_1(F_2 - F_2^*) - \gamma_0\int_0^t (F_2 - F_2^*)d\tau. \tag{16}$$

Thus, it is clear that with the selection (15) and (16), the control objective is achieved. Since, after replacing (15) and (16) in (13) and (14), respectively, the tracking errors' dynamics of the closed-loop system are:

$$0 = \ddot{e}_v + \beta_2\ddot{e}_v + \beta_1\dot{e}_v + \beta_0 e_v, \tag{17}$$

$$0 = \ddot{e}_\omega + \gamma_2\ddot{e}_\omega + \gamma_1\dot{e}_\omega + \gamma_0 e_\omega, \tag{18}$$

where the tracking errors are defined as

$$\begin{aligned} e_v &= F_1 - F_1^*, \\ e_\omega &= F_2 - F_2^*. \end{aligned} \tag{19}$$

The characteristic polynomials associated with (17) and (18) are determined by

$$p_v(s) = s^3 + \beta_2 s^2 + \beta_1 s + \beta_0, \tag{20}$$

$$p_\omega(s) = s^3 + \gamma_2 s^2 + \gamma_1 s + \gamma_0. \tag{21}$$

A convenient selection of the controls gains $(\beta_2, \beta_1, \beta_0)$ and $(\gamma_2, \gamma_1, \gamma_0)$ are given by

$$\begin{aligned} \beta_2 &= a_1 + 2\xi_1\omega_{n1}, \\ \beta_1 &= 2\xi_1\omega_{n1}a_1 + \omega_{n1}^2, \\ \beta_0 &= a_1\omega_{n1}^2, \\ \gamma_2 &= a_2 + 2\xi_2\omega_{n2}, \\ \gamma_1 &= 2\xi_2\omega_{n2}a_2 + \omega_{n2}^2, \\ \gamma_0 &= a_2\omega_{n2}^2, \end{aligned} \tag{22}$$

which are imposed when matching (20) and (21), term to term, with the following Hurwitz polynomials:

$$p_{v_d}(s) = (s + a_1)\left(s^2 + 2\xi_1\omega_{n1}s + \omega_{n1}^2\right), \tag{23}$$

$$p_{\omega_d}(s) = (s + a_2)\left(s^2 + 2\xi_2\omega_{n2}s + \omega_{n2}^2\right), \tag{24}$$

with $a_1, a_2 > 0$, $\xi_1, \xi_2 > 0$, and $\omega_{n1}, \omega_{n2} > 0$.

In consequence, the controls (11) and (12), as long as $v > 0$, accomplish $v \to v^*$ and $\omega \to \omega^*$, respectively.

2.3. Flatness-Based Hierarchical Controller: Separate Dynamics. In this section, the second flatness control strategy that executes the bidirectional angular velocity trajectory tracking for the DC/DC Buck converter-inverter-DC motor system (1), (2), (3) and (4) is designed. This strategy is on the basis of a hierarchical control scheme that takes into account the system dynamics separately, that is, a flatness control for the motor and another for the converter. By initially considering that the DC/DC Buck converter and the DC motor operate separately, the hierarchical control structure is the following:

(1) High-level control: this flatness control carries out the bidirectional angular velocity trajectory tracking in the DC motor shaft, that is, $\omega \to \omega^*$.

(2) Low-level control: this flatness control executes the DC/DC Buck converter output voltage tracking, that is, $v \to v^*$.

(3) Integration: this allows the connection between the controls (1) and (2) through the hierarchical control scheme.

(1) DC Motor Control. Since, initially, it is assumed that the Buck converter and DC motor operate separately. Then, from (3) and (4), the motor model is transformed in

$$\begin{aligned} L_{\mathrm{a}} \frac{di_{\mathrm{a}}}{dt} &= \vartheta - R_{\mathrm{a}} i_{\mathrm{a}} - k_{\mathrm{e}} \omega, \\ J \frac{d\omega}{dt} &= k_{\mathrm{m}} i_{\mathrm{a}} - b\omega, \end{aligned} \tag{25}$$

where

$$\vartheta = v u_{2\mathrm{av}}. \tag{26}$$

According to [18], the system (25) has as flat output to ω. In consequence, the control ϑ allows the following representation:

$$\vartheta = \frac{JL_{\mathrm{a}}}{k_{\mathrm{m}}} \ddot{\omega} + \frac{1}{k_{\mathrm{m}}} (bL_{\mathrm{a}} + JR_{\mathrm{a}}) \dot{\omega} + \left(\frac{bR_{\mathrm{a}}}{k_{\mathrm{m}}} + k_{\mathrm{e}} \right) \omega. \tag{27}$$

From (27), after proposing the motor control as

$$\vartheta = \frac{JL_{\mathrm{a}}}{k_{\mathrm{m}}} \mu + \frac{1}{k_{\mathrm{m}}} (bL_{\mathrm{a}} + JR_{\mathrm{a}}) \dot{\omega} + \left(\frac{bR_{\mathrm{a}}}{k_{\mathrm{m}}} + k_{\mathrm{e}} \right) \omega, \tag{28}$$

the angular velocity tracking problem is reduced to control the system:

$$\mu = \ddot{\omega}. \tag{29}$$

If ω^* is the desired angular velocity, a selection of μ that accomplishes $\omega \to \omega^*$ is given by

$$\mu = \ddot{\omega}^* - \gamma_2 (\dot{\omega} - \dot{\omega}^*) - \gamma_1 (\omega - \omega^*) - \gamma_0 \int_0^t (\omega - \omega^*) d\tau, \tag{30}$$

where γ_0, γ_1, and γ_2 are the gains of the auxiliary control μ. Defining the tracking error as $e_\omega = \omega - \omega^*$, after replacing (30) in (29), the error dynamics in closed-loop is obtained

$$\ddot{e}_\omega + \gamma_2 \ddot{e}_\omega + \gamma_1 \dot{e}_\omega + \gamma_0 e_\omega = 0, \tag{31}$$

whose characteristic polynomial is

$$p_\omega(s) = s^3 + \gamma_2 s^2 + \gamma_1 s + \gamma_0, \tag{32}$$

which is imposed to be stable, via its matching with the Hurwitz polynomial (24), that is,

$$p_{\omega_d}(s) = (s + a_2)\left(s^2 + 2\xi_2 \omega_{n2} s + \omega_{n2}^2\right), \tag{33}$$

with $a_2 > 0$, $\xi_2 > 0$, and $\omega_{n2} > 0$. Therefore, the gains γ_2, γ_1, and γ_0 are given by

$$\begin{aligned} \gamma_2 &= a_2 + 2\xi_2 \omega_{n2}, \\ \gamma_1 &= 2\xi_2 \omega_{n2} a_2 + \omega_{n2}^2, \\ \gamma_0 &= a_2 \omega_{n2}^2. \end{aligned} \tag{34}$$

With the aforementioned approach, $\omega \to \omega^*$ when $t \to \infty$ is achieved.

(2) Buck Converter Control. As it is assumed that there is no connection between the converter and motor. Then, $i_{\mathrm{a}} = 0$, from (1) and (2) the Buck converter model is

$$\begin{aligned} L \frac{di}{dt} &= E u_{1\mathrm{av}} - v, \\ C \frac{dv}{dt} &= i - \frac{v}{R}. \end{aligned} \tag{35}$$

According to [18], the flat output of the system (35) is v. Thus, $u_{1\mathrm{av}}$ can be written as:

$$u_{1\mathrm{av}} = \frac{LC}{E} \ddot{v} + \frac{L}{RE} \dot{v} + \frac{1}{E} v. \tag{36}$$

Choosing the control input $u_{1\mathrm{av}}$, from (36), as

$$u_{1\mathrm{av}} = \frac{LC}{E} \eta + \frac{L}{RE} \dot{v} + \frac{1}{E} v. \tag{37}$$

Then, the voltage tracking in the converter output is reduced to

$$\eta = \ddot{v}. \tag{38}$$

Thus, a convenient proposal of η so that $v \to v^*$, with v^* being the converter desired voltage, is

$$\eta = \ddot{v}^* - \beta_2 (\dot{v} - \dot{v}^*) - \beta_1 (v - v^*) - \beta_0 \int_0^t (v - v^*) d\tau, \tag{39}$$

where β_2, β_1, and β_0 are the gains of the auxiliary control η. Thus, the control (37), with (39), achieves $\upsilon \to \upsilon^*$ when $t \to \infty$. This is quickly verified when (39) is replaced in (38). Since, after defining the tracking error $e_\upsilon = \upsilon - \upsilon^*$, the closed-loop dynamics is obtained

$$\ddot{e}_\upsilon + \beta_2 \ddot{e}_\upsilon + \beta_1 \dot{e}_\upsilon + \beta_0 e_\upsilon = 0, \tag{40}$$

whose characteristic polynomial is

$$p_\upsilon(s) = s^3 + \beta_2 s^2 + \beta_1 s + \beta_0, \tag{41}$$

which is imposed to be stable through matching it with the Hurwitz polynomial

$$p_{\upsilon_d}(s) = (s + a_1)\left(s^2 + 2\xi_1 \omega_{n1} s + \omega_{n1}^2\right), \tag{42}$$

where $a_1 > 0$, $\xi_1 > 0$, and $\omega_{n1} > 0$. Hence, the auxiliary control gains are determined by

$$\begin{aligned} \beta_2 &= a_1 + 2\xi_1 \omega_{n1}, \\ \beta_1 &= 2\xi_1 \omega_{n1} a_1 + \omega_{n1}^2, \\ \beta_0 &= a_1 \omega_{n1}^2. \end{aligned} \tag{43}$$

(3) Hierarchical Controller. Having carried out the separate control of the subsystems integrating the DC/DC Buck converter-inverter-DC motor system. Now, the hierarchical controller that executes the bidirectional angular velocity trajectory tracking is proposed.

For the DC motor, it was found that the control ϑ achieving $\omega \to \omega^*$ is determined by

$$\vartheta = \frac{JL_a}{k_m}\mu + \frac{1}{k_m}(bL_a + JR_a)\dot{\omega} + \left(\frac{bR_a}{k_m} + k_e\right)\omega, \tag{44}$$

with μ defined as

$$\mu = \ddot{\omega}^* - \gamma_2(\dot{\omega} - \dot{\omega}^*) - \gamma_1(\omega - \omega^*) - \gamma_0 \int_0^t (\omega - \omega^*) d\tau. \tag{45}$$

In turn, ϑ defined in (26) as

$$\vartheta = \upsilon u_{2av}, \tag{46}$$

considers that the voltage υ is the power supply of the DC motor inverter circuit. Therefore, the control associated with the inverter is determined by

$$u_{2av} = \frac{\vartheta}{\upsilon}. \tag{47}$$

On the other hand, the control accomplishing $\upsilon \to \upsilon^*$ was defined as

$$u_{1av} = \frac{LC}{E}\eta + \frac{L}{RE}\dot{\upsilon} + \frac{1}{E}\upsilon, \tag{48}$$

with η given by

$$\eta = \ddot{\upsilon}^* - \beta_2(\dot{\upsilon} - \dot{\upsilon}^*) - \beta_1(\upsilon - \upsilon^*) - \beta_0 \int_0^t (\upsilon - \upsilon^*) d\tau. \tag{49}$$

Thus, the hierarchical controller is determined by (48) and (47), as long as $\upsilon > 0$, obtaining $\upsilon \to \upsilon^*$ and $\omega \to \omega^*$, respectively.

3. Experimental Results in Closed-Loop

Here, the experimental results in closed-loop of the flatness controls designed in Section 2 are presented. The controls robustness is verified under abrupt variations in the system parameters. In the experimental development, MATLAB-Simulink and a dSPACE DS1104 board are used.

3.1. Experimental Setup. The experimental setup was developed using the general connection diagram shown in Figure 2. In the diagram presented in Figure 2 the following blocks are distinguished:

(i) *Bidirectional DC/DC Buck converter-DC motor system*: this block corresponds to the system under study and is composed of three stages, namely, a Buck power converter, an inverter, and a DC motor. The nominal values of the Buck converter parameters are as follows:

$$\begin{aligned} L &= 4.94\,\text{mH}, \\ R &= 64\,\Omega, \\ C &= 114.4\,\mu\text{F}, \\ E &= 42\,\text{V}. \end{aligned} \tag{50}$$

The inverter allows obtaining the bidirectional angular velocities in the motor shaft. The driving of the inverter transistors is carried out by two IR2113. Lastly, the used DC motor corresponds to the GNM5440E-G3.1 whose nominal parameters are as follows:

$$\begin{aligned} L_a &= 2.22\,\text{mH}, \\ k_e &= 120.1 \times 10^{-3}\,\text{N} \cdot \text{m/A}, \\ R_a &= 0.965\,\Omega, \\ k_m &= 120.1 \times 10^{-3}\,\text{V} \cdot \text{s/rad}, \\ J &= 118.2 \times 10^{-3}\,\text{kg} \cdot \text{m}^2, \\ b &= 129.6 \times 10^{-3}\,\text{N} \cdot \text{m} \cdot \text{s/rad}. \end{aligned} \tag{51}$$

(ii) *Flatness controls*: in this block, the differential flatness controls are programmed via MATLAB-Simulink. That is, the controls (11) and (12) (based on the complete dynamics) and (47) and (48) (based on the separate dynamics of the system) are experimentally implemented. The gain parameters associated with the differential flatness controls, (11), (12) and (47), (48), are defined as

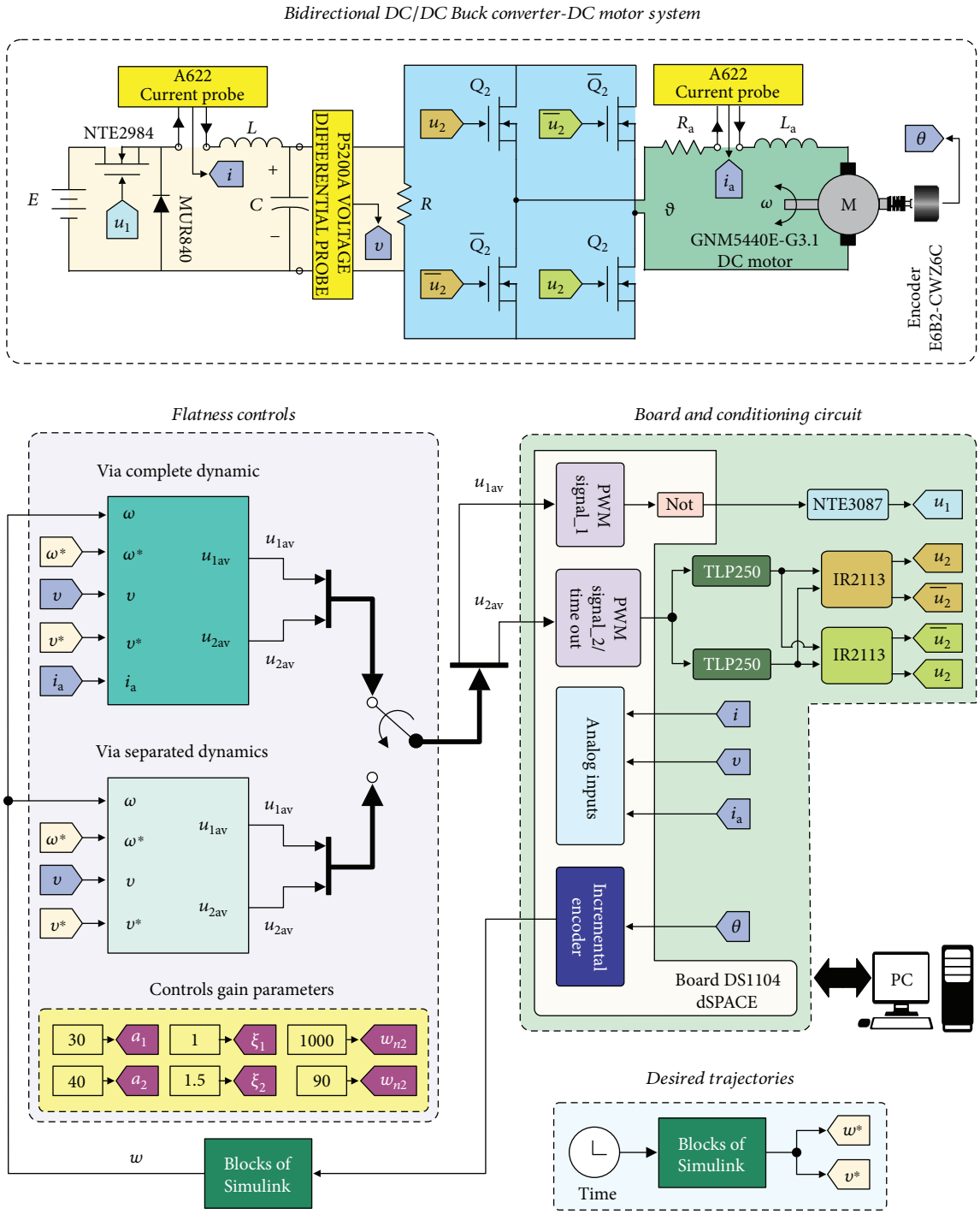

Figure 2: General diagram of the experimental setup connections.

$$\begin{aligned} a_1 &= 30, \\ \xi_1 &= 1, \\ \omega_{n1} &= 1000, \\ a_2 &= 40, \\ \xi_2 &= 1.5, \\ \omega_{n2} &= 90. \end{aligned} \tag{52}$$

Notice that the gain definitions related to the controls, given by (22), (34), and (43) are equal.

(iii) *Desired trajectories*: in this block, the desired trajectories ω^* and v^* are programmed. For the DC motor, the following bidirectional trajectory is proposed:

$$\omega^*(t) = A \sin\left(\frac{2\pi}{P} t\right), \tag{53}$$

with a period $P = 20/3$ s and an amplitude $A = 13$ rad/s. Whereas for the Buck converter, the trajectory is defined as

$$v^*(t) = \bar{v}_i(t_i) + \left[\bar{v}_f(t_f) - \bar{v}_i(t_i)\right]\psi(t, t_i, t_f). \quad (54)$$

That is, the desired trajectory v^* smoothly interpolates between the initial voltage $\bar{v}_i = 24$ V and the final one $\bar{v}_f = 30$ V in the time interval $[t_i, t_f] = [1\text{ s}, 2\text{ s}]$ through the Bézier polynomial ψ, defined by

$$\psi(t, t_i, t_f) = \begin{cases} 0, & t \le t_i, \\ \left(\dfrac{t - t_i}{t_f - t_i}\right)^3 \left[20 - 45\left(\dfrac{t - t_i}{t_f - t_i}\right) + 36\left(\dfrac{t - t_i}{t_f - t_i}\right)^2 - 10\left(\dfrac{t - t_i}{t_f - t_i}\right)^3\right], & t \in (t_i, t_f), \\ 1, & t \ge t_f. \end{cases} \quad (55)$$

(iv) *Board and conditioning circuit*: this block electrically isolates the DS1104 board from the power stage, through the NTE3087 and TLP250 optocouplers. Furthermore, this block properly drives the Buck converter and inverter when generating, by means of the PWM1 and PWM2, the switched inputs u_1 and u_2, respectively. Also, in this block, the measurement of the variables i, v, i_a, and ω is carried out. Two current probes A622 are used to measure i and i_a. While the voltage probe P5200A is employed to read the voltage v. Lastly, ω is obtained via the E6B2-CWZ6C encoder and Simulink blocks.

3.2. Experimental Results. In order to obtain the experimental results, the connection diagram shown in Figure 2 has been used. This shows the interconnections of the bidirectional DC/DC Buck converter-DC motor system with MATLAB-Simulink and the DS1104 board.

With the intention of evaluating the performance of the designed controls, the following abrupt changes in the system parameters E, R, L, and C have been considered:

$$E_m = \begin{cases} E, & 0\text{ s} \le t < 2.5\text{ s}, \\ 70\%E, & 2.5\text{ s} \le t < 5\text{ s}, \\ E, & 5\text{ s} \le t \le 20\text{ s}, \end{cases}$$

$$R_m = \begin{cases} R, & 0\text{ s} \le t < 7.5\text{ s}, \\ 14\%R, & 7.5\text{ s} \le t < 10\text{ s}, \\ R, & 10\text{ s} \le t \le 20\text{ s}, \end{cases} \quad (56)$$

$$L_m = \begin{cases} L, & 0\text{ s} \le t < 12.5\text{ s}, \\ 30\%L, & 12.5\text{ s} \le t < 15\text{ s}, \\ L, & 15\text{ s} \le t \le 20\text{ s}, \end{cases}$$

$$C_m = \begin{cases} C, & 0\text{ s} \le t < 17.5\text{ s}, \\ 300\%C, & 17.5\text{ s} \le t \le 20\text{ s}. \end{cases}$$

Figure 3 shows the experimental results in closed-loop when the abrupt changes (56) are considered. Whereas, Figure 4 depicts the experimental results when an abrupt load variation, via a brake system, is applied in $8\text{ s} \le t \le 15\text{ s}$. In both figures, the results associated with the control based on the *complete dynamics*, that is, (11) and (12), correspond to ω_{cd}, $i_{a_{cd}}$, $u_{2av_{cd}}$, v_{cd}, i_{cd}, and $u_{1av_{cd}}$. While the results related to the control based on the *separate dynamics*, that is, (47) and (48), are ω_{sd}, $i_{a_{sd}}$, $u_{2av_{sd}}$, v_{sd}, i_{sd}, and $u_{1av_{sd}}$.

As can be observed in Figures 3 and 4, the results are satisfactory for both controls, since it is achieved that $\omega \to \omega^*$ and $v \to v^*$ even when abrupt changes in the system parameters and an abrupt load variation are taken into account. Thus, the robustness of the controls is shown. On the other hand, the controls u_{1av} and u_{2av} are not saturated when executing the system tracking task. That is, $u_{1av} \in [0, 1]$ and $u_{2av} \in [-1, 1]$ in all the experimental results.

Lastly, although in general the two controls show good performance, the authors consider that the scheme based on the hierarchical approach, that is, (47) and (48), is more simple to design because the system (1), (2), (3), and (4) is separated in two subsystems.

4. Conclusions

In this paper, two flatness-based robust controls for the bidirectional angular velocity trajectory tracking problem of the DC/DC Buck converter-inverter-DC motor system were proposed. The first control considers the system complete dynamics. Whereas, the second separates the dynamics of the system, which later are joined through a hierarchical controller. The performance of the proposed controls was verified through experiments with a built prototype, MATLAB-Simulink, and a DS1104 board. The results shown that the proposed controls satisfactorily execute the trajectory tracking task even when abrupt changes on the system parameters are considered. Thus, the robustness of the flatness-based controls was exhibited. It is noteworthy that the tested uncertainties do not simultaneously occur in practice. However, they were presented with the purpose of

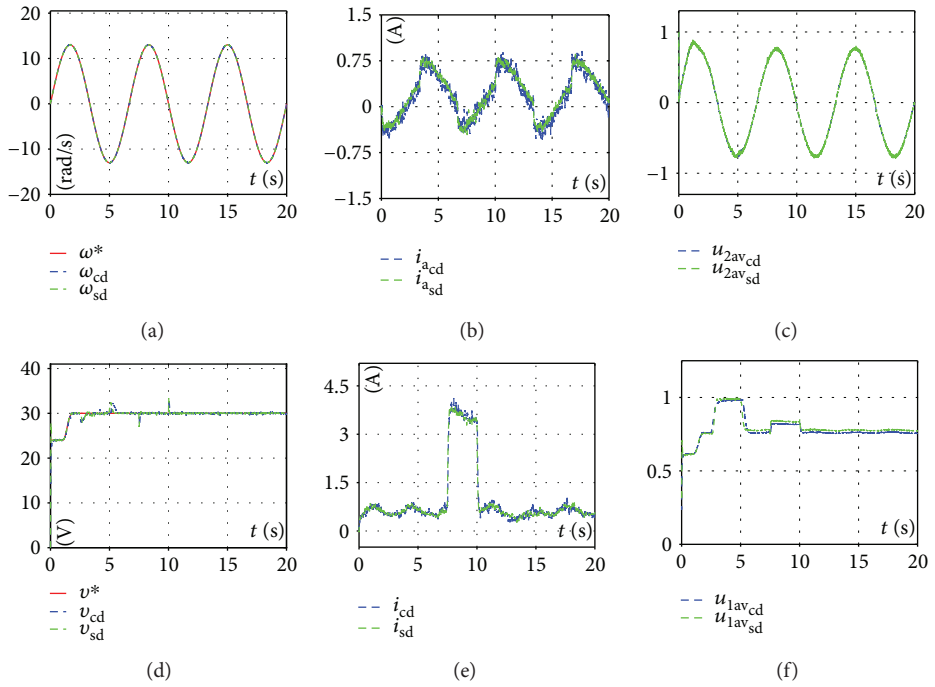

Figure 3: Experimental results of controls (11), (12) and (47), (48) when abrupt changes in E_m, R_m, L_m, and C_m are considered.

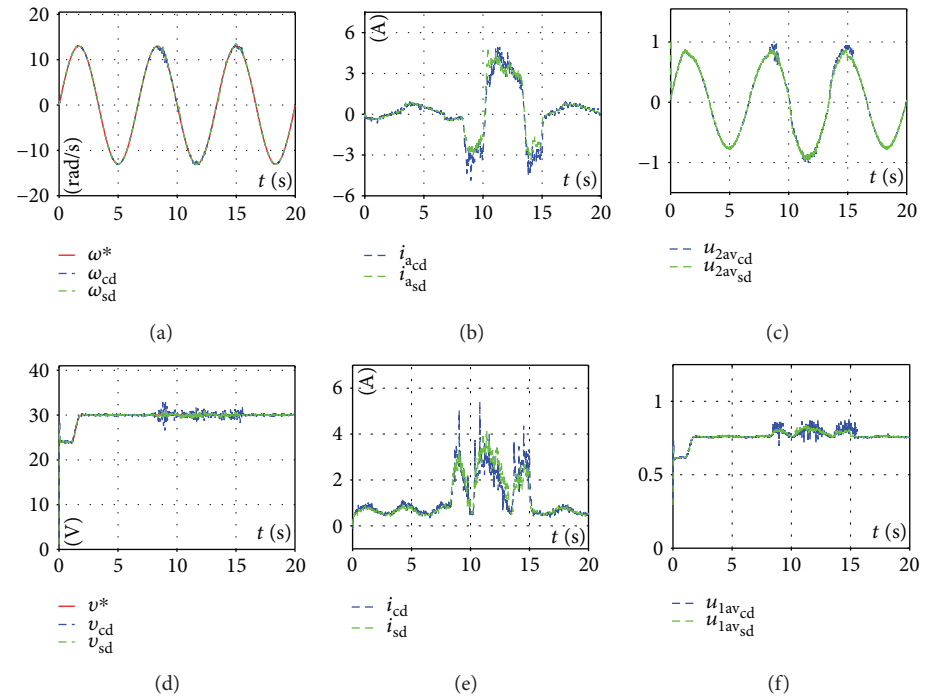

Figure 4: Experimental results of controls (11), (12) and (47), (48) when an abrupt load change is applied.

showing the possible industrial application of the herein designed controls.

Data Availability

The data used to support the findings of this study are available from the corresponding author upon request.

Conflicts of Interest

The authors declare that the research was conducted in the absence of any commercial, financial, or personal relationships that could be construed as a potential conflict of interests.

Acknowledgments

The authors thank the editor and the anonymous reviewers for the time spent in the revision of the manuscript. Their valuable comments helped to significantly improve the quality of the paper. This work was supported by Secretaría de Investigación y Posgrado del Instituto Politécnico Nacional, México. The work of Eduardo Hernández-Márquez, José Rafael García-Sánchez, and Mayra Antonio-Cruz has been supported by CONACYT-México and BEIFI scholarships. Likewise, Eduardo Hernández-Márquez thanks the Instituto Tecnológico Superior de Poza Rica for the support given to study Ph.D. program at CIDETEC-IPN. Ramón Silva-Ortigoza, Hind Taud, and Mariana Marcelino-Aranda acknowledge financial support from IPN programs EDI and SIBE and from SNI-México. Finally, Victor Manuel Hernández-Guzmán thanks the SNI-México for financial support.

References

[1] J. Popović-Gerber, J. A. Oliver, N. Cordero et al., "Power electronics enabling efficient energy usage: energy savings potential and technological challenges," *IEEE Transactions on Power Electronics*, vol. 27, no. 5, pp. 2338–2353, 2012.

[2] R. Fuger, A. Matsekh, J. Kells, D. B. T. Sercombe, and A. Guina, "A superconducting homopolar motor and generator–new approaches," *Superconductor Science and Technology*, vol. 29, no. 3, article 034001, 2016.

[3] H. Sira-Ramírez and R. Silva-Ortigoza, *Control Design Techniques in Power Electronics Devices*, Springer-Verlag, London, UK, 2006.

[4] T. Strasser, F. Andrén, J. Kathan et al., "A review of architectures and concepts for intelligence in future electric energy systems," *IEEE Transactions on Industrial Electronics*, vol. 62, no. 4, pp. 2424–2438, 2015.

[5] S. Jain, A. K. Thopukara, R. Karampuri, and V. T. Somasekhar, "A single-stage photovoltaic system for a dual-inverter-fed open-end winding induction motor drive for pumping applications," *IEEE Transactions on Power Electronics*, vol. 30, no. 9, pp. 4809–4818, 2015.

[6] X. Z. Gao, Z. X. Hou, Z. Guo, and X. Q. Chen, "Reviews of methods to extract and store energy for solar-powered aircraft," *Renewable and Sustainable Energy Reviews*, vol. 44, pp. 96–108, 2015.

[7] P. A. Plonski, J. V. Hook, and V. Isler, "Environment and solar map construction for solar-powered mobile systems," *IEEE Transactions on Robotics*, vol. 32, no. 1, pp. 70–82, 2016.

[8] M. Gadalla and S. Zafar, "Analysis of a hydrogen fuel cell-PV power system for small UAV," *International Journal of Hydrogen Energy*, vol. 41, no. 15, pp. 6422–6432, 2016.

[9] S. Ademi and M. Jovanovic, "Control of doubly-fed reluctance generators for wind power applications," *Renewable Energy*, vol. 85, pp. 171–180, 2016.

[10] J. R. García-Sánchez, R. Silva-Ortigoza, S. Tavera-Mosqueda et al., "Tracking control for mobile robots considering the dynamics of all their subsystems: experimental implementation," *Complexity*, vol. 2017, Article ID 5318504, 18 pages, 2017.

[11] S. E. Lyshevski, *Electromechanical Systems, Electric Machines, and Applied Mechatronics*, CRC Press, Boca Raton, FL, USA, 1999.

[12] I. Boldea and S. A. Nasar, *Electric Drives*, CRC Press, Boca Raton, FL, USA, 1999.

[13] J. Linares-Flores, *Control Suave de Velocidad de Motores de CD Mediante Convertidores de Potencia CD/CD, [Ph.D. thesis]*, Sección de Mecatrónica del Departamento de Ingeniería Eléctrica del CINVESTAV-IPN, Mexico City, Mexico, 2006.

[14] M. A. Ahmad, R. M. T. Raja Ismail, and M. S. Ramli, "Control strategy of Buck converter driven DC motor: a comparative assessment," *Australian Journal of Basic and Applied Sciences*, vol. 4, no. 10, pp. 4893–4903, 2010.

[15] O. Bingöl and S. Paçaci, "A virtual laboratory for neural network controlled DC motors based on a DC-DC Buck converter," *International Journal of Engineering Education*, vol. 28, no. 3, pp. 713–723, 2012.

[16] H. Sira-Ramírez and M. A. Oliver-Salazar, "On the robust control of Buck-converter DC-motor combinations," *IEEE Transactions on Power Electronics*, vol. 28, no. 8, pp. 3912–3922, 2013.

[17] R. Silva-Ortigoza, J. R. García-Sánchez, J. M. Alba-Martínez et al., "Two-stage control design of a Buck converter/DC motor system without velocity measurements via a Σ−Δ-modulator," *Mathematical Problems in Engineering*, vol. 2013, Article ID 929316, 11 pages, 2013.

[18] R. Silva-Ortigoza, C. Márquez-Sánchez, F. Carrizosa-Corral, M. Antonio-Cruz, J. M. Alba-Martínez, and G. Saldaña-González, "Hierarchical velocity control based on differential flatness for a DC/DC Buck converter-DC motor system," *Mathematical Problems in Engineering*, vol. 2014, Article ID 912815, 12 pages, 2014.

[19] R. Silva-Ortigoza, V. M. Hernández-Guzmán, M. Antonio-Cruz, and D. Muñoz-Carrillo, "DC/DC Buck power converter as a smooth starter for a DC motor based on a hierarchical control," *IEEE Transactions on Power Electronics*, vol. 30, no. 2, pp. 1076–1084, 2015.

[20] V. M. Hernández-Guzmán, R. Silva-Ortigoza, and D. Muñoz-Carrillo, "Velocity control of a brushed DC-motor driven by a DC to DC Buck power converter," *International Journal of Innovative Computing, Information and Control*, vol. 11, no. 2, pp. 509–521, 2015.

[21] S. G. Kumar and S. H. Thilagar, "Sensorless load torque estimation and passivity based control of Buck converter fed DC motor," *The Scientific World Journal*, vol. 2015, Article ID 132843, 15 pages, 2015.

[22] S. Khubalkar, A. Chopade, A. Junghare, M. Aware, and S. Das, "Design and realization of stand-alone digital fractional order PID controller for Buck converter fed DC motor," *Circuits, Systems, and Signal Processing*, vol. 35, no. 6, pp. 2189–2211, 2016.

[23] G. Rigatos, P. Siano, P. Wira, and M. Sayed-Mouchaweh, "Control of DC-DC converter and DC motor dynamics using differential flatness theory," *Intelligent Industrial Systems*, vol. 2, no. 4, pp. 371–380, 2016.

[24] T. K. Nizami, A. Chakravarty, and C. Mahanta, "Design and implementation of a neuro-adaptive backstepping controller for Buck converter fed PMDC-motor," *Control Engineering Practice*, vol. 58, pp. 78–87, 2017.

[25] A. Chakravarty, T. K. Nizami, and C. Mahanta, "Real time implementation of an adaptive backstepping control of Buck

converter PMDC-motor combinations," in *2017 Indian Control Conference (ICC)*, pp. 277–282, Guwahati, India, January 2017.

[26] T. K. Roy, L. C. Paul, M. I. Sarkar, M. F. Pervej, and F. K. Tumpa, "Adaptive controller design for speed control of DC motors driven by a DC-DC Buck converter," in *2017 International Conference on Electrical, Computer and Communication Engineering (ECCE)*, pp. 100–105, Cox's Bazar, Bangladesh, February 2017.

[27] M. A. Ahmad and R. M. T. Raja Ismail, "A data-driven sigmoid-based PI controller for Buck-converter powered DC motor," in *2017 IEEE Symposium on Computer Applications & Industrial Electronics (ISCAIE)*, pp. 81–86, Langkawi Island, Malaysia, April 2017.

[28] T. K. Nizami, A. Chakravarty, and C. Mahanta, "A fast learning neuro adaptive control of Buck converter driven PMDC motor: design, analysis and validation," *IFAC-PapersOnLine*, vol. 50, no. 1, pp. 37–42, 2017.

[29] H. Wu, L. Zhang, J. Yang, and S. Li, "Model predictive control for DC-DC Buck power converter-DC motor system with uncertainties using GPI observer," in *2017 36th Chinese Control Conference (CCC)*, pp. 4906–4911, Dalian, China, July 2017.

[30] J. Linares-Flores, J. Reger, and H. Sira-Ramirez, "Load torque estimation and passivity-based control of a Boost-converter/DC-motor combination," *IEEE Transactions on Control Systems Technology*, vol. 18, 2010.

[31] A. T. Alexandridis and G. C. Konstantopoulos, "Modified PI speed controllers for series-excited DC motors fed by DC/DC Boost converters," *Control Engineering Practice*, vol. 23, pp. 14–21, 2014.

[32] G. C. Konstantopoulos and A. T. Alexandridis, "Enhanced control design of simple DC-DC Boost converter-driven DC motors: analysis and implementation," *Electric Power Components and Systems*, vol. 43, no. 17, pp. 1946–1957, 2015.

[33] J. Linares-Flores, J. L. Barahona-Avalos, H. Sira-Ramírez, and M. A. Contreras-Ordaz, "Robust passivity-based control of a Buck–Boost-converter/DC-motor system: an active disturbance rejection approach," *IEEE Transactions on Industry Applications*, vol. 48, no. 6, pp. 2362–2371, 2012.

[34] E. E. Jiménez-Toribio, A. A. Labour-Castro, F. Muñiz-Rodríguez, H. R. Pérez-Hernández, and E. I. Ortiz-Rivera, "Sensorless control of Sepic and Cuk converters for DC motors using solar panels," in *2009 IEEE International Electric Machines and Drives Conference*, pp. 1503–1510, Miami, FL, USA, May 2009.

[35] R. S. Ortigoza, J. N. A. Juarez, J. R. G. Sanchez, M. A. Cruz, V. M. H. Guzman, and H. Taud, "Modeling and experimental validation of a bidirectional DC/DC Buck power electronic converter-DC motor system," *IEEE Latin America Transactions*, vol. 15, no. 6, pp. 1043–1051, 2017.

[36] R. S. Ortigoza, J. N. A. Juarez, J. R. G. Sanchez, V. M. H. Guzman, C. Y. S. Cervantes, and H. Taud, "A sensorless passivity-based control for the DC/DC Buck converter-inverter–DC motor system," *IEEE Latin America Transactions*, vol. 14, no. 10, pp. 4227–4234, 2016.

[37] V. H. García-Rodríguez, R. Silva-Ortigoza, E. Hernández-Márquez, J. R. García-Sánchez, M. Ponce-Silva, and G. Saldaña-González, "A DC motor driven by a DC/DC Boost converter-inverter: modeling and simulation," in *2016 International Conference on Mechatronics, Electronics and Automotive Engineering (ICMEAE)*, pp. 78–83, Cuernavaca, Morelos, Mexico, November 2016.

[38] R. S. Ortigoza, V. H. G. Rodriguez, E. H. Marquez et al., "A trajectory tracking control for a Boost converter–inverter–DC motor combination," *IEEE Latin America Transactions*, vol. 16, no. 4, pp. 1008–1014, 2018.

[39] E. H. Marquez, R. S. Ortigoza, J. R. G. Sanchez, V. H. G. Rodriguez, and J. N. A. Juarez, "A new "DC/DC Buck-Boost converter–DC motor" system: modeling and experimental validation," *IEEE Latin America Transactions*, vol. 15, no. 11, pp. 2043–2049, 2017.

[40] E. Hernández-Márquez, R. Silva-Ortigoza, C. A. Avila-Rea et al., "Regulation of the DC/DC Buck-Boost converter-inverter-DC motor system: sensorless passivity based control," in *2017 International Conference on Mechatronics, Electronics and Automotive Engineering (ICMEAE)*, pp. 88–92, Cuernavaca, Mexico, November 2017.

[41] J. Linares-Flores, H. Sira-Ramírez, E. F. Cuevas-López, and M. A. Contreras-Ordaz, "Sensorless passivity based control of a DC motor via a solar powered Sepic converter-full bridge combination," *Journal of Power Electronics*, vol. 11, no. 5, pp. 743–750, 2011.

Hindawi
Complexity
Volume 2018, Article ID 8261413, 8 pages
https://doi.org/10.1155/2018/8261413

Research Article

Investigation and Optimization of Grounding Grid Based on Lightning Response by Using ATP-EMTP and Genetic Algorithm

Saeid Gholami Farkoush,[1] Tahir Khurshaid,[1] Abdul Wadood,[1] Chang-Hwan Kim,[1] Kumail Hassan Kharal,[1] Kyu-Ho Kim,[2] Namhun Cho,[3] and Sang-Bong Rhee[1]

[1]*Department of Electrical Engineering, Yeungnam University, Gyeongsan, Republic of Korea*
[2]*Department of Electrical Engineering, Hankyong National University, 327 Chungang-ro, Anseong-si, Kyonggi-do 17579, Republic of Korea*
[3]*Korea Electric Power Research Institute (KEPRI), Korea Electric Power Company (KEPCO), 105 MunjiRo, Yuseong-gu, Daejeon 34056, Republic of Korea*

Correspondence should be addressed to Sang-Bong Rhee; rrsd@yu.ac.kr

Received 26 January 2018; Revised 19 April 2018; Accepted 10 May 2018; Published 5 August 2018

Academic Editor: Hugo Morais

A large number of electromagnetic transient studies have been analyzed for finding the overvoltage behavior of power system. A grounding grid of power system is so important for reducing the effect of overvoltage phenomena during a short-circuit event. Two sections are important in grounding system behavior: soil ionization and inductive behavior; this paper focuses on the inductive manner of grounding grid. The grounding grid is considered as a conductor segment; each conductor segment acts as a grounding unit. In this paper, the transient methodology is introduced to investigate the lightning effect on grounding body at each point of grounding grid in normal and optimized conditions. Genetic algorithm is applied for regular and irregular grounding grid to obtain best values of mesh size with the lower ground potential rise (GPR) as compared with the normal condition for more safety. The grounding grid is a combination of inductance, resistance, and capacitance. This model is suitable for practical applications related to fault diagnosis. Several voltages on different positions of grounding grid are described in this paper using ATP-EMTP and genetic algorithm. The computer simulation shows that the proposed scheme is highly feasible and technically attractive.

1. Introduction

In daily life, electricity plays a vital role. Electrical power system consists of generation, transmission, and distribution. It is very important to secure this transmission and distribution for the safety of customers. For more safety, the grounding system at specific points has been predicted in a power grid. A number of articles had been discussed about human safety in the surroundings of grounding system or other electrical devices [1–3]. There are two important sections for improving performance at the grounding grid, firstly reducing fault current and secondly optimizing the grid configuration. Reducing fault current is so difficult or impractical in the grounding grid [4, 5]. Then, the modification of grounding grid configuration is frequently used, which can be reached by changing of the grid mesh and adding vertical grounding rods for getting more efficiency [6–8]. The behavior of grounding grids under lightning stroke is explained with more details and analysis in [9]. The purpose of the ground system is twofold: the first is to provide safety against electric shock, which can cause harm to people and the second is to provide the proper operating level for the power system when a fault occurs. For managing safety in a ground grid against fault, problems like lightning need to be simulated with the different software; for example, TRAGSYS is used to simulate and to analyze the transient on transformer terminals by taking into account the grounding effects [10]. ETAP software was proposed for ground grid mesh designing by using the latest IEEE 81 2013 standard for ground grid mesh data [11]. The rigorous

electromagnetic model was suggested for analyzing the lightning surge efficiency of grounding grids. The result of the proposed model shows that values of the grounding grid impulse coefficients are nearly linear dependent on the side length of square grids [12]. The author at [13] proposed the external charge method to design for grounding grids. For estimation of grounding grid parameters, boundary element method is used. The advantages of these methods are the ability to calculate parameters of complex groundings in homogeneous and double-layered soil with parallel boundaries of discontinuity of the soil electrical conductivity under lightning stroke [14–16]. In some papers, the transient electromagnetic (TEM) method is used to draw the configuration of a substation for optimization of grounding grid under lightning stroke [17–19].

In this paper, we achieve to figure out the configuration of grounding grids using ATP-EMTP. Firstly, we show a simulation of grounding in ATP-EMTP under lightning stroke in normal computation. Secondly, genetic algorithm is suggested to a system for optimization of grounding grids. The complete configuration of grounding grids will be clearly and accurately shown on the map. Surface voltages and mesh size before and after optimization will be investigated under lightning stroke in a grounding grid. Each stroke lasts normally less than one millisecond, and the separation time between the strokes is typically a few tens of milliseconds.

2. Analytical Lightning Current in ATP-EMTP

When lightning attaches to the substation, two current waves distribute in the substation. The first one is moving upwards to reach a maximum value of lightning current, and the second one goes down towards zero value. The speed of the lightning current in the first section as shown in Figure 1 is very close to the speed of light, and in the second section, it gradually decreases with the speed less than that of light (usually 1/3 to 2/3 of the speed of light). The analytical expression is usually adopted to represent the injected current $i_o(t)$ in the Heidler function, defined as

$$i_o(t) = I \frac{(t/\tau_1)^n}{1 + (t/\tau_1)^n} e^{-(t/\tau_1)}, \quad (1)$$

where I is a control of the current amplitude, τ_1 is the front time constant, τ_2 is the decay time constant, and n is an exponent having values between 1.1 to 20.

Figure 1 shows the example of the lightning current curve when the lightning happens.

3. Grounding Grid in Power System

The substation grounding system comprises a grid (earth mat) formed by a horizontal buried conductor. The functions of grounding systems or earth mat include the following:

(1) To ensure safety to personnel in substations against electrical shocks

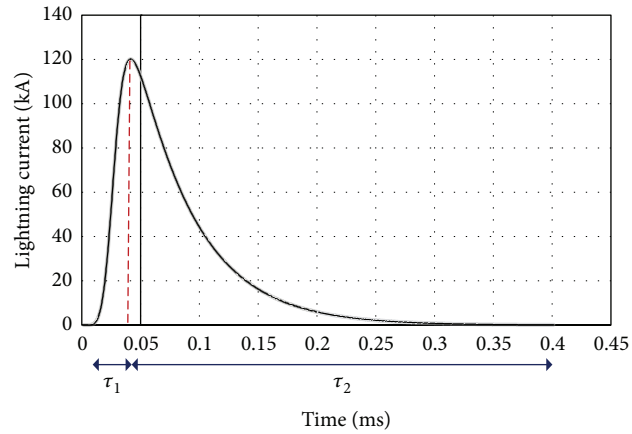

Figure 1: Lightning current.

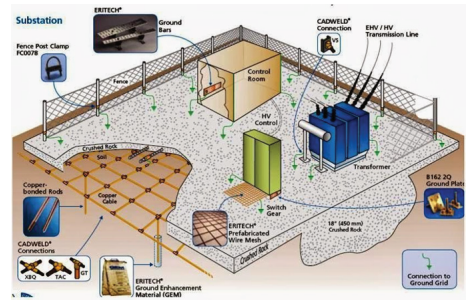

Figure 2: General arrangement of an earth electrode system at an electrical substation [20].

(2) To provide the ground connection for connecting the neutrals of star-connected transformer winding to earth (neutral earthing)

(3) To discharge the overvoltages from overhead ground wires or the lightning mats to earth

(4) To provide a path for discharging the charge between phase and ground by means of earthing switches

(5) To provide earth connections to structures and other noncurrent carrying metallic objects in the substation (equipment grounding)

Figure 2 shows the general arrangement of an earth electrode system at an electrical substation.

4. Computation Test Cases

The mesh is formed by placing mild steel bars arranged in x and y directions in the soil at a depth of about 0.5 m below the surface of the substation floor in the entire substation area except for the foundations. A typical conductor spacing ranges from 3 to 20 m. The crossings of the horizontal bars in the x and y directions are welded. The earthing rods can also be placed downside the mesh at each point including the points in building foundations as well as the transformer

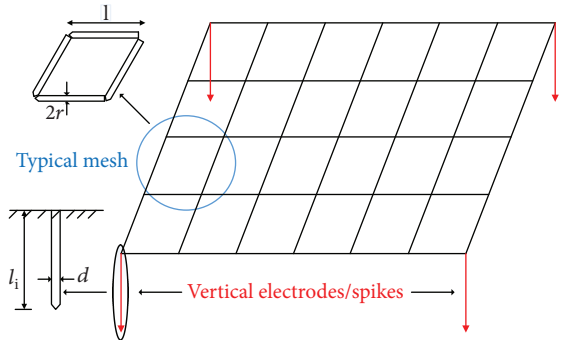

Figure 3: Three-dimensional view of the earthing system.

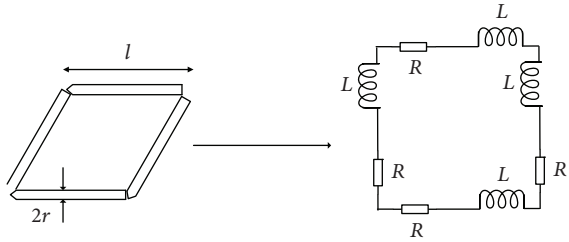

Figure 4: Parameter model of elementary grounding electrode segment.

foundations and inside fenced areas and so on. Figure 3 shows the three-dimensional view of the earthing system.

The proposed model representation of grounding electrodes includes properly arranged size of inductances and resistances. Figure 4 shows the parameter model of elementary grounding electrode segment.

The longitudinal resistance "R" and self-inductance "L" for each elementary cell is obtained by using the following classical expressions:

$$R = \frac{l}{\pi . r^2} \cdot \rho_{cu}\ [\Omega], \tag{2}$$

$$L = \frac{\mu_0 \cdot l}{2 \cdot \pi} \cdot \left[\ln\left(\frac{2 \cdot l}{\sqrt{2 \cdot r \cdot h}}\right) - 1\right]\ [\mathrm{H}], \tag{3}$$

where "l" is the length of the elementary cell, "r" is the radius of the electrode, "ρ_{cu}" is the resistivity of the material, and "h" is the buried depth, and the magnetic permeability of the material has been assumed equal to the vacuum permeability, $\mu_0 = 4 \cdot \pi \cdot 10^{-7}$ [21].

$$\begin{aligned} \rho_{cu} &= 1.77 \times 10^{-8}, \\ \mu_0 &= 4 \cdot \pi \cdot 10^{-7}, \\ r &= 0.015\ \mathrm{m}, \\ l &= 15\ \mathrm{m}, \\ R &= 37.56 \times 10^{-5}\ \Omega, \\ L &= 13.5\ \mu\mathrm{H}, \\ h &= 0.5\ \mathrm{m}. \end{aligned} \tag{4}$$

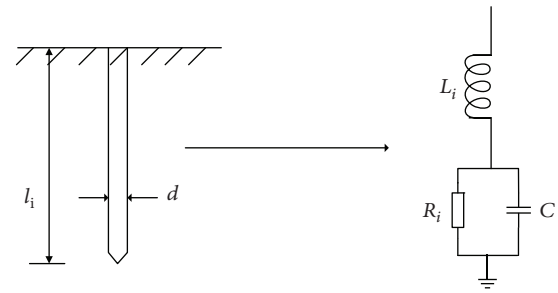

Figure 5: The equivalent circuit for ground rod.

An equivalent circuit of the ground rod is shown in Figure 5. The resistance, inductance, and capacitance of the under transient phenomenon are calculated by [22]

$$\begin{aligned} R_i &= \frac{\rho}{l_i}\left(\ln\frac{8l_i}{d} - 1\right)\ [\Omega], \\ L_i &= 2l_i\left(\ln\frac{4l_i}{d} \times 10^{-7}\right)\ [\mathrm{H}], \\ C &= \frac{\varepsilon_r l_i}{18 \ln\left(4l_i/d\right)} \times 10^{-9}\ [\mathrm{F}], \end{aligned} \tag{5}$$

where "ρ" is solid resistivity (Ω-m), "l_i" is the total length of ground rod (m), "d" is the diameter of the ground rod (m), and "ε_r" is the relative permittivity of solid.

$$\begin{aligned} \rho_{\mathrm{copper}} &= 1.68 \times 10^{-8}, \\ l_i &= 1\ \mathrm{m}, \\ d &= 0.016\ \mathrm{m}, \\ L_i &= 0.0011\ \mathrm{mH}, \\ R_i &= 8.7 \times 10^{-8}\ \Omega, \\ \varepsilon_r &= 250, \\ C &= 0.0025\ \mu\mathrm{F}. \end{aligned} \tag{6}$$

Also, stoke current pulse has a peak value of $I_m = 30$ kA, and a zero to peak time is 4 μs.

16-grounding-mesh model is simulated by implementing all data in ATP-EMTP. Randomly, three points are selected for analyzing the effect of the grounding grid when lightning happens in the substation. Figure 6 shows the 16-mesh model of regular grounding.

The grid is hit by lightning current pulse $I_m = 30$ kA as shown in Figure 7. The dimensions of the grid have a $60 \times 60\ \mathrm{m}^2$ and $15 \times 15\ \mathrm{m}^2$ mesh and are buried in soil with 30 Ωm resistivity.

As shown in Figure 8, three selected points are investigated.

Figure 9 shows the ground potential rise (GPR) at points A, B, and C in ATP-EMTP. It can be seen that voltages in points are different when lightning happens in the grounding system.

The next case study included in this paper is for analyzing irregular grounding grid when lightning hit in the system.

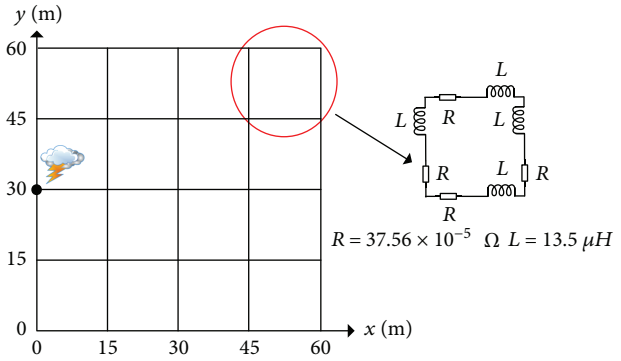

Figure 6: 16-mesh simulation model of regular grounding.

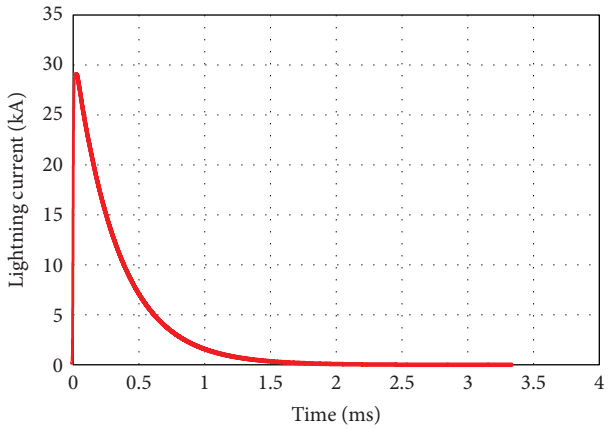

Figure 7: Lightning current hit in grounding grid.

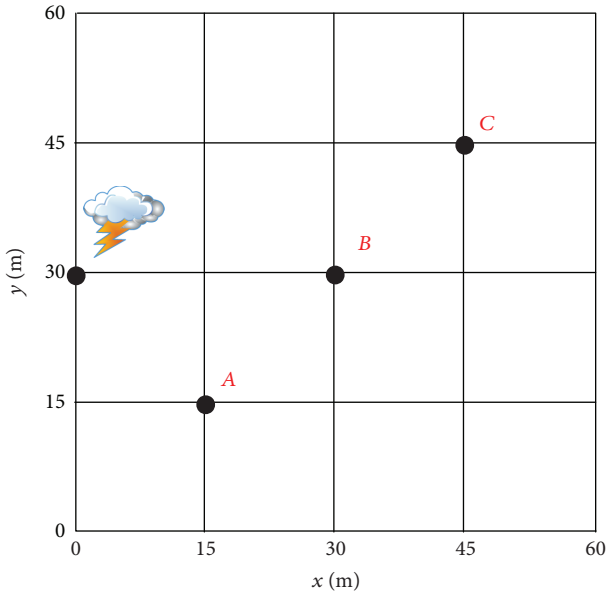

Figure 8: Three selected points for investigation of lightning effect.

16-grounding-irregular-mesh model is designed and simulated in ATP-EMTP. In this case, three points are selected for analyzing the effect of the grounding grid randomly,

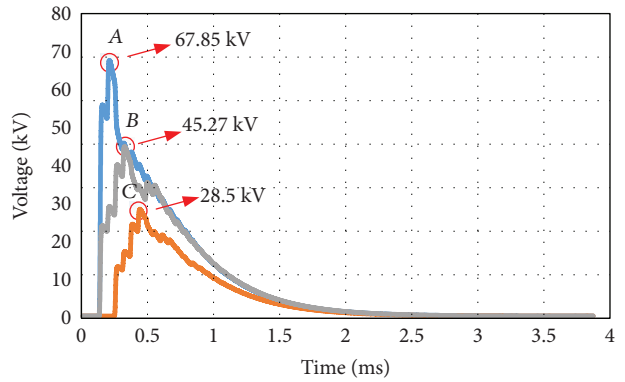

Figure 9: Ground potential rise at points A, B, and C after lightning in the regular ground grid.

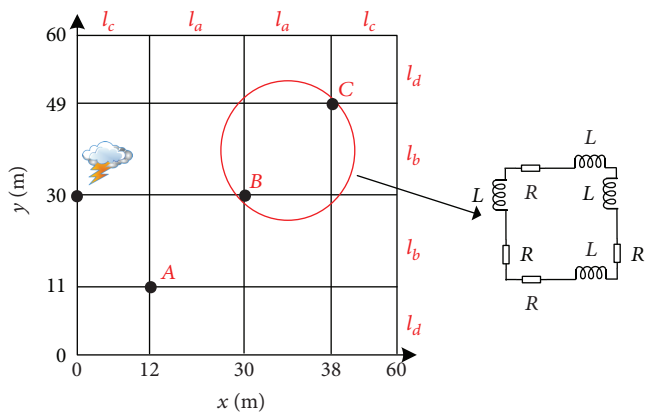

Figure 10: 16-mesh simulation model of the irregular grounding grid.

when lightning happens in the substation earlier discussed in Figure 6. Figure 10 shows the 16-irregular-mesh grounding grid. The dimension of the grid has a $60 \times 60\,m^2$, $11 \times 12\,m^2$, $11 \times 18\,m^2$, and $12 \times 19\,m^2$ meshes and is buried in soil with $30\,\Omega m$ resistivity.

The length of elementary cells of the irregular mesh is listed below.

$$l_a = 18\,m,\ l_b = 19\,m,\ l_c = 12\,m,\ l_d = 11\,m. \tag{7}$$

Based on the (2) and (3), all the longitudinal resistance "R" and self-inductance "L" for each elementary cell of the irregular mesh are obtained as shown below.

$$\begin{aligned} R_a &= 45 \times 10^{-5}\,\Omega, \\ L_a &= 16.86\,\mu H, \\ R_b &= 47.57 \times 10^{-5}\,\Omega, \\ L_b &= 18\,\mu H, \\ R_c &= 30 \times 10^{-5}\,\Omega, \\ L_c &= 10.26\,\mu H, \\ R_d &= 27.54 \times 10^{-5}\,\Omega, \\ L_d &= 9.2\,\mu H. \end{aligned} \tag{8}$$

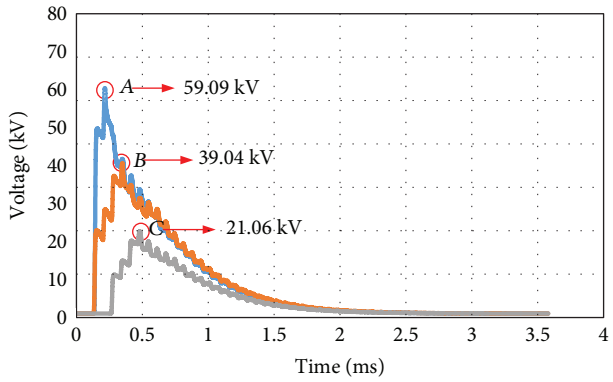

FIGURE 11: GPR at points A, B, and C after lightning in the irregular ground grid.

Figure 11 shows the GPR at points *A*, *B*, and *C* as shown in Figure 10. As it can be seen, voltages in points are different with the irregular ground grid when lightning hit the grounding grid.

Reducing maximum voltage of regular and irregular grounding grid after lightning hit in the system is so important for safety. For that reason, it is better to change the size of the mesh with the same total area of the grounding grid. For obtaining best mesh size, it is suggested to use algorithm methods. Few algorithm methods are applied in the lightning field in the power system [23, 24]. But in this case, for optimization of mesh size and reduction of maximum ground potential rise, genetic algorithm is suggested.

5. Minimization of GPR Using Genetic Algorithm

For designing an optimal grounding grid with more safety, genetic algorithm [25, 26] is applied in ATP-EMTP. The representation of each possible grid is made by means of a string of bits V. This string is made of two substrings V_x and V_y with lengths N_x and N_y, respectively. Each substring represents the conductors arranged in each possible direction. N_x and N_y are the maximum numbers of wires parallel to the y- and x-axes, respectively, forming the grid. Hence, the minimum possible distance between any two wires parallel to the y-axis is

$$D_x = \frac{L_x}{N_x} \tag{9}$$

and to the x-axis is

$$D_y = \frac{L_y}{N_y}, \tag{10}$$

where L_x and L_y are the total dimensions of the grid. Each bit corresponds to one possible situation of a wire in the grounding grid. If the grid has a conductor in the i position, the respective bit value is 1. Otherwise, the bit value is 0 (see Figure 12).

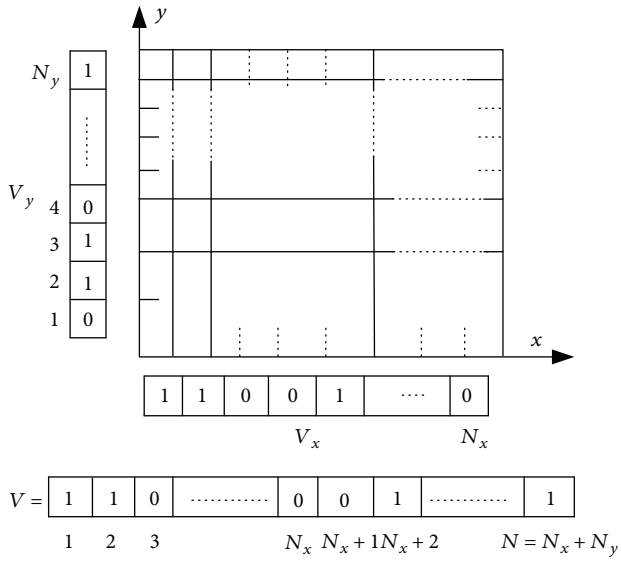

FIGURE 12: Representation of individuals.

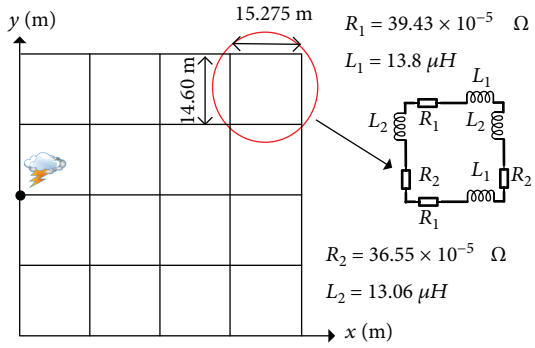

FIGURE 13: 16-mesh simulation model of regular grounding grid after applying a genetic algorithm.

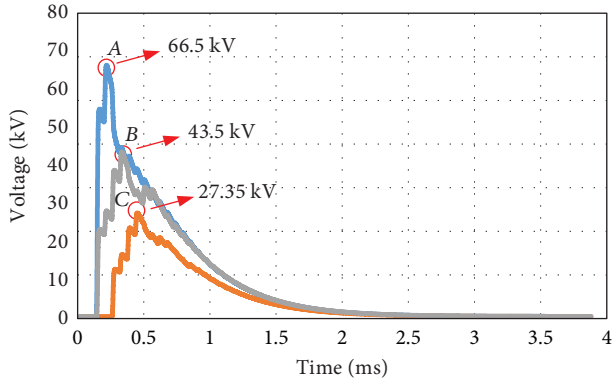

FIGURE 14: Ground potential rise at points A, B, and C after lightning genetic algorithm optimization in the ground grid.

Table 1: Simulation data comparison before and after optimization in regular grounding grid.

	Point A		Point B		Point C	
	Max (kV)	$T = 500$ (μs)	Max (kV)	$T = 500$ (μs)	Max (kV)	$T = 500$ (μs)
Before optimization	67.85	9.17 (V)	45.27	9.42 (V)	28.5	7.035 (V)
After optimization	66.5	9.085 (V)	43.5	9.34 (V)	27.35	6.967 (V)

First of all, a population is generated in a random way. Starting from this population and by means of the basic crossover and mutation operators, the following new populations are generated. In each generation, all the individuals are analyzed to evaluate their fitness as optimum solution to the problem. The model used in the analysis of the grounding grids is independent of the genetic algorithm. In this case, a typical method for studying grounding systems at low frequency is used. This method, named "Combined Integration/Matrix Method" is based on subdividing the conductors of the grounding grid into smaller segments. The density of leaking current in each segment may be considered constant. So, a matrix relationship between the currents and the corresponding potentials in all the segments can be calculated. The elements of the abovementioned matrix are obtained by integration. If the grid is assumed equipotential, the values of the leaking currents can be calculated. Knowing the leaking currents, the potential at any point on the earth's surface can be calculated. In order to take into account the effect of the boundary ground air, the traditional method of images is used.

The objective function to be minimized is GPR. The constraints of step and touch voltages which must be strictly observed could be introduced by assigning a null value to the fitness function for the grids which do not meet them [27].

Genetic parameters, for example, population size, crossover rate, and mutual rate, are the entities that assist in tuning the genetic algorithm performance. All of the data is applied in ATP-EMTP for optimization of the grounding grid. The genetic algorithm defined new mesh size for reducing GPR in the grounding grid.

For new mesh size, new R and L should be defined in ATP-EMTP using (2) and (3), new data obtained for grounding grid shown in below equations.

$$\begin{aligned} R_1 &= 39.43 \times 10^{-5}\ \Omega, \\ L_1 &= 13.8\ \mu\text{H}, \\ R_2 &= 36.55 \times 10^{-5}\ \Omega, \\ L_2 &= 13.06\ \mu\text{H}. \end{aligned} \tag{11}$$

After applying the genetic algorithm in ATP-EMTP, the mesh size in the regular ground grid is changed to a new value but the total area of the grounding grid is the same. Figure 13 shows the new value of mesh size in the regular grounding grid system.

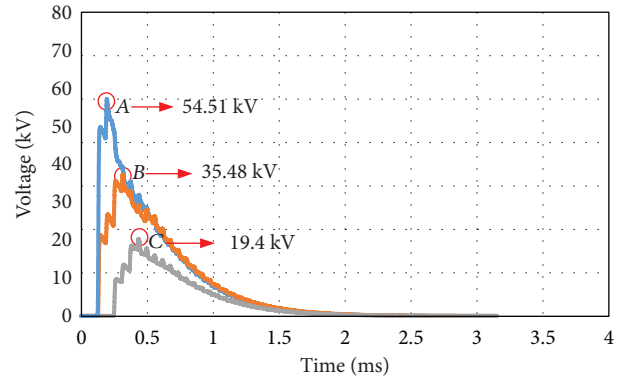

Figure 15: Ground potential rise at point A, B and C after lightning genetic algorithm optimization in the irregular ground grid.

Figure 14 shows the ground potential rise (GPR) at points A, B, and C in ATP-EMTP after applying genetic algorithm with new mesh sizes. It can be seen that voltages in points are less than those in Figure 9 when lightning hits the grounding grid system. As the size of mesh changes, the value of GPR decreases. For obtaining best results, a genetic algorithm is applied in the grid using ATP-EMTP. Decreasing GPR causes increasing safety in the grounding grid. Also, voltage dead time is reduced by genetic algorithm optimization in comparison with normal conditions.

Table 1 shows the values of GPR before and after optimization of a genetic algorithm using ATP-EMTP when the grounding grid mesh sizes are regular.

As shown in Table 1 at point A, the maximum GPR is reduced from 67.85 kV to 66.5 kV, at point B from 45.27 kV to 43.5 kV, and at point C from 28.5 kV to 27.35 kV, respectively. Also for voltage, the dead time at point A is decreased from 9.17 V to 9.085 V, at point B from 9.42 V to 9.34 V, and at point C from 7.035 V to 6.967 V, respectively.

In the other case study for irregular grounding grid, after applying the genetic algorithm in ATP-EMTP, all elementary cells of irregular mesh changed in optimum value that is written below.

$$\begin{aligned} l_a &= 19.46\ \text{m}, \\ l_b &= 18.68\ \text{m}, \\ l_c &= 11.65\ \text{m}, \\ l_d &= 10.24\ \text{m}. \end{aligned} \tag{12}$$

Table 2: Simulation data comparison before and after optimization in irregular grounding grid.

	Point A		Point B		Point C	
	Max (kV)	$T = 500$ (μs)	Max (kV)	$T = 500$ (μs)	Max (kV)	$T = 500$ (μs)
Before optimization	59.09	11.54 (V)	39.04	12.78 (V)	21.06	9.4 (V)
After optimization	54.51	9.28 (V)	35.48	10.24 (V)	19.4	6.9 (V)

Based on (2) and (3), all the new longitudinal resistance "R" and self-inductance "L" for each elementary cell of the irregular mesh after optimizing are obtained below.

$$\begin{aligned} R_a' &= 48.72 \times 10^{-5}\ \Omega, \\ L_a' &= 18.53\ \mu\text{H}, \\ R_b' &= 46.77 \times 10^{-5}\ \Omega, \\ L_b' &= 17.63\ \mu\text{H}, \\ R_c' &= 29.17 \times 10^{-5}\ \Omega, \\ L_c' &= 9.9\ \mu\text{H}, \\ R_d' &= 25.64 \times 10^{-5}\ \Omega, \\ L_d' &= 8.43\ \mu\text{H}. \end{aligned} \tag{13}$$

Figure 15 shows the GPR at points A, B, and C that is determined in Figure 10.

It can be seen that voltages in points are different with irregular ground grid after applying the genetic algorithm in ATP-EMTP when lightning hit the grounding grid. All sizes of meshes are optimized but the total area of the grounding grid is the same as the original size.

Table 2 shows the values of GPR before and after optimization of a genetic algorithm using ATP-EMTP when grounding grid mesh sizes are irregular.

As shown in Table 2 at point A, the maximum GPR is reduced from 59.095 kV to 54.51 kV, at point B from 39.04 kV to 35.48 kV, and at point C from 21.06 kV to 19.4 kV, respectively. Also for voltage, the dead time at point A is decreased from 11.54 V to 9.28 V, at point B from 12.78 V to 10.24 V, and at point C from 9.4 V to 6.9 V, respectively.

6. Conclusions

This paper proposed the transient methodology to investigate the lighting stroke effect on grounding grid by calculating various voltages at different nodes using ATP-EMTP toolbox and optimizing ground grid size by using a genetic algorithm. The simulation result acknowledges the behavior and impedance of grounding based on mesh size grid when lightning happened.

Grounding grid data is simulated in ATP-EMTP for investigation of lightning effect; also, to measure GPR and mesh grid size, both are simulated in the ATP-EMTP for checking surface voltage at the grounding grid. Achieving the best result of GPR and mesh grid size is a target for more safety. For getting this condition, genetic algorithm is applied in ATP-EMTP. Also after optimization, there is a minor change in the value of grid impedance but the amplitude of mesh size is so important for reducing GPR. Analysis and optimization result of regular and irregular grounding shows that irregular grounding is safe than regular grounding grid. The total GPR in irregular grounding grid is lower than that in regular grounding grid in terms of safety condition. Changing amplitude of mesh changed the value of GPR. GPR and grounding mesh size are optimized up to an optimum value by using genetic algorithm than normal condition without optimization. Also, irregular grounding grid system is better than regular grounding grid; it should be recommended.

Data Availability

The data used to support the findings of this study are available from the corresponding author upon request.

Conflicts of Interest

The authors declare that there is no conflict of interests regarding the publication of this paper.

Acknowledgments

This research was supported by Korea Electric Power Corporation, Grant no. (R17XA05-38).

References

[1] Substations Committee of the IEEE Power Engineering Society, *IEEE Guide for Safety in AC Substation Grounding*, IEEE, 2000.

[2] M. Mitolo, "Of electrical distribution systems with multiple grounded neutrals," *IEEE Transactions on Industry Applications*, vol. 46, no. 4, pp. 1541–1546, 2010.

[3] F. Freschi, A. Guerrisi, M. Tartaglia, and M. Mitolo, "Numerical simulation of heart-current factors and electrical models of the human body," *IEEE Transactions on Industry Applications*, vol. 49, no. 5, pp. 2290–2299, 2013.

[4] L. M. Popović, "Influence of metal installations surrounding the feeding cable line on the ground fault current distribution in supplied substations," *IEEE Transactions on Power Delivery*, vol. 23, no. 4, pp. 2583–2590, 2008.

[5] E. Pons, P. Colella, R. Napoli, and R. Tommasini, "Impact of MV ground fault current distribution on global earthing systems," *IEEE Transactions on Industry Applications*, vol. 51, no. 6, pp. 4961–4968, 2015.

[6] E. S. M. El-Refaie, S. E. Elmasry, M. K. Abd Elrahman, and M. H. Abdo, "Achievement of the best design for unequally spaced grounding grids," *Ain Shams Engineering Journal*, vol. 6, no. 1, pp. 171–179, 2015.

[7] Y. Gao, R. Zeng, X. Liang, J. He, W. Sun, and Q. Su, "Safety analysis of grounding grid for substations with different structure," in *PowerCon 2000. 2000 International Conference on Power System Technology. Proceedings (Cat. No.00EX409)*, vol. 3, pp. 1487–1492, Perth, WA, Australia, December 2000.

[8] F. Nedi, "A new evolutionary method for designing grounding grids by touch voltage control," in *2004 IEEE International Symposium on Industrial Electronics*, vol. 2, pp. 1501–1505, Ajaccio, France, May 2004.

[9] B. R. Gupta and B. Thapar, "Impulse impedance of grounding grids," *IEEE Transactions on Power Apparatus and Systems*, vol. PAS-99, no. 6, pp. 2357–2362, 1980.

[10] M. Popov, L. Grcev, H. K. Hoidalen, B. Gustavsen, and V. Terzija, "Investigation of the overvoltage and fast transient phenomena on transformer terminals by taking into account the grounding effects," *IEEE Transactions on Industry Applications*, vol. 51, no. 6, pp. 5218–5227, 2015.

[11] M. U. Aslam, M. U. Cheema, M. B. Cheema, and M. Samran, "Design analysis and optimization of ground grid mesh of extra high voltage substation using an intelligent software," in *2014 The 1st International Conference on Information Technology, Computer, and Electrical Engineering*, pp. 339–345, Semarang, Indonesia, November 2014.

[12] L. Grcev, "Lightning surge efficiency of grounding grids," *IEEE Transactions on Power Delivery*, vol. 26, no. 3, pp. 1692–1699, 2011.

[13] E. Bendito, A. Carmona, A. M. Encinas, and M. J. Jimenez, "The extremal charges method in grounding grid design," *IEEE Transactions on Power Delivery*, vol. 19, no. 1, pp. 118–123, 2004.

[14] A. Mujezinović, A. Muharemović, A. Muharemović, I. Turković, and Z. Bajramović, "Application of finite element method in calculation of large and complex grounding systems," in *2012 International Conference and Exposition on Electrical and Power Engineering*, pp. 688–692, Iasi, Romania, October 2012.

[15] I. Colominas, F. Navarrina, and M. Casteleiro, "Analysis of transferred earth potentials in grounding systems: a BEM numerical approach," *IEEE Transactions on Power Delivery*, vol. 20, no. 1, pp. 339–345, 2005.

[16] H. Zildžo, A. Muharemović, H. Matoruga, and A. Mujezinović, "Application of coupled 1D and 2D isoparametric discontinuous boundary elements in the calculation of large grounding systems," in *2011 XXIII International Symposium on Information, Communication and Automation Technologies*, pp. 1–7, Sarajevo, Bosnia and Herzegovina, October 2011.

[17] C. Yu, Z. Fu, Q. Wang, H. M. Tai, and S. Qin, "A novel method for fault diagnosis of grounding grids," *IEEE Transactions on Industry Applications*, vol. 51, no. 6, pp. 5182–5188, 2015.

[18] C. Yu, Z. Fu, X. Hou, H. M. Tai, and X. Su, "Break-point diagnosis of grounding grids using transient electromagnetic apparent resistivity imaging," *IEEE Transactions on Power Delivery*, vol. 30, no. 6, pp. 2485–2491, 2015.

[19] C. Yu, Z. Fu, G. Wu, L. Zhou, X. Zhu, and M. Bao, "Configuration detection of substation grounding grid using transient electromagnetic method," *IEEE Transactions on Industrial Electronics*, vol. 64, no. 8, pp. 6475–6483, 2017.

[20] "Substation earthing system design," 2014, http://www.electricalknowhow.com/2014/01/course-ee-5-grounding-system-design.html.

[21] G. Celli, E. Ghiani, and F. Pilo, "Behaviour of grounding systems: a quasi-static EMTP model and its validation," in *2010 30th International Conference on Lightning Protection (ICLP)*, pp. 1–6, Cagliari, Italy, September 2010.

[22] K. Supanus, W. Thansiphraserth, N. Rugthaicharoencheep, and A. Phayomhom, "External grounding design to reduce effects of lightning damage in distribution system," in *7th IET International Conference on Power Electronics, Machines and Drives (PEMD 2014)*, pp. 1–6, Manchester, UK, April 2014.

[23] Y. Lu, Y. Zhou, and X. Wu, "A hybrid lightning search algorithm-simplex method for global optimization," *Discrete Dynamics in Nature and Society*, vol. 2017, Article ID 8342694, 23 pages, 2017.

[24] V. Javor, K. Lundengård, M. Rančić, and S. Silvestrov, "Application of genetic algorithm to estimation of function parameters in lightning currents approximations," *International Journal of Antennas and Propagation*, vol. 2017, Article ID 4937943, 11 pages, 2017.

[25] F. Baccichetti, F. Bordin, and F. Carlassare, "λ-Prophage induction by furocoumarin photosensitization," *Experientia*, vol. 35, no. 2, pp. 183-184, 1979.

[26] Z. Michalewicz, "Genetic algorithms + data structures = evolution programs," *Computational Statistics & Data Analysis*, vol. 24, no. 3, pp. 372-373, 1996.

[27] A. F. Otero, J. Cidras, and C. Garrido, "Genetic algorithm based method for grounding grid design," in *1998 IEEE International Conference on Evolutionary Computation Proceedings. IEEE World Congress on Computational Intelligence (Cat. No.98TH8360)*, pp. 120–123, Anchorage, AK, USA, May 1998.

Hindawi
Complexity
Volume 2018, Article ID 2340628, 32 pages
https://doi.org/10.1155/2018/2340628

Review Article

Survey on Complex Optimization and Simulation for the New Power Systems Paradigm

João Soares[1], **Tiago Pinto**[2], **Fernando Lezama**[3] and **Hugo Morais**[4]

[1]*GECAD-Research Group on Intelligent Engineering and Computing for Advanced Innovation and Development-Polytechnic of Porto (IPP), R. Dr. António Bernardino de Almeida, 431, 4200-072 Porto, Portugal*
[2]*BiSITE, University of Salamanca, Calle Espejo, 2, 37007 Salamanca, Spain*
[3]*National Institute of Astrophysics, Optics and Electronics (INAOE), Puebla, Mexico*
[4]*Électricité de France R&D, Paris, France*

Correspondence should be addressed to João Soares; jan@isep.ipp.pt

Received 25 January 2018; Revised 4 May 2018; Accepted 30 May 2018; Published 1 August 2018

Academic Editor: Pietro De Lellis

This survey provides a comprehensive analysis on recent research related to optimization and simulation in the new paradigm of power systems, which embraces the so-called smart grid. We start by providing an overview of the recent research related to smart grid optimization. From the variety of challenges that arise in a smart grid context, we analyze with a significance importance the energy resource management problem since it is seen as one of the most complex and challenging in recent research. The survey also provides a discussion on the application of computational intelligence, with a strong emphasis on evolutionary computation techniques, to solve complex problems where traditional approaches usually fail. The last part of this survey is devoted to research on large-scale simulation towards applications in electricity markets and smart grids. The survey concludes that the study of the integration of distributed renewable generation, demand response, electric vehicles, or even aggregators in the electricity market is still very poor. Besides, adequate models and tools to address uncertainty in energy scheduling solutions are crucial to deal with new resources such as electric vehicles or renewable generation. Computational intelligence can provide a significant advantage over traditional tools to address these complex problems. In addition, supercomputers or parallelism opens a window to refine the application of these new techniques. However, such technologies and approaches still need to mature to be the preferred choice in the power systems field. In summary, this survey provides a full perspective on the evolution and complexity of power systems as well as advanced computational tools, such as computational intelligence and simulation, while motivating new research avenues to cover gaps that need to be addressed in the coming years.

1. Introduction

Energy is essential to assure most of the activities in developed societies [1]. Looking to the energy vectors, electricity consumption is rising significantly and changing the global paradigm of the energy mix [2]. The emerging and developed countries are also changing the primary sources to obtain the electricity, supporting the increase of the use of renewable primary sources, such as wind and the sun and the use of more clean sources like the natural gas [3]. The growing responsibility of each country regarding environmental aspects is also contributing to this paradigm change [4].

Other important aspects of modern societies are the efficiency in the use of energy, and electricity in particular, and the transparency in electricity negotiation [5]. These concerns have led to the adoption and development of competitive electricity markets. The rules and policies of electricity markets are very different worldwide, reflecting, in many cases, the reality of power systems in different regions [1]. Due to the significant changes in the power systems both in the production and in new usages of electricity, the markets and the power systems control itself are evolving in order to meet the present and future needs. New players and energy resources are emerging—notably electric vehicles (EV) [6],

consumption flexibility and demand response (DR) [7], large penetration of renewable based generation [8], energy efficiency measures [9], and building energy management parties [10], among many others. Several types of aggregator players, taking advantage on concepts such as the smart grid and microgrid [11], as discussed in Section 2 are also emerging in order to boost the potential of smaller players and resources. This new paradigm in power systems has increased the complexity to manage and operate the transmission and distribution networks and the interactions between the traditional and new players. The uncertainties associated with renewable based generation, electricity market prices, energy consumption, or electrical vehicles trips are just a few examples of the increased sources of complexity brought to the power and energy sector. Now that the planning and operation must consider the small resources of new players, rather than just looking at the overall picture of overall consumption and generation, makes the problem-solving in this domain an increasingly complex task. To address this complexity, new approaches have been proposed in the research field, for instance, considering hierarchical management with the inclusion of increased intelligence at each level of the hierarchical control [12]. In such approaches, the main idea is to have a good balance between the complexity of the problems to be solved at each level and the number of iterations and quantity of information needed to exchange between each level of the hierarchy. However, multiple alternative solutions should take into account the reality of each region.

The development of new algorithms using advanced optimization techniques and artificial intelligence are being proposed and tested to enable dealing with the increased complexity allowing a cyber-physical representation of the reality [13]. These two worlds, the real and the virtual, should run in parallel, considering and learning from past experiences to forecast and estimate the future. The new large-scale and complex models that are required to model the power and energy system under the new paradigm cannot be solved in due time without the support of new intelligent simulation and optimization approaches.

This paper provides a survey on the latest advances on optimization and simulation in the new paradigm of power systems. The main focus is centered on (i) the optimization of power systems under the new smart grid context, analyzing energy resource management models that deal with the increased complexity brought by the large number of new players and energy resources in this domain, and especially by the uncertainty associated to the variability and fluctuation of prices, generation, and consumption. Optimization models including stochastic modeling, robust analysis, and innovative business models are discussed and compared; (ii) the discussion and analysis of the application of computational intelligence approaches as means to solve the complex optimization problems, while guaranteeing an adequate balance between the execution time, the use of computational resources, and the quality of the achieved results. Evolutionary computation techniques are discussed in detail, as one of the most widely used approaches to solve the complex optimization models; (iii) the analysis of large-scale simulation of electricity markets and smart grid. Multiagent-based approaches are especially relevant in this domain, which includes the interaction between purely virtual environments, and hybrid approaches combining software agents and physical resources.

This paper is organized as follows. After this introduction, Section 2 introduces and explains the main concepts that are used throughout the paper. Section 3 presents a general overview of the recent research work related to new arisen challenges in the scope of smart grid and power systems optimization. In addition, a critic analysis is given to research work on energy resource scheduling, seen as one of the most complex and challenging research problems faced in power systems optimization. Section 4 provides an overview of the application of computational intelligence techniques for solving complex optimization problems in the energy domain. An extensive analysis of evolutionary computation applications for optimization in the energy domain is provided, followed by a brief review on artificial neural networks and fuzzy systems applications. Section 5 reviews the current state of the art in complex large-scale simulation in power and energy systems. The section emphasizes two main topics, namely, electricity market simulation and smart grid simulation, and covers both simulation models and studies proposed in the literature, as well as large-scale simulators resulting from relevant international research projects. Finally, the conclusion provided in Section 6 summarizes the most relevant points identified throughout the document, including the main advances in the literature and the main limitations that lead to new emerging research paths.

2. Preliminaries

Power systems are one of the backbones of our modern society. In fact, the electric grid is considered one of the greatest inventions of the 20th century. Despite the big challenge that the generation, control, and management of electricity represent, speaking in an elevated level of abstraction, the process from the generation of electricity to the delivery of it to end-user was somehow simple to understand. For instance, Figure 1 shows a simplified design of electric grids. In the early days of the electric grid, the flow of electricity was well defined from generation facilities, traveling through the transmission and distribution grid, until reaching end-users. Simple communication capabilities were required for control and monitoring. So, despite that some of the processes inside the electric grid were complex, looking at the electric grid as a whole, and compared with the electric grid of today, one could say that its design presents low complexity and it is easy to understand.

The truth is that without the electric infrastructure, it would be hard to imagine our days. However, nowadays due to recent reforms in the energy sector, unprecedented changes have been observed in this field, most notably the proliferation of renewable energy sources, mainly wind and solar generation and increasing penetration of EVs [14]. In this context, we are witnessing the appearance of new terms in the power systems arena, such as smart grid and

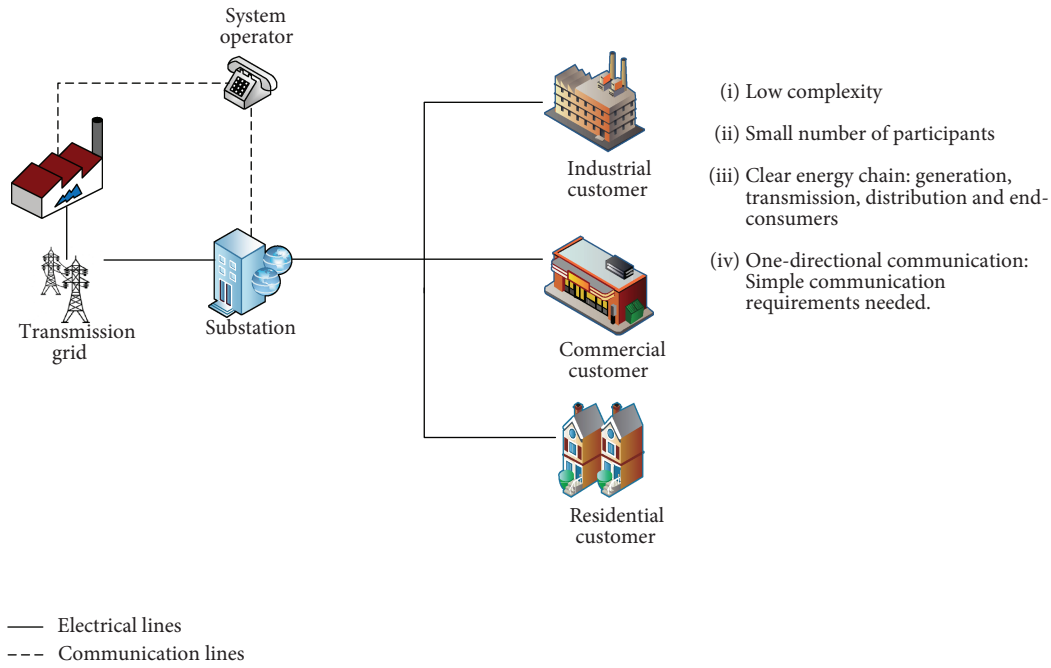

Figure 1: The past of the electricity system. One of the greatest inventions of the 20th century.

microgrid, which have distinct meaning. Although the definition of those terms is still evolving, it is accepted that smart grid refers to the merge of advanced computing technologies and communications with the electricity network. Equipment such as smart meters and phasor measurement units will contribute to an increase in observability and improvement in decision-making and situational awareness. Ultimately, the goal of smart grid is to provide a safe, reliable, and flexible grid operation, which is able to accommodate large number of renewables and other resources without sacrificing the reliability and cost of grid operation [15, 16]. On the other hand, microgrid represents a group of interconnected loads and generation resources with defined grid boundaries that can be controlled as a single entity. A microgrid in its pure definition should be able to operate isolated from the main grid, that is, in islanded mode. A university campus or a residential building can constitute an independent microgrid if the above definition is met. Since the microgrid relies on advanced computation technologies, it is possible to generalize that a microgrid is "smart" or part of a larger smart grid.

In this paper, we refer to the abovementioned changes as the new paradigm of power systems. On the one hand, these changes are contributing to reduction in the carbon footprint and increase in sustainability [17, 18]; on the other hand, power systems are becoming more complex and difficult to understand [19–22]. For instance, the electric grid from Figure 1 is evolving to something like the smart grid shown in Figure 2. The complexity of the smart grid is attributed to multiple players that interact and operate with independent behaviors and goals in a physical constrained network. These decisions impact the physical layer, and the overall result is difficult to be inferred from analyzing individual behavior. Moreover, no single entity can control, monitor, and manage in real time, which furthers contributes to higher system complexity.

If those new considerations were not enough, the technical constraints in modeling power systems are increasingly complex due to new societal challenges such as pollution and health impacts, ecological changes, multiple uses of land and water resources, and safety. These constraints are specific and translate into specific mathematical equations in optimization problems, making them harder to solve [23]. The current framework of smart grid involves several layers from the component parts (grid lines, equipment, and resources), including communication, management, and business layers.

In addition, smart grid design and implementation need to embed broader social and cultural considerations in order for smart grids to be successful. Not only do smart grids need to be understood as complex techno-socio-economic systems with multiple physical, cyber, social, policy, and decision-making layers; also, the interaction of those layers with changing external conditions (economic cycles, technological innovation, and prevailing and changing weather and climatic conditions) needs to be properly studied.

3. Recent Research to Tackle Challenges in the New Paradigm of Power Systems

3.1. Overview and Status of Recent Research. In the last years, research has been devoted to deal with this complexity and overcome the challenges brought by the new paradigm of modern power systems. We have looked at scientific research over the last few years (since 2010) in the SCOPUS database [24] (i.e., in December 2017) using different search terms to analyze the number of publications produced and provide

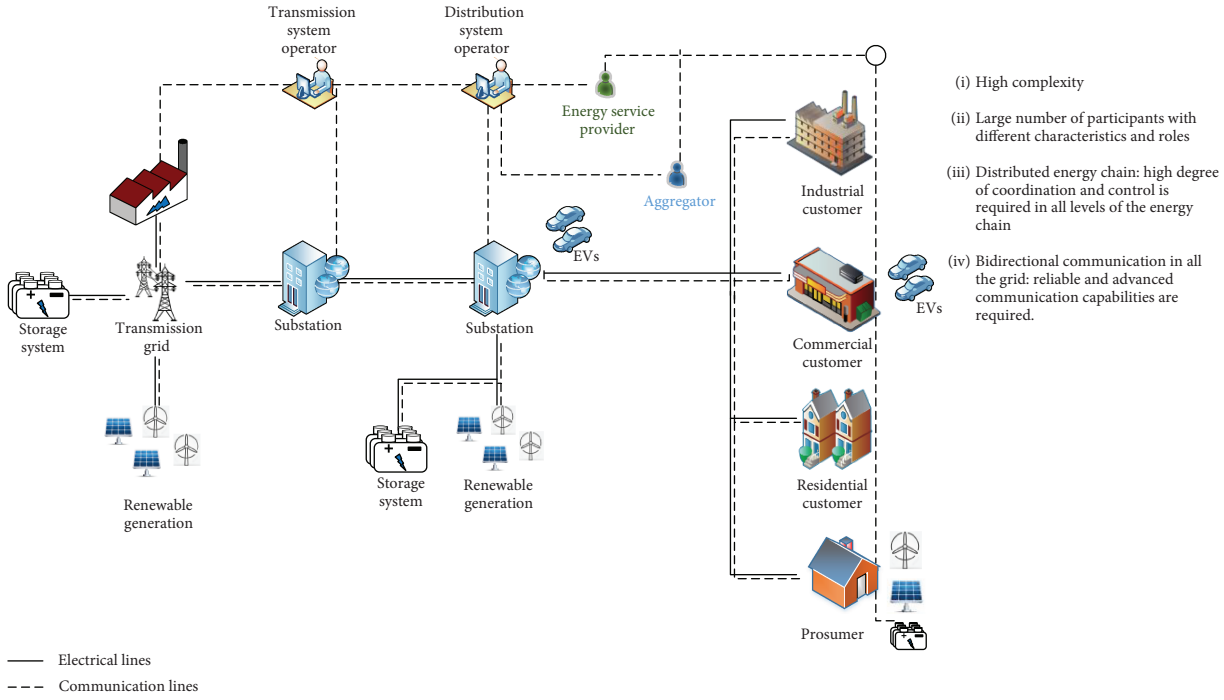

Figure 2: The present and future of the electricity grid. The so-called smart grid.

an overview of the recent research. Table 1 shows the overview of research documents produced since 2010 (excluding 2018) analyzed by different search terms. The search terms have been combined with similar variants within the power systems field to observe results as accurately as possible. We looked for each search term in the abstract, title, and paper's keywords. In addition, we investigate the most cited articles in each search criterion as well as the most noticeable research authors by the number of articles produced. A total of 23,619 documents between 2010 and 2017 are found in the SCOPUS database by using search term "smart grid" OR "smart distribution network" alone in the abstract, title, and keywords and 17,757 if the search term is "renewable generation" OR "renewable energy sources." The search term "smart grid" AND "electric vehicle" produced the least number of documents when compared with the other search terms. In spite of their complementary, EVs in the smart grid context are yet a growing research field not as mature as the research observed in other topics, such as DR.

The most cited article we came across while looking at the produced research documents is [25] (3057 citations). The interest in grid storage applications is noticeable and considered the holy grail of modern power systems, since it can solve many problems and challenges arisen in smart grid. In particular, Dunn et al. [25] review battery systems for grid applications including redox flow, sodium-sulfur, and lithium batteries. The interest of storage for grid applications is related to diversified factors, including management of peak demands and grid reliability, postponement of grid investments, and integration of renewable energy sources.

Regarding "smart grid" OR "smart distribution network" term, the most cited articles we found are [11, 26, 27]. In [26] (1393 citations), an important advance is proposed in order to allow smartness and flexibility of smart grid based on ISA-95 standards. The system is more flexible and expandable using the proposed control. Farhangi [11] (1186 citations) highlights ingredients, drivers, and standards for the success and path of smart grid. Cabana et al. [27] (1144 citations) review the literature concerned with the materials used in lithium batteries, strong enablers of smart grids, and renewable technologies.

In "Renewable generation" OR "renewable energy sources" research topic, we could conclude that the 3 most cited articles are [25, 28, 29]. Blaabjerg et al. [28] (2256 citations) give an overview of the structures of distributed generation (DG) renewable sources based on fuel cell, photovoltaic (PV), and wind turbines. Carrasco et al. [29] (1989 citations) present a review of the appropriate storage system technology used for the integration of intermittent renewable energy sources. New trends in power electronics for the integration of wind and PV generators are presented.

In "smart grid" AND "electric vehicle" research topic, the most cited articles are [30–32]. Ipakchi and Albuyeh [30] (905 citations) provide an overview of the future of the power grid, namely, the necessary transformations to accommodate large number of EVs and other resources such as DR. Kamaya et al. and Skyllas-Kazacos et al. [31, 32] (856 and 574 citations) are related to this topic since they present progress related to lithium and flow batteries, which are fundamental and intrinsically related to the development and success of EVs. Lower battery costs and higher energy density are fundamental to leverage attractiveness and competitiveness of electric cars.

Regarding "demand response" OR "demand-side management" research topic, the 3 most cited articles are [30, 33, 34]. Mohsenian-Rad et al. [33] (1097 citations)

Table 1: Research documents produced since 2010 analyzed by search term according to SCOPUS.

Search term	Documents since 2010*	3 most cited articles Reference	Citations	Top 5 authors with most articles Author (number of articles)
"Smart grid" OR "smart distribution network"	23,619	[26]	1393	Vale, Z. (125); Mouftahm, H.T. (78); Morais, H. (76), Li, H. (64); Javaid, N. (59)
		[11]	1186	
		[27]	1144	
"Renewable generation" OR "renewable energy sources"	17,757	[25]	3057	Guerrero, J.M. (58); Senjuy, T. (57); Duic, N. (49); Blaabjer, F. (48); Andersson, G. (42)
		[28]	2256	
		[29]	1989	
"Smart grid" AND "electric vehicle"	2331	[30]	905	Vale, Z. (40); Morais, H. (26); Mouftah, H.T. (25); Masoum, M.A.S. (24); Soares, J. (24)
		[31]	856	
		[32]	574	
"Demand response" OR "demand-side management"	6195	[33]	1097	Vale, Z. (115); Faria, P. (85); Morais, H. (59); Lehtonen, M. (52); Javaid, N. (49)
		[30]	905	
		[34]	830	
"Smart grid" AND "optimization"	3840	[33]	1097	Javaid, N. (44); Vale, Z. (43); Morais, H. (27); Giannakis, G.B. (26); Khan, Z.A. (26)
		[35]	836	
		[36]	872	
"Energy resource management" OR "energy management system"	5206	[11]	1186	Anon (69); Vale, Z. (64); Zhang, B. (58); Sun, H. (47); Morais, H. (46)
		[33]	1097	
		[1]	505	

*Excluding documents already available for 2018. 2017 maybe incomplete.

propose a distributed demand-side management maintaining user privacy and details of energy consumption. The highly cited work emphasizes that the proposed approach may reduce the peak-to-average ratio of the total demand, the total costs, and each user's individual daily electricity charges. Palensky and Dietrich [34] (830 citations) provide an outlook and taxonomy to demand-side management and several successful demonstration projects that have been implemented until the time of publication.

In the topic of "smart grid" AND "optimization," the results in SCOPUS revealed that [33, 35, 36] are the most cited articles. Cheng and Chen [35] (836 citations) provide an outlook at the current state of the art in smart grid communications and open research issues in the field of information and communication technology (ICT). ICT is a key part of the successful deployment of optimization applications in the smart grid. In the search term "energy resource management" OR "energy management system", [1, 11, 33] are the most cited works. Siano [1] (505 citations) provides a comprehensive survey on energy management, including DR potentials and benefits in smart grids. Figure 3 depicts the number of documents produced between 2010 and 2016 by search term according to the same terms previously depicted and analyzed in Table 1. It can be observed that the increase has been significant and well supported since 2010 when analyzing most of the search topics, except from the search term "smart grid" AND "electric vehicle." There is substantial research work on EVs, which is not directly related to the "smart grid" topics (cf. [37]). If compared to "demand response" or other search terms, the number of documents suggests a much more active and mature development. This analysis also suggests that research on EVs in the smart grid context is yet in the early stage. Although many theoretical concepts and ideas have been proposed (e.g., dynamic pricing [38, 39] and vehicle-to-grid [6, 40]), both EVs and smart grid are yet in the early stage of introduction and lessons have to be learned to better understand how EVs can realize the full smart grid potential. Energy resource management-related research has increased steadily along with the research in DR topics since its importance to the new paradigm of power systems (see Section 3.2). In fact, energy resource management is key to smart grid operation in order to attain acceptable costs with reduced impact from uncertainty of intermittent generation and load sources of difficult anticipation such as EVs.

Figure 4 shows the number of conference papers and journal articles produced between 2010 and 2016 (primary axis) by search term "energy resource management" OR "energy management system" in the SCOPUS database. In the secondary axis, the conference papers per journal article indicator are shown (green cross). Other publications such as book chapters are not included in this comparison. The number of journal articles produced per year has increased substantially from 89 in 2010 to 428 in 2016 (more than 4-fold increase). However, the number of conference papers per journal article has reduced significantly in the last three years to 1.27 from more than 2.23 in 2011 to 1.27 in 2016. This suggests that more journal articles are being published for each paper presented at an international conference. In our opinion, this is a potential indicator that energy resource management-related research is getting more mature in the last years and ready for publication in journal.

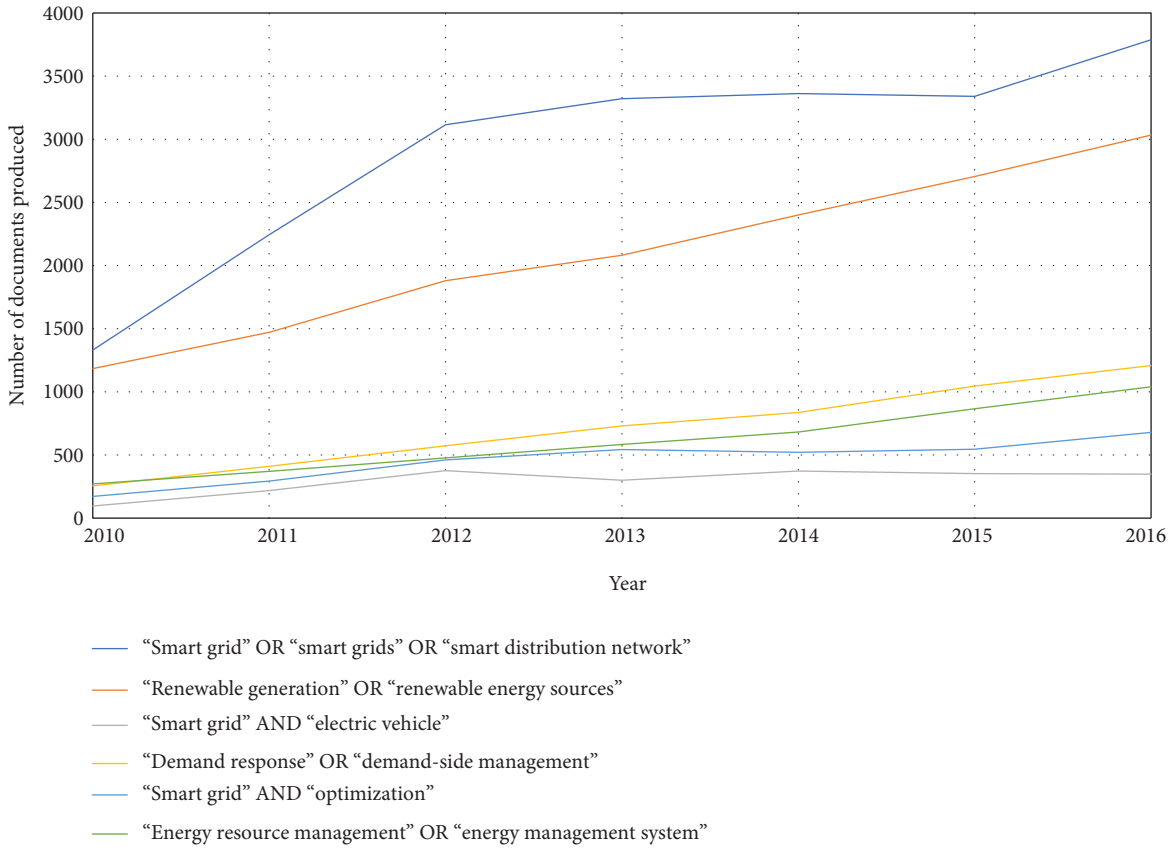

Figure 3: Documents produced between 2010 and 2016 by search term in the SCOPUS database.

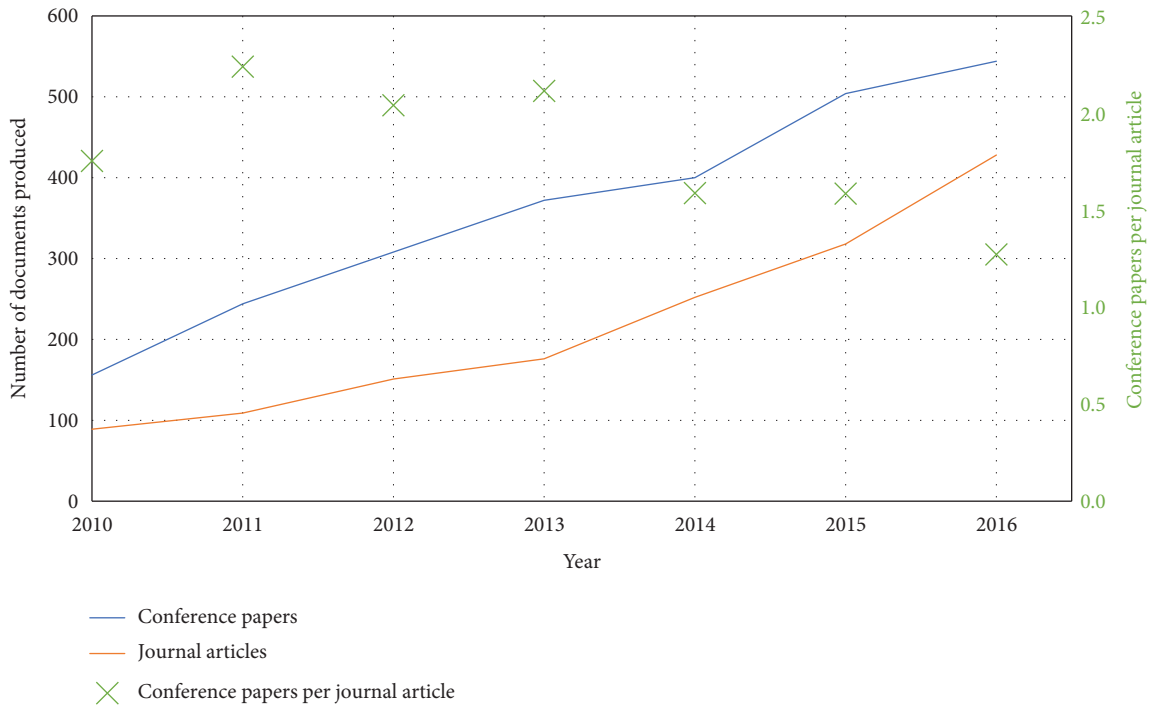

Figure 4: Conference papers and journal articles produced between 2010 and 2016 (primary axis) by search term ("energy resource management" OR "energy management system") in the SCOPUS database.

3.2. Review of Works in the Energy Resource Management. Energy resource management has been considered by some researchers as one of the most complicated optimization problems in power systems due to its combinatorial nature, nonlinearities, and large number of energy resources which leads to high dimensionality and highly constrained problems [23, 41–43]. Adequate optimization frameworks are a key part of the new paradigm brought by the smart grid operation. The literature has a relevant amount of publications in this field that we selected and revised in this section. Since consideration of uncertainty is crucial for smart grid models [44], we investigated in detail this component in the studied models. We also include papers published in 2017 (55 publications appear in the SCOPUS database with the search term "energy resource management" OR "energy scheduling" AND ("uncertainty" OR "uncertain" OR "variability") between 2010 and 2017, of which 22 are from 2017). However, we could observe that the majority of the proposals still lack the consideration of full component uncertainty and/or DR in the model. Table 2 identifies the characteristics of the main publications we selected in what regards the considered energy resources and in terms of uncertainty consideration in the model.

As can be observed in Table 2, very few works attempt to consider most sources of uncertainty in a joint energy scheduling model [45, 46]. Moreover, it is yet not common to see works that incorporate vehicle-to-grid (V2G), DG, DR, and energy storage systems (ESS) simultaneously as in [45–48]. However, [47, 48] do not include consideration of uncertainty of the energy resources.

The work developed in [49] approaches the problem of day-ahead electricity market bidding to minimize charging costs and satisfy EV demand of the aggregator. The work considers the presence of uncertainty, but V2G is not considered in the problem. Results suggest that controlling EV charging is important to lower energy costs, while the aggregator has limited market potential with reasonable amount of EVs. A related work can be seen in [50] where a bidding and power scheduling is proposed to maximize the expected benefit of a microgrid. The stochastic model captures several sources of uncertainty, and the novelty lies in the exploitation of thermal characteristics of the buildings to mitigate renewable imbalances. Also, works [51–53] propose to tackle the optimal bidding in the market of the aggregator using multistage stochastic [51, 53] and robust approaches [52]. The work in [54] introduces the reliability of the fuel cell outages in the microgrid energy scheduling, but the uncertainty considered in the model lies only in the fuel cell outages.

The model in [55] proposes a scheduling model for microgrids under uncertainty. The work implements a two-stage stochastic model with one external power flow algorithm to calculate power losses. EV uncertainty, DR, and V2G are not considered though. To overcome this, [45] propose an improved two-stage stochastic model that addresses several sources of uncertainty, namely, wind, PV, EVs, demand, and market price, in a joint model yet not accounting for power losses. Later, a new model is proposed in [46], which adds network constraints, namely, power line capacity and voltage control to the original problem in [45]. The problem is solved using a Benders decomposition scheme. The results suggest that the large-scale problem with uncertainty can be solved in its most complex form, dealing at the same time with the number of resources and the DSO technical constraints as part of the equation.

The two-stage stochastic model introduced in [56] adds to the previous stochastic microgrid energy scheduling works, a hybrid AC/DC microgrid setting. However, the work does not consider DR application. The model in [57] proposes a day-ahead energy and reserve scheduling for the aggregator. The uncertainties are modeled via a point estimate method. The work does not consider EVs as an intelligent load. The work in [58] proposes a similar work but considering compressed air ESS. EVs are not considered as well.

Most of these works have implemented a two-stage stochastic model, which requires knowledge about the distribution of the uncertain data, usually possible if historical records are available. However, it is fair to recognize that most of these models require large amounts of computational resources to be able to solve the stochastic model with an adequate number of scenarios (even if scenario reduction techniques are adopted). In fact, scenario reduction techniques decrease the accuracy of the uncertainty representation. Since smart grid operation is dealing with an increasing number of energy resources and consequently more components associated with uncertainty, it remains a major challenge to tackle these optimization models under uncertainty with adequate representation. A solution may lie in metaheuristics and decomposition techniques combined with uncertainty models and/or robust optimization models that deal with a range of uncertainties instead of probabilistic scenarios. Another solution may lie in distributed real-time energy scheduling as proposed in [59], which transforms the problem into a distributed and tractable problem, using rolling horizon optimization and Gaussian approximation. However, we believe the work is still limited since it considers only a single energy source and one source of uncertainty.

Alternatively to stochastic models, Ju et al. [60] propose a robust model for the energy aggregator with DR, ESS, and renewables, which does not require to know the distribution of uncertain parameters such as the forecasts. Still, EVs are not considered in the work as well. Another robust model is adopted in [61] which tackles market price and load demand uncertainty for aggregators that are new entrants to the market and have little knowledge on the behavior of the market and their customers. In [48], authors propose an energy resource management for domestic loads that considers uncertainty in the PV power for the day-ahead and real-time approach. The work considers EVs, DR as flexible loads, and ESS units. Two different stochastic methods are compared and evaluated using a realistic case study.

Table 3 classifies the works reported regarding its main purpose, namely, technical, economic, and environmental aspects. It can be seen that most of the works related to uncertainty deal with economic aspects. Technical aspects are often common and related to power losses and voltage control (when network constraints are considered) such as in [49, 56]. Some of the works consider environmental,

Table 2: Summary of energy scheduling models: resources and uncertainty sources.

Ref.	Resources/components present in the work				Considered sources of uncertainty
	V2G	DG	DR	ESS	
[49]	No	Yes	No	No	Driving patterns and market bids
[55]	No	Yes	No	Yes	Only in wind and PV
[59]	No	Yes	No	No	Only in energy demand
[54]	No	Yes	No	Yes	Only in the fuel cell outages
[50]	No	Yes	Yes	Yes	Load, renewable generation, and electricity price
[56]	Yes	Yes	No	Yes	Load, renewable generation, EV demand, and price
[57]	No	Yes	No	No	Renewable generation, load, and electricity price
[58]	No	Yes	Yes	Yes	Wind/PV, load demand, and market price
[60]	No	Yes	Yes	Yes	Wind/PV only
[51]	No	Yes	No	No	Wind, market bids, and price rivals' offers
[52]	No	Yes	No	No	Wind and market price
[53]	No	Yes	No	Yes	Intermittent source and market price
[45]	Yes	Yes	Yes	Yes	Wind, PV, EVs, load demand, and market price
[62]	No	No	Yes	Yes	—
[38]	No	Yes	Yes	Yes	Wind, PV, EVs, and load demand
[47]	Yes	Yes	Yes	Yes	—
[7]	No	Yes	Yes	No	—
[46]	Yes	Yes	Yes	Yes	Wind/PV, EVs, load demand, and market price
[61]	No	Yes	Yes	No	Market price and load demand via robust model
[48]	Yes	Yes	Yes	Yes	PV power

Table 3: Summary of energy scheduling models: technical and economic aspects.

Ref.	Technical aspects			Economic aspects
	Power losses	Voltage control	Other[1]	
[55]	No	No	No	The goal of the aggregator is to minimize purchases in the spot market.
[49]	Yes	Yes	No	Expected operational costs over the next 24 hours.
[59]	No	No	No	Maximize system utility.
[54]	No	No	Yes	Financial aspects (costs) but also environmental and reliability.
[50]	No	No	Yes	Maximize profits of microgrid considering building dynamics.
[56]	Yes	Yes	No	Expected operation costs over the next 24 hours.
[57]	No	No	No	Maximize expected profits over the next 24 hours.
[58]	No	No	No	Minimize expected costs.
[60]	No	No	No	Maximize operation revenue.
[51]	No	No	No	Maximize profit over the scheduling horizon.
[52]	No	No	No	Maximize utility function in day-ahead and real-time markets.
[53]	No	No	No	Maximize profit in the day-ahead and balancing market.
[45]	No	No	No	Minimize expected operation costs.
[62]	No	No	No	Minimize household energy costs under DR programs.
[38]	No	No	No	Maximize aggregator profit and EV user charging opportunity.
[47]	Yes	Yes	Yes	Maximize aggregator profit.
[7]	No	No	No	Minimize aggregator operation costs and suitable remuneration groups.
[46]	Yes	Yes	No	Minimize operation costs considering market transactions.
[61]	No	No	No	Maximize aggregator payoff considering price risk.
[48]	No	No	No	Maximize domestic energy profit.

[1]Fault location, network restoration, and island operation.

reliability, and building dynamic aspects such as in [50, 54]. Soares et al. and Soares et al. [46, 47] include both technical and economic aspects. However, [47] does not incorporate the resources' uncertainty as formulated later in [46], despite not including environmental aspects as in [47].

4. Computational Intelligence for Complex Optimization Problem in the Energy Domain

Computational intelligence (CI) is usually referred to a family of problem-solving and problem-stating techniques that attempt to exhibit or mimic the "intelligence" observed in nature. It includes some of the most popular paradigms in the applications of computer science, namely, evolutionary computation (EC), artificial neural networks (ANN), and fuzzy systems (FS).

Despite its popularity nowadays, the term CI has had different definitions through the years in the scientific community and typically is seen as a separate area of artificial intelligence (AI) very related with soft computing or natural computation. For instance, the first CI definition is typically attributed to J.C. Bezdek who defined CI in 1992 as "Computational systems that depend on numerical data supplied by manufactured sensors and do not rely upon knowledge" [63]. Later, in 2002, Engelbrecht defined CI as "the study of adaptive mechanisms which enable or facilitate intelligent behavior in complex and changing environments" [64]. Therefore, in an abstract sense, CI can be defined as intelligent computational tools to solve, or model, complex problems. However, two main questions arise regarding this statement, namely, what is a complex problem? And more importantly, why should we use CI to address such issues?

To answer the first question, notice that many real-world problems are highly constrained by nature and face issues related to high dimensionality, lack of information, noisy and corrupted data, real-time requirements, and so on. Due to these characteristics, exact mathematical formulations sometimes fail in providing solutions because of either restriction of time, lack of memory to deal with large-scale problems, or other factors. In other words, problems that cannot be efficiently solved by traditional mathematical approaches can be seen as complex problems.

On the other hand, and answering the second question, CI is strictly related to the subfield of computer sciences known as soft computing. Soft computing (Soft computing became a formal area of study in computer science in the early 1990s and in a broader sense includes topics such as computation intelligence (CI), machine learning (ML), and probabilistic reasoning (PR). In this paper, however, we focus our attention to the main three subfields of CI; namely, an extensive analysis of EC applications for optimization in power systems is provided, with a brief review on optimization-related ANN and FS applications.) is used to solve complex problems (i.e., with characteristics such as the ones previously stated) in which exact methods cannot compute a solution in polynomial time. Different from hard computing, soft computing is tolerant to imprecision, uncertainty, and approximation. Even when soft computing cannot guarantee an optimal outcome, it can return near-optimal solutions in acceptable computational times and with low memory requirements, imitating the role model of the human mind.

It is important to point out that despite the conditions mentioned above, CI has demonstrated satisfactory performance in a wide variety of application fields such as power systems, portfolio optimization, transportation, smart grid, and telecommunications.

As you might notice, this section is devoted to the application of CI for solving the wide variety of complex problems that arise in the new paradigm of power systems. As it was stated in Section 2, current smart grids are evolving to a very fast pace, and the interaction between a considerable number of new participants and elements (with their inherent socioeconomic and technological aspects) makes the analysis of such systems very complex for traditional mathematical tools and management and control models. In addition, the same logic applies to different areas of engineering since CI is a paradigm that is acquiring significant importance these days.

4.1. Computational Intelligence Classification and Application Target. CI is commonly used for different purposes, but we can devise three main categories of its application, namely, optimization, learning/modeling, and control. Moreover, some problems require the use of a combination of these categories to devise practical solutions. Despite the vast synergies existent in the application targets of CI, such targets are strongly related with the three main paradigms of CI. For instance, evolutionary computation (EC) is applied to optimization problems; artificial neural networks (ANN) is extensively used for learning/modeling and forecasting, and fuzzy systems (FS) is typically implemented for control. The relation of EC, ANN, and FS, to the target applications is used to envisage application areas in a broader sense somehow. However, many real-world applications may require synergies between methods belonging to the three fields to obtain an acceptable solution.

With the evolution of technology in diverse engineering fields, real-world problems are becoming more challenging, limiting the use of exact methods. Due to this, CI has emerged as a powerful tool to provide acceptable solutions in different domains. As a proof in the increasing interest of the research community regarding CI applications, Figure 5 shows the number of publications in the main three topics of CI from 2000 to 2016 (17-year span), obtained after a search in the SCOPUS database [24]. The search was done putting as a filter the terms shown in Figure 5, and considering all areas of applications. As a result, 24,706 publications in total were found when searching for "evolutionary computation OR evolutionary algorithms," 23,995 publications using "Artificial Neural Networks," and 49,623 when searching for "Fuzzy systems."

It is evident that CI is gaining interest mainly for its effectiveness to solve a large variety of problems in all areas of engineering. Moreover, from the total number of papers found in the three analyzed areas, 10% (2601 publications of EC), 22% (5299 publications of ANN), and 2% (1410 publications of FS) of the published works correspond to studies in the energy domain. To narrow our review into the topic of

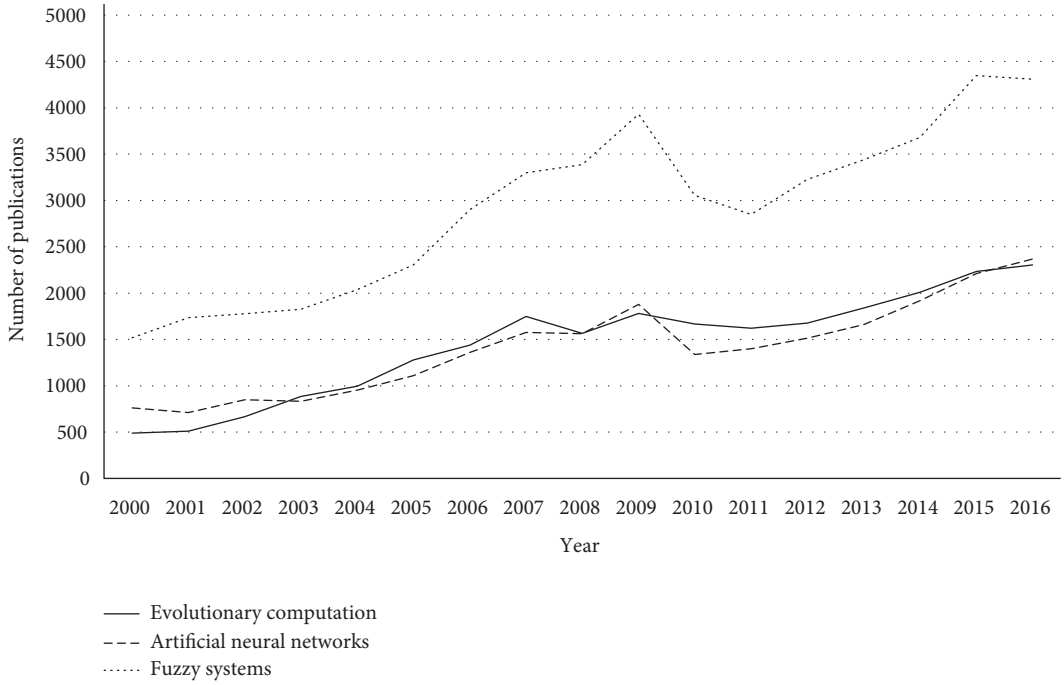

Figure 5: Publications of the main topics of computational intelligence.

interest, that is, CI applied in the energy domain, we have filtered the search focusing on the publications regarding CI in the energy domain.

Figure 6 shows the ratio between the number of publications devoted to the energy domain and the total of publications by the CI paradigm (i.e., EC, ANN, and FS). It is worth noticing that the three areas of CI show a trend that reflects more publications in the energy domain. From the three main topics of CI, EC is the one that shows the most pronounced increment in the ratio in the last years.

In the following subsections of Section 4, we include a brief analysis of the taxonomy of EC, and through Tables 4–7, we group the most cited works of the CI paradigm applied to the energy domain. The tables include the CI techniques, the problem to be solved in the energy domain, and the main mathematical characteristics that make such problems complex and justify the use of advance computational approaches such as CI.

4.2. Evolutionary Computation (EC) Taxonomy. Evolutionary computation (EC) is a fundamental part of CI and encompasses a set of algorithms for global optimization mostly inspired by biological and evolutionary processes. CI is arguably one of the most successful branches of CI, used by a large number of practitioners all over the world and in all areas of engineering [65] (see Figures 5 and 6). It is worth noticing that EC is not only limited to the study of evolutionary algorithms (EA), as it is sometimes wrongly assumed, but also covers some of the most exciting trends in computer sciences, namely, swarm intelligence (SI), nature-inspired algorithms, and bioinspired or natural computation.

The family of algorithms belonging to the class of "evolutionary algorithms" (EA) shares some common characteristics that distinguish them from other metaheuristics. In technical terms, EAs are population-based problem-solvers. Commonly, EAs act over an initial set of candidate solutions (i.e., a population) that is iteratively updated through generations. The performance of the solutions is measured by a given fitness function, and at each generation, solutions with inferior performance are stochastically removed, whereas new solutions (generated through a specific operation particular for different EAs) are introduced into the population. As a result, it is expected that by the principles of natural selection (or artificial selection in this case), the population gradually will evolve towards the optimal fitness value.

The field of EAs is broad, and the techniques typically differ in implementation details or the genetic representation they use. Among the existing techniques of EA, the three main subfields (source of inspiration for many developments in this paradigm) correspond to genetic algorithms (GA) [66, 67], genetic/evolutionary programming (GP) [68, 69], and evolutionary strategies (ES) [70, 71]. In the last decades, differential evolution (DE) [72], a particular case of ES, has been the subject of an entire line of research. DE is arguably one of the most popular and effective EAs with a considerable number of successful applications in the engineering domain [131].

On the other hand, SI and nature/bioinspired computation are metaheuristics inspired in the observation of the collective behavior of agents or natural/biological processes, respectively. For instance, SI takes advantage of the interaction of simple agents with each other on the environment to achieve collectively "intelligence," similarly to natural systems such as ant colonies or bird flocking. Examples of SI algorithms are the ant colony optimization (ACO) [73],

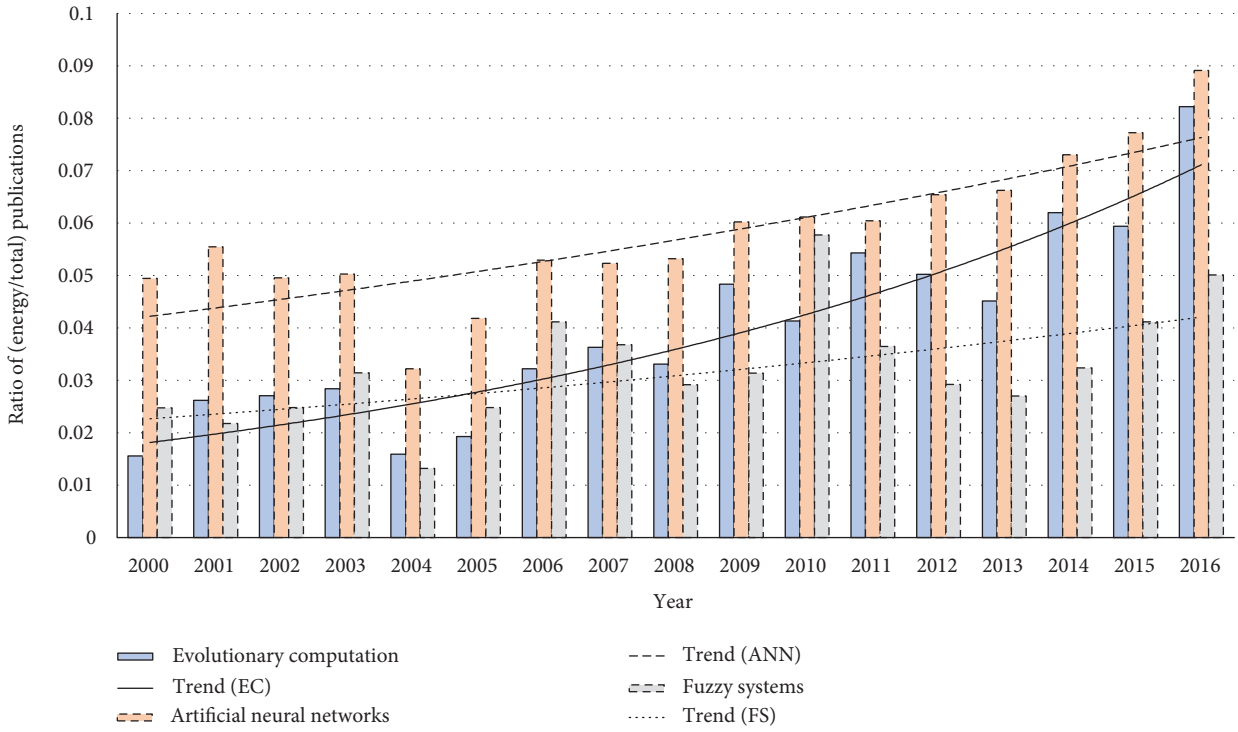

Figure 6: Ratio between energy domain and total of publications by main fields of computational intelligence. The trends suggest an increase in the applications of EC in the energy domain.

particle swarm optimization (PSO) [74], artificial bee colony (ABC) [75], or cuckoo search (CS) [76]. Nature-inspired algorithms go further in the design of algorithms inspired by natural, physical, or even chemical phenomena. Examples of this type of algorithms are gravitational search algorithms (GSA), simulate annealing (SA), harmony search (HS), and others. A very well-conducted taxonomy and classification of nature-inspired algorithms can be found in [77].

4.3. Evolutionary Computation (EC) in the Energy Domain. EC can be applied to problems of all areas of engineering. In this review, however, we are interested in applications related to complex problems in the energy domain. Therefore, in Table 4, we have grouped the most cited works of the EC paradigm applied to the energy domain in the span 2010–2017. The table is organized from the top 1 cited paper to the top 10 according to the SCOPUS database. We show the specific EC approach used, the problem that was solved, and some characteristics related to the work.

In general terms, Table 4 confirms that EC is mainly used to solve optimization problems. Problems such as economic load dispatch (ELD), optimal power flow (OPF), and optimal operation of microgrids are addressed by the most influential works, mainly due to the key role that those problems play in power systems. With the evolution of the electrical grid led by the penetration of distributed resources, and the deployment of smart grid technologies, EC has attracted the attention of many practitioners due to its effectiveness in providing acceptable solutions when exact traditional methods fail. It is also interesting to appreciate the correspondence between some of the most studied algorithms in the field of EA and the most cited papers of EC in the energy domain. For instance, we can find the application of the strength Pareto evolutionary algorithm (SPEA) [78], an algorithm that has been cited more than 6000 times according Google Scholar, into three problems of the energy domain, namely, wind turbine placement, turbine layout design, and the optimization of a stand-alone PV-wind-diesel system with battery storage. The nondominated sorting genetic algorithm NSGA-II [79], another well-known and highly used EA, was applied to the combined cycle power plant (CCPP) optimization problem in [80]. DE, well-known for its simplicity and effectiveness in continuous global optimization, has been used to solve the OPF problem [81] and the optimization of PV systems [82].

In general, Table 4 shows that the majority of the problems in which EC is applied corresponds to complex optimization problems that cannot be solved efficiently by traditional techniques. Such complex problems present common characteristics, namely, multiobjective nature, constrained optimization, convex and nonconvex problems, nonlinear formulations, and so on. Because of the advances in technology, it is expected that the complexity of the systems will increase in the years to come, and therefore, the complexity of the mathematical formulations required to solve related problems is expected to grow as well. In this likely scenario, EC seems a viable and logic option for application into the field, despite the fact that optimal solutions cannot be guaranteeing.

The search of the most cited papers was done in the time span 2010–2017. However, the top ten cited papers

Table 4: Most cited papers between 2010 and 2017 of EC applied to energy-related problems.

Ref.	Year	EC approach	Problem (optimization)	Characteristics
[83]	2010	Strength Pareto evolutionary algorithm (SPEA)	Wind turbine placement Turbine layout design	Constrained optimization problem transformed to bicriterion optimization problem. Objective: maximize the expected energy output and minimize the constraint violations.
[84]	2010	Hybrid algorithm: differential evolution combined with biogeography-based optimization (DE/BBO).	Economic load dispatch (ELD) problems of thermal power units.	Convex and nonconvex problems. The ELP considers thermal power units, transmission losses, and constraints such as ramp rate limits, valve-point loading, and prohibited operating zones.
[85]	2013	Review: fuzzy logic control (FLC), artificial neural network (ANN), and evolutionary algorithms (EA).	Maximum power point tracking (MPPT) techniques for PV applications.	The paper focuses on the applications of CI techniques during partial shading conditions.
[80]	2011	Genetic algorithms (GAs) and second version of nondominated sorting genetic algorithm (NSGA-II).	Combined cycle power plant (CCPP) optimization problem.	Multiobjective optimization. Objective: determine the best design parameters, considering three objectives: (a) CCPP exergy efficiency, (b) total cost rate of the system products, and (c) CO_2 emissions of the overall plant.
[86]	2011	Strength Pareto evolutionary algorithm (SPEA).	Optimization of a stand-alone PV-wind-diesel system with battery storage.	Multiobjective optimization. Objective: optimize the levelized cost of energy (LCOE) and the equivalent carbon dioxide (CO_2) life cycle emissions.
[81]	2010	Differential evolution (DE).	Optimal power flow (OPF) problem	Different objective functions and nonsmooth piecewise quadratic cost functions are considered. Objectives: minimization of fuel cost, voltage profile improvement, and voltage stability enhancement.
[87]	2011	Adaptive modified particle swarm optimization (AMPSO) algorithm.	Optimal operation of a MG with renewable energy sources accompanied by a back-up microturbine/fuel cell/battery hybrid power source.	Nonlinear constraint multiobjective optimization problem Objective: minimization of total operating cost and the net emission simultaneously.
[82]	2011	Differential evolution (DE)	PV modeling techniques.	DE is applied to simultaneously compute all the model parameters at different irradiance and temperature points.
[88]	2010	Fuzzy adaptive hybrid PSO algorithm.	Economic dispatch problem considering the valve-point effect.	Nonsmooth and nonconvex problem when valve-point effects of generation units are taken into account.
[89]	2012	Review: evolutionary algorithms.	Stand-alone hybrid renewable energy systems.	The review focuses on multiobjective methods using evolutionary algorithms for hybrid renewable energy systems.

correspond only to the span 2010–2013. To give a glimpse into more recent works and envisage the research directions of the application of EC nowadays, Table 5 includes the three most cited papers of the years 2015, 2016, and 2017.

In general aspects, it can be appreciated in Table 5 that the tendency of recent influential works lays on the hybridization of EC algorithms. Combinations of DE and PSO into DEPSO [90], ACO and ABC into ACO-ABC [91], or a multistep approach using cuckoo search (CS) algorithm, fuzzy system (FS), weather research and forecasting (WRF), and ensemble forecast (CS-FS-WRF-E) [92] are some examples of the synergies that can be produced between EC algorithms for solving more challenging problems.

On the other hand, in the recent applications of EC, we still can find the application of pure popular EC algorithms. For instance, DE was recently applied to the optimization of combined cooling, heating, and power-based compressed air energy storage. A GA was used in [93] to determine optimal sizing of components in microgrids, while MILP was then used to solve the unit commitment problem (UCP), which is considered of paramount importance in the management and operation of microgrids. NSGA-II was used in [94] to solve a multiobjective optimization problem of solar driven Stirling heat engine with regenerative heat losses. In addition, new algorithms are under development, and their application is also very welcome in the energy domain.

Table 5: Recent most cited papers of EC applied to energy-related problems. The three most cited papers from 2015, 2016, and 2017 are included.

Ref.	Year	EC approach	Problem (optimization)	Characteristics
[90]	2015	Hybrid algorithm: differential evolution combined with particle swarm optimization (DEPSO).	Maximum power point tracking (MPPT) techniques for PV applications.	Simulation and hardware implementation of DEPSO for MPPT.
[91]	2015	Hybrid algorithm: ant colony optimization combined with artificial bee colony (ACO-ABC).	Optimal location and sizing of distributed energy resources.	Multiobjective optimization. Objectives: minimization of power losses, total emissions, total electrical energy cost, and improvement of voltage stability.
[96]	2015	Brainstorm optimization algorithm (BSOA).	Optimal location and setting of flexible AC transmission system (FACTS) devices.	Discrete, multiobjective, multimodal, and constrained optimization. BSOA is compared with PSO, GA, DE, SA, hybrid of genetic algorithm and pattern search (GA-PS), backtracking search algorithm (BSA), gravitational search algorithm (GSA), and asexual reproduction optimization (ARO).
[92]	2016	Multistep approach: cuckoo search (CS) algorithm, fuzzy system (FS), weather research and forecasting (WRF), and ensemble forecast (CS-FS-WRF-E).	Forecasting of wind speed.	CS optimization is used to construct the final model adjusting and correcting the results obtained based on physical laws. The final model yields to best forecasting performance and outperforming all the other models used for comparison.
[97]	2016	Chaotic bat algorithm (CBA).	Economic dispatch problem (EDP).	Consideration of equality and inequality constraints (e.g., such as power balance, prohibited operating zones, and ramp rate limits). Also, transmission losses and multiple fuel options are taken into account.
[94]	2016	Second version of the nondominated sorting genetic algorithm (NSGA-II).	Optimization of solar driven Stirling heat engine with regenerative heat losses.	Multiobjective optimization. Objectives: power output, overall thermal efficiency, and thermo-economic function. A selection of the best solution in the Pareto front by Fuzzy Bellman-Zadeh, Shannon's entropy, LINMAP, and TOPSIS is also implemented.
[98]	2017	Differential evolution (DE).	Optimization of combined cooling, heating, and power-based compressed air energy storage.	Multiobjective optimization. Objectives: maximization of system exergy efficiency and minimization of total product unit cost.
[93]	2017	Genetic algorithm (GA).	Optimal size of microgrid components. Unit commitment problem (UCP).	Leader-follower problem. The leader problem focuses on sizing. The follower problem, that is, the energy management issue, is solved with a mixed-integer linear program.
[99]	2017	Multiobjective quantum-behaved particle swarm optimization (MOQPSO).	Economic environmental hydrothermal scheduling problem.	Multiobjective, nonlinear, and constrained optimization. A constraint handling method is designed to adjust the constraint violation of hydro and thermal plants.

Brainstorm optimization algorithm (BSOA) and chaotic bat algorithm (CBA) [95] are only two examples of successful applications of such new algorithms. BSOA was recently applied to the optimal location and setting of flexible AC transmission system (FACTS) devices in [96], whereas CBA was used to solve the well-known economic dispatch problem (EDP) considering equality and inequality constraints [97].

4.4. Artificial Neural Networks (ANN) and Fuzzy Systems (FS) as Complementary Tools for Optimization. ANN and FS are two important paradigms of CI used mainly for forecasting/modeling and control, respectively. Since the scope of this review is on complex optimization and simulation, the extensive analysis of the applications of ANN and FS is somehow out of the scope of what this review is intended for. However, these two paradigms are also widely used in combination with EC for solving some optimization problems. Moreover, some applications of ANN or FS, such as the ANN weight selection or the definition of the parameter of membership functions of an FS, are indeed highly complex optimization problems that cannot be solved with deterministic methods suitably. Therefore, this section revises some of the hybrid applications in which ANN, FS, and EC are used in combination to solve complex tasks.

The pure application of ANN in power systems is commonly used to solve forecasting problems. Forecasting of solar irradiance or PV power [100–103], wind speed [104–106], or load [107] are just some examples of successful applications of ANN in the energy domain. On the other

Table 6: Some selected highly cited papers of hybrid approaches applied to energy-related problems.

Ref.	Year	CI approach	Problem (optimization)	Characteristics
[85]	2013	Review: fuzzy logic control (FLC), artificial neural network (ANN), and evolutionary algorithms (EA)	Maximum power point tracking (MPPT) techniques for PV applications.	The paper focus on the applications of CI techniques during partial shading conditions.
[109]	2011	Fuzzy logic controller (FLC).	Maximum power point tracking (MPPT) techniques for PV applications.	The near optimum design for membership functions and control rules were found simultaneously by genetic algorithms (GAs).
[111]	2011	Adaptive-network-based fuzzy inference system combined with wavelet transform, and particle swarm optimization.	Forecasting of wind power.	Comparison with seven other approaches (persistence, NRM, ARIMA, NN, NNWT, NF, and WNF) is presented.
[112]	2011	Adaptive-network-based fuzzy inference system combined with wavelet transform and particle swarm optimization.	Forecasting of short-term electricity prices.	Comparison with ten other approaches (ARIMA, mixed-model, NN, wavelet-ARIMA, WNN, FNN, HIS, AWNN, NNWT, and CNEA) are presented.
[113]	2010	Fuzzy adaptive modified particle swarm optimization (FAMPSO).	Nonconvex economic dispatch problem (NEDP).	The fuzzy system is used to tune PSO parameters (i.e., inertia weight and learning factors).

Table 7: Some selected recent highly cited papers of hybrid approaches applied to energy related problems (span of 2015–2017).

Ref.	Year	EC approach	Problem (optimization)	Characteristics
[107]	2015	Review: artificial intelligence- (AI-) based techniques.	Forecasting of short-term load.	Comprehensive and systematic literature review of AI-based short-term load forecasting techniques.
[102]	2015	Hybridizing the support vector machines (SVMs) with firefly algorithm (FFA).	Forecasting of solar radiation.	A comparison with artificial neural networks (ANN) and genetic programming (GP) models is provided.
[114]	2016	Ensemble empirical mode decomposition (EEMD) and GA-backpropagation neural network.	Forecasting of wind speed.	EEMD can effectively handle the mode-mixing problem and decompose the original data into more stationary signals with different frequencies. Each signal is taken as an input to the GA-BP neural network model.
[115]	2015	Mutual information, wavelet transform, evolutionary particle swarm optimization (EPSO), and adaptive neurofuzzy inference system.	Forecasting of wind power.	Integration of existing models and algorithms, which jointly show an advancement over the present state of the art, is provided. Results show a significant improvement over other reported methodology.
[116]	2016	Least square support vector machine (LSSVM) and adaptive neurofuzzy inference system (ANFIS).	Forecasting/prediction of dew point temperature of moist air at atmospheric pressure.	GA was applied to optimize the corresponding parameters of these models. Predictions are performed over an extensive range of temperature and relative humidity.
[92]	2016	Multistep approach: cuckoo search (CS) algorithm, fuzzy system (FS), weather research and forecasting (WRF), and ensemble forecast (CS-FS-WRF-E).	Forecasting of wind speed.	CS optimization is used to construct the final model adjusting and correcting the results obtained based on physical laws. The final model yields to best forecasting performance and outperforming all the other models used for comparison.
[117]	2017	Artificial neural network (ANN) coupled with fuzzy clustering method (FCM). Additive linear interdependent fuzzy multiobjective optimization (ALIFMO). Second version of the nondominated sorting genetic algorithm (NSGA-II).	Exergetic optimization of continuous photobiohydrogen production process from syngas by *Rhodospirillum rubrum* bacterium.	Multiobjective optimization. Objectives: minimization of the normalized exergy destruction and maximization of the rational and process exergetic efficiencies. The solutions of the proposed approach were also compared with conventional fuzzy multiobjective optimization procedures with independent objectives.

hand, FS are more commonly applied as operation and control strategies. For instance, in [108], a fuzzy logic controller (FLC) was designed for operation and control of an offshore wind farm interconnected to a high-voltage DC (HVDC) system. The maximum power point tracking (MPPT) for PV, a problem sometimes solved by ANN, was addressed using FLCs in [109, 110].

Nevertheless, ANN and FS are also commonly coupled with EC, giving, as a result, some hybrid approaches that attract the attention of the research community to a significant extent. In an effort to synthesize such pieces of work, in Table 6 we have selected some of the most cited works regarding hybrid models using ANN and FS in the span 2010–2017. A combination of fuzzy inference systems, wavelet transform, and PSO is used [111, 112] for forecasting. In this case, the definition of the parameters associated with the membership functions of the fuzzy inference system is a complex optimization problem, and therefore, PSO is used to this end, obtaining more accurate results. On the contrary, in [113], a fuzzy system is used to tune the parameters of PSO, giving place to the so-called fuzzy adaptive modified particle swarm optimization (FAMPSO), which is used for solving the nonconvex economic dispatch problem (NEDP). These two examples show how the interactions between ANN, FS, and EC might go into different directions, giving place to the envisage of more refined techniques when a good knowledge of the strengths and weaknesses of the involved approaches exists.

We have also selected some recent hybrid approaches corresponding to highly cited papers related to ANN and FS applications. Table 7 presents such selection, and it is interesting to notice that the majority of the selected work is related to forecasting techniques [92, 102, 107, 114–116]. This trend is highly motivated by the necessity of a more efficient integration of renewable generation into existing electrical grids. Since forecasting techniques will never guarantee a perfect match between realizations and estimations (or at least we seem to be far from that goal), the improvement of existing techniques is of paramount importance in the operation of power systems.

Overall, the revised literature shows that CI has a strong potential for solving complex tasks in the energy domain. The use of hybrid techniques, along with some other powerful available resources, such as super computers or parallelism, opens a window of opportunity to refine existing techniques and make them more accurate and reliable tools.

5. Complex Large-Scale Simulation in Power and Energy Systems

5.1. Electricity Market Simulation. Renewable energy sources such as wind and solar variable and intermittent nature pose new challenges to the power sector and also to electricity markets. Many different market approaches have been experimented all around the world, and all have been subject to multiple revisions. The primary focus is on adapting electricity markets to deliver their intended economic efficiency and reliability outcomes under the new paradigm of growing share of renewable energy sources [118]. One of the main European Union (EU) priorities concerns the formation of a pan-European energy market. The majority of European countries have already joined together into common market operators, resulting in joint regional electricity markets composed of several countries. Additionally, in early 2015, several of these regional European electricity markets have been coupled in a common market platform, operating on a day-ahead basis [119]. That achievement has been enabled by the multiregional coupling (MRC), a pan-European initiative dedicated to the integration of power spot markets in Europe. The common market platform has resulted from an initiative of seven European power exchanges, called price coupling of regions (PCR) [119], which have joined efforts to develop a single price coupling solution used to calculate electricity prices across Europe and allocate cross-border capacity on a day-ahead basis. This is a crucial step to achieve the overall EU target of a harmonized European electricity market.

This type of initiative is being accommodated by the European Commission, which has created the basis for a significant number of European projects that have been giving substantial contributions to deal with some of the most prominent issues in the field, as discussed in [120] and summarized as follows. One of the main hurdles for the operation of a pan-European market concerns the European power network constraints. The e-Highway2050 project aims at developing and applying a methodology for the long-term development of the pan-European transmission network able to ensure a reliable power delivery from renewable sources, and their integration in the pan-European market. The Optimate (An Open Simulation Platform to Test Integration in MArkeT design of massive intermittent Energy) project had a simulation platform as output, which accommodates the simulation of the pan-European electricity market. In the scope of CASSANDRA (a multivariate platform for assessing the impact of strategic decisions in electrical power systems), the participation of small consumers in the electricity market has been modeled, including the assessment of their strategic decisions. eBADGE (Development of Novel ICT tools for integrated Balancing Market Enabling Aggregated DR and DG Capacity) is developing a simulation and modeling tool for integrated balancing and reserve markets. EMELIE (electricity market liberalisation in Europe) focused on the liberalisation of the European electricity market and its potential impacts on market developments; this project has resulted in a modeling and decision support tool for analysis of various strategic behaviors in the scope of the European electricity market. E-PRICE (Price-based Control of Electrical Power Systems) approached the issue of errors in the prediction of both production and demand and their impact on ancillary services and reserve capacity. Renewable portfolio addresses market players' optimal scheduling under integrating renewables in EU electricity markets, considering a stochastic dynamic market environment.

These initiatives are, however, strongly directed to the perspective of market operators and regulators, which results in valuable advances in what concerns market mechanisms, and market operation and validation, but, apart from a few exceptions, almost entirely disregard the decision support of market participant players, and the impact that the

interaction between these entities has on the market. This decision support is, however, essential, since the complexity and the constantly changing environment of electricity markets makes the decision-making process of the involved entities a very difficult task. Operators and regulators need to foresee market developments and experiment and test new market rules and mechanisms. Market players need to understand how and when to participate in each market.

Due to the rising needs, several electricity market simulators have been developed, as can be consulted in [5, 121–124], which provide interesting reviews on electricity market simulators. In fact, a total of 2454 documents related to electricity market simulation can be found in the SCOPUS database, until the end of 2017. Such works start emerging slowing from 1981, and several peaks of interest in this theme are well highlighted throughout the years, as can be seen from Figure 7.

As can be seen from Figure 7, there has been a significant increase in the interest in research on electricity market simulation in the beginning of the millennium, with a huge increase in the number of documents published during these few years. In fact, the 10 most cited documents in this area all refer to the first decade of the 2000s, as depicted in Table 8. An overview of the most cited documents and top authors related to electricity market simulation is shown in Table 8. The tendency keeps on increasing from that point onwards, but there are several obvious peaks of interest, which are closely related to the most relevant changes in electricity market policies, as well as market model restructuring all around the globe.

Some relevant examples of electricity market simulators resulting from these works are [5, 122] the Simulator for Electric Power Industry Agents (SEPIA) [135], which is a Microsoft Windows-oriented platform; Power Web [136], a Web-based market simulator that allows participants to interact from very distinct zones of the globe; and The short-medium run electricity market simulator (SREMS) [137], which is based on game theory and is able to support scenario analysis in the short-medium term and to evaluate market power. These simulators present a common limitation, as they lack flexibility in order to deal with dynamic environments with complex interactions between the involved entities. Multiagent systems are computer systems composed of autonomous agents that interact to solve problems beyond the individual capabilities of each agent [138]. In the last decade, a number of multiagent electricity market simulators have emerged [124, 139].

An agent-based simulation model of the England and Wales electricity market is presented in [140]. The simulation model enables comparing alternative market mechanisms, including different settlement systems and bidding periods. The same model is applied to the German electricity market in [141]. The proposed simulation model defines agents through several attributes. Reinforcement learning is used to support agents' decisions. The analysis of alternative auction models is an important asset of this simulator; however, the complete functionalities of electricity markets are not modeled, and market participation is restricted to producers [142]. A wholesale market simulation model has also been developed by the MIT [143]. In this simulator, a static number of three generator agents use the derivative following strategy [144] to learn the best bids to apply in order to maximize the profits. The market model is very simple, with only generators being able to act dynamically. These agents can bid their complete generation capacity or just a part depending on the expected profits [145]. A simulated market model based on double auction is presented in [146, 147]. The market model matches consumers and generator bids pairwise [148]. The focus of this simulator is on the learning process of agents' bidding behavior, with the application of the Roth-Erev reinforcement learning algorithm [147] and genetic algorithms [146]. An electricity market simulation study that compares three alternative pricing methods in electricity market auctions is presented in [149]. Agents in this simulation model submit bids for the entire generation capacity, and they learn to bid mark-ups on top of their marginal costs. A model consisting in three sequential energy markets representing, namely, a gas market, a wholesale electricity market, and a retail electricity market, is presented in [150]. All these market models are modeled as uniform-price auctions, in which only supply agents submit their bids. The focus is on the study and analysis of the dynamics of reward interdependence in the different markets [151]. An electricity market simulation study directed to Nash equilibrium analysis is presented in [152]. Q-Learning is used to provide learning capabilities to the involved agents, considering a market pool considering transmission grid constraints. Social welfare implications are analyzed for several congestion management approaches. A multiagent simulation system to model the UK electricity market is introduced in [153]. This simulator includes several different pricing calculation schemes, and the focus of the study is on producer agents' learning behavior. The role of other relevant involved agents, such as consumers or the independent system operator (ISO), is, however, not considered. Additionally, the simulated market model represents the UK electricity market before its restructuring process of 2001; hence, this model is severely outdated.

The Genoa Artificial Power Exchange (GAPEX) [154] is an agent-based framework for modeling and simulating power exchanges. GAPEX is implemented in MATLAB and allows the creation of artificial power exchanges reproducing exact market clearing procedures of the most important European power exchanges [155]. The Electricity Market Complex Adaptive System (EMCAS) [156] uses an agent-based approach with agents' strategies based on learning and adaptation. Different agents are used to capture the restructured market heterogeneity, including generation, demand, transmission and distribution companies, independent system operators, consumers, and regulators. It allows undertaking electricity market simulations in a time continuum ranging from hours to decades, including several pool and bilateral contract markets [157, 158]. Agent-based modeling of electricity systems (AMES) [159] is an open-source computational laboratory for the experimental study of wholesale power markets restructured in accordance with US Federal Energy Regulatory Commission (FERC)'s market design. It uses an agent-based test bed strategically learning

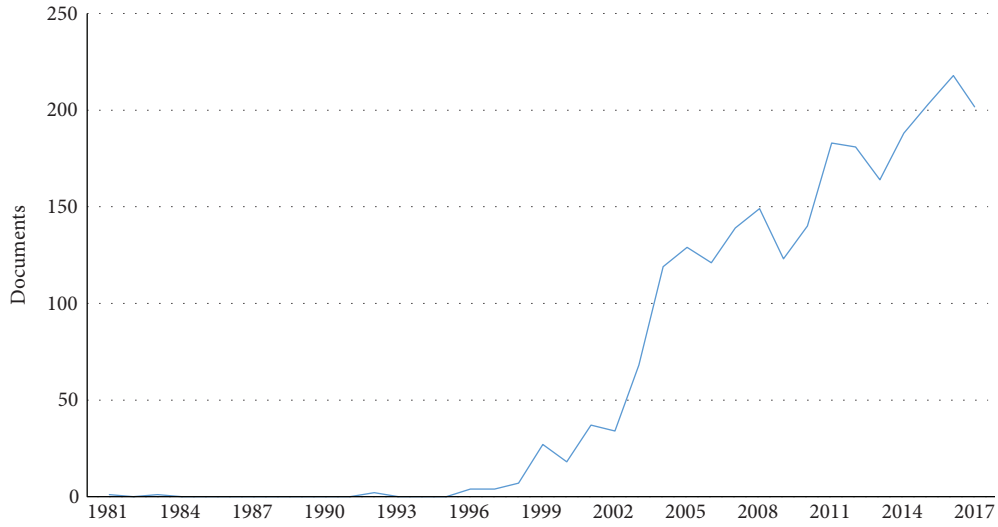

Figure 7: Documents related to electricity market simulation in the SCOPUS database until 2017.

Table 8: Overview of the most cited documents and top authors related to electricity market simulation.

Search term	Documents until 2017	10 most cited articles		Top 5 authors with most articles Author (number of articles)
		Reference	Citations	
Electricity market simulation	2447	[125]	881	Vale, Z. (79) Pinto, T. (59) Praça, I. (48) Morais, H. (43) Wen, F. (34)
		[126]	373	
		[127]	330	
		[128]	287	
		[129]	282	
		[130]	264	
		[131]	240	
		[132]	220	
		[133]	212	
		[134]	195	

electric power traders to experimentally test the extent to which commonly used seller market power and market efficiency measures are informative for restructured wholesale power markets. The wholesale power market includes an independent system operator, load-serving entities, and generation companies, distributed across the busses of the transmission grid. Each generation company agent uses stochastic reinforcement learning to update the action choice probabilities currently assigned to the supply offers in its action domain.

The Multiagent Simulator of Competitive Electricity Markets (MASCEM) is a simulator developed by the Polytechnic of Porto, Portugal [160, 161]. MASCEM supports the simulation of several market models, including the simulation of the market models of MIBEL (Iberian market), EPEX (central EU market), and Nord Pool (northern European market), as well as some other specific market models, for example, CAISO's. The network validation is also possible, although in a simplistic manner. Agents in MASCEM are endowed with machine learning and decision support capabilities through its integration with the Adaptive Decision Support for Electricity Markets Negotiations (AiD-EM) system [162]. The participation of DG, small consumers, DR, and EVs, among other resources, is enabled through the connection of MASCEM with the Multiagent Smart Grid Platform (MASGriP) [163]. The integration between the several systems is achieved through the use of ontologies to support the communications between the agents of the different systems. The National Electricity Market Simulation System (NEMSIM) is an agent-based electricity market simulator developed specifically for simulating Australia's electricity market. The agents considered in NEMSIM are electricity producers, network service providers, retailers, and the National Electricity Market Management Company (NEMMCO) [164]. The market models in NEMSIM include bidding and bilateral contracts. The technical constraints of the transmission network are considered, even if only in a superficial way. Negotiating agents have independent learning capabilities, based on the agents' specific goals. However, since NEMSIM is designed particularly for the Australian market, its model is too specific to be easily adapted to other market models. Another simulation model that follows the Australian market rules is presented in [165]. This model includes two bidding mechanisms, namely, stepwise and piecewise linear bidding. Simulations are restricted to a couple of generators in order to study the learning process of tacitly collusive strategies [166].

The short-term electricity market simulator-real time (STEMS-RT) has been developed by the Electric Power Research Institute (EPRI) [167, 168]. STEMS-RT models the market and accommodates both human participants and computer agents. Human and simulated agents represent buyers and sellers and are able to set up and submit their bids. Two autonomous biding strategies are available for suppliers, namely, a conservative approach, consisting in bidding all generations at the marginal cost. The second approach

tries to maximize the profit on a short-term basis [169]. STEMS-RT, however, does not include some important electricity market participants such as consumers, aggregators, or the ISO. Also, STEMS-RT is restricted to the bidding process in the pool market, and although it provides two autonomous bidding strategies, there is no actual learning process for agents' decision support. A two-settlement market composed by one forward market and one spot market is simulated in [170]. The agents present in this simulator are consumers, generators, transmission line provider agents, and the ISO. The focus of simulations is put on the decision-making of generators and the ISO. The problem is formulated as an equilibrium problem with equilibrium constraints. The strategy for representing the decision-making and solving it mathematically is similar to that of STEMS-RT. PowerACE is an agent-based simulation tool developed to study the CO_2 emission trading market [171]. PowerACE is composed by several types of agents, namely, producers, consumers, traders, long-term planners, market operators, certificate traders, load serving entities, and consumers. The market model includes a market for CO_2 emission allowance that complements the usual pool and bilateral markets. The capability of PowerACE investigating environmental issues (such as CO_2 emission) is an important asset in upcoming simulators or in the improvement of existing ones, as it can largely affect the long-term investment decisions of generation companies. A multiagent architecture for decision-making in decentralized electricity markets called EMMAS (Electricity Market Multiagent System) is presented in [172]. Agents are introduced as (i) basic (atomistic), which can be a consumer, generator, transmission system operator, distributor, market operator, wholesaler, retailer, or a regulator, and (ii) synthetic (combined), which are combinations of different basic agents. EMMAS agents are able to learn from past experiences or directly from the domain of expertise. Both the distribution and transport grids are modeled.

Electricity market simulation is an area that has been attracting a significant interest during the last years. Many of the existing simulators have been discontinued, while others have been adopted or purchased by governmental entities. Tracking of their recent developments has been proven to be a difficult task, as it is possible to observe by the publication year of many of the review works. Some further relevant works related to electricity market simulation can be consulted in [173], which presents an electricity market simulator for mainland Spain; [174] presents the Marketecture from Los Alamos National Laboratory; [175] details the N-ABLE™, the Agent-Based Laboratory for Economics developed at Sandia National Laboratory; and [176] presents some simulations for coupled systems using the GridWise™ system, at the Pacific Northwest National Laboratory. Table 9 provides a comparison of the main characteristics of the most relevant reviewed electricity market simulators.

From Table 9, it is visible that most of the existing simulators include some types of agent learning capabilities, although these are almost entirely exclusively directed to generation agents. Many of these simulators also consider grid constraints, making them suitable for simulation under operators' and regulators' perspective. However, the study of the integration of distributed renewable generation and integration of DR or even of aggregators in the market is still very poor. This deficiency makes most of these simulators still unable to provide a valuable support for the study of the evolution of the power system in accommodating the targeted large amounts of renewable generation and to incentivize the active participation from the consumers' side.

5.2. Microgrid and Smart Grid Simulation. One of the main achievements of the power and energy sector in recent years is the common acceptance by the involved stakeholders that power systems require major changes to accommodate in an efficient and secure way an intensive use of renewable-based DG [177]. The conclusion that the so-called smart grids are required is a crucial foundation for the work to be done in the coming years towards the modernization and restructuring of the power sector according to the new paradigms [20]. Huge investments have already been made in projects concerning smart grids, including research and development projects, pilot installations, and rollout of smart metering. A list of a total of 950 projects related to smart grids starting from 2002 up until today, amounting to €5 billion investment, is published in [178]. The domains with the highest investment are smart network management, demand-side management, and integration of DG and storage, together accounting for around 80% of the total investment. The large number of smart grid-related projects is resulting in important advances in the field, namely, concerning demonstration pilots and management and control methodologies.

The European Technologic Platform Smart Grids (ETPSG) for future electric networks is the main European forum for the establishment of R&D policies for the intelligent electricity grid sector [179]. The mission of ETPSG is (i) to create and maintain a shared sight for the future of electricity networks in Europe and serve as a catalyzer for their implementation and (ii) promote research, development, demonstration, and implementation projects related to intelligent electricity networks [120].

Under the ETPSG and due to the increase in funding from the EU in this field, several large-scale European projects have been providing a substantial contribution to deal with some of the most prominent issues in the field, as discussed in [120]. The e-Highway2050 project aims at developing and applying a methodology for the long-term development of the pan-European transmission network, with the objective of guaranteeing a reliable power delivery from renewable sources, and their integration in the pan-European market. This project adopts a top-down methodology to support the planning from 2020 to 2050. In this context, the output of this work should potentiate the idealization of a possible super European power network, which interconnects the large part of European countries. IRENE-40 is a European project that aims at providing an Infrastructure Roadmap for Energy Networks in Europe. The objectives of IRENE-40 are to identify strategies for investors and regulators to build a more secure, ecologically sustainable, and competitive European electricity system, which are presented in a roadmap, that is, a timeline with actions

Table 9: Comparison of the main characteristics of some of the most relevant electricity market simulators.

Work	Demand response	Distributed generation	Aggregators	Grid constraints	Agent learning	Market details	Other
[141]	+				++	Study of alternative market models; impact on German electricity market	
[143]		+			++		
[146]	++				+	Double auction	
[147]					++		Comparison of bidding strategies
[149]					++	Comparison of alternative market mechanisms	
[150]		++	++		+	Wholesale, retail, and natural gas markets	
[152]		+		++	++	Congestion management	
[153]		++			++	Models the old UK electricity market	
[154]			+		+	Models GME—the Italian electricity market	
[156]				++	++	Realistic modeling of the Australian electricity market	
[159]	+	++		++	++	Models the US MISO, ISO-NE, NYISO, PJMB, CAISO, SPP, and ERCOT market areas	
[160]		+	++	+	++	Market models of MIBEL, EPEX, and Nord pool	Demand response, electric vehicles, and distributed generation are modeled through the connection to the MASGriP simulator
[164]				+	+	Models the Australia National Electricity Market (NEM)	
[165]					++		Analysis of collusive strategies
[167]		+				Day-ahead auction-based market	
[170]	+	+		++	+	Spot market and forward market	
[171]					++	Balancing market	
[172]			+	+	+	Day-ahead simple auction and with uniform price	

and a description of development stages towards future electricity networks over the coming 40 years.

WILMAR (Wind Power Integration in Liberalised Electricity Markets) has focused on the study of the impact of large-scale penetration of wind-based generation and its accommodation in EM, while TRADEWIND—Wind Power Integration and Exchange in the Trans-European Power Market—led by EWEA (European Wind Energy Association) aims at facilitating the dismantling of barriers for the large-scale integration of wind energy in European power systems, on transnational and European levels, and to formulate recommendations for policy development, market rules, and interconnector allocation methods to support wind power integration. TRADEWIND explores the benefits that a European grid with better interconnections and an improved power market design can have on the integration of large amounts of wind power. EWIS—European Wind Integration Study—towards a successful integration of large-scale wind power into European electricity grids provided a market model that represents the idealized operation of existing day-ahead markets respecting declared cross-border transfer capabilities. It simulated daily actions of transmission system operators (TSOs) to redispatch generation to meet actual network physical limits and respond to emerging information concerning demand, wind output, and other generation changes [120].

IDE4L focuses on providing flexibility services and distributed control for aggregators. The role of the distribution system operator is the core entity of this project, addressing several distinct market models. PV-Prosumers4Grid is studying novel self-consumption and aggregation models for prosumers, with the aim of supporting large-scale PV integration in the system. EU-SysFlex aims at achieving an efficient coordinated use of flexibility to enable the wide spread of renewable generation. This requires defining the right amount of flexibility and system services to support transmission system operators. iDistributedPV is developing affordable solutions to increase the penetration of distributed solar PV based on the effective integration of solar PV equipment, including the exploration of several related concepts

and approaches. The main goal is to enhance the role of the prosumer.

The significant work being developed in the scope of the multiple projects in the field is resulting in several relevant works in the domain of smart grid and microgrid simulation. In fact, an astonishing number of 15,723 documents are found in the SCOPUS database when searching for Microgrid OR Smart Grid OR Energy Systems Simulation, until the end of 2017. Most of these works have been published in the last decade, as can be seen by Figure 8.

As Figure 8 shows, although these topics have been briefly mentioned for more than 50 years, the interest in microgrid and smart grid simulation has just boosted in the last decade, following the large increase of investment in smart grids, and the worldwide definition of ambitious targets for renewable generation integration in the system, which requires the exploration of approaches such as the smart grid and microgrid, and their simulation. Table 10 shows the details on the most cited articles and most relevant authors in this domain.

As Table 10 shows, a significant number of documents related to microgrid and smart grid simulation can be easily found. A document discussing the requirements of smart grid simulation tools, including grid constraints, markets, legislation, communication infrastructure, regulation, and legislation, can be consulted in [190], paving the path for development ways of future simulators. Also, a relevant list of smart grid simulation tools can be consulted in [191]. In many of these works, a multiagent approach is commonly applied. Many of the advantages of using multiagent systems in the energy system are discussed in [124]. These advantages are mainly related to the large-scale accommodation of renewable energy sources. The distributed architecture is one of the emphasized advantages, due to the distributed nature of renewable energy sources and their need for local decisions and information. The flexibility is another core asset, since a multiagent system can easily accommodate new agents and exclude agents (both software and physical resources) without compromising the simulated system. This is closely related to the resiliency of the system, as a distributed approach usually has a better response to changes and failure in the network, thus helping to improve its stability and efficiency [192].

In [193], three main types of approaches for smart grid and microgrid simulation using multiagent systems are identified, namely, centralized, distributed, and hierarchical approached. The centralized approach refers to the collection of homogeneous agents that are managed by centralized control and management agents. These two types of agents are described in [194] as reactive and cognitive, respectively. Reactive agents only respond to requests with their standard actions, and cognitive agents incorporate enhanced management and/or control capabilities. Another relevant work considering a centralized approach for agent-based control of microgrids is [195].

In a distributed approach, each agent detains the knowledge about his share of the system, and they interact with each other in order to coordinate and manage the operations in a distributed way, as well as to cooperate and share services that respecifies to each agent. A distributed system for self-organization of generation sources, consumption, and storage is proposed in [196]. The simulation of a test microgrid with DG, consumers, and storage is used in [197] to demonstrate the advantages of a distributed control using multiagent systems.

An hierarchical model considers the authority of some agents over others [198]. This approach requires classifying each individual agent as being of a certain type, which facilitates the definition of agents' roles and also improves the scalability and robustness of real-time operational control [199]. The work presented in [200] proposes a three-level agent-based hierarchical approach for distributed power flow control. A simulation model based on a two-level hierarchical approach is presented in [201] to enable distributed microgrid control. The upper level comprises the central controller, which coordinates and manages the information from the network perspective. The bottom layer includes microsource controllers and load controllers, which perform their control and management locally. Market participation is also included in [202]. Agents in the higher levels are responsible for the decision-making regarding the complex tasks, while the lower-level agents are accommodated to simpler tasks. Some other applications of hierarchal agent-based systems for smart grid and microgrid simulation are discussed in [203–209].

A decentralized approach for the management of storage devices is proposed in [210]. An agent-based simulation infrastructure is used to support negotiations in order to optimize the operation of storage units in a decentralized manner. Another market-driven simulation system for storage device management and operation is introduced in [211]. This problem is defined as a multiplayer game, and the Nash equilibrium is used to minimize the energy cost by reducing the peak demand. Energy transaction patterns are analyzed through agent-based simulation in [212]. The load scheduling is addressed using genetic algorithms and considering the consumer comfort. The integration of renewable based generation in the electricity market is explored through simulation in [213]. This work explores potential business models considering the alternative models of DR for buildings. The market-based control of imbalances using a multiagent simulator is addressed by [214]. This simulator includes the control of different units and combines DR and several distributed energy sources.

An agent-based simulation approach for microgrid control is presented in [215], focusing on the distribution grid control decisions. The interaction between multiple microgrids is simulated and studied in [216]. This simulation model enables studying the coordinated control of multiple integrated microgrids, as well as incorporating relevant aspects such as reserve regulation. The simulation model presented in [217] focuses on large-scale modeling of transportation assets in smart grids. Namely, the simulator addresses the demand management of EVs through the simulation of the power grid and transport.

A simulation system for different types of consumers and their behavior in a smart grid setting is presented in [218]. This simulation system enables consumer agents to define

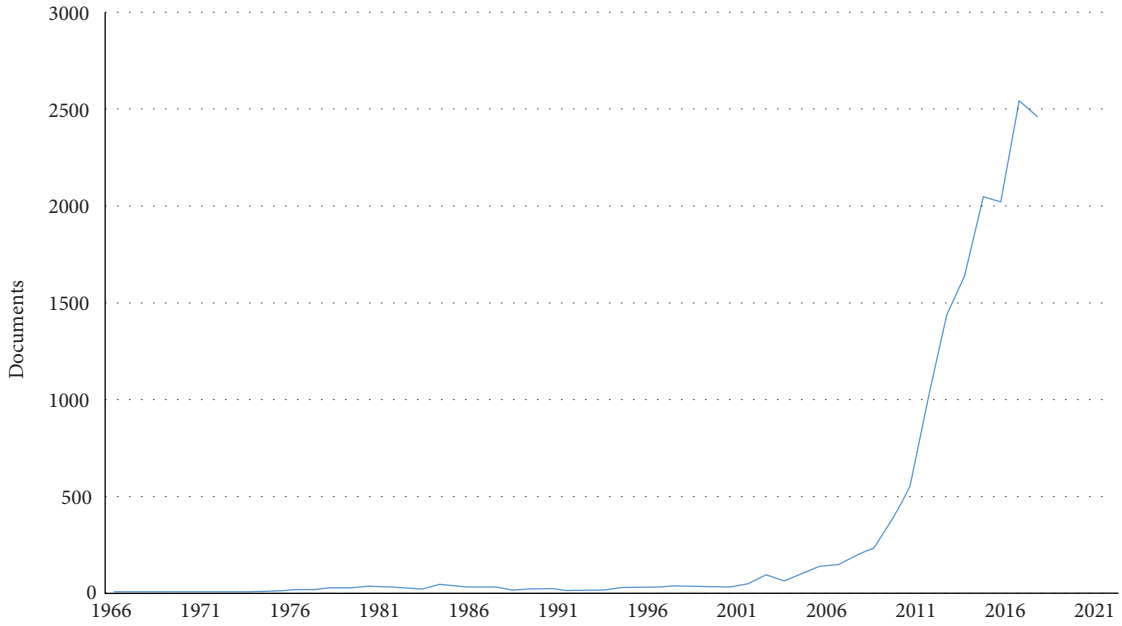

Figure 8: Documents related to microgrid, smart grid, and energy systems simulation in the SCOPUS database until 2017.

Table 10: Overview of the most cited documents and top authors related to microgrid and smart grid simulation.

Search term	Documents until 2017	3 most cited articles		Top 5 authors with most articles
		Reference	Citations	Author (number of articles)
Smart grid simulation	5781	[33]	1110	Vale, Z. (38); Li, H. (37); Javaid, N. (36); Senjyu, T. (31); Han, Z. (28);
		[180]	475	
		[181]	472	
Microgrid simulation	4929	[182]	936	Guerrero, J.M. (141); Vasquez, J.C. (61); Li, P. (55); Wang, C. (41); Ghosh, A. (39);
		[183]	870	
		[184]	668	
Energy systems simulation	5808	[185]	667	Senjyu, T. (20); Streblow, R. (20); Anon (19); Müller, D. (19); Lehnhoff, S. (16);
		[186]	586	
		[187]	471	
Power systems simulation	59,305	[188]	1657	Senjyu, T. (152); Sun, Y. (131); Blaabjerg, F. (123); Malik, O.P. (121); Wen, J. (121);
		[189]	1483	
		[182]	936	

their actions at each time, deciding among use of local generation, reduction of their consumption, trade of energy with utilities or their neighbors, and use of their batteries.

An agent-based simulation system for local energy systems named energy cultures is presented in [219]. The multiagent model integrates several types of agents, which are represented by aggregators in the wholesale market. This simulator has been used in the CASCADE project to address different issues, all related to the future role of the aggregator in future power and energy systems [220].

A flexible large-scale agent-based simulation tool for smart grids is presented in [221]. This simulator, named GridLAB-D, is open-source and considers different smart grid resources such as DR, storage, EVs, and the retail market. The flexibility of the simulator enables it to be used to study multiple questions in the field, related to energy trading, flexibility, management, and operation of smart grids.

The Multiagent Smart Grid Platform (MASGriP) is a large-scale simulator of microgrids and smart grids [163] that combines agent-based simulation with real-time simulation and physical emulation. This simulator can be used as a stand-alone application, using the agent-based system to simulate different types of smart grid players and management, operation, and interaction models, or it can be used in a physical setting to control a microgrid in real time, combining real resources with simulated players and assets. This simulator is connected to the MASCEM electricity market simulator [160], which enables combining the smart grid operation with market simulation.

A smart grid simulator that uses the AnyLogic simulation environment is presented in [222]. This simulator models

local energy communities considering buildings with self-generation and storage devices. Different configurations are allowed in order to enable the study of a multiplicity of issues in the smart grid domain. The simulator introduced in [223] uses the HLA architecture to simulate multiple environments, among which is the smart grid. The proposed architecture connects different ICT components and applies it to power systems modeling. Additionally, the proposed architecture is integrated with models in Simulink, Omnet++, and JADE to enhance the modeling of smart grid applications.

The large-scale simulation of smart grids using Modelica is addressed in [224]. This object-oriented equation-based modeling tool enables increasing the flexibility, efficiency, and scalability of simulation frameworks. This work suggests that using such an approach may prove to be a relevant step forward in the simulation of large-scale systems such as the smart grid. The work presented in [225], in turn, applies the Discrete Event System Specification (DEVS) formalism for modeling and simulation of the smart grid. The proposed approach considers several distinct smart grid resources and shows that such a model enables specifying components as well as developing event-driven simulations.

The work presented in [226] proposes a cosimulation framework of the smart grid including the modeling of the power and communication networks. In [227], the same cosimulation subject is addressed, but this time focused on enabling direct load control in the smart grid. Issues such as the data volume, timing questions, and reliability issues are addressed. The PSS SINCAL and OPNET simulators are combined to enable the real application of the proposed simulation model in a German distribution network.

The large number of works related to microgrid and smart grid simulation leads to a rather vast and complementary simulation focus in this field. Table 11 presents a comparison of the main top-level characteristics of some of the most relevant simulators discussed in this paper.

As can be seen from Table 11, the main focus of microgrid and smart grid simulators is the study of the integration of renewable energy generation in the system. Grid modeling is almost always available, and DR is also being increasingly addressed by most recent works. On the other hand, the simulation study of EVs, the role of the aggregator, and the market interaction with the local grid are issues that, although addressed by some simulators, still lack a significant wide spread in terms of simulation modeling. The modeling and simulation of agent learning capabilities is still very poor in this domain, contrarily to what can be seen from the field of electricity market simulation. It is a fact that most of the least explored areas that are discussed here are addressed in dedicated works, which does not mean these areas are not being addressed. However, their integration in complete simulation frameworks is still showing to be taking its first steps.

6. Final Remarks and Future Research Directions

This survey analyzed recent research (mostly from 2010) on complex optimization and in the new paradigm of power systems and the smart grid era. The main focus is centered on (i) the optimization of power systems under the new smart grid context, (ii) the discussion and analysis of the application of computational intelligence approaches as means to solve the complex optimization problems, and (iii) the analysis of large-scale simulation of electricity markets and smart grid.

It started with a preliminary section with a brief explanation of basic concepts in the new power systems paradigm. After that is an overview of research work to tackle challenges brought by the smart grid technologies. Then, it focused on research related to energy resource management due to its particularly complex case in this field. This study realized that smart grid optimization is starting to adopt methods to tackle sources of uncertainty in the mathematical models. However, it is found that most of the work relies on traditional approaches and lacks ability to scale to real systems (due to limited computer resources with the adopted approaches). As a consequence, they are also limited in covering all sources of uncertainty and considering different problem horizons.

The survey also analyzed CI due to its large potential to tackle the challenges introduced early in this survey related to smart grid optimization. In fact, CI encompasses some of the most existing paradigms of computer sciences. Among them, EC is one of the most prominent paradigms, with some very mature algorithms applied to a wide variety of complex optimization problems. In the energy domain, hybrid techniques that make use of the three main paradigms of CI (i.e., EC, ANN, and FS) are currently used as a tool to model and solve some of the arising issues in power systems. The evolution of complex energy systems is pushing into the limits on the application of the most accepted exact solutions, which in some cases are not suitable to deal with these new complex scenarios. It is in this context that motivates the use of CI as an efficient tool to deal with this challenging scenario. However, despite the successful applications of CI in a wide variety of problems, the portfolio of algorithms belonging to CI has the drawback of being unable of guaranteeing optimal solutions. The use of additional resources, such as supercomputers or parallelism, open a window to refine the application of CI, and it is expected that in the near future, CI solutions will be sufficiently mature to be adopted as the preferred solutions to power systems.

Due to its importance to the new paradigm of power systems, we analyzed electricity market simulators, which together with smart grid optimization are also a complex case of power systems studies. We realized in this study that those simulators are valuable but still limited solutions, as they are usually directed to specific market environments and present limitations in coping with the interaction with external systems. This hardens the possibility for cosimulation of distinct and complementary environments, such as the coexistence and simultaneous participation of players in multiple electricity markets. Most of the existing simulators include some agent learning capabilities, although these are almost entirely exclusively directed to generation agents. Many of these simulators also consider grid constraints, making them suitable for simulation under operators' and regulators' perspective.

Table 11: Comparison of the main characteristics of some of the most relevant microgrid and smart grid simulators.

Work	Demand response	Distributed generation	Electric vehicles	Aggregators	Market participation	Grid modeling	Agent learning	Other
[163]	++	++	+	++	++	+	+	Real-time simulation and emulation
[210]		++				++		Storage
[211]	++	++				+	+	Microstorage and reserve regulation
[213]	++			++				
[214]	++	++			++			Reduction of local imbalances
[215]		++				++	+	
[218]	++				++			P2P trading
[221]	++	++		+		++		
[222]	+	++			+			Transactions with neighbors
[223]	+	++		+		++		Ontologies for domain knowledge
[224]		++				++		Physical modeling of smart grid components
[225]		++				+	+	
[226]	+	+				++		Co-simulation with communication network
[227]	++	++				++		Co-simulation with communication network

However, the study of the integration of distributed renewable generation, integration of DR, of electric vehicles, or even of aggregators in the market, is still very poor. This deficiency makes most of these simulators still unable to provide a valuable support for the study of the evolution of the power system in accommodating the targeted large amounts of renewable generation and to incentivize the active participation from the consumers' side.

Effective solutions should rapidly appear, so that current and alternative market models can be easily simulated and assessed using realistic models regarding not only electricity markets but also the present and future penetration of diverse types of energy resources. The main problems of the field such as the massive integration of renewable energy sources in electricity markets, the inadequate models to support the active participation of consumers, and the consequent need for modeling alternative and innovative market models that enable accommodating new types of players, remain, therefore, unaddressed.

On the other hand, the quick emergence of the process of smart grids is showing not to be entirely free of problems. A large number of practical applications, although very expensive, are enabling solutions that present serious limitations and provide little return of investment. It is not clear that the rolled-out equipment is sufficiently open and flexible to be useful for the next generation of smart grid solutions that should appear in the coming years. Additionally, although important contributions are being achieved, these still remain as solutions for partial problems. In highly dynamic and codependent areas, such as power networks, smart grids, and electricity markets, the cooperation between different systems becomes essential in order to look at the global problem as a whole. Most of the smart grid-related works consist in practical implementations, highly industry driven, and involving almost exclusively large stakeholders in the field, such as regulators, operators, and utilities, resulting in an almost complete focus on achieving fast ways to overcome present problems. This is, however, leading to an absence of pure research exploitation in the field, which is essential to reaching innovative findings to enable the scientific breakthrough that is required to provide advanced solutions, not only to the current and most prominent problems that are arising but also to future issues that are inevitable.

The focus of current microgrid and smart grid simulators can be said to be quite diversified. The study of the integration of renewable energy generation in the system is the main addressed question, while grid modeling is usually addressed, and DR begins to be considered in large scale. On the other hand, relevant issues such as the simulation of electric vehicles, aggregator models, and the interaction with the market are still not sufficiently addressed by current large-scale simulators. Additionally, most simulation approaches are based on multiagent systems. Although this paradigm is showing to be suitable for the task, it still presents several limitations, as identified in [193]. The emergent or unexpected behavior from autonomous agents in dynamic environments is one of the main sources of uncertainty, as the same level of behavior cannot be guaranteed under different settings, scenarios, and contexts. The portability of agents is another issue, which relates to agents' physical integration. Although many advances have been accomplished in recent years, issues with standardization and difficulties of communication with different types of devices and resources are still proving to be an arduous challenge to overcome. The scalability is another

Table 12: Number of citations and *h-index* for selected countries ranked by total number of citations between 2010 and 2016 for the same search term.

Affiliation country	Number of citations								*h-index*
	2010	2011	2012	2013	2014	2015	2016	Total	
United States	13	35	275	543	781	1232	1539	4481	35
China	5	31	208	439	610	762	1094	3214	31
Canada	48	22	260	390	521	685	941	2976	22
Italy	0	27	72	176	329	497	663	1756	27
Spain	4	22	111	196	348	452	600	1756	22
South Korea	1	21	142	219	296	426	552	1686	21
France	5	18	61	154	190	313	415	1164	18
Portugal	6	22	51	110	161	290	406	1038	22
United Kingdom	0	20	62	128	152	240	330	931	20
Germany	9	16	40	76	133	236	283	799	16
India	0	13	23	48	81	116	246	523	13
Japan	0	12	40	58	67	132	180	488	12

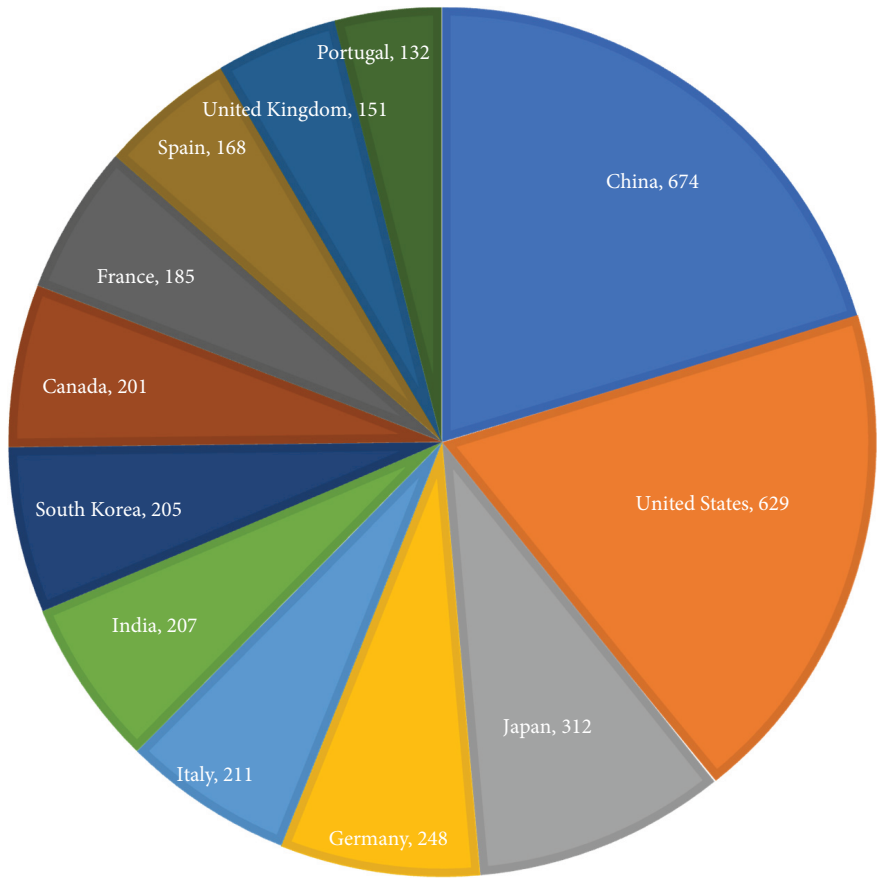

Figure 9: Documents produced between 2010 and 2016 by affiliation country (top 12) for search term ("energy resource management" OR "energy management system") in the SCOPUS database.

important aspect in large-scale simulation. There are multiple approaches devoted to guaranteeing the scalability of the simulation environment; however, these are still always dependent on the processing machines when it comes to increasing the number of agents and integrated smart grids or microgrids. Finally, the security component is another important limitation when considering the real application of agent-based systems or their simulation using real data. Security in communications, data storage, and management still need to be highly improved and standardized so as to

Table 13: Citations per paper and number of documents by country (ranked by citations per paper) for the same search term, 2010–2016.

Affiliation country	Citations per paper	Number of documents produced	Position if ranked by number of documents
Canada	14.8	201	8
Spain	10.5	168	10
Italy	8.3	211	5
South Korea	8.2	205	7
Portugal	7.9	132	12
United States	7.1	629	2
France	6.3	185	9
United Kingdom	6.2	151	11
China	4.8	674	1
Germany	3.2	248	4
India	2.5	207	6
Japan	1.6	312	3

enable the wide-scale application of agent-based simulators in real environments.

Appendix

Statistic of recent research in the scope of energy resource management

Additional information is given in this appendix regarding statistics of recent research in scope of energy resource management. Figure 8 shows the number of documents produced between 2010 and 2016 by affiliation country (top 12) for the search term "energy resource management" OR "energy management system" in the SCOPUS database. China-affiliated researchers lead the number of documents produced so far with 674 documents, which combined with United States, Japan, and Germany represent more than 50% of the documents produced in this research field. Portugal appears in the 12th position of this list (6th European country) with 132 research documents.

For the same search term, we also investigated the research impact of the documents produced in this field, that is, number of citations and citations per paper, which can be interpreted as quality indicator. Table 12 shows the total number of citations by country (the same as appears in Figure 9), and Table 13 shows the citations per paper for the same countries. It can be seen that United States, China, and Canada are the research affiliations with the highest impact translated by the total number of citations between 2010 and 2016 (51% of top 12 global citations). It is interesting to remark that in spite of Japan ranking third in the total number of documents (312, see Figure 9), the total number of citations of those documents is only 488, which puts Japan as the last in this list regarding the total number of citations, with 1.6 citations per paper (see Table 13). Data suggests that Canada and Spain perform quite well in the research impact for the advances in the energy resource management, figuring with 14.8 and 10.5 citations per paper, respectively, which are significantly apart from the other countries in this list. Portugal also presents very interesting impact results ranking 5th in the citations per paper list, in spite of being in the 12th position when ranked by number of documents (see Table 13). Portugal is ahead of United Kingdom and Germany, India, and Japan when seen by for the total citations (see Table 12). This data is accurate on how research affiliations have performed in the past, namely, between 2010 and 2016, and according to SCOPUS database. But we understand that highly cited articles related to the search term of energy resource management, such as [11] (Canada), [33] (Canada and USA), and [1] (Italy), contribute to improve the country affiliation rank.

Conflicts of Interest

The authors declare that they have no conflicts of interest.

Acknowledgments

The present work has been developed in part under the EUREKA-ITEA2 Project M2MGrids (ITEA-13011) and Project SIMOCE (ANI|P2020 17690) and has received funding from FEDER funds through COMPETE program and from national funds through Fundação para a Ciência e a Tecnologia under the project UID/EEA/00760/2013. In addition, it was supported in part by Grant agreement no. 703689 (project ADAPT). Additionally, this work has profited from ideas from the proposal of the recently funded project with ref. 02/SAICT/2017/28983 from CENERGETIC. This work has been also partially supported by Consejo Nacional de Ciencia y Tecnologia (CONACYT), Mexico.

References

[1] P. Siano, "Demand response and smart grids—a survey," *Renewable and Sustainable Energy Reviews*, vol. 30, pp. 461–478, 2014.

[2] EC, European Commission, *2030 Framework for Climate and Energy Policies*, European Commission, 2014.

[3] X. Zhang, M. Shahidehpour, A. Alabdulwahab, and A. Abusorrah, "Hourly electricity demand response in the stochastic day-ahead scheduling of coordinated electricity and natural gas networks," *IEEE Transactions on Power Systems*, vol. 31, no. 1, pp. 592–601, 2016.

[4] M. S. Hossain, N. A. Madlool, N. A. Rahim, J. Selvaraj, A. K. Pandey, and A. F. Khan, "Role of smart grid in renewable energy: an overview," *Renewable and Sustainable Energy Reviews*, vol. 60, pp. 1168–1184, 2016.

[5] A. Weidlich and D. Veit, "A critical survey of agent-based wholesale electricity market models," *Energy Economics*, vol. 30, no. 4, pp. 1728–1759, 2008.

[6] K. M. Tan, V. K. Ramachandaramurthy, and J. Y. Yong, "Integration of electric vehicles in smart grid: a review on vehicle to grid technologies and optimization techniques," *Renewable and Sustainable Energy Reviews*, vol. 53, pp. 720–732, 2016.

[7] P. Faria, J. Spinola, and Z. Vale, "Aggregation and remuneration of electricity consumers and producers for the definition of demand response programs," *IEEE Transactions on Industrial Informatics*, vol. 12, no. 3, pp. 952–961, 2016.

[8] D. Pinheiro Neto, E. G. Domingues, A. P. Coimbra, A. T. de Almeida, A. J. Alves, and W. P. Calixto, "Portfolio optimization of renewable energy assets: hydro, wind, and photovoltaic energy in the regulated market in Brazil," *Energy Economics*, vol. 64, pp. 238–250, 2017.

[9] B. Zhou, W. Li, K. W. Chan et al., "Smart home energy management systems: concept, configurations, and scheduling strategies," *Renewable and Sustainable Energy Reviews*, vol. 61, pp. 30–40, 2016.

[10] European commisssion, *Accelerating Clean Energy in Buildings*, European Commission, 2016.

[11] H. Farhangi, "The path of the smart grid," *IEEE Power and Energy Magazine*, vol. 8, no. 1, pp. 18–28, 2010.

[12] T. Strasser, F. Andrén, J. Kathan et al., "A review of architectures and concepts for intelligence in future electric energy systems," *IEEE Transactions on Industrial Electronics*, vol. 62, no. 4, pp. 2424–2438, 2015.

[13] M. Iqbal, M. Azam, M. Naeem, A. S. Khwaja, and A. Anpalagan, "Optimization classification, algorithms and tools for renewable energy: a review," *Renewable and Sustainable Energy Reviews*, vol. 39, pp. 640–654, 2014.

[14] S. Oren, "Renewable energy integration and the impact of carbon regulation on the electric grid," in *2012 IEEE Power and Energy Society General Meeting*, San Diego, CA, USA, July 2012.

[15] H. Abdi, S. D. Beigvand, and M. L. Scala, "A review of optimal power flow studies applied to smart grids and microgrids," *Renewable and Sustainable Energy Reviews*, vol. 71, pp. 742–766, 2017.

[16] N. Soares, J. Bastos, L. D. Pereira et al., "A review on current advances in the energy and environmental performance of buildings towards a more sustainable built environment," *Renewable and Sustainable Energy Reviews*, vol. 77, pp. 845–860, 2017.

[17] European Commission, *EU Energy, Transport and GHG Emissions Trends to 2050: Reference Scenario 2016*, European Commission, Luxembourg, 2016.

[18] V. Foster and D. Bedrosyan, *Understanding CO2 Emissions from the Global Energy Sector*, World Bank, Washington, DC, USA, 2014.

[19] N. B. Arias, J. F. Franco, M. Lavorato, and R. Romero, "Metaheuristic optimization algorithms for the optimal coordination of plug-in electric vehicle charging in distribution systems with distributed generation," *Electric Power Systems Research*, vol. 142, pp. 351–361, 2017.

[20] I. Colak, S. Sagiroglu, G. Fulli, M. Yesilbudak, and C. F. Covrig, "A survey on the critical issues in smart grid technologies," *Renewable and Sustainable Energy Reviews*, vol. 54, pp. 396–405, 2016.

[21] H. Liang and W. Zhuang, "Stochastic modeling and optimization in a microgrid: a survey," *Energies*, vol. 7, no. 4, pp. 2027–2050, 2014.

[22] S. Y. Abujarad, M. W. Mustafa, and J. J. Jamian, "Recent approaches of unit commitment in the presence of intermittent renewable energy resources: a review," *Renewable and Sustainable Energy Reviews*, vol. 70, pp. 215–223, 2017.

[23] M. De Lara, P. Carpentier, J. Chancelier, and V. Leclère, "Optimization methods for the smart grid," *Report Commissioned by the Conseil Français de l'Energie*, Ecole des Ponts ParisTech, 2016.

[24] Elsevier, "Scopus database," July 2018, https://www.scopus.com/.

[25] B. Dunn, H. Kamath, and J. M. Tarascon, "Electrical energy storage for the grid: a battery of choices," *Science*, vol. 334, no. 6058, pp. 928–935, 2011.

[26] J. M. Guerrero, J. C. Vasquez, J. Matas, L. G. De Vicuña, and M. Castilla, "Hierarchical control of droop-controlled AC and DC microgrids - a general approach toward standardization," *IEEE Transactions on Industrial Electronics*, vol. 58, no. 1, pp. 158–172, 2011.

[27] J. Cabana, L. Monconduit, D. Larcher, and M. R. Palacín, "Beyond intercalation-based li-ion batteries: the state of the art and challenges of electrode materials reacting through conversion reactions (Adv. Mater. 35/2010)," *Advanced Materials*, vol. 22, no. 35, 2010.

[28] F. Blaabjerg, R. Teodorescu, M. Liserre, and A. V. Timbus, "Overview of control and grid synchronization for distributed power generation systems," *IEEE Transactions on Industrial Electronics*, vol. 53, no. 5, pp. 1398–1409, 2006.

[29] J. M. Carrasco, L. G. Franquelo, J. T. Bialasiewicz et al., "Power-electronic systems for the grid integration of renewable energy sources: a survey," *IEEE Transactions on Industrial Electronics*, vol. 53, no. 4, pp. 1002–1016, 2006.

[30] A. Ipakchi and F. Albuyeh, "Grid of the future," *IEEE Power and Energy Magazine*, vol. 7, no. 2, pp. 52–62, 2009.

[31] N. Kamaya, K. Homma, Y. Yamakawa et al., "A lithium superionic conductor," *Nature Materials*, vol. 10, no. 9, pp. 682–686, 2011.

[32] M. Skyllas-Kazacos, M. H. Chakrabarti, S. A. Hajimolana, F. S. Mjalli, and M. Saleem, "Progress in flow battery research and development," *Journal of the Electrochemical Society*, vol. 158, no. 8, p. R55, 2011.

[33] A. H. Mohsenian-Rad, V. W. S. Wong, J. Jatskevich, R. Schober, and A. Leon-Garcia, "Autonomous demand-side management based on game-theoretic energy consumption scheduling for the future smart grid," *IEEE Transactions on Smart Grid*, vol. 1, no. 3, pp. 320–331, 2010.

[34] P. Palensky and D. Dietrich, "Demand side management: demand response, intelligent energy systems, and smart loads," *IEEE Transactions on Industrial Informatics*, vol. 7, no. 3, pp. 381–388, 2011.

[35] F. Cheng and J. Chen, "Metal–air batteries: from oxygen reduction electrochemistry to cathode catalysts," *Chemical Society Reviews*, vol. 41, no. 6, pp. 2172–2192, 2012.

[36] V. C. Güngör, D. Sahin, T. Kocak et al., "Smart grid technologies: communication technologies and standards," *IEEE Transactions on Industrial Informatics*, vol. 7, no. 4, pp. 529–539, 2011.

[37] L. Lu, X. Han, J. Li, J. Hua, and M. Ouyang, "A review on the key issues for lithium-ion battery management in electric vehicles," *Journal of Power Sources*, vol. 226, pp. 272–288, 2013.

[38] J. Soares, M. A. F. Ghazvini, N. Borges, and Z. Vale, "Dynamic electricity pricing for electric vehicles using stochastic programming," *Energy*, vol. 122, pp. 111–127, 2017.

[39] C. M. Flath, J. P. Ilg, S. Gottwalt, H. Schmeck, and C. Weinhardt, "Improving electric vehicle charging

coordination through area pricing," *Transportation Science*, vol. 48, no. 4, pp. 619–634, 2014.

[40] R. C. Green II, L. Wang, and M. Alam, "The impact of plug-in hybrid electric vehicles on distribution networks: a review and outlook," *Renewable and Sustainable Energy Reviews*, vol. 15, no. 1, pp. 544–553, 2011.

[41] J. Soares, H. Morais, T. Sousa, Z. Vale, and P. Faria, "Day-ahead resource scheduling including demand response for electric vehicles," *IEEE Transactions on Smart Grid*, vol. 4, no. 1, pp. 596–605, 2013.

[42] J. Soares, M. A. Fotouhi Ghazvini, M. Silva, and Z. Vale, "Multi-dimensional signaling method for population-based metaheuristics: solving the large-scale scheduling problem in smart grids," *Swarm and Evolutionary Computation*, vol. 29, pp. 13–32, 2016.

[43] A. Mahor, V. Prasad, and S. Rangnekar, "Economic dispatch using particle swarm optimization: a review," *Renewable and Sustainable Energy Reviews*, vol. 13, no. 8, pp. 2134–2141, 2009.

[44] D. T. Ton and W.-T. P. Wang, "A more resilient grid: the U.S. Department of Energy joins with stakeholders in an R&D plan," *IEEE Power and Energy Magazine*, vol. 13, no. 3, pp. 26–34, 2015.

[45] J. Soares, M. A. Fotouhi Ghazvini, N. Borges, and Z. Vale, "A stochastic model for energy resources management considering demand response in smart grids," *Electric Power Systems Research*, vol. 143, pp. 599–610, 2017.

[46] J. Soares, B. Canizes, M. A. F. Ghazvini, Z. Vale, and G. K. Venayagamoorthy, "Two-stage stochastic model using benders' decomposition for large-scale energy resource management in smart grids," *IEEE Transactions on Industry Applications*, vol. 53, no. 6, pp. 5905–5914, 2017.

[47] J. Soares, N. Borges, Z. Vale, and P. B. Oliveira, "Enhanced multi-objective energy optimization by a signaling method," *Energies*, vol. 9, no. 10, p. 807, 2016.

[48] A. Gazafroudi, F. Prieto-Castrillo, T. Pinto, J. Prieto, J. Corchado, and J. Bajo, "Energy flexibility management based on predictive dispatch model of domestic energy management system," *Energies*, vol. 10, no. 9, 2017.

[49] M. Gonzalez Vaya and G. Andersson, "Optimal bidding strategy of a plug-in electric vehicle aggregator in day-ahead electricity markets under uncertainty," *IEEE Transactions on Power Systems*, vol. 30, no. 5, pp. 2375–2385, 2015.

[50] D. T. Nguyen and L. B. Le, "Optimal bidding strategy for microgrids considering renewable energy and building thermal dynamics," *IEEE Transactions on Smart Grid*, vol. 5, no. 4, pp. 1608–1620, 2014.

[51] H. Pandzic, J. M. Morales, A. J. Conejo, and I. Kuzle, "Offering model for a virtual power plant based on stochastic programming," *Applied Energy*, vol. 105, pp. 282–292, 2013.

[52] M. Rahimiyan and L. Baringo, "Strategic bidding for a virtual power plant in the day-ahead and real-time markets: a price-taker robust optimization approach," *IEEE Transactions on Power Systems*, vol. 31, no. 4, pp. 2676–2687, 2016.

[53] L. Baringo and A. J. Conejo, "Offering strategy of wind-power producer: a multi-stage risk-constrained approach," *IEEE Transactions on Power Systems*, vol. 31, no. 2, pp. 1420–1429, 2016.

[54] G. Cardoso, M. Stadler, A. Siddiqui et al., "Microgrid reliability modeling and battery scheduling using stochastic linear programming," *Electric Power Systems Research*, vol. 103, pp. 61–69, 2013.

[55] W. Su, J. Wang, and J. Roh, "Stochastic energy scheduling in microgrids with intermittent renewable energy resources," *IEEE Transactions on Smart Grid*, vol. 5, no. 4, pp. 1876–1883, 2014.

[56] A. A. Eajal, M. F. Shaaban, K. Ponnambalam, and E. F. El-Saadany, "Stochastic centralized dispatch scheme for AC/DC hybrid smart distribution systems," *IEEE Transactions on Sustainable Energy*, vol. 7, no. 3, pp. 1046–1059, 2016.

[57] A. G. Zamani, A. Zakariazadeh, and S. Jadid, "Day-ahead resource scheduling of a renewable energy based virtual power plant," *Applied Energy*, vol. 169, pp. 324–340, 2016.

[58] A. N. Ghalelou, A. P. Fakhri, S. Nojavan, M. Majidi, and H. Hatami, "A stochastic self-scheduling program for compressed air energy storage (CAES) of renewable energy sources (RESs) based on a demand response mechanism," *Energy Conversion and Management*, vol. 120, pp. 388–396, 2016.

[59] C. Gong, X. Wang, W. Xu, and A. Tajer, "Distributed real-time energy scheduling in smart grid: stochastic model and fast optimization," *IEEE Transactions on Smart Grid*, vol. 4, no. 3, pp. 1476–1489, 2013.

[60] L. Ju, Z. Tan, J. Yuan, Q. Tan, H. Li, and F. Dong, "A bi-level stochastic scheduling optimization model for a virtual power plant connected to a wind–photovoltaic–energy storage system considering the uncertainty and demand response," *Applied Energy*, vol. 171, pp. 184–199, 2016.

[61] M. Fotouhi Ghazvini, J. Soares, H. Morais, R. Castro, and Z. Vale, "Dynamic pricing for demand response considering market price uncertainty," *Energies*, vol. 10, no. 9, 2017.

[62] M. A. Fotouhi Ghazvini, J. Soares, O. Abrishambaf, R. Castro, and Z. Vale, "Demand response implementation in smart households," *Energy and Buildings*, vol. 143, pp. 129–148, 2017.

[63] J. C. Bezdek, "On the relationship between neural networks, pattern recognition and intelligence," *International Journal of Approximate Reasoning*, vol. 6, no. 2, pp. 85–107, 1992.

[64] A. Engelbrecht, *Computational Intelligence: an Introduction*, Halsted Press, New York, NY, USA, 2002.

[65] D. B. Fogel, *Evolutionary Computation*, John Wiley & Sons, Inc., Hoboken, NJ, USA, 2005.

[66] J. H. Holland, "Outline for a logical theory of adaptive systems," *Journal of the ACM*, vol. 9, no. 3, pp. 297–314, 1962.

[67] D. E. Golberg, *Genetic Algorithms*, Pearson Education India, 2006.

[68] J. R. Koza, *Genetic Programming: On the Programming of Computers by Means of Natural Selection*, MIT Press, 1992.

[69] L. J. Fogel, A. J. Owens, and M. J. Walsh, *Artificial Intelligence through Simulated Evolution*, John Wiley & Sons, Oxford, England, 1966.

[70] I. Rechenberg, "Evolutionsstrategien," in *Simulationsmethoden in der Medizin und Biologie. Medizinische Informatik und Statistik, vol 8*, B. Schneider and U. Ranft, Eds., pp. 83–114, Springer, Berlin, Heidelberg, 1978.

[71] H.-G. Beyer and H.-P. Schwefel, "Evolution strategies – a comprehensive introduction," *Natural Computing*, vol. 1, no. 1, pp. 3–52, 2002.

[72] K. Price, R. Storn, and J. Lampinen, *Differential Evolution*, Springer-Verlag, Berlin/Heidelberg, 2005.

[73] M. Dorigo and G. Di Caro, "Ant colony optimization: a new meta-heuristic," in *Proceedings of the 1999 Congress on Evolutionary Computation-CEC99 (Cat. No. 99TH8406)*, pp. 1470–1477, Washington, DC, USA, July 1999.

[74] R. Eberhart and J. Kennedy, "A new optimizer using particle swarm theory," in *MHS '95. Proceedings of the Sixth International Symposium on Micro Machine and Human Science*, pp. 39–43, Nagoya, Japan, October 1995.

[75] D. Karaboga and B. Basturk, "A powerful and efficient algorithm for numerical function optimization: artificial bee colony (ABC) algorithm," *Journal of Global Optimization*, vol. 39, no. 3, pp. 459–471, 2007.

[76] X.-S. Yang and S. Deb, "Cuckoo search via levy flights," in *2009 World Congress on Nature & Biologically Inspired Computing (NaBIC)*, pp. 210–214, Coimbatore, India, December 2009.

[77] I. Fister Jr, X. S. Yang, I. Fister, J. Brest, and D. Fister, "A brief review of nature-inspired algorithms for optimization," p. 4, 2013, http://arxiv.org/abs/1307.4186.

[78] E. Zitzler and L. Thiele, "Multiobjective evolutionary algorithms: a comparative case study and the strength Pareto approach," *IEEE Transactions on Evolutionary Computation*, vol. 3, no. 4, pp. 257–271, 1999.

[79] K. Deb, A. Pratap, S. Agarwal, and T. Meyarivan, "A fast and elitist multiobjective genetic algorithm: NSGA-II," *IEEE Transactions on Evolutionary Computation*, vol. 6, no. 2, pp. 182–197, 2002.

[80] P. Ahmadi, I. Dincer, and M. A. Rosen, "Exergy, exergoeconomic and environmental analyses and evolutionary algorithm based multi-objective optimization of combined cycle power plants," *Energy*, vol. 36, no. 10, pp. 5886–5898, 2011.

[81] A. A. Abou El Ela, M. A. Abido, and S. R. Spea, "Optimal power flow using differential evolution algorithm," *Electric Power Systems Research*, vol. 80, no. 7, pp. 878–885, 2010.

[82] K. Ishaque and Z. Salam, "An improved modeling method to determine the model parameters of photovoltaic (PV) modules using differential evolution (DE)," *Solar Energy*, vol. 85, no. 9, pp. 2349–2359, 2011.

[83] A. Kusiak and Z. Song, "Design of wind farm layout for maximum wind energy capture," *Renewable Energy*, vol. 35, no. 3, pp. 685–694, 2010.

[84] A. Bhattacharya and P. K. Chattopadhyay, "Hybrid differential evolution with biogeography-based optimization for solution of economic load dispatch," *IEEE Transactions on Power Systems*, vol. 25, no. 4, pp. 1955–1964, 2010.

[85] K. Ishaque and Z. Salam, "A review of maximum power point tracking techniques of PV system for uniform insolation and partial shading condition," *Renewable and Sustainable Energy Reviews*, vol. 19, pp. 475–488, 2013.

[86] R. Dufo-López, J. L. Bernal-Agustín, J. M. Yusta-Loyo et al., "Multi-objective optimization minimizing cost and life cycle emissions of stand-alone PV–wind–diesel systems with batteries storage," *Applied Energy*, vol. 88, no. 11, pp. 4033–4041, 2011.

[87] A. A. Moghaddam, A. Seifi, T. Niknam, and M. R. Alizadeh Pahlavani, "Multi-objective operation management of a renewable MG (micro-grid) with back-up micro-turbine/fuel cell/battery hybrid power source," *Energy*, vol. 36, no. 11, pp. 6490–6507, 2011.

[88] T. Niknam, "A new fuzzy adaptive hybrid particle swarm optimization algorithm for non-linear, non-smooth and non-convex economic dispatch problem," *Applied Energy*, vol. 87, no. 1, pp. 327–339, 2010.

[89] M. Fadaee and M. A. M. Radzi, "Multi-objective optimization of a stand-alone hybrid renewable energy system by using evolutionary algorithms: a review," *Renewable and Sustainable Energy Reviews*, vol. 16, no. 5, pp. 3364–3369, 2012.

[90] M. Seyedmahmoudian, R. Rahmani, S. Mekhilef et al., "Simulation and hardware implementation of new maximum power point tracking technique for partially shaded PV system using hybrid DEPSO method," *IEEE Transactions on Sustainable Energy*, vol. 6, no. 3, pp. 850–862, 2015.

[91] M. Kefayat, A. Lashkar Ara, and S. A. Nabavi Niaki, "A hybrid of ant colony optimization and artificial bee colony algorithm for probabilistic optimal placement and sizing of distributed energy resources," *Energy Conversion and Management*, vol. 92, pp. 149–161, 2015.

[92] J. Zhao, Z.-H. Guo, Z.-Y. Su, Z.-Y. Zhao, X. Xiao, and F. Liu, "An improved multi-step forecasting model based on WRF ensembles and creative fuzzy systems for wind speed," *Applied Energy*, vol. 162, pp. 808–826, 2016.

[93] B. Li, R. Roche, and A. Miraoui, "Microgrid sizing with combined evolutionary algorithm and MILP unit commitment," *Applied Energy*, vol. 188, pp. 547–562, 2017.

[94] R. Arora, S. C. Kaushik, R. Kumar, and R. Arora, "Multi-objective thermo-economic optimization of solar parabolic dish Stirling heat engine with regenerative losses using NSGA-II and decision making," *International Journal of Electrical Power & Energy Systems*, vol. 74, pp. 25–35, 2016.

[95] A. H. Gandomi and X.-S. Yang, "Chaotic bat algorithm," *Journal of Computational Science*, vol. 5, no. 2, pp. 224–232, 2014.

[96] A. Rezaee Jordehi, "Brainstorm optimisation algorithm (BSOA): an efficient algorithm for finding optimal location and setting of FACTS devices in electric power systems," *International Journal of Electrical Power & Energy Systems*, vol. 69, pp. 48–57, 2015.

[97] B. R. Adarsh, T. Raghunathan, T. Jayabarathi, and X.-S. Yang, "Economic dispatch using chaotic bat algorithm," *Energy*, vol. 96, pp. 666–675, 2016.

[98] E. Yao, H. Wang, L. Wang, G. Xi, and F. Maréchal, "Multi-objective optimization and exergoeconomic analysis of a combined cooling, heating and power based compressed air energy storage system," *Energy Conversion and Management*, vol. 138, pp. 199–209, 2017.

[99] Z.-K. Feng, W.-J. Niu, and C.-T. Cheng, "Multi-objective quantum-behaved particle swarm optimization for economic environmental hydrothermal energy system scheduling," *Energy*, vol. 131, pp. 165–178, 2017.

[100] A. Mellit and A. M. Pavan, "A 24-h forecast of solar irradiance using artificial neural network: application for performance prediction of a grid-connected PV plant at Trieste, Italy," *Solar Energy*, vol. 84, no. 5, pp. 807–821, 2010.

[101] C. Chen, S. Duan, T. Cai, and B. Liu, "Online 24-h solar power forecasting based on weather type classification using artificial neural network," *Solar Energy*, vol. 85, no. 11, pp. 2856–2870, 2011.

[102] L. Olatomiwa, S. Mekhilef, S. Shamshirband, K. Mohammadi, D. Petković, and C. Sudheer, "A support vector machine-firefly algorithm-based model for global solar radiation prediction," *Solar Energy*, vol. 115, pp. 632–644, 2015.

[103] C. Voyant, G. Notton, S. Kalogirou et al., "Machine learning methods for solar radiation forecasting: a review," *Renewable Energy*, vol. 105, pp. 569–582, 2017.

[104] G. Li and J. Shi, "On comparing three artificial neural networks for wind speed forecasting," *Applied Energy*, vol. 87, no. 7, pp. 2313–2320, 2010.

[105] S. S. Soman, H. Zareipour, O. Malik, and P. Mandal, "A review of wind power and wind speed forecasting methods with different time horizons," in *North American Power Symposium 2010*, Arlington, TX, USA, September 2010.

[106] R. Ata, "RETRACTED: artificial neural networks applications in wind energy systems: a review," *Renewable and Sustainable Energy Reviews*, vol. 49, pp. 534–562, 2015.

[107] M. Q. Raza and A. Khosravi, "A review on artificial intelligence based load demand forecasting techniques for smart grid and buildings," *Renewable and Sustainable Energy Reviews*, vol. 50, pp. 1352–1372, 2015.

[108] S. M. Muyeen, R. Takahashi, and J. Tamura, "Operation and control of HVDC-connected offshore wind farm," *IEEE Transactions on Sustainable Energy*, vol. 1, no. 1, pp. 30–37, 2010.

[109] A. Messai, A. Mellit, A. Guessoum, and S. A. Kalogirou, "Maximum power point tracking using a GA optimized fuzzy logic controller and its FPGA implementation," *Solar Energy*, vol. 85, no. 2, pp. 265–277, 2011.

[110] C. Ben Salah and M. Ouali, "Comparison of fuzzy logic and neural network in maximum power point tracker for PV systems," *Electric Power Systems Research*, vol. 81, no. 1, pp. 43–50, 2011.

[111] J. P. S. Catalão, H. M. I. Pousinho, and V. M. F. Mendes, "Hybrid wavelet-PSO-ANFIS approach for short-term wind power forecasting in Portugal," in *2011 IEEE Power and Energy Society General Meeting*, vol. 2, pp. 50–59, Detroit, MI, USA, July 2011.

[112] J. P. S. Catalão, H. M. I. Pousinho, and V. M. F. Mendes, "Hybrid wavelet-PSO-ANFIS approach for short-term electricity prices forecasting," in *2011 IEEE Power and Energy Society General Meeting*, vol. 26, pp. 137–144, Detroit, MI, USA, July 2011.

[113] T. Niknam, H. D. Mojarrad, and M. Nayeripour, "A new fuzzy adaptive particle swarm optimization for non-smooth economic dispatch," *Energy*, vol. 35, no. 4, pp. 1764–1778, 2010.

[114] S. Wang, N. Zhang, L. Wu, and Y. Wang, "Wind speed forecasting based on the hybrid ensemble empirical mode decomposition and GA-BP neural network method," *Renewable Energy*, vol. 94, pp. 629–636, 2016.

[115] G. J. Osório, J. C. O. Matias, and J. P. S. Catalão, "Short-term wind power forecasting using adaptive neuro-fuzzy inference system combined with evolutionary particle swarm optimization, wavelet transform and mutual information," *Renewable Energy*, vol. 75, pp. 301–307, 2015.

[116] A. Baghban, M. Bahadori, J. Rozyn et al., "Estimation of air dew point temperature using computational intelligence schemes," *Applied Thermal Engineering*, vol. 93, pp. 1043–1052, 2016.

[117] S. Hosseinpour, M. Aghbashlo, M. Tabatabaei, H. Younesi, M. Mehrpooya, and S. Ramakrishna, "Multi-objective exergy-based optimization of a continuous photobioreactor applied to produce hydrogen using a novel combination of soft computing techniques," *International Journal of Hydrogen Energy*, vol. 42, no. 12, pp. 8518–8529, 2017.

[118] F. P. Sioshansi, *Evolution of Global Electricity Markets: New Paradigms, New Challenges, New Approaches*, Academic Press, 2013.

[119] PCR, "EUPHEMIA: description and functioning," 2016, August 2016, https://www.epexspot.com/document/35377/Euphemia.

[120] T. Pinto, H. Silva, Z. Vale, G. Santos, and I. Praça, "Pan-European electricity market simulation considering the European power network capacities," in *2015 26th International Workshop on Database and Expert Systems Applications (DEXA)*, pp. 91–95, Valencia, Spain, September 2015.

[121] F. Sensuß, M. Genoese, M. Ragwitz, and D. Möst, "Agent-based simulation of electricity markets - a literature review-," *Energy Studies Review*, vol. 15, no. 2, 2007.

[122] Z. Zhou, W. K. (. V.). Chan, and J. H. Chow, "Agent-based simulation of electricity markets: a survey of tools," *Artificial Intelligence Review*, vol. 28, no. 4, pp. 305–342, 2007.

[123] E. Guerci, M. A. Rastegar, and S. Cincotti, "Agent-based modeling and simulation of competitive wholesale electricity markets," in *Handbook of Power Systems II. Energy Systems*, S. Rebennack, P. Pardalos, M. Pereira, and N. Iliadis, Eds., Springer, Berlin, Heidelberg, 2010.

[124] P. Ringler, D. Keles, and W. Fichtner, "Agent-based modelling and simulation of smart electricity grids and markets - a literature review," *Renewable and Sustainable Energy Reviews*, vol. 57, pp. 205–215, 2016.

[125] A. H. Mohsenian-Rad and A. Leon-Garcia, "Optimal residential load control with price prediction in real-time electricity pricing environments," *IEEE Transactions on Smart Grid*, vol. 1, no. 2, pp. 120–133, 2010.

[126] L. Wu, M. Shahidehpour, and T. Li, "Stochastic security-constrained unit commitment," *IEEE Transactions on Power Systems*, vol. 22, no. 2, pp. 800–811, 2007.

[127] M. Ventosa, Á. Baíllo, A. Ramos, and M. Rivier, "Electricity market modeling trends," *Energy Policy*, vol. 33, no. 7, pp. 897–913, 2005.

[128] F. Sensfuß, M. Ragwitz, and M. Genoese, "The merit-order effect: a detailed analysis of the price effect of renewable electricity generation on spot market prices in Germany," *Energy Policy*, vol. 36, no. 8, pp. 3086–3094, 2008.

[129] F. Wen and A. K. David, "Optimal bidding strategies and modeling of imperfect information among competitive generators," *IEEE Transactions on Power Systems*, vol. 16, no. 1, pp. 15–21, 2001.

[130] M. Korpaas, A. T. Holen, and R. Hildrum, "Operation and sizing of energy storage for wind power plants in a market system," *International Journal of Electrical Power & Energy Systems*, vol. 25, no. 8, pp. 599–606, 2003.

[131] H. Nikkhajoei and R. H. Lasseter, "Distributed generation interface to the CERTS microgrid," *IEEE Transactions on Power Delivery*, vol. 24, no. 3, pp. 1598–1608, 2009.

[132] C. P. Rodriguez and G. J. Anders, "Energy price forecasting in the Ontario competitive power system market," *IEEE Transactions on Power Systems*, vol. 19, no. 1, pp. 366–374, 2004.

[133] K. Bhattacharya and J. Zhong, "Reactive power as an ancillary service," *IEEE Transactions on Power Systems*, vol. 16, no. 2, pp. 294–300, 2001.

[134] P. L. Joskow and E. Kohn, "A quantitative analysis of pricing behavior in California's wholesale electricity market during summer 2000," *The Energy Journal*, vol. 23, no. 4, 2002.

[135] S. A. Harp, S. Brignone, B. F. Wollenberg, and T. Samad, "SEPIA: a simulator for electric power industry agents," *IEEE Control Systems Magazine*, vol. 20, no. 4, pp. 53–69, 2000.

[136] R. D. Zimmerman and R. J. Thomas, "POWERWEB: a tool for evaluating economic and reliability impacts of electric power market designs," in *IEEE PES Power Systems*

Conference and Exposition, 2004, pp. 1562–1567, New York, NY, USA, October 2004.

[137] G. Migliavacca, "SREMS: a short-medium run electricity market simulator based on game theory and incorporating network constraints," in *2007 IEEE Lausanne Power Tech*pp. 813–818, Lausanne, Switzerland, July 2007.

[138] M. Wooldridge and N. R. Jennings, "Intelligent agents: theory and practice," *The Knowledge Engineering Review*, vol. 10, no. 02, p. 115, 1995.

[139] P. Hernandez-Leal, M. Kaisers, T. Baarslag, and E. Munoz de Cote, "A survey of learning in multiagent environments: dealing with non-stationarity," 2017, http://arxiv.org/abs/1707.09183.

[140] J. Bower and D. W. Bunn, "Model-based comparisons of pool and bilateral markets for electricity," *The Energy Journal*, vol. 21, no. 3, 2000.

[141] J. Bower, D. W. Bunn, and C. Wattendrup, "A model-based analysis of strategic consolidation in the German electricity industry," *Energy Policy*, vol. 29, no. 12, pp. 987–1005, 2001.

[142] N. C. Figueiredo, P. P. D. Silva, and D. Bunn, "Weather and market specificities in the regional transmission of renewable energy price effects," *Energy*, vol. 114, pp. 188–200, 2016.

[143] P. Visudhiphan and M. D. Ilic, "Dynamic games-based modeling of electricity markets," in *IEEE Power Engineering Society. 1999 Winter Meeting (Cat. No.99CH36233)*, pp. 274–281, New York, NY, USA, February 1999.

[144] A. R. Greenwald, J. O. Kephart, and G. J. Tesauro, "Strategic pricebot dynamics," in *Proceedings of the 1st ACM conference on Electronic commerce - EC '99*, pp. 58–67, Denver, Colorado, USA, November 1999.

[145] P. Visudhiphan, M. D. Ilic, and R. Neck, "Chapter 68 – an agent-based approach to modeling electricity spot markets," in *Modeling and Control of Economic Systems 2001, A Proceedings volume from the 10th IFAC Symposium*, pp. 407–412, Klagenfurt, Austria, September 2001.

[146] J. Nicolaisen, M. Smith, V. Petrov, and L. Tesfatsion, "Concentration and capacity effects on electricity market power," in *Proceedings of the 2000 Congress on Evolutionary Computation. CEC00 (Cat. No.00TH8512)*, pp. 1041–1047, La Jolla, CA, USA, July 2000.

[147] V. Petrov and G. Sheblé, "Building electric power auctions with improved Roth-erev reinforced learning," in *Proceedings of the North American Power Symposium*, College Station, TX, USA, 2001.

[148] F. Gao, G. B. Sheble, K. W. Hedman, and C.-N. Yu, "Optimal bidding strategy for GENCOs based on parametric linear programming considering incomplete information," *International Journal of Electrical Power & Energy Systems*, vol. 66, pp. 272–279, 2015.

[149] B. Zou, M. Yan, and X. Xie, "The comparisons between pricing methods on pool-based electricity market using agent-based simulation," in *2004 IEEE International Conference on Electric Utility Deregulation, Restructuring and Power Technologies. Proceedings*, pp. 285–289, Hong Kong, China, April 2004.

[150] A. R. Micola, A. Banal-Estañol, and D. W. Bunn, "Incentives and coordination in vertically related energy markets," *Journal of Economic Behavior & Organization*, vol. 67, no. 2, pp. 381–393, 2008.

[151] A. Banal-Estañol and A. Rupérez Micola, "Behavioural simulations in spot electricity markets," *European Journal of Operational Research*, vol. 214, no. 1, pp. 147–159, 2011.

[152] T. Krause and G. Andersson, "Evaluating congestion management schemes in liberalized electricity markets using an agent-based simulator," in *2006 IEEE Power Engineering Society General Meeting*, Montreal, QC, Canada, June 2006.

[153] A. J. Bagnall and G. D. Smith, "A multiagent model of the UK market in electricity generation," *IEEE Transactions on Evolutionary Computation*, vol. 9, no. 5, pp. 522–536, 2005.

[154] S. Cincotti and G. Gallo, "The genoa artificial power-exchange," in *Agents and Artificial Intelligence. ICAART 2012. Communications in Computer and Information Science, Vol 358*, J. Filipe and A. Fred, Eds., pp. 348–363, Springer, Berlin, Heidelberg, 2013.

[155] L. Ponta, M. Raberto, A. Teglio, and S. Cincotti, "An agent-based stock-flow consistent model of the sustainable transition in the energy sector," *Ecological Economics*, vol. 145, pp. 274–300, 2018.

[156] V. S. Koritarov, "Real-world market representation with agents," *IEEE Power and Energy Magazine*, vol. 2, no. 4, pp. 39–46, 2004.

[157] P. Thimmapuram, T. D. Veselka, V. Koritarov, S. Vilela, R. Pereira, and R. F. Silva, "Modeling hydro power plants in deregulated electricity markets: integration and application of EMCAS and VALORAGUA," in *2008 5th International Conference on the European Electricity Market*, Lisboa, Portugal, May 2008.

[158] G. Conzelmann, G. Boyd, V. Koritarov, and T. Veselka, "Multi-agent power market simulation using EMCAS," in *IEEE Power Engineering Society General Meeting, 2005*, pp. 2829–2834, San Francisco, CA, USA, June 2005.

[159] H. Li and L. Tesfatsion, "Development of open source software for power market research: the AMES test bed," *The Journal of Energy Markets*, vol. 2, no. 2, pp. 111–128, 2009.

[160] G. Santos, T. Pinto, I. Praça, and Z. Vale, "MASCEM: optimizing the performance of a multi-agent system," *Energy*, vol. 111, pp. 513–524, 2016.

[161] I. Praça, C. Ramos, Z. Vale, and M. Cordeiro, "MASCEM: a multiagent system that simulates competitive electricity markets," *IEEE Intelligent Systems*, vol. 18, no. 6, pp. 54–60, 2003.

[162] T. Pinto, Z. Vale, T. M. Sousa, I. Praça, G. Santos, and H. Morais, "Adaptive learning in agents behaviour: a framework for electricity markets simulation," *Integrated Computer-Aided Engineering*, vol. 21, pp. 399–415, 2014.

[163] P. Oliveira, T. Pinto, H. Morais, and Z. Vale, "MASGriP — a multi-agent smart grid simulation platform," in *2012 IEEE Power and Energy Society General Meeting*, pp. 1–8, San Diego, CA, USA, July 2012.

[164] G. Grozev and D. Batten, "NEMSIM: practical challenges for agent-based simulation of energy markets," in *CSIRO Complex Syst. Sci. Annu. Work. CSIRO Manuf. Infrastruct. Technol.*, Melbourne, Australia, 2005.

[165] T. D. H. Cau and E. J. Anderson, "A co-evolutionary approach to modelling the behaviour of participants in competitive electricity markets," in *IEEE Power Engineering Society Summer Meeting*, pp. 1534–1540, Chicago, IL, USA, July 2002.

[166] E. J. Anderson and T. D. H. Cau, "Implicit collusion and individual market power in electricity markets," *European Journal of Operational Research*, vol. 211, no. 2, pp. 403–414, 2011.

[167] R. Entriken, *Using Automated Agents with Probe: Interface Requirements Specification*, Technical Report 1012157, EPRI, Palo Alto, 2005.

[168] R. L. Hu, R. Skorupski, R. Entriken, and Y. Ye, "A mathematical programming formulation for optimal load shifting of electricity demand for the smart grid," *IEEE Transactions on Big Data*, p. 1, 2016.

[169] R. Audouin, F. Hermon, and R. Entriken, "Extending a spot market multi-agent simulator to model investment decisions," in *2006 IEEE PES Power Systems Conference and Exposition*, pp. 1190–1197, Atlanta, GA, USA, November 2006.

[170] D. J. Veit, A. Weidlich, J. Yao, and S. S. Oren, "Simulating the dynamics in two-settlement electricity markets via an agent-based approach," *International Journal of Management Science and Engineering Management*, vol. 1, no. 2, 2006.

[171] A. Weidlich, F. Sensfuß, M. Genoese, and D. Veit, "Studying the effects of CO_2 emissions trading on the electricity market: a multi-agent-based approach," in *Emissions Trading*, R. Antes, B. Hansjürgens, and P. Letmathe, Eds., pp. 91–101, Springer, New York, NY, USA, 2008.

[172] E. Gnansounou, S. Pierre, A. Quintero, J. Dong, and A. Lahlou, "A multi-agent approach for planning activities in decentralized electricity markets," *Knowledge-Based Systems*, vol. 20, no. 4, pp. 406–418, 2007.

[173] J. L. Bernal-Agustín, J. Contreras, R. Martín-Flores, and A. J. Conejo, "Realistic electricity market simulator for energy and economic studies," *Electric Power Systems Research*, vol. 77, no. 1, pp. 46–54, 2007.

[174] K. Atkins, C. L. Barrett, C. M. Homan, A. Marathe, M. V. Marathe, and S. Thite, "Agent based economic analysis of deregulated electricity markets," in *6th IAEE European Energy Conference on Modelling in Energy Economics and Policy*, Zürich, Switzerland, September 2004.

[175] M. A. Ehlen, A. J. Scholand, and K. L. Stamber, "The effects of residential real-time pricing contracts on transco loads, pricing, and profitability: simulations using the N-ABLE™ agent-based model," *Energy Economics*, vol. 29, no. 2, pp. 211–227, 2007.

[176] S. E. Widergren, J. M. Roop, R. T. Guttromson, and Z. Huang, "Simulating the dynamic coupling of market and physical system operations," in *IEEE Power Engineering Society General Meeting, 2004*, pp. 748–753, Denver, CO, USA, June 2004.

[177] M. Ayar, S. Obuz, R. D. Trevizan, A. S. Bretas, and H. A. Latchman, "A distributed control approach for enhancing smart grid transient stability and resilience," *IEEE Transactions on Smart Grid*, vol. 8, no. 6, pp. 3035–3044, 2017.

[178] JCR, "Smart grid projects outlook," 2017, http://ses.jrc.ec.europa.eu/smart-grids-observatory.

[179] ETP, "European technologic platforms," http://cordis.europa.eu/technology-platforms.

[180] Q.-C. Zhong and G. Weiss, "Synchronverters: inverters that mimic synchronous generators," *IEEE Transactions on Industrial Electronics*, vol. 58, no. 4, pp. 1259–1267, 2011.

[181] A. J. Conejo, J. M. Morales, and L. Baringo, "Real-time demand response model," *IEEE Transactions on Smart Grid*, vol. 1, no. 3, pp. 236–242, 2010.

[182] N. Pogaku, M. Prodanović, and T. C. Green, "Modeling, analysis and testing of autonomous operation of an inverter-based microgrid," *IEEE Transactions on Power Electronics*, vol. 22, no. 2, pp. 613–625, 2007.

[183] F. Katiraei and M. R. Iravani, "Power management strategies for a microgrid with multiple distributed generation units," *IEEE Transactions on Power Systems*, vol. 21, no. 4, pp. 1821–1831, 2006.

[184] F. Katiraei, M. R. Iravani, and P. W. Lehn, "Micro-grid autonomous operation during and subsequent to islanding process," *IEEE Transactions on Power Delivery*, vol. 20, no. 1, pp. 248–257, 2005.

[185] D. G. Erbs, S. A. Klein, and J. A. Duffie, "Estimation of the diffuse radiation fraction for hourly, daily and monthly-average global radiation," *Solar Energy*, vol. 28, no. 4, pp. 293–302, 1982.

[186] D. B. Crawley, J. W. Hand, M. Kummert, and B. T. Griffith, "Contrasting the capabilities of building energy performance simulation programs," *Building and Environment*, vol. 43, no. 4, pp. 661–673, 2008.

[187] H. Lund and B. V. Mathiesen, "Energy system analysis of 100% renewable energy systems-the case of Denmark in years 2030 and 2050," *Energy*, vol. 34, no. 5, pp. 524–531, 2009.

[188] B. Gustavsen and A. Semlyen, "Rational approximation of frequency domain responses by vector fitting," *IEEE Transactions on Power Delivery*, vol. 14, no. 3, pp. 1052–1061, 1999.

[189] R. D. Zimmerman, C. E. Murillo-Sánchez, and R. J. Thomas, "MATPOWER: steady-state operations, planning, and analysis tools for power systems research and education," *IEEE Transactions on Power Systems*, vol. 26, no. 1, pp. 12–19, 2011.

[190] S. Rohjans, S. Lehnhoff, S. Schütte, F. Andrén, and T. Strasser, "Requirements for smart grid simulation tools," in *2014 IEEE 23rd International Symposium on Industrial Electronics (ISIE)*, pp. 1730–1736, Istanbul, Turkey, June 2014.

[191] S. F. Bush, "Appendix: smart grid simulation tools," in *Smart Grid*, p. 576, John Wiley & Sons, 2013.

[192] S. Kakran and S. Chanana, "Smart operations of smart grids integrated with distributed generation: a review," *Renewable and Sustainable Energy Reviews*, vol. 81, pp. 524–535, 2018.

[193] A. Kantamneni, L. E. Brown, G. Parker, and W. W. Weaver, "Survey of multi-agent systems for microgrid control," *Engineering Applications of Artificial Intelligence*, vol. 45, pp. 192–203, 2015.

[194] A. L. Dimeas and N. D. Hatziargyriou, "Control agents for real microgrids," in *2009 15th International Conference on Intelligent System Applications to Power Systems*, pp. 1–5, Curitiba, Brazil, November 2009.

[195] Z. Wang, R. Yang, and L. Wang, "Intelligent multi-agent control for integrated building and micro-grid systems," in *ISGT 2011*, pp. 1–7, Anaheim, CA, USA, January 2011.

[196] Z. Jiang, "Agent-based control framework for distributed energy resources microgrids," in *2006 IEEE/WIC/ACM International Conference on Intelligent Agent Technology*, pp. 646–652, Hong Kong, China, December 2006.

[197] C. M. Colson and M. H. Nehrir, "Comprehensive real-time microgrid power management and control with distributed agents," *IEEE Transactions on Smart Grid*, vol. 4, no. 1, pp. 617–627, 2013.

[198] H. E. Farag, E. F. El-Saadany, and L. El Chaar, "A multilayer control framework for distribution systems with high DG penetration," in *2011 International Conference on Innovations in Information Technology*, pp. 94–99, Abu Dhabi, UAE, April 2011.

[199] Z. Xiao, T. Li, M. Huang et al., "Hierarchical MAS based control strategy for microgrid," *Energies*, vol. 3, no. 9, pp. 1622–1638, 2010.

[200] M. Cossentino, C. Lodato, S. Lopes, M. Pucci, G. Vitale, and M. Cirrincione, "A multi-agent architecture for simulating and managing microgrids," in *2011 Federated Conference on Computer Science and Information Systems (FedCSIS)*, pp. 619–622, Szczecin, Poland, September 2011.

[201] J. Oyarzabal, J. Jimeno, J. Ruela, A. Engler, and C. Hardt, "Agent based micro grid management system," in *2005 International Conference on Future Power Systems*, Amsterdam, Netherlands, November 2005.

[202] H. S. V. S. Kumar Nunna and S. Doolla, "Multiagent-based distributed-energy-resource management for intelligent microgrids," *IEEE Transactions on Industrial Electronics*, vol. 60, no. 4, pp. 1678–1687, 2013.

[203] E. L. Karfopoulos, P. Papadopoulos, S. Skarvelis-Kazakos et al., "Introducing electric vehicles in the microgrids concept," in *2011 16th International Conference on Intelligent System Applications to Power Systems*, pp. 1–6, Hersonissos, Greece, September 2011.

[204] T. Logenthiran, D. Srinivasan, and A. M. Khambadkone, "Multi-agent system for energy resource scheduling of integrated microgrids in a distributed system," *Electric Power Systems Research*, vol. 81, no. 1, pp. 138–148, 2011.

[205] T. Logenthiran, D. Srinivasan, A. M. Khambadkone, and H. N. Aung, "Multiagent system for real-time operation of a microgrid in real-time digital simulator," *IEEE Transactions on Smart Grid*, vol. 3, no. 2, pp. 925–933, 2012.

[206] C. M. Colson, M. H. Nehrir, and R. W. Gunderson, "Multi-agent microgrid power management," *IFAC Proceedings Volumes*, vol. 44, no. 1, pp. 3678–3683, 2011.

[207] F. Y. S. Eddy and H. B. Gooi, "Multi-agent system for optimization of microgrids," in *8th International Conference on Power Electronics - ECCE Asia*, pp. 2374–2381, Jeju, South Korea, June 2011.

[208] Z. Wang, B. Chen, J. Wang, M. M. Begovic, and C. Chen, "Coordinated energy management of networked microgrids in distribution systems," *IEEE Transactions on Smart Grid*, vol. 6, no. 1, pp. 45–53, 2015.

[209] Z. Jun, L. Junfeng, W. Jie, and H. W. Ngan, "A multi-agent solution to energy management in hybrid renewable energy generation system," *Renewable Energy*, vol. 36, no. 5, pp. 1352–1363, 2011.

[210] D. Unger and J. M. A. Myrzik, "Agent based management of energy storage devices within a virtual energy storage," in *2013 IEEE Energytech*, Cleveland, OH, USA, May 2013.

[211] P. Vytelingum, T. D. Voice, S. D. Ramchurn, A. Rogers, and N. R. Jennings, "Agent-based micro-storage management for the smart grid," in *Proceedings of the 9th International Conference on Autonomous Agents and Multiagent Systems: Volume 1-Volume 1*, pp. 39–46, Toronto, Canada, May 2010.

[212] M. N. Faqiry, R. Kundu, R. Mukherjee, S. Das, and A. Pahwa, "Game theoretic model of energy trading strategies at equilibrium in microgrids," in *2014 North American Power Symposium (NAPS)*, Pullman, WA, USA, September 2014.

[213] S. Dave, M. Sooriyabandara, and M. Yearworth, "System behaviour modelling for demand response provision in a smart grid," *Energy Policy*, vol. 61, pp. 172–181, 2013.

[214] K. Kok, Z. Derzsi, J. Gordijn et al., "Agent-based electricity balancing with distributed energy resources, a multiperspective case study," in *Proceedings of the 41st Annual Hawaii International Conference on System Sciences (HICSS 2008)*, Waikoloa, HI, USA, January 2008.

[215] S. Rumley, E. Kägi, H. Rudnick, and A. Germond, "Multi-agent approach to electrical distribution networks control," in *2008 32nd Annual IEEE International Computer Software and Applications Conference*, pp. 575–580, Turku, Finland, August 2008.

[216] E. Trinklein, G. Parker, W. Weaver et al., "Scoping study: networked microgrids," Tech. Rep. 1433071, Sandia National Laboratories, Albuquerque, NM, USA, 2014.

[217] M. D. Galus, "Agent-based modeling and simulation of large scale electric mobility in power systems," Ph.D. Thesis, ETH Zurich Research Collection, 2012.

[218] S. Kahrobaee, R. A. Rajabzadeh, L.-K. Soh, and S. Asgarpoor, "Multiagent study of smart grid customers with neighborhood electricity trading," *Electric Power Systems Research*, vol. 111, pp. 123–132, 2014.

[219] J. Stephenson, B. Barton, G. Carrington, D. Gnoth, R. Lawson, and P. Thorsnes, "Energy cultures: a framework for understanding energy behaviours," *Energy Policy*, vol. 38, no. 10, pp. 6120–6129, 2010.

[220] M. Rylatt, R. Gammon, P. Boait et al., "Cascade: an agent based framework for modeling the dynamics of smart electricity systems," *Emergence: Complexity and Organization*, vol. 15, pp. 1–13, 2013.

[221] S. Behboodi, D. P. Chassin, N. Djilali, and C. Crawford, "Transactive control of fast-acting demand response based on thermostatic loads in real-time retail electricity markets," *Applied Energy*, vol. 210, pp. 1310–1320, 2018.

[222] J. Delamare, B. Bitachon, Z. Peng, Y. Wang, B. R. Haverkort, and M. R. Jongerden, "Development of a smart grid simulation environment," *Electronic Notes in Theoretical Computer Science*, vol. 318, pp. 19–29, 2015.

[223] A. N. Albagli, D. M. Falcão, and J. F. De Rezende, "Smart grid framework co-simulation using HLA architecture," *Electric Power Systems Research*, vol. 130, pp. 22–33, 2016.

[224] F. Casella, A. G. Bartolini, and A. Leva, "Equation-based object-oriented modelling and simulation of large-scale smart grids with Modelica," *IFAC-PapersOnLine*, vol. 50, no. 1, pp. 5542–5547, 2017.

[225] M. Jarrah, "Modeling and simulation of renewable energy sources in smart grid using DEVS formalism," *Procedia Computer Science*, vol. 83, pp. 642–647, 2016.

[226] A. Razaq, B. Pranggono, H. Tianfield, and H. Yue, "Simulating smart grid: co-simulation of power and communication network," in *2015 50th International Universities Power Engineering Conference (UPEC)*, Stoke on Trent, UK, September 2015.

[227] R. Alishov, M. Spähn, and R. Witzmann, "Co-simulation architecture for centralised direct load control in smart grid," in *CIRED Workshop 2016*, Helsinki, Finland, June 2016.

Hindawi
Complexity
Volume 2018, Article ID 7276585, 15 pages
https://doi.org/10.1155/2018/7276585

Research Article

An Elitist Transposon Quantum-Based Particle Swarm Optimization Algorithm for Economic Dispatch Problems

Angus Wu[1] **and Zhen-Lun Yang**[2]

[1]*Department of Electronic Engineering, City University of Hong Kong, Tat Chee Ave, Kowloon Tong, Hong Kong*
[2]*School of Information Engineering, Guangzhou Panyu Polytechnic, Guangzhou 511483, China*

Correspondence should be addressed to Angus Wu; angus.wu@cityu.edu.hk

Received 23 February 2018; Revised 7 May 2018; Accepted 21 May 2018; Published 17 July 2018

Academic Editor: Fernando Lezama

Population-based optimization algorithms are useful tools in solving engineering problems. This paper presents an elitist transposon quantum-based particle swarm algorithm to solve economic dispatch (ED) problems. It is a complex and highly nonlinear constrained optimization problem. The proposed approach, double elitist breeding quantum-based particle swarm optimization (DEB-QPSO), makes use of two elitist breeding strategies to promote the diversity of the swarm so as to enhance the global search ability and an improved efficient heuristic handling technique to manage the equality and inequality constraints of ED problems. Investigating on 15-unit, 40-unit, and 140-unit widely used test systems, through performance comparison, the proposed DEB-QPSO algorithm is able to obtain higher-quality solutions efficiently and stably superior than the other the state-of-the-art algorithms.

1. Introduction

Economic dispatch (ED) of electric power generation is used to determine an optimal combination of power output from the units in the system for a minimal total generation cost meeting the load demand while satisfying all equality and inequality constraints of the units and system. The constraints involved discontinuous prohibited zones, unit power limits, and ramp rate limits making the practical ED problem a highly constrained nonconvex and nonlinear optimization problem [1]. The cost function of ED problems can be represented by a quadratic function and solved by conventional methods such as the gradient method, dynamic programming, and the lambda-iteration method [2, 3]. However, none of these conventional optimization methods is able to provide an optimal solution as they are fast but easily getting stuck at the local optima as confirmed with past experience of researchers.

In recent decades, a wide variety of metaheuristic optimization methods such as genetic algorithm (GA) [4, 5], artificial immune system (AIS) [6, 7], particle swarm optimization (PSO) [8–16], differential evolution (DE) [17–19], gravitational search algorithm (GSA) [20], Tabu Search (TS) [21, 22], neural network (NN) [23, 24], evolutionary programming (EP) [25], bacterial foraging algorithm (BFA) [26], biogeography-based optimization (BBO) [27], and other population-based optimization algorithms [28–32] have been applied with success in solving the ED problems and been able to obtain better solutions compared to using conventional optimization methods.

Recently, a variant of PSO with guaranteed global convergence ability, quantum-behaved particle swarm optimization (QPSO) algorithm, is proposed by Sun et al. [33, 34]. QPSO outperforms PSO in global search ability and is a promising optimizer for complex problems [35–37]. QPSO demonstrates its superiority in solving ED problems comparing to other population-based optimization algorithms [38, 39]. Although various QPSO approaches have been successful in solving ED problems as reported in literature, they still lack the efficient mechanism to treat the constraints effectively [39]. The most commonly used method to handle constraints in ED problem with QPSO is the use of penalty

functions [39, 40]. The simple implementation of combining the constraints with the objective function is the advantage of this approach. However, an additional tuning parameter called penalty factor is needed to penalize those solutions violating the constraints. It is rather difficult to choose the appropriate penalty factor for the penalty function approaches. A small penalty factor is not effective to handle the ED problem. Conversely, a large penalty factor will make the ED problem feasible but is distorting the solution space. As a result, it will converge to a weak local optimum. Recently, some heuristic constraint handling strategies have been proposed to modify infeasible solutions to satisfy the equality constraints, but their heavy computational requirement imposes a challenge for any evolutionary algorithms based on those heuristic strategies to find the global optimal solutions efficiently [41].

To overcome the existing deficiencies of QPSO for the ED problem, this paper proposes a double elitist breeding transposon QPSO (DEB-QPSO) algorithm based on our recent work on EB-QPSO [42] with the extension of an improved constraint handling technique and a cooperative update method for the pbests and gbest. The proposed approach makes use of two elitist breeding methods with transposon to enhance the diversity of the population in the QPSO mechanism. The transposon operators can improve the global search ability by preventing the premature convergence through increased diversity of the population as demonstrated in our previous work [42]. The current work is to extend our EB-QPSO technique to solve the ED problems. Moreover, one of the proposed elitist breeding schemes aims to assist the constraint handling while improving the diversity of the population. An improved dedicated efficient heuristic handling technique is proposed to manage the equality and inequality constraints of ED problems. The proposed algorithm is applied on three different widely used ED test problems and compared to various the state-of-the-art population-based optimization algorithms. The rest of this paper is organized as follows: the mathematical formulation of the ED problem is given in Section 2. Section 3 briefly describes the PSO, QPSO, and EB-QPSO algorithms that related to the proposed approach. The proposed DEB-QPSO algorithm for solving ED problems is presented in Section 4. Section 5 gives the implementation of the proposed algorithm for solving ED problems. Section 6 provides the case studies and results of the DEB-QPSO algorithm for three nonconvex ED problems and is compared to the state-of-the-art approaches from literature. Conclusion is given in Section 7.

2. Problem Formulation

The objective of ED is to reduce the operation cost of the system while fulfilling the load demand within the limit of constraints. The nonsmooth/nonconvex ED problem takes into account valve-point loading effects, prohibited operating zones and multifuel options along with system power demand, transmission loss, and operational limit constraints. The overall ED problem can be formulated as a nonlinear optimization programming problem:

$$\text{Minimize} \quad C_T = \sum_{i=1}^{Ng} F_i(P_i), \tag{1}$$

$$F_i(P_i) = \mathrm{a}_i + b_i P_i + c_i P_i^2, \tag{2}$$

where C_T, $F_i(P_i)$, and N_g are the total fuel cost, cost function of generator i, and the number of generators in the system, respectively; a_i, b_i, and c_i are the cost coefficients of the ith generator and P_i is the power output of the ith generator.

The generating units with multiple valves in steam turbines are available. The opening and closing of these valves may add the ripples in the cost function which makes the objective function highly nonlinear [5]. The cost function in (2) is modified as

$$F_i(P_i) = a_i + b_i P_i + c_i P_i^2 + \left| e_i \sin\left(f_i \times (P_{i,\min} - P_i)\right)\right|, \tag{3}$$

where $P_{i,\min}$ is the minimum output of the ith generator, e_i and f_i are two coefficients of the ith generator with valve-point loading effect.

ED problem is subjected to the following constraints:

(i) Power balance constraint

$$\sum_{i=1}^{N_g} P_i - P_L - P_D = 0, \tag{4}$$

where P_L and P_D are the total transmission network losses and the total load demand, respectively.

Normally, P_L is represented by way of Kron's loss formula [1] given as

$$P_L = \sum_{i=1}^{N_g}\sum_{j=1}^{N_g} P_i B_{ij} P_j + \sum_{i=1}^{N_g} B_{0i} P_i + B_{00}, \tag{5}$$

where B_{ij}, B_{i0}, and B_{00} are known as the loss coefficients determined by the situation of a specified power system.

(ii) Power output limit and amp rate limit constraint

Considering the inequality constraints of power output limit and ramp rate limit simultaneously, the generator operation constraint can be expressed as follows:

$$\max\left\{P_{i,\min}, P_i^0 - DR_i\right\} \le P_i \le \min\left\{P_{i,\max}, P_i^0 + UR_i\right\}, \tag{6}$$

where $P_{i,\min}$, $P_{i,\max}$, P_i^0, UR_i, and DR_i are the minimum output, maximum output, previous output power, the upramp limit, and downramp limit of the ith generator, respectively.

(iii) Prohibited operating zone constraint

The feasibility operation zones of a unit with prohibited operation zones lead to additional constraints on the unit operating range as follows:

$$P_i \in \begin{cases} P_i^{\min} \le P_i \le P_{i,1}^{l}, \\ P_{i,k-1}^{u} \le P_i \le P_{i,k}^{l}, \\ P_{i,n_{pz}}^{u} \le P_i \le P_i^{\max}, \\ k = 2, 3, \ldots, n_{pz}, \end{cases} \tag{7}$$

where n_{gz}, $P_{i.k}^{l}$, and $P_{i.k}^{u}$ are the number of prohibited zones, the lower bound of the kth prohibited zone of the ith generator, and upper bound of the kth prohibited zone of the ith generator, respectively.

3. PSO, QPSO, and EB-QPSO

Particle swarm optimization (PSO) was proposed by Kennedy and Eberhart [34, 43] and is acknowledged as one of the most popular stochastic algorithms. In the past two decades, the PSO algorithm has undergone many improvements or modifications in an effort to compete more effectively on solving complicated problems [34, 43].

3.1. The Original PSO Algorithm. The PSO algorithm is inspired by the social behavior of bird flocking. Each particle is defined by a position vector $\mathbf{x} = (x_1, x_2, \ldots, x_D)$ which signifies a solution responsible for the exploration of the search space. Let N denote the swarm size and D be the dimensionality of the search space; during the search process, the position of each particle is evolved through the velocity and position equations:

$$v_i^{t+1} = wv_i^t + c_1 r_1 \left(\text{pbest}_i - \mathbf{x}_i^t\right) + c_2 r_2 \left(\text{gbest} - \mathbf{x}_i^t\right), \tag{8}$$

$$\mathbf{x}_i^{t+1} = v_i^{t+1} + \mathbf{x}_i^t, \tag{9}$$

where v_i^t and $\mathbf{x}_i^t$ are the velocity and position of the ith $(i = 1, 2, \ldots, N)$ particle in generation t. pbest_i, the personal best, is the previous position having the best objective function value of the ith particle. gbest called global best particle is the position of the best particle among all particles in the swarm. r_1 and r_2 are two uniformly distributed random numbers generated in the range $[0, 1]$. c_1 and c_2 are the learning factors called acceleration coefficients, and w is the inertia weight introduced into (8) by Shi and Eberhart [34, 43, 44] which is decreased linearly from 0.9 to 0.4 through the evolutionary process to enhance the capacity of exploring the solution space. Without loss of generality, for minimization, with the objective function, f, the pbest_i is updated according to

$$\text{pbest} = \begin{cases} \mathbf{x}_i^t & \text{if } f\left[\mathbf{x}_i^t\right] < f\left[p_i^{t-1}\right], \\ \text{pbest}_i^{t-1} & \text{if } f\left[\mathbf{x}_i^t\right] > f\left[p_i^{t-1}\right]. \end{cases} \tag{10}$$

Consequently, gbest is found by

$$\begin{aligned} \text{gbest}^t &= \text{pbest}_g^t, \\ \text{pbest}_g^t &= \arg \min_{1 \le i \le N} \left\{ f\left[\text{pbest}_i^t\right] \right\}. \end{aligned} \tag{11}$$

Although PSO converges fast and many attempts have been made to improve the performances of PSO [42, 43], it is prone to be trapped into local optima and not guaranteed to be global convergent as demonstrated in [45].

3.2. QPSO. A widely used PSO using alternative particle evolution formulae is QPSO. Inspired by the quantum mechanics, Sun et al. developed the quantum-behaved particle swarm optimization algorithm based on the trajectory analysis of the PSO, which is theoretically proved to be global convergent [33, 34, 46]. In the evolutionary process, the position of each particle is updated with the following rules:

$$\begin{aligned} \mathbf{x}_i^{t+1} &= p_i^t + \alpha \left| \mathbf{x}_i^t - \text{mbest}^t \right| \ln\left(\frac{1}{u_i^t}\right), \quad \text{if randv} \ge 0.5, \\ \mathbf{x}_i^{t+1} &= p_i^t - \alpha \left| \mathbf{x}_i^t - \text{mbest}^t \right| \ln\left(\frac{1}{u_i^t}\right), \quad \text{if randv} < 0.5, \end{aligned} \tag{12}$$

where p_i^t, mbest^t, and α are the local attractor of the particle in iteration t, the mean best position in iteration t, and the contraction-expansion coefficient, respectively; both u_i^t and randv are random numbers generated using the uniform probability distribution functions in the range of $[0, 1]$. The local attractor is defined as

$$p_i^t = \varphi^t \times \text{pbest}_i^t + \left(1 - \varphi^t\right) \times \text{gbest}^t, \tag{13}$$

where φ^t is a uniformly distributed random parameter chosen within the interval $[0, 1]$, $\text{pbest}_\text{i}^\text{t}$ and gbest^t are the personal best of the ith particle and global best of the swarm, respectively. The mean best position is defined as the mean of the pbest position of all particles:

$$\text{mbest}^t = \frac{1}{N} \sum_{i=1}^{N} \text{pbest}_i^t. \tag{14}$$

α is the contraction-expansion coefficient used to control convergence rate of QPSO, which is usually adjusted with a time-varying decreasing method [47] defined as follows:

$$\alpha = \frac{\alpha_1 + (T - t) \times (\alpha_0 - \alpha_1)}{T}, \tag{15}$$

where T is the maximum iteration number and t is the current search iteration number. α_0 and α_1 are the initial and final values of α, respectively.

QPSO is theoretically guaranteed the global convergence of the algorithm; however, upon the assumption of infinite number of search iteration, such requirement is impractical in solving complex engineering problems like ED problems.

3.3. EB-QPSO. To alleviate the problem of QPOS, numerous strategies have been proposed in recent literatures to improve the exploration efficiency and quality of solution. These strategies can be classified as improvements by parameter selection, control swarm diversity, cooperative methods, using probability distribution function, novel search methods, and hybrid methods [32, 46, 48, 49, 51–57] Recently, a EB-QPSO algorithm based on transposon was proposed [42, 58]. The basic idea of the approach is to make better use of the elitists consisting of the pbests and

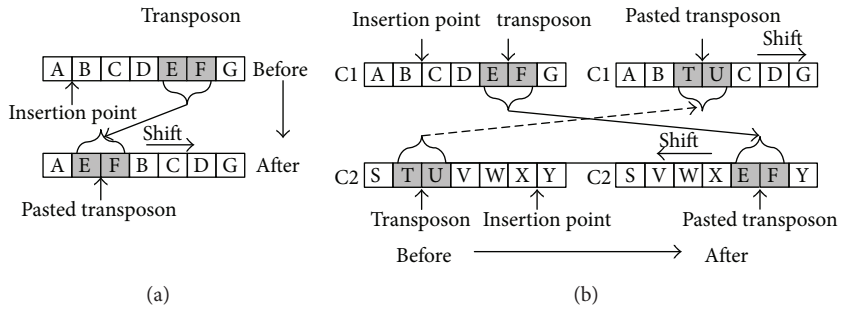

Figure 1: Cut-and-paste transposon operator. (a) Cut-and-paste in same chromosome. (b) Cut-and-paste in different chromosomes.

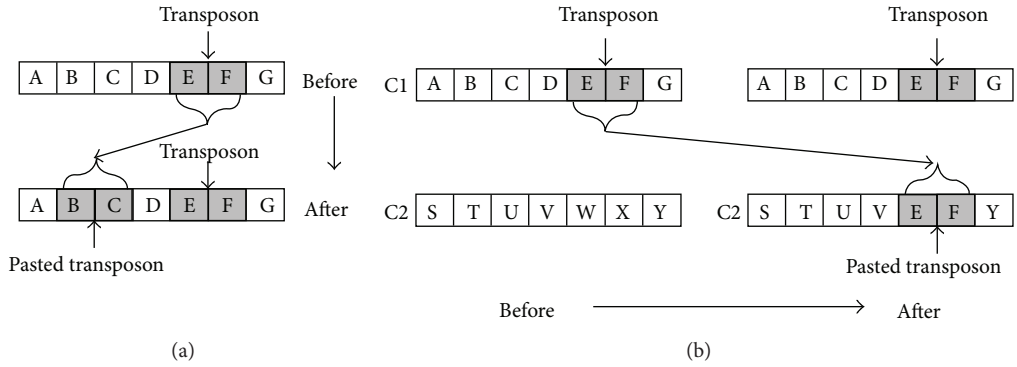

Figure 2: Copy-and-paste transposon operator. (a) Copy-and-paste in same chromosome. (b) Copy-and-paste in different chromosomes.

gbest in aiding to aggrandize the diversity of the swarm that is essential to the exploration and exploitation for the search of the global optima [59, 60].

An elitist exploration strategy, namely, elitist transposon breeding, is incorporated with the basic evolutionary processes of QPSO in the EB-QPSO algorithm. In the elitist transposon breeding scheme, an elitist pool consisting of pb ests and gbest is constructed. New particles are generated from the elitist pool with the transposon operators, having the ability to enhance the diversity of solutions, to explore the elitist memory and extract some more potential essences from the elitist individuals and thus to improve the search efficiency. Moreover, the update of elitists with the newbred better-fitted individuals will provide a more efficient and precise search guidance for the swarm.

Transposon operators were firstly proposed by Tang et al. [50] and mainly used in multiobjective evolutionary algorithms and applied in population-based optimization algorithm in our works [42, 58, 61]. A transposon is made of consecutive genes located in the randomly assigned position in each chromosome while the transposon operators are lateral movement operations that happen in one chromosome or between different ones. In general, there exist two types of transposon operators, cut-and-paste and copy-and-paste, which are shown in Figures 1 and 2. The transposon operations conducted within an individual chromosome or on a different chromosome are chosen randomly. Moreover, the size of each transposon can be greater than one and is decided by a parameter called jumping

Figure 3: An example of the particle is represented as a chromosome.

percentage while the number of transposons is also a predefined parameter. Another parameter, the jumping rate, is assigned to determine the probability of the activation of transposon operations.

As demonstrated in Figure 3, each particle which can be regarded as a chromosome consists of the same number of genes as the size of its position vector and each gene holds a real number of the corresponding decision variable.

Comparing with other the state-of-the-art PSO and QPSO variants, EB-QPSO performs more competitively in solving unconstrained optimization problems in terms of better global search capability and faster convergence rate as demonstrated in our recent work [42, 58] and has been applied in solving practical problems like cancer gene classification [62, 63].

4. DEB-QPSO for ED Problems

In this section, we will propose a DEB-QPSO algorithm based on our recent work of using elitist breeding to solve the ED problem. A double elitist breeding strategy is designed to improve the search efficiency and manage the constraint requirement of the complex ED problems. In addition, an improved heuristic technique infeasible particle

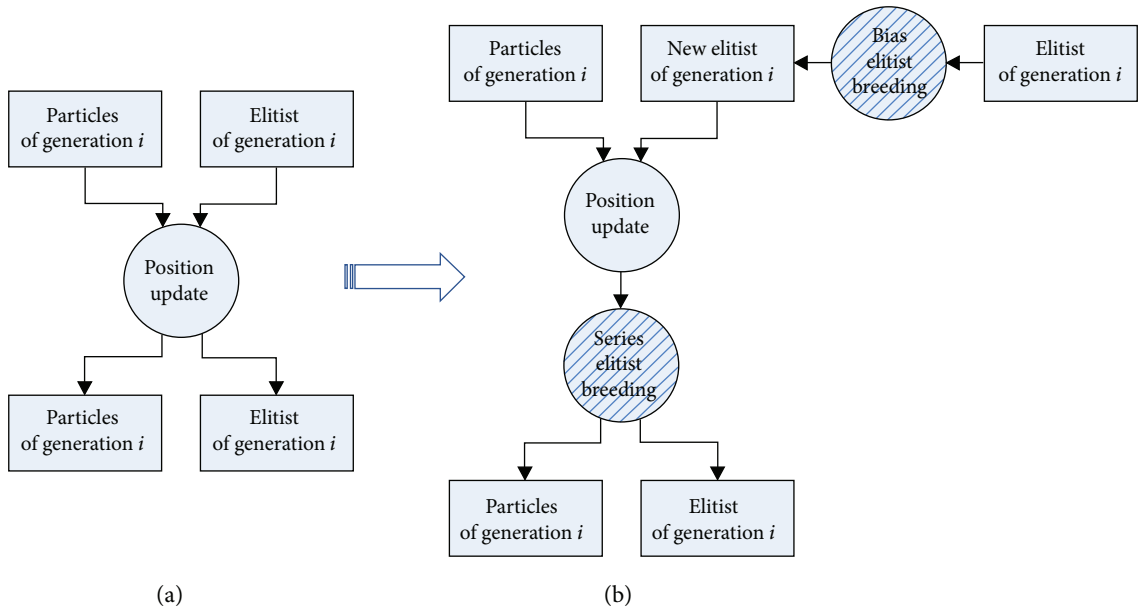

Figure 4: Integration of the double elitist breeding into the evolutionary processes of QPSO.

repositioning is proposed to treat the equality and inequality constraints of ED problems efficiently. Moreover, a novel update method for the pbests and gbest of the swarm is proposed to cooperate with the constraint handling technique. In the rest of the section, the double elitist breeding strategy catered for solving constrained optimization problem is described and is followed by how to use the proposed approach to solve ED problem.

4.1. Elitist Breeding Strategies. The elitists have a major effect on the exploration behavior of the swarm, thus impinging the exploration performance. Obviously, making good use of the elitists is beneficial to promote the exploration for optimal solution. In DEB-QPSO, an elitist pool, epool, consisting of pbests and gbest is constructed. Two elitist breeding strategies are used to improve the global search ability of the algorithm. Generally, the main idea of breeding is to make good use of the elitists to generate new particles through transposon operations. There are two types of elitist breeding operations used: the bias elitist breeding and the series elitist breeding differentiated according to their execution sequences in the proposed DEB-QPSO algorithm and the selection of the type of elitists for breeding. Figure 4 shows the relationship between the elitist breeding and the normal algorithmic operation of QPSO. In Figure 4(a), it gives the relationship between particles and the elitists of the swarm in the original QPSO while Figure 4(b) illustrates the integration of two elitist breeding with the exploration operations of QPSO.

4.2. Bias Elitist Breeding. The bias elitist breeding aims at improving the search efficiency of the algorithm through promoting the particle diversity and assists the constraint handling capability. The bias elitist breeding is not executed on every search cycle but once at the interval of every λ iteration. It places impact to particles by substituting the elitist individuals in memory with better-fitted new-bred individuals. Breeding operation will be conducted on every particle in the swarm. New particles will be generated through the transposon with an elitist selected randomly from the original elitist pool made up of the pbests and the gbest of the swarm. Only the feasible elitists are selected for transposon. If the newly generated particle has a better fitness evaluated by the objective function, it will become the personal best of that particle and be kept in the elitist pool; otherwise, the original personal best of that particle will be kept in the elitist pool. In other words, the pbest of each particle and the gbest will be substituted by the corresponding better solutions in the newly generated subswarm. Such elitist breeding scheme is biased towards the generation of elitists in the feasible zone. The idea is illustrated in Figure 5.

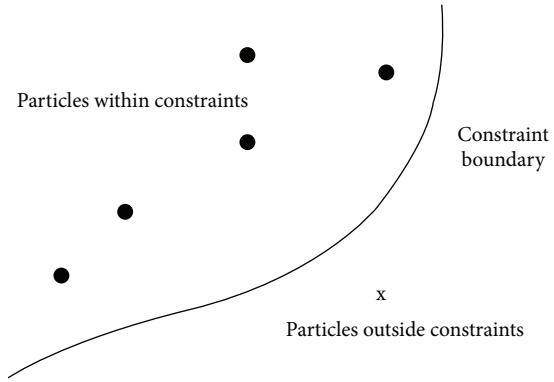

Figure 5: Particles participated in transposon: an infeasible particle undergoes transposon with a feasible elitist randomly selected from the elitist pool.

```
1.  Procedure of Bias elitist breeding
2.  for i = 1 to swarm size N
3.      epool_eb = transposon (epool, particle[i];);
4.      evaluate (epool_eb);
5.      if f (epool_eb[i]) < f (pbest[i]);
6.          pbest [i] = epool_eb [i];
7.      endif
8.  endfor
```

Pseudocode 1. The pseudocodes for bias elitist breeding operation.

For an infeasible particle, located outside the constraint boundary, undergoing the bias elitist breeding with a randomly selected elitist located within the constraint boundary, it is more likely to have a feasible particle generated for the infeasible particle through the transposon with a feasible elitist chosen from epool. In such a way, the bias elitist breeding not only promotes the diversity of the swarm but also is able to assist the constraint handling capability in order to enhance the global search exploration in return. The pseudocodes of bias elitist breeding operation are given in Pseudocode 1.

4.3. Series Elitist Breeding. The series elitist breeding is performed right after the position update procedure of each particle. It will be conducted for every search cycle. Different from the bias elitist breeding, the newly updated particle undergoes transposon with an elitist selected randomly among all elitists from epool to generate a trial vector so as to effectively exploit and explore the search space. The purpose of the series elitist breeding is to promote the diversity of the swarm. The epool is updated accordingly with the newly generated particle. The procedure of series elitist breeding is the same as the bias one, but all the elitists participated in the random selection of transposon.

4.4. Constraint Handling with Particle Repositioning. To keep the particle search in the correct direction, it is essential to satisfy the equality and inequality constraints simultaneously. The standard penalty function method is not effective in handling the equality constraints. Researches have focused on the heuristic strategies to modify infeasible solutions to satisfy the equality constraints. Emphasis is on adjusting the value of the elements in each solution in every search iteration meticulously to satisfy the constraints [9, 64, 65]; obviously, such strategies are computationally expensive and inefficient in finding the optimum solution. As mentioned, the infeasible particle which resulted from the position update may have a chance to migrate to the feasible zone through the series elitist breeding. Therefore, an improved heuristic technique based on the heuristic strategy presented in [64] and combined with the complementary update method for pbests and gbest for infeasible particle repositioning to satisfy the constraints is proposed. If the infeasible particle cannot be corrected through the series elitist breeding, it will be repositioned to a new location satisfying the constraints through the method described as follows:

Step 1. If necessary, to satisfy the inequality constraint of power output limit given by (6), modify the value of the jth element in the ith individual as follows:

$$P_{i,j} = \begin{cases} P_{i,j}, & \text{if } P_{j,\min}{}' \le P_{i,j} \le P_{j,\max}{}', \\ P_{j,\min}{}', & \text{if } P_{i,j} < P_{j,\min}{}', \\ P_{j,\max}{}', & \text{if } P_{i,j} > P_{j,\max}{}'. \end{cases} \tag{16}$$

Step 2. If any element in the ith individual falls within its kth prohibited zone, the value of this element will be adjusted to satisfy the inequality constraint given by (7) as follows:

$$P_{i,j} = \begin{cases} P_{i,k}^{l}, & \text{if } \left(P_{j,k}^{u} - P_{i,j}\right) > \left(P_{i,j} - P_{j,k}^{l}\right), \\ P_{i,k}^{u}, & \text{if } \left(P_{j,k}^{u} - P_{i,j}\right) \le \left(P_{i,j} - P_{j,k}^{l}\right). \end{cases} \tag{17}$$

Step 3. Set $P_i^{l} = P_i$ and set each of the repairing flag RF_j of element j to 0.

Step 4. Calculate P_L (i.e., transmission network loss) using the coefficient formula given by (5).

Step 5. Calculate the equality constraint violation using the following formula:

$$P_{cv} = \sum_{i=1}^{N_g} P_i - P_L - P_D. \tag{18}$$

If the absolute value of P_{cv} is less than the predefined demand tolerance ε, then go to Step 8; otherwise, go to Step 6.

Step 6. From the current individual, randomly select an element j with $RF_j = 0$ (it means the element was not selected so far) and set $RF_j = 1$; if all the elements have been selected before, then go to Step 8.

Step 7. Adjust the value of element j to satisfy the power balance constraint given by (4) as follows:

$$P_{i,j} = \begin{cases} P_{i,j} - \min\left(P_{cv}, \left(P_{i,j} - P_{j,\min}{}'\right) \times \text{randv}\right), & \text{if } P_{cv} > 0, \\ P_{i,j} + \max\left(P_{cv}, \left(P_{j,\max}{}' - P_{i,j}\right) \times \text{randv}\right), & \text{if } P_{cv} \le 0, \end{cases} \tag{19}$$

where randv is a random number uniformly distributed on $[0, 1]$.
If element j falls within its kth prohibited zone, the value of this element will be adjusted to satisfy the prohibited zone constraint as Step 2. Repeat the actions listed in Step 5.

Step 8. If $\max_{\forall j}\{|P_{i,j} - P'_{i,j}|\} < \delta$, then go to Step 9; otherwise, go to Step 3. Here, δ is a temporal adaptive solution convergence tolerance and can be calculated as follows:

$$\delta = \frac{\delta_1 + (T - t) \times (\delta_0 - \delta_1)}{T}, \tag{20}$$

where T is the maximum iteration number and t is the current search iteration number; δ_0 and δ_1 are the initial and final values of δ, respectively.

Step 9. End.

The improved constraint handling method lays on the time-varying δ together with the cooperative update method for pbests and gbest described below to reduce the computational cost and enhance the search efficiency. To handle the constraints effectively, the solution convergence tolerance δ is normally set to a small fixed value in those approaches adopting the heuristic technique as in [64] and thereby leads to heavy computational cost. Apparently, it is unnecessary to use the meticulous method to handle the constraints for each of the individual particles in the whole search procedure. Hence, the time-varying decrement δ is proposed to improve the efficiency of constraint handling. In the early iterations, more infeasible solutions are allowed to appear so as to increase the diversity of the search. Combined with the elitist breeding strategies, the exploration ability of the solution algorithm is thereby enhanced. Conversely, in the later iterations, a stricter criterion is beneficial for generating the feasible solutions so as to enhance the convergence speed of the search.

4.5. pbests *and* gbest *Update.* It is clear that the equality constraint is not guaranteed to be satisfied through the heuristic repairing procedure. To cooperate with the constraint handling method, a novel update method for pbests and gb est is introduced following the constraint handling step. The method is as shown below.

Step 1. Calculate P_L using coefficient (5).

Step 2. Calculate the absolute value of equality constraint violation (called constr) according to the formula as follows:

$$\text{constr} = abs\left(\sum_{i=1}^{N_g} P_i - P_L - P_D\right). \tag{21}$$

If constr is less than the demand tolerance ε, then set constr to 0; otherwise, calculate the probability (called prob) to accept the infeasible solutions as the elitist (pbest and gbest) as follows:

$$\text{prob} = \frac{t}{T}, \tag{22}$$

where T is the maximum iteration number and t is the current search iteration number.Then recontribute the value of constr with the equation below:

$$\text{constr} = \begin{cases} 0, & \text{if randv} > \text{prob}, \\ \text{constr}, & \text{if randv} \le \text{prob}, \end{cases} \tag{23}$$

where randv is a random value chosen uniformly within the interval $[0, 1]$.

Step 3. Update pbest of each particle with the following rules:

(1) If constr of the current particle is less than constr of its pbest, set the current particle as its updated pbest.

(2) If constr of the current particle is equal to constr of its pbest and the objective function value of the current particle is less than the objective function value of its pbest, set the current particle as its updated pbest.

(3) Otherwise, keep the pbest of the current particle unchanged.

Step 4. Update gbest with the following rule: select the pbest with the smallest constr as the new gbest of the current iteration; if more than one pbest have the same smallest value of constr, use the pbest with the smallest objective function value as the new pbest.

Step 5. Stop the pbest and gbest update procedure.

Obviously, the probability of accepting infeasible solution as elitists is decreasing with respect to the search iteration. Such scheme aims to enhance the solution diversity in the early search iterations and promotes the search efficiency in the feasible area in the later search stage.

5. Implementation of the DEB-QPSO Algorithm

The decision variables in ED problems are the real power output of the units in the systems. A particle is a set of real number elements corresponding to the units' output represented particle by the position vector $\mathbf{x} = (x_1, x_2, \ldots, x_D)$ where D is the number of units, which signifies a solution in the search responsible for the exploration of the search space. The proposed DEB-QPSO algorithm is summarized as in Table 1:

5.1. Initialization of Population. According to (6), the minimum and maximum outputs of the ith generator are defined as follows:

$$\begin{aligned} P'_{i,\min} &= \max\left\{P_{i,\min}, P_i^0 - DR_i\right\}, \\ P'_{i,\max} &= \min\left\{P_{i,\max}, P_i^0 + UR_i\right\}. \end{aligned} \tag{24}$$

Table 1: The process of DEB-QPSO.

Step 1. Randomly initialize the position of a population while satisfying the constraints.
Step 2. Update the positions of particles according to (12).
Step 3. Perform the series elitist breeding operation.
Step 4. If necessary, repair the position of particles to satisfy the constraints.
Step 5. Update pbests and gbest.
Step 6. Perform the bias elitist breeding operation when the criterion is met.
Step 7. Go to step 2 until the stopping criterion is met.

Therefore, a set of particles is initialized randomly as follows:

$$P_{i,j}^{\text{init}} = P_{j,\min}{}' + \text{randv}_{i,j} \times \left(P_{j,\max}{}' - P_{j,\min}{}'\right), \tag{25}$$

where $\text{randv}_{i,j}$ is the random number generated using the uniform probability distribution function in the range $[0, 1]$.

5.2. Position Update. For each particle, the position update is conducted according to the QPSO algorithm signified by (8).

5.3. Series Elitist Breeding. The series elitist breeding is performed on each particle with the elitist randomly selected from epool. New subswarm is generated. Since the resulting subswarm is not always guaranteed to satisfy the constraints, the improved particle repositioning is conducted.

5.4. Update of pbests *and* gbest. The pbests of each particle at iteration $t + 1$ is updated according to the described updating procedures. Obviously, gbest is set as the best evaluated position among all the pbests.

5.5. Bias Elitist Breeding. To bias the swarm towards the feasible region, each particle is going through the bias elitist breeding for every λ iteration.

5.6. Stopping Criteria. The proposed DEB-QPSO algorithm is terminated if the iteration reaches a predefined maximum number.

6. Case Studies and Results

The proposed DEB-QPSO approach is applied to three different widely used test case power systems posing different difficulties to optimization algorithms: (i) a 15-unit system with prohibited operating zones, ramp rate limits, and transmission network losses, (ii) a 40-unit system with valve-point effects, prohibited operating zones, and ramp rate limits, and (ii) a 140-unit Korean power system with valve-point effects, prohibited operating zones, and ramp rate limits.

To evaluate the solution quality and robustness fairly, 50 independent runs are conducted for each case. The setup for the proposed DEB-QPSO algorithm is as follows:

Table 2: Best solution obtained using the proposed DEB-QPSO (case I).

Bus number	Output	Bus number	Output
P_1 (MW)	454.9997	P_9 (MW)	60.5887
P_2 (MW)	380	P_{10} (MW)	159.9958
P_3 (MW)	129.9998	P_{11} (MW)	80
P_4 (MW)	130	P_{12} (MW)	79.9992
P_5 (MW)	170	P_{13} (MW)	25
P_6 (MW)	459.9998	P_{14} (MW)	15
P_7 (MW)	430	P_{15} (MW)	15
P_8 (MW)	68.7781		
ΣP_i (MW)		2660. 3611	
P_{loss} (MW)		30.3611	
F_{total} (\$/h)		32701.1557	

(1) The maximum object function evaluation numbers (FEs) are 6000, 20,000, and 20,000 for test systems 1, 2, and 3, respectively.

(2) The population size is 20.

(3) The contraction-expansion coefficient α decreases linearly from 0.6 to 0.5.

(4) CR in serial elitist breeding is fixed at 0.6.

(5) λ is 2.

(6) ε is set to $1 \times 10^{-10} \times$ (total power load demand), and it is much stricter than the parameter setting in [24].

(7) δ_0 and δ_1 are set at 1×10^{-2} and 1×10^{-3}, respectively.

To make a direct comparison, simulation experiments of the three test systems are conducted with the QPSO and its two variants, QPSO-DM(1) and QPSO-DM(2), proposed to solve the ED problem in [39] with the same population size and FEs as set in the DEB-QPSO algorithm. In addition, to assess the efficiency of the proposed elitist breeding strategies and the proposed constraint handling method, the proposed constraint handling and the one proposed in IPSO [64] are applied, respectively, to the original QPSO under the same parameter settings as in the DEB-QPSO algorithm to form two other algorithms, namely, QPSO-EDP(1) and QPSO-EDP(2), for comparison. Furthermore, the computational results found by some other the state-of-the-art methods reported in the literature are compared as well. All the simulations are conducted under the computing environment with a notebook PC, 4 GB RAM, Core i3 2.13GHz CPU clock speed, Microsoft Windows 7, and MATLAB 2010a.

For each test case, there are two tables showing the simulation results: one for the best fuel cost values obtained by DEB-QPSO with the corresponding generation power outputs after 50 independent runs (Tables 2, 3, and 4 for case I, case II, and case III, resp.) and the other for the result summary of the best, average, and

Table 3: Best solution obtained using the proposed DEB-QPSO (case II).

Bus number	Output	Bus number	Output	Bus number	Output	Bus number	Output
P_1 (MW)	110.7998	P_{11} (MW)	168.7821	P_{21} (MW)	523.2794	P_{31} (MW)	190.0000
P_2 (MW)	110.7998	P_{12} (MW)	168.0552	P_{22} (MW)	523.2794	P_{32} (MW)	190.0000
P_3 (MW)	97.3999	P_{13} (MW)	214.7598	P_{23} (MW)	523.2794	P_{33} (MW)	190.0000
P_4 (MW)	179.7331	P_{14} (MW)	400.0000	P_{24} (MW)	523.2794	P_{34} (MW)	164.7998
P_5 (MW)	87.7999	P_{15} (MW)	394.2794	P_{25} (MW)	523.2794	P_{35} (MW)	164.7998
P_6 (MW)	140.0000	P_{16} (MW)	304.5196	P_{26} (MW)	523.2794	P_{36} (MW)	164.7998
P_7 (MW)	259.5997	P_{17} (MW)	489.2794	P_{27} (MW)	10.0000	P_{37} (MW)	110.0000
P_8 (MW)	284.5997	P_{18} (MW)	489.2794	P_{28} (MW)	10.0000	P_{38} (MW)	110.0000
P_9 (MW)	284.5997	P_{19} (MW)	511.2794	P_{29} (MW)	10.0000	P_{39} (MW)	110.0000
P_{10} (MW)	130.0000	P_{20} (MW)	511.2794	P_{30} (MW)	87.7999	P_{40} (MW)	511.2794
ΣP_i (MW)		10500.0000			F_{total} (\$/h)		121472.7668

Table 4: Best solution obtained for the 140-unit system using DEB-QPSO (case III).

Bus number	Output	Bus number	Output	Bus number	Output	Bus number	Output	Bus number	Output
P_1 (MW)	117.2970	P_{29} (MW)	500.9966	P_{57} (MW)	103.8112	P_{85} (MW)	115.0175	P_{113} (MW)	94.1953
P_2 (MW)	188.7133	P_{30} (MW)	501	P_{58} (MW)	198.0444	P_{86} (MW)	207.0494	P_{114} (MW)	94.0038
P_3 (MW)	189.8084	P_{31} (MW)	506	P_{59} (MW)	311.5666	P_{87} (MW)	207.0172	P_{115} (MW)	244
P_4 (MW)	190	P_{32} (MW)	505.9437	P_{60} (MW)	285.0454	P_{88} (MW)	177.3728	P_{116} (MW)	244.2227
P_5 (MW)	168.5109	P_{33} (MW)	505.9441	P_{61} (MW)	163.5463	P_{89} (MW)	176.1600	P_{117} (MW)	244.0369
P_6 (MW)	188.1695	P_{34} (MW)	505.9737	P_{62} (MW)	95.4018	P_{90} (MW)	175.0217	P_{118} (MW)	95.1762
P_7 (MW)	489.9914	P_{35} (MW)	499.8883	P_{63} (MW)	160.7681	P_{91} (MW)	175.1082	P_{119} (MW)	95.0278
P_8 (MW)	489.9733	P_{36} (MW)	499.9484	P_{64} (MW)	165.9874	P_{92} (MW)	579.9638	P_{120} (MW)	116.0736
P_9 (MW)	495.9999	P_{37} (MW)	240.9973	P_{65} (MW)	487.1185	P_{93} (MW)	644.9552	P_{121} (MW)	175.0168
P_{10} (MW)	495.9738	P_{38} (MW)	240.9804	P_{66} (MW)	197.9387	P_{94} (MW)	983.9236	P_{122} (MW)	2.1429
P_{11} (MW)	495.9997	P_{39} (MW)	773.9365	P_{67} (MW)	488.8266	P_{95} (MW)	978	P_{123} (MW)	4.0436
P_{12} (MW)	495.9950	P_{40} (MW)	768.9871	P_{68} (MW)	490	P_{96} (MW)	681.9999	P_{124} (MW)	15
P_{13} (MW)	505.9779	P_{41} (MW)	3.0000	P_{69} (MW)	130.1504	P_{97} (MW)	719.9820	P_{125} (MW)	9.0005
P_{14} (MW)	508.9738	P_{42} (MW)	3.0091	P_{70} (MW)	234.8483	P_{98} (MW)	718	P_{126} (MW)	12.0286
P_{15} (MW)	505.9993	P_{43} (MW)	249.7749	P_{71} (MW)	137.3286	P_{99} (MW)	719.9486	P_{127} (MW)	10.0056
P_{16} (MW)	504.9864	P_{44} (MW)	242.9736	P_{72} (MW)	325.2732	P_{100} (MW)	963.9992	P_{128} (MW)	112.1078
P_{17} (MW)	505.9858	P_{45} (MW)	249.9237	P_{73} (MW)	195.6645	P_{101} (MW)	957.9839	P_{129} (MW)	4.0005
P_{18} (MW)	505.8171	P_{46} (MW)	249.3941	P_{74} (MW)	175.3521	P_{102} (MW)	1006.9750	P_{130} (MW)	5.0025
P_{19} (MW)	504.8906	P_{47} (MW)	244.7004	P_{75} (MW)	186.0201	P_{103} (MW)	1005.9920	P_{131} (MW)	5
P_{20} (MW)	504.9952	P_{48} (MW)	248.0422	P_{76} (MW)	175.1273	P_{104} (MW)	1012.9910	P_{132} (MW)	50.3038
P_{21} (MW)	504.9956	P_{49} (MW)	249.8546	P_{77} (MW)	175.5258	P_{105} (MW)	1019.9920	P_{133} (MW)	5.0258
P_{22} (MW)	504.9881	P_{50} (MW)	249.7768	P_{78} (MW)	330.9662	P_{106} (MW)	953.9933	P_{134} (MW)	42.0002
P_{23} (MW)	504.9728	P_{51} (MW)	169.2291	P_{79} (MW)	530.8824	P_{107} (MW)	952	P_{135} (MW)	42.0500
P_{24} (MW)	504.9863	P_{52} (MW)	165.0001	P_{80} (MW)	530.9256	P_{108} (MW)	1006	P_{136} (MW)	41.0118
P_{25} (MW)	536.9815	P_{53} (MW)	165.7448	P_{81} (MW)	366.5174	P_{109} (MW)	1012.9980	P_{137} (MW)	17.0102
P_{26} (MW)	536.7416	P_{54} (MW)	165.5105	P_{82} (MW)	56.01368	P_{110} (MW)	1021	P_{138} (MW)	7
P_{27} (MW)	548.9839	P_{55} (MW)	180.0231	P_{83} (MW)	115.1456	P_{111} (MW)	1014.9750	P_{139} (MW)	7.1937
P_{28} (MW)	548.7910	P_{56} (MW)	180	P_{84} (MW)	115.0067	P_{112} (MW)	94.1349	P_{140} (MW)	26.9094
ΣP_i (MW)		49342.0000			F_{total} (\$/h)		1559989.4523		

worst cost found by the proposed DEB-QPSO and its FEs together with the corresponding result of the other state-of-the-art methods in literatures (Tables 5, 6, and 7 for case I, case II, and case III, resp.). In addition, to access the effectiveness of the proposed constraint handling method in reducing the computational time, the average

Table 5: Results obtained by optimization methods (case I).

Methods	Best cost ($/h)	Worst cost ($/h)	Mean cost ($/h)	FEs	CPU time (s)
PSO [11]	32858.00	33331.00	33105.00	20,000	/
GA [11]	33113.00	33337.00	33228.00	20,000	/
SA-PSO [12]	32708.00	32789.00	32732.00	20,000	/
IPSO [13]	32,709	—	32784.5	10,000	/
DSPSO-TSA [14]	32715.06	32730.39	32724.63	6000	/
MTS [22]	32716.87	32796.13	32767.4	100,000	/
IA_EDP [7]	**32698.20***	32823.78	32750.22	20,000	/
QPSO [39]	33014.21	33342.30	33148.77	6000	/
QPSO-DM(1) [39]	32970.85	33406.27	33163.26	6000	/
QPSO-DM(2) [39]	32927.93	33353.23	33156.34	6000	/
QPSO-EDP(1)	32707.99	32718.39	32712.02	6000	4.27
QPSO-EDP(2)	32710.14	32719.27	32716.94	6000	6.35
DEB-QPSO	**32701.16**	**32701.18**	**32701.17**	6000	4.68

*In the case of IA_EDP, power balance constraint is not satisfied.

Table 6: Results obtained by optimization methods (case II).

Methods	Best cost ($/h)	Worst cost ($/h)	Mean cost ($/h)	FEs	CPU time (s)
NAPSO [15]	121491.0662	121491.5261	121491.2756	100,000	/
FAPSO [15]	122261.3706	122597.5196	122471.0751	100,000	/
PSO [15]	124875.8523	125368.9204	125162.7011	100,000	/
IABC [16]	121491.2751	121582.3865	121539.4175	100,000	/
IABC-LS [16]	121488.7636	121582.2525	121526.0333	100,000	/
QPSO [39]	126615.4498	128679.5909	128621.1241	20,000	/
QPSO-DM(1) [39]	131291.9433	131586.1562	131368.4071	20,000	/
QPSO-DM(2) [39]	131318.4412	133393.5961	131739.5250	20,000	/
QPSO-EDP(1)	121681.46	121708.01	121693.42	20,000	5.38
QPSO-EDP(2)	121875.23	121907.26	121895.49	20,000	7.96
DEB-QPSO	**121472.77**	**121483.67**	**121477.52**	20,000	6.15

Table 7: Results obtained by optimization methods (case III).

Methods	Best cost ($/h)	Worst cost ($/h)	Mean cost ($/h)	FEs	CPU time (s)
IPSO [64]	1657962.73	1657962.73	1657962.73	300,000	/
CQGSO [40]	1657962.72	1657962.77	1657962.74	120,000	/
DEL [18]	1657962.71	—	1658001.70	225,000	/
DE [19]	1566264.99	1566308.37	1566285.56	250,000	/
IDE [19]	1564648.66	1564682.73	1564663.54	250,000	/
QPSO [39]	1795570.26	1896439.75	1837102.23	20,000	/
QPSO-DM(1) [39]	1826727.13	1926994.21	1882621.38	20,000	/
QPSO-DM(2) [39]	1836848.28	1925476.87	1883407.62	20,000	/
QPSO-EDP(1)	1562612.57	1564828.72	1564105.64	20,000	7.21
QPSO-EDP(2)	1563052.83	1565314.23	1564482.81	20,000	10.39
DEB-QPSO	**1559989.45**	**1560739.23**	**1560215.43**	20,000	8.48

CPU time required by the DEB-QPSO, QPSO-EDP(1), and QPSO-EDP(2) algorithms are listed in Tables 5, 6, and 7 for case I, case II, and case III, respectively.

Moreover, the convergence characteristics of the median results obtained in the 50 runs with the proposed DEB-QPSO algorithm and the compared QPSO-EDP(1) and QPSO-

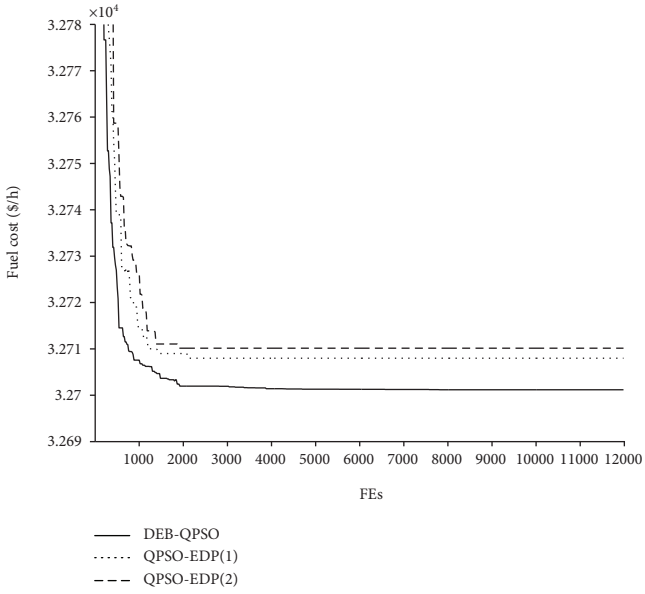

Figure 6: Convergence properties for case I.

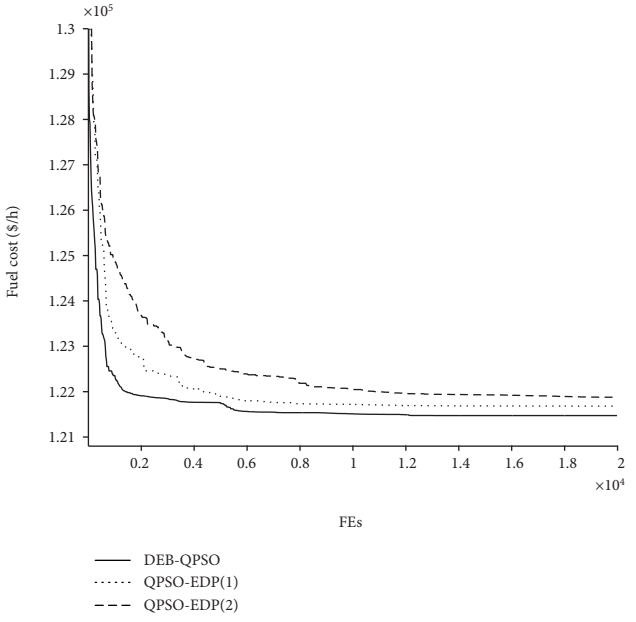

Figure 7: Convergence properties for case II.

EDP(2) algorithms for the three test systems are illustrated in Figures 6, 7, and 8, respectively.

6.1. Case I: 15-Unit System. The test system consists of 15 generating units. The expected load demand is 2630 MW. The system parameters and the B coefficients can be found in [10]. The main difficulties of this system for any optimization algorithm are the nonlinear and noncontinuous decision space and the power balance constraint with network transmission losses.

From Table 5, it clearly shows that the proposed method obtains the best result with lowest FEs than other techniques

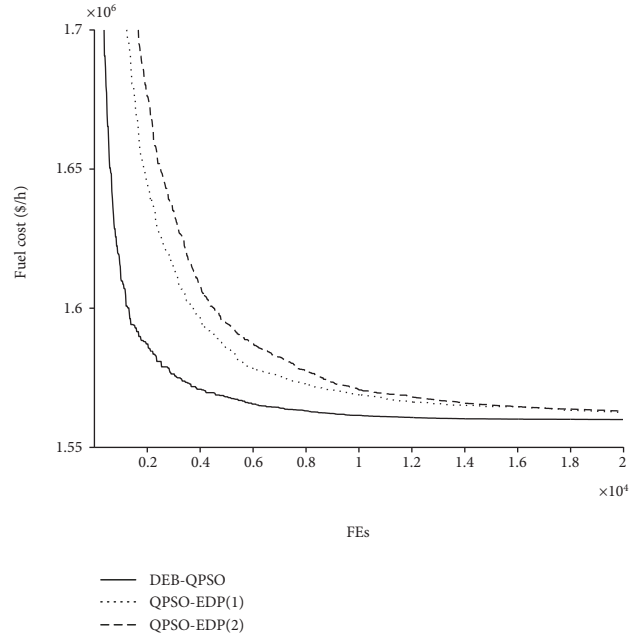

Figure 8: Convergence properties for case III.

except for IA_EDP [7] in the 15-generating-unit test systems. However, it should be noted that the exact power loss computed from the best solution found by IA_EDP [7] is actually 30.2825 instead of 30.0187 as reported in the corresponding literature, which shows that the total generated power of the schedule is much less than the total load demand plus its total line loss; obviously, the best solution reported in [7] is in fact infeasible. It can be concluded that the elitist breeding strategy of the proposed DEB-QPSO algorithm is not only capable of locating the optimal solution but also capable of being computationally effective as fewer functional evaluations are required comparing to other algorithms in the 15-generating-unit test system.

Moreover, the robustness of DEB-QPSO is confirmed with the evidence that the difference between worst cost and the best cost obtained by DEB-QPSO is no more than 0.01% of the best cost. The impact of the two key components of DEB-QPSO towards the search of optimal solution is also revealed individually from the simulation results. On one hand, it can be concluded from the results obtained by DEB-QPSO and QPSO-EDP(1) that the proposed elitist breeding strategies are beneficial for improving the global search capability of QPSO since QPSO-EDP(1) employed the same constraint handling as in the proposed DEB-QPSO. On the other hand, the efficiency of the proposed constraint handling method is validated not only with the results obtained by QPSO-EDP(1), which are better than those obtained by QPSO-EDP(2) using the IPSO's constraint handling method in [64], but also required less computational time to locate the solutions. Furthermore, the extra processing for elitist breeding is computational effective as the DEB-QPSO only increases less than 10% of the computational time when comparing with QPSO-EDP(1).

Besides, the simulation results also reveal that algorithms with heuristic constraint handling such as QPSO-EDP(1),

QPSO-EDP(2), IPSO, and the proposed DEB-QPSO have better performance and computational effectiveness than those using penalty function for constraint handling.

It can be observed from Figure 6 that the DEB-QPSO algorithm converges to the result very close to the final optimal solution in early iterations and has a better convergence property than QPSO-EDP(1) and QPSO-EDP(2) algorithms in test case I.

6.2. Case II: 40-Unit System. The test system consists of 40 thermal units and 5 of which exhibit prohibited zones. The transmission losses are not considered and the expected load demand is 10,500 MW. All the generators in this system are subjected to valve-point effects resulting in a solution space with multiple minima. Because of the large dimension and multiple minima, it is hard to locate the global minimum. The fuel cost function coefficients and active power generation limits for this system can be obtained from Table 7 in reference [15] and the prohibited operation zones from Table 12 in reference [15].

It can be observed from Table 4 that the DEB-QPSO algorithm has generated very satisfactory stable solutions in the 40-generating-unit test system. The DEB-QPSO algorithm is able to obtain the best costs among the compared approaches with the lowest FEs; besides, the best cost and the worst cost are all within ±0.01% of the cost mean. Similarly, the efficiencies of the proposed elitist breeding strategies and the constraint handling method are both demonstrated positively in the test results in terms of the solution obtained and the computational efforts required to reach to the solution comparing to the compared algorithms. Moreover, the QPSO-EDP(1) algorithm with the proposed constraint handling outperforms the QPSO-EDP(2) algorithm while the DEB-QPSO algorithm has better solution than both QPSO-EDP(1) and QPSO-EDP(2) algorithms as in case I. It is obvious that the proposed DEB-QPSO algorithm has the best convergence performance among the three compared algorithms as shown in Figure 7.

6.3. Case III: 140-Unit System. To demonstrate the capability of the DEB-QPSO algorithm to the large-scale power systems, the proposed method is evaluated on a Korean power system consisting of 140 generators with ramp rate limits with the hydro and pump storage plants not being considered. Twelve of the generating units have the cost function with valve-point effects, and four generating units have the prohibited operating zones.

Since the 140-unit system is a larger system with more nonlinear elements and so as local minima; it is far more difficult to find the global solution than case II. System parameters of the test system are taken from [64] with the load demand set at 49,342 MW. It can be observed in Table 7 that the proposed DEB-QPSO algorithm outperforms the compared methods. Moreover, even the worst result found by the DEB-QPSO algorithm is less costly than the best result of other compared methods, which reveals that the proposed algorithm is able to solve the large-scale ED problems with valve-point effect and prohibited zones effectively.

In addition, the robustness of the DEB-QPSO algorithm is obviously demonstrated by the fact that all the costs obtained by the DEB-QPSO algorithm are within ±0.01% of the mean value. Comparison of the computational time needed for the ED problem by the DEB-QPSO, QPSO-EDP(1), and QPSO-EDP(2) algorithms supports the efficiencies of the proposed elitist breeding strategies and constraint handling method. In Figure 8, the proposed DEB-QPSO algorithm exhibits better convergence properties in solving the large-scale nonconvex ED problems.

7. Conclusion

This paper proposes a DEB-QPSO approach for solving nonconvex, nonsmooth, and nonlinear ED problems. It combines the basic evolutionary processes of QPSO with two elitist breeding strategies, and an efficient improved heuristic constraint handling technique is proposed to solve the ED problems. The bias elitist breeding combined with the series elitist breeding is devised to improve the search efficiency of the algorithm. To handle the constraints, the improved heuristic technique for repairing position of particles and a novel pbests and gbest update method are proposed. These strategies reduce the computational efforts and improve the search efficiency of the solution algorithm for solving ED problems. Such characteristics are demonstrated consistently in all test cases.

The proposed DEB-QPSO method was tested on the ED problems of three widely used power system instances of 15 units, 40 units, and 140 units, respectively, with nonconvex, nonsmooth, and nonlinear characteristics of the generators such as valve-points prohibited operating zones with ramp rate limits as well as transmission network losses. The results of the case studies clearly illustrate the superior features of the proposed DEB-QPSO method such as high-quality solutions, robustness properties, and computational effectiveness. Comparing with other algorithms, the DEB-QPSO algorithm can locate better solution effectively. It is mainly because the proposed elitist breeding scheme can aggrandize the diversity of the swarm that is essential to the exploration and exploitation for the search of the global optima. The framework of the DEB-QPSO algorithm can be used as an efficient optimizer providing satisfactory solutions for ED problems with various features. Future researches will be followed to perfect the DEB-QPSO algorithm for solving ED problems under dynamic environment.

Data Availability

The data used to support the findings of this study are available from the corresponding author upon request.

Conflicts of Interest

The authors declare that they have no conflicts of interest.

Acknowledgments

This work is supported by the CityU SRG Research Grant no. 7004541.

References

[1] A. J. Wood and B. F. Wollenberg, *Power Generation, Operation, and Control*, John Wiley & Sons, 2012.

[2] S. Granville, "Optimal reactive dispatch through interior point methods," *IEEE Transactions on Power Systems*, vol. 9, no. 1, pp. 136–146, 1994.

[3] Z.-X. Liang and J. D. Glover, "A zoom feature for a dynamic programming solution to economic dispatch including transmission losses," *IEEE Transactions on Power Systems*, vol. 7, no. 2, pp. 544–550, 1992.

[4] C.-L. Chiang, "Improved genetic algorithm for power economic dispatch of units with valve-point effects and multiple fuels," *IEEE Transactions on Power Systems*, vol. 20, no. 4, pp. 1690–1699, 2005.

[5] D. C. Walters and G. B. Sheble, "Genetic algorithm solution of economic dispatch with valve point loading," *IEEE Transactions on Power Systems*, vol. 8, no. 3, pp. 1325–1332, 1993.

[6] S. Hemamalini and S. P. Simon, "Dynamic economic dispatch using artificial immune system for units with valve-point effect," *International Journal of Electrical Power & Energy Systems*, vol. 33, no. 4, pp. 868–874, 2011.

[7] V. S. Aragón, S. C. Esquivel, and C. A. Coello Coello, "An immune algorithm with power redistribution for solving economic dispatch problems," *Information Sciences*, vol. 295, pp. 609–632, 2015.

[8] B. K. Panigrahi, V. Ravikumar Pandi, and S. Das, "Adaptive particle swarm optimization approach for static and dynamic economic load dispatch," *Energy Conversion and Management*, vol. 49, no. 6, pp. 1407–1415, 2008.

[9] Y. Zhang, D.-w. Gong, N. Geng, and X.-y. Sun, "Hybrid bare-bones PSO for dynamic economic dispatch with valve-point effects," *Applied Soft Computing*, vol. 18, pp. 248–260, 2014.

[10] J. Cai, X. Ma, L. Li, and P. Haipeng, "Chaotic particle swarm optimization for economic dispatch considering the generator constraints," *Energy Conversion and Management*, vol. 48, no. 2, pp. 645–653, 2007.

[11] Z.-L. Gaing, "Particle swarm optimization to solving the economic dispatch considering the generator constraints," *IEEE Transactions on Power Systems*, vol. 18, no. 3, pp. 1187–1195, 2003.

[12] C.-C. Kuo, "A novel coding scheme for practical economic dispatch by modified particle swarm approach," *IEEE Transactions on Power Systems*, vol. 23, no. 4, pp. 1825–1835, 2008.

[13] A. Safari and H. Shayeghi, "Iteration particle swarm optimization procedure for economic load dispatch with generator constraints," *Expert Systems with Applications*, vol. 38, no. 5, pp. 6043–6048, 2011.

[14] S. Khamsawang and S. Jiriwibhakorn, "DSPSO–TSA for economic dispatch problem with nonsmooth and noncontinuous cost functions," *Energy Conversion and Management*, vol. 51, no. 2, pp. 365–375, 2010.

[15] T. Niknam, H. D. Mojarrad, and H. Z. Meymand, "Non-smooth economic dispatch computation by fuzzy and self adaptive particle swarm optimization," *Applied Soft Computing*, vol. 11, no. 2, pp. 2805–2817, 2011.

[16] S. Özyön and D. Aydin, "Incremental artificial bee Colony with local search to economic dispatch problem with ramp rate limits and prohibited operating zones," *Energy Conversion and Management*, vol. 65, pp. 397–407, 2013.

[17] L. dos Santos Coelho and V. C. Mariani, "Combining of chaotic differential evolution and quadratic programming for economic dispatch optimization with valve-point effect," *IEEE Transactions on Power Systems*, vol. 21, no. 2, pp. 989–996, 2006.

[18] L. dos Santos Coelho, T. C. Bora, and V. C. Mariani, "Differential evolution based on truncated Lévy-type flights and population diversity measure to solve economic load dispatch problems," *International Journal of Electrical Power & Energy Systems*, vol. 57, pp. 178–188, 2014.

[19] M. Basu, "Improved differential evolution for economic dispatch," *International Journal of Electrical Power & Energy Systems*, vol. 63, pp. 855–861, 2014.

[20] U. Güvenç, Y. Sönmez, S. Duman, and N. Yörükeren, "Combined economic and emission dispatch solution using gravitational search algorithm," *Scientia Iranica*, vol. 19, no. 6, pp. 1754–1762, 2012.

[21] W.-M. Lin, F.-S. Cheng, and M.-T. Tsay, "An improved Tabu search for economic dispatch with multiple minima," *IEEE Transactions on Power Systems*, vol. 17, no. 1, pp. 108–112, 2002.

[22] S. Pothiya, I. Ngamroo, and W. Kongprawechnon, "Application of multiple Tabu search algorithm to solve dynamic economic dispatch considering generator constraints," *Energy Conversion and Management*, vol. 49, no. 4, pp. 506–516, 2008.

[23] J. H. Park, Y. S. Kim, I. K. Eom, and K. Y. Lee, "Economic load dispatch for piecewise quadratic cost function using Hopfield neural network," *IEEE Transactions on Power Systems*, vol. 8, no. 3, pp. 1030–1038, 1993.

[24] R. Naresh, J. Dubey, and J. Sharma, "Two-phase neural network based modelling framework of constrained economic load dispatch," *IEE Proceedings - Generation, Transmission and Distribution*, vol. 151, no. 3, pp. 373–378, 2004.

[25] N. Sinha, R. Chakrabarti, and P. K. Chattopadhyay, "Evolutionary programming techniques for economic load dispatch," *IEEE Transactions on Evolutionary Computation*, vol. 7, no. 1, pp. 83–94, 2003.

[26] B. K. Panigrahi and V. Ravikumar Pandi, "Bacterial foraging optimisation: Nelder–Mead hybrid algorithm for economic load dispatch," *IET Generation, Transmission & Distribution*, vol. 2, no. 4, pp. 556–565, 2008.

[27] A. Bhattacharya and P. K. Chattopadhyay, "Biogeography-based optimization for different economic load dispatch problems," *IEEE Transactions on Power Systems*, vol. 25, no. 2, pp. 1064–1077, 2010.

[28] L. D. Le, L. D. Ho, D. N. Vo, and P. Vasant, "Hybrid differential evolution and gravitational search algorithm for non-convex economic dispatch," in *Proceedings of the 18th Asia Pacific Symposium on Intelligent and Evolutionary Systems - Volume 2*, pp. 89–103, Springer, 2015.

[29] N. Jayakumar, S. Subramanian, S. Ganesan, and E. B. Elanchezhian, "Grey wolf optimization for combined heat and power dispatch with cogeneration systems," *International Journal of Electrical Power & Energy Systems*, vol. 74, pp. 252–264, 2016.

[30] D. N. Vo, P. Schegner, and W. Ongsakul, "Cuckoo search algorithm for non-convex economic dispatch," *IET Generation, Transmission & Distribution*, vol. 7, no. 6, pp. 645–654, 2013.

[31] L. Srivastava and H. Singh, "Hybrid multi-swarm particle swarm optimisation based multi-objective reactive power dispatch," *IET Generation, Transmission & Distribution*, vol. 9, no. 8, pp. 727–739, 2015.

[32] M. R. AlRashidi and M. E. El-Hawary, "A survey of particle swarm optimization applications in electric power systems," *IEEE Transactions on Evolutionary Computation*, vol. 13, no. 4, pp. 913–918, 2009.

[33] J. Sun, B. Feng, and W. Xu, "Particle swarm optimization with particles having quantum Behavior," in *Proceedings of the 2004 Congress on Evolutionary Computation (IEEE Cat. No.04TH8753)*, pp. 325–331, Portland, OR, USA, 2004.

[34] J. Sun, C.-H. Lai, and X.-J. Wu, *Particle Swarm Optimisation: Classical and Quantum Perspectives*, CRC Press, 2011.

[35] S. M. Mikki and A. A. Kishk, "Quantum particle swarm optimization for electromagnetics," *IEEE Transactions on Antennas and Propagation*, vol. 54, no. 10, pp. 2764–2775, 2006.

[36] S. Li, R. Wang, W. Hu, and J. Sun, "A new QPSO based BP neural network for face detection," in *Fuzzy Information and Engineering*, pp. 355–363, Springer, 2007.

[37] S. N. Omkar, R. Khandelwal, T. V. S. Ananth, G. Narayana Naik, and S. Gopalakrishnan, "Quantum behaved particle swarm optimization (QPSO) for multi-objective design optimization of composite structures," *Expert Systems with Applications*, vol. 36, no. 8, pp. 11312–11322, 2009.

[38] H. M. Dubey, B. K. Panigrahi, and M. Pandit, "Bio-inspired optimisation for economic load dispatch: a review," *International Journal of Bio-Inspired Computation*, vol. 6, no. 1, pp. 7–21, 2014.

[39] J. Sun, W. Fang, D. Wang, and W. Xu, "Solving the economic dispatch problem with a modified quantum-behaved particle swarm optimization method," *Energy Conversion and Management*, vol. 50, no. 12, pp. 2967–2975, 2009.

[40] M. Moradi-Dalvand, B. Mohammadi-Ivatloo, A. Najafi, and A. Rabiee, "Continuous quick group search optimizer for solving non-convex economic dispatch problems," *Electric Power Systems Research*, vol. 93, pp. 93–105, 2012.

[41] Y. Wang, B. Li, G. M. Jing, P. Wang, and J. Wang, "Research of constraint handling techniques for economic load dispatch of power System," in *IEEE Congress on Evolutionary Computation*, pp. 1–8, Barcelona, Spain, 2010.

[42] Z.-L. Yang, A. Wu, and H.-Q. Min, "An improved quantum-behaved particle swarm optimization algorithm with elitist breeding for unconstrained optimization," *Computational Intelligence and Neuroscience*, vol. 2015, Article ID 326431, 12 pages, 2015.

[43] K. E. Parsopoulos and M. N. Vrahatis, *Particle Swarm Optimization and Intelligence: Advances and Applications*, IGI Global, 2010.

[44] Y.-l. Zheng, L.-h. Ma, L.-y. Zhang, and J.-x. Qian, "Empirical study of particle swarm optimizer with an increasing inertia weight," in *The 2003 Congress on Evolutionary Computation, 2003. CEC '03*, pp. 221–226, Canberra, ACT, Australia, 2003.

[45] F. Van den Bergh, *An Analysis of Particle Swarm Optimizers, [Ph.D. thesis]*, University of Pretoria, Pretoria, South Africa, 2006.

[46] J. Sun, X. Wu, V. Palade, W. Fang, C.-H. Lai, and W. Xu, "Convergence analysis and improvements of quantum-behaved particle swarm optimization," *Information Sciences*, vol. 193, pp. 81–103, 2012.

[47] J. Sun, W. Fang, X. Wu, V. Palade, and W. Xu, "Quantum-behaved particle swarm optimization: analysis of individual particle behavior and parameter selection," *Evolutionary Computation*, vol. 20, no. 3, pp. 349–393, 2012.

[48] W. Fang, J. Sun, Y. Ding, X. Wu, and W. Xu, "A review of quantum-behaved particle swarm optimization," *IETE Technical Review*, vol. 27, no. 4, pp. 336–348, 2010.

[49] J. Sun, W. Xu, and W. Fang, "A diversity-guided quantum-behaved particle swarm optimization algorithm," in *Asia-Pacific Conference on Simulated Evolution and Learning*, pp. 497–504, Springer, Berlin, Heidelberg, 2006.

[50] K. S. Tang, T. M. Chan, R. J. Yin, and K. F. Man, *Multiobjective Optimization Methodology: A Jumping Gene Approach*, CRC Press, 2018.

[51] J. Sun, W. Xu, and J. Liu, "Parameter selection of quantum-behaved particle swarm optimization," in *Advances in Natural Computation*, pp. 543–552, Springer, Berlin, Heidelberg, 2005.

[52] W. Fang, J. Sun, and X. Wen-bo, "Improved quantum-behaved particle swarm optimization algorithm based on differential evolution operator and its application," *Journal of System Simulation*, vol. 20, no. 24, pp. 6740–6744, 2008.

[53] K. Yang and H. Nomura, "Quantum-behaved particle swarm optimization with chaotic search," *IEICE Transactions on Information and Systems*, vol. E91-D, no. 7, pp. 1963–1970, 2008.

[54] W. Fang, J. Sun, and W. Xu, "Analysis of mutation operators on quantum-behaved particle swarm optimization algorithm," *New Mathematics and Natural Computation*, vol. 05, no. 02, pp. 487–496, 2009.

[55] J. Sun, W. Fang, V. Palade, X. Wu, and W. Xu, "Quantum-behaved particle swarm optimization with Gaussian distributed local attractor point," *Applied Mathematics and Computation*, vol. 218, no. 7, pp. 3763–3775, 2011.

[56] Y. Li, R. Xiang, L. Jiao, and R. Liu, "An improved cooperative quantum-behaved particle swarm optimization," *Soft Computing*, vol. 16, no. 6, pp. 1061–1069, 2012.

[57] M. Xu, L. Zhang, B. du, L. Zhang, Y. Fan, and D. Song, "A mutation operator accelerated quantum-behaved particle swarm optimization algorithm for hyperspectral endmember extraction," *Remote Sensing*, vol. 9, no. 3, p. 197, 2017.

[58] Z. Yang, A. Wu, H. Liao, and J. Xu, "An elitist promotion quantum-behaved particle swarm optimization algorithm," in *2016 8th International Conference on Intelligent Human-Machine Systems and Cybernetics (IHMSC)*, pp. 347–350, Hangzhou, China, 2016.

[59] S. Cheng, Y. Shi, and Q. Quande, "Population diversity based study on search information propagation in particle swarm optimization," in *2012 IEEE Congress on Evolutionary Computation*, pp. 1–8, Brisbane, QLD, Australia, 2012.

[60] J. Chen, B. Xin, Z. Peng, L. Dou, and J. Zhang, "Optimal contraction theorem for exploration–exploitation tradeoff in search and optimization," *IEEE Transactions on Systems, Man, and Cybernetics - Part A: Systems and Humans*, vol. 39, no. 3, pp. 680–691, 2009.

[61] Z. Yang, A. Wu, and H. Min, "A multi-objective PSO algorithm with transposon and elitist seeding approaches," in *2013 Sixth International Conference on Advanced Computational Intelligence (ICACI)*, pp. 64–69, Hangzhou, China, 2013.

[62] P. Chaudhari and H. Agarwal, "Improving feature selection using elite breeding QPSO on gene data set for cancer classification," in *Intelligent Engineering Informatics*, pp. 209–219, Springer, Singapore, 2018.

[63] H. Agarwal and P. Chaudhari, "Enhancing classification accuracy using elite breeding QPSO on gene dataset," in *2017 International Conference on Advances in Computing, Communication and Control (ICAC3)*, pp. 1–6, Mumbai, India, 2017.

[64] J.-B. Park, Y.-W. Jeong, J.-R. Shin, and K. Y. Lee, "An improved particle swarm optimization for nonconvex economic dispatch problems," *IEEE Transactions on Power Systems*, vol. 25, no. 1, pp. 156–166, 2010.

[65] M. N. Abdullah, A. H. A. Bakar, H. Mokhlis, and J. J. Jamian, "An efficient constraint handling approach for economic load dispatch problem with non-smooth cost function," *Applied Mechanics and Materials*, vol. 785, pp. 490–494, 2015.

Hindawi
Complexity
Volume 2018, Article ID 1640395, 11 pages
https://doi.org/10.1155/2018/1640395

Research Article

A Novel Control Strategy on Multiple-Mode Application of Electric Vehicle in Distributed Photovoltaic Systems

Qianwen Zhong,[1,2] **Yize Sun**,[2] **and Lele Peng**[1]

[1]*School of Urban Railway Transportation, Shanghai University of Engineering Science, Shanghai 201620, China*
[2]*School of Mechanical Engineering, Donghua University, Shanghai 201620, China*

Correspondence should be addressed to Yize Sun; sunyz@dhu.edu.cn

Received 21 November 2017; Revised 14 March 2018; Accepted 3 May 2018; Published 11 July 2018

Academic Editor: Tiago Pinto

Considering the booming development of electric vehicle (EV), this article presents a novel control scheme analyzing EV multiple-mode application in a number of distributed photovoltaic (PV) systems, which rationalizes the energy flow among the energy system participants containing a power grid, a grid-connected PV system, power consumption devices, storage batteries, and EV. Based on the control scheme, the authors propose two day-ahead optimal control strategies with different objective functions: one is minimizing the daily electricity expense of an individual distributed PV system and the other is minimizing the daily total expense of distributed PV systems which EV can be connected to. The model has been verified by the actual data and forecast data, respectively. The results show under the individual objective, in the distributed PV system with EV, the electricity expense can obtain an annual reduction of 27.18%. Furthermore, in the distributed PV system with a storage battery as well as EV, the electricity expense can obtain an annual reduction from 30.67% to 81.49% with a storage battery capacity changing from 1 kWh to 20 kWh. Under the total objective, the total expense and even the individual expense have different degrees of reduction. However, the specific benefits should be rerationally distributed by balancing the interests of all the distributed PV systems. In addition, besides the application in the distributed PV systems, this model may have some potential on the development of a regional energy system.

1. Introduction

Due to electric vehicles (EVs) in the past several years showing an explosive development, researchers have found that these mobile distributed storage units have great potential in energy systems in future power grids, especially when coordinated with renewable energy. Therefore, the literature on the rational planning, optimal operation of EVs, and renewable energy sources has mushroomed these years. Wu et al. [1] briefly analyze the possible scenarios of using renewable energy to charge EVs. Chen and Duan [2] deal with the daily EV mileage uncertainty by Monte Carlo simulation and design an optimization and integration method of EV in microgrids with minimizing the total cost of electricity as the goal. ElNozahy et al. [3] also use Monte Carlo simulation to provide a probabilistic planning and scheduling method for an energy storage system integrating EVs and photovoltaic (PV) arrays in a distributed power grid. Guo et al. [4] discuss a two-stage renewable energy generation parking lot economy framework for EVs. The first stage processes uncertainty of renewable energy, and the second stage controls EV charging operation based on a predictive model. Considering the smart grid with EV and PV power generation in an islanding operation mode, Tang et al. [5] provide an online reinforcement learning method called object representation adaptive dynamic programming, which is for the adaptive islanding control unit in smart grids. Hashemi et al. [6] present a sensitivity analysis on feasibility of users supplying energy into power grids, to determine the minimum storage system capacity with different positions of low voltage power grid configuration. It prevents the overvoltage caused by PV high penetration, which presents a definition named residual power curve (RPC). Paterakis et al. [7] give a detailed family energy management system structure to determine the best home appliance scheduling strategy based on demand response on the following day when the price changes and

power peak limits. Kaschub et al. [8] discuss the impact of different incentives and tariffs on PV storage systems in Germany. Cao [9] compares situations of integrated renewable energy to support the construction of the system with the hydrogen energy vehicles and EVs, respectively, through the reasonable control, which provides a better reference for the implementation of EU's 2050 line integration of renewable energy vehicles. Kampezidou et al. [10] compare the economic effects of two types of energy storage systems including EVs and pumped storage on high-penetration renewable energy systems. Assuncao et al. [11] present a technical and economic evaluation model for the simulation of EV battery, which is for the mismatch between demand and PV power generation and guidance of economic policy. Marra et al. [12] propose an energy storage strategy to reduce voltage rise of PV feeders by coordinating the load of EVs as an energy storage mode. An intelligent charging and discharging random scheduling method is proposed by Honarmand et al. [13], which is for a large number of EVs in a parking lot. Meanwhile, they design a self-scheduling model considering PV power generation system and distributed generators in the intelligent parking lot. For the traditional industrial microgrid, Derakhshandeh et al. [14] put forward a kind of electricity and thermal power generation scheduling coordination method, which considers the microgrid characteristics of traditional industry, also with the application of EVs, PV systems, and PV energy storage systems. Howlader et al. [15] focus on the optimal operation scheme of the smart grid with conventional thermal generators and distributed generation. To solve the optimal scheduling problem for hybrid energy microgrid including PV, wind power generation, heat and power cogeneration, energy storage systems, and EV, Liu et al. [16] present an optimal scheduling model considering demand response, with minimum total operation cost which includes the cost of natural gas, the cost of power grid and EV charging, and the discharging cost. In the study of Ju et al. [17], wind power, PV power generation, EV, and conventional power plants are combined into a virtual power plant; considering the uncertainty and demand response, they give a two-way stochastic optimal scheduling model for the virtual plant. On that basis, they further improve the original optimization scheduling model [18] by minimizing the cost, minimizing the energy consumption, and maximizing the profit. Similarly, Coelho et al. [19] design a multiobjective power dispatch model to minimize the total cost of the microgrid of EVs, battery, maximum peak load, extreme difference, and double Sharpe ratio index, and the problem is formulated as a mixed-integer linear programming problem. Jaramillo and Weidlich [20] also propose a multiobjective microgrid optimal scheduling model; besides operating costs and peak power costs, environmental indicators are also taken into account. Gao et al. [21] start from the comfort and economy of the home users and divide the load into three categories: fixed, shiftable, and adjustable loads, and then optimize the scheduling of the home energy system according to different kinds of load. Zhao et al. [22] from residential customers' and public utilities' views build an integrated demand response simulation optimization framework for high penetration of EVs, PV, and energy storage systems under scenarios of TOU price, real-time price, and curtailment price mechanism. Based on the actual operation of dynamic optimization, Bracco et al. [23] establish an intelligent multipower and sustainable building microgrid test platform with the goal of minimizing cost and CO_2 emissions at the University of Genova, Savona University Campus, and experiments show that reasonable scheduling optimization is feasible and effective.

The above lists the literature that considers the optimal dispatching control of EVs. However, as the research topic is still in its infancy, the specific criteria have not yet been determined. Most of the current studies are based on large-scale or medium-scale renewable energy power stations, so there are still a lot of problems that need to be solved or improved for distributed PV systems. Besides the above problems, there are few studies considering the multiple modes of EV which contain the application of G2V, V2G, off-grid, and driving modes as well as testing them in multiple locations.

The arrangement of this article is as follows: firstly, in Section 2, the models of each participant in the distributed PV system are illustrated. Secondly, the novel day-ahead control strategies are presented in Section 3 with different objective functions: one is minimizing the daily electricity expense of an individual distributed PV system and the other is minimizing the daily total expense of distributed PV systems which EV can be connected to. Thirdly, to verify the effectiveness of optimal control strategies, the actual data of PV generation and electricity demand are used first. Then, the results are also calculated using forecast data which could be used to discuss the feasibility under forecasting models. Finally, the conclusions are summarized and future work is briefly introduced.

2. Distributed PV System Model

A commonly distributed system involves the power grid, the PV system, and the storage system. In this article, due to the explosive development of EV, the authors take the EV with vehicle-to-grid (V2G) function into consideration. To simplify the model, a storage battery is used as a representative of the storage system. The most important role of batteries equipped in the distributed PV system is through charging or discharging energy to improve the stability and economy of the energy system, and contrary to the EV's battery, it can be seen as a fixed storage system. The first application of EV battery must satisfy the normal function of EV as a transport. On this basis, it can more be used as an auxiliary storage system participating in the energy adjustment of a distributed PV system. To better distinguish the fixed battery, here, it is seen as a mobile storage system. In the following, a model of each participant in the distributed PV system is introduced or built, which is required in the optimal scheduling control strategy.

2.1. PV Prediction Model. The PV array power output model is selected from [24, 25]:

$$E_{\mathrm{PV}} = f\left(V_{\mathrm{OC}}, I_{\mathrm{SC}}, V_{\mathrm{M}}, I_{\mathrm{M}}, N, N_{\mathrm{s}}, N_{\mathrm{p}}, G, \mathrm{Temp}, t_{\mathrm{in}}\right), \quad (1)$$

where V_{OC} is the open-circuit voltage, I_{SC} is the short-circuit current, V_M is the voltage at maximum power point, I_M is the current at maximum power point, N is the serial number of PV cells in one panel, N_s is the serial number of PV array, N_p is the parallel number of PV array, G represents the solar irradiance, Temp represents the temperature, and t_{in} represents the time interval of the recorded data.

As there must be the difference between the PV model built with parameters from the manufacturer and data recorded in the actual outside environment and the error information of the historical data is missing in this paper, here in this model, the authors assumed that the error of PV power generation forecasting model is consistent with the Gaussian distribution,

$$\mathrm{Er}_{PV} = \frac{\left|E_{PV} - \widehat{E_{PV}}\right|}{E_{PV}} \sim N(\mu, \sigma). \tag{2}$$

In the above equation, Er_{PV} represents the error between the PV forecasting value $\widehat{E_{PV}}$ and the actual generation E_{PV}. Through setting the mean error μ and mean square deviation σ, the PV power generation forecasting values are randomly generated under different conditions by MATLAB software.

2.2. Electricity Load Forecast Model. A Bayesian neural network (BNN) model is established to forecast the load values with 16 load-related inputs. The vectors of inputs, $\mathbf{V}_I$, are shown:

$$\begin{aligned}\mathbf{V}_I = \Big[&\mathbf{t}, \mathbf{d}_t, \mathbf{T}, \mathbf{T}_{n-1}, \mathbf{T}_{n-2}, \mathbf{RH}, \mathbf{RH}_{n-1}, \mathbf{RH}_{n-2}, \mathbf{L}_{n-1}, \mathbf{L}_{n-2},\\ &\cdot \mathbf{L}_{n-3}, \mathbf{L}_{n-4}, \mathbf{L}_{n-(24/t_i)}, \mathbf{L}_{n-(24/t_i)\cdot 2}, \mathbf{L}_{n-(24/t_i)\cdot 7}, \mathbf{L}_{n-(24/t_i)\cdot 7\cdot 2}\Big].\end{aligned} \tag{3}$$

To build the electricity demand forecast model, the input factors which are mostly considered in the existing models would be the time type and the meteorological type. Based on the similar consideration, in this article, time of every day, $\mathbf{t}$; day type (which is defined as integers from 1 to 7 to express Monday to Sunday, resp., and 8 to express special holidays), $\mathbf{d}_t$; ambient temperature, $\mathbf{T}$; and relative humidity, $\mathbf{RH}$, are firstly considered as the inputs. n is used to represent the series order number of historical sample data's intervals. For instance, $\mathbf{T}_{n-1}$ means the temperature vector observed from one interval before the n interval, which is actually the data from the previous interval. Due to no record before the historical first interval, here T_1 is used as the initial value to complement the vector. If other vectors lack some items, the same complement method is used. Besides these vectors, historical load data, $\mathbf{L}$, are also used in inputs to increase the accuracy of the forecast model. With a similar meaning of subscript, the eight historical data vectors in the latter half are actual load in the first past interval, the second past interval, the third past interval, the fourth past interval, the same interval of yesterday, the same interval of the day before yesterday, the same interval in last week with the same day type, and the same interval in the week before last week with the same day type, respectively. These eight inputs of the forecast model basically cover the most relevant historical load values within the past two weeks.

2.3. Storage Battery Model. The control algorithm of the storage battery is designed by geometrical-logical control method in another published article of the authors [26]. The key point of this algorithm can be described as follows. Under a time-of-use (TOU) electricity retail tariff, if it satisfies the condition that the tariff is always higher than the feed-in-tariff (FiT) even considering the inefficiencies of energy transformation, ignoring initial capital and maintenance costs of storage battery system, the best size of the battery should equal the sum of the positive values obtained by the load minus the PV generation in every interval within the shoulder and peak time. When the maximum available storage energy of a battery is less than the optimum size but is larger than the surplus PV energy, the controller will fully charge the battery before the peak time. If the available energy of a battery at one day's beginning is less than the surplus PV energy, the beginning capacity should be used firstly during the morning shoulder shortfall, then the rest should be discharged completely during the morning off-peak time, in order to make the battery empty in preparation for the following period of surplus PV generation.

Besides the above control algorithm of storage batteries, the following (4), (5), and (6) are the assumption or basic limitation on the storage batteries which must be satisfied:

$$E_B = E_{B_+} - E_{B_-}, \tag{4}$$

$$\begin{aligned} 0 \le E_{B_+} &\le P_{B_{\max_{charge}}} \cdot t_{in},\\ 0 \le E_{B_-} &\le P_{B_{\max_{discharge}}} \cdot t_{in},\\ -P_{B_{\max_{discharge}}} \cdot t_{in} \le E_B &\le P_{B_{\max_{charge}}} \cdot t_{in}, \end{aligned} \tag{5}$$

$$E_{B_{size}} \cdot \mathrm{SoC}_{B_{min}} \le E_{B_0} + \left(E_B - E_{B_{loss}}\right) \le E_{B_{size}} \cdot \mathrm{SoC}_{B_{max}}, \tag{6}$$

where E_B is the energy change of battery. When this parameter is positive, it means the battery has been charged during that period; on the opposite, when it is negative, it means the battery has been discharged during that time. To better distinguish the charging and discharging energy, the authors define two parameters, E_{B_+} and E_{B_-}, respectively, to represent them, which are limited to greater or equal to 0 and at the same time only one can be greater than 0. If E_B is negative, the battery is discharged and helping to meet the load. Equation (5) gives the limitations of the battery. In order to extend the life of the battery, manufacturers commonly recommend the optimal and the maximum charging and discharging power rates. $P_{B_{\max_{charge}}}$ and $P_{B_{\max_{discharge}}}$ represent the maximum charging and discharging rates of the battery, based on manufacturer recommendations. Under this case, the constraints of the battery are two inequalities limiting the bidirectional energy flow of the battery. Equation (6) further limits the battery's state of charge (SoC) between the lower bound and upper bound if needed. It should be noticed that here the energy change of all the ordered periods from the initial time

interval to the current time interval is accumulated because the SoC must satisfy this constraint in every moment during the entire optimization duration. In this equation, $E_{B_{size}}$ is the specified capacity of the storage battery. E_{B_0} represents the initial battery energy. $SoC_{B_{min}}$ and $SoC_{B_{max}}$ are the minimum and maximum SoC of the battery, respectively. $E_{B_{loss}}$ is the energy loss of the battery, mostly resulting from heat loss.

It is worth noting that all the parameters used to explain the values related to direction in the model in this article are nonnegative values. For the following illustration, a parameter named B_{max} is also given here to represent the maximum energy that could be used in the storage battery when it is fully charged, which is also mentioned and applied in the geometrical logical analysis battery control algorithm.

2.4. EV Battery Model. Similar to the storage battery models, here the following equations of the EV battery can be obtained:

$$E_{EV} = E_{EV_+} - E_{EV_-}, \tag{7}$$

$$\begin{aligned} 0 \le E_{EV_+} &\le E_{EV_{max_{charge}}} \cdot t_{in}, \\ 0 \le E_{EV_-} &\le E_{EV_{max_{discharge}}} \cdot t_{in}, \\ -P_{EV_{max_{discharge}}} \cdot t_{in} \le E_{EV} &\le P_{EV_{max_{charge}}} \cdot t_{in}, \end{aligned} \tag{8}$$

$$\begin{aligned} E_{EV_{size}} \cdot SoC_{EV_{min}} &\le E_{EV_0} + \left(E_{EV} - E_{EV_{loss}} - E_{trip}\right) \\ &\le E_{EV_{size}} \cdot SoC_{EV_{max}}, \end{aligned} \tag{9}$$

where E_{EV} is the energy change of the EV battery. When this parameter is positive, it means the EV battery has been charged during the duration. If this value is negative, the EV battery has been discharged and helping to meet the load. E_{EV_+} is the energy change in G2V mode. E_{EV_-} is the energy export in V2G mode. Equation (7) gives the energy usage of the EV battery. $P_{EV_{max_{charge}}}$ and $P_{EV_{max_{discharge}}}$ represent the maximum charging and discharging rate of the EV battery, respectively, based on manufacturer recommendations. Equation (9) limits the SoC of the EV battery between the lower bound and upper bound. $E_{EV_{size}}$ is the specific size of the EV battery. E_{EV_0} represents the initial battery energy. $SoC_{EV_{min}}$ and $SoC_{EV_{max}}$ are the minimum and maximum SoC values of the EV battery, respectively. $E_{EV_{loss}}$ is the energy loss of the EV battery, mostly resulting from heat loss. E_{trip} represents the energy consumed when the EV is driving on a certain trip between two known locations within some time. Subscripts are used to distinguish the different trips between locations if necessary, for example, $E_{trip_{ab}}$ represents the energy consumption of the EV battery between location a and location b.

Due to the objective in this article which is to obtain the minimum electricity expenses, the bill reductions should compare with the V2G cost of the EV. In [27], this cost can be calculated by the following:

$$C_a = E_{V2G} \cdot N_d \cdot (C_d + r_e). \tag{10}$$

This equation is used to determine the cost to the EV owner for allowing access to the stored energy in their vehicles, where C_a is the annual cost. E_{V2G} is the energy available in each EV per dispatch in kWh. N_d is the number of dispatches per year. C_d is the cost of battery degradation. r_e is the electricity price.

3. Proposed Control Strategies

As the EV has the transport function, it can move from one location to another. In other words, when the EV is connected to the grid of some parking place, its battery can be applied as a small storage unit to that place.

A comprehensive analysis of EVs applied in the distributed PV systems can be shown in Figure 1. The box on the top left shows two scenarios of one PV system, number 1 PV system, in which the left circle is the distributed PV system with EV connected. The basic participants in one distributed PV system include power grid, grid-connected PV generation, storage battery, electricity load, and EV, which would provide or consume electric energy. The top right box illustrates the two probabilities when the EV is out of the number 1 PV system. One is that the EV is in another distributed PV system, the other is that the EV is driving on a trip. The box on the lower left is all the given states of the distributed PV systems when the EV battery is connected to one of them, and the lower right is the state of the distributed PV system when the EV is driving on some trip from one distributed PV system to another or the EV is off-grid.

The main research content of this article is to design the optimal energy flow of distributed PV systems with EV multiple-mode application under the objective of minimizing the electricity expense. Based on the model described in the above section, the control structure of distributed PV systems can be shown in Figure 2.

It can be seen from the figure that the distributed PV system integral model includes PV generation forecast model, BNN load forecast model, control model of storage battery by geometrical logic analysis methodology, and multiple-mode optimal control of EV battery in distributed PV systems. In order to further discuss the control strategy of distributed PV systems, the above diagram describes a proposed two-level storage system control strategy based on the actual situation of the system. That means in a storage system which includes a storage battery and an EV battery, the storage battery is preferred and firstly used. The technological development at this stage makes the storage equipment still limited by a variety of factors, such as its cost, life, and efficiency, so under such condition the authors make the EV battery only as a secondary and auxiliary option for storage purpose with reasonable and practical significance. It can be found from the figure that the input parameters for the second-level storage system are the remaining surplus PV generation or electricity demand after the first-level control process of storage battery system.

A novel optimal model considering the EV-applied multiple modes can be formulated. Suppose there is an EV storage aggregator which can control the EV battery charging

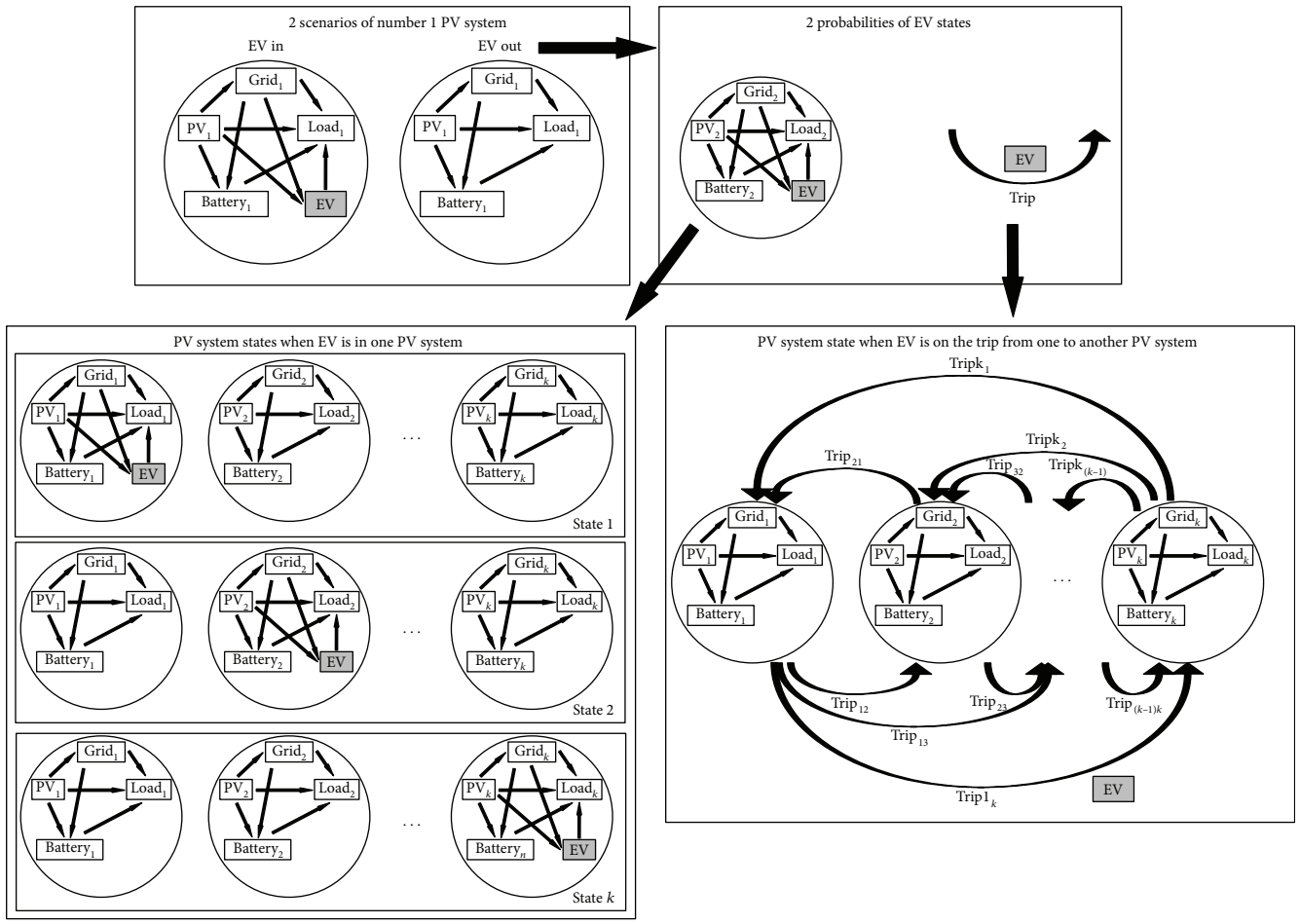

Figure 1: Scenarios of the distributed PV systems with EV multiple-mode application.

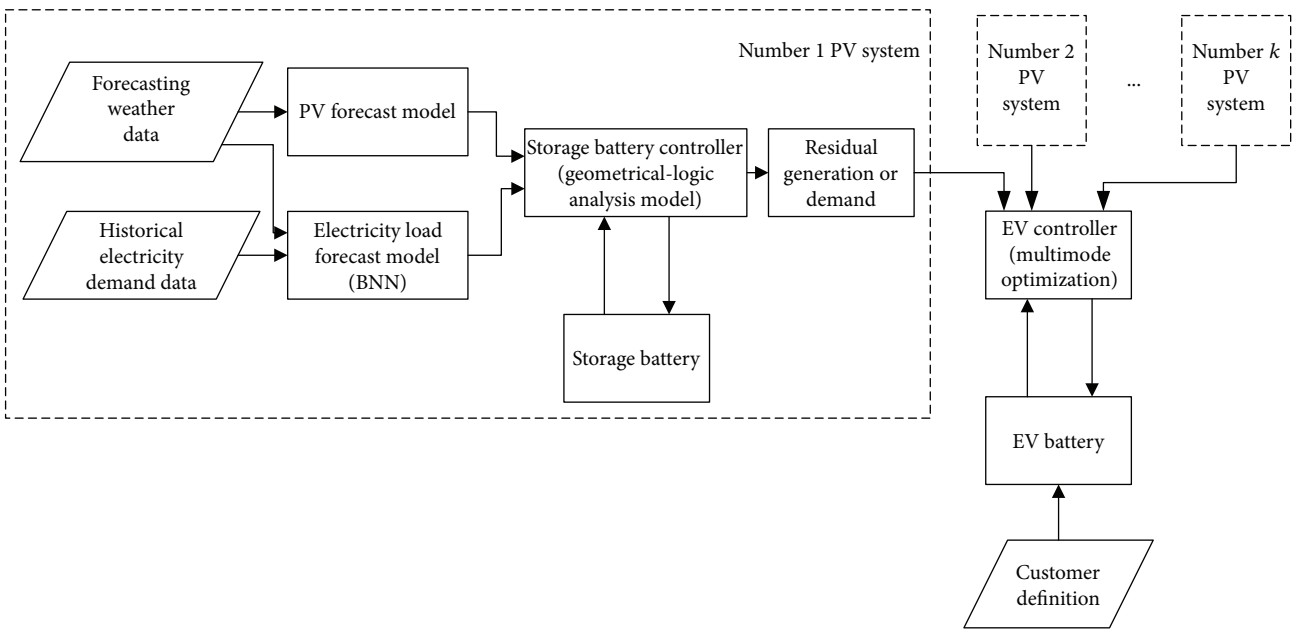

Figure 2: Control schematic of the distributed PV systems with EV multiple-mode application.

and discharging schedule in all the distributed PV systems which the EV can be connected to the grid.

From the above illustration, the following equilibrium equations can be obtained. When the EV is in the number i PV system, the EV battery is deemed as a storage device just like a battery joining the energy flow in one distributed PV system. On the contrary, other distributed PV systems do not have EV battery participating in the energy change.

$$\begin{aligned} &E_{\text{grid}_i}(t) + E_{\text{PV}_i}(t) - E_{\text{B}_i}(t) - E_{\text{load}_i}(t) - E_{\text{EV}}(t) = 0, \\ &E_{\text{grid}_j}(t) + E_{\text{PV}_j}(t) - E_{\text{B}_j}(t) - E_{\text{load}_j}(t) = 0 \ (j \in (1,k) \cap j \neq i). \end{aligned} \tag{11}$$

In the above equation, integer i represents the number i of the ordered distributed PV systems in which the EV battery is being connected to its power grid in time t; (t) represents the corresponding value in ordered period t with observation time interval t_{in}, and the total number of ordered periods is n_{f}; j represents other ordered distributed PV systems without EV connection in time t, and $0 < j < \text{k}$ but $j \neq i$, where k is the number of distributed PV systems. E_{grid}, E_{PV}, E_{load}, E_{B}, and E_{EV} are the energy change of the grid, PV, load, battery, and EV battery in time t, respectively. From an optimal economy view, in this article the proposed optimal control model has been firstly designed with an objective of minimizing electricity cost of one specific distributed PV system.

$$\min \quad C_i = \sum_{t=1}^{n_{\text{f}}} \left(M_i(t) \cdot E_{\text{grid}_{i_+}}(t) - \text{FiT}(t) \cdot E_{\text{grid}_{i_-}}(t) \right), \tag{12}$$

where C_i represents the electricity cost of the number i PV system, n_{f} is the final time order, M_i and FiT are the electricity retail tariff of number i PV system and feed-in-tariff of solar energy, respectively, and E_{grid_+} and E_{grid_-} stand for the energy imported from or exported to the grid in unit interval t_{in}, respectively. From actual condition analysis, this objective is likely to happen when the EV owner wants to obtain the lowest electricity expense of his residence.

Another possible objective may be the minimization of the total electricity cost for all the distributed PV systems in which the EV battery may participate in.

$$\min \quad C_{\text{total}} = \sum_{i=1}^{k} \sum_{t=1}^{n_{\text{f}}} \left(M_i(t) \cdot E_{\text{grid}_{i_+}}(t) - \text{FiT}(t) \cdot E_{\text{grid}_{i_-}}(t) \right). \tag{13}$$

The authors would like to assess, when multiple locations share one EV controller, whether the total electricity cost could be effectively reduced or not. Through the calculations under these two different objectives, the optimal scheduling problem can be analyzed and solved from different views.

The following equations are the constraints of the distributed PV system with net metering when EV is being connected to the grid:

$$\begin{aligned} \text{subject to} \quad & E_{\text{grid}}(t) = E_{\text{grid}_+}(t) - E_{\text{grid}_-}, (t), \\ & E_{\text{grid}_+}(t) \leq E_{\text{load}}(t) + E_{\text{B}}(t) + E_{\text{EV}}(t), \\ & E_{\text{grid}_-}(t) \leq E_{\text{PV}}(t). \end{aligned} \tag{14}$$

This equation gives the limitations of electricity energy from and into the grid. When considering the energy balance, it can be found that the maximum energy import occurs when all the electrical devices simultaneously consume electricity from the grid, and the maximum energy export occurs when all the surplus PV generation is fed into the grid. When the EV is being connected to the grid, the EV battery is available for bidirectional interaction.

On the contrary, when the EV is out of the distributed PV system, the above equation should be

$$\begin{aligned} &0 \leq E_{\text{grid}_+}(t) \leq E_{\text{load}}(t) + E_{\text{B}}(t), \\ &0 \leq E_{\text{grid}_-}(t) \leq E_{\text{PV}}(t). \end{aligned} \tag{15}$$

The constraints should also contain the limitations on the storage battery and EV battery.

Under this way, the total E_{V2G} in this article can be expressed as

$$E_{\text{V2G}} = \sum_{i=1}^{n_{\text{f}}} E_{\text{grid}_{i_+}}. \tag{16}$$

4. Results and Discussion

Here, this verification scenario of two distributed PV systems is assumed as the description in the following. During the working day, the EV owner usually should stay in his workplace, so he drives the EV from home to the workplace and parks the EV there during the working hours. The time of off-grid covering one trip is assumed as half hour. In this article, the working hours are assumed from 9:00 to 17:00. Then, after the working hours, he drives the EV home and leaves the EV connected to the charging pile during the night. That is to say under this scenario, most of time in the working days, the EV is mainly parked in the owner's home or parking area of the workplace. If in these two locations, the EV can both be connected to the grid and participate in the energy systems, the proposed optimal control strategy should effectively reduce the expense of electricity.

The following is a case as an example using a whole year historical data of number 13 in 300 households with PV users from July 1, 2010, to June 30, 2011, which is provided by Ausgrid Company, a utility in Australia [28]. The data includes the electricity load, PV size, PV generation with half-hour interval, and also postcode to express the location. The specific home is with a 2.22 kW PV system, and the average electricity consumption was 11.99 kWh per day, which had a typical load shape with a small peak in the morning and a larger peak in the afternoon. The meteorological correlation parameters are from the Bureau of Meteorology, Australia. To better illustrate and design the economic control strategy, Sydney's actual three-level time of use price is chosen as a whole integrated control strategy for specific operations and result analysis, which includes off-peak time (0:00–7:00 and

22:00–24:00), shoulder time (7:00–14:00 and 20:00–22:00). and peak time (14:00–20:00) in one day. The electricity retail tariff (which is 0.13$ in off-peak time, 0.21$ in shoulder time, and 0.53$ in peak time) and the FiT (0.08%/kWh) are both from the Independent Pricing and Regulatory Tribunal (IPART). The efficiencies of the PV system are the same as [26], which include the efficiency of DC/DC, 0.95; the efficiency of DC/AC or AC/DC, 0.95; the efficiency of the battery charging state, 0.85; and the efficiency of the battery discharging state, 0.9. In the case, EV monitoring data is provided by Smart Grid Smart City [29], which follows 20 EVs of i-MiEV type from Mitsubishi brand. They recorded the data with very detailed information of EV application, such as the parameters of time, state of charge (SoC) of the EV battery, mileage, charging time of every start and end, trip time of every start and end, and also distance, average velocity, and simple description of trip destination. In the following computation, the authors apply the average value of EV trip as the common trip features in which the average trip time is 18 minutes and the average battery consumption of one trip is 1.88 kWh and assume that the charging efficiency is the same as discharging efficiency, which is 74.6% from the EV brochure supplied by the manufacturer. Due to the consideration of battery reasonable application, the SoC of the storage battery and the EV battery is controlled within 20%~100%. The actual load data used for the workplace is calculated, the average half-hour load value of the Chemical and Biomolecular Engineering Building in Sydney University in one year from Dec 1, 2007, to Nov 30, 2008. Because there is no PV system in this building and the goal of the validation is to show the effectiveness of the proposed optimal control strategy, here the second distributed PV system is simplified to energy system with power grid and load only.

The test scenario only contains two distributed systems and one EV application in a whole year; therefore, it is not a very big problem, and the authors simply chose the self-contained function "fmincon" in MATLAB software to solve it, and in order to ensure the correctness of the solutions, we assumed the initial battery and EV battery as fully charged ($\mathrm{SoC_B}(0) = 100\%$ and $\mathrm{SoC_{EV}}(0) = 100\%$). The program of the proposed control model has been run on Dell XPS13 laptop, with the Intel Core i7 and 1.9 GHz of CPU master frequency. The average running time is around half an hour once for the whole year. The memory features after the program running are 3937 MB of physical memory (RAM), 4963 MB of page file (swap space), and 6990 MB of virtual memory (address space) in use.

The results of annual electricity expense under different conditions are listed in Table 1. The different conditions include the storage battery capacity changes, with or without EV, and the objective function changes. $B_{\max}$ as abovementioned represents the available capacity of the storage battery. The results show that if the distributed PV system only with the storage battery capacity increases from 1 kWh to 20 kWh and without EV application, the electricity expense can obtain a reduction from 13.44% to 58.39%. If the distributed PV system with the storage battery capacity increases from 1 kWh to 20 kWh and with an EV application, the electricity expense can obtain a reduction from 30.67% to 81.49%. From the table, under the condition of only with EV as a mobile storage equipment and not equipped with other storage equipment, the customer residential electricity expense could get a 27.18% saving when the objective is $\min(C_i)$. With the storage battery capacity increasing, electricity consumption saving values gradually increased. However, in the actual energy system design and application, the storage capacity leads to the cost increasing of storage system. Under this way, the designer must compare the saving with the cost and take the degradation, life, and other related factors of storage system into consideration to determine the reasonable storage system capacity which can generate the maximum benefit.

Table 1: Computing result comparison of the whole year under different conditions.

$B_{\max}$ (kWh)	Electricity expense without EV ($)	Electricity expense reduction without EV (%)	Electricity expense with EV ($)		Electricity expense reduction under objective $\min(C_i)$ (%)
			$\min(C_{\text{total}})$	$\min(C_i)$	
0	891.34	0	819.35	649.03	27.18
1	771.53	13.44	727.18	618.00	30.67
2	683.08	23.36	645.87	540.77	39.33
3	618.34	30.63	591.47	476.57	45.97
4	570.86	35.95	543.69	429.24	51.84
5	536.24	39.84	510.92	393.86	55.81
10	436.47	51.03	393.78	270.21	69.68
15	388.23	56.44	333.45	201.17	77.43
20	370.93	58.39	300.54	164.99	81.49

The results obtained above are calculated by the actual historical data of PV generation and electricity demand and mainly discuss the relevant conclusions and effectiveness of the optimization control under the designed distributed PV system control strategy in this article. While the EV battery is parking in the workplace energy system, it could play a role in shifting load. It indicates that the EV battery is charged during the lower price period and discharged in the higher price period in order to reduce the workplace electricity consumption. Under this control, the workplace applies the EV battery as a storage unit to reduce the expense on electricity, and the EV battery is charged by the workplace grid power to a certain degree. This can be seen as the application of EV, a mobile storage system, achieves a win-win situation. However, the specific benefits should be rerationally distributed by balancing the interests of all participants.

Further, the feasibility and effectiveness of the control strategy are analyzed with day-ahead predicted PV generation and demand. Due to the missing information of PV modules, here the authors assume the error of PV prediction model conforming to the Gaussian distribution which is introduced in Section 2.1, and to simplify the calculation, the average error μ is set as 0. Since in the selected customer's

Table 2: Performance of the load forecast model.

Samples (17520)	MSE	R^2
Training set (10512, 60%)	3.77e−2	8.55e−1
Validation set (3504, 20%)	0	0
Test set (3504, 20%)	5.29e−2	7.85e−1

energy system, the recorded PV generation is generally less than 1 kWh in the recorded time interval of half an hour, the standard deviation σ is set as 0.1 and 0.2, respectively. To realize the above settings, the MATLAB software is chosen to generate the forecasting PV power values under our assumptions and different deviations by a function named "random."

The BNN method is introduced to establish the customer's electricity load forecasting model, which has been illustrated in Section 2.2. The data used to calculate is still from Ausgrid company as the above descriptions. The total number of samples is 17520 and is randomly divided into 60% as the training set, 20% as the validation set, and 20% as the test set by MATLAB software, respectively. The MSE and R-squared values of the electricity demand forecast model are shown in Table 2.

From the historical data of this chosen sample, the repeatability and regularity of the electricity consumption way are relatively weak. For this type of user, higher prediction accuracy may require the customer to provide relevant factors as detailed as possible or supply own defined schedule of electricity demand. However, it is very difficult to realize such requirements. Thus, here even the prediction performance is lower compared to some other customers' from the 300 households of Ausgrid, it roughly could be seen to meet the basic test needs.

In order to compare the designed control strategy performance using actual historical data and predicted values as inputs, respectively, the authors calculate the results of six different input conditions under the objective function $\min(C_i)$. The results are listed in Table 3; $\mathbf{L}_{\mathrm{H}}$ is the historical data of load and PV_{H} expresses the historical data of PV generation, respectively; $\mathbf{L}_{\mathrm{F}}$ is the forecasting data of load and PV_{F} expresses the forecasting data of PV, respectively. It can be seen from the table that, as discussed above, the customer's power consumption mode has a relatively weak repeatability and strong randomness and the performance with demand prediction is inferior to other cases, which leads to a bigger difference than with other inputs. When the standard deviation of the PV generation error increases, the difference between the actual and the forecasting inputs increases, which is consistent with the assumption of the model performance.

In order to compare the above results intuitively, Figure 3 illustrates the customer annual consumption varied with the increasing storage battery capacity. It is obvious that the minimum residential annual electricity expense under $\min(C_i)$ is lower than $\min(C_{\mathrm{total}})$. Under the $\min(C_{\mathrm{total}})$, the EV owner's residential electricity expense also significantly reduced compared to the case without EV. This indicates that EV as a mobile storage system to participate the energy conversion of multiple parking places can obtain significant economic benefits through reasonable optimal scheduling control.

From the figure, it is also evident that the increase of the storage battery capacity could reduce the difference between the actual consumption and the calculated consumption by the forecast inputs. This indicates that the storage battery has a certain role to improve the overall optimal control performance in the distributed PV system. This improvement in performance can be converted to economic benefits, so as to provide a reference when the designers consider the cost of storage system.

Through the above calculation and discussion, the error of annual electricity expense with forecast inputs is less than 10% by comparison with actual inputs. Here, the authors go a step further to discuss the control model with predicted inputs. In the following, Table 4 shows some situations to see when the model would be out of work with increasing deviation.

As the performance of the electricity demand is already known by the forecast load model, a simple way to change the predicted input is just to assume the forecasting PV generation with different σ values. Table 4 shows the results under different assumptions with $B_{\max} = 5$ kWh and $\min(C_i)$. Due to the PV generation values used in the computing which are almost all smaller than 1, the assumed value range of σ is big enough under this condition. That means when the σ value is assumed as 0.5, the average error will be greater than 50%, and when σ is assumed as 1.0, the average error will be greater than 100%. That is already the most extreme situation and nearly would not happen. From the results listed in the table, it can be seen that even when σ is 0.5, the annual electricity expense under the designed control scheme is still very close to the results obtained with the actual data. However, when σ is 1.0, the results are greatly deviated from the actual input operation. Thus, under this extreme condition, the control strategy is invalid. It is noteworthy that this failure situation is basically impossible to happen. Therefore, the overall scheme of the distributed systems established can meet the practical application and has notable economic benefits.

5. Conclusion

Considering the booming development of the electric vehicle (EV), this article presents a novel control scheme analyzing EV multiple-mode application in a number of distributed photovoltaic (PV) systems, which rationalizes the energy flow among the energy system participants containing power grid, grid-connected PV system, power consumption devices, storage battery, and EV. In this article, the EV with V2G mode is seen as a mobile storage system, and multiple mode represents the EV that can be applied with G2V, V2G, off-grid, and driving modes and also can be used in multiple locations. In the control scheme, the PV prediction model with an error satisfying Gaussian distribution and load forecast model based on Bayesian neural network learning method are used as the inputs of the control framework. According to the inputs, the authors propose two day-

Table 3: Results of annual electricity expenses under $\min(C_i)$ with different inputs.

$\min(C_i)$ (\$)		L_H & PV_H	L_F & PV_H	L_H & PV_F $\sigma = 0.1$	L_H & PV_F $\sigma = 0.2$	L_H & PV_F $\sigma = 0.1$	L_H & PV_F $\sigma = 0.2$
B_{max} (kWh)	0	649.03	583.42	636.96	611.67	571.56	547.15
	5	393.86	330.41	391.14	376.48	397.54	400.62
	10	270.21	234.42	268.12	255.34	231.26	221.16
	15	201.17	186.59	198.10	188.73	184.55	175.44
	20	164.99	163.09	164.20	155.98	160.89	152.13

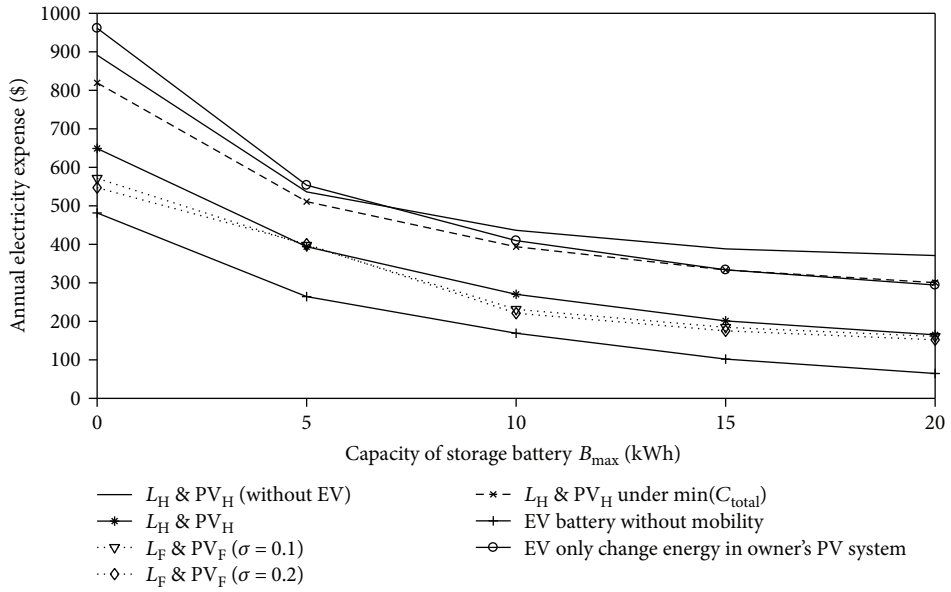

Figure 3: Change of annual consumption on electricity with varied available storage battery capacity.

Table 4: Results of annual electricity expense with $B_{max} = 5$ kWh and $\min(C_i)$ under different σ of forecasting PV model.

Assumed σ in PV prediction model	0.01	0.05	0.1	0.2	0.5	1
Annual electricity expense under the objective function $\min(C_i)$	393.86	394.77	397.54	400.62	399.54	2.41

ahead optimal control strategies with different objective functions; one is minimizing the daily electricity expense of individual distributed PV system and the other is minimizing the daily total expense of distributed PV systems which EV can be connected to. The control structure makes the customer obtain a lowest expense on electricity through the storage battery system control in the first level by geometrical logic analysis methodology and EV optimal scheduling control with multiple-mode application in the second level. The model has been verified and analyzed by the actual historical data and forecast data, respectively. The results show that if the distributed PV system only with the storage battery and without EV application is being used, the electricity expense can obtain a reduction from 13.44% to 58.39% with the battery capacity increasing from 1 kWh to 20 kWh. If the distributed PV system without storage battery and with EV application is being used, the electricity expense can obtain a reduction of 27.18%. Furthermore, when the distributed PV system with the storage battery increases as well as EV application, the electricity expense can obtain a reduction from 30.67% to 81.49%. Under the total objective, the total expense and even the individual expense have different degrees of reduction. However, the specific benefits should rerationally distributed by balancing the interests of all distributed PV systems. Besides economic consideration, the models explained in this article can be easily introduced into the environment and energy conservation goals. In addition, this model may have some potential on the development of regional energy system. Future work will focus on further improving the performance of PV generation forecast model and the electricity demand forecast model and supplementing reasonable real-time control strategy to obtain a higher benefit.

Nomenclature

E_{PV}: The forecasting PV output in unit time interval (kWh)
V_{OC}: The open-circuit voltage (V)
I_{SC}: The short-circuit current (A)

V_M: The voltage at maximum power point (V)
I_M: The current at maximum power point (A)
N: The serial number of PV cells in one panel
N_s: The serial number of PV array
N_p: The parallel number of PV array
G: The solar irradiance (kW/m^2)
Temp: The temperature (°C)
t_{in}: Unit time interval, which is 30 min in this paper
Er_{PV}: The error between the PV forecasting value and the actual PV generation (kWh)
$\widehat{E_{PV}}$: The forecasting PV value (kWh)
E_{PV}: The actual PV generation (kWh)
μ: The mean error
σ: Mean square deviation
$\mathbf{V}_I$: Vectors of inputs in BNN load forecasting model
t: Time of every day
$\mathbf{d}_t$: Day type
T: Ambient temperature (°C)
RH: Relative humidity (%)
n: The series order number of historical sample data's intervals
L: Historical load data (kWh)
E_B: The battery energy change (kWh)
E_{B_+}: The charging energy (kWh)
E_{B_-}: The discharging energy (kWh)
$P_{B_{max_{charge}}}$: The maximum charging rates of battery (kW/h)
$P_{B_{max_{discharge}}}$: The maximum discharging rates of battery (kW/h)
$E_{B_{size}}$: The specified capacity of the storage battery (kWh)
E_{B_0}: The initial battery energy (kWh)
$SoC_{B_{min}}$: The minimum SoC of battery
$SoC_{B_{max}}$: The maximum SoC of battery
$E_{B_{loss}}$: The energy loss of the battery (kWh)
B_{size}: The capacity of the storage battery (kWh)
B_{max}: The maximum energy could be used in the storage battery when it is fully charged (kWh)
E_{EV}: The battery energy change of EV battery (kWh)
E_{EV_+}: The energy change by G2V mode (kWh)
E_{EV_-}: The energy export by V2G mode (kWh)
$P_{EV_{max_{charge}}}$: The maximum charging rate of the EV battery (kW/h)
$P_{EV_{max_{discharge}}}$: The maximum discharging rate of the EV battery (kW/h)
E_{EV_0}: The initial state of battery (kWh)
$SoC_{EV_{min}}$: The minimum SoC of EV battery
$SoC_{EV_{max}}$: The maximum SoC of EV battery
$E_{EV_{loss}}$: The energy loss of the EV battery (kWh)
E_{trip}: The energy consumed when the EV is driving on a certain trip between two known locations within some time (kWh)
C_a: The annual cost of V2G ($)
E_{V2G}: The energy available in each EV per dispatch (kWh)
N_d: The number of dispatches per year
C_d: The cost of battery degradation ($)
r_e: The electricity price ($/kWh)
k: The number of distributed PV systems
i: The ordered distributed PV systems in which the EV battery is being connected to its power grid in time t
j: The other ordered distributed PV systems without EV connection in time t
n_f: The final time order
t: The ordered period with observation time interval t_{in}
C_i: The minimizing electricity cost of one specific distributed PV system ($)
C_{total}: The minimization of the total electricity costs for all the distributed PV systems which an EV battery may participate in ($)
L_H: The historical data of load
PV_H: The historical data of PV generation
L_F: The forecasting data of load
PV_F: The forecasting data of PV generation.

Conflicts of Interest

The authors declare that they have no conflicts of interest.

Acknowledgments

The authors would like to thank Ausgrid, the Australian Bureau of Meteorology, and the Smart Grid Smart City project for the data applied in this paper. This work was supported by the National Natural Science Foundation of China (Grant No. 51478258, 51405287), Shanghai Committee of Science and Technology (Grant No. 18030501300).

References

[1] W. Shengjun, X. Qingshan, L. Qun, Y. Xiaodong, and C. Bing, "Optimal EV charging control strategy based on DC microgrid," *Energy Procedia*, vol. 100, pp. 243–247, 2016.

[2] C. Chen and S. Duan, "Optimal integration of plug-in hybrid electric vehicles in microgrids," *IEEE Transactions on Industrial Informatics*, vol. 10, no. 3, pp. 1917–1926, 2014.

[3] M. S. ElNozahy, T. K. Abdel-Galil, and M. M. A. Salama, "Probabilistic ESS sizing and scheduling for improved integration of PHEVs and PV systems in residential distribution systems," *Electric Power Systems Research*, vol. 125, pp. 55–66, 2015.

[4] Y. Guo, J. Xiong, S. Xu, and W. Su, "Two-stage economic operation of microgrid-like electric vehicle parking deck," *IEEE Transactions on Smart Grid*, vol. 7, no. 3, pp. 1703–1712, 2016.

[5] Y. Tang, J. Yang, J. Yan, and H. He, "Intelligent load frequency controller using GrADP for island smart grid with electric vehicles and renewable resources," *Neurocomputing*, vol. 170, pp. 406–416, 2015.

[6] S. Hashemi, J. Ostergaard, and G. Yang, "A scenario-based approach for energy storage capacity determination in LV grids with high PV penetration," *IEEE Transactions on Smart Grid*, vol. 5, no. 3, pp. 1514–1522, 2014.

[7] N. G. Paterakis, O. Erdinc, A. G. Bakirtzis, and J. P. S. Catalao, "Optimal household appliances scheduling under day-ahead

pricing and load-shaping demand response strategies," *IEEE Transactions on Industrial Informatics*, vol. 11, no. 6, pp. 1509–1519, 2015.

[8] T. Kaschub, P. Jochem, and W. Fichtner, "Solar energy storage in German households: profitability, load changes and flexibility," *Energy Policy*, vol. 98, pp. 520–532, 2016.

[9] S. Cao, "Comparison of the energy and environmental impact by integrating a H_2 vehicle and an electric vehicle into a zero-energy building," *Energy Conversion and Management*, vol. 123, pp. 153–173, 2016.

[10] S. I. Kampezidou, E. Polymeneas, and S. Meliopoulos, "The economic effect of storage in systems with high penetration of renewable sources," in *2015 North American Power Symposium (NAPS)*, pp. 1–6, Charlotte, NC, USA, 2015.

[11] A. Assuncao, P. S. Moura, and A. T. de Almeida, "Technical and economic assessment of the secondary use of repurposed electric vehicle batteries in the residential sector to support solar energy," *Applied Energy*, vol. 181, pp. 120–131, 2016.

[12] F. Marra, G. Y. Yang, Y. T. Fawzy et al., "Improvement of local voltage in feeders with photovoltaic using electric vehicles," *IEEE Transactions on Power Systems*, vol. 28, no. 3, pp. 3515-3516, 2013.

[13] M. Honarmand, A. Zakariazadeh, and S. Jadid, "Self-scheduling of electric vehicles in an intelligent parking lot using stochastic optimization," *Journal of the Franklin Institute*, vol. 352, no. 2, pp. 449–467, 2015.

[14] S. Y. Derakhshandeh, A. S. Masoum, S. Deilami, M. A. S. Masoum, and M. E. Hamedani Golshan, "Coordination of generation scheduling with PEVs charging in industrial microgrids," *IEEE Transactions on Power Systems*, vol. 28, no. 3, pp. 3451–3461, 2013.

[15] H. O. R. Howlader, H. Matayoshi, and T. Senjyu, "Distributed generation incorporated with the thermal generation for optimum operation of a smart grid considering forecast error," *Energy Conversion and Management*, vol. 96, pp. 303–314, 2015.

[16] Z. Liu, C. Chen, and J. Yuan, "Hybrid energy scheduling in a renewable micro grid," *Applied Sciences*, vol. 5, no. 3, pp. 516–531, 2015.

[17] L. Ju, Z. Tan, J. Yuan, Q. Tan, H. Li, and F. Dong, "A bi-level stochastic scheduling optimization model for a virtual power plant connected to a wind–photovoltaic–energy storage system considering the uncertainty and demand response," *Applied Energy*, vol. 171, pp. 184–199, 2016.

[18] L. Ju, H. Li, J. Zhao, K. Chen, Q. Tan, and Z. Tan, "Multi-objective stochastic scheduling optimization model for connecting a virtual power plant to wind-photovoltaic-electric vehicles considering uncertainties and demand response," *Energy Conversion and Management*, vol. 128, pp. 160–177, 2016.

[19] V. N. Coelho, I. M. Coelho, B. N. Coelho et al., "Multi-objective energy storage power dispatching using plug-in vehicles in a smart-microgrid," *Renewable Energy*, vol. 89, pp. 730–742, 2016.

[20] L. B. Jaramillo and A. Weidlich, "Optimal microgrid scheduling with peak load reduction involving an electrolyzer and flexible loads," *Applied Energy*, vol. 169, pp. 857–865, 2016.

[21] F. Gao, W. Tang, T. Yan et al., "Day-ahead energy optimal scheduling of household microgrid considering the user satisfaction," *2015 IEEE PES Asia-Pacific Power and Energy Engineering Conference (APPEEC)*, 2015, pp. 1–5, Brisbane, QLD, Australia, 2015.

[22] J. Zhao, S. Kucuksari, E. Mazhari, and Y.-J. Son, "Integrated analysis of high-penetration PV and PHEV with energy storage and demand response," *Applied Energy*, vol. 112, pp. 35–51, 2013.

[23] S. Bracco, F. Delfino, F. Pampararo, M. Robba, and M. Rossi, "A dynamic optimization-based architecture for polygeneration microgrids with tri-generation, renewables, storage systems and electrical vehicles," *Energy Conversion and Management*, vol. 96, pp. 511–520, 2015.

[24] J. A. Gow and C. D. Manning, "Development of a photovoltaic array model for use in power-electronics simulation studies," *IEE Proceedings - Electric Power Applications*, vol. 146, no. 2, pp. 193–200, 1999.

[25] G. R. Walker, "Evaluating MPPT converter topologies using a Matlab PV Model," *Journal of Electrical & Electronics Engineering Australia*, vol. 21, no. 1, pp. 49–55, 2001.

[26] Q. Zhong, R. Khalilpour, A. Vassallo, and Y. Sun, "A logic-based geometrical model for the next day operation of PV-battery systems," *Journal of Energy Storage*, vol. 7, pp. 181–194, 2016.

[27] C. Zhou, K. Qian, M. Allan, and W. Zhou, "Modeling of the cost of EV battery wear due to V2G application in power systems," *IEEE Transactions on Energy Conversion*, vol. 26, no. 4, pp. 1041–1050, 2011.

[28] "Solar home electricity data notes. Sydney: Ausgrid," https://www.ausgrid.com.au/Common/About-us/Corporate-information/Data-to-share/Solar-home-electricity-data.aspx.

[29] "Research and Markets: Australia-Smart Grid-Smart City Project-2011," https://trove.nla.gov.au/work/160745433?q&versionId=175242047.

Hindawi
Complexity
Volume 2018, Article ID 9842025, 20 pages
https://doi.org/10.1155/2018/9842025

Research Article

Optimal Scheduling of a Microgrid Including Pump Scheduling and Network Constraints

Ashok Krishnan,[1] **L. P. M. I. Sampath**,[2] **Y. S. Foo Eddy**,[1] **and H. B. Gooi**[1]

[1]*School of Electrical and Electronic Engineering, Nanyang Technological University, 50 Nanyang Avenue, Singapore 639798, Singapore*
[2]*Interdisciplinary Graduate School, Nanyang Technological University, 21 Nanyang Link, Singapore 637371, Singapore*

Correspondence should be addressed to Ashok Krishnan; ashok004@e.ntu.edu.sg

Received 26 January 2018; Accepted 3 April 2018; Published 10 July 2018

Academic Editor: João Soares

This paper proposes an efficient energy management system (EMS) for industrial microgrids (MGs). Many industries deploy large pumps for their processes. Oftentimes, such pumps are operated during hours of peak electricity prices. A lot of industries use a mix of captive generation and imported utility electricity to meet their energy requirements. The MG considered in this paper includes diesel generators, battery energy storage systems, renewable energy sources, flexible loads, and interruptible loads. Pump loads found in shipyard dry docks are modelled as exemplar flexible industrial loads. The proposed EMS has a two-stage architecture. An optimal MG scheduling problem including pump scheduling and curtailment of interruptible loads (ILs) is formulated and solved in the first stage. An optimal power flow problem is solved in the second stage to verify the feasibility of the MG schedule with the network constraints. An iterative procedure is used to coordinate the two EMS stages. Multiple case studies are used to demonstrate the utility of the proposed EMS. The case studies highlight the efficacy of load management strategies such as pump scheduling and curtailment of ILs in reducing the total electricity cost of the MG.

1. Introduction

Industrial power networks may comprise distributed generators, battery energy storage systems (BESSs), and different types of loads. As such, industrial power networks can be treated as grid-connected MGs. An EMS facilitates efficient MG operation by minimizing the overall electricity cost. The EMS determines an optimal schedule and dispatch for each distributed generator, BESS, flexible load, and interruptible load (IL) in the MG while respecting various technical and operational constraints. The EMS is also capable of incorporating load management strategies in its optimal scheduling problem formulation. Furthermore, the EMS needs to consider power flow equations and system security constraints while optimally dispatching the MG components. This is considered in an optimal power flow (OPF) problem incorporated in the EMS architecture. Thus, formulating an efficient energy management (EM) problem is a complex task due to the need to integrate both unit commitment (UC) and OPF problems. This normally results in the EM problem being formulated by ignoring network losses and system security constraints. The EM problem then simplifies to a UC problem which is usually formulated as a mixed integer linear programming (MILP) or mixed integer quadratic programming (MIQP) problem. However, the feasibility of results obtained using such formulations is questionable owing to potential violations of the network constraints and the absence of power losses in the formulation.

In Singapore, the wholesale electricity prices are updated every 30 minutes. Large industrial customers have the option of sourcing their electricity requirements directly from the wholesale electricity market through SP Services Limited. In this scenario, industries need to contend with the risk of increased costs due to volatile electricity prices. The contestable consumers' electricity bills usually comprise two segments: (i) energy charge and (ii) capacity charge. The energy charge is calculated by taking the product of electricity charge and energy consumed. The capacity charge is computed on a monthly basis. The capacity charge is calculated by taking the product of contracted capacity and contracted capacity price. A huge uncontracted capacity charge is incurred if the maximum power demand exceeds the contracted capacity at

any point of time. Large pumps constitute a major portion of the electrical load demand in many industrial facilities. Due to the large pumping requirements in many industries, pump capacities are typically in the region of several MWs. In other words, pump usage has a significant bearing on the maximum load demand in many industrial facilities. Pump usage is also constrained by operational requirements in many industries whereby a certain quantity of water or other liquid needs to be pumped within a defined time frame. Optimal planning and scheduling of pump usage along with timely curtailment of ILs can help in lowering the maximum demand of the industrial facility, thereby leading to a reduction in the electricity cost.

With the advent of deregulated power systems, load management strategies have recently attracted wide research interest. A recent survey of existing demand response models and approaches can be found in [1]. Load management strategies have been proposed for rural water pumping stations [2] and flour mills [3, 4] among other applications. An optimal pump scheduling problem formulation for a rural two-stage water pumping station was developed in [2]. A generic optimal industrial load management scheme compatible with energy hub management systems was developed in [3] for process scheduling in industries such as flour mills and water pumping facilities. The mixed logical dynamical (MLD) approach was used to formulate and solve an optimal scheduling problem for district heating networks including generation sources, thermal energy storage systems, and flexible thermal loads in [5]. A load management strategy meeting objectives such as maximum user comfort or minimum cost for thermostatically controlled household appliances was presented in [6]. A recent work also developed an EMS for district heating networks including flexible loads while ensuring adequate user comfort at minimal cost [7].

Development of EMSs for MGs has been an active research area in recent years. In this context, model predictive control (MPC) based schemes have been widely adopted in recent years for power system scheduling applications. A few typical examples of such schemes can be found in [8–10]. However, as mentioned earlier, most of these schemes including [8, 9] do not account for network constraints due to the difficulties involved in solving the optimization problem. In other words, most of these schemes consider the UC and OPF problems separately. A few works have integrated the UC and OPF problems. The authors of [11] integrated the UC and OPF problems for a conventional power system without considering the presence of BESSs, renewable energy sources (RESs), and ILs. More recent works such as [12, 13] consider centralized cooperative schemes for standalone MGs. A centralized controller addresses the power sharing problem among interconnected MGs in [14]. The authors of [15] proposed a jump and shift method for integrating the UC and OPF problems while including BESSs and RESs in the network. This approach was adapted for a multimicrogrid scenario in the authors' recent work [16]. However, these works do not consider load management strategies in the problem formulation.

In this paper, comprehensive, component wise models of exemplar MGs are first developed. The MGs modelled in this paper comprise diesel generators (DGs), BESSs, RESs, flexible pump loads, and ILs. The MLD framework is used to model the DGs, BESSs, and ILs. Subsequently, an EMS is proposed for optimally scheduling the MG. The proposed EMS has a two-stage architecture along the lines of [15] to minimize operational costs while ensuring that the network constraints are not violated. The proposed EMS also incorporates efficient load management strategies such as pump scheduling and curtailment of ILs. The pump scheduling scheme is formulated to save electricity costs while respecting certain operational constraints. The incorporation of load management strategies such as pump scheduling into the overall two-stage MG EMS architecture is the key contribution of this paper. This result is a new optimal MG scheduling problem formulation which helps in reducing the overall cost of operation for the MG while respecting various technical and operational constraints. The efficacy of the proposed EMS is demonstrated through case studies under different operational scenarios. The case studies also demonstrate the effectiveness of including ILs in the overall optimal scheduling problem.

The remainder of this paper is organized as follows: Section 2 develops first principle models of all the MG components. Section 3 describes the formulation of the EM problem. An overview of the iterative solution approach implemented in the EMS is also presented in Section 3. Section 4 presents numerical results obtained from different case studies performed to demonstrate the efficacy of the proposed optimization model. Section 5 provides some concluding remarks and directions for future work.

2. Industrial Microgrid Model

This section develops first principle models of the DGs, BESSs, RESs, flexible pump loads, and ILs considered in this paper.

2.1. Diesel Generators. DGs are controllable in nature. The fuel cost of DG f is determined by a quadratic function of its real power output as shown below [15]. Furthermore, start-up costs are imposed on the DGs. Minimum uptime (UT) and downtime (DT) constraints also restrict the operation of the DGs.

$$C_{\mathrm{DG}} = \sum_{\substack{k\in\mathcal{K}\\ f\in\mathcal{F}}} \left(b^f_{\mathrm{SU},k} C^f_{\mathrm{SU}} + b^f_{\mathrm{DG},k} \left(c^f_0 + c^f_1 P^f_{\mathrm{DG},k} + c^f_2 \left(P^f_{\mathrm{DG},k} \right)^2 \right) \right). \quad (1)$$

In (1), the first term represents the start-up cost while the second term represents the fuel cost of the corresponding DG. All the technical parameters of the 3 DGs considered in this paper are provided in Table 1.

2.2. Battery Energy Storage Systems. In this work, a realistic BESS model is considered including intertemporal constraints on the state of charge (SOC). A battery degradation cost function accounts for the impact of charging and

Table 1: Technical parameters of the DGs in the MGs.

DG #	c_0^f ($)	c_1^f ($/MW)	c_2^f ($/MW^2)	min $P_{DG,k}^f$ (MW)	max $P_{DG,k}^f$ (MW)	C_{SU}^f ($)	min UT/DT (h)
1	80	30	1	0.1	3	50	3
2	200	60	2	0.1	3	30	3
3	1000	50	3	0.1	3	5	3

discharging events on the cost of purchasing the BESS. The overall BESS model is presented below [17].

$$\mathrm{SOC}_{k+1}^e = \mathrm{SOC}_k^e + \frac{\left(\eta_c^e P_{bc,k}^e - P_{bd,k}^e/\eta_d^e\right)}{P_{1C}^e}, \quad \forall k \in \mathcal{K},\ \forall e \in \mathcal{E} \tag{2}$$

$$\mathrm{SOC}_{min}^e \le \mathrm{SOC}_{k+1}^e \le \mathrm{SOC}_{max}^e, \quad \forall k \in \mathcal{K},\ \forall e \in \mathcal{E} \tag{3}$$

$$0 \le P_{bc,k}^e \le P_{bc,max}^e, \quad \forall k \in \mathcal{K},\ \forall e \in \mathcal{E} \tag{4}$$

$$0 \le P_{bd,k}^e \le P_{bd,max}^e, \quad \forall k \in \mathcal{K},\ \forall e \in \mathcal{E}. \tag{5}$$

The evolution of the BESS SOC is described by (2). The SOC evolution depends on the charging and discharging powers and the charging and discharging efficiencies. A binary variable is used to distinguish between the charging and discharging events to prevent simultaneous charging and discharging. Interested readers may refer to [8] for more details. Intertemporal constraints on the SOC evolution are expressed in (3) while the bounds on charging and discharging powers are expressed in (4) and (5), respectively. The overall BESS cost function is expressed as follows:

$$C_{BESS} = \sum_{\substack{k\in\mathcal{K}\\ e\in\mathcal{E}}} \frac{I^e}{2B_{cap}^e N^e}\left(\frac{P_{bc,k}^e}{T_{bc}^e} + \frac{P_{bd,k}^e}{T_{bd}^e}\right). \tag{6}$$

In this paper, all the BESSs are considered to have the following parameters: $P_{bc,max}^e = P_{bd,max}^e = 300$ kW, $B_{cap}^e = 1020$ kWh, $N^e = 6000$ h, $P_{1C}^e = 1020$ kW, $\mathrm{SOC}_{min} = 0.2$, $\eta_c^e = \eta_d^e = 0.95$, $\mathrm{SOC}_{max} = 0.9$, and $I^e = \$408{,}000$. Furthermore, BESS operation is constrained by the following [18, 19]:

$$\mathrm{SOC}_1^e = \mathrm{SOC}_{25}^e, \quad \forall e \in \mathcal{E}. \tag{7}$$

In this work, the load profiles used for the MG scheduling problems were adapted from the IEEE RTS-96 load profiles provided in [20]. As such, in many cases, the system load profile may not differ significantly between two consecutive days. In this scenario, it is important to ensure that the flexibility provided by the BESS scheduling is available every day to the system operator. To provide this flexibility, the initial and final SOCs of the BESSs are constrained to be equal as shown in (7).

2.3. Renewable Energy Sources. Renewable energy sources such as solar photovoltaic (PV) and wind power plants are included as components of the MGs which are modelled in this paper. The operating costs of these RESs are assumed to be 0 [16]. The following paragraphs describe the modelling of the solar PV and wind power plants.

The power output from the wind power plant is proportional to the cube of the wind velocity and is calculated using the following equation:

$$P_{wind} = 0.5 C_p k \rho A \left(v_{wind}\right)^3. \tag{8}$$

Among other PV performance models, the five-parameter array performance model has been extensively used by researchers [21]. The PV performance model is used to extract the current-voltage (I-V) curve and the maximum power point (MPP) which can help in improving the performance of the PV system. The steady-state PV module performance is described as follows [22]:

$$I_L - I_S\left\{\exp\left[\alpha\left(v_{pv} + R_S i_{pv}\right)\right] - 1\right\} - \frac{v_{pv} + R_S i_{pv}}{R_{Sh}} - i_{pv} = 0$$
$$P_{pv} = v_{pv} i_{pv}, \tag{9}$$

where $\alpha = q/n_s kT$ is the ideality factor. Furthermore, $k = 1.38 \times 10^{23}$ J/K is the Boltzmann's constant, $q = 1.6022 \times 10^{19}$ is the electronic charge, $K = 298$ K is the temperature, and n_s is the number of cells in series. Interested readers may refer to [22] and the references therein for further details about the solar PV and wind power plant models. In this work, the solar PV and wind power plant generation forecasts were obtained from [23]. In this paper, $P_{RES,k}^z$ is used to represent the electrical power produced by RES z (either P_{pv} or P_{wind}) during hour k.

2.4. Interruptible Loads. These are loads in the MG which are considered to be less important. ILs provide the EMS with a lot of flexibility while scheduling the MG components. The ILs may be shed if sufficient monetary compensation is paid. The total cost associated with the curtailment of all the ILs in a MG is calculated as follows [24]:

$$C_{IL} = \sum_{\substack{k\in\mathcal{K}\\ h\in\mathcal{H}}} p_k^h b_{IL,k}^h P_{IL,k}^h. \tag{10}$$

Three ILs (IL 1, IL 2, and IL 3) are considered to be a part of the MGs modelled in this paper. The curtailment of each IL is constrained by the following:

$$0 \le P_{IL,k}^h \le 0.4\,\mathrm{MWh}, \quad \forall k \in \mathcal{K},\ \forall h \in \mathcal{H} \tag{11}$$

$$\sum_{k\in\mathcal{K}} P_{IL,k}^h \le 2\,\mathrm{MWh}, \quad \forall h \in \mathcal{H}. \tag{12}$$

The constraints in (11) and (12) basically restrain the EMS from indiscriminately using the ILs to relax the scheduling problem. Equation (11) imposes an hourly constraint while (12) imposes a daily limit on the curtailment of individual ILs.

2.5. Pump Loads. Pump loads found in shipyard dry docks have been used as exemplar industrial loads in this paper. The power consumed by pump m during hour k, $P^m_{\text{Pump},k}$, is defined as follows [25]:

$$P^m_{\text{Pump},k} = C^m b^m_k, \quad \forall k \in \mathcal{K},\ \forall m \in \mathcal{M}. \tag{13}$$

Equation (13) implies that all the pumps run at fixed speeds and operate at rated power if scheduled. The constraints associated with the operation of the pumps are described in the following paragraphs.

Pumps are required to pump a certain amount of water or other liquid within the specified optimization period. This constraint is expressed as follows:

$$\sum_{\substack{k\in\mathcal{K}\\ m\in\mathcal{M}}} Q^m \tau * b^m_k \geq V_{\text{d}}. \tag{14}$$

Large pumps cannot be started up or shutdown too frequently during the optimization period due to their large inertias. This constraint is expressed as follows:

$$\sum_{k\in\mathcal{K}} b^m_{\text{SU},k} \geq b^m_{\text{SU,max}}, \quad \forall m \in \mathcal{M} \tag{15}$$

$$b^m_{\text{SU},k} = b^m_k \left(b^m_k - b^m_{k-1}\right), \quad \forall k \in \mathcal{K},\ \forall m \in \mathcal{M}. \tag{16}$$

Equation (16) is linearized as follows [26]:

$$\begin{aligned} b^m_{\text{SU},k} &\leq \frac{\left(b^m_k + 1 - b^m_{k-1}\right)}{2}, \quad \forall k \in \mathcal{K},\ \forall m \in \mathcal{M} \\ b^m_{\text{SU},k} &\geq \frac{\left(b^m_k - b^m_{k-1}\right)}{2}, \quad \forall k \in \mathcal{K},\ \forall m \in \mathcal{M}. \end{aligned} \tag{17}$$

This work considers a total of 7 pumps including 3 main pumps and 4 auxiliary pumps. For the main pumps: $Q^m = 24{,}000\ \text{m}^3/\text{h}$, $C^m = 1.45\ \text{MW}$, and $b^m_{\text{SU,max}} = 1$. For the auxiliary pumps: $Q^m = 1{,}200\ \text{m}^3/\text{h}$, $C^m = 0.11\ \text{MW}$ and $b^m_{\text{SU,max}} = 10$. Finally, $V_d = 200{,}000\ \text{m}^3$, and $\tau = 1\ \text{h}$. It may be pertinent to mention here that despite the greater flexibility offered by the auxiliary pumps, they are inefficient compared to the main pumps. As a result, the advantage offered by the greater flexibility of the auxiliary pumps is diminished to a certain extent.

2.6. MLD Modelling Approach. The MLD formalism is a class of hybrid dynamical systems which has been used by several researchers for formulating power system scheduling problems. A few examples of such problems can be found in [8, 10, 27] and the references therein. The main advantage of using the MLD formalism to model the MG components is that the final optimal scheduling problem turns out to be an MILP or MIQP problem [8, 10, 27]. Numerous commercial solvers are available to efficiently solve MILP and MIQP problems. HYSDEL (Hybrid System Description Language) permits application engineers to formulate hybrid system models in a descriptive fashion [28]. A compiler generates the MLD models from the descriptive HYSDEL models. The MLD models are subsequently used in optimization problems or for synthesizing controllers. In this paper, MLD models of all the DGs, BESSs, and ILs are obtained using HYSDEL. In the MLD framework, the overall system model is described using the following equations [29]:

$$x(k+1) = Ax(k) + B_{\text{u}}u(k) + B_{\text{aux}}w(k) + B_{\text{aff}} \tag{18}$$

$$E_{\text{x}}x(k) + E_{\text{u}}u(k) + E_{\text{aux}}w(k) \leq E_{\text{aff}}, \tag{19}$$

where $x = \begin{bmatrix} x_{\text{c}} & x_{\text{b}} \end{bmatrix}^{\text{T}}$, $x_{\text{c}} \in \mathbb{R}^{n^{\text{c}}_{\text{x}}}$, $x_{\text{b}} \in \{0,1\}^{n^{\text{b}}_{\text{x}}}$, represents continuous and binary system states; $u = \begin{bmatrix} u_{\text{c}} & u_{\text{b}} \end{bmatrix}^{\text{T}}$, $u_{\text{c}} \in \mathbb{R}^{n^{\text{c}}_{\text{u}}}$, $u_{\text{b}} \in \{0,1\}^{n^{\text{b}}_{\text{u}}}$, represents continuous and binary system inputs; $w = \begin{bmatrix} w_{\text{c}} & w_{\text{b}} \end{bmatrix}^{\text{T}}$, $w_{\text{c}} \in \mathbb{R}^{n^{\text{c}}_{\text{w}}}$, $w_{\text{b}} \in \{0,1\}^{n^{\text{b}}_{\text{w}}}$, represents continuous and binary auxiliary variables. Auxiliary variables are used in the MLD framework to convert propositional logic to linear inequalities of the form shown in (19). A, B_{u}, B_{aux}, B_{aff}, E_{x}, E_{u}, E_{aux}, and E_{aff} are constant matrices of suitable dimensions which are used to describe the interactions between the system states, system inputs, and auxiliary variables. The auxiliary variables are solved with (19) using the current state of the system $x(k)$ and input $u(k)$, thereby determining the time evolution of the model described in (18) and (19). A well posed MLD system has a unique solution for the auxiliary variables $w(k)$ from (19) for a given state $x(k)$ and input $u(k)$. Interested readers may refer to [29] for a detailed description of the MLD framework. A detailed description of the modelling of thermal units and BESSs using the MLD approach can be found in [8] and [27], respectively.

3. Energy Management System Architecture

The proposed EMS comprises two sequential stages for minimizing the total MG operating cost. The motivation behind adopting this two-stage approach is to decrease the complexity of the overall optimization problem, thereby ensuring that it is solved within a reasonable time. The two stages of the proposed EMS are described below.

3.1. Stage 1: Unit Commitment. The UC problem for the MG is solved in Stage 1 wherein all the DGs, BESSs, pumps, and ILs are optimally scheduled to satisfy the active power demand. The overall optimization problem solved at this stage is described below.

$$\begin{aligned} \min_{u,x,w} \quad & J = C_{\text{DG}} + C_{\text{BESS}} + C_{\text{UCC}} + C_{\text{Grid}} + C_{\text{IL}} \\ \text{subject to} \quad & (18), (19) \\ & u_{\min} \leq u \leq u_{\max}; \\ & x_{\min} \leq x \leq x_{\max}; \\ & w_{\min} \leq w \leq w_{\max} \end{aligned}$$

$$P_{\mathrm{D},k} - \sum_{h\in\mathscr{H}} P^{h}_{\mathrm{IL},k} + P^{\mathrm{loss}}_{\mathrm{e},k} + \sum_{m\in\mathscr{M}} P^{m}_{\mathrm{Pump},k} = \sum_{f\in F} P^{f}_{\mathrm{DG},k} + P_{\mathrm{eb},k} - P_{\mathrm{es},k} + \sum_{e\in\mathscr{E}} \left(P^{e}_{\mathrm{bd},k} - P^{e}_{\mathrm{bc},k}\right) + \sum_{z\in\mathscr{Z}} P^{z}_{\mathrm{RES},k}, \quad \forall k \in \mathscr{K}, \tag{20}$$

where the first constraint refers to the bounds on the system states, system inputs, and auxiliary variables. Equation (20) is the power balance constraint for the UC problem. The unexplained terms of (20) are described in the following paragraphs.

C_{Grid} calculates the cost incurred by the MG due to the purchase of electricity from the utility grid. C_{Grid} also accounts for the revenue earned from the sale of electricity to the utility grid. C_{Grid} is calculated as follows:

$$C_{\mathrm{Grid}} = \sum_{k\in K} \left(C_{\mathrm{p},k} P_{\mathrm{eb},k} - C_{\mathrm{s},k} P_{\mathrm{es},k}\right). \tag{21}$$

C_{UCC} is the cost incurred by the MG due to the import of uncontracted capacity from the utility grid. The uncontracted capacity is calculated based on the maximum demand as follows [25]:

$$P_{\mathrm{UC}} = \max\left\{0, \max_{1\le k\le 24}\left\{P_{\mathrm{eb},k} - P_{\mathrm{CC}}\right\}\right\}. \tag{22}$$

Equation (22) is linearized as follows:

$$\begin{aligned} &P_{\mathrm{UC}} \ge P_{\mathrm{eb},k} - P_{\mathrm{CC}}, \quad \forall k \in \mathscr{K} \\ &P_{\mathrm{UC}} \ge 0, \\ &C_{\mathrm{UCC}} = U_{\mathrm{CC}} P_{\mathrm{UC}}, \end{aligned} \tag{23}$$

where U_{CC} = \$12,860/MW/month and $P_{\mathrm{CC}} = 0.7$ MW. Due to its exorbitant pricing, uncontracted capacity needs to be avoided as much as possible. Efficient load management strategies can aid the EMS in achieving this target.

The overall optimization problem is solved in an MPC framework with a prediction horizon of 24. In Stage 1, the overall optimization problem turns out to be an MIQP problem. The optimization problem is described in MATLAB using YALMIP [30] and solved using CPLEX.

3.2. Stage 2: Optimal Power Flow. Optimal power flow (OPF) is a key optimization problem in power system operations. It is used to determine optimal setpoints for the system variables while satisfying power demand and respecting generator and network constraints. The main objective of the OPF problem is usually to minimize the power generation cost of the system. Importantly, the OPF problem also accounts for power losses in the system. Thus, the OPF problem can also be formulated to minimize power losses in the system. As the system load demand varies with time, it is essential to solve the OPF problem within a reasonable time. However, OPF is a nonconvex, nonlinear optimization problem which is NP-hard to solve [16]. Global optimization procedures to solve the OPF problem are computationally expensive. Notwithstanding their suboptimal results, gradient based methods have been widely adopted by researchers to solve the OPF problem due to their fast computational speeds. Among these, the quadratic programming method [31] and the interior point method (and its variants) [15, 32, 33] are popular due to their fast computational speeds.

3.2.1. Network Model. Let $\mathscr{N}$ and $\mathscr{L}$ represent the sets of N buses and L lines in the MG respectively. The generators are connected to a subset of $\mathscr{N}$. In this paper, multiple OPF problems are solved during different hours. Thus, all the variables and parameters of the OPF problem during hour k are denoted by $(\cdot)_k$. In this formulation, the polar form of the complex bus voltage $v_k \in \mathbb{C}^N$ is used as $v^i_k = V^i_k e^{j\delta^i_k}$, where V^i_k and δ^i_k are the magnitude and phase angle, respectively, of the voltage phasor v^i_k at bus $i \in \mathscr{N}$. The complex power injection vector is denoted by $s_k \in \mathbb{C}^N$ such that $s^i_k = P^i_{\mathrm{e},k} + jQ^i_{\mathrm{e},k}$ for bus $i \in \mathscr{N}$, where $P^i_{\mathrm{e},k}$ is the generated real power and $Q^i_{\mathrm{e},k}$ is the generated reactive power. All the transmission lines in the MG are modelled using the standard π-model. For transmission line l connecting buses i and j; $l = (i, j) \in \mathscr{L}$, let $Y \in \mathbb{C}^L$ be the branch admittance matrix having components $Y_{ij} = g_{ij} + jb_{ij}$, where g_{ij} and b_{ij} are the series conductance and susceptance, respectively, and b^{sh}_{ij} is the line charging susceptance. Also $d_k \in \mathbb{C}^N$ such that $d^i_k = P^i_{\mathrm{d},k} + \mathrm{j}Q^i_{\mathrm{d},k}$ for bus i, where $P^i_{\mathrm{d},k}$ and $Q^i_{\mathrm{d},k}$ are the active and reactive power demands at bus i, respectively, such that $P_{\mathrm{D},k} = \sum_{i\in\mathscr{N}} P^i_{\mathrm{d},k}$ and $Q_{\mathrm{D},k} = \sum_{i\in\mathscr{N}} Q^i_{\mathrm{d},k}$.

3.2.2. OPF Problem Formulation. The constraints for the OPF problem mainly adhere to Kirchhoff's laws and are formulated to ensure that the active and reactive powers are balanced at each bus while satisfying generation capability margins and voltage bounds. The constraints for the OPF problem are enumerated below.

(1) Active power balance at bus i is

$$P^{ij}_{\mathrm{e},k} = g_{ij}\left(V^i_k\right)^2 - g_{ij}V^i_k V^j_k \cos\left(\delta^{ij}_k\right) + b_{ij}V^i_k V^j_k \sin\left(\delta^{ij}_k\right); \quad i, j \in \mathscr{N}, \ \forall l \in \mathscr{L} \tag{24a}$$

$$P^i_{\mathrm{e},k} = \sum_{f\in\mathscr{F}(i)} P^f_{\mathrm{DG},k} + \sum_{e\in\mathscr{E}(i)} P^e_{\mathrm{BESS},k} + P_{\mathrm{Grid},k} + \sum_{z\in\mathscr{Z}(i)} P^z_{\mathrm{RES},k} - P^i_{\mathrm{d},k} + \sum_{h\in\mathscr{H}(i)} P^h_{\mathrm{IL},k} - \sum_{m\in\mathscr{M}(i)} P^m_{\mathrm{Pump},k} \tag{24b}$$

$$P^i_{\mathrm{e},k} = \sum_{j\in\mathscr{N}(i)} P^{ij}_{\mathrm{e},k}; \quad \forall i \in \mathscr{N} \tag{24c}$$

$$P^{e}_{\mathrm{BESS},k} = P^{e}_{\mathrm{bd},k} - P^{e}_{\mathrm{bc},k}; \quad \forall e \in \mathscr{E} \tag{24d}$$

$$P_{\mathrm{Grid},k} = P_{\mathrm{eb},k} - P_{\mathrm{es},k}. \tag{24e}$$

(2) Reactive power balance at bus i is

$$Q^{ij}_{\mathrm{e},k} = \left(b_{ij} + \frac{b^{\mathrm{sh}}_{ij}}{2}\right)\left(V^{i}_{k}\right)^{2} - b_{ij}V^{i}_{k}V^{j}_{k}\cos\left(\delta^{ij}_{k}\right) - g_{ij}V^{i}_{k}V^{j}_{k}\sin\left(\delta^{ij}_{k}\right); \quad i, j \in \mathscr{N},\ \forall l \in \mathscr{L} \tag{25a}$$

$$Q^{i}_{\mathrm{e},k} = \sum_{f\in\mathscr{F}(i)} Q^{f}_{\mathrm{DG},k} + \sum_{e\in\mathscr{E}(i)} Q^{e}_{\mathrm{BESS},k} + Q_{\mathrm{Grid},k} + \sum_{z\in\mathscr{Z}(i)} Q^{z}_{\mathrm{RES},k} - Q^{i}_{\mathrm{d},k} + \sum_{h\in\mathscr{H}(i)} Q^{h}_{\mathrm{IL},k} - \sum_{m\in\mathscr{M}(i)} Q^{m}_{\mathrm{Pump},k} \tag{25b}$$

$$Q^{i}_{\mathrm{e},k} = \sum_{j\in\mathscr{N}(i)} Q^{ij}_{\mathrm{e},k}; \quad \forall i \in \mathscr{N} \tag{25c}$$

$$Q^{e}_{\mathrm{BESS},k} = Q^{e}_{\mathrm{bd},k} - Q^{e}_{\mathrm{bc},k}; \quad \forall e \in \mathscr{E} \tag{25d}$$

$$Q_{\mathrm{Grid},k} = Q_{\mathrm{eb},k} - Q_{\mathrm{es},k}, \tag{25e}$$

where the active power flow ($P^{ij}_{\mathrm{e},k}$) and reactive power flow ($Q^{ij}_{\mathrm{e},k}$) through line l connecting buses i and j can be represented in (24a) and (25a) satisfying the physical laws of the power flow and $\delta^{ij}_{k} = \delta^{i}_{k} - \delta^{j}_{k}$. $P^{i}_{\mathrm{e},k}$ and $Q^{i}_{\mathrm{e},k}$ are the amounts of active and reactive power injections (if positive) or extractions (if negative) at bus i, respectively. It may be noted that all the reactive power variables (denoted using Q) follow a similar notation to the real power variables (denoted using P).

It is assumed that the pump loads and ILs consume reactive power equivalent to 50% of their active power consumption and that the converters of the BESSs and RESs at the PCC are capable of maintaining a power factor greater than 0.7. The sets of DGs, BESSs, RESs, ILs, and pumps connected to bus i are denoted by $\mathscr{F}(i), \mathscr{E}(i), \mathscr{Z}(i), \mathscr{H}(i)$, and $\mathscr{M}(i)$, respectively; the set of buses connected to bus i with transmission lines are denoted by $\mathscr{N}(i)$, where $\mathscr{F}(i) \subset \mathscr{F}, \mathscr{E}(i) \subset \mathscr{E}, \mathscr{Z}(i) \subset \mathscr{Z}, \mathscr{H}(i) \subset \mathscr{H}, \mathscr{M}(i) \subset \mathscr{M}$, and $\mathscr{N}(i) \subset \mathscr{N}$. Constraints (24c) and (25c) represent the active and reactive power balances at each bus, respectively. However, the additional variables $P^{ij}_{\mathrm{e},k}, Q^{ij}_{\mathrm{e},k}, P^{i}_{\mathrm{e},k}$, and $Q^{i}_{\mathrm{e},k}$ are omitted in the implementation.

(3) Active and reactive power injection limits of each power source are discussed in Section 3.3.

(4) Voltage bounds at bus i are

$$V^{i}_{k} \in \left[V^{i}_{\min}, V^{i}_{\max}\right]; \quad \forall i \in \mathscr{N}, \tag{26}$$

where $(\cdot)_{\min}$ and $(\cdot)_{\max}$ indicate the lower and upper bounds of the corresponding decision variable, respectively.

3.3. Coordination between Stage 1 and Stage 2. The EMS solves Stage 1 and Stage 2 alternately. In Stage 1, binary statuses and dispatch values for all the DGs, BESSs, pumps, and ILs in the MG are determined. In addition to this, a schedule for exchanging power with the utility grid is also determined. The power exchange schedule and dispatch values of the DGs, BESS, pumps, and ILs are shared with the OPF problem in Stage 2. The OPF problem is formulated by permitting a small degree of freedom around the scheduled power exchange values and dispatch values of the DGs and BESSs generated in Stage 1. In Stage 2, the network power losses are determined and power flow convergence is checked. The power losses are shared with Stage 1 which solves the UC problem including the power losses. The dispatch and power exchange values are shared with Stage 2. This iterative process continues till convergence. This process is illustrated in the flowchart shown in Figure 1. The first UC problem in Stage 1 is solved with an initial ($P^{\mathrm{loss}}_{e,k}$) = 0 MW for each hour. The status and dispatch vectors are then passed to Stage 2. Based on these values, the bounds of the controllable generator dispatch variables in the OPF subproblems are modified as shown below. Here, the DGs, BESSs, and the main grid supply are considered as controllable generators. Let $\widehat{P}^{g}_{\mathrm{e},k}, \widehat{u}^{g}_{k}$, and $\widehat{P}^{e}_{\mathrm{BESS},k}$ be the dispatch value, the commitment status for generator g, and the power flow from BESS e during hour k, respectively, received from Stage 1.

For f^{th} DG,

$$P^{f}_{\mathrm{e},k} \geq \widehat{u}^{f}_{k} \max\left\{(1-\alpha)\,\widehat{P}^{f}_{\mathrm{e},k}, P^{f}_{\mathrm{e,min}}\right\}, \quad \forall k \in K,\ \forall f \in \mathscr{F} \tag{27a}$$

$$P^{f}_{\mathrm{e},k} \leq \widehat{u}^{f}_{k} \min\left\{(1+\alpha)\,\widehat{P}^{f}_{\mathrm{e},k}, P^{f}_{\mathrm{e,max}}\right\}, \quad \forall k \in K,\ \forall f \in \mathscr{F} \tag{27b}$$

$$\widehat{u}^{f}_{k} Q^{f}_{\mathrm{e,min}} \leq Q^{f}_{\mathrm{e},k} \leq \widehat{u}^{f}_{k} Q^{f}_{\mathrm{e,max}}, \quad \forall k \in K,\ \forall f \in \mathscr{F}. \tag{27c}$$

The power supplies from the grid and the BESSs are bidirectional. Therefore, based on the power flow direction, the shifted domain is defined as follows.

For e^{th} BESS,

$$Q^{e}_{\mathrm{BESS,min},k} \leq Q^{e}_{\mathrm{BESS},k} \leq Q^{e}_{\mathrm{BESS,max},k}; \quad \forall e \in \mathscr{E}. \tag{28}$$

(1) If $\widehat{P}^{e}_{\mathrm{bd},k} \geq 0$ ($\widehat{P}_{\mathrm{BESS},k} \geq 0$),

$$P^{e}_{\mathrm{BESS},k} \geq \max\left\{(1-\alpha)\,\widehat{P}^{e}_{\mathrm{BESS},k}, 0\right\} \tag{29a}$$

$$P^{e}_{\mathrm{BESS},k} \leq \min\left\{(1+\alpha)\,\widehat{P}^{e}_{\mathrm{BESS},k}, P^{e}_{\mathrm{bd,max}}\right\}. \tag{29b}$$

(2) If $\widehat{P}^{e}_{\mathrm{bc},k} \geq 0$ ($\widehat{P}_{\mathrm{BESS},k} \leq 0$),

$$P^{e}_{\mathrm{BESS},k} \geq \min\left\{(1-\alpha)\,\widehat{P}^{e}_{\mathrm{BESS},k}, 0\right\} \tag{30a}$$

$$P^{e}_{\mathrm{BESS},k} \leq \max\left\{(1+\alpha)\,\widehat{P}^{e}_{\mathrm{BESS},k}, -P^{e}_{\mathrm{bc,max}}\right\}. \tag{30b}$$

Note that the shifted domains for the grid supply also can be defined similar to (28), (29a), (29b), (30a), and (30b) based on

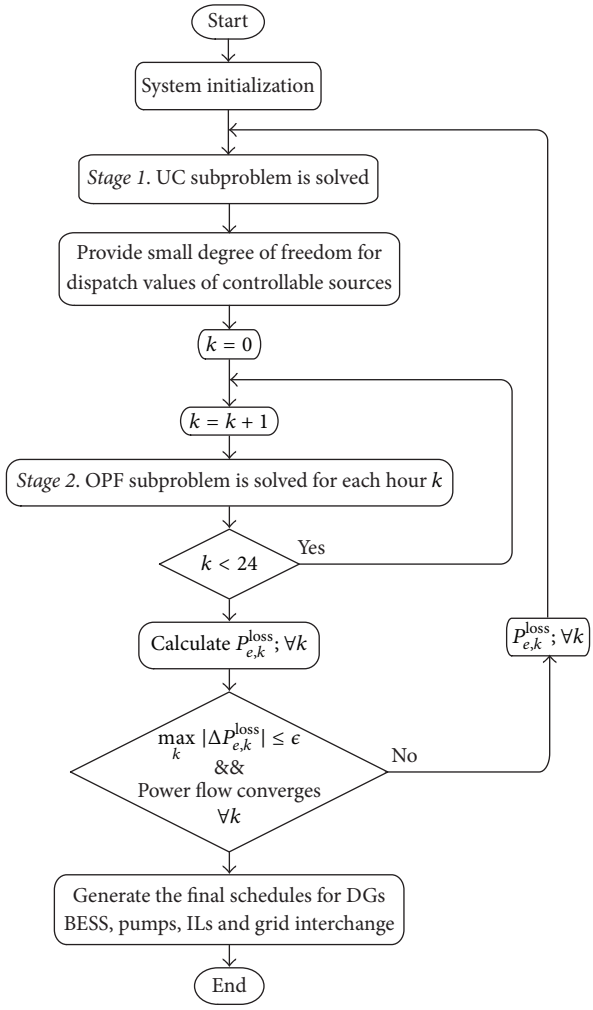

Figure 1: Flowchart for EMS layer computations.

the power flow direction. Here, α is a positive parameter value denoting the small degree of freedom permitted around the optimal dispatch values calculated in Stage 1. This parameter should be wisely chosen as a lower α leads to slower convergence and a higher α will result in the connection between Stage 1 and Stage 2 being lost. In this paper, α is taken as 0.03. The uncontrollable sources such as the RESs are fixed in a similar manner to Stage 1.

Importantly, the OPF problems solved in Stage 2 are decoupled from each other. Hence, parallel solving techniques can be used to further increase the computational performance if necessary. The OPF problem in Stage 2 computes the power loss during each hour. This calculation is shown below in (31a). The total power loss ($P^{loss}_{e,k}$) during each hour k is conveyed to the UC problem in Stage 1 for the next iteration. Thereafter, the UC problem is solved once again in Stage 1 with losses included and the dispatch values are shared with Stage 2.

$$P^{\text{loss}}_{\text{e},k} = \sum_{l \in \mathscr{L}} \left[P^{ij}_{\text{e},k} + P^{ji}_{\text{e},k} \right]; \quad i, j \in \mathscr{N},\ \forall l = (i, j) \in \mathscr{L},\ \forall k \in \mathscr{K}. \tag{31a}$$

The algorithm progresses iteratively till the power losses and the dispatch values converge. The proof of convergence for this method was demonstrated in [15].

4. Case Studies

Two exemplar MGs are modelled in this paper. First, the optimal scheduling of a modified IEEE 30-bus system is performed under the following operational scenarios to demonstrate the efficacy of the proposed EMS and pump scheduling formulations:

(1) Without optimal pump scheduling and ILs, water is pumped in the shortest possible time using only the 3 main pumps.

(2) Optimal pump scheduling is performed using the 3 main pumps alone.

(3) Optimal pump scheduling is performed using only the 3 main pumps and the 4 auxiliary pumps.

(4) Optimal pump scheduling is performed using only the 3 main pumps and the 3 ILs.

(5) Optimal pump scheduling is performed using the 3 main pumps, the 4 auxiliary pumps, and the 3 ILs.

Subsequently, to further validate the versatility and efficacy of the proposed EMS for different networks, the optimal scheduling of a modified IEEE 57-bus system is performed under Scenario 5.

4.1. Case Study 1: Optimal Scheduling of a Modified IEEE 30-Bus System. A modified IEEE 30-bus system is adopted as an exemplar MG for this case study. The base value is considered as 8000 kVA and the line resistance and reactance values are increased to 3 and 1.5 times the p.u. values provided in the standard MATPOWER case file for the IEEE 30-bus system, respectively [34]. In the 30-bus system used in this paper, the three DGs are connected to buses 27, 2, and 3, respectively, while the BESS and wind farm are connected to bus 22. The solar PV plant is connected to bus 13 while bus 1 serves as the point of common coupling (PCC) with the main utility grid. The 3 main pumps are connected to bus 27 while the 4 auxiliary pumps are connected to bus 29. Finally, the summation of ILs is distributed among the load buses in proportion to their nominal load demand.

4.1.1. System Initialization. For all the simulation scenarios, it was assumed that the main pumps were switched off prior to the start of the optimization period. For Scenarios 3 and 5, it was assumed that the auxiliary pumps were switched off prior to the start of the optimization period. Furthermore, it was assumed that $\text{SOC}^e_1 = 0.6$. Finally, it was assumed that all the DGs in the MG were switched off prior to the start of the optimization period.

All the scenarios were simulated under the assumption that accurate point forecasts for load demand (excluding pump loads), electricity prices, and RES generation were available. The electricity price forecasts in this paper were adapted from [35, 36]. The forecasts for load demand (excluding pump loads), RES generation, and electricity prices in

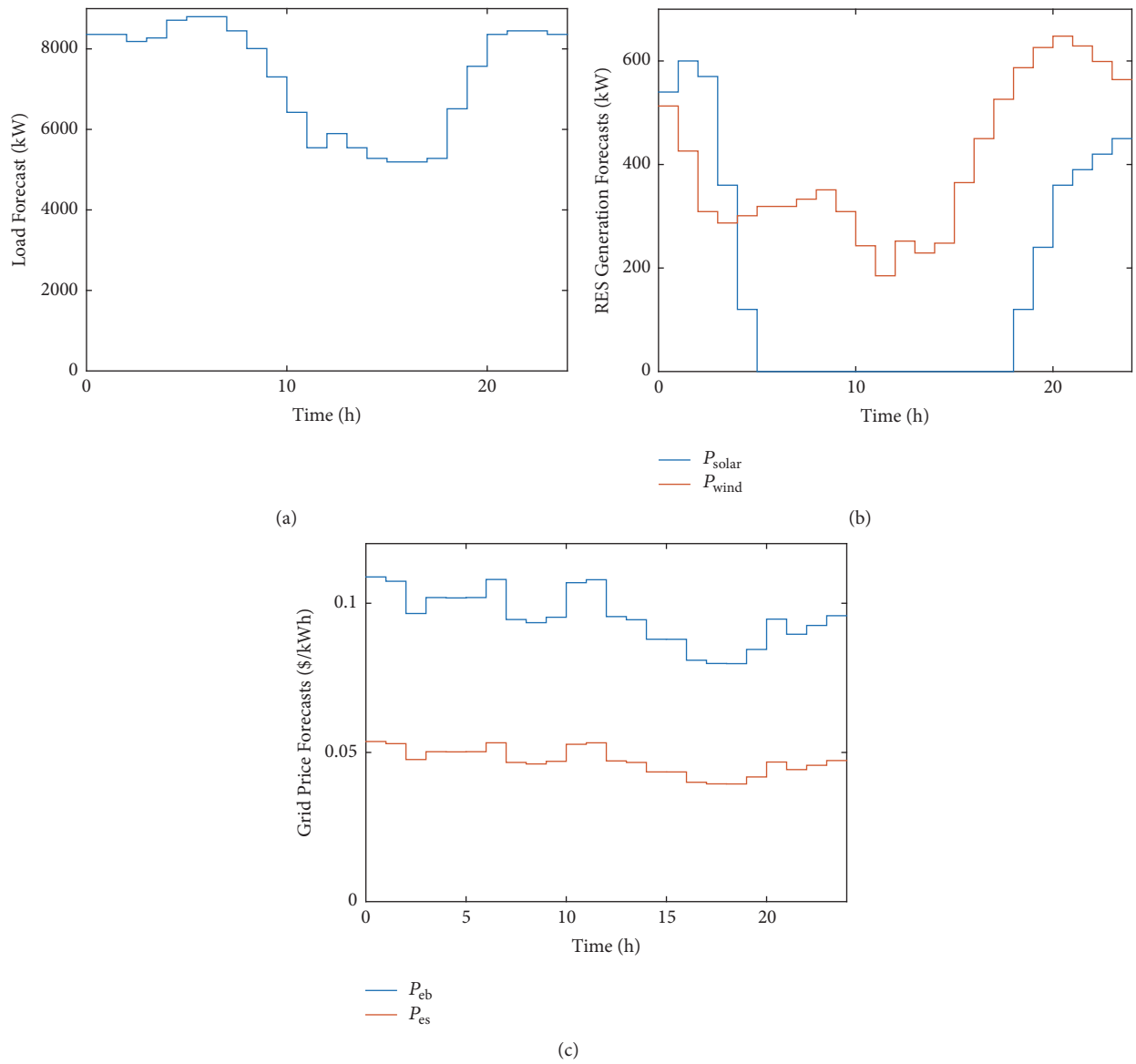

Figure 2: Forecasts of (a) load demand, (b) RES generation, and (c) electricity price.

this case study are shown in Figures 2(a), 2(b), and 2(c), respectively.

4.1.2. Optimal Scheduling Results. The final dispatch values of the DGs in Scenarios 1–5 are shown in Figures 3(a), 4(a), 5(a), 6(a), and 7(a), respectively. The BESS charge and discharge profiles in Scenarios 1–5 are shown in Figures 3(b), 4(b), 5(b), 6(b), and 7(b), respectively. The power purchased from the main grid, P_{eb}, in Scenarios 1–5 is shown in Figures 3(c), 4(c), 5(c), 6(c), and 7(c), respectively. The schedules for the main pumps in Scenarios 1–5 are shown in Table 3. The auxiliary pump schedules are provided in Table 4. The IL curtailment schedules in Scenarios 4 and 5 have been illustrated in Figures 8 and 9, respectively.

In Scenario 1, it is assumed that the 3 main pumps are switched on during the first 3 hours of the day in order to pump the water in the shortest possible time. This action has major cost implications since the overall system load demand is high during the first 3 hours of the day. This is evidenced by the results shown in Table 2. From Figure 3(c), it is observed that P_{eb} exceeds the contracted capacity of 0.7 MW during the first 3 hours. As a result, an uncontracted capacity charge of \$11,991.5 is incurred. It is also observed from Figure 3(c) that the EMS purchases electricity from the utility grid beyond the contracted capacity even during hours when the total load demand is lesser. This can be attributed to the methodology used to calculate the uncontracted capacity cost shown in (22) and (23). Consequently, from Figure 3(a), it is seen that DG 3 is shutdown from hour 6 onwards and DG 2 is shutdown between hours 14 and 17. From hour 18 onwards, when load demand starts increasing, DG 2 is once again started up and operated at full capacity. The relatively cheaper DG 1 is operated at full capacity throughout the day.

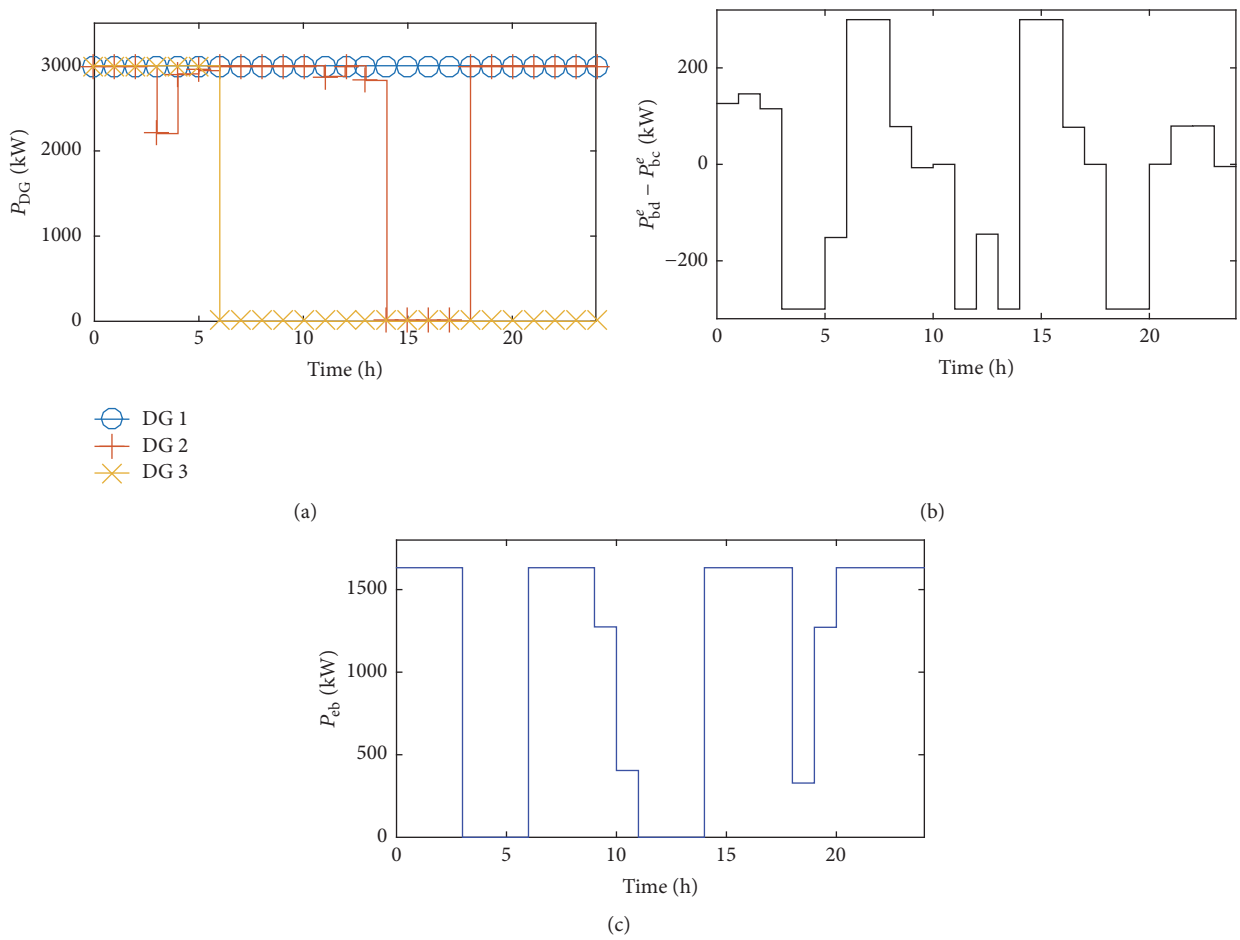

Figure 3: Scenario 1: (a) dispatch values of DG 1, DG 2, and DG 3, (b) BESS charge and discharge profiles, and (c) P_{eb}.

Table 2: Cost breakdown and computational times for Scenarios 1–5.

Scenario #	Uncontracted capacity cost ($)	Interruptible load cost ($)	Total cost ($)	Percentage reduction in total cost	Computational time (s)
1	11,991.50	-	34,710.10	-	38.11
2	0	-	29,997.80	13.58%	60.59
3	0	-	29,945.11	13.73%	136.04
4	0	864.21	22,995.63	33.75%	60.81
5	0	861.90	22,911.79	33.99%	108.53

From Table 2, it is observed that the introduction of pump scheduling in Scenario 2 eliminates the uncontracted capacity charge incurred in Scenario 1. From Figure 4(a), it is observed that all 3 DGs are operated during the hours of peak load demand (hours 0–10 and 20–24). From Figure 4(c), it is clear that the maximum power imported from the main grid does not exceed 0.7 MW. From Figure 4(b), it is seen that the BESS usage in Scenario 2 is much lower than what is observed in Scenario 1. In Scenario 1, it was observed that the MG was forced to import uncontracted capacity during the first 3 hours of the day to meet the high load demand. Due to this, the EMS continued importing power from the main grid during the later hours of the day as well. Due to the elimination of the uncontracted capacity in Scenario 2, DG 2 is operated throughout the day. It is clear from Table 3 that the pump scheduling ensures that only 1 pump is operated at a time to avoid uncontracted capacity. Moreover, from Table 3, it is observed that main pumps 1 and 3 are operated during the first 4 hours and last 4 hours, respectively. During these hours, all 3 DGs are operational thereby ensuring that the MG has enough running capacity to accommodate the main pumps.

Compared to Scenario 2, a reduction of 1 hour in main pump usage is observed in Scenario 3 due to the introduction of auxiliary pumps. Consequently, as observed in Table 2, there is a marginal reduction of $53 in the total cost for

Table 3: Schedule of main pumps for Scenarios 1–5.

Scenario	Main Pump 1	Main Pump 2	Main Pump 3
1	[1,1,1,0,0,0,0,0,0,0,0,0,0,0,0,0,0,0,0,0,0,0,0,0]	[1,1,1,0,0,0,0,0,0,0,0,0,0,0,0,0,0,0,0,0,0,0,0,0]	[1,1,1,0,0,0,0,0,0,0,0,0,0,0,0,0,0,0,0,0,0,0,0,0]
2	[0,0,0,0,0,0,0,0,0,1,0,0,0,0,0,0,0,0,0,0,0,0,0,0]	[1,1,1,1,0,0,0,0,0,0,0,0,0,0,0,0,0,0,0,0,0,0,0,0]	[0,0,0,0,0,0,0,0,0,0,0,0,0,0,0,0,0,0,0,0,1,1,1,1]
3	[0,0,0,0,0,0,0,0,0,1,0,0,0,0,0,0,0,0,0,0,0,0,0,0]	[0,0,0,0,0,0,0,0,0,0,0,0,0,0,0,0,0,0,0,0,1,1,1,1]	[1,1,1,0,0,0,0,0,0,0,0,0,0,0,0,0,0,0,0,0,0,0,0,0]
4	[0,0,0,0,0,0,0,1,1,0,0,0,0,0,0,0,0,0,0,0,0,0,0,0]	[0,0,0,0,0,0,0,0,0,0,0,0,1,1,1,1,1,0,0,0,0,0,0,0]	[0,0,0,1,1,0,0,0,0,0,0,0,0,0,0,0,0,0,0,0,0,0,0,0]
5	[0,0,0,1,0,0,0,0,0,0,0,0,0,0,0,0,0,0,0,0,0,0,0,0]	[0,0,0,0,0,0,0,0,0,0,0,0,1,1,1,1,1,0,0,0,0,0,0,0]	[0,0,0,0,0,0,0,1,1,0,0,0,0,0,0,0,0,0,0,0,0,0,0,0]

Table 4: Schedules of auxiliary pumps for Scenarios 3 and 5.

Scenario	Aux. Pump 1	Aux. Pump 2	Aux. Pump 3	Aux. Pump 4
3	[0,0,0,1,0,0,0,0,0,0,0,0,0,0,0,0,0,0,0,0,0,0,0,0]	[0,0,0,1,0,0,0,0,1,0,0,0,0,0,0,0,0,0,0,0,0,0,0,0]	[0,0,0,0,0,0,0,0,0,0,0,0,0,0,0,0,1,0,0,0,0,0,0,0]	[0,0,0,0,0,0,0,0,1,0,0,0,0,0,0,1,0,1,0,0,0,0,0,0]
5	[0,0,0,0,1,0,0,0,0,0,0,1,0,0,0,0,0,0,0,1,0,0,0,0]	[0,0,0,0,0,0,0,0,0,0,0,1,0,0,0,0,0,0,0,1,0,0,0,0]	[0,0,0,0,0,0,0,0,0,0,0,0,0,0,0,0,0,0,0,1,0,0,0,0]	[0,0,0,0,0,0,0,0,0,0,0,0,0,0,0,0,0,0,0,0,1,0,0,0]

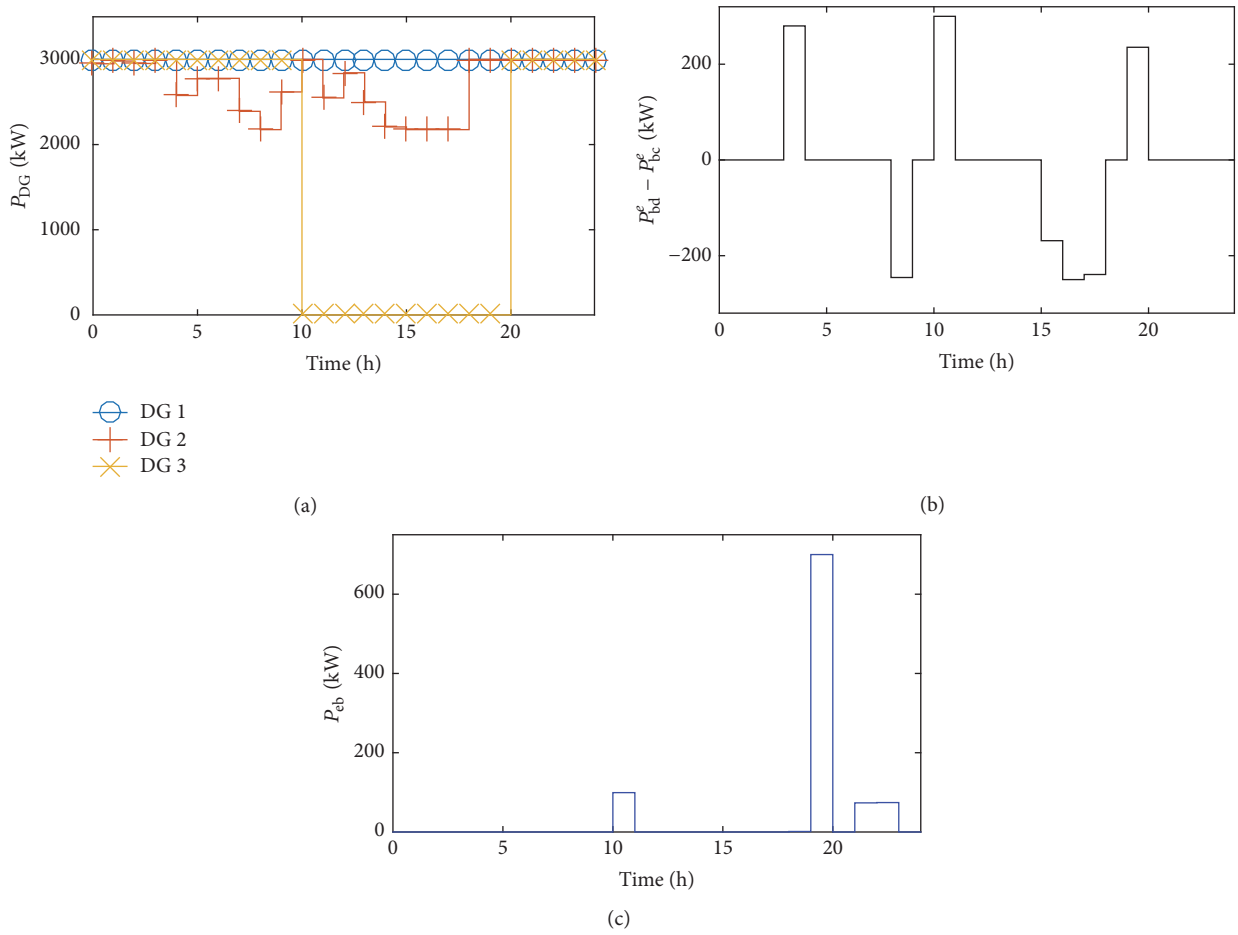

FIGURE 4: Scenario 2: (a) dispatch values of DG 1, DG 2, and DG 3, (b) BESS charge and discharge profiles, and (c) P_{eb}.

Scenario 3 when compared with Scenario 2. The schedules of main pumps, dispatch of DGs, BESS charge and discharge profiles, and trends in electricity purchase from the main grid in Scenario 3 are similar to Scenario 2.

As observed from Table 2, the introduction of ILs in Scenario 4 leads to a reduction of $6,949 in the total cost when compared with Scenario 3. From Figure 8, it is clear that the ILs are mainly utilized during the first 3 hours and the last 5 hours of the day when the load demand is quite high. Compared to the previous scenarios, the usage of the relatively expensive DG 3 is significantly reduced in Scenario 4. As observed from Figure 6(a), the EMS keeps the relatively expensive DG 3 switched off during the first 3 hours. However, DG 3 needs to be switched on at hour 4 since the total curtailment permitted for each IL in a day is capped at 2 MWh. As shown in Figure 6(c), the main grid electricity makes up for any shortfall without exceeding the contracted capacity as and when required. It is observed from Table 3 that the main pumps are mostly used during the valleys in the load profile.

The trends in Figures 7(a)–7(c) are quite similar to Figures 6(a)–6(c). As with Scenario 3, the inclusion of auxiliary pumps leads to a marginal decrease in the total cost of Scenario 5 when compared with Scenario 4. However, from Table 2, it is seen that the total cost in Scenario 5 (lowest cost scenario) is 33.99% lower than the total cost in Scenario 1 which is the worst case. In Scenario 5, unlike Scenario 4, a main pump is not operated during hour 5. From Figures 7(b) and 9, it is seen that this eliminates the need to import power from the main grid and curtail ILs during hour 5 as was the case in Scenario 4.

Figure 10 illustrates the convergence of the 2-stage EMS computations described in Section 3. From Figure 10, it is observed that Scenario 3 takes more number of iterations to converge. From Figure 10, it is observed that the total operating costs of all the scenarios reach close to their final values after 3 iterations. It may be noted that the trajectories followed by both total operating cost and total power loss are similar. Finally, the sale of electricity to the utility grid was not observed in any of the scenarios considered.

4.2. Case Study 2: Optimal Scheduling of a Modified IEEE 57-Bus System. A modified IEEE 57-bus system is adopted as an exemplar MG for this case study. The optimal scheduling of the modified 57-bus MG is performed under Scenario 5. The base value is considered as 7000 kVA and the line reactance values are decreased by 50% when compared with the p.u. values provided in the standard MATPOWER case file for the IEEE 57-bus system [34]. In the 57-bus system used in this paper, the three DGs are connected to buses 1, 8, and 9,

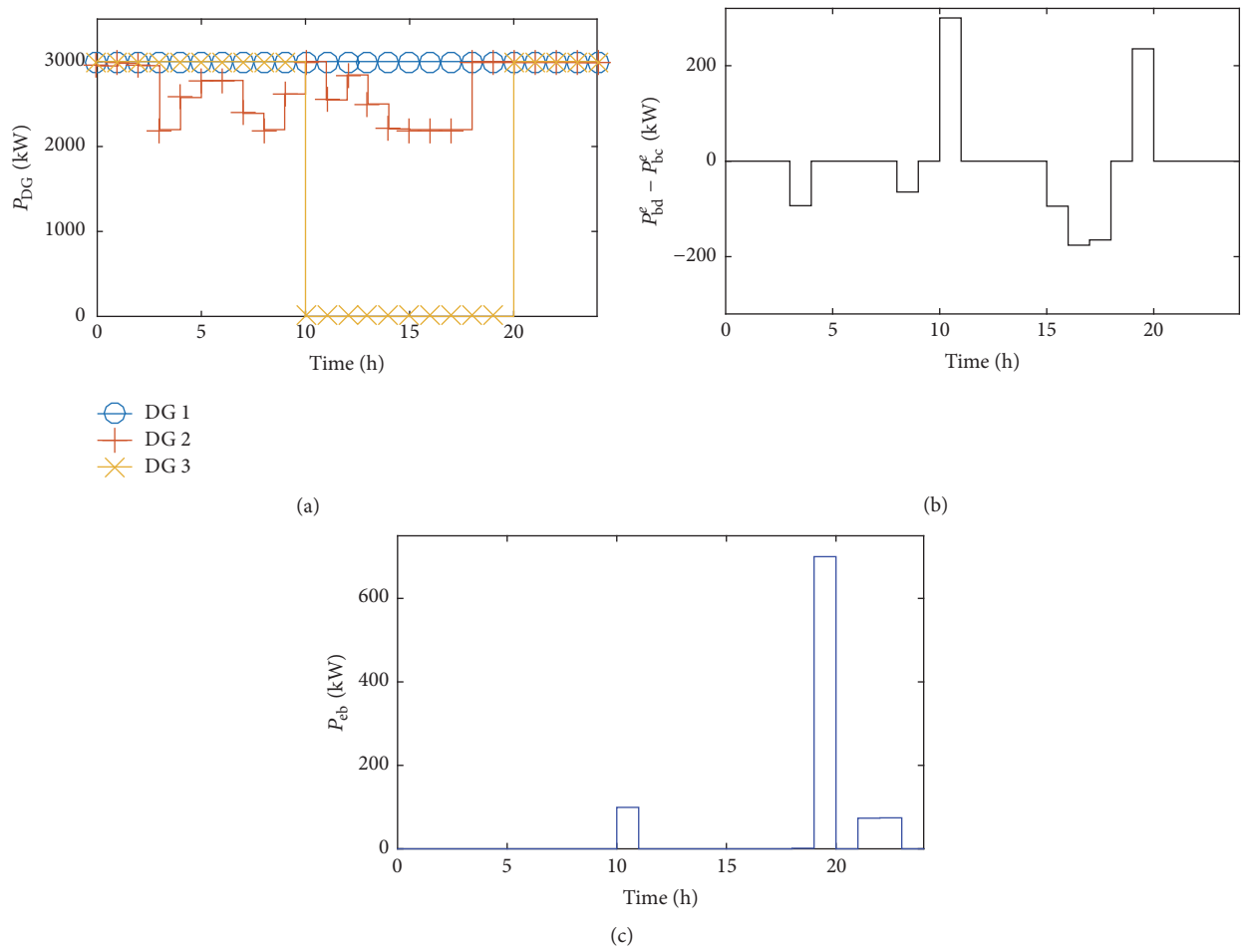

FIGURE 5: Scenario 3: (a) dispatch values of DG 1, DG 2, and DG 3, (b) BESS charge and discharge profiles, and (c) P_{eb}.

respectively, while the wind farms are connected to buses 2 and 12. BESSs are connected to buses 2 and 12. A solar PV plant is connected to bus 3 while bus 6 serves as the point of common coupling (PCC) with the main utility grid. The 3 main pumps are connected to bus 2 while the 4 auxiliary pumps are connected to bus 1. Finally, the summation of ILs is distributed among the load buses in proportion to their nominal load demand.

4.2.1. System Initialization. For this case study, it was assumed that all the main pumps and auxiliary pumps were switched off prior to the start of the optimization period. Furthermore, it was assumed that initial SOCs for the two BESSs in the MG were 0.6 and 0.5, respectively. Finally, it was assumed that all the DGs in the MG were switched off prior to the start of the optimization period.

This case study was performed under the assumption that accurate point forecasts for load demand (excluding pump loads), electricity prices, and RES generation were available. The load demand forecast for this case study is shown in Figure 11. Forecasts of the solar PV plant and one wind power plant in this case study are shown in Figure 2(b) while the forecast for the second wind power plant in this case study is also shown in Figure 11.

4.2.2. Optimal Scheduling Results. The final dispatch values of the DGs in this case study are shown in Figure 12(a). The charge and discharge profiles of the BESSs in this case study are shown in Figure 12(b). The power purchased from the main grid in this case study, P_{eb}, is shown in Figure 12(c). In this case study, Main Pump 1 operates between hours 16 and 18; Main Pump 2 operates only during hour 19; Main Pump 3 operates between hours 12 and 15. Auxiliary Pump 1 operates during hours 15, 17, and 18; Auxiliary Pump 2 operates during hours 11 and 15; Auxiliary Pump 3 operates during hour 15; and Auxiliary Pump 4 operates during hour 11.

The results of this case study largely agree with those of Case Study 1. The pumps are generally operated during the valley periods in the load profile which coincide with the late night hours. A clear indication of this is the operation of 1 main pump and 3 auxiliary pumps during hour 15. From Figure 11, it is observed that the load demand is at its lowest during hour 15. The EMS avoids using the expensive DG 3 due to the higher contribution from the RESs in this case study. DGs 1 and 2 are used at nearly their full capacities throughout the 24-hour period. From Figure 13, it is observed that the ILs are utilized during the hours when the load demand is at its peak. During these hours, the EMS also imports power from the utility grid without exceeding the contracted capacity of

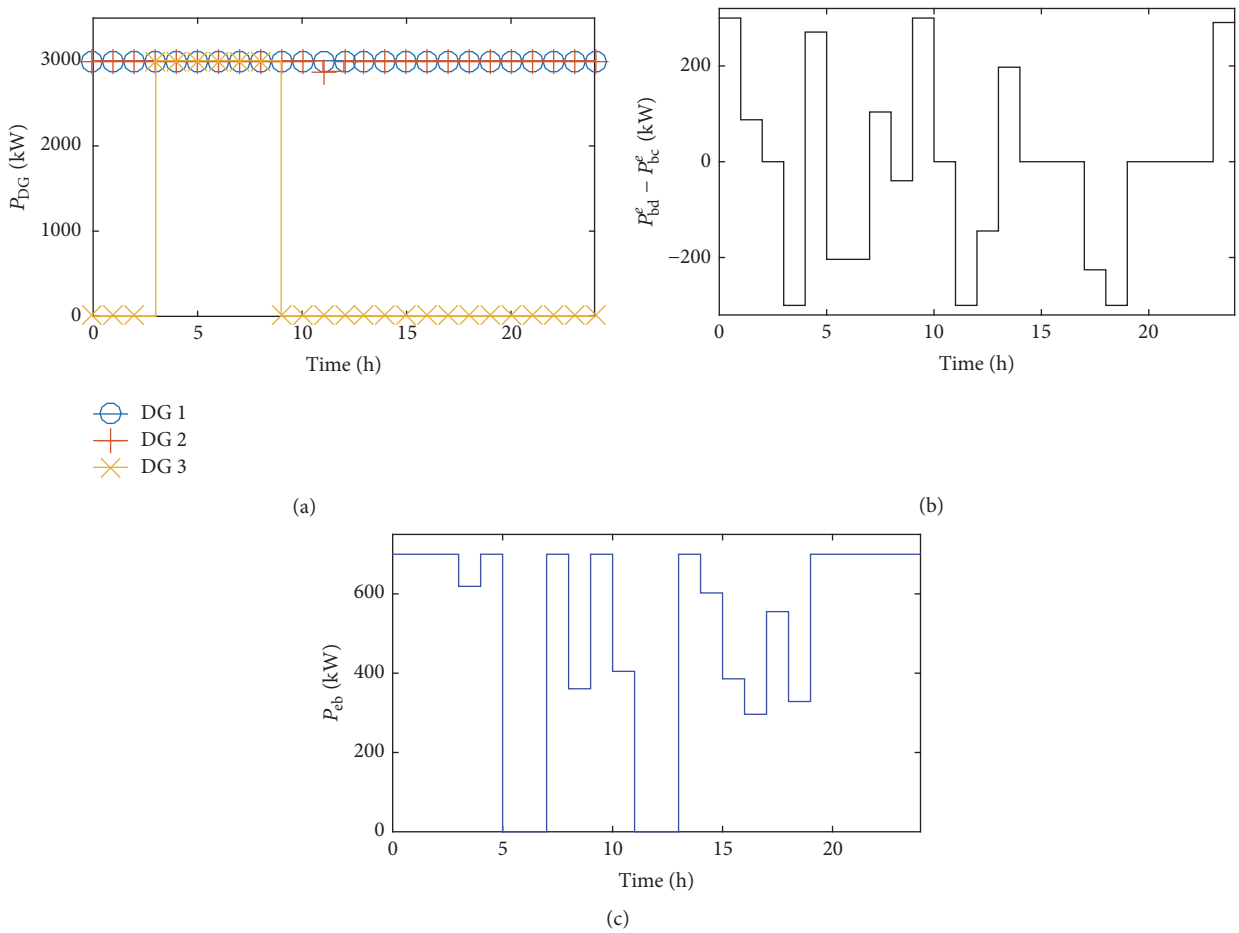

FIGURE 6: Scenario 4: (a) dispatch values of DG 1, DG 2, and DG 3, (b) BESS charge and discharge profiles, and (c) P_{eb}.

0.8 MW. From Figure 12(b), it is observed that the BESSs discharge during some peak loading hours while charging during the valley periods in the load profile. The overall MG cost in this case study was $15842.79 while the computational time taken to solve the problem was 154.49 s. The higher contribution from the RESs results in a lower cost in this case study.

Finally, Figure 14 illustrates the convergence of the 2-stage EMS computations. From Figure 14, it is observed that the EMS takes more number of iterations to converge compared to all the scenarios in Case Study 1 except Scenario 3. Finally, the sale of electricity to the utility grid was not observed in this case study.

4.3. Discussions and Scope for Future Work. This section discusses the limitations of this paper and how the assumptions made could potentially impact the optimal MG scheduling results. Furthermore, some possible future research directions are also presented. Case Study 1 clearly established the potential of load management strategies in reducing the MG operating cost. In Scenario 1, it was assumed that the main pumps would be switched on during the first 3 hours of the day to pump out the water in the fastest possible time. Even if this assumption was not true, load management strategies such as pump scheduling and curtailment of ILs still provide the maximum reduction in operation cost without compromising on any operational requirements.

The MG models in this paper were developed using the MLD approach which essentially results in a state-space representation of the system as shown in (18). Consequently, the system states need to be initialized before starting the simulation. The initial system states provide a snapshot of the MG prior to the start of the simulation. The initialization of the system states needs to be done carefully to ensure that all the constraints are respected and the overall tractability of the problem is not affected. In line with these requirements, the authors had randomly selected a set of values to initialize the system states. However, it is clear that the selection of different initial states for the system would result in different system evolution according to (18) and (19) and consequently different scheduling results.

In this paper, the optimal MG scheduling is performed on the basis of fixed forecasts for RES generation, electricity price, and load demand. In case of any uncertainties in the RES generation and electricity price forecasts, the resulting MG schedules which are generated by the EMS may be suboptimal. One way to deal with the uncertainties is to introduce spinning reserve constraints in the scheduling problem which would enable the MG to manage the loss of the largest RES. The objective of this paper was to present

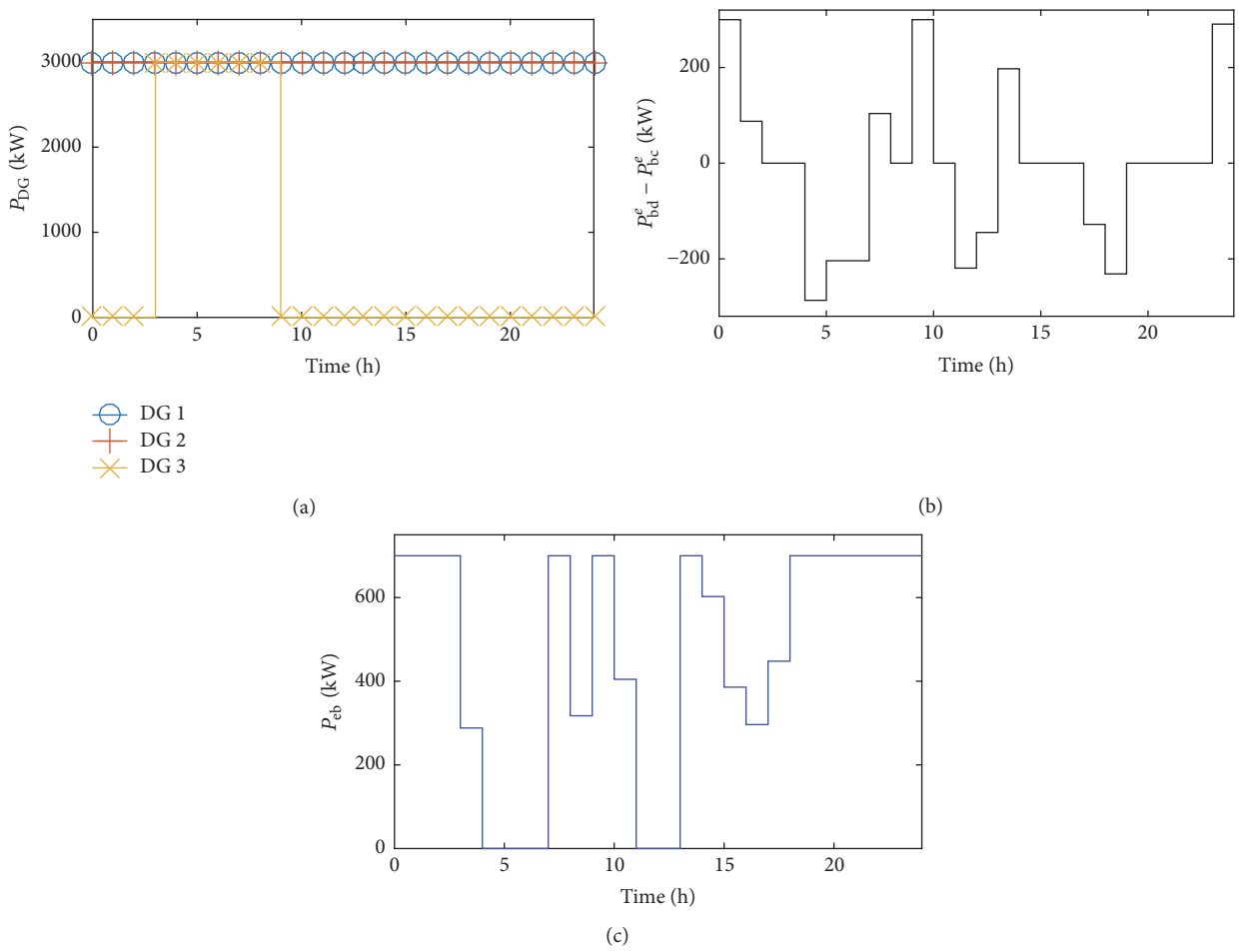

Figure 7: Scenario 5: (a) dispatch values of DG 1, DG 2, and DG 3, (b) BESS charge and discharge profiles, and (c) P_{eb}.

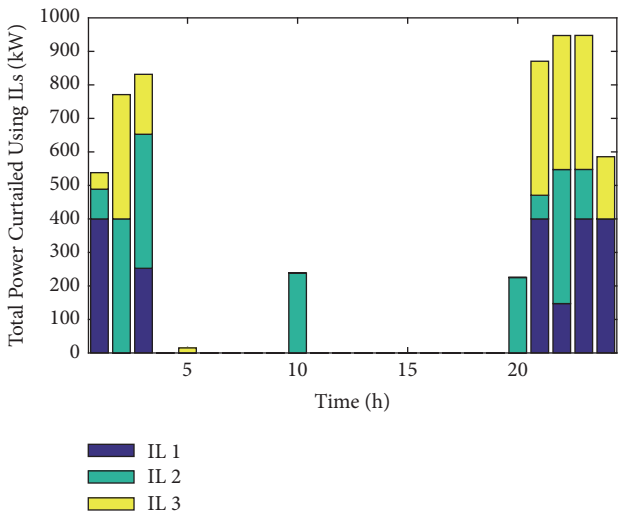

Figure 8: Curtailment of ILs in Scenario 4.

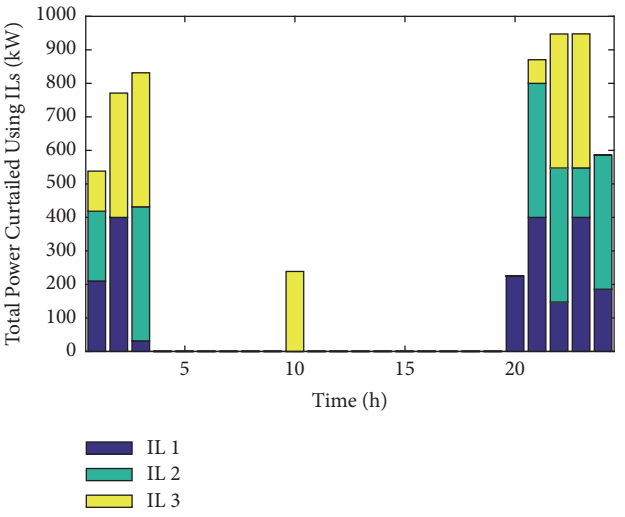

Figure 9: Curtailment of ILs in Scenario 5.

the EMS architecture and problem formulation. The authors have not focused on handling uncertainties in this work. In this context, one possible direction for future work is to develop a scenario-based robust optimization approach for handling forecast uncertainties in the optimal scheduling of MGs while also respecting the network constraints using the EMS architecture explained in this paper.

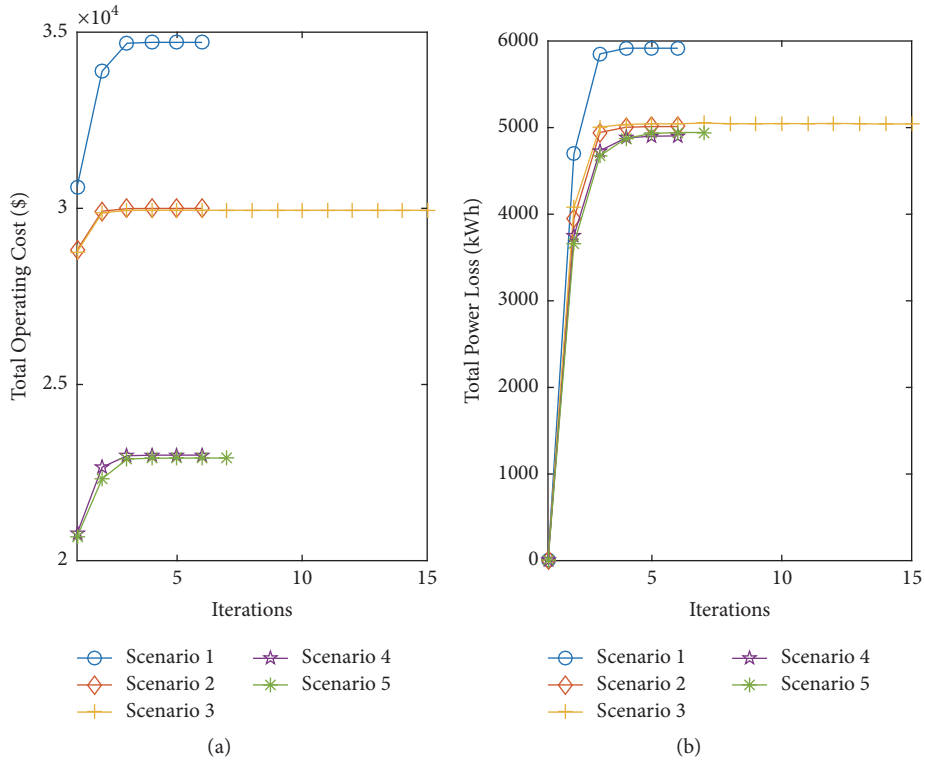

Figure 10: Evolution of (a) total operating cost and (b) total power loss over 24 hours.

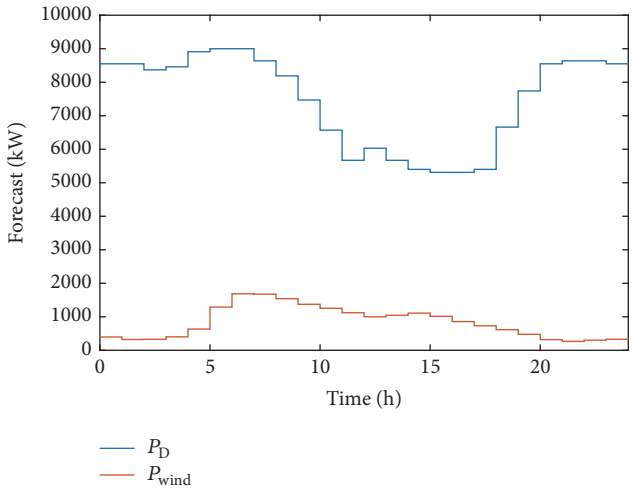

Figure 11: Forecasts of load demand and wind power plant generation for Case Study 2.

The concept of eco-industrial parks (EIPs) has been recently gaining research attention. A significant attribute of EIPs is the sharing of energy between different business entities. Typically, industrial parks consume and produce both heat and electricity. In future, the framework proposed in this paper could be integrated with an industrial park level waste heat recovery network with combined cycle gas turbines bridging the electrical and thermal energy streams. Future studies could also focus on designing efficient load management strategies for such multienergy networks.

5. Conclusions

This paper developed a first principle model of industrial MGs including DGs, BESSs, pump loads, and ILs. Subsequently, a 2-stage EMS was proposed for optimally scheduling the MGs. The EMS adopted an iterative procedure to integrate the UC and OPF problems, thereby satisfying network constraints. Load management strategies including pump scheduling and curtailment of ILs were adopted by the EMS to reduce the total electricity cost. The efficacy of the EMS including load management strategies was demonstrated on a 30-bus exemplar MG system under five operational scenarios. From the scheduling results obtained for the 5 scenarios, it was observed that the nonadoption of efficient load management strategies led to significant uncontracted capacity charges. The results also demonstrated the potential of optimal pump scheduling in realizing significant cost savings through the reduction or elimination of uncontracted capacity charges. The impact of auxiliary pumps and curtailment of ILs on the total cost of the system was also analyzed. It was found that while auxiliary pumps had a marginal impact on the total cost, curtailment of ILs realized significant cost savings. Finally, the scalability and efficacy of the EMS were demonstrated on an exemplar 57-bus MG. The 57-bus case study demonstrated the scalability of the EMS architecture

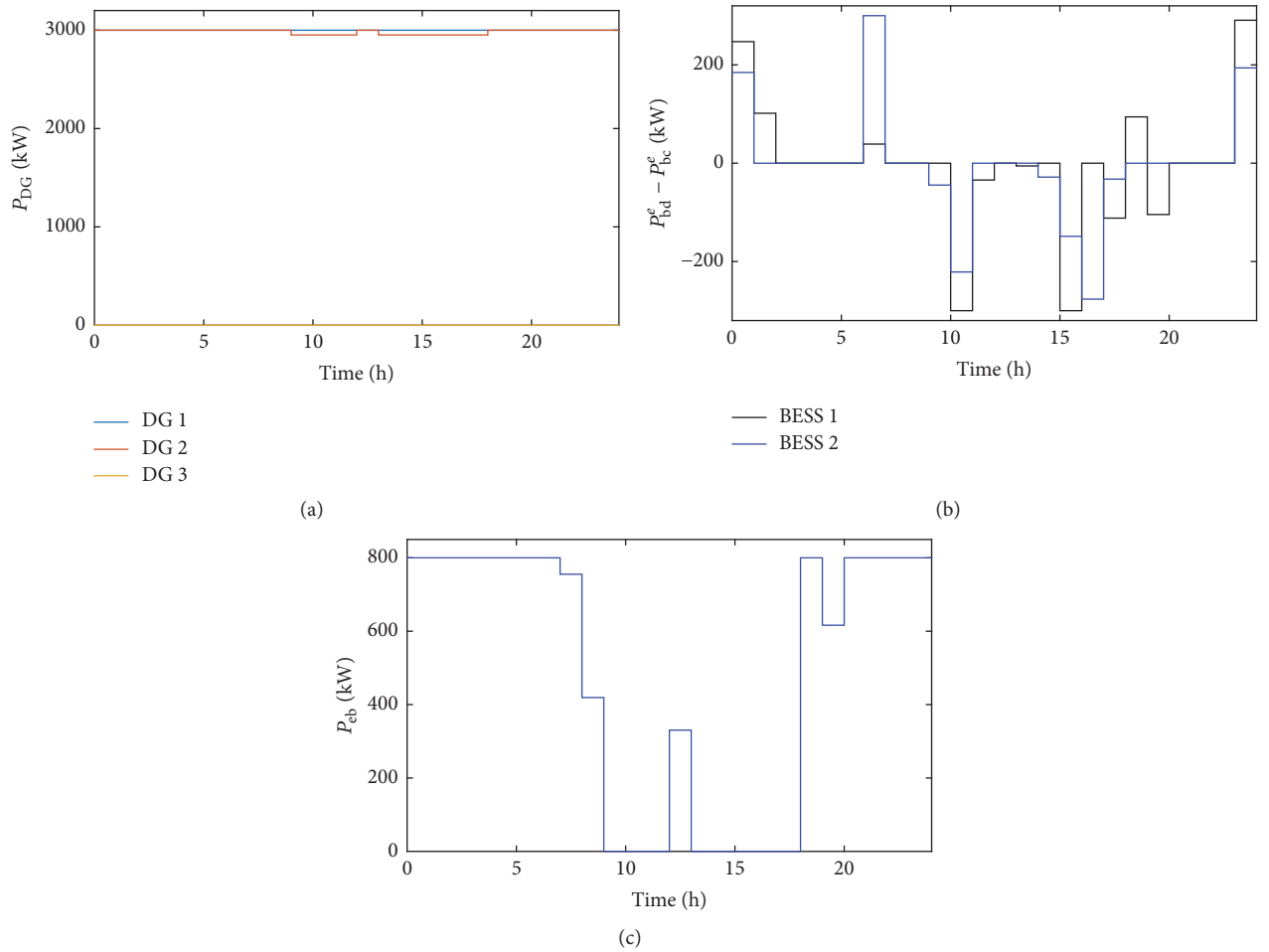

FIGURE 12: Optimal scheduling of modified IEEE 57-bus system: (a) dispatch values of DG 1, DG 2, and DG 3, (b) charge and discharge profiles of BESSs, and (c) P_{eb}.

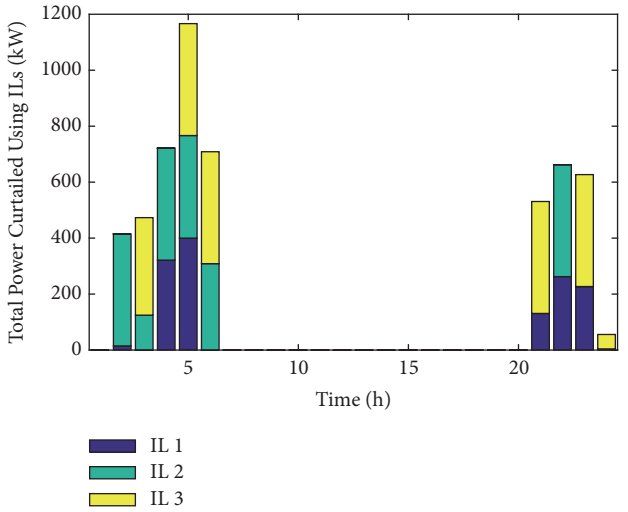

FIGURE 13: Curtailment of ILs in modified IEEE 57-bus system.

while also validating the results obtained in the 30-bus case study.

Nomenclature

A. Indices

k: Index for time (hours)
f: Index for diesel generators (DGs)
e: Index for battery energy storage systems (BESSs)
h: Index for interruptible loads (ILs)
m: Index for pumps
z: Index for renewable energy sources (RESs)
l: Index for lines
i, j: Index for buses.

B. Sets

$\mathcal{K}$: Set of all hours in a day; that is, $\mathcal{K} = \{1, 2, 3, \ldots, 24\}$
$\mathcal{F}$: Set of DGs in the MG
$\mathcal{E}$: Set of BESSs in the MG
$\mathcal{H}$: Set of ILs in the MG
$\mathcal{M}$: Set of pumps in the MG
$\mathcal{Z}$: Set of RESs in the MG
$\mathcal{N}$: Set of buses in the MG
$\mathcal{L}$: Set of lines in the MG.

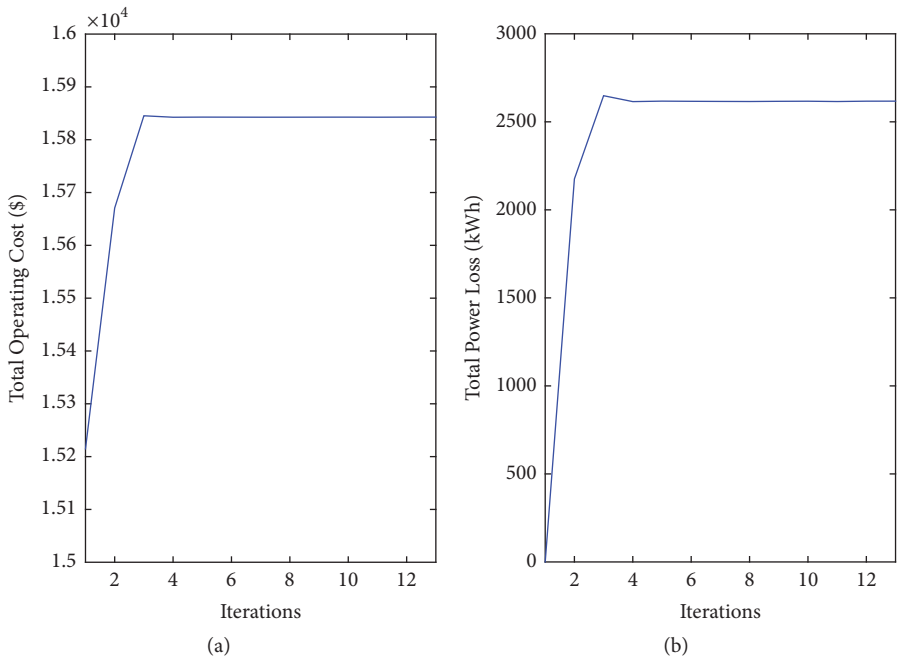

Figure 14: Evolution of (a) total operating cost and (b) total power loss over 24 hours.

C. Parameters

$(\cdot)_{\min}$: Lower bound of the corresponding parameter
$(\cdot)_{\max}$: Upper bound of the corresponding parameter
C^f_{SU}: DG start-up cost coefficient ($)
c^f_0, c^f_1, c^f_2: Fuel cost curve coefficients in $/MW^2, $/MW, and $, respectively
η^e_c/η^e_d: BESS charging/discharging efficiency percentages
P^e_{1C}: Power required by the BESS to charge 100% in one hour (kW)
I^e: BESS purchase cost ($)
B^e_{cap}: BESS capacity (kWh)
N^e: Number of cycles for BESS to reach end of life (h)
$T^e_{\text{bc}}/T^e_{\text{bd}}$: Average number of hours BESS charges/discharges in a day
C_p: Power coefficient which is a function of the tip speed ratio
ρ: Air density
A: Area swept by the rotor blades
I_L,I_S: Light current and diode saturation current, respectively
R_S,R_{Sh}: Series and shunt resistances, respectively
C^m: Pump capacity in MW
Q^m: Pump flow rate in m^3/h
τ: Optimization interval
V_d: Volume of liquid to be pumped in 24 h in m^3
P_{CC}: Contracted capacity in MW
U_{CC}: Uncontracted capacity cost coefficient in $/MW/month
g_{ij},b_{ij}: Series conductance and susceptance, respectively
b^{sh}_{ij}: Line charging susceptance.

D. Variables

$b^f_{\text{SU},k}$: Binary variable indicating DG start-up status
$b^f_{\text{DG},k}$: Binary variable indicating DG commitment status
$P^f_{\text{DG},k}$: Real power output of DG (kW)
SOC^e_k: BESS state of charge (SOC) (scale of 0-1)
$P^e_{\text{bc},k}/P^e_{\text{bd},k}$: BESS charging/discharging power (kW)
v_{wind}: Wind velocity
v_{pv},i_{pv}: Operating voltage and current of PV module, respectively
p^h_k: Compensation paid in $/MWh to IL
$b^h_{\text{IL},k}$: Binary variable indicating IL status
$P^h_{\text{IL},k}$: Amount of IL curtailed (kW)
b^m_k: Binary variable indicating pump status
$b^m_{\text{SU},k}$: Binary variable indicating pump start-up status
$P^z_{\text{RES},k}$: Real power produced by RES in kW
$C_{\text{p},k}$: Price at which electricity is purchased from the utility grid in $/kWh
$P_{\text{eb},k}$: Real power purchased from the utility grid in kW
$C_{\text{s},k}$: Price at which electricity is sold to the utility grid in $/kWh
$P_{\text{es},k}$: Real power sold to the utility grid in kW
P_{UC}: Uncontracted capacity in MW
V^i_k: Magnitude of the voltage phasor v^i_k

δ_k^i: Phase angle of the voltage phasor v_k^i
s_k: Complex power injection in MVA
$P_{e,k}^i$: Generated active power in kW
$Q_{e,k}^i$: Generated reactive power in kvar
$P_{d,k}^i$: Active power demand in kW
$Q_{d,k}^i$: Reactive power demand in kvar
$P_{e,k}^{ij}$: Active power flow through line l connecting buses i and j in kW
$Q_{e,k}^{ij}$: Reactive power flow through line l connecting buses i and j in kvar
$P_{e,k}^{\text{loss}}$: Total power loss in kW
$\widehat{P}_{e,k}^g$: Dispatch value of generator g received by Stage 2 from Stage 1 in kW
$\widehat{u}_k^g$: Commitment status of generator g received by Stage 2 from Stage 1
$\widehat{P}_{\text{BESS},k}^e$: Value of power flow from the BESS received by Stage 2 from Stage 1 in kW.

Conflicts of Interest

The authors declare that they have no conflicts of interest.

Acknowledgments

The authors would like to acknowledge funding support from NTU Start-Up Grant. The work of L. P. M. I. Sampath was supported by the International Center of Energy Research (ICER), established by Nanyang Technological University (NTU), Singapore, and Technische Universität München (TUM), Germany.

References

[1] R. Deng, Z. Yang, M. Chow, and J. Chen, "A survey on demand response in smart grids: mathematical models and approaches," *IEEE Transactions on Industrial Informatics*, vol. 11, no. 3, pp. 570–582, 2015.

[2] G. Zheng and Q. Huang, "Energy optimization study of rural deep well two-stage water supply pumping station," *IEEE Transactions on Control Systems Technology*, vol. 24, no. 4, pp. 1308–1316, 2016.

[3] S. Paudyal, C. A. Cañizares, and K. Bhattacharya, "Optimal operation of industrial energy hubs in smart grids," *IEEE Transactions on Smart Grid*, vol. 6, no. 2, pp. 684–694, 2015.

[4] S. Ashok and R. Banerjee, "An optimization mode for industrial load management," *IEEE Transactions on Power Systems*, vol. 16, no. 4, pp. 879–884, 2001.

[5] M. P. Fanti, A. M. Mangini, M. Roccotelli, and W. Ukovich, "A district energy management based on thermal comfort satisfaction and real-time power balancing," *IEEE Transactions on Automation Science and Engineering*, vol. 12, no. 4, pp. 1271–1284, 2015.

[6] P. Du and N. Lu, "Appliance commitment for household load scheduling," *IEEE Transactions on Smart Grid*, vol. 2, no. 2, pp. 411–419, 2011.

[7] F. Verrilli, S. Srinivasan, G. Gambino et al., "Model predictive control-based optimal operations of district heating system with thermal energy storage and flexible loads," *IEEE Transactions on Automation Science and Engineering*, vol. 14, no. 2, pp. 547–557, 2017.

[8] A. Parisio, E. Rikos, and L. Glielmo, "A model predictive control approach to microgrid operation optimization," *IEEE Transactions on Control Systems Technology*, vol. 22, no. 5, pp. 1813–1827, 2014.

[9] A. Parisio, E. Rikos, G. Tzamalis, and L. Glielmo, "Use of model predictive control for experimental microgrid optimization," *Applied Energy*, vol. 115, pp. 37–46, 2014.

[10] A. Krishnany, B. V. Patilx, H. B. Gooiy, and K. V. Lingy, "Predictive control based framework for optimal scheduling of combined cycle gas turbines," in *Proceedings of the 2016 American Control Conference, (ACC '16)*, pp. 6066–6072, USA, July 2016.

[11] Y. Fu, M. Shahidehpour, and Z. Li, "Security-constrained unit commitment with ac constraints," *IEEE Transactions on Power Systems*, vol. 20, no. 3, pp. 1538–1550, 2005.

[12] M. Kahl, C. Freye, and T. Leibfried, "A Cooperative Multi-Area Optimization with Renewable Generation and Storage Devices," *IEEE Transactions on Power Systems*, vol. 30, no. 5, pp. 2386–2395, 2015.

[13] P. Fortenbacher, A. Ulbig, S. Koch, and G. Andersson, "Grid-constrained optimal predictive power dispatch in large multi-level power systems with renewable energy sources, and storage devices," in *Proceedings of the 2014 IEEE PES Innovative Smart Grid Technologies Conference Europe, ISGT-Europe 2014*, Turkey, October 2014.

[14] A. Ouammi, H. Dagdougui, L. Dessaint, and R. Sacile, "Coordinated Model Predictive-Based Power Flows Control in a Cooperative Network of Smart Microgrids," *IEEE Transactions on Smart Grid*, vol. 6, no. 5, pp. 2233–2244, 2015.

[15] S. X. Chen and H. B. Gooi, "Jump and shift method for multi-objective optimization," *IEEE Transactions on Industrial Electronics*, vol. 58, no. 10, pp. 4538–4548, 2011.

[16] L. P. Sampath, A. Krishnan, K. Chaudhari, H. B. Gooi, and A. Ukil, "A control architecture for optimal power sharing among interconnected microgrids," in *Proceedings of the 2017 IEEE Power & Energy Society General Meeting (PESGM)*, pp. 1–5, Chicago, IL, July 2017.

[17] K. Chaudhari, A. Ukil, K. N. Kumar, U. Manandhar, and S. K. Kollimalla, "Hybrid Optimization for Economic Deployment of ESS in PV-Integrated EV Charging Stations," *IEEE Transactions on Industrial Informatics*, vol. 14, no. 1, pp. 106–116, 2018.

[18] Z. Bao, Q. Zhou, Z. Yang, Q. Yang, L. Xu, and T. Wu, "A multi time-scale and multi energy-type coordinated microgrid scheduling solution - Part I: model and methodology," *IEEE Transactions on Power Systems*, vol. 30, no. 5, pp. 2257–2266, 2015.

[19] Z. Li and Y. Xu, "Optimal coordinated energy dispatch of a multi-energy microgrid in grid-connected and islanded modes," *Applied Energy*, vol. 210, pp. 974–986, 2018.

[20] C. Grigg, P. Wong, P. Albrecht, R. Allan, M. Bhavaraju, and R. Billinton, "The IEEE reliability test system -1996 a report prepared by the reliability test system task force of the application of probability methods subcommittee," *IEEE Transactions on Power Systems*, vol. 14, no. 3, pp. 1010–1020, 1999.

[21] W. de Soto, S. A. Klein, and W. A. Beckman, "Improvement and validation of a model for photovoltaic array performance," *Solar Energy*, vol. 80, no. 1, pp. 78–88, 2006.

[22] X. Wang, A. Palazoglu, and N. H. El-Farra, "Operational optimization and demand response of hybrid renewable energy systems," *Applied Energy*, vol. 143, pp. 324–335, 2015.

[23] "Renewables.ninja," https://www.renewables.ninja/.

[24] M. Alipour, K. Zare, and M. Abapour, "MINLP Probabilistic Scheduling Model for Demand Response Programs Integrated Energy Hubs," *IEEE Transactions on Industrial Informatics*, vol. 14, no. 1, pp. 79–88, 2017.

[25] A. Krishnan, L. P. M. I. Sampath, F. Y. S. Eddy, and B. V. Patil, "Multi-energy scheduling using a hybrid systems approach," in *Analysis and Design of Hybrid Systems*, 2018, https://www.researchgate.net/publication/323905991.

[26] C. A. Floudas, *Nonlinear and Mixed-Integer Optimization: Fundamentals and Applications*, Oxford University Press, NY, USA, 1995.

[27] A. Krishnan, F. Y. S. Eddy, and B. V. Patil, "Hybrid Model Predictive Control Framework for the Thermal Unit Commitment Problem including Start-up and Shutdown Power Trajectories," *IFAC-PapersOnLine*, vol. 50, no. 1, pp. 9329–9335, 2017.

[28] F. D. Torrisi and A. Bemporad, "HYSDEL—A tool for generating computational hybrid models for analysis and synthesis problems," *IEEE Transactions on Control Systems Technology*, vol. 12, no. 2, pp. 235–249, 2004.

[29] A. Bemporad and M. Morari, "Control of systems integrating logic, dynamics, and constraints," *Automatica*, vol. 35, no. 3, pp. 407–427, 1999.

[30] J. Löfberg, "YALMIP: a toolbox for modeling and optimization in MATLAB," in *Proceedings of the IEEE International Symposium on Computer Aided Control System Design*, pp. 284–289, Taipei, Taiwan, September 2004.

[31] M. Q. Wang, H. B. Gooi, S. X. Chen, and S. Lu, "A mixed integer quadratic programming for dynamic economic dispatch with valve point effect," *IEEE Transactions on Power Systems*, vol. 29, no. 5, pp. 2097–2106, 2014.

[32] F. Capitanescu and L. Wehenkel, "Experiments with the interior-point method for solving large scale Optimal Power Flow problems," *Electric Power Systems Research*, vol. 95, pp. 276–283, 2013.

[33] E. J. Oliveira, L. W. Oliveira, J. Pereira, L. M. Hon, I. C. Silva, and A. Marcato, "An optimal power flow based on safety barrier interior point method," *International Journal of Electrical Power & Energy Systems*, vol. 64, pp. 977–985, 2015.

[34] R. D. Zimmerman, C. E. Murillo-Sánchez, and R. J. Thomas, "MATPOWER: steady-state operations, planning, and analysis tools for power systems research and education," *IEEE Transactions on Power Systems*, vol. 26, no. 1, pp. 12–19, 2011.

[35] "Energy market company, price information," https://www.emcsg.com/marketdata/priceinformation.

[36] X. Zhang, J. Bao, R. Wang, C. Zheng, and M. Skyllas-Kazacos, "Dissipativity based distributed economic model predictive control for residential microgrids with renewable energy generation and battery energy storage," *Journal of Renewable Energy*, vol. 100, pp. 18–34, 2017.

Hindawi
Complexity
Volume 2018, Article ID 9597158, 11 pages
https://doi.org/10.1155/2018/9597158

Research Article

An Evaluation of a Metaheuristic Artificial Immune System for Household Energy Optimization

Maria Navarro-Caceres,[1] **Pramod Herath**,[2] **Gabriel Villarrubia**,[1] **Francisco Prieto-Castrillo**,[1,2] **and G. Kumar Venyagamoorthy**[3,4]

[1]*University of Salamanca, s/n. Salamanca, 37003 Espejo, Spain*
[2]*Media Lab, Massachusetts Institute of Technology, 20 Amherst St, Cambridge, MA, USA*
[3]*Holcombe Department of Electrical and Computer Engineering, Real-Time Power and Intelligent Systems Laboratory and Clemson University, Clemson, SC 29634, USA*
[4]*School of Engineering, University of KwaZulu-Natal, Durban, South Africa*

Correspondence should be addressed to Maria Navarro-Caceres; maria90@usal.es

Received 25 October 2017; Accepted 4 March 2018; Published 2 July 2018

Academic Editor: Hugo Morais

Devices in a smart home should be connected in an optimal way; this helps save energy and money. Among numerous optimization models that can be found in the literature, we would like to highlight artificial immune systems, which use special bioinspired algorithms to solve optimization problems effectively. The aim of this work is to present the application of an artificial immune system in the context of different energy optimization problems. Likewise, a case study is performed in which an artificial immune system is incorporated in order to solve an energy management problem in a domestic environment. A thorough analysis of the different strategies is carried out to demonstrate the ability of an artificial immune system to find a successful optima which satisfies the problem constraints.

1. Introduction

A Home Energy Management System (HEMS) is a key element in a domestic environment that improves household economy through automated technologies.

In the recent years, different domestic buildings equipped with communication channels (*smart houses*) have actively participated in electrical networks [1] as building blocks in smart grids (SGs). Therefore, they play an important role in optimizing the scheduling of electric power [1, 2].

There are a number of strategies that employ different techniques to optimize the scheduling of energy use in the home. Among many other strategies, statistical models are one example of them. We can see how they are leveraged in the work of [3], which models controllable loads using a Markovian approach. These loads depend on weather conditions. In [4], a demand-response program is automatically applied from classical methods to control the devices connected to the network under the uncertainty of the outside temperature and the price of electricity. In [5], three problems related to HEMS have been solved by applying an observable Markovian decision process. This work made it possible to reduce domestic energy costs in the electricity price market.

Classical approaches had some limitations [6]; thus, new paradigms have been applied to solve HEMS. One successfully developed paradigm is that which uses bioinspired algorithms to solve optimization problems. These algorithms try to mimic the behavior of some biological entities to find solutions which, applying classical computation, would be too costly or even implausible in terms of time and resources. Some widely used and noteworthy algorithms are artificial neural networks (ANN), genetic algorithms (GA), or swarm intelligence [7]. Some bioinspired algorithms work in different contexts, and they render good results. One of these algorithms is the artificial immune system (AIS) which follows

the principles of the vertebrae immune system to find solutions in an optimization problem. The AIS algorithm can be designed in a variety of ways. From the different variants, in this work, it is decided to use Opt-aiNet [8], which has been used successfully for the optimization of functions in different contexts [8]. Opt-aiNet allows finding several solutions in parallel. By using operations such as mutation, cloning, and suppression, each solution corresponds to different optima (maxima or minima) points in the optimization function.

In the area of intelligent network optimization, several works that follow the bioinspired paradigm have been proposed. These include [9], who propose an energetic services modeling method based on the particle swarm optimization (PSO) algorithm. Soares et al. [10] propose a multiobjective genetic approach for scheduling domestic charge in an energy management system. Yuce et al. [11] present a neural network with a genetic algorithm (ANN-GA) to optimize energy management in the domestic sector. However, to the authors' knowledge, AIS has only been implicated in some preliminary achievements in power management, such as solving power supply problems, or electrical reconfigurations. For example, in [12], an AIS is used to control thermal units in residential buildings, and in [13], the authors optimize a wind energy-generating system also with an AIS.

In this paper, an in-depth review of the AIS concept and its application to different electrical problems is made. From the results of this review, a case study on a problem of home energy management optimization is described and solved using this algorithm. We aim to demonstrate that AIS can be successfully applied to electrical management problems in domestic settings. Part of our objective has been to adapt the Opt-aiNet algorithm to include complex constraints on the optimization problem and to work efficiently with a large number of variables.

This paper presents a simple electric context with different devices, namely, a photovoltaic panel (PV), a battery system, a space heater or heater, a water heater, and must-run services. All of them are connected in a smart home, within an electrical system. It is aimed at optimizing the scheduling for the next 24 hours so that the electrical benefit is maximized between the energy that is sold and the energy that is bought.

Two strategies are designed in our case study to represent two different electrical situations. In strategy 1, the HEMS manages the electric power with the electricity grid without considering any internal restriction. In other words, we do not consider any variable related to the maintenance of the domestic electric charge through the electrical energy produced by the PV system. Therefore, this strategy only seeks to optimize energy benefits. However, strategy 2 is aimed at supplying the electricity demand autonomously whenever possible. Therefore, the surplus generated by the PV is stored in the battery. HEMS will sell electricity to the grid when the battery is fully charged. Also, the battery is discharged when the electrical demand is greater than the power generated by the PV. If the battery cannot supply all the electrical charge, then the HEMS must buy electricity from the power grid. Based on these two strategies, three different experiments were developed. Firstly, a comparison of AIS with two different bioinspired algorithms is made, namely, the classical genetic algorithm (GA) and the particle swarm optimization (PSO). Secondly, both strategies are compared to analyze the influence of the battery in the home network. Finally, a deep analysis is carried out with different situations of the battery charge in the home network. The results obtained in all situations are expected to validate the AIS as an appropriate algorithm for the optimization of HEMS.

This document is structured as follows. Section 2 provides an overview of the design of AIS and a review about its involvement in electrical problems. Section 3 describes the technical details of the addressed electrical problem. Section 4 presents the configuration of AIS and its application to the electrical problem. In Section 5, the results obtained in the three case studies are outlined and discussed. Finally, Section 6 presents the conclusions of our research and future work.

2. Artificial Immune Systems

The organisms of many species have developed immune systems to protect them from external agents. Above all, vertebrate immune systems consist of different molecules, cells, and organs that are distributed throughout the body and are not controlled by any central entity. From an immunological point of view, any element present in the immune system is called an antigen. If this antigen belongs to the internal organism to protect the body, it is called self-antigen or antibody. Otherwise, the antigens from the external environment are called non-self-antigens and can provoke different diseases. Therefore, immune systems are aimed at distinguishing between self-antigens and non-self-antigens through a pattern recognition process, attacking only those that are harmful for the body [14].

Drawing on the concept of the immune system, [15] developed the *CLONALG* algorithm, a clonal selection procedure that allows mutating some antibodies according to their affinity to an external antigen; therefore, in order to perform pattern recognition, it generates copies of the antibodies according to their affinity with the antigen. The copies are mutated following a rate δ inversely proportional to their affinity with the antigen (1).

$$\delta = \frac{e^{f_i}}{\beta}, \tag{1}$$

where β is a constant obtained empirically to normalize the effect of the fitness value f_i of each cell. These new individuals are added to the general population and reevaluated to be reproduced and mutated again.

In order to give a new solution for the optimization of functions, [8] developed Opt-aiNet, an artificial immune system (AIS) based on the *CLONALG* behavior. The information is encoded as antigens which should be recognized by the antibodies of our immune system. Then, the fitness value of an antigen is defined as the affinity between the antigen and the antibody and can be compared with a distance

metric. Henceforth, small distances between an antigen and an antibody represent high affinity, whereas longer distances represent lower affinity.

The Opt-aiNet algorithm follows the general description of an artificial immune system. Firstly, antibodies, which represent the different data to optimize, are randomly generated. Then, they are presented to the antigens, which encode the objective function, in order to calculate the affinity between them when the data are applied to the function. If one antibody obtains a good rating in the objective function, that means it has high affinity and therefore is selected. These chosen antibodies are reproduced and mutated based on their fitness value according to the *CLONALG* algorithm and the β parameter. In order to preserve diversity, antibodies whose affinity is lower than a given threshold t_s are removed from the population.

Artificial immune systems, in particular Opt-aiNet, are able to find several optima of the objective function in parallel. This means that AIS can find a set of good candidates for the solution of optimization problems that are different from one another. Additionally, AIS can preserve those individuals that are good enough to be reproduced and mutated in consecutive iterations.

2.1. AIS Applications in Energy Contexts. The concept of a next-generation power system such as smart grid, efficient energy management, and better power system planning cannot be achieved without electrical load forecasting [16]. Consequently, multiple time horizons which are associated with the regulation, dispatching, scheduling, and unit commitment of the power grid are analyzed and solved using different methods. Artificial intelligence (AI) is widely applied to a variety of applications, as it can handle the complexity derived from such electrical problems. In particular, bioinspired algorithms, such as artificial neural networks or swarm intelligence, are especially effective in solving this kind of problems. In this section, a brief but comprehensive literature review of a special bioinspired algorithm, the artificial immune systems, is provided. AIS was applied in different contexts with positive results: when solving combinatorial problems [17, 18], to detect intrusions in wireless sensor networks [19], or even to generate chord progressions [20]. The major goal of this section is to review, identify, evaluate, and analyze the performance of AIS in power systems and model research.

Regarding the electrical context, there are plenty of proposals focusing on diverse fields. One of them is related to the control of variables and configuration of an electrical system. de Mello Honorio et al. [21] model an optimal power flow (OPF), which is a nonlinear, nonconvex, and large-scale problem with both continuous and discrete control variables, using a modified artificial immune system (AIS). The AIS makes use of hypermutation, which is responsible for local search, and receptor edition, which explores different areas in the solution space. The proposed AIS is combined with a gradient vector to improve the final results. This combination is also aimed at collecting valuable information during the hypermutation process, decreasing the number of generations and clones, and, consequently, speeding up the convergence process while reducing the computational time. Belkacemi and Feliachi [22] use a multiagent system (MAS) which follows the human immune system behavior to propose a new technique for power system reconfiguration and restoration, applied to a model of Southern California Edison's Circuit of the Future. Each element of the MAS represents a natural immunological element that interacts with the other elements to heal the body. Similarly, the MAS is able to detect and isolate faults and restore power to the affected loads taking into consideration line capacity, voltage profile, and power losses [22]. de Oliveira et al. [23] present a methodology for the reconfiguration of radial electrical distribution systems to minimize energy losses making use of the bioinspired metaheuristic artificial immune system. The AISs have to plan the system operation considering both radiality and connectivity constraints and different load levels. Consequently, the AIS algorithm is adapted to accommodate the features of the problem better and to improve the search process. The algorithm developed is tested in well-known distribution systems, with very successful results. Souza et al. [24] solve the reconfiguration problem of electrical distribution systems (EDSs) with variable demand, using the artificial immune algorithm. As the reconfiguration problem with variable demand is a complex problem of a combinatorial nature, Copt-aiNet (artificial immune network for combinatorial optimization), which is a combinatorial version of the algorithm Opt-aiNet, is applied to identify the best radial topology for an EDS in order to minimize the cost of energy losses in a given operation period. A specialized sweep load flow for radial systems was used to evaluate the feasibility of the topology with respect to the operational constraints of the EDS and to calculate the active power losses for each demand level. The obtained results were compared with those in the literature in order to validate and prove the efficiency of the proposed algorithm. Souza et al. [25] also aim to solve the reconfiguration problem of EDS by comparing the results of the Copt-aiNet (artificial immune network for combinatorial optimization) and the Opt-aiNet (artificial immune network for optimization) algorithms. A specialized forward/backward radial power flow was used to evaluate each of the proposed solutions in order to determine its power losses and its feasibility regarding the operational constraints of the EDS. To validate the use of an AIS, the final results were compared with other solutions obtained with other algorithms in the literature.

Other important field of application is the forecasting of electrical variables (loads and power generation or consumption). Abdul Hamid and Abdul Rahman [26] propose an artificial neural net (ANN) trained following the behavior of an artificial immune system (AIS) to generate a short-term load forecasting model. Two sets of electrical energy demand data were used to test the capability of the proposed algorithm. The results presented in the manuscript show that the proposed AIS learning algorithm is capable of providing a forecast comparable to that of an artificial neural network with an integrated back propagation (BP) algorithm. Consequently, the AIS is an alternative learning algorithm for an artificial neural network. The work proposed by [27] is one

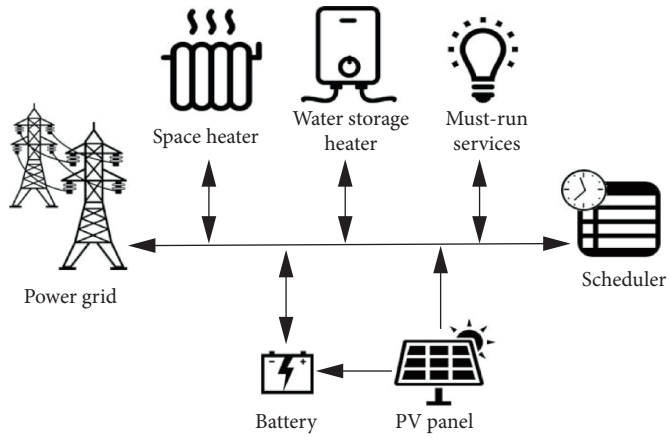

Figure 1: Schematic image of domestic electrical system.

of the first studies using an integrated AIS simulation for improved forecasting of electricity consumption with random variations. They develop a new system with different algorithms, namely, AIS, genetic algorithm (GA), and particle swarm optimization (PSO), to simulate annual electricity consumptions in selected countries. The mean absolute percentage error (MAPE) is applied to evaluate the results and select the best forecasting model. A case study with data of the annual electricity consumptions for 16 countries from 1980 to 2006 is analyzed. For the selected countries, the AIS method with the clonal selection algorithm (CLONALG) shows satisfactory results when applied with simulated data and has been selected as the preferred method. Hernandez et al. [28] model a hybrid artificial immune system (AIS) combining the back propagation method with the artificial immune system, to achieve higher accuracy, lesser input load data requirement, and faster convergence. The hybrid approach is implemented, and its results are compared with a GA and a PSO. This analysis reveals that AIS solves the problem in a more efficient way than do GA and PSO.

Dudek [29] proposes a short-term load forecast model based on an AIS to predict the hourly load demand of a week. In this proposed technique, each antigen of AIS, which contains the time series load sequences (some part is a forecast sequence), is compared with historical load patterns. MAPE is also used to evaluate the performance of the proposed forecast model. The system achieves a minimum MAPE of 1.77%, which means the AIS obtains very successful results. AISs are also applied for economic optimization in an electrical environment. Dynamic economic dispatch determines the optimal scheduling of online generator outputs with predicted load demands over a certain period of time taking into consideration the ramp rate limits of the generators [30]. Basu [31] presents an artificial immune system algorithm that solves a heat and power economic optimization problem. The AIS is adapted to this problem, adding new operations such as hypermutation and tournament, and is then used in a preliminary test system.

Basu [30] implements adaptive cloning, hypermutation, aging operation, and tournament selection. In order to validate the new AIS, numerical results of a ten-unit system with fuel cost function have been developed. The results obtained from the proposed algorithm are compared with those obtained from particle swarm optimization and evolutionary programming. From numerical results, it is shown that the proposed AIS provides a more efficient solution than do particle swarm optimization and evolutionary programming in terms of minimum cost and computation time. Aragón et al. [32] present an AIS-inspired algorithm, called IA EDP, which tries to solve an economic dispatch problem. It makes use of two versions of a redistribution power operator which tries to keep the solutions that it finds. The proposal is applied to eight problems taken from the literature. The results are compared with those derived from several other approaches to determine the advantages of the IA EDP against classical evolutionary computing.

This brief background leads us to the conclusion that AIS can be applied to a variety of electrical contexts with very successful results. This fact encourages us to work with a specific AIS, called Opt-aiNet, also leveraged in different papers [24, 25] and to adjust it specifically to our case study. The classical Opt-aiNet usually works with a low number of variables (each individual contains about 6 variables at most) and without constraints encoded as mathematical functions. In the present work, this algorithm is adjusted to admit up to 336 variables and 25 linear constraints (inequalities and equations).

3. Home Energy Management Problem

In the designed case study, we consider a home electrical system that has some household appliance connected to it (Figure 1).

The context can be thought as a domestic grid with a generation part and a consumption part, connected to the power grid. As shown in Figure 1, the generation system or the PV system includes the PV generator and the battery. The consumption parts are the electric loads which contain the following appliances: a space heater, a storage water heater, and must-run services. To balance the profit of energy services between the PV system and the loads, the scheduler is connected to the grid. The scheduler aims at maximizing the profit of energy services provided in a

domestic energy management system through (2) OF, which is the objective function to optimize.

$$\mathrm{OF} = \sum_{t} (\lambda_{\mathrm{sold}} P_{\mathrm{sold}}(t) - \lambda_{\mathrm{bought}} P_{\mathrm{bought}}(t) - \sum_{j \in \mathrm{ELs}} \mathrm{VOLL}_j L_j(t)^{\mathrm{shed}} - V^{s}_{\mathrm{pv}}(t)). \quad (2)$$

OF is a linear combination of four electrical factors. λ_{sold}, $\lambda_{\mathrm{bought}}$, VOLL_j and V_{pv} are constants that provide the prices per unit of energy load and are given by the market. The first term $\lambda_{\mathrm{sold}} P_{\mathrm{sold}}(t)$ represents the income from the sale of energy produced by the PV panel to the electricity grid. The second factor is the total cost of electrical energy that is bought from the network, $\lambda_{\mathrm{bought}} P_{\mathrm{bought}}(t)$. The value of electrical energy is not served, meaning the lo is encoded in the third part, $\sum_{j \in \mathrm{ELs}} \mathrm{VOLL}_j L_j(t)^{\mathrm{shed}}$. Finally, the spillage costs of PV panels, $V^{s}_{\mathrm{pv}} S_{\mathrm{pv}}(t)$, are represented in the last term of the equation.

We need to balance the loads between the energy generated (the PV system $P_{\mathrm{pv}}(t)$, the energy provided by the battery $P_{b,\mathrm{out}}(t)$, and the energy bought from the power grid $P_{\mathrm{bought}}(t)$) and the energy consumed, meaning the electrical loads of the different services $L_j(t) - L_j(t)^{\mathrm{shed}}$ (heater, storage water heater, and mustrung services) and the battery charge $P_{b,\mathrm{in}}(t)$ (3). Additionally, the power flow limitation through the distribution line is stated in (4), where $f_{\max}$ is a constant set to 6 according to [33].

$$P_{\mathrm{bought}}(t) + P_{\mathrm{pv}}(t) + P_{b,\mathrm{out}}(t) = \sum_{j \in \mathrm{ELs}} \left(L_j(t) - L^{\mathrm{shed}}_j(t) \right) + P_{b,\mathrm{in}}(t), \quad (3)$$

$$-f_{\max} \leq P_{\mathrm{bought}}(t) - P_{\mathrm{sold}}(t) \leq f_{\max}. \quad (4)$$

The specific definitions for all domestic appliances are described in the following subsections.

3.1. PV System. The PV system can generate the power output $P_{\mathrm{pv}}(t)$ of the grid, which can be modelled through Equation 5.

$$P_{\mathrm{pv}}(t) = P_{\mathrm{pv},p}(t) - S_{\mathrm{pv}}(t), \quad (5)$$

where S refers to the spillage costs of the PV system and $P_{\mathrm{pv},p}(t)$ is the potential power generation for the PV system. $P_{\mathrm{pv},p}(t)$ is limited to maximum and minimum bands due to the prediction of the PV power generation, following (6). $\sigma^{\mathrm{down}}_{\mathrm{pv}}$ and $\sigma_{\mathrm{pv}}{}^{\mathrm{up}}$ are down and up prediction variances for the PV system, respectively, and are calculated following [34]. $P^{\mathrm{pred}}_{\mathrm{pv}}(t)$ is the predicted power generated by the PV system. This amount is positive or equal to zero and is limited to the actual power generation of the PV, $P_{\mathrm{pv},p}(t)$, as represented in (7). In other words, the PV system can potentially generate this power but HEMS cannot operate it because of economic and technical constraints.

$$P^{\mathrm{pred}}_{\mathrm{pv}}(t) - \sigma^{\mathrm{down}}_{\mathrm{pv}} \leq P_{\mathrm{pv},p}(t) \leq P^{\mathrm{pred}}_{\mathrm{pv}}(t) - \sigma^{\mathrm{up}}_{\mathrm{pv}}, \quad (6)$$

$$0 \leq S_{\mathrm{pv}}(t) \leq P_{\mathrm{pv},p}(t). \quad (7)$$

3.2. Electrical Loads. Electrical loads include loads that can be controllable and/or shiftable. In this case study, three types of loads are modelled: space heater, $L_{\mathrm{sh}}(t)$, which is a controllable load, storage water heater, $L_{\mathrm{swh}}(t)$, which is a shiftable load, and must-run services, $L_{\mathrm{mrs}}(t)$, which are noncontrollable-shiftable loads. Equations 8 and 9 define the total electrical load and total load shedding of our domestic grid, respectively. These loads are described in the following subsections.

$$\sum_{j \in ELs} L_j(t) = L_{\mathrm{sh}}(t) + L_{\mathrm{swh}}(t) + L_{\mathrm{mrs}}(t), \quad (8)$$

$$\sum_{j \in ELs} L^{\mathrm{shed}}_j(t) = L^{\mathrm{shed}}_{\mathrm{sh}}(t) + L^{\mathrm{shed}}_{\mathrm{swh}}(t) + L^{\mathrm{shed}}_{\mathrm{mrs}}(t). \quad (9)$$

3.2.1. Space Heater. The space heater provides the desired indoor temperature. Equation 10 represents the performance of the space heater based on the relationship between the indoor temperature and its electrical load. In (10), θ_0 is the initial indoor temperature in time $t = 1$, which is assumed to be equal to the desired temperature. R is the thermal resistance, and C is the thermal capacity of

$$\theta_{\mathrm{in}}(t+1) = \theta_{\mathrm{in}}(t) e^{-1/RC} + L_{\mathrm{sh}}(t) R \left(1 - e^{-1/RC}\right) + \theta^{\mathrm{pred}}_{\mathrm{out}}(t) \left(1 - e^{-1/RC}\right), \quad t \geq 2 \quad \theta_{\mathrm{in}}(t) = \theta_0 = \theta_{\mathrm{des}}, \quad t = 1. \quad (10)$$

Equation 11 represents the limitation of the indoor temperature. In our case study, this limitation is set to 1°C more or less than the desired temperature. Finally, due to physical factors, the loads and the load sheddings are both limited by their maximum and minimum constraints (12) and (13).

$$-1 \leq \theta_{\mathrm{in}}(t) - \theta_{\mathrm{des}} \leq 1, \quad (11)$$

$$L^{\min}_{\mathrm{sh}}(t) \leq L_{\mathrm{sh}}(t) \leq L^{\max}_{\mathrm{sh}}(t), \quad (12)$$

$$0 \leq Ls^{\mathrm{shed}}_{\mathrm{sh}}(t) \leq L_{\mathrm{sh}}(t). \quad (13)$$

3.2.2. Storage Water Heater. The storage water heater is responsible for preserving the heat in the water tanks. The maximum and minimum limitations of the storage water heater's load are stated in (14). The maximum energy consumption of the storage water heater should be less than the maximum capacity of the tank U_{swh}, according to (15). Finally, the maximum of the load shedding of the storage water heater is always less than the energy consumption of the appliance (16).

$$L^{\min}_{\mathrm{swh}}(t) \leq L_{\mathrm{swh}}(t) \leq L^{\max}_{\mathrm{swh}}(t), \quad (14)$$

$$\sum_{t=1}^{N_t} L_{\mathrm{swh}}(t) = U_{\mathrm{swh}}, \quad (15)$$

$$0 \leq L_{\text{swh}}^{\text{shed}}(t) \leq L_{\text{swh}}(t). \quad (16)$$

3.2.3. Must-Run Services. Must-run services consist of loads that should be provided quickly, and therefore, it is not easy to predict them, for example, lighting and entertainment. For the purposes of this paper, it is assumed that there is no uncertainty in predicting the electrical loads of must-run services (17). As in the storage water heater, the maximum of the load shedding $L_{\text{mrs}}^{\text{shed}}(t)$ must always be less than the energy consumed $L_{\text{mrs}}(t)$ (18).

Also, the load shedding constraint is stated in (18).

$$L_{\text{mrs}}(t) = L_{\text{mrs}}^{\text{pred}}(t), \quad (17)$$

$$o \leq L_{\text{mrs}}^{\text{shed}}(t) \leq L_{\text{mrs}}(t). \quad (18)$$

3.3. Battery System. The battery system can be used to apply the charge and discharge strategies in the HEMS. A flowchart (Figure 2) is designed to operate with the battery in the domestic environment. The system aims at providing the required electrical demand, maximizing its benefits. When there is a surplus $P_{b,\text{in}}(t)$ of the energy generated (i.e., the PV panel generates more energy $P_{\text{pv}}(t)$ than the total load TL(t) demands), it is stored in the battery ($C_b(t)$). If the battery is fully charged $C_b(t) > C_b^{\max}$, then it is sold to the grid $P_{\text{sold}}(t)$. On the contrary, the system makes use of the energy stored in the battery $P_{b,\text{out}}(t)$ when the electrical demand is higher than the power generation of the PV panel. Additionally, if the battery cannot provide the energy needed (i.e., is unavailable or completely discharged, $C_b(t) > C_b^{\min}$), the system will buy the electricity $P_{\text{bought}}(t)$ from the power grid.

4. Experimental Setting

To assess the performance of the proposed HEMS, some parameters have been set to optimize the system. The maximum power produced by the PV system is 2 kW. The battery can store between $C_{\min}^b$ 48 and $C_{\max}^b$ 2.4 kWh. The maximum heating power of the space heater (SH) $L_{\text{sh}}^{\max}(t)$ equals 2 kW to maintain the temperature of the house within ±1 of the desired temperature (θ_{des} 23°C). The thermal resistance, R, of the building shell is equal to 18°C/kW, and the capacity C equals 0.525 kWh/°C. The energy capacity of the storage water heater (U_{swh}) is 10.46 kWh (180 L) which has 2 kW as maximum of heating elements $L_{\text{swh}}^{\max}$. Table 1 displays the predicted data that has been used in [33]. Table 2 gives the price data of the system. VOLL and spillage costs of PV power generation are shown in Table 3.

These data are used in our HEMS to optimize the function (2). The objective function is integrated into Opt-aiNet to get an optimized schedule of 24 hours in a domestic environment. Following the Opt-aiNet procedure, the initial population randomly generated, where each individual is a set of electrical values for 24 hours, must comply with the constraints modelled in the electrical management problem. For this purpose, each datum of the individual is considered as an electrical parameter to optimize for 24 hours. Initially, the parameters which only depend on some fixed boundaries (6), (7), (12), (14), and (17) are generated. Then, these parameters are used as new boundaries for those electrical parameters that depend on them (the rest of the equations are given in the model of Section 3). This methodology is recursively applied until all the parameters needed for each individual are generated. Finally, to obtain the parameters related to the battery load, the parameters previously calculated and the flowchart of Figure 2 are applied to generate the new ones.

With the individuals generated, Opt-aiNet work follows these steps:

(1) Initiate N population following the method above, to respect the linear constraints and the flowchart if it is the case.

(2) Evaluate each individual according to the optimization function given in (2).

(3) Create N_c clones of each individual. The elements of each clone should be slightly changed according to the mutation equation (1).

(4) For each cell or antibody, select the best clone with the highest objective value.

(5) If the mean objective of the last iteration and the present one are below a limit, then similar individuals are suppressed according to the similarity threshold t_s that measures distances between two antibodies.

(6) If some individuals are suppressed, then it is needed to add a new random population. These new solutions are generated following the method given above to respect the constraints and the flowchart if that is the case.

(7) This work flow is repeated until the convergence criterion (maximum number of iterations *gen*). The result is one or more individuals with an optimum objective value.

As we can see, AIS contains five parameters, namely, number of individuals N, number of clones N_c, similarity threshold t_s, maximum number of generations *gen*, and the mutation parameter β. Depending on the problem, they can take several values and are essential for a correct operation. AIS needs some parameters to be set beforehand in order to optimize a problem correctly. These parameters are related to the cloning and mutation process, the suppression algorithm, and the convergence criterion. For each iteration, a number of clones N_c is generated per cell. This number N_c is set empirically and can influence the final results. Generally, if N_c is set with a very low value, the convergence criterion can be delayed, as we are not able to find enough diversity to select better individuals for each cell. Otherwise, if too many clones are generated, the time upon convergence might be longer than expected.

We empirically set the AIS parameters according to Table 4, which gave the optimal performance in terms of fitness and time.

The next section will describe the simulations and results with Opt-aiNet configured for the presented HEMS.

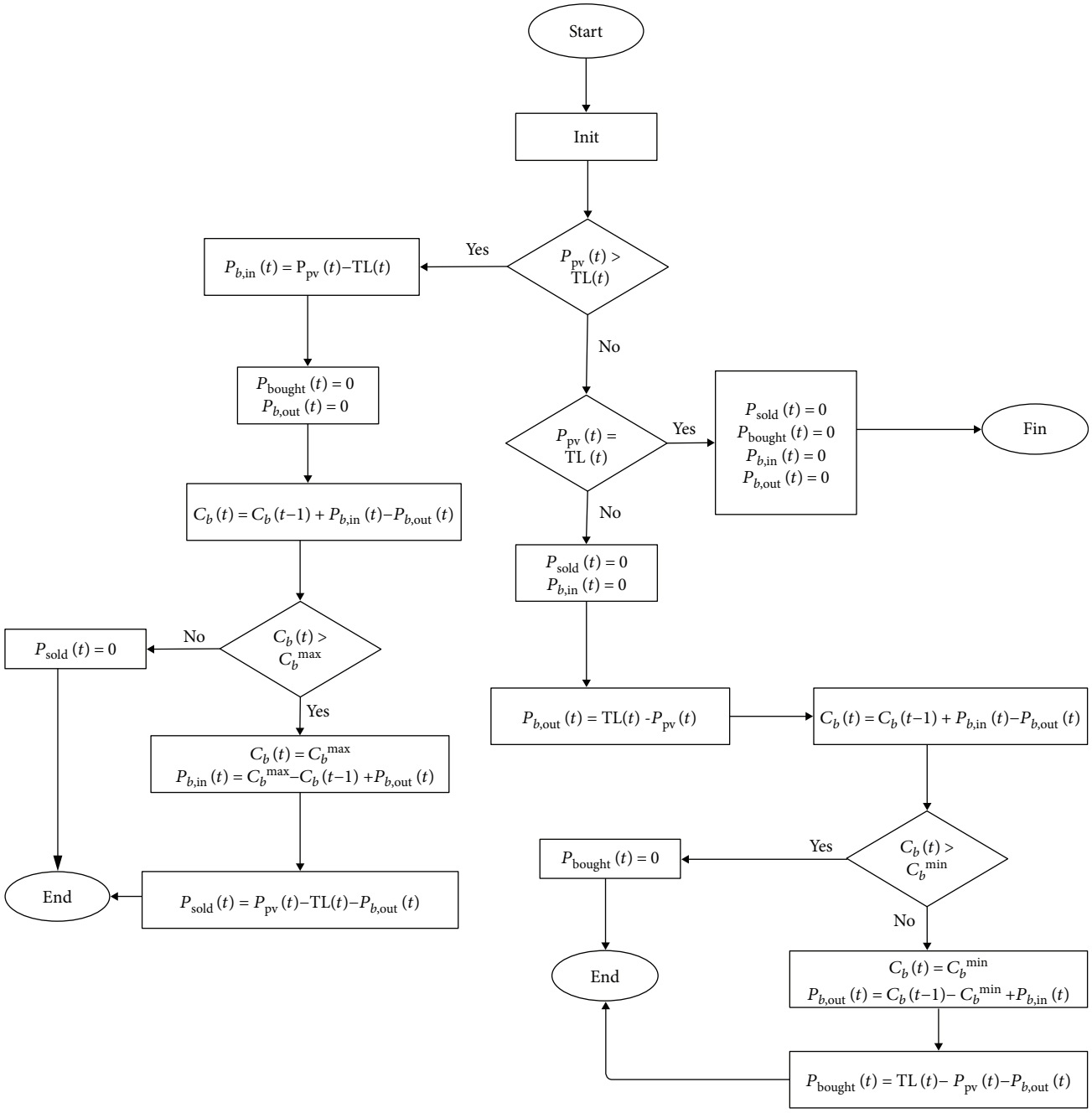

Figure 2: Flowchart modelling the battery parameters.

5. Simulation Results

The evaluation is twofold. Firstly, it is expected that Opt-aiNet obtains positive results in solving optimization problems in the created setting and comparing them with other classical bioinspired approaches. Consequently, a comparative analysis was carried out between a classical genetic algorithm (GA) and a particle swarm optimization (PSO). Additionally, we analyzed the impact of the flowchart (Figure 2) on our system, when the battery was involved. Therefore, two strategies that represent two electrical situations are designed. In the first strategy (strategy 1), the domestic environment does not consider any variable related to the maintenance of the domestic electric charge through the electrical energy produced by the PV system. This strategy only aims at optimizing its energy benefits. In the second strategy (strategy 2), the home environment aims at supplying the electricity demand autonomously. Therefore, the surplus generated by the PV is stored in the battery. In this strategy, the electricity could be sold to the grid if the battery is completely charged. On the contrary, if the battery cannot supply all the electrical charge, then the HEMS must buy electricity from the power grid.

Table 1: Predicted data of uncertain variables.

t	${}^{P}_{\text{pv}}\text{pred}(t)$	$\sigma_{\text{pv}}{}^{\text{up}}$	$\sigma_{\text{pv}}\text{down}$	$\theta\text{outpred}(t)$	$L\text{pred}_{\text{mrs}}(t)$
1	0	0.03	0.01	5.5	0.3
2	0	0.03	0.01	5.5	0.3
3	0	0.03	0.01	5.2	0.3
4	0	0.03	0.01	5.2	0.3
5	0	0.03	0.01	4.8	0.4
6	0	0.03	0.01	5.5	0.6
7	0.25	0.03	0.01	6.5	0.8
8	0.75	0.03	0.01	7.5	0.8
9	1.25	0.03	0.01	9.8	0.7
10	1.75	0.03	0.01	10.1	0.55
11	1.9	0.03	0.01	11.5	0.5
12	1.9	0.03	0.01	12	0.5
13	1.9	0.03	0.01	12.5	0.5
14	1.75	0.03	0.01	12	0.5
15	1.25	0.03	0.01	11.5	0.6
16	0.75	0.03	0.01	10	0.8
17	0.25	0.03	0.01	9	1.5
18	0	0.03	0.01	8.5	1.8
19	0	0.03	0.01	8	1.7
20	0	0.03	0.01	7.5	1.1
21	0	0.03	0.01	7	0.9
22	0	0.03	0.01	6.5	0.7
23	0	0.03	0.01	6.2	0.6
24	0	0.03	0.01	6	0.4

Table 2: Price data of the system.

	Price ($/MW)	
Time (hour)	λ_i	λnet
23–7	2.2	0.0814
8–14	2.2	0.1408
15–20	2.2	0.3564
21-22	2.2	0.1408

Table 3: VOLL and spillage costs.

	VOLL ($/MW)			Spillage cost ($/MW)
Time (hour)	SH	SWH	MRS	PV
22–7	1	1	2.2	4
8–21	1	1	2.2	4

Based on these two main goals, three different experiments are considered:

(i) *Experiment I: comparative study between GA, PSO, and AIS*

(ii) *Experiment II: comparison between strategy 1 and strategy 2*

Table 4: Optima values set for N, N_c, gen, t_s, and β in both strategies.

	N	N_c	gen	ts	β
Strategy I	250	12	250	10	100
Strategy II	250	18	300	3	10

(iii) *Experiment III: analysis of strategy 2 when the battery is disconnected or connected*

Experiment I makes a comparison between GA, PSO, and AIS. Experiment II optimizes the parameters related to the PV system, the space heater, the water heater, and the must-run services; therefore, the parameters related to the battery charge are not considered (strategy I). The results obtained from the optimization process are compared with the results that are retrieved when the parameters of the battery are included in the system, although all are set to 0. That means the battery is disconnected from the home environment but the AIS follows the flowchart to optimize the system.

Finally, experiment III performed two different analyses: when the battery was disconnected and when the battery was connected, to study the impact of this device on the system.

5.1. Comparison between GA, PSO, and AIS. In this section, we aim to compare the results obtained with three different bioinspired algorithms: genetic algorithm, particle swarm optimization, and artificial immune system. The genetic algorithm (GA) is widely used in optimization problems with many configurations. In this paper, a classical approach of GA is applied so that the mutation and crossover as well as the number of generations are empirically set to 0.3, 0.8, and 2000, respectively. Additionally, the selection function chosen was the roulette algorithm.

The particle swarm optimization (PSO) was first introduced by Eberhart and Kennedy [35] and consists of a population-based optimization algorithm which is deemed to be a nature-inspired optimization methodology. PSO employs a set of particles which would move through the search space at every iteration and would calculate the fitness value at each point. After a termination condition is met, the best optimized value is selected by choosing the best value found in the history of particles. The success of PSO lies in its "velocity equation"; this equation decides on the next point in space that each particle would move to. The velocity equation can be shown as

$$V_{id,k+1} = wV_{id,k} + c_1 \times \text{rand}_1 \times \left(X_{p\text{best}id,k} - X_{id,k}\right) + c_2 \times \text{rand}_2 \times \left(X_{g\text{best}d,k} - X_{id,k}\right). \quad (19)$$

Here, $V_{id,k+1}$ is the velocity of the dth dimension of the ith particle in the next iteration (k + 1st), w is the inertia of the particle, $V_{id,k}$ is the velocity of the dth dimension of the ith particle in the current iteration (kth iteration), c_1 is the cognitive acceleration constant, c_2 is the social acceleration constant, $X_{p\text{best}id,k}$ is the position of the particle in the dth dimension at which the best solution was

found so far by the ith particle, $X_{gbestd,k}$ is the value of the dth dimension at which the best solution so far was found by the whole system, $X_{id,k}$ is the current position of the ith particle in the dth dimension, and c_1 and c_2 are random numbers. Using the velocity calculated, the next position to be evaluated is calculated as

$$X_{id,k+1} = X_{id,k} + V_{id,k}. \quad (20)$$

The above velocity equation works well when the system is under no constraints. However, when there are constraints, some of the particles might fall off the feasible region. In this case, the particles should not update their personal best when a particle is outside the feasible region. Neither should the global best be updated in case of a particle being outside the feasible boundary, having a better value than the current global best. In case a particle has not found a personal best that falls in the feasible region, the particle should rely only on global best to guide its movement. In this case, the calculation of velocity would change to

$$V_{id,k+1} = wV_{id,k} + (c_1 + c_2) \times \text{rand} \times \left(X_{gbestd,k} - X_{id,k}\right). \quad (21)$$

However, equality constraint satisfaction is more difficult than the inequality constraint satisfaction. To solve this problem, a mending procedure is carried out at every iteration to make sure all particles satisfy the equality constraint. The mending procedure calculates the overshoot of each of the particle and adds a correction value to correct the error. The correction is equally added to each of the intervals of the particle.

In order to demonstrate the efficiency of the artificial immune system in the energy management optimization problem, we performed a comparative test with a version of constrained PSO adopted from [36] and an approach of the genetic algorithm. The goal was to predict the optimum values for each variable during 24 hours, following strategy 1 and strategy 2. The linear constraints proposed in the electrical model are applied, and subsequently, the objective function for the optimized variables is measured.

Table 5 shows the results obtained when the objective function and the energy are bought and consumed when AIS, GA, and PSO are applied with an optimal setting.

As Table 5 shows, AIS obtains slightly better results in the objective function for both strategies when both settings are optimal to solve this problem. That means AIS is a better configuration of the electrical parameters to optimize the problem stated. Likewise, AIS is able to find lower values for the amount of energy bought, which means the algorithm allows saving energy and money to the customer. The results of the AIS for the energy sold are lesser than in PSO and in GA. That could be explained because in PSO and in GA, the mean amounts of energy that are managed are greater than in AIS. However, PSO also obtained positive results (at least, better than with the classical approach of GA); therefore, we propose to make a deeper comparison with more complex problems to validate both algorithms and study the limitations of each one.

Table 5: Results of the objective function and the energy bought and consumed when AIS and PSO are applied with an optimal setting.

		Objective value	Energy bought	Energy sold
Strategy 1	**PSO**	23.52	46.61	14.12
	GA	22.48	46.94	14.09
	AIS	23.86	45.66	14.22
Strategy 2	**PSO**	4.86	37.60	5.40
	GA	4.92	32.66	5.22
	AIS	5.11	26.53	4.64

5.2. Analysis of the Energy Management Strategy. In this section, the two strategies described below are deeply analyzed and compared. The first strategy looks for maximizing the domestic energy profit. However, the second strategy aims at maximizing energy profit and acting as an autonomous energy system. It is expected that strategy II obtains better results, as this strategy pursues the autonomous management of energy, saving more money than in strategy I.

Opt-aiNet worked with individuals or vector of 264 elements with equality and inequality constraints, as each individual contains all the variables for 24 hours. Each value corresponds to the different electric loads and powers described in Section 3 for the PV panel, the storage water heater, the space heater, and the must-run services. We run the algorithm with two different configurations, one with strategy 1, excluding all the constraints related to battery management, and one with strategy 2, including all the constraints related to battery management, but with the battery variables set to 0. Table 6 shows the results according to the fitness value of the objective function OF and the parameters of sold and bought energy.

As we can see, the value of the objective function in strategy 1 is higher than that of strategy 2. However, the transacted energy between home and power grid is lesser in strategy 1, which means that Strategy 2 allows for the autonomous management of energy at home.

5.3. Impact of the Battery. In this analysis, strategy 2 is applied to study the influence of the battery in the domestic environment. In this case particularly, individuals in the AIS have 336 elements because the parameters corresponding to the battery charge and load are set as elements of optimization. Each individual is constructed following the linear constraints and the flowchart before being inserted into the population. Two different executions are made, firstly, with all the variables related to the battery management set to 0. In the second execution, the variables of the battery could change according to the corresponding equations and flowchart (Figure 2). The results obtained are shown in Table 7.

From the data in Table 7, we can see that the battery system can improve the value of the objective function. Table 7 also considers a situation in which the battery increases the amount of electrical energy sold from the smart home to the grid, and it decreases the amount of electrical energy that a home buys from the network.

Table 6: Impact of energy management strategies on the amount of sold/bought electrical energy to/from power grid and OF.

	Strategy 1	Strategy 2
OF	23.8613	5.11
E_{sold}	14.22	4.64
E_{bought}	45.66	26.53

Table 7: Impact of battery system on the amount of sold/bought electrical energy to/from power grid and OF.

	Strategy 2	
	With battery	Without battery
OF	12.31	5.11
E_{sold}	6.22	4.64
E_{bought}	10.47	26.53

6. Conclusions

Artificial immune systems are a bioinspired algorithm that is capable of optimizing problems in a variety of research fields. This paper focused specifically on the application of AIS to electrical problems, such as demand response and scheduling optimization.

A specific AIS called Opt-aiNet is selected, which is an improved version of an AIS used in different contexts [8], and it is applied to solve a power system optimization problem efficiently.

We modelled a domestic environment with different appliances connected to the network, namely, a PV panel, a space heater, a storage water heater, a battery, and must-run services. Subsequently, the Opt-aiNet algorithm is adapted to include complex constraints in the optimization problem and to work with a large number of variables derived from this domestic environment.

Two strategies have been developed to test Opt-aiNet. The first one aimed at maximizing the energy profit of a home. The main purpose of the second strategy is to maximize its energy profit and act as an autonomous energy system simultaneously and independently of whether the battery variables are considered or not.

In order to demonstrate the validity of this proposal, three different experiments were carried out. The first one consisted of a formal comparison between the application of a GA and a PSO in the same context. The results were very positive as Opt-aiNet obtained a better solution than did GA with a classical configuration. This encourages the use of Opt-aiNet as a solution that gives very good results.

The second experiment aimed at comparing two different electrical strategies. The final results showed that strategy II, which aims at maximizing the autonomy of the system, increases the efficiency of the model in terms of energy saving and therefore household economy.

Finally, another experiment is performed to analyze the impact of the battery considering two different situations: when the battery is available (can be filled and used in our system) or unavailable (the battery is full and cannot be used). This last comparison showed the importance of using a battery for improving the general profit of our residential electrical system. In fact, the final results led us to conclude that the battery helps to maximize the profit of the whole system.

Future work will consist of improving the results of the optimization problem with the GA and presenting a more complex case considering the uncertainty of predicted variables to encourage the use of evolutionary computing.

Conflicts of Interest

The authors declare that they have no conflicts of interest.

Acknowledgments

This work has been partially supported by the European Commission H2020 MSCA-RISE-2014: DREAM-GO Project (Marie Sklodowska-Curie grant agreement no. 641794) and by the National Science Foundation (NSF) of the United States, Grant IIP no. 1312260.

References

[1] M. A. A. Pedrasa, T. D. Spooner, and I. F. MacGill, "The value of accurate forecasts and a probabilistic method for robust scheduling of residential distributed energy resources," in *2010 IEEE 11th International Conference on Probabilistic Methods Applied to Power Systems*, pp. 587–592, Singapore, July 2010.

[2] A. Molderink, V. Bakker, M. G. C. Bosman, J. L. Hurink, and G. J. M. Smit, "Domestic energy management methodology for optimizing efficiency in smart grids," in *2009 IEEE Bucharest PowerTech*, pp. 1–7, Bucharest, Romania, July 2009.

[3] M. Nistor and C. H. Antunes, "Integrated management of energy resources in residential buildings-a markovian approach," *IEEE Transactions on Smart Grid*, vol. 9, no. 1, pp. 240–251, 2018.

[4] S. Althaher, P. Mancarella, and J. Mutale, "Automated demand response from home energy management system under dynamic pricing and power and comfort constraints," *IEEE Transactions on Smart Grid*, vol. 6, no. 4, pp. 1874–1883, 2015.

[5] T. M. Hansen, E. K. P. Chong, S. Suryanarayanan, A. A. Maciejewski, and H. J. Siegel, "A partially observable markov decision process approach to residential home energy management," *IEEE Transactions on Smart Grid*, vol. 9, no. 2, pp. 1271–1281, 2018.

[6] T. G. Kolda, R. M. Lewis, and V. Torczon, "Optimization by direct search: new perspectives on some classical and modern methods," *SIAM Review*, vol. 45, no. 3, pp. 385–482, 2003.

[7] J. L. Fernandez-Marquez, G. Di Marzo Serugendo, S. Montagna, M. Viroli, and J. L. Arcos, "Description and composition of bioinspired design patterns: a complete overview," *Natural Computing*, vol. 12, no. 1, pp. 43–67, 2013.

[8] L. N. De Castro and J. Timmis, "An artificial immune network for multimodal function optimization," in *Proceedings of the 2002 Congress on Evolutionary Computation. CEC'02 (Cat. No.02TH8600)*, pp. 699–704, Honolulu, HI, USA, May 2002.

[9] M. A. Pedrasa, E. D. Spooner, and I. F. MacGill, "Improved energy services provision through the intelligent control of distributed energy resources," in *2009 IEEE Bucharest PowerTech*, Bucharest, Romania, July 2009.

[10] A. Soares, C. H. Antunes, C. Oliveira, and A. Gomes, "A multi-objective genetic approach to domestic load scheduling in an energy management system," *Energy*, vol. 77, pp. 144–152, 2014.

[11] B. Yuce, Y. Rezgui, and M. Mourshed, "Ann–ga smart appliance scheduling for optimised energy management in the domestic sector," *Energy and Buildings*, vol. 111, pp. 311–325, 2016.

[12] J. Zhu, F. Lauri, A. Koukam, V. Hilaire, and M. G. Simoes, "Improving thermal comfort in residential buildings using artificial immune system," *2013 IEEE 10th International Conference on Ubiquitous Intelligence and Computing and 2013 IEEE 10th International Conference on Autonomic and Trusted Computing*, 2013, pp. 194–200, Vietri sul Mere, Italy, December 2013.

[13] K. Lakshmi and S. Vasantharathna, "Gencos wind–thermal scheduling problem using artificial immune system algorithm," *International Journal of Electrical Power & Energy Systems*, vol. 54, pp. 112–122, 2014.

[14] L. N. De Castro and J. Timmis, *Artificial Immune Systems: A New Computational Intelligence Approach*, Springer Science & Business Media, 2002.

[15] L. N. De Castro and F. J. Von Zuben, *The Clonal Selection Algorithm with Engineering Applications*, Proceedings of GECCO, 2000.

[16] M. Q. Raza and A. Khosravi, "A review on artificial intelligence based load demand forecasting techniques for smart grid and buildings," *Renewable and Sustainable Energy Reviews*, vol. 50, pp. 1352–1372, 2015.

[17] M.-H. Chen, P.-C. Chang, and C.-H. Lin, "A self-evolving artificial immune system ii with t-cell and b-cell for permutation flow-shop problem," *Journal of Intelligent Manufacturing*, vol. 25, no. 6, pp. 1257–1270, 2014.

[18] L.-F. Hsu, C.-C. Hsu, and T.-D. Lin, "An intelligent artificial system: artificial immune based hybrid genetic algorithm for the vehicle routing problem," *Applied Mathematics & Information Sciences*, vol. 8, no. 3, pp. 1191–1200, 2014.

[19] S. Shamshirband, N. B. Anuar, M. L. M. Kiah et al., "Co-fais: cooperative fuzzy artificial immune system for detecting intrusion in wireless sensor networks," *Journal of Network and Computer Applications*, vol. 42, pp. 102–117, 2014.

[20] M.'ı. Navarro, M. Caetano, G. Bernardes, L. N. de Castro, and J. M. Corchado, "Automatic generation of chord progressions with an artificial immune system," in *International Conference on Evolutionary and Biologically Inspired Music and Art*, pp. 175z–1186, Springer, 2015.

[21] L. de Mello Honorio, A. M. Leite da Silva, and D. A. Barbosa, *A Gradient-Based Artificial Immune System Applied to Optimal Power Flow Problems*, Artificial Immune Systems, 2007.

[22] R. Belkacemi and A. Feliachi, "Multi-agent design for power distribution system reconfiguration based on the artificial immune system algorithm," in *Proceedings of 2010 IEEE International Symposium on Circuits and Systems*, pp. 3461–3464, Paris, France, June 2010.

[23] L. W. de Oliveira, E. J. de Oliveira, F. V. Gomes, I. C. Silva Jr, A. L. M. Marcato, and P. V. C. Resende, "Artificial immune systems applied to the reconfiguration of electrical power distribution networks for energy loss minimization," *International Journal of Electrical Power & Energy Systems*, vol. 56, pp. 64–74, 2014.

[24] S. S. F. Souza, R. Romero, J. Pereira, and J. T. Saraiva, "Artificial immune algorithm applied to distribution system reconfiguration with variable demand," *International Journal of Electrical Power & Energy Systems*, vol. 82, pp. 561–568, 2016.

[25] S. S. F. Souza, R. Romero, and J. F. Franco, "Artificial immune networks copt-ainet and opt-ainet applied to the reconfiguration problem of radial electrical distribution systems," *Electric Power Systems Research*, vol. 119, pp. 304–312, 2015.

[26] M. B. Abdul Hamid and T. K. Abdul Rahman, "Short term load forecasting using an artificial neural network trained by artificial immune system learning algorithm," in *2010 12th International Conference on Computer Modelling and Simulation*, pp. 408–413, Cambridge, UK, March 2010.

[27] A. Azadeh, M. Taghipour, S. M. Asadzadeh, and M. Abdollahi, "Artificial immune simulation for improved forecasting of electricity consumption with random variations," *International Journal of Electrical Power & Energy Systems*, vol. 55, pp. 205–224, 2014.

[28] L. Hernandez, C. Baladron, J. M. Aguiar et al., "A multi-agent system architecture for smart grid management and forecasting of energy demand in virtual power plants," *IEEE Communications Magazine*, vol. 51, no. 1, pp. 106–113, 2013.

[29] G. Dudek, *Artificial Immune System for Short-Term Electric Load Forecasting*, Artificial Intelligence and Soft Computing–ICAISC, 2008.

[30] M. Basu, "Artificial immune system for dynamic economic dispatch," *International Journal of Electrical Power & Energy Systems*, vol. 33, no. 1, pp. 131–136, 2011.

[31] M. Basu, "Artificial immune system for combined heat and power economic dispatch," *International Journal of Electrical Power & Energy Systems*, vol. 43, no. 1, pp. 1–5, 2012, ISSN 0142-0615.

[32] V. S. Aragón, S. C. Esquivel, and C. A. Coello Coello, "An immune algorithm with power redistribution for solving economic dispatch problems," *Information Sciences*, vol. 295, pp. 609–632, 2015.

[33] A. S. Gazafroudi, F. Prieto-Castrillo, and J. M. Corchado, "Residential energy management using a novel interval optimization method," in *2017 4th International Conference on Control, Decision and Information Technologies (CoDIT)*, pp. 0196–0201, Barcelona, Spain, April 2017.

[34] M. Pedrasa, T. D. Spooner, and I. F. MacGill, "Scheduling of demand side resources using binary particle swarm optimization," *IEEE Transactions on Power Systems*, vol. 24, no. 3, pp. 1173–1181, 2009.

[35] R. Eberhart and J. Kennedy, "A new optimizer using particle swarm theory," in *MHS'95. Proceedings of the Sixth International Symposium on Micro Machine and Human Science*, pp. 39–43, Nagoya, Japan, October 1995.

[36] Y. del Valle, J. Perkel, G. K. Venayagamoorthy, and R. G. Harley, *Optimal Allocation of Facts Devices: Classical versus Metaheuristic Approaches*, Transactions of the South Institute of Electrical Engineers, 2009.

Hindawi
Complexity
Volume 2018, Article ID 5905932, 16 pages
https://doi.org/10.1155/2018/5905932

Research Article

An Ising Spin-Based Model to Explore Efficient Flexibility in Distributed Power Systems

Francisco Prieto-Castrillo,[1,2,3] **Amin Shokri Gazafroudi**,[3] **Javier Prieto**,[3] **and Juan Manuel Corchado**[3]

[1]*Media Laboratory, Massachusetts Institute of Technology, Cambridge, MA 02139-4307, USA*
[2]*Harvard T.H. Chan School of Public Health, Harvard University, Boston, MA 02115, USA*
[3]*University of Salamanca, BISITE Research Group, Edificio I+D+i, 37008 Salamanca, Spain*

Correspondence should be addressed to Francisco Prieto-Castrillo; franciscop@usal.es

Received 25 January 2018; Accepted 19 March 2018; Published 8 May 2018

Academic Editor: João Soares

This paper analyses customers' demand flexibility in a local power trading scenario through an Ising spin-based model. We look at quantitative information on the two-way relationships between power exchanges and spin dynamics. To this end, a modified version of the Metropolis-Hastings algorithm was implemented, including a gradient descent through the constraint surface. This allowed us to analyse the system on a large scale (considering the cumulated benefit of all the actors involved) and also from the perspective of total aggregation. In a maximum flexibility scenario, the total aggregation profit increases with the number of aggregators. We also investigate numerically the effect of aggregator boundaries on the spin dynamics.

1. Introduction

How can customers' collective behaviour affect the efficiency of distributed power systems? Furthermore, could the outcomes of this collective behaviour be exploited in the forthcoming self-organised power systems? In this work, we explore these matters analytically and numerically. An Ising spin-based model allowed us to provide quantitative criteria to couple system's performance and customers' standpoint on being flexible or not in their demand.

Distributed power systems (DPSs) are complex ecosystems encompassing machines, networks, procedures, operators, and customers organised in hierarchical layers [1]. After restructuring the power systems, new players have appeared, such as Distribution System Operators (DSOs) which provide electrical demand to local customers [2]. Also, customers are increasingly changing their roles from passive (only consumer) to active (generators). Moreover, recent Demand Response (DR) programs require customers to make a timely adjustment of their demand [3]. In this interwined subsystems, customers are also exposed to social interactions that can influence their decision as in any other community. In particular, users' flexibility in power consumption has a major influence on the performance of the whole system [4, 5]. In turn, DPSs powerful restrictions to maintain quality of service and security cause new constraint forces applied to customer behaviour.

On the other hand, collective behaviour has features which are hard to explain by classical statistical methods [6]. For example, the so-called *herding* behaviour or the economic bubbles are phenomena lying outside analyses that neglect large correlations and self-organisation occurring near the critical point [7]. In regard to DPSs, a sharp transition in customer's behaviour (i.e., *emergence*) can trigger dramatic consequences. To the best of our knowledge however, a quantitative analysis of the complexity of customers behaviour in DPSs has not yet been provided. Ising-based models are a promising approach as we demonstrate here.

The Lenz-Ising spin model is known since 1925 [8]. In short, the model consists of an arrangement of interacting agents which have two possible states (i.e., *up* and *down*). Agents interact with their neighbours locally and are also

exposed to external action and to thermal noise. In the physics metaphor of a ferromagnetic material, the atoms tend to align their quantum *spins* to minimise energy. However, for high temperatures, the agents flip their spins randomly. There is a critical temperature T_c (known as Curie temperature) for which the system suffers a sharp change—second-order phase transition—from order to disorder. Near T_c the system has anomalous behaviour and the correlations among spin states propagate fast to the entire system. As we will show in Section 2, this model is fairly simple but powerful enough to capture most of the features of complex systems (e.g., phase transitions and *universality*) [9]. This has motivated many researchers to apply the Ising model to different fields ranging from ecology [10] to language evolution [11] (see [12] for a discussion of the physical motivation of the model and its limitations).

Given that social systems are both finite and heterogeneous, the Ising model has been exported in different flavours to capture the phenomena under investigation. Perhaps the most known of these Ising-like models is Tom Schelling's model of segregation [13] which has been shown to provide insight into the mechanisms under segregation in U.S. cities. This model has been shown to roughly correspond to an Ising model at $T = 0$ [14]. In this regard, the temperature has been understood as a proxy of tolerance in binary *thermodynamic societies*; solubility corresponds to integration (i.e., mixing) and the miscibility gap to segregation [15]. Ising inspired systems have also been applied to financial markets to explain expectation bubbles and economic crashes [16]. For instance, the authors in [17] create a synthetic market where agents can take three actions: *buy*, *sell,* or *stay inactive*. Also, researchers in the power systems and electricity markets domain have made an effort to include part of this complex behaviour in the problem. For instance, in [18] bilateral electricity markets are analysed as complex networks. In [19], the authors use a game theoretic approach to understand the cooperation between small-scale electricity production and consumers. Multiagent systems (MAS) have also been applied to electricity markets to allow decentralized decision-making [20]. See, for instance, [21], where authors modelled the behaviour of local consumers and producers as active agents in the electricity market based on the distributed control approach. More recently, the entity of *aggregators* has entered into the modelling scene. These are agents mediating between customers and distribution companies to offer demand bulks at competitive price. In this context, the authors in [22] define a bilevel problem where the upper-level maximises the profit of the DSO, while the lower-level maximises the profit of each aggregator. Finally, in [23] the authors use a Hopfield neural network to optimise control in power systems and make the whole system self-controlled. Here, there is a super-system composed of several power subsystems which are in turn aggregations of customers. Each customer is simulated as a node in the neural network with two possible states: generation and consumption. Since the Hopfield network is formally equivalent to a spin-glass model, the problem has some formal resemblance with our work. However, our approach is very different. In [23], the aim is to adjust demand and supply to balance the system and let it work autonomously; agent interactions are determined to maintain proper frequency and voltage values only and there is no market. In our work, spins are agents in a decision environment with power exchanges among aggregators, the DSO, and the real-time electricity market (RTEM). Moreover, in this paper, we assume that DSOs act as agents able to participate in the real-time electricity markets to trade real-time power in a two-way fashion. Notice that here we follow the same approach as in [22], where DSO behaves as a proactive market agent able to transact power with the real-time electricity market. This way, besides the RTEM, the DSO is able to trade power with local agents (e.g., aggregators and nodal consumers). Therefore, consumers can play as virtual generation agents according to their behaviour in terms of flexibility.

For the first time, we couple the local power trading problem with an Ising-based model and analyse the interrelationships between them. The Ising model provides quantitative criteria regarding how the diffusion of flexible/nonflexible behaviour impacts the required constraints in the optimisation problem.

This paper is structured as follows. First we describe the local power exchange problem in Section 2 and how the Ising model can be linked to it in Section 3. Then in Section 4 we analyse the problem at the large scale—the social welfare—where we find how the power exchange problem constrains the Ising model in different ways. In Section 5 we decrease the scale and we focus on the problem from the demand aggregator's perspective. Finally we conclude and make our final remarks in Section 6.

2. Hierarchical Model and Agent Interactions in the Distributed Power Grid

In our setting, we consider a real-time interplay structure among five kinds of actors: consumers, bus-loads, aggregators, DSOs, and RTEM. In Figure 1, we describe schematically the power exchange problem and how it couples with the spin model. The power system at distribution level involves a hierarchical structure as shown in (a). Here, only DSO is able to exchange power P_t^{RT} with the RTEM at price λ_t^{RT}. At time t each bus j interchanges power with both DSO (P_{jt}^{DSO2L}) and aggregator k (P_{jt}^{L2A}) at prices λ^{DSO2L} and $\lambda_{kt}^{\mathrm{L2A}}$, respectively. Then, a generic aggregator k exchanges an amount of P_{kt}^{A2DSO} power with DSO at price $\lambda_{kt}^{\mathrm{A2DSO}}$. In this way, the power transaction between bus-loads and aggregators is two-way according to the flexibility behaviour from the demand side. Moreover, there are two-way power exchanges between aggregator and DSO. However, the power transaction between DSO and bus-loads is one-way: only from DSO to bus-loads. In other words, bus-loads can only buy real-time power from the DSO, while they are able to buy/sell power from/to aggregators. Also, only DSO can participate in the RTEM.

Each bus-load connects a set of customers whose state in terms of demand corresponds to a binary state of a spin (here represented as an arrow up/down mimicking the spin

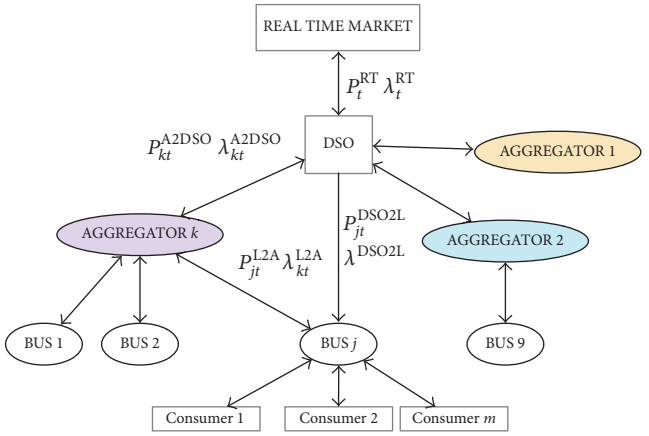

(a) Hierarchical structure in the DPS

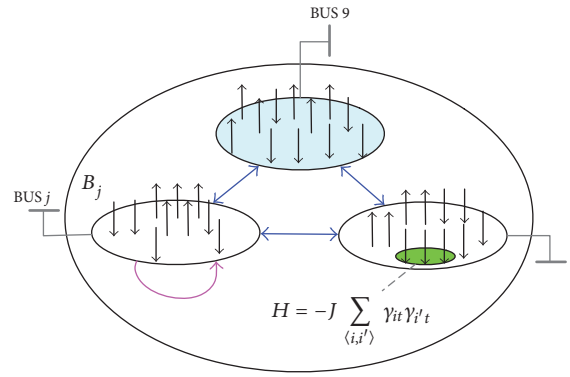

(b) Bus-loads and spin interactions

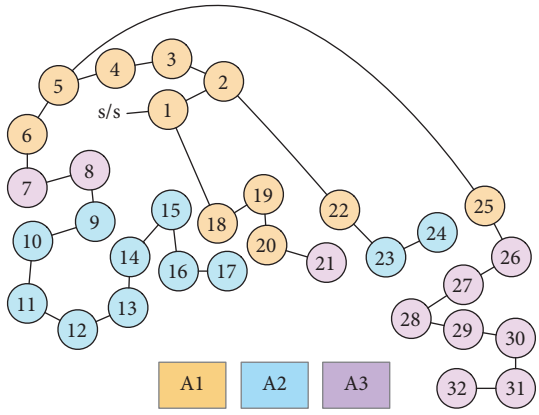

(c) 33-bus reference system and aggregators

1	3	6	7	8	12	15	18	20	23	23	24	24	25	28	29	31
1	3	6	7	9	12	15	18	20	23	23	24	24	26	28	30	31
1	3	6	7	9	13	15	18	20	23	23	24	24	26	28	30	31
1	3	6	7	9	13	15	18	21	23	23	24	24	26	29	30	31
1	3	6	7	9	13	16	18	21	23	23	24	24	26	29	30	31
1	3	6	7	9	13	16	18	21	23	23	24	24	26	29	30	31
1	3	6	7	10	13	16	19	21	23	23	24	24	27	29	30	31
1	4	6	7	10	13	16	19	21	23	23	24	24	27	29	30	31
2	4	6	7	10	13	16	19	21	23	23	24	24	27	29	30	31
2	4	6	7	11	13	17	19	21	23	23	24	24	27	29	30	31
2	4	6	7	11	13	17	19	22	23	23	24	24	27	29	30	31
2	4	6	7	11	14	17	19	22	23	23	24	24	28	29	30	31
2	5	6	7	11	14	17	19	22	23	23	24	24	28	29	30	32
2	5	6	8	11	14	17	20	22	23	23	24	25	28	29	31	32
2	5	6	8	12	14	17	20	22	23	23	24	25	28	29	31	32
3	5	7	8	12	14	17	20	22	23	24	24	25	28	29	31	32
3	5	7	8	12	15	18	20	22	23	24	24	25	28	29	31	32

(d) Lattice arrangement of customers

FIGURE 1: Power exchange and the spin model. Each bus in (a), (c) groups customers interacting through the Ising Hamiltonian with binary states represented by up/down arrows (b). Aggregators share the demand in the bus-loads (c) and customers are arranged into a 2D lattice (d) in a way that preserves the bus distance partially.

metaphor). From the demand side, different types of power balancing or other constraints can force cooperation among customers either at interbus level (blue arrows) or at intrabus level (pink arrow) in Figure 1(b). In this work, we use a 33-bus reference system (Figure 1(c)) from [1]. This is composed of 32 loads and an entry bus—indicated as "s/s"—playing the role of a slack bus connected to the main grid; power exchanges between the DSO and RTEM are done through this slack bus. The whole demand in the distributed power system is partitioned by aggregators. In our schematic we show the case of three operators as in [22]. In this work, we will use the data in [1] (shown in Table 1) as a reference for the maximum scheduled loads at each bus. From this data and assuming that a home might consume around 13 kW [24], we estimate the approximate number of customers per bus (assuming one customer per home) which makes a total of $N \approx 289$ customers. Finally in Figure 1(d), we show a 2D grid arrangement where each of the $17 \times 17 = 289$ cells represents a customer. Furthermore, we assume that in the bus-loads there exists some notion of topological closeness (e.g., spatial or electrical proximity) which is partially mapped onto the square lattice.

More rigorously, given a set C of N consumers $C = \{1, \ldots, N\}$, a set B of n_J electrical buses $B = \{1, \ldots, n_J\}$, and a set A of n_A potential aggregators $A = \{1, \ldots, n_A\}$, we arrange two partitions: in-bus-communities $C = \biguplus_{j \in B} B_j$ and bus-aggregations $B = \biguplus_{k \in A} A_k$. This way B_j represents the subset of consumers with loads electrically connected to bus j and A_k stands for the subset of buses whose load is aggregated by aggregator k. These quantities enable us to define the following maps: (1) customer-bus map: $\Delta_{cb} : C \times B \to \{0, 1\}$; $(i, j) \mapsto \chi_{(B_j)}(i)$ and (2) bus-aggregator map: $\Delta_{ba} : B \times A \to \{0, 1\}$; $(j, k) \mapsto \chi_{(A_k)}(j)$, where $\chi_A(x)$ represents the indicator function. To lighten notation, we will use Δ_{ij} or Δ_{jk} to represent $\Delta_{cb}(i, j)$ or $\Delta_{ba}(j, k)$, respectively, depending on

Table 1: Bus maximum scheduled load from [1] and number of homes assuming that each home demands approximately 13 kW as in [24].

Bus	$L_j^{\max}$ [kW]	Homes
1	100	8
2	90	7
3	120	9
4	60	5
5	60	5
6	200	15
7	200	15
8	60	5
9	60	5
10	45	3
11	60	5
12	60	5
13	120	9
14	60	5
15	60	5
16	60	5
17	90	7
18	90	7
19	90	7
20	90	7
21	90	7
22	90	7
23	420	32
24	420	32
25	60	5
26	60	5
27	60	5
28	120	9
29	200	15
30	150	12
31	210	16
32	60	5

the context. Notice that because B_j and A_k partition the sets C and B, respectively, it holds that

$$\sum_{j\in B}\Delta_{ij} = 1,$$
$$\sum_{k\in A}\Delta_{jk} = 1, \quad (1)$$
$$\forall i, j \in C, B.$$

This means that each customer is linked at least to one bus which is in turn connected to at least one aggregator. Below, we describe each agent in the system, specifying both its constraints and its objective function.

2.1. Bus-Loads and Consumers. Each consumer $i \in C$ has an associated load l_{it} at time t. Since each bus $j \in B$ connects $|B_j|$ customers, the load at each bus j at time t is $L_{jt} = \sum_{i\in B_j} l_{it}$. Additionally, each consumer load can be split into a scheduled amount l_{it}^c and a flexible portion l_{it}^f, which represents how customers can act as either upward or downward flexible loads: $l_{it} = l_{it}^c - l_{it}^f$, $\forall i \in C, t$. The sign convention here is that a positive flexibility $l_{it}^f > 0$ tends to reduce the scheduled load, whereas a negative flexibility $l_{it}^f < 0$ would increase customer's expected demand. In other words, if $l_{it}^f > 0$ the corresponding customer decreases his day-ahead scheduled electrical demand in the real time. However, if $l_{it}^f < 0$ his real-time electrical demand is more than his day-ahead scheduled demand. From these expressions, we find that

$$L_{jt} = L_{jt}^c - L_{jt}^f, \quad \forall j \in B, t, \quad (2)$$

where we have introduced consistently $L_{jt}^c = \sum_{i\in B_j} l_{it}^c$ and $L_{jt}^f = \sum_{i\in B_j} l_{it}^f$. For the scheduled load at each bus j, we use the expression:

$$L_{jt}^c = P_t^s \frac{L_j^{\max}}{\sum_{j\in B} L_j^{\max}}, \quad \forall j \in B, t, \quad (3)$$

where P_t^s represents the power at the source bus and $L_j^{\max}$ is the normalised expected load at bus j (see Table 1). The per-bus flexible component splits itself into the power exchanged with both DSO (P_{jt}^{DSO2L}) and aggregator (P_{jt}^{L2A}):

$$L_{jt}^f = P_{jt}^{\mathrm{L2A}} - P_{jt}^{\mathrm{DSO2L}}, \quad \forall j \in B, t. \quad (4)$$

According to the schematic shown in Figure 1(a) loads can only buy from the DSO and hence we have

$$P_{jt}^{\mathrm{DSO2L}} \geq 0, \quad \forall j \in B, t. \quad (5)$$

On the other hand, the bus-aggregator power exchanges are bidirectional. If $P_{jt}^{\mathrm{L2A}} < 0$ demand at bus j is buying from aggregator, the flexibility decreases. However, if $P_{jt}^{\mathrm{L2A}} > 0$ then the flexibility of the bus is increased. This can be interpreted as *virtual generation* injected into the aggregator decreasing the scheduled load at time t.

Eventually, the amount of flexibility would be constrained in different ways to ensure self-sustainability and dynamic flexibility of all loads. In this work, we allow two types of flexibility constraint:

$$\sum_{j\in B} L_{jt}^f = 0, \quad \forall t, \quad (6)$$

$$\sum_{t} L_{jt}^f = 0, \quad \forall j \in B. \quad (7)$$

On one hand, (7) is the definition of the shiftable-loads (i.e., loads that can be shifted over time). On the other hand, (6) increases the self-sustainability of the distributed power system and converges the problem to the optimum social

welfare. As we will see both constraints lead to different scenarios.

The optimisation at each bus j can be expressed as the trade-off between load bought from DSO at price λ^{DSO2L} and virtual generation sold to its aggregator k at price $\lambda_{kt}^{\mathrm{L2A}}$ integrated over time:

$$\mathrm{OF}_{j\in A_k} = \lambda^{\mathrm{DSO2L}} \sum_t P_{jt}^{\mathrm{DSO2L}} - \sum_t \lambda_{kt}^{\mathrm{L2A}} P_{jt}^{\mathrm{L2A}}. \tag{8}$$

This function must be minimised from the perspective of the loads' profit. However, both aggregators and DSO have their own priorities as we show below.

2.2. Aggregators. The first thing to notice is that each aggregator is able to sell to the DSO all the virtual generation collected among the set of buses he operates on:

$$P_{kt}^{\mathrm{A2DSO}} = \sum_{j\in A_k} P_{jt}^{\mathrm{L2A}}, \quad \forall k \in A, t. \tag{9}$$

Also there is a price model for these exchanges which is constrained in the following way:

$$\delta_{kt} \lambda_{kt}^{\mathrm{L2A}} \leq \lambda_{kt}^{\mathrm{A2DSO}} \leq \lambda_t^{\mathrm{RT}}, \tag{10}$$

where $\delta_{kt} \geq 1$ represents a lower bound threshold for the aggregator-to-DSO price compared to load-to-aggregator price. This ensures aggregators' profit, which makes it reasonable for them to be part of the market. Also, the aggregator-to-DSO price is limited by the DSO-to-market price; this upper bound acts as a price control, limiting the bidding price of aggregators below the real-time price. Here we will use reference values from [22] for $\delta_{kt} = 1.1$, $\lambda_{kt}^{\mathrm{L2A}}$ and λ_t^{RT} related to the NordPool market. We summarise the respective values in Tables 2 and 3.

The optimisation function for each aggregator k can be expressed as the accumulated balance over time between power P_{kt}^{A2DSO} sold to DSO at price $\lambda_{kt}^{\mathrm{A2DSO}}$ and power P_{jt}^{L2A} bought from demand j, at price λ_{kt}^{L2A}:

$$\mathrm{OF}_k = \sum_t \sum_{j\in A_k} \lambda_{kt}^{\mathrm{L2A}} P_{jt}^{\mathrm{L2A}} - \sum_t \lambda_{kt}^{\mathrm{A2DSO}} P_{kt}^{\mathrm{A2DSO}} \tag{11}$$

which as in the case of demand must be minimised to reach a profitable situation from the aggregators' perspective.

2.3. Distribution System Operator. In our model, DSO is an agent able to exchange power directly with all other agents in the system. As stressed, the DSO is the only player who can exchange power with the RTEM. In the power-flow balance, the power sold by the DSO to the whole demand—bus-loads—arrives from the power transacted with both aggregators and market. We express this in the following equation:

$$P_t^{\mathrm{RT}} + \sum_{k\in A} P_{kt}^{\mathrm{A2DSO}} = \sum_{j\in B} P_{jt}^{\mathrm{DSO2L}}. \tag{12}$$

Table 2: Day-ahead market power transactions P_t^s and real-time market price λ_t^{RT} obtained from [22].

Time (h)	P_t^s [kW]	λ_t^{RT} [€/kW]
1	1114,50	0,13
2	1114,50	0,12
3	1300,25	0,15
4	1114,50	0,11
5	2972,00	0,30
6	2972,00	0,32
7	3343,50	0,35
8	3715,00	0,40
9	3715,00	0,42
10	6315,50	0,66
11	6687,00	0,71
12	6687,00	0,74
13	6315,50	0,69
14	3715,00	0,50
15	3715,00	0,41
16	3715,00	0,40
17	3715,00	0,42
18	5572,50	0,60
19	5944,00	0,65
20	6315,50	0,67
21	6501,25	0,70
22	2972,00	0,35
23	1857,50	0,28
24	1486,00	0,15

Therefore, the DSOs optimisation function can be expressed as the accumulated trade-off among these quantities, times the respective prices over time:

$$\begin{aligned}\mathrm{OF}_{\mathrm{DSO}} = &\sum_t \sum_{k\in A} \lambda_{kt}^{\mathrm{A2DSO}} P_{kt}^{\mathrm{A2DSO}} + \sum_t \lambda_t^{\mathrm{RT}} P_t^{\mathrm{RT}} \\ &- \lambda^{\mathrm{DSO2L}} \sum_t \sum_{j\in B} P_{jt}^{\mathrm{DSO2L}}.\end{aligned} \tag{13}$$

This function will be minimised from the DSO's perspective to maximise its profit.

So far we have described the main actors in the power exchange scenario with power balance and price constraints along with the respective optimisation functions for each agent. Now we describe the Ising model and our interpretation of its constituents in this context.

3. An Ising Spin Model for Customers' Flexibility

The Ising Hamiltonian (14) describes the interaction among entities (i.e., agents or spins) given their state $s_i \in \{-1, 1\}$ and between each spin and a global magnetic field b. The coupling constant J measures the strength of spin-to-spin interactions.

$$H = -J \sum_{\langle i,j\rangle} s_i s_j - b \sum_i s_i. \tag{14}$$

Table 3: Aggregator prices table obtained from [22].

Time (h)	$\lambda^{\text{L2A}}_{k=1,t}$ [€/kW]	$\lambda^{\text{L2A}}_{k=2,t}$ [€/kW]	$\lambda^{\text{L2A}}_{k=3,t}$ [€/kW]
1	0,05	0,08	0,06
2	0,05	0,08	0,07
3	0,05	0,09	0,07
4	0,04	0,07	0,05
5	0,11	0,18	0,15
6	0,12	0,20	0,16
7	0,13	0,22	0,17
8	0,15	0,24	0,19
9	0,16	0,25	0,20
10	0,24	0,41	0,33
11	0,26	0,42	0,36
12	0,28	0,43	0,37
13	0,25	0,40	0,32
14	0,18	0,26	0,21
15	0,15	0,24	0,20
16	0,14	0,22	0,18
17	0,15	0,25	0,19
18	0,20	0,36	0,30
19	0,21	0,36	0,29
20	0,22	0,41	0,30
21	0,24	0,42	0,33
22	0,12	0,22	0,16
23	0,11	0,19	0,15
24	0,06	0,09	0,07

The notation $\langle i, j\rangle$ refers to pairs of spins belonging to the same radius of action or neighbourhood. When $J > 1$ (ferromagnetism) spins tend to align in the same direction and if $J < 1$ (antiferromagnetism) the spins tend to align in opposite directions. For $J = 0$, there is no spin-to-spin interaction. The external action of a positive field $b > 0$ will also foster positive spin alignments (and the other way around for $b < 0$). For a given temperature T the probability for finding a spin configuration $\Gamma = \{s_i\}$ is proportional to the Boltzmann factor: $\exp(-H/k_BT)$, where k_B stands for the Boltzmann constant. It is usual to take units such that $J = 1$ and $k_B = 1$. An important magnitude is the magnetisation $M = (1/N)\sum_{i=1}^{N} s_i$ which measures the macroscopic effect of the spin states. In the so-called Mean Field approximation its value is $T_c = 2J/(k_b \log(1 + \sqrt{(2)}))$.

One way to implement the Ising model numerically is through the Metropolis-Hastings algorithm [25], which belongs to the family of the Markov Chain Monte Carlo (MCMC) methods. Applied to our case it can be understood as a random walk over the configuration space $\Omega = \{\Gamma\}$ that converges to the Boltzmann distribution. In Algorithm 1 we show the pseudocode of a slight variant of the classical algorithm where we have included the possibility for implementing a constraint f at each step. Here f can represent the constraints in (6) and (7). The idea is that the spin shift is performed also when the constraint is minimised in absolute value. The number of iterations is chosen so that the final configuration reaches *equilibrium*. In operative terms this means that the correlations among the spin states are negligible at this point.

The size of the lattice is another important factor when using the model. On one hand, a small lattice with free boundary conditions—the one used here—shows border effects which are not present in large systems or in systems with other boundary conditions (e.g., periodic). In particular, this can affect the number of iterations to decorrelate the system and the potential transitions of state. There is an interesting debate on whether finite systems can undergo phase transitions or not [26]. Clearly, a finite system cannot reproduce a singularity in a purely mathematical sense using a finite number of sums. As it is shown in [26] phase transitions in finite systems tend to be rounded and smoothed near the critical points. In Figure 2 we show the autocorrelation function for the spin states between the initial and evolved configuration for increasing number of iterations. We start with a random initial configuration for the 17×17 spin system shown in Figure 1(d). For $> 5k$ iterations it is possible to achieve a reasonable value of decorrelation. In the inset, we show the phase transition in M beyond T_c. Notice how the numerical implementation is still able to reproduce qualitatively the transition $M = \pm 1 \rightarrow 0$ although in a smoothed and rounded way.

When using this model one has to fix the interpretation for the following elements: (1) spin states, (2) spin-to-spin interactions, (3) external field, (4) magnetisation, and (5) temperature. In our setting, we can parametrize the eagerness of consumer i to follow the flexibility program at time t with two state variables: (1) flexible $\gamma_{it} = 1$ and (2) not flexible: $\gamma_{it} = -1$. A possible and simple model for l^f_{it} is then

$$l^f_{it} = l^c_{it}\gamma_{it}. \tag{15}$$

The spin-to-spin interaction can be a proxy for communication among customers and the external field b can simulate a top-down directive forcing customers to follow some policies or Demand Response (DR) programs that are adopted by players in the top layers of the system (e.g., DSO and aggregators). On the other hand, in the context of financial markets [27] interprets M as a measure for the deviation from the fundamental value; if M is large agents are afraid of trading unless they have strong support from their private opinions or from their neighbours. In our case $M = 1$ and $M = -1$ represent that the system has either maximum or minimum flexibility. A value of M close to 0 is interpreted as a perfect balance where half of the customers are flexible and the other half is not. Finally, the temperature can represent customers' uncertainty about the effectiveness of the flexibility program that can impact on the reliability and security of the system. We can also associate T with noise in customers' information channels; too much noise destroys the spontaneous magnetisation (max/min flexibility previously achieved) [15]. Also, when the "social temperature" [28] is high it destroys large domains (subpopulations) and hence it favours the mixing of options.

Let us also assume that all consumers connected to a bus have the same amount of scheduled load: $l^c_{it} = l^c_{jt} > 0$, $\forall i \in$

INPUT: Δ_{cb}, Γ, f, T, *num.Iters*
OUTPUT: Γ'_t
(1) $iter \leftarrow 0$
(2) **while** $iter \leq num.Iters$ **do**
(3) $n \leftarrow$ pick a random spin from Γ
(4) $\Delta E \leftarrow 2\gamma_{nt} \sum_{\langle i,n \rangle} \gamma_{it}$ {energy change if spin flipped}
(5) $P(\Delta E) \leftarrow \exp(-\Delta E/T)$ {Boltzmann's probability for ΔE}
(6) $\gamma'_{it} \leftarrow \gamma_{it}(1 - 2\delta_{in})$ {new configuration if spin flipped}
(7) $M'_{jt} \leftarrow (1/n_j) \sum_{B_j} \gamma'_{it}$ {bus magnetization in new configuration}
(8) **if** $|f(M'_{jt})| \leq |f(M_{jt})|$ **then**
(9) $x \leftarrow$ random number $\in [0, 1]$ from uniform distribution
(10) **if** ($\Delta E \leq 0$ **or** $x \leq P(\Delta E)$) **then**
(11) $\Gamma'_t \leftarrow \Gamma_t \setminus \{\gamma_{nt}\} \cup \{-\gamma_{nt}\}$ {flip spin}
(12) **end if**
(13) **end if**
(14) $iter \leftarrow iter + 1$
(15) **end while**

Algorithm 1: Constrained Metropolis-Hastings (CMH).

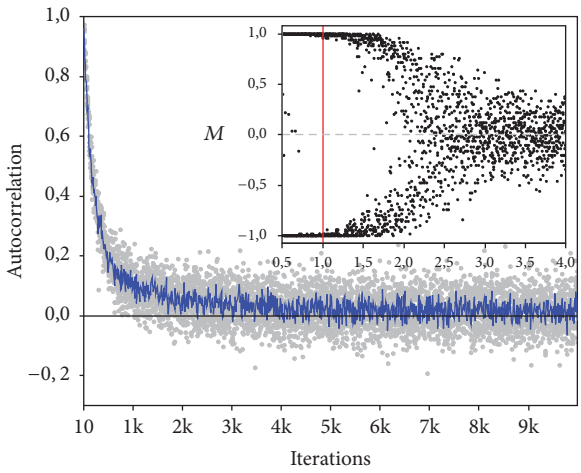

Figure 2: Autocorrelation function for the spin states between initial and evolved configurations. Grey dots represent numerical realisations and the blue line represents the average. The inset shows the phase transition in M beyond T_c (red line).

B_j, j, t (notice that this does not reduce the generality of the problem; we can always adjust the number of customers per bus to represent the scheduled per-bus load L^c_{jt}). Therefore, the flexible component of the load at bus j at time t renders

$$L^f_{jt} = l^c_{jt} M_{jt} n_j, \tag{16}$$

where $n_j = |B_j|$ represents the number of customers in bus j and M_{jt} stands for the *bus magnetisation* $M_{jt} \equiv (1/n_j) \sum_{i \in B_j} \gamma_{it}$. Let us also define dimension-free variables $\forall j \in B, t$ as follows: $\eta_{jt} \equiv P^{\text{L2A}}_{jt}/L^c_{jt}$ and $\psi_{jt} \equiv P^{\text{DSO2L}}_{jt}/L^c_{jt}$. Further, we assume that the real-time power exchanged from DSO and RTEM is a factor of the total load the DSO has to supply to buses. $P^{\text{RT}}_t \equiv \sum_{j \in B} \theta_{jt} L^c_{jt}$. With these definitions and (4), we find

$$\eta_{jt} - \psi_{jt} = M_{jt}, \quad \forall j \in B, t. \tag{17}$$

Notice that the power flow from aggregator k to DSO in (9) can be expressed as

$$P^{\text{A2DSO}}_{kt} = \sum_{j \in B} \Delta_{jk} l^c_{jt} \eta_{jt} n_j. \tag{18}$$

Also, from (1), (12), and (18) one can express the DSO power constraints as

$$\sum_{j \in B} n_j l^c_{jt} \left(\theta_{jt} + \eta_{jt} - \psi_{jt}\right) = 0, \quad \forall t. \tag{19}$$

Since $l^c_{jt} \geq 0$, $\forall j \in B, t$ and $nj \geq 0$, $\forall j \in B$, inequality 5 is expressed as

$$\psi_{jt} \geq 0, \quad \forall j \in B, t. \tag{20}$$

Notice that constraints (17) and (19) can be combined into

$$\sum_{j \in B} n_j l^c_{jt} \left(\theta_{jt} + M_{jt}\right) = 0, \quad \forall t. \tag{21}$$

Finally, flexibility constraints in (6), (7) can be expressed through (16) as

$$\sum_{j \in B} l^c_{jt} n_j M_{jt} = 0, \quad \forall t, \tag{22}$$

$$\sum_{t} l^c_{jt} M_{jt} = 0, \quad \forall j \in B. \tag{23}$$

By combining constraints (10), (17), (19), (20), with either (22) or (23) and different objective functions, we can build scenarios from different perspectives and scales as we show below.

4. Large Scale Optimisation: Flexibility and Social Welfare

With the definitions above and from (8), we find the optimisation for each bus j:

$$\mathrm{OF}_j = \sum_{t,k\in A} n_j l^c_{jt} \Delta_{kj} \left(\lambda^{\mathrm{DSO2L}} \psi_{jt} - \lambda^{\mathrm{L2A}}_{kt} \eta_{jt}\right), \quad \forall j \in B, t, \tag{24}$$

(where we have used $\mathrm{OF}_j = \sum_{k\in A} \Delta_{kj} \mathrm{OF}_{j\in A_k}$). The optimisation functions for each aggregator from (9) and (11) render

$$\mathrm{OF}_k = \sum_{t,j\in B} n_j l^c_{jt} \Delta_{kj} \left(\lambda^{\mathrm{L2A}}_{kt} - \lambda^{\mathrm{A2DSO}}_{kt}\right) \eta_{jt}, \quad \forall k \in A, t, \tag{25}$$

where we have used $\sum_{j\in A_k}[\cdot] = \sum_{j\in B} \Delta_{kj}[\cdot]$. Finally, from (9) and (13), we find

$$\mathrm{OF}_{\mathrm{DSO}} = \sum_{t,k\in A, j\in B} n_j l^c_{jt} \left[\Delta_{kj} \lambda^{\mathrm{A2DSO}}_{kt} \eta_{jt} + \frac{\lambda^{\mathrm{RT}}_t}{n_A} \theta_{jt} - \frac{\lambda^{\mathrm{DSO2L}}}{n_A} \psi_{jt}\right], \quad \forall t. \tag{26}$$

By defining $\mathrm{OF}_L \equiv \sum_{j\in B} \mathrm{OF}_j$ and $\mathrm{OF}_A \equiv \sum_{k\in A} \mathrm{OF}_k$, the total load and total aggregation objective functions are found straightforward. Finally our objective is to maximise the *social welfare* of the distributed power system. Hence, the optimisation function is defined as $\mathrm{OF}_W = \mathrm{OF}_L + \mathrm{OF}_A + \mathrm{OF}_{\mathrm{DSO}}$ to ensure the maximised profits of all players (DSO, aggregator, and bus-loads) in the distributed power system. The global optimisation function OF_W can be expressed as

$$\mathrm{OF}_W = \sum_t \lambda^{\mathrm{RT}}_t \sum_{j\in B} n_j l^c_{jt} \theta_{jt}. \tag{27}$$

Notice how from this global scale the specifics about power exchanges between DSO-to-demand, demands-to-aggregators, and aggregators-to-DSO cancel out. The only relevant quantity which remains is the aggregated power exchanges between the DSO and RTEM integrated over time. From constraint (21) it holds

$$\mathrm{OF}_W = -\sum_t \lambda^{\mathrm{RT}}_t \sum_{j\in B} n_j l^c_{jt} M_{jt} \tag{28}$$

which links the objective function to the spin flexibility.

What this equation is telling us is that social welfare increases (OF_W is minimised) when flexibility increases. Now depending on which additional constraint we use for the flexible amount ((22) or (23)), there are two main scenarios to analyse:

$$S1(\text{Shiftable-Loads}): \begin{cases} \mathrm{OF}_W = -\sum_{j\in B} n_j \sum_t \lambda^{\mathrm{RT}}_t l^c_{jt} M_{jt} \\ \sum_t l^c_{jt} M_{jt} = 0, \ \forall j \in B, \end{cases} \tag{29}$$

$$S2(\text{Self-Sustainability}): \begin{cases} \mathrm{OF}_W = 0 \\ \sum_{j\in B} n_j l^c_{jt} M_{jt} = 0, \ \forall t. \end{cases} \tag{30}$$

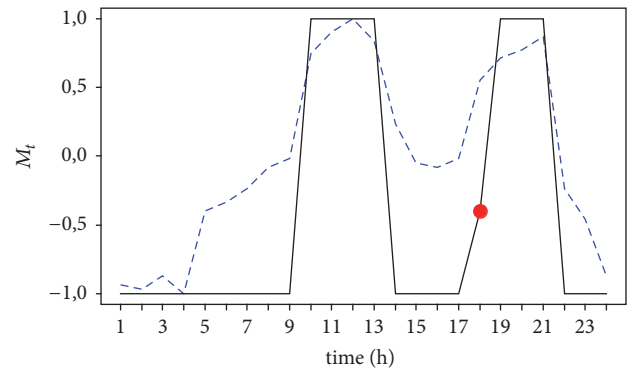

Figure 3: Resulting per-bus magnetisations. Blue dotted line shows the values for the normalised RTEM prices $\bar{\lambda}^{\mathrm{RT}}_t$. The red dot represents a situation where the discrete spin system is unable to comply with the electrical constraint by flipping spin states.

These two forms for constraining customers' flexibility lead to very different strategies in terms of consumers' interaction and cooperation (see arrows in Figure 1(b)). The constraint in $S1$ can be achieved by asking spin communities to adjust their flexibility over time independently of other communities; the only requirement is that at the end of the 24 h cycle each bus j renders $\sum_t l^c_{jt} M_{jt} = 0$. This can be set into a linear programming problem for the variables M_{jt}. On the other hand, in scenario $S2$ the objective function vanishes regardless of consumer's flexibility. However, in-bus-communities (i.e., spin communities) are forced to constrain their spin state every hour so that the whole system renders $\sum_{j\in B} n_j l^c_{jt} M_{jt} = 0$. This requires a level of coordination among the bus communities at every hour t.

4.1. Shiftable-Loads. The constraint in (29) can be implemented as follows. First we solve the optimisation problem in (29). The output is the per-bus magnetisations M_{jt}. Notice that the constraint can be factorised in j. This way, minimising OF_W is equivalent to solving

$$\begin{aligned} \min \quad & -\sum_t \lambda^{\mathrm{RT}}_t P^s_t M_{jt} \\ \text{s.t.} \quad & \sum_t P^s_t M_{jt} = 0. \end{aligned} \tag{31}$$

For all $j \in B$. Therefore the solutions M_{jt} do not depend on j and we can write $M_t \equiv M_{jt}, \forall j \in B$. In Figure 3 we show the solution along with the RTEM prices scaled in the following way: $\bar{\lambda}^{\mathrm{RT}}_t = 2(\lambda^{\mathrm{RT}}_t - \min(\lambda^{\mathrm{RT}}_t))/(\max(\lambda^{\mathrm{RT}}_t) - \min(\lambda^{\mathrm{RT}}_t)) - 1 \in [-1, 1]$. This scaling makes both quantities comparable. Notice how the bus-flexibility solution follows the RTEM prices over time. This means that at demand peak times (10–13 h) and from (18–21 h) it is necessary to increase customers' flexibility.

Then we might ask how the spin system can comply with the total magnetisation imposed by the electrical constraints

at every time t (see Figure 3). We need each spin-community γ_{it}, $\forall i \in B_j$ to follow the constraint:

$$\sum_{i \in B_j} \gamma_{it} = n_j M_t, \quad \forall j, t. \tag{32}$$

This must hold for each bus-community of size n_j for all times. By redefining the spin states as $s_{it} \equiv (1 + \gamma_{it})/2$ with $s_{it} \in \{0, 1\}$, the constraint in (32) is equivalent to

$$\sum_{i \in B_j} s_{it} = \frac{n_j}{2}(1 + M_t), \quad \forall j, t. \tag{33}$$

Since the spin system is discrete, the left hand side of (33) is a positive natural number: $\mathbb{N}^+ \ni x \equiv \sum_{i \in B_j} s_{it}$. Therefore, there is no solution if M_t is not a rational number: $M_t \notin \mathbb{Q}$. If $M_t \in \mathbb{Q}$ (i.e., $M_t = a/b$; $a, b \in \mathbb{Z}$, $a, b \neq 0$), there is a solution when

(1) $a = 0$ and n_j is even; the solution consists in having half of the spins up and half down;

(2) $a = b$ with solution $s_{it} = 1, \forall i$;

(3) $a = -b$ with solution $s_{it} = 0, \forall i$;

(4) $a/b \in (-1, 0)$ and n_j is a multiple of $2b$.

Notice that in Figure 3 all solutions are $M_t = \pm 1$ for all times except for $t = 18$, where we found $M_t = -0.4$. In the first case the only possible solutions are $s_{it} = 1, \forall i$ if $M_t = 1$ and $s_{it} = 0$, $\forall i$ if $M_t = -1$. However, in the latter case of $M_t = -0.4 = -2/5$ customers will not be able to flip their states in order to attain this magnetisation; although we are in case (4), none of the available buses connects a number of homes which is a multiple of 5 (Table 1).

This evidences a potential limitation of a discrete model when it is coupled to the local power exchange problem. In the presence of electrical constraints, a discrete system will in general not be able to follow the continuum limit every time. A possible strategy to cope with this situation is to include an external effect (field) in the customer interactions to force their flexibility. In the Ising parlance, this is equivalent to setting $b > 0$ in the Ising Hamiltonian of (14). Then we can measure how customer's flexibility increases by setting $M_{t=18} = -1$, evolve the system for different field intensities, and see if we reach $M_{t=19} = 1$. In Figure 4 we show the final magnetisation for a pair of (T, b) reached from a starting configuration with all spins down ($M = -1$) after 10k iterations using the Metropolis algorithm without any constraint. Magnetisations are averaged from 5000 Monte Carlo runs for each (T, b) combination. As a reference we find the field strength $b = 1.5$ that makes the system reach $M_t = 1$ at the theoretical critical temperature T_c (blue dotted line in the inset). This is a way of forcing the so-called *herding* behaviour by imposing a top-down approach. Notice how the external action ramps up customers' flexibility. However, if temperature is high, the noise will destroy these dynamics and the intended constraint can not be reached.

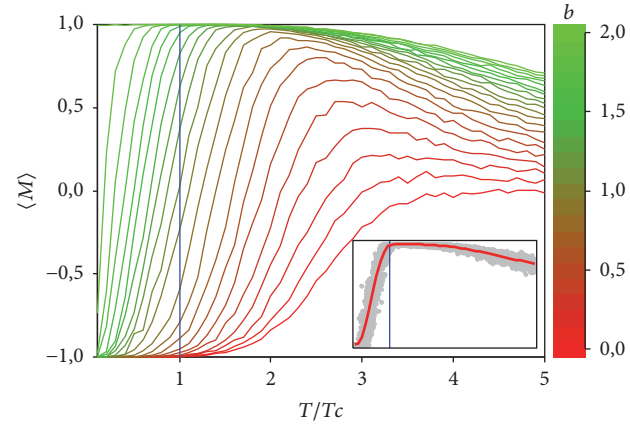

Figure 4: Ramping up to meet maximum flexibility. Each curve represents the final magnetisation for a pair of (T, b) reached from a starting configuration with all spins down ($M = -1$). The inset shows the curve for $b = 1.5$ (grey dots are numerical realisations and red line represents the averaged value) and the critical temperature (blue vertical line).

4.2. Self-Sustainability. Now let us explore a different situation where loads are forced to adjust so that $\sum_{j \in B} n_j l^c_{jt} M_{jt} = 0$ at every time. A simple way to tackle this problem is by seeking solutions where the total magnetisation is either maximised or minimised. Hence, the problem can be set in terms of an Integer Linear Programming (ILP) problem of the form:

$$\begin{aligned} \max\,(\min) \quad & \sum_j M_{jt} \\ \text{s.t.} \quad & \sum_j n_j l^c_{jt} M_{jt} = 0 \\ & -1 \leq M_{jt} \leq 1 \\ & M_{jt} \in \mathbb{Z}. \end{aligned} \tag{34}$$

Analogous for j in the shiftable-loads case, now the optimal solutions M_{jt} do not depend on time and we can set $M_j \equiv M_{jt}, \forall t$. For each case (max or min) we have the range of values for $M_j = \{-1, 0, 1\}$. In Figures 5(a) and 5(b) we show both solutions with our spin arrangement (Figure 1(c)). The maximisation solutions from the system in (34) result in 125 locations with $M_j = -1$, 132 with $M_j = 1$, and 32 with $M_j = 0$. On the other hand, the minimisation results in 132 locations with $M_j = -1$, 125 with $M_j = 1$, and also 32 with $M_j = 0$. Therefore, the total magnetisation in both cases is 7 and -7 for the maximisation or minimisation problem, respectively.

As in Scenario *S*1, spin communities with constraints $M_j = 1$ or $M_j = -1$ can be obtained by switching the spin states regardless of the size of the community. However for the $M_j = 0$ communities (shown in white color in Figure 5), a solution is only found when n_j is even. Therefore, buses $j = 10, 28$ in the maximisation and $j = 3, 10$ for the minimisation, respectively, will lack a solution as indicated by a red label in the figure. We have also verified this numerically by solving the following simple Binary Linear Programming (BLP)

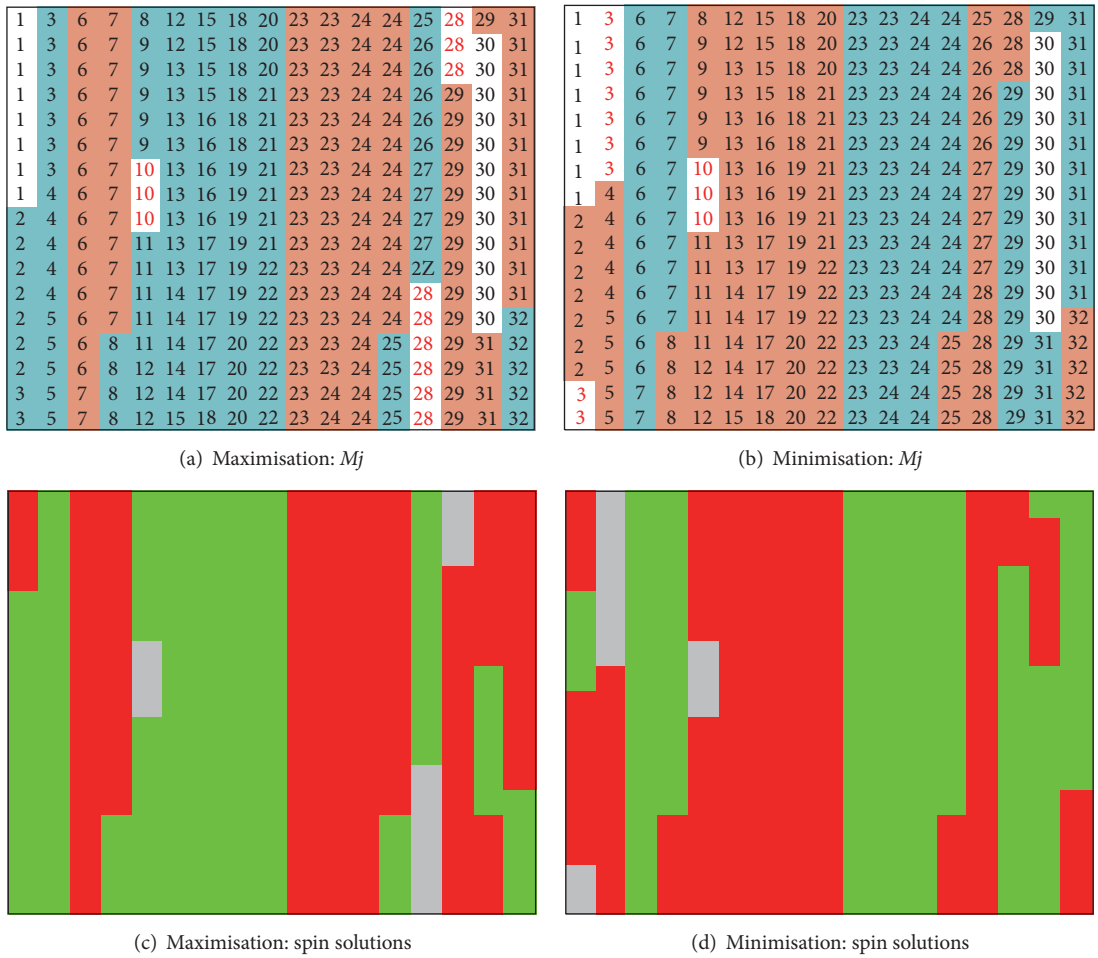

(a) Maximisation: *Mj*

(b) Minimisation: *Mj*

(c) Maximisation: spin solutions

(d) Minimisation: spin solutions

FIGURE 5: Electrical constraints and spin solutions in a self-sustainability scenario. (a, b) Max/min solutions with $M_j = -1$ (red), $M_j = 0$ (white), and $M_j = 1$ (blue); numbers indicate the bus number the customers belong to. (c, d) Spin solutions with $\gamma_{jt} = -1$ (red), $\gamma_{jt} = 1$ (green), and grey color if there is no solution.

problem for each bus-community (notice that minimising instead of maximising the problem will provide the same result; the only difference among solutions is the switching of states in the bus communities when n_j is an even number).

$$\begin{aligned} \max \quad & \sum_{i=1}^{n_j} s_i \\ \text{s.t.} \quad & \sum_{i=1}^{n_j} s_i = \frac{n_j}{2}\left(1 + M_j\right) \\ & s_i \in \{0, 1\}. \end{aligned} \tag{35}$$

We show the spin solutions from (35) in Figures 5(c) and 5(d).

Since these constraints must hold for all times, it is interesting to check how *robust* the system is for complying with such magnetisations. To this end we test the robustness as follows:

(1) Regularise buses with $M_j = 0$ and n_j odd by rewiring a random customer from another bus with $M_j \neq 0$. This results in a feasible spin configuration compatible with the constraints in (30).

(2) Perturb the feasible spin solution with strength q by switching the state of round$(q/N \cdot 100)$ spins.

(3) Evolve the spin system with both the unconstrained Metropolis and with the CMH algorithm for a range of temperatures $T/T_c = 0.5, 0.6, \ldots, 1.5$.

(4) Measure the value of the constraint $F = \sum_j n_j l^c_{jt} M_j$ in both cases.

(5) In the resulting ensemble find the realisation with minimum F and monitor how $|F|$ deviates from 0.

We found that the constraints-free evolution renders F values of 3 orders of magnitude larger than those obtained with the constrained version (CMH). The results of this experiment are shown in Figure 6. Here we compare on a normalised scale how the constraints deviate from 0 as we perturb the feasible spin solution with increasing perturbation strength. We measure the perturbation by the Hamming distance between the original and the perturbed configuration. Every

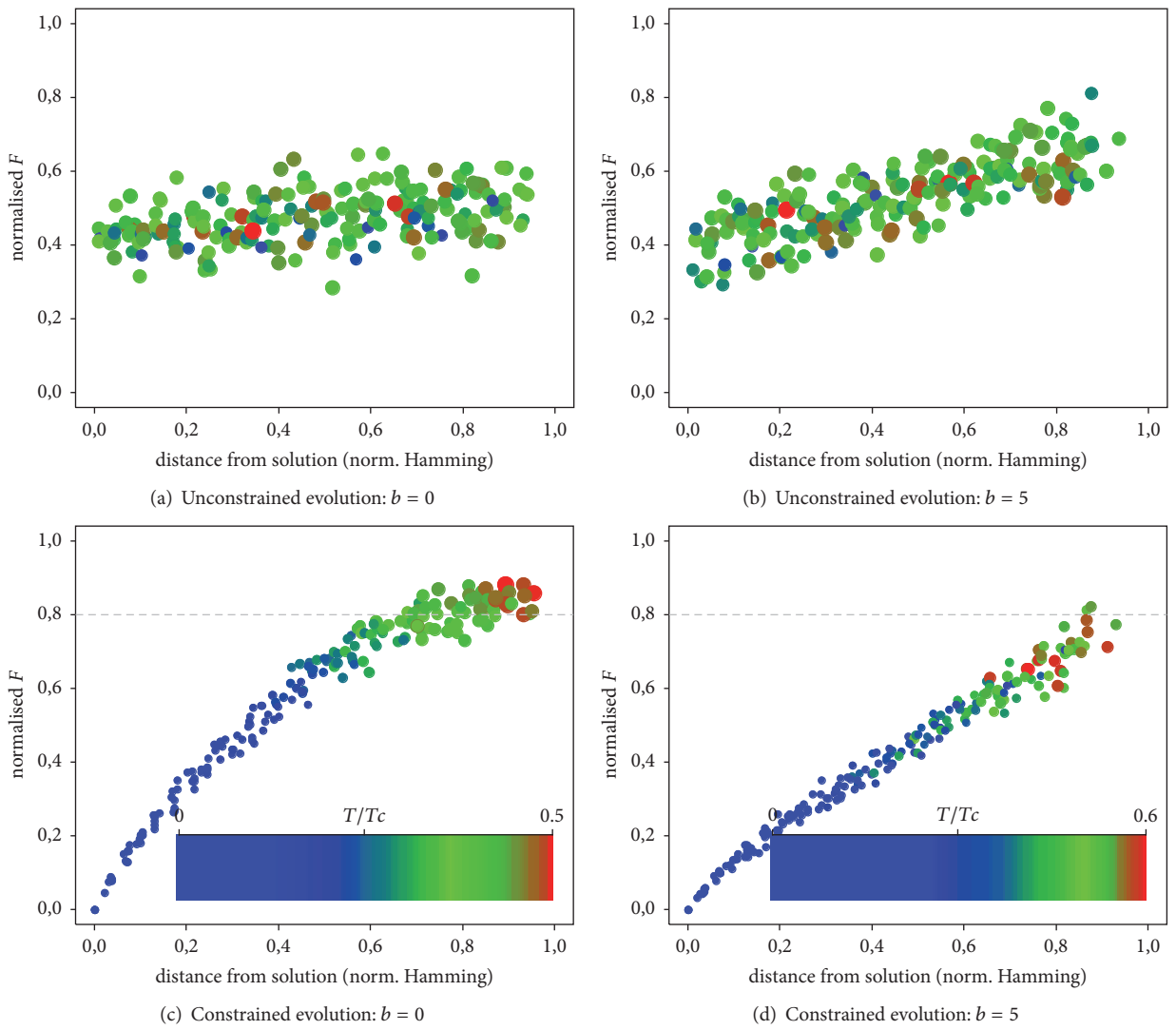

(a) Unconstrained evolution: $b = 0$

(b) Unconstrained evolution: $b = 5$

(c) Constrained evolution: $b = 0$

(d) Constrained evolution: $b = 5$

FIGURE 6: Constraint robustness in a self-sustainability scenario. (a, b) Unconstrained evolution. (c, d) Evolution with the CMH version. The size of the points is proportional to the temperature where the minimum value of $|F|$ is found.

point represents the average value of 20 Monte Carlo replicas for the same parameters. As expected, the unconstrained evolution fails to provide a systematic trend in these dynamics since once the constraint is broken, there are no mechanisms to bend the spin dynamics towards regions with increasing feasibility. However, we find a pattern for the constrained evolution: as we deviate from the solution the value for F increases monotonically (worsening the feasibility). Notice that if perturbations are large, the minimum F is only found for high temperatures, since as we increase thermal fluctuations, the system will be able to explore different configurations and discover lower F values.

The effect of the external field is different in both cases. In the unconstrained case the field only tilts up the values and reduces the noise. This is useless in our case since the field action reinforces the perturbations worsening the constraint. In the constrained case, however, the field linearises the point pattern on our scaling (we have added a dotted grey line for reference) and this improves feasibility. Therefore, an external action in the community would not be useful for recovering flexibility unless additional mechanisms are implemented to penalise deviations from the feasible region. These actions can be implemented smoothly because the drift from optimality increases monotonically with the perturbation.

5. The Aggregators' Perspective

From (17) and (25) we find that the total aggregation optimisation function renders

$$\mathrm{OF}_A = \sum_{tj} n_j I_{jt}^c \left(\psi_{jt} + M_{jt}\right) \sum_k \Delta_{kj} \left(\lambda_{kt}^{\mathrm{L2A}} - \lambda_{kt}^{\mathrm{A2DSO}}\right) \quad (36)$$

which must attain a minimum value to maximise total aggregation profit. Each aggregator-to-DSO transaction has a price $\lambda_{kt}^{\mathrm{A2DSO}}$ bounded by constraint (10) and as stressed before:

$\lambda_{kt}^{\text{A2DSO}} \geq \delta_{kt}\lambda_{kt}^{\text{L2A}}$. Since we also have $\psi_{jt} \geq 0$, this problem will be in general unbounded in ψ_{jt} (the power that customers buy from DSO). From the aggregator's profit perspective, the larger the quantity $(\psi_{jt} + M_{jt})$, the higher their benefit (notice that in this case the flexibility constraints in (22) and (23) do not bound the ψ_{jt} values). This way, maximum flexibility and maximum ψ_{jt} will render an optimal benefit to aggregators without considering the optimum profit of the bus-loads. Hence, optimising the problem from the aggregators' point of view propels a bottom-up power transaction from bus-loads to aggregators, from aggregators to DSO, and from DSO to the real-time market, hierarchically. Moreover, the exchanged power benefit between the DSO and bus-loads is missing because this is irrelevant to aggregators. Consequently, as (36) shows, aggregators ask for the maximum loads' flexibility. In other words, the power flexibility is balanced with the power exchanged between the bus-loads to aggregators and with the power sent from DSO to bus-loads. Hence, from the aggregators' perspective, this will push the system to increase the flexibility from demand side and transacted power from the DSO to the loads. Notice that although this case is profitable for the DSO, it is not a profitable way for bus-loads to join this energy management approach.

One way to motivate bus-loads to join this setting is by letting ψ_{jt} be a parameter instead of a variable in this optimisation problem. In particular—and without loss of generality—we can set $\psi_{jt} = 0$. Also notice that, in optimality conditions, the variables $\lambda_{kt}^{\text{A2DSO}}$ will attain their maximum values in (10): $\lambda_{kt}^{\text{A2DSO}} = \lambda_t^{\text{RT}}$. The modified aggregation optimisation function is then expressed as

$$\overline{\text{OF}}_A = \sum_{tj} n_j l_{jt}^c M_{jt} \sum_k \Delta_{kj} \left(\lambda_{kt}^{\text{L2A}} - \lambda_t^{\text{RT}}\right). \tag{37}$$

Below we explore two analytical limits of (37) and how flexibility constraints in (22) and (23) affect the respective solutions.

(1) Aggregator Homogeneous Prices Limit. If all aggregators offer the same price for their transactions with the bus-loads, $\lambda_{kt}^{\text{L2A}} \to \lambda_t^{\text{L2A}}$ (i.e., there is no heterogeneity in the distributed power system), the optimisation function does not depend on the load-to-bus mapping $\overline{\text{OF}}_A \to \sum_t (\lambda_t^{\text{L2A}} - \lambda_t^{\text{RT}}) \sum_j n_j l_{jt}^c M_{jt}$. Also, if the self-sustainability flexibility constraint (22) is added to the problem, the function will be zeroed. This way, self-sustainability constraints do not have any effect on the total aggregation benefit because it makes the distributed power system an independent energy system. Hence, the system does not depend on the real-time electricity market to provide its local demand.

(2) Stationary Limit in Aggregator Prices. On the other hand, consider a situation where there is no price evolution over time (i.e., a fixed tariff scenario). In this case we get $\lambda_{kt}^{\text{L2A}} \to \lambda_k^{\text{L2A}}$, $\lambda_t^{\text{RT}} \to \lambda^{\text{RT}}$, and the optimisation function in (37) renders $\overline{\text{OF}}_A \to \sum_{kj} \Delta_{jk} n_j (\lambda_k^{\text{L2S}} - \lambda_{\text{RT}}) \sum_t l_{jt}^c M_{jt}$. In this case the function is zeroed and again independent of the load-to-bus mapping if we impose the shiftable-loads flexibility constraint (23). This is because in a fixed tariff scenario shifting demand over time is not rational, and it does not render any extra profit for the distributed power system.

5.1. Optimal Load-to-Aggregator Mappings. If we assume that customers are maximally flexible we can set $M_{jt} = 1$ in the optimisation function and conjecture which bus-to-aggregator mappings are more effective in different scenarios. In [22] the authors analysed the problem with 3 aggregators and other different configurations built by merging these 3 operators with aggregator prices in Table 3. Since for all times aggregator A_1 always holds the minimum price, the optimal solution will map all buses to A_1. However, this is unrealistic since it is unlikely that all demand can be monopolised by a single aggregator. One way to cope with this is to force aggregators to split load as $\forall k \sum_j \Delta_{jk} \leq \text{round}(n_J/n_A) + q$, where $q \in \mathbb{N}$ is a slack threshold for the uniform bus-to-aggregator mapping. By adding this constraint, the optimisation can be tackled by solving the BLP problem in the Δ_{jk} variables

$$\begin{aligned} \min \quad & z = \sum_{tj} n_j l_{jt}^c \sum_k \Delta_{kj} \left(\lambda_{kt}^{\text{L2A}} - \lambda_t^{\text{RT}}\right) \\ \text{s.t.} \quad & \sum_k \Delta_{jk} = 1, \quad \forall j \\ & \sum_j \Delta_{jk} \leq \text{round}\left(\frac{n_J}{n_A}\right) + q, \quad \forall k \\ & \Delta_{jk} \in \{0, 1\}. \end{aligned} \tag{38}$$

In Figure 7 we show the normalised value of the objective function in (38) as we increase the number of aggregators (in %) and for different q values. First we notice a global trend: the optimisation increases (lower objective function values) with the number of aggregators. Also q helps in this reduction by pulling the solutions downwards and by smoothing the peaks as it increases. For low q values the constraints are more stiff and the feasible space becomes fragmented. In the limit $q = 0$ (maximum homogeneity of load split) we find that for combinations of $\{5, 6, 10, 13, 14, 15, 22, 23, 24, 25, 26, 27, 28, 29, 30, 31\}$ aggregators there are no optimal solutions (black dots). The reason for this is that for $q = 0$ and, say, $n_A = 5$, we are forcing to evenly distribute 32 buses among 5 aggregators so that at least one bus belongs to one aggregator. But each aggregator can only group round$(32/5) = 6$ buses at maximum. On the other hand, as q increases the peaks are smoothed, since the feasible space increases too. To test our model we compare our results (39) with the mapping in [22] displayed in Figure 1(d). The cardinality of $A_1, A_2, A_3 = (11, 11, 10)$ corresponds to our optimal solution from (38) for $q = 0$ and $n_A = 3$:

$$\begin{aligned} A_1 &= \{1, 3, 6, 7, 13, 23, 24, 28, 29, 30, 31\}, \\ A_2 &= \{2, 4, 5, 8, 9, 17, 18, 19, 20, 21, 22\}, \\ A_3 &= \{10, 11, 12, 14, 15, 16, 25, 26, 27, 32\}. \end{aligned} \tag{39}$$

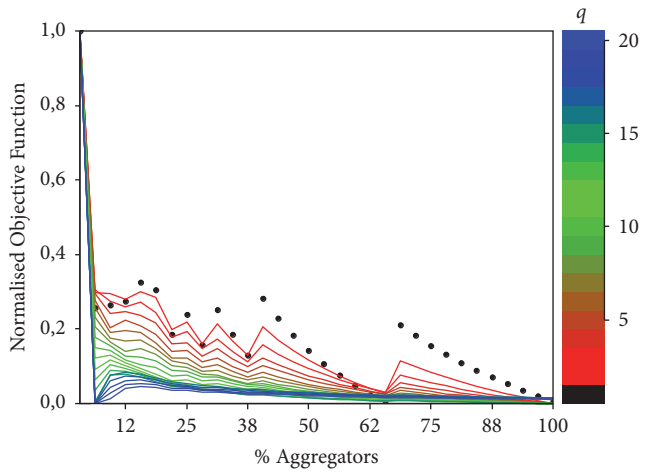

FIGURE 7: Bus-to-aggregator map efficiency. The normalised value of z for the optimal solution is shown for different number of aggregators and q. Black circles represent feasible solutions for $q = 0$.

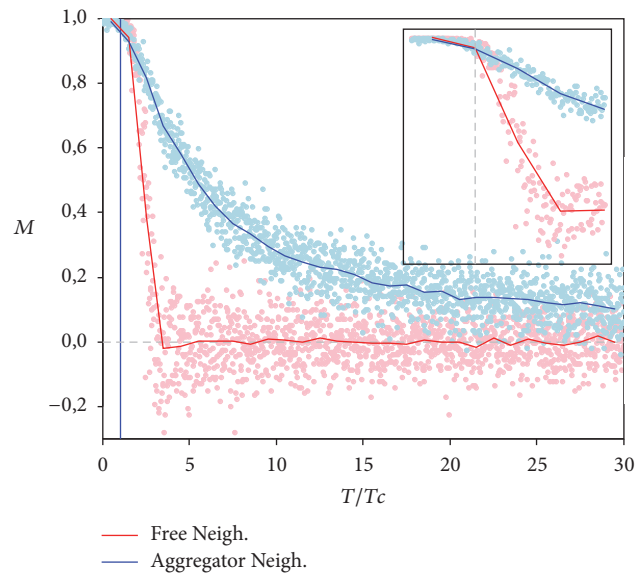

FIGURE 8: Aggregator boundaries and total magnetisation. Standard evolution (red) compared with another evolution where spins interact only with neighbours belonging to the same aggregator (blue). Dots represent 100 realisations for each T and lines show averaged values (T_c shown in blue vertical line). The inset zooms in the solutions where there is a phase-like transition at T/T_c (grey dotted line).

From these results we conclude that, in a maximum flexibility scenario, the total aggregation profit increases with the number of aggregators. In general, depending on the bus scheduled loads and the number of aggregators, demand cannot be split 100% evenly among aggregators; there must be some slack mechanisms to allow for flexibility in this mapping. Since customers group into buses and buses are mapped to aggregators, this discussion is relevant to the customer's flexibility as we show below with our Ising model.

5.2. Aggregator Boundaries and Their Effects. Since aggregators operate on bus-load collections they might impose certain *boundaries* on the customers (and hence, in the associated spin system). These boundaries can be, for instance, by-contract forcing actions or other rules which have a greater or lesser influence on the customers' behaviour. The effect of this on the spin model is that agents will prefer to interact with neighbours who share the same aggregator. In our final experiment we measure the effect of aggregator boundaries by comparing a standard evolution (neighbourhood-free) with another evolution where spins interact only with neighbours belonging to the same aggregator. We start with a feasible solution for maximum flexibility $M = 1$ and then we measure how thermal noise worsens the solution.

In Figure 8 we show these results by comparing the boundary-free evolution with the aggregators' boundary dynamics with the reference boundaries shown in Figure 1(d). As expected, with very high temperature, noise will dominate interactions and the system will reach the $M = 0$ equilibrium as shown in Figure 2 (inset). However, the interesting dynamics occur precisely near criticality. Here we can monitor how sharply the flexibility (M) drops as T increases. The free-neighbourhood solution drops fast to $M = 0$ for $T/T_c > 1.5$ (shown as a grey dotted line in the inset of the figure). However, notice how the neighbourhood constrained evolution slows down the worsening of the flexibility. Following our interpretation of temperature as uncertainty (lack of information), as T grows, shared opinions as to whether demand should be increased (spin-to-spin interactions) will not be strong enough to keep customers' confidence level in the flexibility program. Consequently, they will randomly decide whether to increase or decrease their demand and the constraint for maximum flexibility will start to deteriorate. However, when the information flow among customers is bounded within regions in the configuration space, this drop is smoothed, since the information does not propagate to the entire system in the same way. From our previous discussion about the limitations of a finite model for reproducing a phase transition, one might attempt to provide a *semicritical* exponent to these phase-like transitions. However, that is left for a future work.

6. Summary and Discussion

In this work we have analysed the customers' demand flexibility in a local power trading problem through an Ising spin-based model. We interpret spin states as customers' standpoint on following a flexibility program or not, which translates into an increase or decrease of their scheduled load. Spin-to-spin interactions simulate how these customer attitudes can change when information is retrieved from neighbouring customers. An external field is a proxy of top-down directives to enforce flexibility criteria and we associate the temperature in the spin system with uncertainty about the flexibility program. Further, we have addressed quantitative information about the two-way relationships between power

exchanges and spin dynamics. These are formalised in terms of constraints, which force the spin system to evolve in different ways. To this end we provide a modified version of the Metropolis-Hastings algorithm including a gradient descent through the constraint surface. This implementation allowed us to analyse the system on a large scale (considering the cumulated benefit of all the actors involved) and also from the perspective of total aggregation.

At the global scale—welfare—we made two reasonable assumptions to limit customers' flexibility (shiftable-loads and self-sustainability). Each leads to two different scenarios which in turn motivate different types of analyses in our spin system. In the shiftable-loads scenario the maximum welfare requires each bus-community to meet a given value of flexibility every time. However, in general this is not possible in a discrete system. We provide conditions for this and also measure how an external field can force customers' flexibility.

Maximum welfare in the self-sustainability scenario requires all customers to meet the flexibility criteria every hour. We monitor the robustness of a feasible solution by perturbing the spin matrix and then measuring the feasibility of the perturbed magnetisation. When spins evolve by decreasing the constraint, there is an improvement of 3 orders of magnitude in the solutions with respect to the classical Metropolis evolution. An external action in the community would not be useful for recovering flexibility unless additional mechanisms are implemented to penalise deviations from the feasible region.

On the aggregation scale we analyse two limits: homogeneous and fixed electricity tariff of aggregators. These are interesting cases since flexibility constraints set the total aggregation optimisation function to zero: shiftable-loads in the fixed tariff case and self-sustainability in the case of homogeneous prices. Here we also address quantitative results of how aggregators can effectively split the total demand in the system and which are the implications of aggregator subcommunities in the spreading of flexible behaviour. We find that, in a maximum flexibility scenario, the total aggregation profit increases with the number of aggregators. In general, depending on the bus scheduled loads and the number of aggregators, demand cannot be split 100% evenly among aggregators; there must be some slack mechanisms to allow flexibility in this mapping. Finally, we check the effect of aggregator boundaries on spin dynamics following our interpretation of temperature as uncertainty (lack of information); as T grows shared opinions as to whether demand should be increased will not be strong enough to keep customers' confidence level in the flexibility program. Consequently, they will randomly decide whether demand should be increased or decreased and the constraint for maximum flexibility will start to deteriorate. However, when the information flow among customers is bounded within regions in the configuration space, it is smoothed, since the information does not propagate to the entire system in the same way.

In a future work we will make a more in-depth analysis of the relationships between more general spin system topologies and the flexibility constraints. Also we will develop a more thorough study of the phase transitions in presence of aggregator boundaries and their implications.

Nomenclature

N: Number of customers
C: Set of customers
B: Set of bus-loads
B_j: Customers connected to bus j
A: Set of aggregators
A_k: Buses managed by aggregator k
n_J: Number of buses
n_A: Number of aggregators
n_T: Number of hours
n_j: Number of customers connected at bus j
Δ_{ij}: = 1(0) if customer i is connected (not connected) to bus j
Δ_{jk}: = 1(0) if bus j is managed (not managed) by aggregator k
H: Ising Hamiltonian
γ_i: Flexibility for customer i
s_i: State of spin i
E: Energy of the spin system
T: Temperature of the spin system
T_c: Critical temperature
J: Spin-to-spin interaction strength
b: Magnetic external field
M: Magnetisation of the spin system
Γ: One configuration in the spin system
Ω: Set of possible spin configurations
l_{it}: Load of customer i at time t
l_{it}^c: Expected load of customer i at time t
l_{it}^f: Flexible proportion of load of customer i at time t
L_{jt}^c: Expected load in bus j at time t
L_{jt}^f: Flexible proportion of load in bus j at time t
P_t^s: Power at the source bus at time t
$L_j^{\max}$: Normalised expected load at bus j
P_{jt}^{L2A}: Power exchange for buy/sell between bus j and aggregator t
P_t^{RT}: Real-time power exchange between DSO and RTM at time t
P_{kt}^{A2DSO}: Power exchange or buy/sell between aggregator k and aggregator DSO
P_{jt}^{DSO2L}: Power bought to DSO by demand at bus j (customers connected to bus j)
ψ_{jt}: Normalised power bought to DSO by demand at bus j at time t
η_{jt}: Normalised power exchange for buy/sell between bus j and aggregator at time t
θ_{jt}: Fraction of power exchange between DSO and RTM reaching bus j in time t
$\lambda_{kt}^{\mathrm{L2A}}$: Price for buy/sell between demand at bus and aggregator k at time t
$\lambda_{kt}^{\mathrm{RT}}$: Real-time market price for DSO and RTM power exchanges
λ^{DSO2L}: Price for DSO and load power exchanges
$\lambda_{kt}^{\mathrm{A2DSO}}$: Real-time market price for DSO and aggregator k power exchanges

δ_{kt}: Profit guarantee factor of aggregator k at time t
f: Additional constraint imposed to the Metropolis-Hastings algorithm
OF_j: Optimisation function for bus-load j
OF_L: Optimisation function for all buses
OF_k: Optimisation function for aggregator k
OF_A: Optimisation function for all aggregators
OF_W: Optimisation function in the social welfare scenario
q: Slack threshold to relax constraints in (38).

Conflicts of Interest

The authors declare that they have no conflicts of interest.

Acknowledgments

This research was partially supported by the Regional Ministry of Education from Castilla y León (Spain) and the European Social Fund under the *MOVIURBAN* project with Ref. SA070U16. The authors also acknowledge the European Commission H2020 MSCA-RISE-2014: Marie Sklodowska-Curie project *DREAM-GO; Enabling Demand Response for Short and Real-Time Efficient and Market Based Smart Operation; An Intelligent and Real-Time Simulation Approach* with Ref. 641794. Amin Shokri Gazafroudi also acknowledges the support by the Ministry of Education of Junta de Castilla y León and the European Social Fund through a grant from predoctoral recruitment or research personnel associated with the research project "Arquitectura Multiagente para la Gestión Eficaz de Redes de Energía a Través del Uso de Técnicas de Inteligencia Artificial" of the University of Salamanca.

References

[1] N. Mithulananthan, Q. Duong Hung, and Y. Kwang, *Intelligent Network Integration of Distributed Renewable Generation*, Springer International Publishing, 2017.

[2] A. S. Gazafroudi, F. Prieto-Castrillo, T. Pinto, and J. M. Corchado, "Organization-based multi-agent system of local electricity market: Bottom-up approach," *Advances in Intelligent Systems and Computing*, vol. 619, pp. 281–283, 2017.

[3] M. A. Fotouhi Ghazvini, J. Soares, O. Abrishambaf, R. Castro, and Z. Vale, "Demand response implementation in smart households," *Energy and Buildings*, vol. 143, pp. 129–148, 2017.

[4] S. S. Torbaghan, N. Blaauwbroek, P. Nguyen, and M. Gibescu, "Local market framework for exploiting flexibility from the end users," in *Proceedings of the 13th International Conference on the European Energy Market, EEM 2016*, pp. 1–6, Portugal, June 2016.

[5] A. Gazafroudi, F. Prieto-Castrillo, T. Pinto, J. Prieto, J. Corchado, and J. Bajo, "Energy flexibility management based on predictive dispatch model of domestic energy management system," *Energies*, vol. 10, no. 9, p. 1397, 2017.

[6] G. Ajmone Marsan, N. Bellomo, and A. Tosin, *Complex Systems and Society Modeling and Simulation*, Springer International Publishing, New York, NY, USA, 2013.

[7] A. Carro, R. Toral, and M. S. Miguel, "Markets, herding and response to external information," *PLoS ONE*, vol. 10, no. 7, Article ID e0133287, 2015.

[8] S. G. Brush, "History of the Lenz-Ising model," *Reviews of Modern Physics*, vol. 39, no. 4, pp. 883–893, 1967.

[9] R. V. Sole, *Phase Transitions*, Springer International Publishing, 2011.

[10] R. Schlicht and Y. Iwasa, "Forest gap dynamics and the Ising model," *Journal of Theoretical Biology*, vol. 230, no. 1, pp. 65–75, 2004.

[11] D. Nettle, "Is the rate of linguistic change constant?" *Lingua*, vol. 108, no. 2-3, pp. 119–136, 1999.

[12] A. M. Guenault, *Statistical Physics*, Springer International Publishing, Dordrecht, Netherlands, 2007.

[13] T. C. Schelling, "Dynamic models of segregation," *Journal of Mathematical Sociology*, vol. 1, pp. 143–186, 1971.

[14] D. Stauffer, "Social applications of two-dimensional Ising models," *American Journal of Physics*, vol. 76, no. 4-5, pp. 470–472, 2008.

[15] J. Mimkes, "Binary alloys as a model for the multicultural society," *Journal of Thermal Analysis and Calorimetry*, vol. 43, no. 2, pp. 521–537, 1995.

[16] S. Bornholdt, "Expectation bubbles in a spin model of markets: Intermittency from frustration across scales," *International Journal of Modern Physics C*, vol. 12, no. 5, pp. 667–674, 2001.

[17] P. Sieczka and J. A. Holyst, "A threshold model of financial markets," *Acta Physica Polonica A*, vol. 114, no. 3, pp. 525–530, 2008.

[18] E. Bompard and Y. Ma, "Modeling bilateral electricity markets: A complex network approach," *IEEE Transactions on Power Systems*, vol. 23, no. 4, pp. 1590–1600, 2008.

[19] W. Lee, L. Xiang, R. Schober, and V. W. S. Wong, "Direct electricity trading in smart grid: A coalitional game analysis," *IEEE Journal on Selected Areas in Communications*, vol. 32, no. 7, pp. 1398–1411, 2014.

[20] S. M. Sajjadi, P. Mandal, T.-L. Tseng, and M. Velez-Reyes, "Transactive energy market in distribution systems: A case study of energy trading between transactive nodes," in *Proceedings of the 48th North American Power Symposium, NAPS 2016*, pp. 1–6, Springer International Publishing, USA, September 2016.

[21] A. Jokic, P. P. J. Van Den Bosch, and R. M. Hermans, "Distributed, price-based control approach to market-based operation of future power systems," in *Proceedings of the 2009 6th International Conference on the European Energy Market, EEM 2009*, pp. 1–6, Leuven, Belgium, May 2009.

[22] C. Zhang, Q. Wang, J. Wang, P. Pinson, J. M. Morales, and J. Ostergaard, "Real-time procurement strategies of a proactive distribution company with aggregator-based demand response," *IEEE Transactions on Smart Grid*, vol. 3053, no. c, p. 1, 2016.

[23] T. Ishii and K. Yasuda, "Hierarchical decentralized autonomous control in super-distributed energy systems," *IEEJ Transactions on Electrical and Electronic Engineering*, vol. 2, no. 1, pp. 63–71, 2007.

[24] B. Canizes, T. Pinto, J. Soares, Z. Vale, P. Chamoso, and D. Santos, "Smart city: A GECAD-BISITE energy management case study," *Advances in Intelligent Systems and Computing*, vol. 619, pp. 92–100, 2017.

[25] L. David and B. Kurt, *A Guide to Monte Carlo Simulations in Statistical Physics*, Springer International Publishing, New York, NY, USA, 2005.

[26] V. E. Brkzin, "The Onset of Phase Transitions in Finite Systems," *Physikertagung Heidelberg*, vol. 42, no. 7, pp. 6–8, 1986.

[27] S. Bornholdt and F. Wagner, "Stability of money: Phase transitions in an Ising economy," *Physica A: Statistical Mechanics and its Applications*, vol. 316, no. 1-4, pp. 453–468, 2002.

[28] D. O. Cajueiro, "Enforcing social behavior in an Ising model with complex neighborhoods," *Physica A: Statistical Mechanics and its Applications*, vol. 390, no. 9, pp. 1695–1703, 2011.

Hindawi
Complexity
Volume 2018, Article ID 3683969, 21 pages
https://doi.org/10.1155/2018/3683969

Research Article

Simulation Study on Clustering Approaches for Short-Term Electricity Forecasting

Krzysztof Gajowniczek and Tomasz Ząbkowski

Department of Informatics, Warsaw University of Life Sciences (SGGW), Warsaw, Poland

Correspondence should be addressed to Krzysztof Gajowniczek; krzysztof_gajowniczek@sggw.pl

Received 22 December 2017; Revised 21 February 2018; Accepted 11 March 2018; Published 26 April 2018

Academic Editor: Tiago Pinto

Advanced metering infrastructures such as smart metering have begun to attract increasing attention; a considerable body of research is currently focusing on load profiling and forecasting at different scales on the grid. Electricity time series clustering is an effective tool for identifying useful information in various practical applications, including the forecasting of electricity usage, which is important for providing more data to smart meters. This paper presents a comprehensive study of clustering methods for residential electricity demand profiles and further applications focused on the creation of more accurate electricity forecasts for residential customers. The contributions of this paper are threefold: (1) using data from 46 homes in Austin, Texas, the similarity measures from different time series are analyzed; (2) the optimal number of clusters for representing residential electricity use profiles is determined; and (3) an extensive load forecasting study using different segmentation-enhanced forecasting algorithms is undertaken. Finally, from the operator's perspective, the implications of the results are discussed in terms of the use of clustering methods for grouping electrical load patterns.

1. Introduction

Throughout the EU, there is considerable interest in smart electricity networks, where increased control over electricity supply and consumption is achieved by investments and improvements in new technologies such as advanced metering infrastructure. Smart metering is part of this movement and is perceived as a necessary step in achieving the EU's energy policy goals by the year 2020 (i.e., cut greenhouse gas emissions by 20%, improve energy efficiency by 20%, and ensure that 20% of the EU's energy demand is supplied by renewable sources) [1].

Clustering analysis is an unsupervised learning technique that has been widely used to identify different energy consumption patterns, particularly among commercial customers, individual industries, or large aggregations of residential customers [2]. Recently, the fast-growing stream of meter data has motivated further research on the application of clustering techniques to individual residential customers [3]. By clustering time series of hourly load data, each customer can be represented by a number of load patterns, thus allowing variability information to be derived. Clustering can therefore serve as a valuable preprocessing step, providing fine-grained information on customer attributes and sources of variation for subsequent modeling and customer segmentation.

Many dissimilarity measures between time series have been proposed in the literature. They can be grouped into four categories [4, 5]:

(i) Shape: Minkowski distance, short time series distance, and dynamic time warping distance.

(ii) Editing: edit distance for real sequences and longest common subsequence distance.

(iii) Features: autocorrelation-based distances, short time series distance, Fourier coefficients-based distance, TQuest distance, and periodogram-based distances.

(iv) Structure: Maharaja distance and Piccolo distance.

This study examines the first three categories, as they can be used in the majority of cases. The fourth category requires

some a priori assumptions that affect the obtained results. For instance, they assume that the observed time series is the result of a certain parametric base model, mainly the autoregressive integrated moving-average (ARIMA) model. This implies the need to prioritize the relevant parameters of the model in advance.

Dissimilarity between time series can be also computed using information theory. For instance, Kullback–Leibler (KL) divergence is a measure of how one time series probability distribution diverges from a second (expected) probability distribution [6]. This measure is distribution-wise and asymmetric and thus does not qualify as a statistical metric of spread. In the simple case, a KL divergence of 0 indicates that we can expect similar, if not the same, behavior of two time series distributions, while a KL divergence of 1 indicates that the two time series distributions behave in such a different manner that the expectation given the first distribution approaches zero. The second example is mutual information (MI) of two time series which is a measure of the mutual dependence between two investigated time series [7]. Intuitively, mutual information measures the information that two time series share: it gives the idea of how one of these time series reduces uncertainty about the other. For example, if two time series are independent, then knowing the first time series does not give any information about the second time series and vice versa, so their mutual information is zero. At the other extreme, if the first time series is a deterministic function of the second one, then the mutual information is maximal.

As their input, most clustering algorithms take parameters such as the number of clusters, density of clusters, or, at least, the number of points in a cluster. Nonhierarchical procedures usually require the user to specify the number of clusters before any clustering is accomplished, whereas hierarchical methods routinely produce a series of solutions ranging from q clusters to only a single cluster [8]. As such, the problems of determining a suitable number of clusters for a dataset and evaluating the clustering results have been considered by several researchers. The procedure of evaluating the results of a clustering algorithm is known as cluster validity analysis [9].

In general, there are three approaches for investigating the cluster validity. The first, based on external criteria, compares the cluster analysis results to some known results, such as externally provided class labels. The second approach, based on internal criteria, uses information obtained from within the clustering process to evaluate how well the results fit the data without reference to external information. The third approach is based on relative criteria and consists of evaluating a clustering structure by comparing it with other structures given by the same algorithm using different parameter values (e.g., the number of clusters). In this paper, we consider this third class of measures [10].

Based on the selected time series similarity measures and hierarchical clustering algorithms, this study developed forecasting models for the aggregate electricity demand of individual groups of households. The predictions given by these models were compared with the results of a base model built for all households (aggregate over 46 consumers for *WikiEnergy* data [11]). In particular, using smart metering data, we aim to answer the following research questions:

(1) To what extent is it possible to provide accurate 24-hour load forecasting for the group of households?

(2) Which of the proposed time series similarity measures and the measures determining the relevant number of clusters gives the greatest increase in forecast accuracy?

(3) What kind of forecasting methods and algorithms is appropriate to address highly volatile data?

The remainder of this paper is organized as follows. In Section 2, various time series similarity measures, grouped into three categories, are introduced. As different clustering algorithms usually lead to different numbers of clusters, Section 3 discusses several measures for determining the relevant number of clusters. In Section 4, based on *WikiEnergy* data gathered from 46 households, various numerical experiments regarding the clustering of these households are presented. Section 5 describes the methods used in our forecasting experiments, and Section 6 presents the results from a number of numerical experiments that provide 24-hour forecasts at different data aggregation levels. Finally, Section 7 concludes the paper.

2. Time Series Similarity Measures

The following subsections briefly describe three categories of time series similarity measures. In the remainder of this section, unless otherwise specified, $z_g = (z_1, z_2, \ldots, z_n)^T$ and $y_g = (y_1, y_2, \ldots, y_n)^T$ denote partial realizations from two real-valued processes $\{Z_g,\ g \in \mathbb{N}\}$ and $\{Y_g,\ g \in \mathbb{N}\}$, respectively. Note that serial realizations of the same length n are initially assumed, although this limitation can be omitted in some cases.

2.1. Measures Based on the Shape of Time Series. A simple approach for measuring the similarity between z_g and y_g is to consider conventional metrics based on the closeness of their values at specific points in time. Some commonly used raw-values-based dissimilarity measures are introduced below.

2.1.1. Minkowski Distance. The Minkowski distance of order p, where p is a positive integer, is also known as the L_p-norm distance [12]. This measure is typically used with $p = 2$, giving the Euclidean distance, and is very sensitive to signal transformations such as shifting or time scaling (stretching or shrinking of the time axis). The proximity notion relies on the closeness of the values observed at corresponding points in time, so that the observations are treated as if they were independent. In particular, L_p is invariant to permutations over time [4, 5].

2.1.2. Short Time Series Distance. The short time series (STS) distance was introduced by Möller-Levet et al. [13] as a metric that adapts to the characteristics of irregularly sampled series [4, 5].

2.1.3. Dynamic Time Warping Distance. The goal of dynamic time warping (DTW) is to find patterns in time series [14]. The DTW distance determines a mapping between the series which minimizes a specific distance measure between the coupled observations. This allows similar shapes to be recognized, even in the presence of signal transformations such as shifting and/or scaling, and ignores the temporal structure of the values because the proximity is based on the differences, regardless of the behavior around these values [4, 5].

2.2. Measures Based on Editing the Time Series. The edit distance, which was initially developed to calculate the similarity between two sequences of strings, is based on the idea of counting the minimum number of edit operations (delete, insert, and replace) that are necessary to transform one sequence into the other. The problem of working with real numbers is that it is difficult to find exact matching points in two different sequences and, therefore, the edit distance is not directly applicable.

2.2.1. Edit Distance for Real Sequences. The distance between points in the time series is reduced to 0 or 1 [15]. If two points z_g and y_g are closer to each other in the absolute sense than some user-specified threshold ε, they are considered to be equal. On the contrary, if they are further apart, they are considered to be distinct and the distance between them is set to 1. As an additional property, the edit distance for real sequences (EDR) permits gaps or unmatched regions in the time series but penalizes them with a value equal to their length values [4, 5].

2.2.2. Longest Common Subsequence Distance. In this metric, the similarity between two time series is quantified in terms of the longest common subsequence (LCSS), with gaps or unmatched regions permitted [16]. As with EDR, the initial mapping between the series uses the Euclidean distance between two points, which is reduced to 0 or 1 depending on some threshold ε values [4, 5].

2.3. Measures Based on the Time Series Features. Instead of using the raw data values in the series, this category of distance measures aims to extract a set of features from the time series and calculate the similarity between these features.

2.3.1. Distance Based on the Cross-Correlation. This distance is based on the cross-correlation between two time series. The maximum lag considered in the calculation should not exceed the length of the series values [4, 5].

2.3.2. Autocorrelation-Based Distances. Several researchers have considered measures based on the estimated autocorrelation functions [17]. These rely on the autocorrelation between two time series with a maximum lag of L values [4, 5].

2.3.3. Periodogram-Based Distances. Most of the measures discussed so far operate in the same domain, that is, the time domain. However, the signal representation in the frequency domain provides a good alternative for measuring the similarity between time series. The key idea is to assess the similarity between the corresponding spectral representations of the time series values [4, 5, 18].

2.3.4. Fourier Coefficients-Based Distances. This measure is based on comparing the discrete Fourier transform coefficients of the series [19]. The value of each coefficient measures the contribution of its associated frequency to the series. Based on this, the inverse Fourier transform provides a means of representing the sequences as a combination of sinusoidal forms. Note that the Fourier coefficients are complex numbers that can be expressed as $z_{g_f} = a_f + b_f i$. In the case of real sequences such as time series, the discrete Fourier transform is symmetric, and therefore it is sufficient to study the first $n/2 + 1$ coefficients. Furthermore, it is commonly considered that most of the information is found within the first n Fourier coefficients, where $t < n/2+1$. Based on this information, the distance between two time series is given by the Euclidean distance between the first t coefficients [4, 5].

2.3.5. TQuest Distance. The fundamental idea of the TQuest distance [20] is to define a set of intervals in a time series in which the stochastic processes exceed a predetermined threshold τ. The final distance between two time series is defined in terms of the similarity between sets of intervals based on this threshold value. Intuitively, two time intervals are said to be similar if they have similar start and end points. TQuest is independent of the size of the individual time series; this is important because time series exhibiting similar properties can be converted into intervals of different lengths. Another advantage is that this measure only takes into account the local similarity, with the remaining (continued) intervals not affecting the final result [4, 5].

3. Measures for Determining the Relevant Number of Clusters

Different clustering algorithms usually lead to different clusters of data; even for the same algorithm, the selection of different parameters or the order in which data objects are presented can greatly affect the final clustering partitions. Thus, effective evaluation standards and criteria are critically important to ensure confidence in the clustering results. At the same time, these assessments provide meaningful insights into how many clusters are hidden in the data. In most real-life clustering situations, users face the dilemma of selecting the number of clusters or partitions in the underlying data. As such, numerous indices for determining the number of clusters in a dataset have been proposed.

3.1. CH Index. The value of q that maximizes CH(q) specifies the number of clusters [21].

3.2. C Index. The minimum value of C [21] is considered to be the relevant number of clusters in a given dataset.

3.3. Duda Index. Reference [21] proposed the ratio Je(2)/Je(1) as a criterion, where Je(2) is the sum of squared errors within clusters when the data are partitioned into two clusters and Je(1) is the squared error when only one cluster is present. The optimal number of clusters is that which gives the smallest value of this ratio.

3.4. Ptbiserial Index. This index [21] is simply a point-biserial correlation between the raw input dissimilarity matrix and a corresponding matrix consisting of 0s or 1s. A value of 0 is assigned if the two corresponding points are clustered together by the algorithm; a value of 1 is assigned otherwise. Given that larger positive values reflect a better fit between the data and the obtained partition, the maximum value of the index is used to select the optimal number of clusters in the dataset.

3.5. DB Index. This index [21] is a function of the ratio of within-cluster scatter to between-cluster separation. The q value that minimizes the index is considered to be the optimal number of clusters in a given dataset.

3.6. Frey Index. The Frey index [21] can only be applied to hierarchical methods; it is the ratio of difference scores from two successive levels in the hierarchy. The numerator is the difference between the mean between-cluster distances from the two hierarchy levels (level j and level $j + 1$), whereas the denominator is the difference between the mean within-cluster distances of levels j and $j+1$.

3.7. Hartigan Index. The maximum difference between hierarchy levels is taken to indicate the correct number of clusters in the data [21].

3.8. Ratkowsky Index. Charrad et al. [21] proposed a criterion for determining the optimal number of clusters based on $\overline{S}/q^{0.5}$. The value of $\overline{S}$ is the average of the ratios of $(\mathrm{BGSS}_j/\mathrm{TSS}_j)$, where BGSS is the sum of squares between the clusters (groups) for each variable and TSS is the total sum of squares for each variable. The optimal number of clusters is the value of q that maximizes $\overline{S}/q^{0.5}$.

3.9. Ball Index. Ball and Hall [21] proposed an index based on the average distance between data items and their respective cluster centroids. The largest difference between levels is used to indicate the optimal solution.

3.10. McClain Index. The McClain and Rao index [21] is the ratio of the average within-cluster distance divided by the number of within-cluster distances to the average between-cluster distance divided by the number of cluster distances. The minimum value of this index indicates the optimal number of clusters.

3.11. KL Index. The value of q that maximizes KL(q) [21] specifies the optimal number of clusters.

3.12. Silhouette Index. The maximum value of this index is used to determine the optimal number of clusters in the data [21].

3.13. Dunn Index. The Dunn index [21] is the ratio between the minimal intercluster distance and the maximal intracluster distance. If the dataset contains compact and well-separated clusters, the diameter of the clusters is expected to be small and the distance between the clusters is expected to be large. Thus, the Dunn index should be maximized.

3.14. SD Index. The SD validity index is based on the concepts of average scattering for clusters and total separation between clusters [21]. The number of clusters q that minimizes this index gives the optimal value for the number of clusters in the dataset.

4. Splitting Households into Clusters

4.1. Data Characteristics. Numerical analyses were performed using data from 46 households taken from *WikiEnergy*. The *WikiEnergy* dataset, constructed by Pecan Street Inc., is a large database of consumer energy information. This database is highly granular, including usage measurements collected from up to 24 circuits within the home. The households considered in the analysis are located in Austin, Texas, USA. We extracted 14 months of data (March 2013–April 2014) from 46 households in nearby neighborhoods at a granularity level of 1 hour. Thus, it was possible to aggregate the hourly demand values and divide the consumers into homogeneous groups [1]. From the aggregated data (Figure 1), we could see that the highest electricity consumption takes place in summer, between June and August, most likely due to air conditioning.

To analyze the volatility of the load, we prepared the box and whisker plots, for each of the 24 hours over the whole year, for two customers: one with quite stable load profile and the second with highly volatile characteristics (see Figures 2 and 3 for details). The whiskers show the minimum and maximum value in a given hour and the box encloses 50% of the total data (top edge represents the 75th quartile and bottom edge the 25th quartile, and the line in the middle is the median). For instance, the household, as shown in Figure 2, on average consumes 1.5 kWh in each hour while the volatility is rather low. The other household, as shown in Figure 3, can be characterized as the one using, on average, only 0.2 kWh in each hour; however, the volatility of the load is very high, regardless of the hour.

It should be noted that the source dataset was of relatively high quality. The time series in the dataset had no missing values. In some time series, few outliers were observed; however, they were left in the dataset. Please refer to Table 1 for the descriptive statistics of the electric load observed at each of the households. In the preprocessing step, only normalization of the data was applied. Additionally, only few features describing particular households were available (i.e., structural and building specific data). Those were building type (apartment, single-family home, and town home),

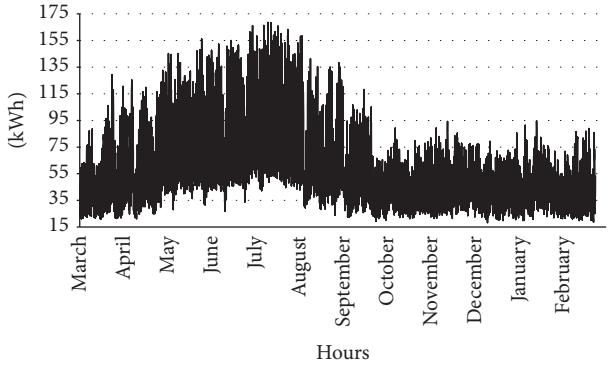

Figure 1: Hourly load data for 46 customers from 1 March 2013 to 28 February 2014.

construction year, total square footage, and incentive program due to the installed photovoltaic systems [22].

The dataset was split into training, validation, and testing samples. The training sample consisted of data from 365 days (8760 observations) between April 5, 2013, and February 28, 2014; the validation sample consisted of 28 days (672 observations) between March 1, 2014, and March 28, 2014; and the testing sample consisted of 14 days (336 observations) between March 29, 2014, and April 11, 2014 [1].

4.2. Determining the Similarity between Time Series. The starting point for the process of partitioning households was the selection of training samples for the period considered in determining the similarity between the electricity consumption time series.

In the second step, using the *R-CRAN* software, matrixes of similarity measures were calculated between all 46 time series. All measures were implemented in the following libraries:

(i) *TSdist* [5]: the *tsDatabaseDistances* function was used with arguments implementing the following similarity measures:

(a) *ccor*: distance based on the cross-correlation.
(b) *edr*: EDR with a threshold value of $\varepsilon = 0.2$.
(c) *dtw*: DTW distance.
(d) *euclidean*: L_p distance.
(e) *fourier*: Fourier coefficients-based distance.
(f) *lcss*: LCSS distance with a threshold value of $\varepsilon = 0.2$.
(g) *sts*: STS distance.
(h) *tquest*: TQuest distance with a threshold value of $\tau = 1$.

(ii) *TSclust* [4]: the *diss* function was used with arguments implementing the following similarity measures:

(a) *ACF*: autocorrelation-based distances with a maximum delay of $L = 50$ and geometrically decaying weights with $p = 0.05$.

Table 1: Descriptive statistics for the electric load observed at each of the households.

Household number	Missing	Min	Max	Mean	CV
1	0	0.05	7.36	0.65	1.24
2	0	0.19	7.41	1.29	0.86
3	0	0.01	13.88	3.67	0.65
4	0	0.00	7.89	1.62	0.65
5	0	0.39	12.62	2.42	0.72
6	0	0.20	11.40	2.07	0.86
7	0	0.19	11.10	1.42	1.14
8	0	0.02	5.36	0.48	1.38
9	0	0.27	5.85	1.34	0.63
10	0	0.00	9.20	1.06	1.27
11	0	0.36	10.55	1.77	0.78
12	0	0.13	9.16	1.06	1.15
13	0	0.08	6.27	0.56	1.08
14	0	0.16	8.13	1.03	0.99
15	0	0.24	10.10	1.41	0.73
16	0	0.00	9.53	1.25	1.15
17	0	0.19	5.44	0.94	1,04
18	0	0.27	7,80	1,33	0,82
19	0	0.00	10.04	1.59	0.98
20	0	0.31	7.33	1.35	0.77
21	0	0.65	11.21	2.69	0.62
22	0	0.11	4.05	0.50	0.65
23	0	0.66	6.72	1.50	0.53
24	0	0.29	8.06	1.09	0.92
25	0	0.08	4.71	0.35	1.32
26	0	0.15	7.02	1.11	0.97
27	0	0.08	5.70	0.51	0.98
28	0	0.00	7.96	1.38	0.83
29	0	0.18	10.55	1.27	1.09
30	0	0.00	14.46	3.01	0.77
31	0	0.08	7.88	0.76	1.17
32	0	0.25	7.23	1.06	0.85
33	0	0.15	7.15	1.12	1.11
34	0	0.26	10.67	1.27	1.01
35	0	0.20	8.14	1.64	0.85
36	0	0.06	5.10	0.48	0.90
37	0	0.21	10.15	1.33	0.92
38	0	0.00	3.81	0.56	0.67
39	0	0.00	11.45	1.40	1.16
40	0	0,00	8,49	1,03	1,08
41	0	0,15	6,58	0,92	0,92
42	0	0.10	3.90	0.43	0.89
43	0	0.00	6.97	1.06	0.94
44	0	0.06	4.31	0.31	1.17
45	0	0.41	13.77	2.45	0.84
46	0	0.10	5.68	0.75	0.91

(b) *INT.PER*: periodogram-based distances in non-standardized version.

The households were divided into clusters using the Ward method, contained in the *hclust* function. Each of the 10

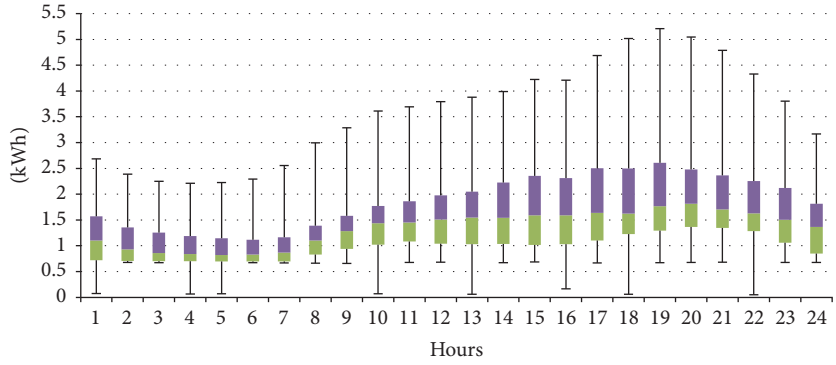

Figure 2: Customer with the least volatile consumption (in kWh) in the analyzed period (1 March 2013 to 28 February 2014).

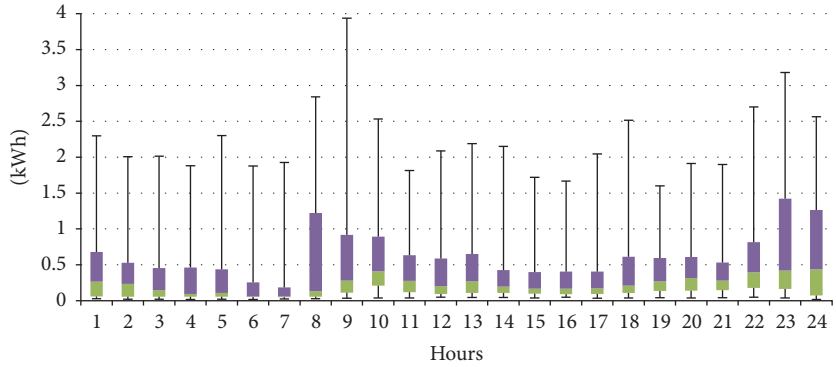

Figure 3: Customer with the most volatile consumption (in kWh) in the analyzed period (1 March 2013 to 28 February 2014).

resulting dendrograms was then divided into the following groups by the *cutree* function:

(i) Partition 1 containing 2 clusters.
(ii) Partition 2 containing 3 clusters.
(iii) Partition 3 containing 4 clusters.
(iv) Partition 4 containing 5 clusters.
(v) Partition 5 containing 6 clusters.
(vi) Partition 6 containing 7 clusters.
(vii) Partition 7 containing 8 clusters.
(viii) Partition 8 containing 9 clusters.

The size of each cluster according to the type of partition and the similarity of hourly time series is listed in Table 2. For the same type of division, the number of households included in the individual clusters varies depending on the similarity measure. The quality of the proposed similarity measures when splitting the data into two clusters is shown in Figure 4.

The most unbalanced group sizes are given by the distance based on cross-correlation (one very large cluster, the others very small), STS distance (two large clusters, the others very small), and TQuest distance (one very large cluster). The most balanced group sizes are given by autocorrelation-based distances (the smallest cluster contains three households), EDR (only in the seventh division do groups with fewer than three households appear), and periodogram-based distances (only in the last split do groups with fewer than three households appear). Other similarity measures generate clusters with a similar number of customers, but small clusters are present at some levels of division.

To determine the similarity between the results of time series clustering (Table 3), Baker's correlation coefficient [23] (function *cor_bakers_gamma*) was implemented in the *dendextend* library. This coefficient measures the similarity between two dendrograms, that is, the results of a hierarchical clustering, by calculating the highest possible value of q (number of groups when cutting a tree) for which two time series still belong to the same subtree. It is known that there are exactly $\binom{46}{2} = 1035$ combinations of such pairs of time series, based on hierarchical clustering. The same operation is then performed on the basis of the second dendrogram. In the next step, these two sets of values (for each dendrogram) are paired according to the order of comparing elements. Eventually, the similarity of the clustering results is assessed on the basis of Spearman's correlation coefficient.

Based on the results presented in Tables 2 and 3, it can be observed that similar clustering results are related to the DTW distance *(dtw)*, L_p distance *(euclidean)*, Fourier coefficients-based distance *(fourier)*, and periodogram-based distances *(int.per)* (denoted by italic font in Table 3). Distances carrying the most dissimilar dendrograms are the autocorrelation-based distances and the longest common subsequence distance.

Table 2: Size of each cluster by the type of partition and time series similarity measure.

Partition number	Autocorrelation-based distances								
1	35	11							
2	26	11	9						
3	23	11	3	9					
4	7	16	11	3	9				
5	7	16	4	7	3	9			
6	7	11	4	5	7	3	9		
7	7	11	4	5	7	3	4	5	
8	3	4	11	4	5	7	3	4	5

Partition number	Fourier coefficients-based distance								
1	40	6							
2	30	6	10						
3	30	2	4	10					
4	30	1	4	10	1				
5	21	1	9	4	10	1			
6	21	1	8	4	10	1	1		
7	13	1	8	8	4	10	1	1	
8	13	1	8	8	3	1	10	1	1

Partition number	Distance based on cross-correlation								
1	40	6							
2	40	5	1						
3	40	1	4	1					
4	39	1	4	1	1				
5	39	1	2	1	2	1			
6	36	3	1	2	1	2	1		
7	35	3	1	2	1	2	1	1	
8	35	3	1	1	1	2	1	1	1

Partition number	Periodogram-based distances								
1	37	9							
2	26	9	11						
3	26	3	6	11					
4	10	3	16	6	11				
5	10	3	11	6	11	5			
6	5	3	11	6	5	11	5		
7	5	3	11	3	5	3	11	5	
8	5	2	11	3	5	3	1	11	5

Partition number	DTW distance								
1	40	6							
2	30	6	10						
3	24	6	6	10					
4	24	2	6	4	10				
5	24	1	6	4	10	1			
6	15	1	6	9	4	10	1		
7	15	1	6	9	1	3	10	1	
8	6	1	9	6	9	1	3	10	1

Partition number	LCSS distance								
1	40	6							
2	38	2	6						
3	9	29	2	6					
4	9	12	2	17	6				
5	4	12	2	17	6	5			
6	4	12	2	16	6	5	1		
7	4	7	2	5	16	6	5	1	
8	4	6	2	5	16	6	5	1	1

Partition number	EDR distance								
1	24	22							
2	24	7	15						
3	18	7	15	6					
4	14	7	15	6	4				
5	14	3	15	4	6	4			
6	12	3	15	4	2	6	4		
7	12	2	15	4	2	6	1	4	
8	12	2	7	4	8	2	6	1	4

Partition number	STS distance								
1	25	21							
2	24	21	1						
3	23	1	21	1					
4	22	1	21	1	1				
5	21	1	21	1	1	1			
6	19	1	21	2	1	1	1		
7	19	1	21	1	1	1	1	1	
8	18	1	21	1	1	1	1	1	1

Partition number	L_p distance								
1	40	6							
2	30	6	10						
3	30	2	4	10					
4	30	1	4	10	1				
5	18	1	12	4	10	1			
6	18	1	11	4	10	1	1		
7	18	1	10	1	4	10	1	1	
8	18	1	6	4	1	4	10	1	1

Partition number	TQuest distance								
1	42	4							
2	42	3	1						
3	41	3	1	1					
4	41	1	2	1	1				
5	39	1	2	1	2	1			
6	35	4	1	2	1	2	1		
7	35	3	1	2	1	2	1	1	
8	35	3	1	2	1	1	1	1	1

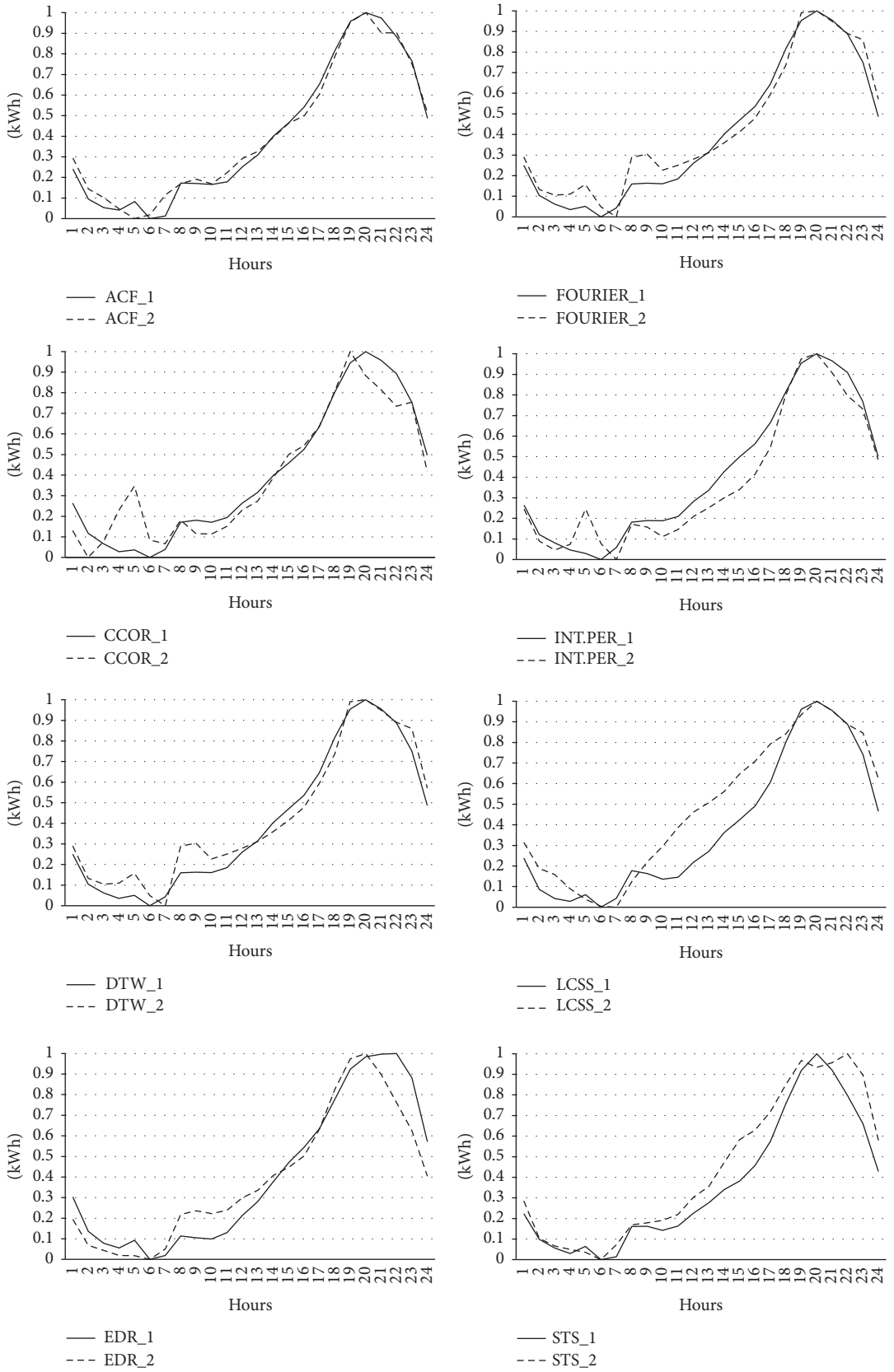

Figure 4: Continued.

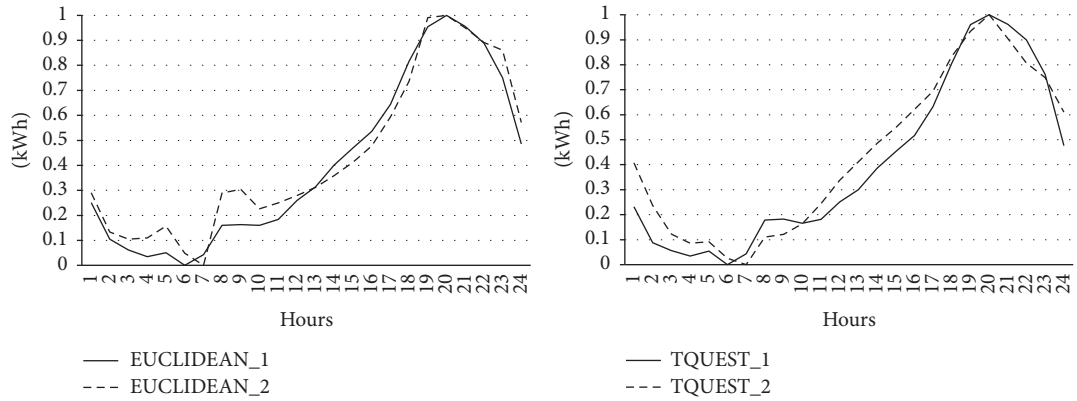

Figure 4: Normalized average hourly load profiles for partition 1 containing 2 clusters.

Table 3: Baker's correlation coefficient between clustering results on the basis of different measures of time series similarity.

	acf	ccor	dtw	edr	euclidean	fourier	int.per	lcss	sts	tquest
acf	*1.000*									
ccor	0.038	*1.000*								
dtw	0.150	0.099	*1.000*							
edr	0.066	0.044	0.315	*1.000*						
euclidean	0.132	0.121	*0.948*	0.292	*1.000*					
fourier	0.158	0.116	*0.951*	0.337	*0.965*	*1.000*				
int.per	0.050	0.110	*0.667*	0.232	*0.715*	*0.699*	*1.000*			
lcss	0.024	−0.053	0.001	−0.039	−0.003	0.003	−0.060	*1.000*		
sts	0.044	0	0.267	0.114	0.236	0.227	0.334	−0.043	*1.000*	
tquest	−0.021	0.350	0.148	0.084	0.174	0.139	0.135	−0.007	−0.024	*1.000*

4.3. Determining the Relevant Number of Clusters. Using the *NbClust* library [21], the relevant number of clusters for all 46 time series was determined. The input arguments of this package are the real-time values of the time series and a similarity array. The optimum number of clusters was determined on the basis of the eight different partitions defined earlier (Table 2). The input parameters for the *NbClust* function were as follows:

(i) *ch*: Calinski and Harabasz index.
(ii) *duda*: Duda index.
(iii) *cindex*: *C* index.
(iv) *ptbiserial*: Ptbiserial index.
(v) *db*: DB index.
(vi) *frey*: Frey index.
(vii) *hartigan*: Hartigan index.
(viii) *ratkowsky*: Ratkowsky index.
(ix) *ball*: Ball index.
(x) *mcclain*: McClain index.
(xi) *kl*: KL index.
(xii) *silhouette*: Silhouette index.
(xiii) *dunn*: Dunn index.
(xiv) *sdindex*: SD index.

The aggregated results for the relevant number of clusters for hourly electricity demand are presented in Table 4. Using a simple majority vote for the relevant number of clusters (partitions in italic font denote the greatest number of measures), it was observed that most measures of time series similarity would split the households into two groups. The LCSS distance gives a very different result, and the EDR and TQuest distances give two equally applicable cluster numbers.

Additionally, it can be realized that Ball's, Frey's, and McClain's measures tend to indicate relatively few clusters. For the remaining measures, some subgroups indicate a similar number of clusters for particular time series similarity measures [24]. For example, Silhouette's, Ptbiserial's, Davies and Bouldin's, Ratkowski's, Dunn's, and SD's measures indicate almost the maximum number of clusters for the LCSS and STS distances, whereas they indicate the minimum number of clusters for DTW, EDR, and the periodogram-based distances.

5. An Approach to Forecasting

5.1. Short-Term Load Forecasting. Recently, with advances in smart metering, there has been a lot of interest in residential power load forecasting and application of analytical techniques to load forecasting on the individual household level [1, 25–27]. However, such a level of granularity is challenging due to the extreme load volatility which is

Table 4: Voting results for the relevant number of clusters based on the partition type and the time series similarity measure.

Measure distance	Number of clusters							
	2	3	4	5	6	7	8	9
Autocorrelation-based distances	*5*	2	3	1	0	0	0	2
Distance based on cross-correlation	*4*	1	1	1	2	0	1	3
DTW distance	*7*	5	1	0	1	0	0	0
EDR distance	*6*	*6*	0	0	0	1	0	0
Lp distance	*8*	2	2	2	0	0	0	0
Periodogram-based distances	*7*	3	0	0	0	0	2	2
Fourier coefficients-based distance	*8*	3	1	2	0	0	0	0
LCSS distance	2	1	0	3	1	0	1	*5*
STS distance	*5*	1	0	1	1	0	1	4
TQuest distance	2	2	1	1	*3*	*3*	0	1

the result of many different dynamic processes observed at individual households, including behavioral and sociodemographic components. Aggregation of individual and to some extent stochastic components reduces the inherent variability of electricity usage resulting in smoother load shapes, and, as a result, the forecasting applied to the higher aggregation levels (power stations or regions) can be achieved with quite low errors.

Different methods have been proposed for forecasting the electric load demand in the last decades. Several modeling techniques are typically used for energy load forecasting. These techniques can be classified into nine categories [28]: (1) multiple regression, (2) exponential smoothing, (3) iterative reweighted least squares, (4) adaptive load forecasting, (5) stochastic time series, (6) ARMAX models based on genetic algorithms, (7) fuzzy logic, (8) artificial neural networks, and (9) expert systems. However, the list is not closed and new techniques are still being adopted and tested for the purpose of accurate electricity load forecasting, including support vector machines or random forests, just to name a few.

Based on literature review, one can conclude that time series analyses are not effective in highly volatile data [29], and therefore time series methods such as regression models, ARIMA models, GARCH, and hybrid models such as the combination of ARIMA and GARCH using wavelet transform are not considered for short-term forecasting when dealing with volatile data [25, 27]. Rather than these, the machine learning techniques like artificial neural networks, support vector machines, or random forests are recently applied in this area with positive outcome [30–33].

Therefore, for the forecasting experiments, we focused on application of machine learning techniques including artificial neural networks, support vector machines, random regression forests, regression trees, and k-NN regression, and as benchmark models, we have selected ARIMA models and some simple techniques like stepwise regression, naive forecast, and random forecasts.

5.2. Accuracy Measures. To assess the forecasting performance of the model, three measures were used: precision, resistant mean absolute percentage error (MAPE), and accuracy [34]. Precision is defined as how well the model is able to forecast the actual load. To measure the precision, the mean squared error (MSE) was used:

$$\mathrm{MSE} = \frac{1}{n}\sum_{i=1}^{n}\left(L_i - P_i\right)^2, \tag{1}$$

where L_i and P_i denote the observed and forecasted load in hour i, respectively [1].

The MAPE satisfies the criteria of reliability, ease of interpretation, and clarity of presentation. However, it does not meet the validity criterion, because the distribution of the absolute percentage errors is usually skewed to the right because of the presence of outliers. In these cases, MAPE can be overinfluenced by some very bad instances, which disrupt otherwise good forecasts [34]. Therefore, we propose the alternative measure of resistant MAPE (r-MAPE) based on the calculation of Huber's M-estimator, which helps to overcome the aforementioned limitation [35].

The M-estimator for the location parameter μ using the maximum likelihood (ML) estimator is defined as a solution θ to

$$\min_{\theta} \quad \sum_{i=1}^{n}\rho\left(\frac{\left|\left(L_i - P_i\right)/L_i\right| - \theta}{\sigma}\right) \times 100\%, \tag{2}$$

or

$$\sum_{i=1}^{n}\varphi\left(\frac{\left|\left(L_i - P_i\right)/L_i\right| - \theta}{\sigma}\right) \times 100\% = 0, \tag{3}$$

where $\varphi = \rho'$ and σ is the scale parameter. For a given positive constant k, Huber's estimator is defined by the following function φ in (3):

$$\varphi(k) = \begin{cases} k & x > k \\ x & -k \le x \le k \\ -k & x < k, \end{cases} \tag{4}$$

where k is a tuning constant that determines the degree of robustness; in this study, we set $k = 1.5$ [36]. The application

Table 5: Feature vector used in forecasting.

Attribute number	Description	Formula
1–24	Hour indicator (dummy variable)	$G_i, i = 1, \ldots, 24$
25–55	Day of the month indicator (dummy variable)	$D_i, i = 1, \ldots, 31$
56–62	Day of the week indicator (dummy variable)	$T_i, i = 1, \ldots, 7$
63–74	Month indicator (dummy variable)	$M_i, i = 1, \ldots, 12$
75	Holiday indicator (dummy variable)	S
76	Sunset indicator (dummy variable)	N
77–100	Load of the previous 24 hours	$Z_{g-i}, i = 1, \ldots, 24$
101–104	Minimum load of the previous 3, 6, 12, and 24 hours	$\min\{Z_{g-1}, \ldots, Z_{g-i}\}, i = 3, 6, 12, 24$
105–108	Maximum load of the previous 3, 6, 12, and 24 hours	$\max\{Z_{g-1}, \ldots, Z_{g-i}\}, i = 3, 6, 12, 24$
109–114	Load in the same hour of the previous week (6 days)	$Z_{g,d-i}, i = 2, \ldots, 7$
115–118	Load in the same hour of the same day in previous weeks (4 weeks)	$Z_{g,d-i}, i = 14, 21, 28, 35$
119–122	Average temperature observed over previous hourly periods	$\text{avg}\{T_{g-i}, \ldots, T_{g-i[+1]}\}, i = 1, 3, 6, 12, 24$
123–128	Average temperature observed in the same hour over the previous 6 days	$T_{g,d-i}, i = 2, \ldots, 7$
129–132	Average weekly temperature observed in the previous i-day periods	$\text{avg}\{T_{g,d-i}, \ldots, T_{g,d-i[+1]}\}, i = 7, 14, 21, 28, 35$
133–136	Average humidity observed over previous hourly periods	$\text{avg}\{W_{g-i}, \ldots, W_{g-i[+1]}\}, i = 1, 3, 6, 12, 24$
137–142	Average humidity observed in the same hour over the previous 6 days	$W_{g,d-i}, i = 2, \ldots, 7$
143–146	Average humidity observed in the previous i-day periods	$\text{avg}\{W_{g,d-i}, \ldots, W_{g,d-i[+1]}\}, i = 7, 14, 21, 28, 35$

Notation [+1] stands for the next element from the set of indices i $\{1, 3, 6, 12, 24\}$, for example, $\text{avg}\{T_{g,d-1}, \ldots, T_{g,d-3}\}$.

of this function is known as metric Winsorizing and brings extreme observations into the range $\mu \mp k$. In practice, σ is not known; thus, a MAD robust estimator is used:

$$\text{MAD} = \text{median}\left(\left|x_i - \text{median}\left(x_i\right)\right|\right). \tag{5}$$

Finally, an accuracy measure was used to identify how many "correct" forecasts the model makes. Correctness is defined by the user, for example, forecasts within a percentage range of the actual load. However, for low loads, a percentage range may become insignificant [1]. For a load of 0.1 kWh, a 15% range would be 0.085–0.115, and a forecast of 0.2 kWh will be considered wrong, whereas such a forecast would be acceptable in practice. To address this false loss of accuracy, we set a 15% range of error to define the general accuracy, but if the load is smaller than 1 kWh, then a range of ±0.15 kWh is considered acceptable [36]. Therefore, the accuracy for hour i is given by

$$\begin{aligned}\text{Accuracy} = &\sum 1\left\{L_i > 1,\ \left|L_i - P_i\right| < P_i * 0.15\right\} \\ &+ \sum 1\left\{L_i < 1,\ \left|L_i - P_i\right| < 0.15\right\}.\end{aligned} \tag{6}$$

5.3. Predictors. In this study, we focus on forecasting the 24-hour-ahead electricity usage. To forecast the load, we constructed a feature vector with the attributes presented in Table 5. These attributes were constructed based on time series of the hourly electricity demand. Additional variables such as temperature, humidity, and date were also collected.

Electricity demand varies depending on the time of day (daily cycles), day of the week (weekly cycles), day of the month (monthly cycles), season (seasonal cycles), and occurrence of holidays. Therefore, we enriched the analysis by considering 76 dummy variables describing the hour (1–24), day of the month (31 variables), day of the week (seven variables), month (12 variables), occurrence of holidays (one variable), and sunset in a particular hour (one variable) [1].

The main variables in the forecasting process are those derived directly from the time series, and they include the maximum, minimum, and actual demand at certain intervals. The features were created by decomposing the time series.

5.4. Implementation. Building predictive models involves huge volumes of data and complex algorithms. Therefore, an efficient computing environment with high-performance computers is necessary. In our case, all the numerical calculations were performed on computing clusters located at the Interdisciplinary Center for Mathematical and Computational Modelling at the University of Warsaw. The HYDRA engine with the Scientific Linux 6 operating system was used with the following nodes and parameters [1]:

(i) Istanbul: AMD Opteron™ 2435 2.6 GHz, 2 CPU × 6 cores, 32 GB RAM.

(ii) Westmere: Intel® Xeon® CPU X5660 2.8 GHz, 2 CPU × 6 cores, 24 GB RAM.

R-CRAN was used as the computing environment. This is an advanced statistical package and an interpreted programming language; it is licensed under the GNU GPL and based on the S language [36].

The starting point for the numerical experiments was the division of the *WikiEnergy* dataset into training (330 days, instead of 365 days, due to up to 35-day time window for attributes construction), validation (28 days), and testing (14 days) samples as described earlier.

The main criterion for training the models is the efficient generalization of knowledge with the least error. The most

commonly used measure to assess the quality of forecasts in the electric power system is MAPE. Therefore, to find the best parameters for all models and ensure their generalization, the following function was minimized:

$$f\left(\mathrm{MAPE}_U, \mathrm{MAPE}_V\right) = \frac{1}{2}\left|\mathrm{MAPE}_U - \mathrm{MAPE}_V\right| + \frac{1}{2}\mathrm{MAPE}_V, \tag{7}$$

where MAPE_U and MAPE_V denote the training and validation errors, respectively [36].

The experiments tested a broad set of machine learning algorithms, including artificial neural networks, regression trees, random forest regression, k-nearest neighbors regression, and support vector regression. In the following subsections, these algorithms are briefly introduced along with their settings. The proposed machine learning algorithms were challenged against some typical approaches used for forecasting (benchmarks), namely, naive forecast, random forecast, the ARIMA model, and stepwise regression [1].

5.4.1. Artificial Neural Networks. Artificial neural networks are mathematical objects in the form of equations or systems of equations, usually nonlinear, for analysis and data processing. The purpose of neural networks is to convert input data into output data with a specific characteristic or to modify such systems of equations to read useful information from their structure and parameters. On the statistical basis, selected types of neural networks can be interpreted in general nonlinear regression categories.

In studies related to forecasting in power engineering, multilayer, one-way artificial neural networks with no feedback are most commonly used. Multilayer perceptron (MLP) networks are one of the most popular types of supervised neural networks. For example, the MLP network (3, 4, 1) means a neural network with three inputs, four neurons in the hidden layer, and one neuron in the output layer. In general, the three-layer MLP neural network (P, M, K) is described by the expression

$$f\left(\mathbf{x}_i, \mathbf{w}\right) = h_2\left(\mathbf{W}_2\left[h_1\left(\mathbf{W}_1\mathbf{x}_i + \mathbf{b}_1\right)\right] + \mathbf{b}_2\right), \tag{8}$$

where $\mathbf{x}_i = (x_1, \ldots, x_p)^T$ represents the input data, $\mathbf{W}_1$ is the matrix of the first layer weights with dimensions $M \times P$, $\mathbf{W}_2$ is the matrix of the second layer weights with dimensions $K \times M$, and $h_i(\mathbf{u})$ and $\mathbf{b}_i$ are nonlinearities (functions of neuron activation, e.g., logistic function) and constant values in subsequent layers, respectively.

The goal of supervised learning of the neural network is to search for such network parameters that minimize the error between the desired values L_i and those received at the output of the network P_i. The most frequently minimized error function is the sum of the squares of differences between the actual value of the explained variable and its theoretical value determined by the model, with the values of the synaptic weight vector set:

$$E\left(\mathbf{w}\right) = \frac{1}{2}\sum_{k=1}^{K}\mathbf{e}^{(k)} = \frac{1}{2}\sum_{k=1}^{K}\left(\sum_{i=1}^{n}\left(P_i^{(k)} - L_i^{(k)}\right)^2\right), \tag{9}$$

where n is the number of training samples, $P_i^{(k)}$ and $L_i^{(k)}$ are the predicted and reference values, and K is the number of training epochs of the neural network.

The neural network learning process involves the iterative modification of the values of the synaptic weight vector $\mathbf{w}$ (all weights are set in one vector), in iteration $k + 1$:

$$\mathbf{w}_{k+1} = \mathbf{w}_k + \eta_k\mathbf{p}_k, \tag{10}$$

where $\mathbf{p}_k$ is the direction of the minimization of the function $E(\mathbf{w})$ and η is the magnitude of the learning error. The most popular optimization methods are undoubtedly gradient methods, which are based on the knowledge of the function gradient:

$$\mathbf{p}_k = -\left[\mathbf{H}\left(\mathbf{w}_k\right)\right]^{-1}\mathbf{g}\left(\mathbf{w}_k\right), \tag{11}$$

where $\mathbf{g}$ and $\mathbf{H}$ denote the gradient and the Hessian of the last known solution $\mathbf{w}_k$, respectively.

In the practical implementations of the algorithm, the exact determination of Hessian $\mathbf{H}(\mathbf{w}_k)$ is abandoned, and its approximation $\mathbf{G}(\mathbf{w}_k)$ is used instead. One of the most popular methods of learning neural networks is the algorithm of variable metrics. In this method, the Hessian (or its reversal) in each step is modified from the previous step by some correction. If by $\mathbf{c}_k$ and $\mathbf{r}_k$ the increments of the vector $\mathbf{w}$ and the gradient $\mathbf{g}$ in two successive iterative steps are marked, $\mathbf{c}_k = \mathbf{w}_k - \mathbf{w}_{k-1}$, $\mathbf{r}_k = \mathbf{g}_k - \mathbf{g}_{k-1}$, and by $\mathbf{V}_k$ the inverse matrix of the approximate Hessian $\mathbf{V}_k = [\mathbf{G}(\mathbf{w}_k)]^{-1}$, $\mathbf{V}_{k-1} = [\mathbf{G}(\mathbf{w}_{k-1})]^{-1}$, according to the most effective formula of Broyden–Fletcher–Goldfarb–Shanno (BFGS) [37], the process of updating the value of the $\mathbf{V}_k$ matrix is described by the recursive relationship

$$\mathbf{V}_k = \mathbf{V}_{k-1} + \left(1 + \frac{\mathbf{r}_k^T\mathbf{V}_{k-1}\mathbf{r}_k}{\mathbf{c}_k^T\mathbf{r}_k}\right)\frac{\mathbf{c}_k\mathbf{c}_k^T}{\mathbf{c}_k^T\mathbf{r}_k} - \frac{\mathbf{c}_k\mathbf{r}_k^T\mathbf{V}_{k-1} + \mathbf{V}_{k-1}\mathbf{r}_k\mathbf{c}_k^T}{\mathbf{c}_k^T\mathbf{r}_k}. \tag{12}$$

As a starting value, $\mathbf{V}_0 = 1$ is usually assumed, and the first iteration is carried out in accordance with the algorithm of the largest slope.

Artificial neural networks are often used to estimate or approximate functions that can depend on a large number of inputs. In contrast to the other machine learning algorithms considered in these experiments, the ANN required the input data to be specially prepared. The vector of continuous variables was standardized, whereas the binary variables were converted such that 0s were transformed into values of –1. Finally, the dependent variable was normalized by zero unitarization. To generate a forecast, the reverse transformation of the dependent variable was applied [1].

To train the neural networks, we used the Broyden–Fletcher–Goldfarb–Shanno (BFGS) algorithm, which is a quasi-Newton optimization method (available in the *nnet* library). The network had an input layer with 146 neurons and a hidden layer with 10, 15, 20, . . . , 50 neurons (i.e., nine sets of experiments).

A logistic function was used to activate all of the neurons in the network, and a regularization factor was introduced to penalize weights that were too high in the network (to control overfitting). Factor values of 0.01, 0.1, and 0.5 were considered [1].

In each experiment, 27 neural networks were learned with various parameters (the number of neurons in the hidden layer multiplied by the number of penalties). To avoid overfitting, after each learning iteration had finished (with a maximum of 50 iterations), the models were checked using the error measure defined in (7). Finally, out of the 27 learned networks, that with the smallest error was chosen as the best for delivering forecasts [36].

5.4.2. k-Nearest Neighbors Regression. The k-nearest neighbors regression [38] is a nonparametric method, which means that no assumptions are made regarding the model that generates the data. Its main advantage is the simplicity of the design and low computational complexity. The forecast of the value of the explained variable L_i on the basis of the vector of explanatory variables $\mathbf{x}_i$ is determined as

$$P_i = \frac{\sum_{k=1}^{K} L_k I\left(\mathbf{x}_i, \mathbf{x}_k\right)}{K}, \tag{13}$$

where

$$I\left(\mathbf{x}_i, \mathbf{x}_k\right) = \begin{cases} 1, & \text{if } \mathbf{x}_k \text{ is one of the } k \text{ nearest neighbors } \mathbf{x}_i \\ 0, & \text{otherwise,} \end{cases} \tag{14}$$

whereas $\mathbf{x}_k$ is one of the k-nearest neighbors $\mathbf{x}_i$, in the case where the distance $d(\mathbf{x}_i, \mathbf{x}_k)$ belongs to k smallest distance between the observations from the set $\mathbf{X}$ and $\mathbf{x}_k$. The most commonly used distance is the Euclid distance.

To improve the algorithm, we normalized the explanatory variables (standardization for quantitative variables and replacement of 0 by −1 for binary variables). The normalization ensures that all dimensions for which the Euclidean distance is calculated have the same importance. Otherwise, a single dimension could dominate the other dimensions [1].

The algorithm was trained with *knnreg* implemented in the *caret* library. Different values of k were investigated in the experiments: {5, 10, 15, 20, 25, 30, 35, 40, 45, 50, 55, 60, 65, 70, 75, 80, 85, 90, 95, 100, 110, 120, 130, 140, 150, 160, 170, 180, 190, 200, 250, 300}. The optimal value, and thus the final form of the model, was determined as that giving the minimum error according to (7).

5.4.3. Regression Trees. Regression trees are popular machine learning induction tools. They approximate target functions in a discreet way and represent them in a tree structure or alternatively in a set of decision rules. Characteristic for decision trees is the division of a multidimensional space of features into disjoint R_k segments, within which a simple model approximating locally the target function within the segment is under consideration [39].

The regression tree in the *CART* version was used in this work. This tree consists of intermediate nodes in which tests are performed on explanatory variables, end nodes (leaves) storing values of the dependent variable L_i (expressed as the average value of objects belonging to a given segment), and branches connecting nodes. The discussed type of model is a binary tree, which means that each branch has two branches (descendants). In the tree construction process, the intermediate sets divide the set of examples into two subsets: positive examples that meet the test assigned to the node and negative examples that do not meet this test. The aim is to ensure that the values of the target function of examples in these subsets have the smallest possible variance:

$$s^2\left(\mathbf{P}\right) = \frac{1}{N_k} \sum_{k \in R_k} \left(L_k - \overline{L}_{R_k}\right)^2, \tag{15}$$

where N_k is the number of observations in the R_k segment and $\overline{L}_{R_k}$ is the average value of the target function of the examples in the set R_k. The variance (15) is a measure of the inhomogeneity of the node (impurity). The division of the set of examples in a node into two subsets as a result of the test is justified if it leads to the reduction of heterogeneity; that is,

$$N_P s^2\left(R_{kP}\right) + N_N s^2\left(R_{kN}\right) < s^2\left(R_k\right), \tag{16}$$

where $(R_k), (R_{kP}), (R_{kN})$ are sets of indexes of examples in the parent node (parent) and in child nodes with positive or negative examples. In addition N_P and N_N are numbers of positive and negative examples in set R_k: $N_P = |R_{kP}|/|R_k|$, $N_N = |R_{kN}|/|R_k|$.

Regression trees are usually built according to the descending scheme. Starting from the start node (root) in which the entire learning set is considered, it moves to the next nodes as a result of dividing the examples into subsets R_{kP} and R_{kN}. The size of the tree depends on the complexity of the problem under consideration. The size of the tree, which implies the degree of its fit to the learning data, can be controlled, for example, using the parameter cp. This parameter indicates to the algorithm how much the general model performance should be increased in each step, so that a given decision node can be divided.

To train regression trees, the *rpart* package was used to implement the CART algorithm. In the process of dividing a multidimensional space, the dispersion (variance) around the mean value of the dependent variable for observations belonging to the same node (leaf) was minimized. At each stage of node splitting, the variable value that minimized the sum of squares was chosen. The minimum number of observations in the node was set to 20, and the leaf was set to at least six observations; otherwise, the node was split [1].

Instead of pruning the tree at the end of the algorithm, we used pruning during the growth stage. Generally, this approach prevents new splits from being created when the previous splits provided only a slight increase in predictive accuracy. The complexity parameter (cp) varied from 0 to 0.1 in increments of 0.001, meaning that if any split did not increase the model's overall coefficient of determination by at least cp, then the split was decreed to be not worth

pursuing. The tree was built up to a depth of 30 levels. Out of 1000 regression trees that were tested, the final structure was chosen based on the error measure defined in (7) [1].

5.4.4. Random Regression Forests. Random forests are an ensemble learning method for regression that operate by constructing a multitude of decision trees at training time and outputting the prediction of the individual trees. Random forests correct for decision trees' habit of overfitting to their training set [40].

The training algorithm for random forests applies the general technique of bootstrap aggregating, or bagging, to tree learners. Given a training set $\mathbf{X}$ with responses $\mathbf{L}$, bagging repeatedly (B times) selects a random sample with replacement of the training set and fits trees T_i to these samples. After training, predictions for unseen samples $\mathbf{X}'$ can be made by averaging the predictions from all the individual regression trees on $\mathbf{X}'$:

$$\mathbf{P} = \frac{1}{B}\sum_{i=1}^{B} T_i\left(\mathbf{X}'\right). \tag{17}$$

This bootstrapping procedure leads to better model performance because it decreases the variance of the model, without increasing the bias. This means that while the predictions of a single tree are highly sensitive to noise in its training set, the average of many trees is not, as long as the trees are not correlated.

The above procedure describes the original bagging algorithm for trees. Random forests differ in only one way from this general scheme: they use a modified tree learning algorithm that selects, at each candidate split in the learning process, a random subset of the features. This process is sometimes called feature bagging. The reason for doing this is the correlation of the trees in an ordinary bootstrap sample: if one or a few features are very strong predictors for the response variable (target output), these features will be selected in many of the B trees, causing them to become correlated. Typically, for a regression problem with p features, $p/3$ (rounded down) features are used in each split.

To train the random regression forest, an algorithm from the *randomForest* library was used. Prior to the training, n-element samples were selected with replacement, and these accounted for approximately 63% of the population. The samples were used to construct the *CART* tree. Each tree was built to its maximum size (without pruning), preventing the occurrence of five or fewer observations in a leaf [1].

A randomized subset of variables was used to construct each tree. The total number of trees in the forest was 500. The final forecast was defined based on Huber's robust estimator [35]. Finally, as in previous cases, the best forest structure was chosen based on the error measure defined in (7).

5.4.5. Support Vector Regression. Support vector learning is based on simple ideas which originated in statistical learning theory [41]. The simplicity comes from the fact that support vector machines (SVMs) apply a simple linear method to the data but in a high-dimensional feature space nonlinearly related to the input space. Moreover, even though we can think of SVMs as a linear algorithm in a high-dimensional space, in practice, it does not involve any computations in that high-dimensional space.

SVMs use an implicit mapping Φ of the input data into a high-dimensional feature space defined by a kernel function, that is, a function returning the inner product $\langle \Phi(\mathbf{x}_i), \Phi(\mathbf{x}_\mathbf{i}')\rangle$ between the images of two data points $\mathbf{x}_i$, $\mathbf{x}_\mathbf{i}'$ in the feature space. The learning then takes place in the feature space, and the data points only appear inside dot products with other points [42]. More precisely, if a projection $\Phi : \mathbf{X} \rightarrow \mathbf{H}$ is used, the dot product $\langle \Phi(\mathbf{x}_i), \Phi(\mathbf{x}_\mathbf{i}')\rangle$ can be represented by a kernel function k:

$$k\left(\mathbf{x}_i, \mathbf{x}_\mathbf{i}'\right) = \left\langle \Phi\left(\mathbf{x}_i\right), \Phi\left(\mathbf{x}_\mathbf{i}'\right)\right\rangle, \tag{18}$$

which is computationally simpler than explicitly projecting $\mathbf{x}_i$ and $\mathbf{x}_\mathbf{i}'$ into the feature space $\mathbf{H}$.

Training an SVM regression involves solving a quadratic optimization problem. Using a standard quadratic problem solver for training an SVM would involve solving a big QP problem even for a moderate sized dataset, including the computation of an $n \times n$ matrix in memory (n training points). In general, predictions correspond to the decision function

$$P_i = \operatorname{sign}\left(\left\langle \mathbf{w}, \Phi\left(\mathbf{x}_i\right)\right\rangle\right), \tag{19}$$

where solution $\mathbf{w}$ has an expansion $\mathbf{w} = \alpha_i \sum_\mathbf{i} \Phi(\mathbf{x}_i)$ in terms of a subset of training patterns that lie on the margin.

Using a different loss function called the ε-insensitive loss function $\|L_i - f(\mathbf{x}_i)\|_\varepsilon = \max\{0, \|L_i - f(\mathbf{x}_i)\| - \varepsilon\}$, SVMs can also perform regression. This loss function ignores errors that are smaller than a certain threshold $\varepsilon > 0$, thus creating a tube around the true output. The primal optimization problem takes the form

$$\begin{aligned}
\text{minimize} \quad & (t, \mathbf{w}) \\
& = \frac{1}{2}\|\mathbf{w}\|^2 \\
& \quad + \frac{C}{n}\sum_{i=1}^{n}\left(\xi_i + \xi_i^*\right), \\
\text{subject to} \quad & \left(\left\langle \Phi\left(\mathbf{x}_i\right), \mathbf{w}\right\rangle + b\right) - L_i \\
& \leq \varepsilon - \xi_i, \\
& L_i - \left(\left\langle \Phi\left(\mathbf{x}_i\right), \mathbf{w}\right\rangle + b\right) \\
& \leq \varepsilon - \xi_i^*, \\
& \quad \xi_i^* \geq 0, \ (i = 1, \ldots, n),
\end{aligned} \tag{20}$$

where C is the cost parameter that controls the penalty paid by the SVM for misclassifying a training point and thus the complexity of the prediction function. A high cost value C will force the SVM to create a complex enough prediction function to misclassify as few training points as possible, while a lower cost parameter will lead to a simpler prediction function.

To construct the support vector regression model, ε-SVR from the *kernlab* library with sequential minimal optimization (SMO) was used to solve the quadratic programming

problem. A linear kernel function was used, and ε (which defines the margin width for which the error function is zero) was arbitrarily taken from the following set: {0.01, 0.05, 0.1, 0.25, 0.5, 0.75, 1} [1].

The regularized parameter C that controls overfitting was arbitrarily set to one of the following values {0.0001, 0.0005, 0.001, 0.005, 0.01, 0.05, 0.1, 0.25, 0.5, 0.75, 1}. Finally, as in all previous cases, the model that minimized the error function (7) was chosen [1].

5.4.6. Naive Forecast. The naive forecast was constructed in the following manner. For the forecasting horizon of 24 h, the value recorded on the previous day at that hour was taken as the forecast [1].

5.4.7. Random Forecast. The random forecast was constructed in the following way. Given the electricity consumption in a given hour on a particular day of the week, empirical distribution functions were computed. Using a *runif* function, a value between 0 and 1 was then drawn from a uniform distribution (p probability). This value was used to estimate the quantile of the empirical distribution (the final value of the forecast) according to a weighted averaging of the order statistic L_i (quantile function):

$$Q_p = (1 - \gamma) L_i + \gamma L_{i+1}, \tag{21}$$

where $\gamma = np + m - g$, n is the number of observations, $g = \text{floor}(np + m)$, and $m = 1 - p$ [1].

5.4.8. ARIMA Model. Autoregressive integrated moving-average model provides a description of a stationary stochastic process in terms of two polynomials, one for the autoregression and the other for the moving average that is applied in some cases where data show evidence of nonstationarity, where an initial differencing step (corresponding to the integrated part of the model) can be applied one or more times to eliminate the nonstationarity [43]. For a given time series of data L_i, an ARIMA(p, d, q) model is given by

$$\left(1 - \sum_{j=1}^{p} \varphi_j B^j\right)(1 - B)^d L_i = \delta + \left(1 + \sum_{j=1}^{q} \theta_j B^j\right)\varepsilon_j, \tag{22}$$

where p is the order (number of time lags) of the autoregressive model, d is the degree of differencing (the number of times the data have had past values subtracted), q is the order of the moving-average model, B^j is the lag operator, φ_j are the parameters of the autoregressive part of the model, θ_j are the parameters of the moving-average part, ε_j are error terms, and finally δ is a drift factor $\delta = \mu(1 - \varphi_1 - \cdots - \varphi_p)$, where μ is the mean of $(1 - B)^d L_i$. The error terms ε_j are generally assumed to be independent, identically distributed variables sampled from a normal distribution with zero mean.

To determine the order of an ARIMA model, a useful criterion is the Akaike information criterion (AIC) written as

$$\text{AIC} = -2\log(L) + 2(p + q + k + 1), \tag{23}$$

where L is the likelihood of the data; the parameter k in this criterion is defined as the number of parameters in the model being fitted to the data. Therefore, this part uses the *auto.arima* function implemented in the *forecast* library. The function identifies and estimates the model by minimizing Akaike's information criterion.

In this model, the maximum values for the AR and MA orders were arbitrarily set to $p = 14$ and $q = 14$. The degree of differencing was tested with the Kwiatkowski–Phillips–Schmidt–Shin (KPSS) test, which examines the null hypothesis that an observable time series is stationary around a deterministic trend [1].

5.4.9. Stepwise Regression. Stepwise linear regression of the form

$$L_i = \mathbf{x}_i^T \boldsymbol{\beta} + \varepsilon_i \tag{24}$$

was used as an automated tool to identify a useful subset of predictors (where $\mathbf{x}_i$ denotes vector of independent variables, $\boldsymbol{\beta}$ is the vector of the models' parameters, and ε_i is the error variable). Two procedures were tested: the first adds the most significant variable (forward selection) and the second removes the least significant variable during each step (backward elimination). The forward approach stops when all variables not in the model have p values that are greater than the specified alpha-to-enter value (5% significance level was used). The backward elimination stops when all variables in the model have p values that are less than or equal to the specified alpha-to-remove value (5% significance level was used) [1].

6. Forecasting Aggregated Electricity Demand

6.1. Forecasting Electricity Demand for the Entire Population. In the first step of the forecasting stage, the hourly (g) values of electricity demand were aggregated by summing all n values of $z_g^{(i)}$ in the entire population:

$$z_g^{\text{population}} = \sum_{i=1}^{n} z_g^{(i)}. \tag{25}$$

For the clarity of the presented results, the following notation is introduced: Z_{24}, naive forecast; F_g, random forecast; ARIMA, ARIMA model; L_f, stepwise regression with forward selection; L_b, stepwise regression with backward elimination; k-NN, k-nearest neighbors regression; RPART, regression trees; RF, random regression forests; NNET, artificial neural network; and SVR, support vector regression [1].

Forecasting results for hourly models with a forecast horizon of 24 h are presented in Table 6. The best results for the test set were obtained by SVR, NNET, and the two comparative methods (L_f and L_b). After examining each of the separate subsets (training, validation, and test) and the error metrics, it is clear that the machine learning models (except for random forests) exhibit good stability. There is also no difference between the MAPE and r-MAPE metrics, which indicates that the forecasts are largely inaccurate.

Table 6: Forecasting results for aggregate models of the entire population.

Model	MAPE (%)	r_MAPE (%)	Acc (%)	MSE	MAPE (%)	r_MAPE (%)	Acc (%)	MSE	MAPE (%)	r_MAPE (%)	Acc (%)	MSE
	Learning sample				Validation sample				Test sample			
Z_{24}	16.05	14.77	57.60	158	16.06	15.40	54.38	75	20.17	18.82	46.43	152
F_g	41.17	36.68	25.98	1059	52.30	44.96	29.87	917	49.19	44.30	25.60	814
ARIMA	9.48	9.01	79.71	45	19.33	18.89	45.77	103	26.28	25.08	39.00	186
L_f	14.76	13.74	61.31	118	18.85	18.80	41.60	91	17.38	16.45	56.85	102
L_b	14.70	13.68	61.74	118	19.96	19.91	36.85	101	17.85	16.91	56.55	103
KNN	14.64	13.39	62.12	131	14.63	14.20	60.77	56	20.41	19.41	47.02	127
RPART	15.58	14.39	59.60	133	16.55	15.48	56.61	72	20.46	19.30	49.40	153
RF	0.50	0.42	100.00	0	14.07	13.69	63.15	49	19.46	18.31	49.70	117
NNET	13.65	12.69	65.34	103	13.62	13.35	61.66	65	17.50	16.76	52.98	110
SVR	14.82	13.62	61.78	126	14.40	14.17	55.42	58	17.03	16.04	57.14	100

6.2. Forecasting Electricity Demand within Clusters. The hourly (g) values of electricity demand were then aggregated by summing all n_k values of $z_g^{(i)}$ in the kth cluster:

$$z_g^{C_k} = \sum_{i=1}^{n_k} z_g^{(i)}. \tag{26}$$

Similar to the previous experiment, the aggregate explanatory variables were determined based on Table 5. For each of the 10 similarity measures and eight possible partitions of household aggregates (total 80 combinations), forecasting models based on machine learning algorithms were developed, as described in Section 5. A total of 440 different "definitive" forecasting models have been developed. Taking into account the number of indirect models developed during the optimization process, the number of models increases to 328680 (32(RPNN) + 102(RPART) + 12(RF) + 27(NNET) + 77(SVR) = 249).

In the next step, the forecasted demand for the whole population was determined as the sum of all q predicted values $p_g^{(k)}$ for the kth cluster:

$$p_g^{\text{population}} = \sum_{k=1}^{q} p_g^{(k)}. \tag{27}$$

For example, let the actual aggregate value of the hourly electricity demand for the entire population at time g be $z_g^{\text{population}} = 46\,\text{kWh}$. Taking into account the second split of households into clusters in terms of the autocorrelation-based distances, the predicted aggregates for these clusters are $p_g^{(1)} = 25\,\text{kWh}$, $p_g^{(2)} = 12\,\text{kWh}$, and $p_g^{(3)} = 10\,\text{kWh}$. By aggregating the above values in accordance with (11), the final forecast for the whole population is $p_g^{\text{population}} = 47\,\text{kWh}$.

To identify situations in which partitioning households into clusters improved the final forecast, we introduced a percentage point sensitivity range and denoted different cases using the following fonts [1]:

(i) Italic font: forecast improves in terms of Acc and MAPE/r-MAPE when determining the final forecast according to (11); for example, for a model with 20% error, the improvement should be at least 0.5 percentage points, so the model error should be less than 19.5%.

(ii) Bold font: forecast worsens in terms of Acc and MAPE/r-MAPE when determining the final forecast according to (11); for example, for a model with 20% error, an increase of at least 0.5 percentage points should be expected, so the model error is greater than 20.5%.

(iii) Roman font: neutral cases in which Acc and MAPE/r-MAPE remain at similar levels; for example, for a model with 20% error, we define a 1 percentage point range (19.5–20.5%) over which no improvement is observed when determining the final forecast according to (11).

Forecasts for the hourly demand models developed in this study, with a 24-hour forecast horizon, are presented in Table 7. This table compares the results of the forecasts for a particular partition against the results of the base model developed for the aggregate of all households (see Table 6).

In the majority of cases, application of k-NN and RPART leads to a deterioration with respect to the baseline models developed for the aggregate population and the same forecasting methods (for the second partition of the TQuest distance and the RPART model, there is some improvement). The RF approach gives improved predictions using EDR, STS, and TQuest. However, the results with RF and SVR are often neutral. The NNET forecasting method generally improves the results for each time series similarity measure (worsening results in only 5% of cases), as presented in Figure 5. Using the distance based on cross-correlation, EDR, L_p, LCSS, and TQuest, the forecast accuracy increased by nearly 1.5 percentage points. In general, the following pattern is observed: the MAPE error decreases when the number of clusters increases (please refer to Average and BASE_NNET labels in Figure 5). This observation suggests that the underlying population was very heterogeneous and splitting it into a number of clusters leads to improved forecast accuracy.

To provide a quantitative summary of the experiments, we tested whether there are statistically significant differences

Table 7: Forecasting results in terms of MAPE error for grouped households using the test set.

Partition number	Autocorrelation-based distance					Partition number	Fourier coefficients-based distance				
	KNN	RPART	RF	NNET	SVR		KNN	RPART	RF	NNET	SVR
1	**21.45**	20.04	19.28	17.20	17.19	1	**21.10**	20.08	19.36	**18.01**	16.88
2	**22.52**	20.83	19.77	*16.67**	17.22	2	**22.23**	**21.70**	19.50	17.32	17.02
3	**23.39**	**21.05**	19.73	17.24	17.10	3	**22.46**	**21.93**	19.16	17.01	16.86
4	**24.51**	**21.85**	19.77	17.14	16.88	4	**22.48**	**21.88**	19.19	*16.88*	16.79
5	**26.00**	**22.66**	19.95	*16.90*	16.70	5	**23.54**	**22.78**	19.28	17.41	*16.39*
6	**26.50**	**22.32**	19.44	*16.49**	16.64	6	**23.99**	**21.98**	19.28	*16.69**	16.56
7	**27.26**	**22.09**	19.28	*16.05**	*16.51*	7	**25.53**	**22.23**	19.18	*16.94*	16.71
8	**28.68**	**21.96**	19.13	*16.25**	16.55	8	**25.72**	**22.49**	19.00	17.33	16.63
Partition number	Distance based on cross-correlation					Partition number	Periodogram-based distance				
	KNN	RPART	RF	NNET	SVR		KNN	RPART	RF	NNET	SVR
1	**21.19**	20.24	19.74	17.20	16.88	1	**20.94**	20.87	19.47	17.61	17.42
2	**21.45**	20.43	19.52	17.58	17.02	2	**22.34**	**21.23**	19.59	*16.75*	16.81
3	**21.78**	20.64	19.24	17.32	17.06	3	**23.30**	**21.62**	19.37	17.11	16.81
4	**21.64**	20.77	19.19	*16.99*	16.90	4	**24.08**	20.61	19.15	17.09	16.74
5	**21.73**	20.56	19.26	*15.65**	16.84	5	**25.50**	**21.22**	19.48	*16.59**	*16.30**
6	**22.21**	**21.00**	**18.90**	*16.32**	16.92	6	**27.19**	**21.90**	19.57	*16.86*	*16.16**
7	**22.51**	20.30	19.21	*16.99*	16.90	7	**27.53**	**21.69**	19.46	*16.67**	*16.07**
8	**22.48**	20.42	19.15	*15.50**	16.87	8	**27.73**	**21.81**	19.60	17.31	*16.09**
Partition number	DTW distance					Partition number	LCSS distance				
	KNN	RPART	RF	NNET	SVR		KNN	RPART	RF	NNET	SVR
1	**21.10**	20.08	19.36	**18.01**	16.88	1	**20.92**	**21.09**	19.18	**19.35**	**17.57**
2	**22.23**	**21.70**	19.50	17.32	17.02	2	**21.19**	**21.17**	19.08	17.24	17.45
3	**23.34**	**21.58**	19.44	*16.52**	17.06	3	**22.79**	**22.36**	*18.91*	*16.81*	17.07
4	**23.57**	**21.85**	19.44	*16.22**	16.90	4	**23.44**	**21.04**	19.06	17.31	16.95
5	**23.59**	**21.82**	19.44	17.36	16.84	5	**24.26**	**20.99**	19.18	*15.95**	16.72
6	**24.88**	**22.66**	19.30	*16.84*	16.92	6	**25.09**	**21.07**	19.08	*16.58**	16.66
7	**24.95**	**22.51**	19.28	17.27	16.90	7	**26.38**	20.70	19.15	*16.40**	*16.47*
8	**26.68**	**22.78**	19.14	*16.47**	16.87	8	**27.06**	20.61	19.32	*16.32**	*16.41*
Partition number	EDR					Partition number	STS distance				
	KNN	RPART	RF	NNET	SVR		KNN	RPART	RF	NNET	SVR
1	20.85	**21.00**	19.06	*16.95*	17.30	1	**20.92**	**21.52**	19.44	17.24	17.49
2	**22.15**	**21.02**	*18.73**	17.31	17.29	2	**21.32**	**21.62**	19.22	*16.90*	17.17
3	**23.39**	**21.08**	18.96	*16.57**	16.94	3	**21.80**	**21.06**	*18.81*	*16.92*	17.00
4	**24.26**	**21.31**	18.99	*15.98**	16.78	4	**22.15**	**22.77**	18.99	17.17	17.05
5	**24.67**	**21.51**	18.98	*16.53**	16.71	5	**22.10**	**22.30**	*18.88*	17.01	17.18
6	**25.95**	**21.99**	*18.69**	*16.57**	16.77	6	**22.41**	**21.78**	*18.92*	*16.76**	16.83
7	**25.92**	**21.77**	*18.50**	*16.54**	16.76	7	**22.44**	**21.80**	*18.79*	*16.56**	16.79
8	**27.86**	**22.02**	19.01	*16.83*	16.68	8	**23.12**	**21.41**	*18.85*	*16.26**	16.73
Partition number	L_p distance					Partition number	TQuest distance				
	KNN	RPART	RF	NNET	SVR		KNN	RPART	RF	NNET	SVR
1	**21.10**	20.08	19.36	**18.01**	16.88	1	**21.08**	20.15	19.27	17.29	16.99
2	**22.23**	**21.70**	19.50	17.32	17.02	2	**21.48**	*19.78*	*18.88*	*16.36**	16.54
3	**22.46**	**21.93**	19.16	17.01	16.86	3	**21.70**	20.01	19.09	*16.58**	*16.41*
4	**22.48**	**21.88**	19.19	*16.88*	16.79	4	**21.88**	20.04	*18.86*	*16.48**	*16.32**
5	**23.74**	**22.43**	19.26	17.03	*16.34*	5	**22.55**	20.84	*18.85*	17.44	*16.35*
6	**24.35**	**22.03**	19.23	*16.02**	*16.50*	6	**23.02**	**21.60**	*18.57**	*15.77**	16.60
7	**24.59**	**22.61**	19.32	*16.38**	16.56	7	**23.09**	**21.65**	*18.64**	*16.03**	16.55
8	**26.33**	**22.41**	19.05	*15.85**	16.61	8	**23.19**	**21.69**	*18.41**	*16.05**	*16.47*

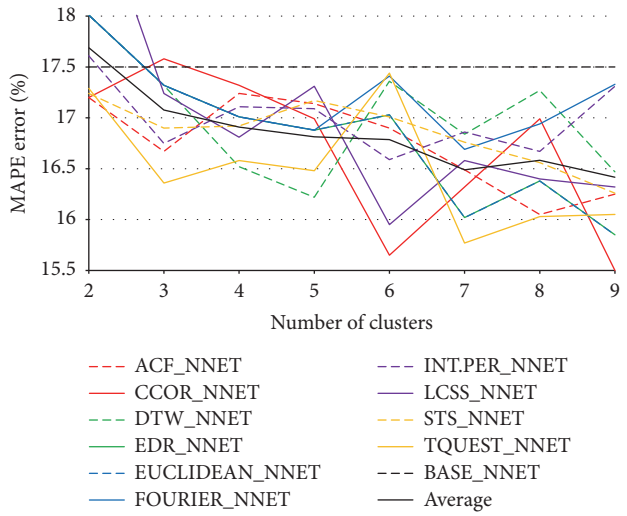

Figure 5: MAPE errors for NNET with respect to the number of clusters and the similarity measure.

in terms of the MAPE errors when forecasting the usage of the entire population against forecasting in segments. The Kolmogorov-Smirnov (K-S) test was used to compare two empirical error distributions with respect to the datasets. The differences were found to be significant at $p < 0.05$ and marked as $*$ in Table 7.

Considering all the partitions that improve the results for NNET (the choice of this forecasting method results from generating the smallest errors), some measures of the optimal number of clusters give the partitions leading to the optimal improvement in prediction quality. The accuracy of these measures is as follows:

(i) Calinski and Harabasz index: 20%.

(ii) Duda index: 40%.

(iii) C index: 50%.

(iv) Ptbiserial index: 40%.

(v) DB index: 80%.

(vi) Frey index: 0%.

(vii) Hartigan index: 20%.

(viii) Ratkowsky index: 20%.

(ix) Ball index: 20%.

(x) McClain index: 10%.

(xi) KL index: 10%.

(xii) Silhouette index: 50%.

(xiii) Dunn index: 40%.

(xiv) SD index: 70%.

The above percentages were calculated according to the number of well-defined subpartitions giving a quality improvement for each similarity measure. For example, the Duda index using the distance based on the cross-correlation, EDR, periodogram-based distances, and LCSS distance gives the optimal number of clusters as 8, 7, 8, and 6, respectively (please refer to Table 8). By applying these values to Table 7 (underlined italic font), it can be seen that they overlap with an improvement in forecasts (four correct cases divided by 10 time series similarity measures).

7. Conclusions

The main objective of this article was to develop an effective method for dealing with short-term forecasts of electricity demand for the whole population and for clusters of households over 24-hour forecasting horizons based on hourly data. To achieve this goal, we investigated the following:

(i) Partitioning of households into disjoint clusters using a hierarchical algorithm based on ten time series similarity measures.

(ii) Determination of the optimum number of clusters for each time series similarity measure.

(iii) Application of different techniques for short-term forecasting using aggregated data and within the groups of homogenous households (segments).

Experiments were designed to answer the research questions concerning load forecasting for a group of customers. In particular, it can be concluded that:

(i) the number of households included in each cluster is very diverse, taking into account the same type of partition and among different time series similarity measures;

(ii) the distances based on cross-correlation, STS, and TQuest give the most unbalanced cluster sizes;

(iii) the results of time series clustering can be divided according to the degree of similarity; we can distinguish a group of four measures with a high degree of similarity (DTW, L_p, Fourier coefficients, and periodogram-based distances) and very low (autocorrelation-based distances and LCSS distance) similarity;

(iv) the optimal number of groups based on the majority vote indicated that the households should be divided into two groups;

(v) there are groups of measures for optimal clustering, indicating a similar number of groups for particular groups of time series similarities;

(vi) models developed based on machine learning algorithms show good stability and can be used in practice to forecast aggregates for the entire population;

(vii) of all the developed methods, neural network models are characterized by the best results for aggregates of the entire population for hourly data;

(viii) the use of artificial neural networks for group forecasting offers, in most cases, increased accuracy of forecasts in relation to the aggregate population;

(ix) for neural networks, the following general pattern is observed: the forecasting error decreases when the number of clusters increases;

Table 8: Results for the relevant number of clusters based on the partition type and the time series similarity measure.

	KL	CH	Hartigan	Cindex	DB	Silhouette	Duda	Ratkowsky	Ball	Ptbiserial	Frey	McClain	Dunn	SDindex
acf	5	4	4	2	9	2	2	4	3	3	2	2	9	2
ccor	2	2	9	9	6	5	8	2	3	6	1	4	9	2
dtw	3	2	3	4	2	2	3	2	3	2	3	2	2	6
edr	3	2	3	2	2	2	7	3	3	3	1	2	3	2
euclidean	2	2	3	4	5	2	4	2	3	2	2	2	2	5
fourier	2	2	3	3	5	2	4	2	3	2	2	2	2	5
int.per	9	2	3	8	2	2	8	2	3	2	2	2	9	3
lcss	5	5	5	2	9	9	6	8	3	9	1	2	9	9
sts	2	2	5	2	9	9	2	6	3	9	1	2	9	8
tquest	7	7	6	9	5	4	2	7	3	6	1	2	6	3

(x) there are groups of measures that select the optimal number of clusters more often than others, with partitions leading to improved forecast quality.

Finally, note that this research was carried out on a sample of 46 households. The conclusions serve as an indication of how the specific measures of time series similarity and optimal clustering, as well as forecasting methods, could behave on a much larger scale.

When load shape clustering is used as a preprocessing step for subsequent household-level segmentation, the requirement for a low number of clusters, which is practical for tariff purposes, should be relaxed to capture the diverse time-of-use behavior in residential hourly consumption. In addition, regarding the size distribution and visual examination conducted in the postcluster checking, future work should evaluate the broader validation of the robustness of the identified clusters using additional data sources, such as household demographic and socioeconomic information and rate structures. In particular, the sources of variability in the identified hourly patterns need to be established and better understood to support more effective demand-side management and behavior-based programs [44].

Conflicts of Interest

The authors declare that they have no conflicts of interest.

Acknowledgments

This study was cofounded by the National Science Centre, Poland, Grant no. 2016/21/N/ST8/02435.

References

[1] K. Gajowniczek and T. Zabkowski, "Electricity forecasting on the individual household level enhanced based on activity patterns," *PLoS ONE*, vol. 12, no. 4, Article ID e0174098, 2017.

[2] G. Chicco, "Overview and performance assessment of the clustering methods for electrical load pattern grouping," *Energy*, vol. 42, no. 1, pp. 68–80, 2012.

[3] L. Jin, D. Lee, A. Sim et al., *Comparison of Clustering Techniques for Residential Energy Behavior using Smart Meter Data*, Lawrence Berkeley National Lab. (LBNL), Berkeley, CA, USA, 2017.

[4] P. Montero and J. A. Vilar, "TSclust: An R package for time series clustering," *Journal of Statistical Software* , vol. 62, no. 1, pp. 1–43, 2014.

[5] U. Mori, A. Mendiburu, and J. A. Lozano, "Distance measures for time series in R," *The TSdist Package R journal*, vol. 8, no. 2, pp. 455–463, 2016.

[6] J. Mei, M. Liu, Y.-F. Wang, and H. Gao, "Learning a Mahalanobis Distance-Based Dynamic Time Warping Measure for Multivariate Time Series Classification," *IEEE Transactions on Cybernetics*, vol. 46, no. 6, pp. 1363–1374, 2016.

[7] E. Bianco-Martinez, N. Rubido, C. G. Antonopoulos, and M. S. Baptista, "Successful network inference from time-series data using mutual information rate," *Chaos: An Interdisciplinary Journal of Nonlinear Science*, vol. 26, no. 4, Article ID 043102, 9 pages, 2016.

[8] P. Berkhin, "A survey of clustering data mining techniques," in *Grouping Multidimensional Data*, J. Kogan, C. Nicholas, and M. Teboulle, Eds., pp. 25–71, Springer, Berlin, Germany, 2006.

[9] D. Xu and Y. Tian, "A comprehensive survey of clustering algorithms," *Annals of Data Science*, vol. 2, no. 2, pp. 165–193, 2015.

[10] M. Halkidi, Y. Batistakis, and M. Vazirgiannis, "On clustering validation techniques," *Journal of Intelligent Information Systems*, vol. 17, no. 2-3, pp. 107–145, 2001.

[11] Pecanstreet, "Dataport," 2014, https://dataport.pecanstreet.org/.

[12] B. Yi and C. Faloutsos, "Fast time sequence indexing for arbitrary *Lp* norms," in *Proceedings of the 26th International Conference on Very Large Data Bases (VLDB '00)*, pp. 385–394, San Francisco, Calif, USA, 2000.

[13] C. S. Möller-Levet, F. Klawonn, K. Cho, and O. Wolkenhauer, "Fuzzy clustering of short time-series and unevenly distributed sampling points," in *Advances in Intelligent Data Analysis V*, vol. 2810 of *Lecture Notes in Computer Science*, pp. 330–340, Springer, Berlin, Germany, 2003.

[14] D. Lin, W. Gu, Y. Wang, X. Yuan, Q. Li, and R. Wang, "Synthetic evaluation of power quality based on dynamic time warping spatial distance measurement," *Power System Technology*, vol. 2, p. 047, 2013.

[15] L. Chen, M. T. Özsu, and V. Oria, "Robust and fast similarity search for moving object trajectories," in *Proceedings of the ACM SIGMOD International Conference on Management of Data (SIGMOD '05)*, pp. 491–502, ACM, June 2005.

[16] M. Vlachos, G. Kollios, and D. Gunopulos, "Discovering similar multidimensional trajectories," in *Proceedings of the 18th International Conference on Data Engineering*, pp. 673–684, San Jose, Calif, USA, March 2002.

[17] P. D'Urso and E. A. Maharaj, "Autocorrelation-based fuzzy clustering of time series," *Fuzzy Sets and Systems*, vol. 160, no. 24, pp. 3565–3589, 2009.

[18] J. Caiado, N. Crato, and D. Peña, "A periodogram-based metric for time series classification," *Computational Statistics & Data Analysis*, vol. 50, no. 10, pp. 2668–2684, 2006.

[19] R. Tolimieri, M. An, and C. Lu, *Algorithms for Discrete Fourier Transform and Convolution*, Springer Science & Business Media, 2013.

[20] J. Aßfalg, H.-P. Kriegel, P. Kröger, P. Kunath, A. Pryakhin, and R. Renz, "Similarity search on time series based on threshold queries," in *Advances in Database Technology—EDBT*, vol. 3896 of *Lecture Notes in Computer Science*, pp. 276–294, Springer, Berlin, Germany, 2006.

[21] M. Charrad, N. Ghazzali, V. Boiteau, and A. Niknafs, "Nbclust: An R package for determining the relevant number of clusters in a data set," *Journal of Statistical Software*, vol. 61, no. 6, pp. 1–36, 2014.

[22] T. Zabkowski and K. Gajowniczek, "Grade analysis for households segmentation based on energy usage patterns," in *Proceedings of the 2017 IEEE International Conference on INnovations in Intelligent SysTems and Applications (INISTA '17)*, pp. 168–173, July 2017.

[23] S. Saraçli, N. Doğan, and I. Doğan, "Comparison of hierarchical cluster analysis methods by cophenetic correlation," *Journal of Inequalities and Applications*, vol. 1, p. 203, 2013.

[24] T. Zabkowski, K. Gajowniczek, and R. Szupiluk, "Grade analysis for energy usage patterns segmentation based on smart meter data," in *Proceedings of the 2nd IEEE International Conference on Cybernetics (CYBCONF '15)*, pp. 234–239, June 2015.

[25] F. Javed, N. Arshad, F. Wallin, I. Vassileva, and E. Dahlquist, "Forecasting for demand response in smart grids: an analysis on use of anthropologic and structural data and short term multiple loads forecasting," *Applied Energy*, vol. 96, pp. 150–160, 2012.

[26] U. Dent, U. Aickelin, and T. Rodden, "The application of a data mining framework to energy usage profiling in domestic residences using UK data," in *Proceedings of the Research Students Conference on Buildings Dont Use Energy, People Do? Domestic Energy Use and CO2 Emissions in Existing Dwellings*, pp. 1–10, Bath, UK, 2011.

[27] Y. G. Yohanis, J. D. Mondol, A. Wright, and B. Norton, "Real-life energy use in the UK: how occupancy and dwelling characteristics affect domestic electricity use," *Energy and Buildings*, vol. 40, no. 6, pp. 1053–1059, 2008.

[28] H. K. Alfares and M. Nazeeruddin, "Electric load forecasting: literature survey and classification of methods," *International Journal of Systems Science*, vol. 33, no. 1, pp. 23–34, 2002.

[29] G. E. P. Box, G. M. Jenkins, and G. C. Reinsel, *Time Series Analysis: Forecasting and Control*, Prentice Hall, Englewood Cliffs, NJ, USA, 3rd edition, 1994.

[30] Z. Aung, J. Williams, A. Sanchez, M. Toukhy, and S. Herrero, "Towards Accurate Electricity Load Forecasting in Smart-Grids," in *Proceedings of the The 4th International Conference on Advances in Databases, Knowledge and Data Applications, DBKDA, SaintGilles*, pp. 51–57, Reunion Island, France, 2012.

[31] K. Amasyali and N. El-Gohary, "Building lighting energy consumption prediction for supporting energy data analytics," *Procedia Engineering*, vol. 145, pp. 511–517, 2016.

[32] G. Mitchell, S. Bahadoorsingh, N. Ramsamooj, and C. Sharma, "A comparison of artificial neural networks and support vector machines for short-term load forecasting using various load types," in *Proceedings of the 2017 IEEE Manchester PowerTech (Powertech '17)*, pp. 1–4, IEEE, Manchester, UK, June 2017.

[33] W. Kong, Z. Y. Dong, D. J. Hill, F. Luo, and Y. Xu, "Short-term residential load forecasting based on resident behaviour learning," *IEEE Transactions on Power Systems*, vol. 33, no. 1, pp. 1087-1088, 2018.

[34] K. Gajowniczek and T. Zabkowski, "Short term electricity forecasting based on user behavior from individual smart meter data," *Journal of Intelligent & Fuzzy Systems: Applications in Engineering and Technology*, vol. 30, no. 1, pp. 223–234, 2016.

[35] M. Huber, M. Lechner, and C. Wunsch, "The performance of estimators based on the propensity score," *Journal of Econometrics*, vol. 175, no. 1, pp. 1–21, 2013.

[36] K. Gajowniczek and T. Zabkowski, "Two-stage electricity demand modeling using machine learning algorithms," *Energies*, vol. 10, no. 10, article 1547, 2017.

[37] N. Andrei, "An adaptive scaled BFGS method for unconstrained optimization," *Numerical Algorithms*, vol. 77, no. 2, pp. 413–432, 2018.

[38] B. Nguyen, C. Morell, and B. De Baets, "Large-scale distance metric learning for k-nearest neighbors regression," *Neurocomputing*, vol. 214, pp. 805–814, 2016.

[39] R. A. Berk, "Classification and regression trees (CART)," in *Statistical Learning from A Regression Perspective*, pp. 129–186, Springer, 2016.

[40] J. Huo, T. Shi, and J. Chang, "Comparison of Random Forest and SVM for electrical short-Term load forecast with different data sources," in *Proceedings of the 7th IEEE International Conference on Software Engineering and Service Science (ICSESS '16)*, pp. 1077–1080, IEEE, August 2016.

[41] F. Davò, M. T. Vespucci, A. Gelmini, P. Grisi, and D. Ronzio, "Forecasting Italian electricity market prices using a Neural Network and a Support Vector Regression," in *Proceedings of the 2016 AEIT International Annual Conference (AEIT '16)*, pp. 1–16, IEEE, October 2016.

[42] K. Muandet, K. Fukumizu, B. Sriperumbudur, and B. Schölkopf, "Kernel mean embedding of distributions: A review and beyond," *Foundations and Trends in Machine Learning*, vol. 10, no. 1-2, pp. 1–141, 2017.

[43] R. J. Hyndman and Y. Khandakar, "Automatic time series forecasting: the forecast package for R," *Journal of Statistical Software* , vol. 27, no. 3, pp. 1–22, 2008.

[44] J. Ling, D. Lee, A. Sim et al., *Comparison of Clustering Techniques for Residential Energy Behavior using Smart Meter Data*, AAAI Workshops & Artificial Intelligence for Smart Grids and Buildings, San Francisco, Calif, USA, 2017.

Hindawi
Complexity
Volume 2018, Article ID 4012740, 14 pages
https://doi.org/10.1155/2018/4012740

Research Article

Dealing with Demand in Electric Grids with an Adaptive Consumption Management Platform

Diego M. Jiménez-Bravo,[1] **Juan F. De Paz**,[1] **Gabriel Villarrubia**,[1] **and Javier Bajo**[2]

[1]*Computer and Automation Department, University of Salamanca, Salamanca, Spain*
[2]*Artificial Intelligence Department, Polytechnic University of Madrid, Madrid, Spain*

Correspondence should be addressed to Diego M. Jiménez-Bravo; dmjimenez@usal.es

Received 24 September 2017; Revised 17 December 2017; Accepted 14 January 2018; Published 25 March 2018

Academic Editor: João Soares

The control of consumption in homes and workplaces is an increasingly important aspect if we consider the growing popularity of smart cities, the increasing use of renewable energies, and the policies of the European Union on using energy in an efficient and clean way. These factors make it necessary to have a system that is capable of predicting what devices are connected to an electrical network. For demand management, the system must also be able to control the power supply to these devices. To this end, we propose the use of a multiagent system that includes agents with advanced reasoning and learning capacities. More specifically, the agents incorporate a case-based reasoning system and machine learning techniques. Besides, the multiagent system includes agents that are specialized in the management of the data acquired and the electrical devices. The aim is to adjust the consumption of electricity in networks to the electrical demand, and this will be done by acting automatically on the detected devices. The proposed system provides promising results; it is capable of predicting what devices are connected to the power grid at a high success rate. The accuracy of the system makes it possible to act according to the device preferences established in the system. This allows for adjusting the consumption to the current demand situation, without the risk of important home appliances being switched off.

1. Introduction

As De Baets et al. [1] report in their paper, European Union member countries made an agreement in October of 2014 in which they set a number of goals for 2030. These goals are related to reducing pollution and obtaining cleaner and more efficient energy. This means that the use of renewable energies should increase in the next years. However, such changes also imply certain challenges; one of them is the adjustment of electrical production to demand. That is why consumption management plays a very crucial role in electric networks and it is becoming an important facet in Smart Grids. The sources of production are very diverse and they are distributed geographically, so it is more complicated to keep an electric network in stable conditions. For these reasons, it is necessary to create a system that will allow for managing consumption automatically, adjusting the generated energy to the requirements of each moment, since the management of short-term production is not feasible. The need for an automatic consumption management system has been reflected in the variety of devices that have been proposed in recent years for the analysis of consumption in electrical networks. We live in an information age where data is highly valuable because of the knowledge that can be extracted from it. For example, a system can obtain the consumption data of a house and analyze it in order to detect behaviour patterns and identify the devices that are connected to that house's electric network. To be able to manage the data of a measurement device a multiagent system has to be implemented.

Up until now several studies addressing this topic have been published. They all focus on identifying the devices connected to an electric network by employing a range of techniques based on NonIntrusive Load Monitoring (NILM); the majority of them are improved versions of standard algorithms. While NILM techniques are used in other works, we use a variety of measuring devices in our proposal in order to extract the consumption data from each line connected to an electric network, and this simplifies the identification of electrical appliances and optimizes the system's performance.

For this reason, we propose a distributed system which will be able to connect with the different measurement systems and obtain the consumption data read by them. By analyzing and extracting important characteristics from the data provided by these measurement systems, the system will be capable of identifying the devices or appliances connected to the electric network. Simultaneously, the system will be able to act on each of the lines connected to the measuring devices.

Furthermore, the proposed system makes use of multiagent technology which provides the distributed architecture with agents who carry out different and specific tasks in the final system. The multiagent system allows creating autonomous entities that work in a coordinated way, providing features such as mobility, dynamic behaviour (the system is capable of creating agents dynamically; this feature makes it possible to modify the goals and behaviour of the system), federation of services, and high-level communication through the transparent management of message queues. This architecture makes it possible to perform different tasks in a coordinated way, improving the system's learning and adaptation capacities. There are numerous agents with different roles; one of the agents, for example, is in charge of communicating with the measuring devices and the acquirement of measurement data. There is also an agent that extracts the home appliances' activation periods from the data obtained by a different agent and another that extracts the main characteristics of activation periods. In addition, one of the agents identifies the home appliances that are connected to the gird. Finally, we have an agent who is responsible for acting on the different lines connected to the measuring systems. These agents act on smart-meter lines or smart plugs in order to interrupt the power supply to these devices; in this way demand can be managed.

The system will identify home appliances by using different supervised machine learning algorithms. To verify the proposal, the system will use several algorithms based on decision rules, decision trees, neural networks, and algorithms based on the Bayes theorem and case-based learning. These methods are tested with a dataset that has been created for the purposes of this study. In order to create the dataset, the principles of the fingerprint algorithm were followed. Fingerprint methods make use of the distances between the maximus of a sound since at these points the sound is purer. When creating the dataset, the maximus of activation periods have been used to extract some of their characteristics and to identify the different algorithms. This allows us to obtain knowledge about the behaviour of the devices. This knowledge is stored on a database in order to subsequently apply advanced reasoning and learning techniques to it.

The article is divided into the following sections. In the background section, we describe some of the studies related to this line of research. The proposed system is outlined in the architecture section. The case study section focuses on particular situations that have been considered during the research. In the results section, the system's performance will be described and analyzed. The last section draws conclusions on the different technological solutions that we had considered for our system; furthermore we discuss future lines of work related to the proposed study.

2. Background

This section is focused on literature that is related to the aims of the present research. All the related works make use of techniques based on NonIntrusive Load Monitoring, described by Hart [12] and by Zoha et al. [13]. Below, the most noteworthy works have been described.

In the year 2014, Belley et al. [2] had already used a smart meter to obtain a house's consumption data. The authors made use of the activation periods of appliances that were in the house. In this study, the authors used the equality between the cases stored in the database and the appliances they analyzed. This methodology entails a high computational cost due to the process of comparing an element with each of the instances stored in the database. In [3] the same authors proposed an improved version of their system using the same algorithm for the identification of devices; however, in the new proposal the system was capable of identifying erratic behaviours related to possible cognitive problems experienced by the users.

Other authors like Lin et al. [4] proposed a new strategy for NILM systems. They suggested that devices should be identified using quadratic programming rules. The results of this research proved that this methodology is effective. The work of De Baets et al. [1] proposed two new algorithms applied to NILM techniques for the identification of devices in electronic networks. The two new methods were as follows: a modified version of the chi-squared goodness-of-fit test and an event detection method based on cepstrum smoothing. Besides, the authors explained that both methods can be optimized using surrogate-based optimization.

Other lines of research focus on improving NILM techniques. The researchers Tang et al. [5] suggested that the state of the building must be taken into account; it can be either occupied or unoccupied. Thus, a system that is capable of considering these two situations will not operate when there are no people in the building. On the contrary, when the building is occupied the system will decide to identify the connected devices in the household. This methodology allows for improving the accuracy of classifiers and reducing computational costs at times when the building is not occupied.

The study conducted by Brown et al. [6] also considers the state of the building. In this work, ultrawideband radar technology was used to determine whether a building is occupied or not. This was done by comparing its results with the data that the system receives from the power monitoring system. Apart from establishing the state of the building, this technique also detects the devices connected to the grid. In addition, this methodology examines the users' behaviour.

The research conducted by Liang et al. in [7] is focused on the construction of a new platform that would provide a better understanding of electrical consumption patterns and that would successfully identify the devices connected to the electrical network. For this purpose, the different activation periods of the devices were analyzed and a number of mathematical programming and pattern recognition techniques were applied to unbundle the load.

A similar task is tackled in the study presented by Lee et al. [8]. In this case, the article leverages already existing

methods for measuring and representing the characteristics of electricity consumption. Moreover, the article considers signal processing as a method of identifying the devices connected to the network by means of disaggregation and filtering techniques.

There are also researches that focus on slightly different aspects, such as electrical demand forecasts for a few days ahead. Examples of works that address this issue are Chen et al. [9] and Chen and Tan [10]. In the first work, daily demand is predicted for each hour using a hybrid clustering algorithm. The second one fulfils the same function but it uses a hybrid algorithm based on support vector regression. Both techniques render great results.

Finally, it is important to list an open source tool that implements several NILM techniques. This tool is called NILMTK (NonIntrusive Load Monitoring ToolKit). It has been developed by Batra et al. [11]. This tool is designed to employ several techniques and shows the results rendered by each of them. It also includes public datasets.

The studies presented above make use of NILM techniques or use a new method to identify the devices connected to an electric network. However, none of them consider the use of smart devices which will be present in our future homes and buildings, and these can measure the consumption of home appliances. In our article, we also propose a new method for the identification of electronic appliances connected to the grid. This new technique makes use of a combination of characteristics of the fingerprint algorithm and NILM techniques. Hence, this proposal sets forth a new methodology for the analysis of data that allows for identifying the devices connected to electric networks. In conclusion, this section summarizes the novel aspects of the work and the main contributions of the work: (a) a management platform that allows for adapting consumption in a network. (b) The identification of household appliances using NILM techniques and their integration with fingerprint algorithm principles. (c) The use of smart meters and relevant communication protocols for obtaining consumption data and switch household appliances on/off in order to adapt consumption. In order to clearly show the features of this proposal, we include a comparison between the proposal and the state of the art (Table 1).

3. Proposed Architecture

The adaptive consumption management system for satisfying demand in electrical networks has to work with different measuring devices in order to read information from them and act accordingly. Information is extracted for the purpose of processing and extracting the knowledge contained in it. The system needs this knowledge in order to identify the household appliances connected to the electric network.

The system works according to the principles of NILM techniques. The NonIntrusive Load Monitoring or NILM systems use a technique that disintegrates the data extracted from meters. Meters are located outside of homes; this is where the name nonintrusive comes form. So, according to a definition proposed by Hart [12], the consumption of a network is composed of the consumption of all the devices connected to it; therefore the goal is to identify as many devices as possible.

In mathematical terms, we could say that, in an instant of time t, the energy is consumed by all the devices n_i, connected to an electric network N in the instant t, as formulated by Zoha et al. [13]:

$$N(t) = n_1(t) + n_2(t) + \cdots + n_n(t). \quad (1)$$

The appliances that are connected to a network are identified by their activation period. Usually, every device has a singular activation period that makes it distinguishable from the rest. So, it can be said that these activation periods are like a signature or a fingerprint; a similar idea is proposed in the work of Haitsma and Kalker [14].

However, we should stress that not all devices behave in the same way; as explained by Kaustav in [15] this makes their identification and distinction easier. Some groups of appliances have a more continuous performance in time than others. Other devices can only have two possible states—on or off. Some appliances, such as a microwave, have a more variable behaviour; this is related to their program or the role they are performing. However, there are also many appliances that have almost infinite behavioural patterns; this depends on the role they perform and on a specific moment in time, such as an LED printer.

Commonly, systems based on NILM techniques can be divided into three successive stages, consisting of three modules: a data acquisition module, a feature extraction module, and finally a learning module. The NILM process is illustrated in Figure 1.

(i) *Data Acquisition.* In this stage, the system obtains the data that allow identifying the different behaviours in an electric network; a meter system is used for this purpose.

(ii) *Feature Extraction.* In this module, the system extracts the connected devices and differentiates between active and inactive devices. That is, it is capable of detecting and extracting the activation periods of household appliances. Diverse techniques are used to extract activation periods; one of them is event-based extraction. These so-called events are the on/off transactions of the different devices. On the contrary, extraction that is not based on events uses sample times to determine whether an appliance is active.

(iii) *System Learning.* This stage consists of training and learning. Learning can be supervised or unsupervised. The systems with supervised learning need a labelled dataset in order to learn and identify devices correctly. Moreover, these systems can also be identified as on-line or off-line systems.

Consequently, to achieve the aim of this work, the system is operated by the different agents. Agents carry out all the subprocesses in the global system. The agents that form part of the system can be divided into two large groups, as shown in Figure 2. These two groups are environmental agents and processing agents.

Table 1: Comparison between the proposal and previous work.

	Belley et al. [2]	Belley et al. [3]	Lin et al. [4]	De Baets et al. [1]	Tang et al. [5]	Brown et al. [6]	Liang et al. [7]	Lee et al. [8]	Chen et al. [9]	Chen and Tan [10]	Batra et al. [11]	Our proposal
Use NILM techniques								X			X	X
New method	X		X	X			X		X	X		X
Improve a method		X										
Consider the state of the building					X	X						
Consumption prediction									X	X		
Toolkit											X	
Uses smart devices												X
Adaptive consumption												X

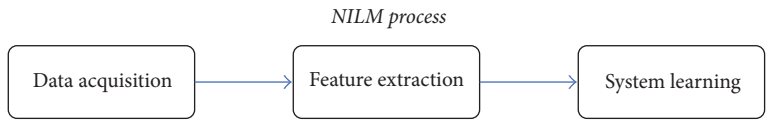

Figure 1: NILM process.

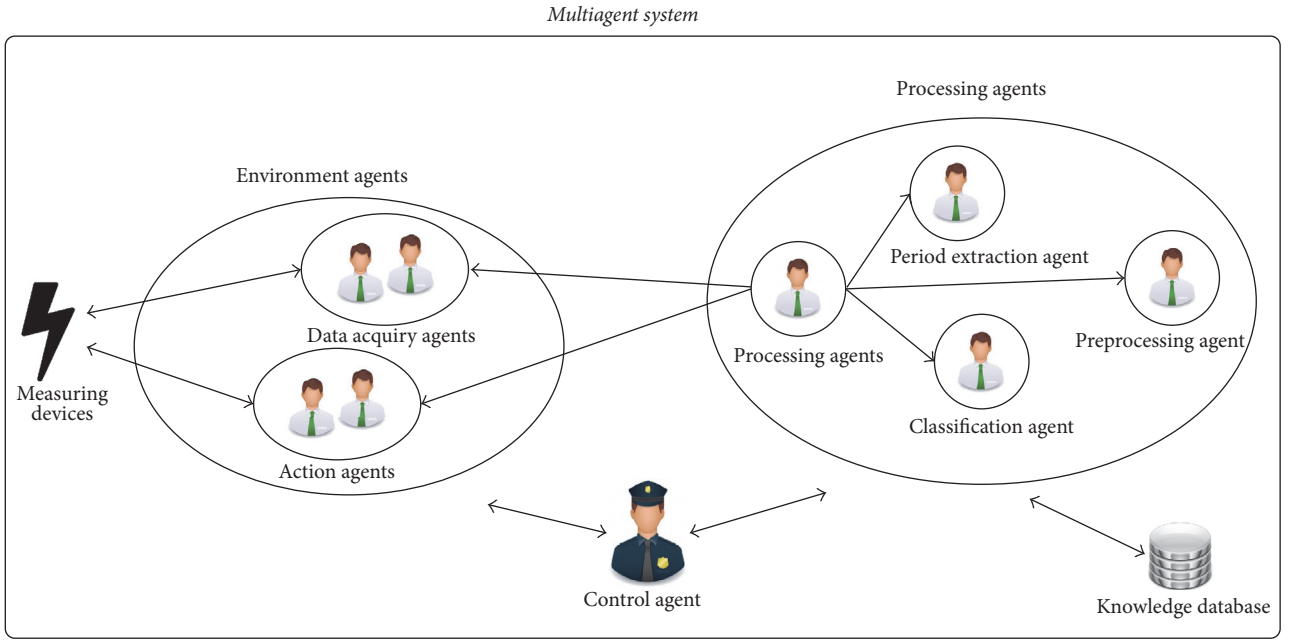

Figure 2: Proposed multiagent system architecture.

(i) *Environmental Agents.* These agents communicate with the measuring systems that are connected to the global system. Their task is to obtain data and work with the measuring system. The agents that acquire data have to communicate with the meters through the required protocols, in order to obtain them, whereas the agents acting on the meters are responsible for turning on/off the different lines of the measuring devices. By acting on the smart meter and the smart plug it is possible to manage demand according to requirements. For efficient demand management, it is necessary to identify the connected devices beforehand. This identification is done in the processing agents organization. In order to determine the order of priority in which these devices have to be switched off, the agent has a prioritized list of how important a device is for daily use and it proceeds to the interruption of supply according to these preferences, until the demand is adjusted.

(ii) *Processing Agents.* They are in charge of the internal processing of information. They carry out a number of actions, such as the pretreatment of data. They are responsible for all the important actions in the system. The processing agent controls the rest of the agents in the same group. The period extraction agent extracts activation periods from the raw data it receives. This agent will extract the consumption values of every activation period, in a way that there are as many groups with consumption values as there are activation periods. These activation periods are detected when the consumption changes in a considerable way. In Figure 3 we can see the agent will extract four activation periods. The preprocessing agent is in charge of extracting the necessary information for identifying the appliances. The extracted features are outlined below.

(a) Mean (m): this characteristic indicates the mean of the consumption values for each activation period; therefore it is the arithmetic mean of consumption of a device in its activation periods:

$$m = \frac{\sum_{t=0}^{n} w(t)}{n}, \tag{2}$$

where $w(t)$ is the set of consumption values in the instant of time t and n indicates the total time instants that compound the activation period.

(b) Maximum (m_x): this value indicates the device's highest consumption value during the activation period:

$$m_x = \max W, \tag{3}$$

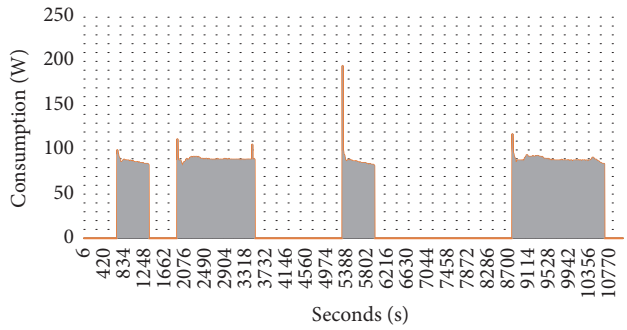

Figure 3: Line connected to a fridge.

where W is the set of consumption values of the activation period.

(c) Minimum (m_n): this feature indicates the minimum consumption value in the activation period of an appliance:

$$m_n = \min W, \tag{4}$$

where W is the set of consumption values of the activation period.

(d) First step (s_1): this value indicates the difference between the first value of the activation period ($w(0)$) and the maximum value (m_x). This "leap" is taken into account:

$$s_1 = m_x - w(0). \tag{5}$$

(e) Second step (s_2): in this case, the value represents the difference between the maximum value of consumption (m_x) and the last value of the period ($w(n)$), so that the second "leap" is also taken into account:

$$s_2 = m_x - w(n). \tag{6}$$

(f) Time (T): it refers to the time during which the device has been active, that is, switched on:

$$T = t(n) - t(0), \tag{7}$$

where $t(n)$ is the final instant of the activation period and $t(0)$ is the initial instant.

The classification agent is in charge of determining what kind of devices it is dealing with. This agent is able to predict what kind of a device exhibits the determined features. In this case, to identify the appliance, case-based reasoning is applied. There are several algorithms that agents can execute (some of them are defined in [16–20]); the process that is followed to determine which of them renders better results will be described in the Results.

Once we obtain a model that is capable of identifying home appliances with a certain level of accuracy, this model will be included in the case-based reasoning system. Every one of those cases will contain all of the features explained before. So, the cases will have the following structure:

$$C = \{m, m_x, m_n, s_1, s_2, T, class\}. \tag{8}$$

The nomenclature of a case is composed of the following values: mean, maximum, minimum, first step, second step, time, and the tag *class* which refers to the device that is represented by the characteristics of C. Thus, the CBR (case-based reasoning) will go through a phase in which it will recover the composed model. The CBR also has a reutilization phase where the recovered model will be used to classify new cases. If the model correctly classifies a new case in the review stage, we move on to the learning stage in which the new case is added to the database. If the user decides it has been incorrectly classified, the model is reconstructed taking into account the new instance added to the database.

(i) Control agent: it is in charge of monitoring the rest of the agents in the system that are found in any of the groups described previously.

The agents from different groups communicate with each other in order to achieve a common goal in the system. This communication between agents is illustrated in Figure 2.

As explained before, the accuracy of several machine learning methods in the identification of appliances was tested. These methods are data mining algorithms based on decision rules, decision trees, case-based learning, neural networks, and the Bayes theorem.

These algorithms can be combined with the fingerprint algorithm for the identification of home appliances. The fingerprint algorithm is used to identify music/songs by their sound wave. Wang [21] and Haitsma and Kalker [14] talk about this in their works. This technique is based on the calculation of hidden Markov models; however the main idea of this technique is the use of distances between the maxims of a sound, since at these points the sound is purer and there is less ambient noise. By finding maximum values and calculating the distances between them, the algorithm can compare these values with the ones stored in a database in order to identify a song; the system then provides the user with an answer containing all the information on the predicted song.

In this way, the relative sound wave maximums allow the algorithm to form a single fingerprint that would be contrasted with those stored in the system database. This algorithm can therefore be used to identify the appliances that are connected to a network once the periods of activation of the consumption network are extracted. The idea is quite similar; the maximums of these activation periods are used to identify the device. However, there is a possibility that difficulties occur in the extraction of relative maxims that contain information; this is because some devices have a continuous or constant activation. Other devices have a variable performance which is what makes them less predictable than others. All this suggests that the task of collating those "fingerprints" with records in the database would be complicated. We therefore have to study and analyze whether using the fingerprint algorithm is practical for this study.

4. Case Studies

For the case study consumption data from different buildings and different users and therefore from different lines of several electric networks were obtained.

Nowadays, there is a great variety of tools that allow measuring the amount of consumed energy in a particular electric network or by a specific appliance that is connected to that network.

Before the study of these technologies, it is important to clarify how they will be integrated in the intelligent system. The first aspect to consider is that this measuring system must offer information in real time; that is to say, the proposed system must be able to communicate with the measuring devices using some kind of protocol that establishes a connection between them. This will allow the intelligent system to communicate with the measuring system, extract information from it, and send it at specific moments.

The intelligent system must be able to manage the information it receives, and this information must regard the consumption of the electric grid or on the consumption of a particular electronic device. This is very important since the extraction of information is necessary for identifying the connected electronic device(s).

Another important feature that this intelligent system must possess is the ability to turn on/off the different devices connected to an electrical grid. Considering the total amount of consumption in a network, at times it may be advisable to turn off devices that are not being used but that continue to consume electricity. That is, the intelligent system must be able to act on the devices using the required communication protocol.

The following measuring and/or actuator devices make communication with the system possible thanks to specialized agents developed for each of them.

(i) *Smart Meter.* Intelligent meters or smart meters are used to measure consumption levels in a home, but in a more detailed and precise way than a traditional electric meter. In addition, these types of counters are capable of communicating the data that they read through some type of a protocol (usually a standard protocol) and in this way consumption can be monitored at all times. If necessary they can interrupt the power supply from a number of lines without interrupting electricity provided by the rest of the lines. This feature allows for the automatic management of demand, suited to the energy needs.

In this study, the German-made "EMH LZQJ XC" smart meter has been used. This device is manufactured by the "EMH metering" company. This smart meter has all of the functions that have been described in the previous paragraph and for this reason it can easily be integrated with any intelligent system. In Figure 4, we can see one particular model.

This model, in particular, communicates through a protocol that uses "TCP/IP" type connections. So, the information stored and managed by this meter can be accessed remotely. It is common for these meters to use standard communication protocols, and specifically the presented model uses the IEC 62056 protocol. Moreover, this smart-meter model has already been installed in many homes in Germany.

Figure 4: Smart-meter LZQJ XC.

(ii) *Smart Plugs.* Smart plugs can be plugged into a standard wall socket and the consumption of any electronic device that is plugged into it can be controlled. Figure 5 shows an example of a smart plug.

These devices allow controlling consumption remotely and in real time. We can operate these devices either through the official developer applications or through third-party APIs that allow establishing a connection with smart plugs.

In this way, smart plugs allow users to obtain consumption data remotely and in real time. It is essential for the intelligent system proposed in this article to be provided with the necessary information. It also allows acting on the devices connected to them, allowing the intelligent system to switch them off or on when necessary or convenient.

With these devices, the necessary information can be extracted and consumption data can be obtained for different electrical devices. To carry out this study ten different home appliances have been used; we have extracted sufficient samples from them to form a dataset. This dataset has been used to test supervised machine learning algorithms and helped us create a classification model that will enable us to identify the behaviour of future appliances. The following devices have been selected to validate the proposed system: a refrigerator, a water pump, a television, a dishwasher, an electric gas heater, a washing machine, a kettle, a freezer, a microwave, and an LED printer. Figure 6 shows an example of the distribution of different devices in a house.

The activation periods of some of these appliances are illustrated on the graphs found in the appendix, where it can be seen that in all cases the appliances have waveform characteristics. Once the characteristics of each activation period are extracted, the identification of devices is, a priori, performed easily. However, given that the behaviour of some of the appliances varies depending on their use over time, identifying them may be more complicated.

Figure 5: Edimax smart plug.

5. Results

This section will analyze the function of the agent organizations illustrated in Figure 2. Furthermore, it will examine the architecture's capability to acquire data from the devices and manage demand. Also, it will evaluate the performance of the processing organization in identifying devices connected to smart plugs. This automatic identification performed by the processing organization is necessary due to the dynamic variations in smart plugs.

The first step is the monitoring and control of the actuators. Firstly, in order to obtain consumption data, we must communicate with the different measurement systems that provide it. To do this, it is necessary to establish a connection with the meters through the specific protocols belonging to each of the meters. In Figure 7, you can see an example of how communication is established with the smart meter to obtain real-time information on energy consumption. Figure 8 shows a fragment of the response to the request for real-time consumption data. The real-time consumption information is located in row seven. Relevant data is then extracted from this information and it is used by the system.

The system uses the same communication protocol to manage the smart meter (Figure 7), thus communication allows for both, the acquirement of data and its management. This scheme is followed in order to reduce energy consumption whenever this is necessary, by acting on the different lines.

The second step is the evaluation of the processing organization. This organization includes the Automatic Device Identification System which uses an algorithm to classify different measuring devices. To choose the most accurate classifier, several supervised machine learning algorithms have been tested and their performance was compared. The following classifiers were used: RIPPER algorithm, PART, C4.5, RandomForest, RandomTree, REPTree, k-NN, KStart, Bayesian networks, and neural networks. These algorithms are provided by the machine learning library Weka. Different databases were used when comparing the algorithms, each database varied in the number of classes and each had one hundred instances per class. Tests have been performed with datasets of four, seven, and ten classes, respectively. Each of the classes is associated with a type of appliance, so that the instances belonging to the same class belong to different models of the same appliance. In order to evaluate the functioning of the identification system, the classifiers were included in the case-based reasoning system's reuse stage and the performance of each of them was analyzed in order to assess the effectiveness of the fingerprint algorithm in the detection of household appliances. After verifying the different algorithms and their classification accuracy, the final system makes use of a dataset of ten classes and one thousand instances, one hundred for each of the classes.

The created dataset has the same characteristics as those described in the architecture section. At the time of tests and experiments, this dataset will help to determine which algorithms offer better results and are the most suitable for the device identification system in a power grid.

In this part of the article we are going to describe the process that we followed to verify and create the final model. Initially a dataset was created, and it contained a total of 400 instances divided among four classes, each containing 100 instances. Therefore, the four classes in the dataset are balanced and represent four different appliances: a refrigerator, a water pump, a television, and a dishwasher. Tests were performed with this dataset, using the 10-fold cross validation method with each of the algorithms mentioned above.

Table 2 shows the results of the tests that were performed on the dataset.

As we can observe, all the proposed algorithms, with the exception of neural networks, offer excellent results. Moreover, the algorithms that work best are the algorithms whose behaviour is based on decision rules: rule algorithms and tree algorithms.

From these results, we can infer that all algorithms render very good results, but we wanted to see how these algorithms would behave if they had to identify more classes. So, three more appliances were introduced to the dataset: a washing machine, a kettle, and a gas heater. For each of these devices 100 new instances were introduced.

Again, we submitted the algorithms to a series of tests with the objective of seeing with what precision they classified the seven appliances. After validating the different models shown in Table 2, we could see that the algorithms that provided the best outcomes were those based on rules. Specifically, the RandomForest algorithm offered the best results and its validation is shown in Table 2, although this time with lower success rate, which is logical since the number of classes and instances has increased. However, if we look at the results of neural networks, their success rate has increased considerably in the second case, from around 0.89 to about 0.925. The improvement in the performance of this algorithm can be caused by a greater number of instances and classes and this leads the weights and the bias assigned to each of the simple neurons to adjust better to the characteristics of the problem. Furthermore, we decided to check if by adding three more appliances—a freezer, a microwave, and an LED printer—the neural network would exhibit further improvement. We also wanted to check if the accuracy of the rest of the classifiers

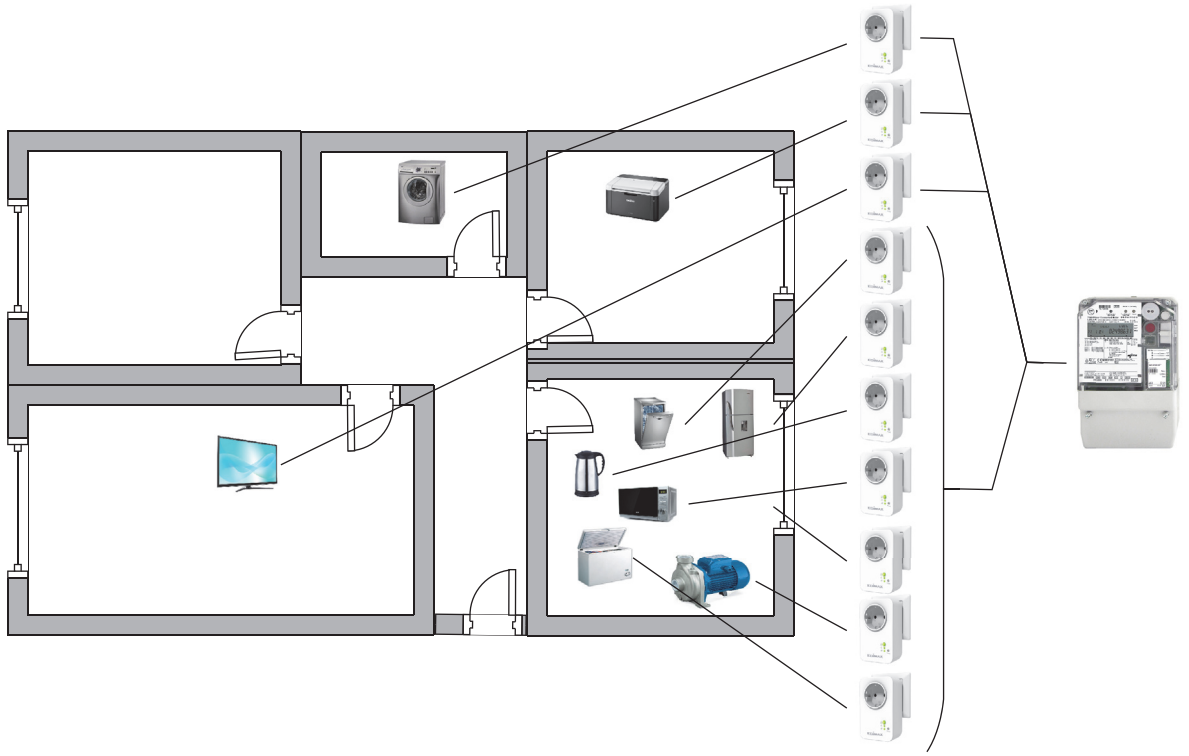

Figure 6: Distribution of the smart meter and smart plug in a house.

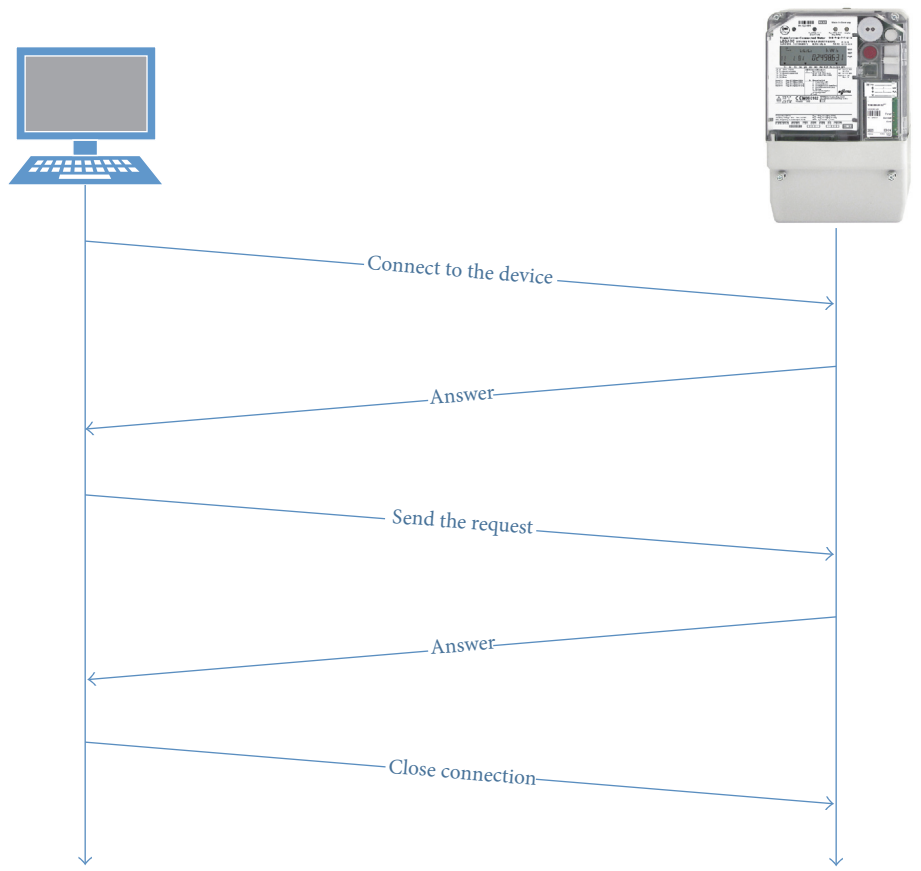

Figure 7: Smart-meter communication sequence.

Table 2: Datasets results.

Algorithm	Four classes' dataset		Seven classes' dataset		Ten classes' dataset	
	Accuracy	Kappa	Accuracy	Kappa	Accuracy	Kappa
RIPPER	0.9775	0.97	0.967143	0.9617	0.928	0.92
PART	0.9875	0.9833	0.975714	0.9717	0.959	0.9544
C4.5	0.9875	0.9833	0.974286	0.97	0.958	0.9533
RandomForest	0.9925	0.99	0.987143	0.985	0.98	0.9778
RandomTree	0.975	0.9667	0.977143	0.9733	0.96	0.9556
REPTree	0.99	0.9867	0.978571	0.975	0.945	0.9389
k-NN	0.97	0.96	0.967143	0.9617	0.952	0.9467
kStart	0.9575	0.9633	0.972857	0.9683	0.966	0.9622
Bayesian networks	0.9575	0.9434	0.94	0.93	0.927	0.9189
Neural networks	0.8875	0.85	0.924286	0.9117	0.853	0.8367

```
/EMH4\@01LZQJL0014F
F.F(00000000)
0.0.0(05439342)
0.0.9(1EMH0005439342)
0.9.1(0111147)
0.9.2(0170320)
1.2.1(000.188*kW)
1.2.2(000.000*kW)
1.2.3(000.000*kW)
1.6.1(0.102*kW)(0170314103000)
1.6.2(0.000*kW)(0000000000000)
1.6.3(0.000*kW)(0000000000000)
1.8.0(00016.722*kWh)
1.8.1(00016.722*kWh)
```

Figure 8: Smart-meter response.

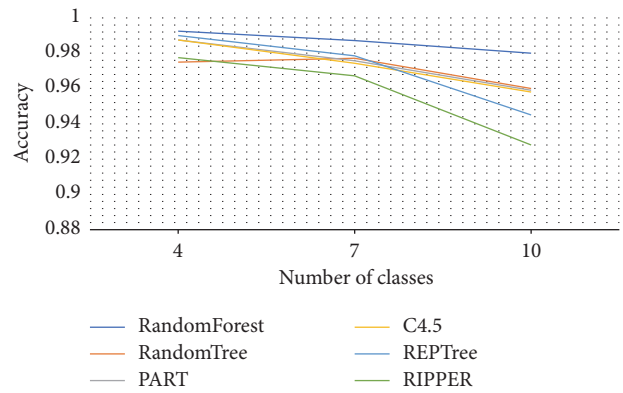

Figure 9: Results of rule-based classifiers in different test.

continued to decline as new appliances were introduced to the dataset. The results of this validation are shown in Table 2.

Interestingly, what we observe in Table 2 is that the accuracy of neural networks lowers significantly with three more classes. The performance of the other algorithms also decreased but to a lesser extent. For the third time, the algorithms that have the greatest accuracy are those that formulate decision rules, specifically RandomForest, which has an accuracy of 98%.

Good results are rendered by techniques that use decision rules and decision trees. We can therefore infer that this kind of algorithms performs well when determining what electronic devices are connected to an electrical network. For this reason, the graph in Figure 9 compares them on the basis of each of the experiments in which they had been tested.

From the graph, we can conclude that all these techniques have very similar behaviour; when the number of instances and classes increases the precision of the classifiers decreases. However, the RandomTree algorithm is an exception because its accuracy increased in the second test, which contained seven classes. Although RandomForest gave outstanding results, it is clear that all the rule-based classifiers performed very well and can be used to predict what devices are connected to an electrical network.

This statement could be confirmed with an ROC analysis. Various techniques can be used to carry out this analysis: the area under the ROC curve or the distance to the point (false positive rate, sensitivity) of each classifier to the point (0, 1); this technique is explained by Fawcett [22]. The second technique has been selected because it allows distinguishing the different classifiers better. In Figure 10, the points of each classifier were represented in a two-dimensional space.

Table 3: ROC analysis of the best algorithms.

Algorithm	Distance to point (0, 1)	Area under the ROC curve
RIPPER	0.0724	0.98
PART	0.0413	0.987
C4.5	0.0423	0.984
RandomForest	0.02	0.998
RandomTree	0.0402	0.978
REPTree	0.0553	0.988

At first sight, the results we see here for the tested algorithms are the same that we saw in the previous plots and tables. However, they are nearer to the point (0, 1). To verify this, we illustrate the results in Table 3, with the distance of each of the points, as shown in the graph in Figure 10, as well as the area under the ROC curve of each algorithm.

In these types of analyses, the distance is closest to 0 and the area under the ROC curve is the closest to 1. In cases where a classifier has these values, it could be considered

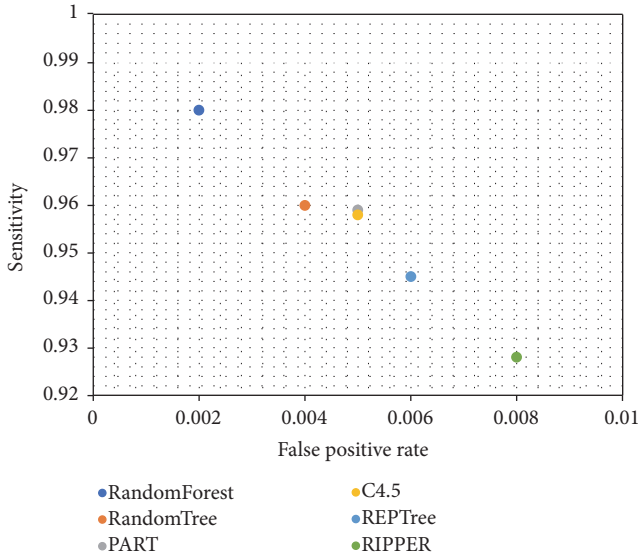

Figure 10: Rank positions (false positive rate, sensitivity) of classifiers.

Table 4: Attribute selection results.

Attribute	Info gain	Correlation
Mean	2.565	0.261
Maximum	2.333	0.248
Minimum	1.005	0.198
First step	2.21	0.289
Second step	2.197	0.289
Time	1.889	0.178

the most suitable classifier for that problem. In the analyzed algorithms, the two values obtained are very close to the objective values, so it can be said that the methods employed are very well coupled to the problem that arises.

However, there is no doubt that the success of these classifiers in the conducted experiments is largely due to the great quality of the dataset. The performance of instances and especially the selection of attributes from the dataset cause the difference in results when executing the machine learning algorithms, as we can see in the tables and the previous plot. For this reason, it would be worthwhile if we made an attribute selection with different techniques, in order to see which of these characteristics are more important when classifying a new instance.

To carry out these studies two different techniques have been used—the info gain and the correlation of attributes in connection with the class. Table 4 and Figure 11 show a comparison of the two techniques mentioned before. The results of these analyses have been normalized with the variable scaling formula, in order to make a clearer comparison between the results of the two techniques.

As can be seen in Figure 11, in the two techniques the most important characteristics that have to be considered in an algorithms' classification of instance are the mean, the maximum value, the first step, and the second one. The

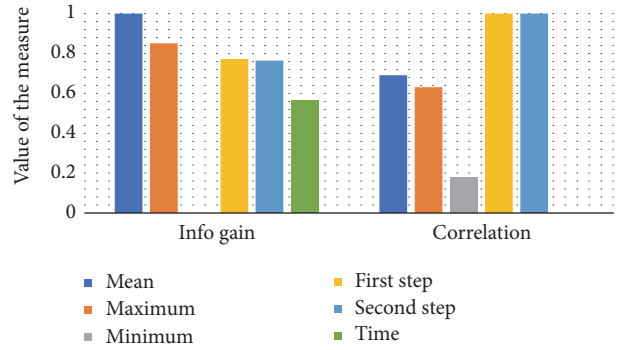

Figure 11: Results of attribute selection with normalized results.

minimum value and time are less important than the other attributes in the classifiers' classification task; however, they are the main reason for which the accuracy of the tested techniques is so high.

6. Conclusions

This work presented the developed adaptive consumption management system, capable of identifying devices connected to an electrical network. In cases where the production of energy is scarce or when excessive energy is being consumed, the user can choose to disconnect some of the devices that are not necessary, in homes, offices, and so forth.

The proposed system has a multiagent architecture, where different types of agents are in charge of carrying out different functions in the process. The agent system also includes the use of case-based reasoning systems.

Different techniques and methods have been studied in order to consider the possibility of implementing them in the proposed system. Above all, we examined the different machine learning techniques that were the most appropriate for the type of problem presented in this work. Specifically, the Results demonstrates that there is a variety of algorithms that offers a more satisfactory behaviour, and for this reason any of these techniques could be used in the proposed system.

Moreover, the work studied the performance of existing devices developed for measuring electrical networks, as well as the home appliances connected to the network itself. The system presented in this work has been developed to act and communicate with two types of devices—smart meters and smart plugs. Thus, the system can obtain data from each of them.

Accordingly, the objectives set forth in the Proposed Architecture have been achieved. The designed platform adapts the consumption of electricity in the networks by interacting with intelligent devices. The purpose of the proposed method is the extraction of knowledge from the electrical network, which allows us to obtain a network's consumption data. It employs NILM techniques to identify the connected household appliances. Subsequently, a method based on the principles of the fingerprint algorithm is used to form a dataset with the identified devices. This dataset allows obtaining excellent results in adapting the electrical

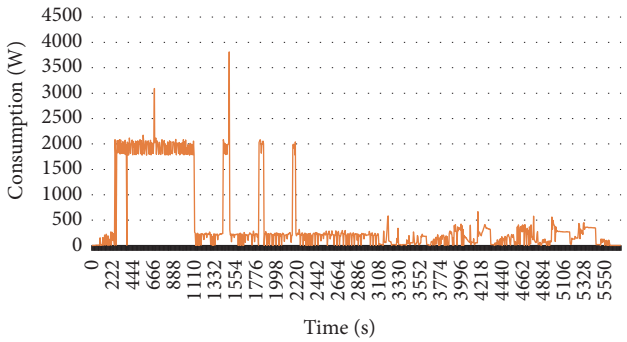

Figure 12: Washing machine activation period.

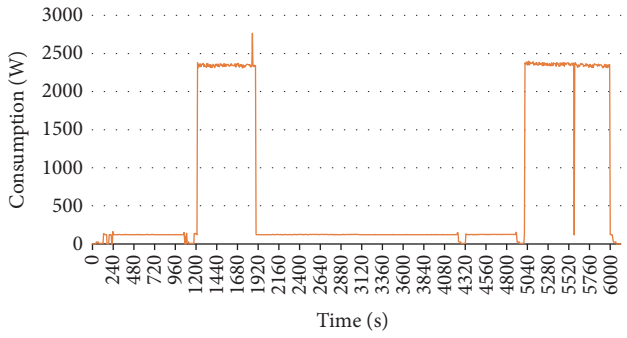

Figure 13: Dishwasher activation period.

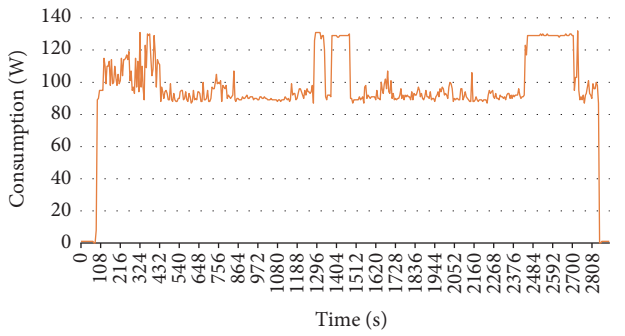

Figure 14: TV activation period.

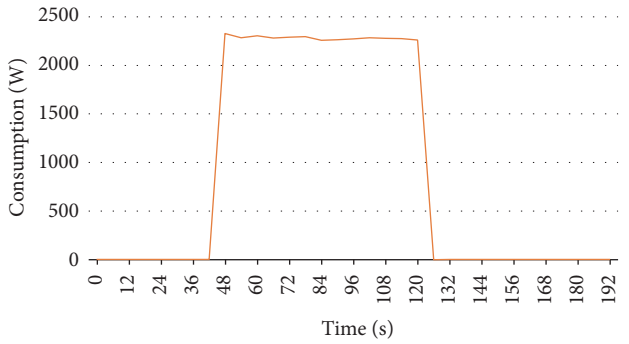

Figure 15: Kettle activation period.

consumption of the devices. Thus, the proposed platform uses a new method that leverages modern technologies for the control of the consumption in the network.

Making our system more effective is an important goal for the coming years. Therefore, future lines of research will include improving the system by adding more devices and appliances to it. This would allow identifying new devices and make the system more complete. The more the appliances in the system's database are, the more robust the system will be.

In addition, a new technique could be added for extracting the activation periods of the devices connected to the network. Some techniques allow withdrawing activation periods, as proposed by Serrà and Arcos [23]. Thus, the effectiveness of this type of techniques for the extraction of patterns in time series could also be verified in a future work.

Security is another aspect that certainly should be considered. The communications established between meters and the system connected to them could be provided with security. The reason for which this improvement is crucial is that transmitted information can be considered important and the privacy of users' data must be guaranteed in intelligent systems.

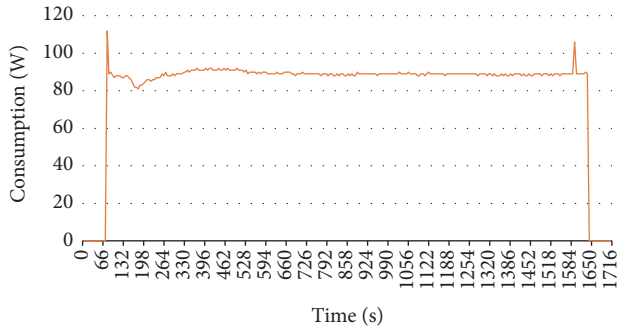

Figure 16: Fridge activation period.

Appendix

In this appendix we introduce the activation periods of the different devices used in the study (see Figures 12–21).

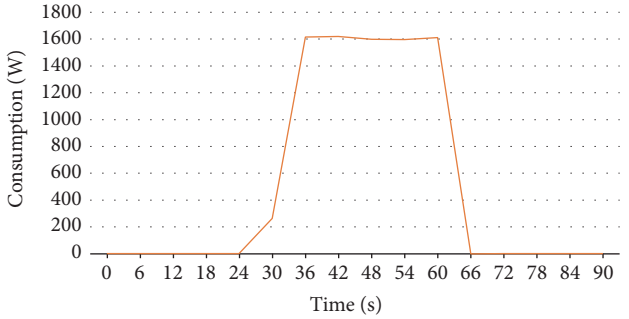

Figure 17: Microwave activation period.

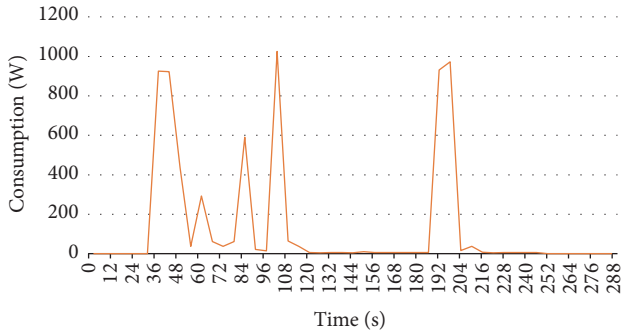

Figure 18: LED printer activation period.

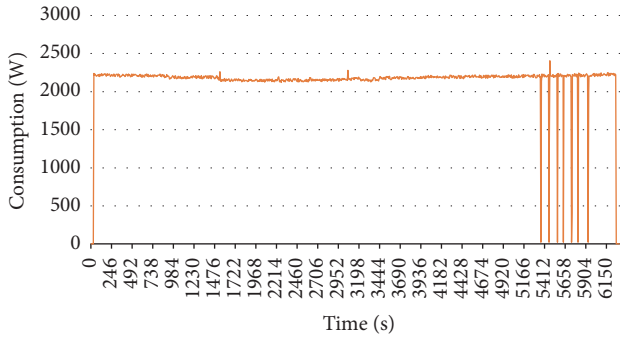

Figure 19: Electrical boiler activation period.

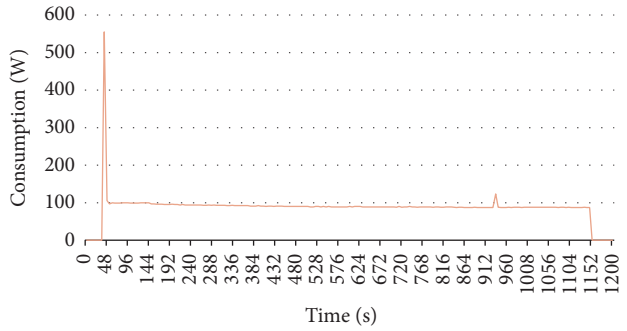

Figure 20: Freezer activation period.

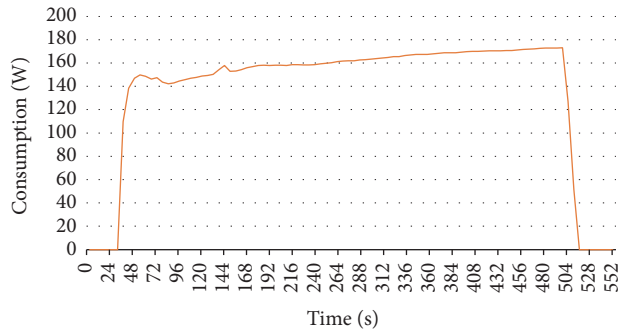

Figure 21: Water pump activation period.

Conflicts of Interest

The authors declare that they have no conflicts of interest.

Acknowledgments

This work has been supported by the European Commission H2020 MSCA-RISE-2014: Marie Skłodowska-Curie project DREAM-GO Enabling Demand Response for short and real-time Efficient And Market based smart Grid Operation—an intelligent and real-time simulation approach ref 641794.

References

[1] L. De Baets, J. Ruyssinck, C. Develder, T. Dhaene, and D. Deschrijver, "On the Bayesian optimization and robustness of event detection methods in NILM," *Energy and Buildings*, vol. 145, pp. 57–66, 2017.

[2] C. Belley, S. Gaboury, B. Bouchard, and A. Bouzouane, "An efficient and inexpensive method for activity recognition within a smart home based on load signatures of appliances," *Pervasive and Mobile Computing*, vol. 12, pp. 58–78, 2014.

[3] C. Belley, S. Gaboury, B. Bouchard, and A. Bouzouane, "Non-intrusive system for assistance and guidance in smart homes based on electrical devices identification," *Expert Systems with Applications*, vol. 42, no. 19, pp. 6552–6577, 2015.

[4] S. Lin, L. Zhao, F. Li, Q. Liu, D. Li, and Y. Fu, "A nonintrusive load identification method for residential applications based on quadratic programming," *Electric Power Systems Research*, vol. 133, pp. 241–248, 2016.

[5] G. Tang, Z. Ling, F. Li, D. Tang, and J. Tang, "Occupancy-aided energy disaggregation," *Computer Networks*, vol. 117, pp. 42–51, 2017.

[6] R. Brown, N. Ghavami, H.-U. Siddiqui, M. Adjrad, M. Ghavami, and S. Dudley, "Occupancy based household energy disaggregation using ultra wideband radar and electrical signature profiles," *Energy and Buildings*, vol. 141, pp. 134–141, 2017.

[7] J. Liang, S. K. K. Ng, G. Kendall, and J. W. M. Cheng, "Load signature studypart i: basic concept, structure, and methodology," *IEEE Transactions on Power Delivery*, vol. 25, no. 2, pp. 551–560, 2010.

[8] W. K. Lee, G. S. K. Fung, H. Y. Lam, F. H. Y. Chan, and M. Lucente, "Exploration on load signatures," in *International Conference on Electronics & Electrical Engineering*, 2004.

[9] Y. Chen, H. Tan, and U. Berardi, "Day-ahead prediction of hourly electric demand in non-stationary operated commercial buildings: A clustering-based hybrid approach," *Energy and Buildings*, vol. 148, pp. 228–237, 2017.

[10] Y. Chen and H. Tan, "Short-term prediction of electric demand in building sector via hybrid support vector regression," *Applied Energy*, vol. 204, pp. 1363–1374, 2017.

[11] N. Batra, J. Kelly, O. Parson et al., "NILMTK: an open source toolkit for non-intrusive load monitoring," in *Proceedings of the 5th ACM International Conference on Future Energy Systems (e-Energy '14)*, pp. 265–276, ACM, Cambridge, UK, June 2014.

[12] G. W. Hart, "Nonintrusive appliance load monitoring," *Proceedings of the IEEE*, vol. 80, no. 12, pp. 1870–1891, 1992.

[13] A. Zoha, A. Gluhak, M. A. Imran, and S. Rajasegarar, "Non-intrusive load monitoring approaches for disaggregated energy sensing: a survey," *Sensors*, vol. 12, no. 12, pp. 16838–16866, 2012.

[14] J. Haitsma and T. Kalker, "A highly robust audio fingerprinting system with an efficient search strategy," *Journal of New Music Research*, vol. 32, no. 2, pp. 211–221, 2003.

[15] B. Kaustav, "Classifcation techniques for non-intrusive load monitoring and prediction of residential loads," https://tel.archives-ouvertes.fr/tel-01162610, 2014.

[16] E. Frank and I. H. Witten, "Generating accurate rule sets without global optimization," in *Proceedings of the Fifteenth International Conference on Machine Learning*, pp. 144–151, 1998.

[17] L. Breiman, "Random forests," *Machine Learning*, vol. 45, no. 1, pp. 5–32, 2001.

[18] L. D. C, "Comparative analysis of random forest, rep tree and j48 classifiers for credit risk prediction," in *Proceedings of the International Conference on Communications, Computer and Information Science Technologies*, vol. ICCCMIT 20, pp. 30–36, 2015.

[19] I. H. Witten, E. Frank, and M. A. Hall, *Data Mining: Practical Machine Learning Tools and Techniques*, Morgan Kaufmann, 2011.

[20] J. G. Cleary and L. E. Trigg, "K*: an instance-based learner using an entropic distance measure," in *Proceedings of the 12th International Conference on Machine Learning*, pp. 108–114, 1995.

[21] A. Wang, "The Shazam music recognition service," *Communications of the ACM*, vol. 49, no. 8, pp. 44–48, 2006.

[22] T. Fawcett, "An introduction to ROC analysis," *Pattern Recognition Letters*, vol. 27, no. 8, pp. 861–874, 2006.

[23] J. Serrà and J. L. Arcos, "Particle swarm optimization for time series motif discovery," *Knowledge-Based Systems*, vol. 92, pp. 127–137, 2016.

Hindawi
Complexity
Volume 2018, Article ID 7154031, 12 pages
https://doi.org/10.1155/2018/7154031

Research Article

A Cosimulation Architecture for Power System, Communication, and Market in the Smart Grid

Markus Mirz,[1] **Lukas Razik**,[1] **Jan Dinkelbach**,[1] **Halil Alper Tokel**,[2] **Gholamreza Alirezaei**,[2] **Rudolf Mathar**,[2] **and Antonello Monti**[1]

[1]*Institute for Automation of Complex Power Systems, RWTH Aachen University, Aachen, Germany*
[2]*Institute for Theoretical Information Technology, RWTH Aachen University, Aachen, Germany*

Correspondence should be addressed to Markus Mirz; mmirz@eonerc.rwth-aachen.de

Received 24 November 2017; Accepted 30 January 2018; Published 28 February 2018

Academic Editor: João Soares

Smart grids evolve rapidly towards a system that includes components from different domains, which makes interdisciplinary modelling and analysis indispensable. In this paper, we present a cosimulation architecture for smart grids together with a comprehensive data model for the holistic representation of the power system, the communication network, and the energy market. Cosimulation is preferred over a monolithic approach since it allows leveraging the capabilities of existing, well-established domain-specific software. The challenges that arise in a multidomain smart grid cosimulation are identified for typical use cases through a discussion of the recent literature. Based on the identified requirements and use cases, a joint representation of the smart grid ecosystem is facilitated by a comprehensive data model. The proposed data model is then integrated in a software architecture, where the domain-specific simulators for the power grid, the communication network, and the market mechanisms are combined in a cosimulation framework. The details of the software architecture and its implementation are presented. Finally, the implemented framework is used for the cosimulation of a virtual power plant, where battery storages are controlled by a novel peak-shaving algorithm, and the battery storages and the market entity are interfaced through a communication network.

1. Introduction

The increase of distributed energy resources (DERs) in power systems and the resulting bidirectional power flows are driving changes in the associated communication infrastructure and market mechanisms. For instance, the ongoing extension of measuring infrastructure in lower voltage layers requires a concurrent deployment of a capable communication network in order to provide for a reliable communication among control centers, substations, and measurement devices. Hence, the planning of electrical grid operation and the underlying communication network should be considered simultaneously, in order to enable the analysis of the impact of interactions between the two domains as it is already shown in [1]. Meanwhile, new market models are developed to support customers taking a more active role in their exchange of power with the grid [2] in such a way that their behavior will also be taken into account in the grid operation [3]. For example, individual users can contribute to a more efficient operation of the grid by putting their battery storage at the disposal of the grid operators, which would require a communication network for the data exchange. Bearing this development in mind, it is interesting to include a market simulation in the analysis as well.

This integration of market mechanisms, the communication network, and the power system complicates studies on future power systems' behavior since a common modelling approach that encompasses the three domains has not been established yet and there are few tools that enable a joint simulation. The comprehensive data model and the cosimulation architecture presented in this work tackle these challenges, enabling the investigation of dynamic interactions between the electrical grid, communication network, and market. These interactions could be technical constraints to the grid that require actions on the market side, communication failures that affect the control loop between the grid and the market, and market decisions that change the behavior of a generation unit or energy consumers connected to the grid.

Therefore, we propose a data model based on the IEC Common Information Model (CIM) [4] that is able to describe an entire smart grid topology including communication and market entities. Besides, the proposed data model allows users to store the whole network topology with components from the three domains in a single well-defined data model, therefore hiding the complexity of the cosimulation from the users. Topology descriptions compliant with this data model can be processed by the presented cosimulation architecture. This architecture and implementation example combines dedicated simulators for the power system, communication network, and energy market whereas previous approaches known to the authors only considered a subset of these three domains or monolithic concepts.

The main contributions of this paper can be summarized as follows:

(i) Analysis of the requirements of a cosimulation combining the three domains and definition of the cosimulation specifications

(ii) Identification of technical challenges of interconnecting the simulators

(iii) Development and the implementation of the cosimulation architecture and the interfaces that implement the specifications

(iv) Validation of the proposed cosimulation environment by simulation results.

The paper is structured as follows: Section 2 gives an overview of the related work on integrated modelling and simulation of smart grids. In Section 3, we identify and describe the use cases for which the proposed cosimulation environment can be used. The challenges for the realization of the cosimulation environment are discussed in Section 4, whereas we present our solutions regarding the designed data model and the software architecture but also its limitations in Section 5. The integrity of the cosimulation environment is validated by the results of a cosimulation in Section 6, where an optimal management of distributed battery storage systems is simulated to improve the voltage stability of a distribution network. We conclude the paper with final remarks in Section 7.

2. Related Work

2.1. Architecture and Data Model. The evolution of traditional power systems towards intelligent power grids has recently triggered efforts for comprehensive modelling and standardization, which aim to include various aspects of a smart grid ecosystem. One major contribution in this context is the *Smart Grid Architecture Model (SGAM)*, which provides a basis for the representation of relationships between entities, functionalities, and subsystems in smart grids [5]. SGAM framework models a smart power grid in five interoperability layers which cover physical components in the network *(component layer)*, protocols for exchange of information between services or systems *(communication layer)*, data models which define the rules for data structures *(information layer)*, functions and services *(function layer)*, and business and market models *(business layer)*. The model further divides the component layer to hierarchical electrical energy conversion and transmission *domains* from *generation* to *customer premises* and to component *zones* such as *field* and *station*. This architectural view aims to accelerate and standardize the development of unified data models, services, and applications in industry and research. In this context, our data model and cosimulation framework in this work build upon the fundamental concept of SGAM, where our focus lies in the following aspects of SGAM:

(i) The unified data model which is presented in Section 5.1 formally defines the structure for data exchange in alignment with the concept of the *information layer* of SGAM.

(ii) The domain-specific simulators of our cosimulation environment include models of power system and communication network components as well as market actors in the *component layer* of SGAM within the *distribution*, *DER*, and *customer premise* domains.

(iii) The communication layer is abstracted by a cosimulation interface and the extensions in the domain-specific simulators in order to enable the data exchange between the components.

(iv) The example use case presented in Section 6, regarding the optimal management of distributed battery storage systems, is an example of a system function which would fall on the *function layer* in the SGAM framework. Besides, the business model that motivates the provision of such a system function, for example, an incentive by the system operator, is defined within the *business layer*.

For the realization of the unified data model in alignment with the SGAM concept, we identify the IEC Common Information Model (CIM) [4] as a well-established basis for extensions in Section 5.1 as it is a widely accepted format to exchange grid data in power systems. Although it includes an extensive list of electrical grid components as well as market-related objects, the communication infrastructure of a power system is hardly included except for a few classes regarding supervisory control and data acquisition (SCADA) links. However, CIM can easily be extended as demonstrated for the market in [6, 7].

2.2. Simulation of Smart Grids. There have been several attempts to build a cosimulation environment with the focus on power grids and communication networks, for example, [1, 8–10]. However, the proposed approaches so far do not account for the market because they focus more on short-term effects caused by limitations of the communication network.

Although MOCES [3] attempts to take a holistic approach to model distributed energy systems, this results in the implementation of a monolithic simulation instead of a cosimulation, with a hybrid simulation for the physical part and an agent-based simulation for the behavioral part which could

represent the market. Therefore, this approach hinders the use of existing domain-specific tools and requires substantial development effort. Instead, in this work, we aim to take advantage of the capabilities that existing tools offer which (i) enhances the credibility of the results and (ii) decreases the effort that is needed to replicate their functionalities.

The proposed simulation framework consists of several simulators, each responsible for a specific domain. The advantage is the possibility of using the best tool for each domain. Besides, the vision is to be able to replace simulators with reasonable effort if the simulation requirements change. For example in Section 6, it is mentioned how [11] could be used to implement a more comprehensive market simulation.

2.3. Classification of Simulations. Schloegl et al. [12] provides a clear classification scheme for energy-related cosimulations. Because our cosimulation environment shall provide holistic simulations, all four categories of simulation elements or models (i.e., continuous processes, discrete processes and events, roles, and statistical elements) defined by Schloegl et al. have to be considered.

In our implementation, the power system is modelled in Modelica as it can be used for physical systems in general [3] and has already proven its capabilities for thermal systems [13] and power systems in particular [14]. Modelica models consist of continuous processes, discrete processes, and events, which makes the power system simulation a hybrid simulation. The communication network is simulated with the available discrete event simulation (DES) tools, such as ns-3. In a DES, the simulation time proceeds with the execution of single events, such as packet arrival and time expiry [15]. The energy market simulation is implemented in Python as DES. Python was chosen as programming language because of its suitability to implement and test different optimization methods [16]. Each market participant aims at optimizing the schedule for its assets, for example, minimizing energy costs and maximizing its profit. Depending on the simulation scenario, the behavior or role of the market participants changes. Examples for statistical elements are wind farm models of the energy grid simulator and communication link models which consider packet losses and the reliability metrics of the communication network simulator.

Furthermore, the proposed cosimulation environment can be formalized as a coupled Discrete Event System Specification (DEVS) as defined in [17] which is why a classification of our architecture in terms of DEVS is given in Section 5.5.

3. Use Cases of the Cosimulation Environment

Our cosimulation solution including the three domains can be used to evaluate different scenarios. To address the physically relevant dependencies, we divide the dynamic interactions between the simulators into two groups:

(i) Fast phenomena in the range of microseconds to seconds, between highly dynamic power system components, for example, power electronics and communication network

(ii) Slow phenomena in the range of minutes to hours which include market entities, power system, and communication network.

In recent literature, the most prominent fast dynamic interactions occur in wide area measurement and control applications as well as remote power electronics devices [10]. Compared to slow phenomena, the simulation of fast phenomena requires relatively smaller simulation time steps due to switching events of electronic components and the fact that the market interactions are not considered. Therefore, in a cosimulation of the fast phenomena, the focus should be more on the efficiency of the cosimulation interface rather than a simplification of the coupling with multiple simulators. The proposed cosimulation environment is intended to support the investigation of fast dynamics but should not be limited to them. This has an influence on our design of the communication interface between the simulators as can be seen in Section 5.4.

On the other hand, slow phenomena are created by closing the loop between the power system and market by means of the communication network. The behavior of market entities may cause changes in the usage of power system components which has an impact on the grid and vice versa and this loop might be impaired by the communication network. The cosimulation environment might be used either to verify the functioning of the control loop given a specific communication network or to plan a communication network that fulfills the requirements of the control mechanisms in power system and market.

Based on this classification of use cases, it can be concluded that all three simulators do not necessarily have to be active at the same time for all scenarios. In this paper, we will focus on the requirements and the implementation for the cosimulation of slow phenomena and confine our discussion on fast phenomena to a description of the adaptions needed for fast phenomena investigations since there already exist several cosimulation environments proposed for these studies [1].

An example use case for slow phenomena is the optimal management of distributed storage systems for peak-shaving to support the grid operation. The proposed cosimulation environment including the communication network allows testing the effects of communication failures on the operation strategy and eventually on the electrical grid, which can provide valuable insights for decision-making. Simulation results for this example are provided in Section 6.

Before the cosimulation is initiated, it is necessary to define and store the topology under investigation along with the scenario-specific parameters. For example, the scenarios can be investigated in which the failures in the communication network are stochastically or deterministically set by the user in the data model. From a user perspective it would be advantageous if all components, their links, and parameters could be defined in one environment rather than splitting this information between different software solutions and formats. Then, the data model for the topology needs to include components that couple different domains.

From these use cases, the following challenges can be identified:

(i) Common data model that includes components of all domains and their interconnections

(ii) Interaction of simulators with different simulation types, for example, event-driven for the communication network and continuous processes for the power system

(iii) Choice of the cosimulation time step which is limited by the synchronization method connecting the simulators.

4. Challenges of the Cosimulation

4.1. Common Data Model. A common data model that covers the electrical market, communication infrastructure, and grid does not exist to the best of our knowledge even though these components are integral part of smart grids. Not only would the user of a simulation software benefit from a common data model during the specification of the simulation scenario but the data exchange would also be simplified. A system description that encompasses all components of smart grids as shown in Figure 1(a) could be either used directly by holistic smart grid simulators or divided into subsystems for a cosimulation as in Figure 1(b).

For many components, this division is straightforward since their parameters are only needed by one domain-specific simulator. For example, electrical lines exist only in the power system domain and have connections only to other power system components. Some components, on the other hand, constitute natural coupling points between the power system, the market, and the communication network. These components are called *interdomain components* in the following. For instance, a battery storage device connected to the grid can act as a market participant that offers its capability to charge or discharge. In order to enable its participation in the energy market, the battery storage needs an interface which is a communication modem in this case. The modem can be seen as a part of the battery storage. Therefore, the data model class associated with the battery storage device has to be able to hold or reference to data on the properties of the battery storage in electrical, market, and communication domains. For a cosimulation, the information on interdomain components have to be split into several parts since their parameters are needed by the simulators and each simulator has to simulate a dedicated part of these components.

4.2. Cosimulation Time and Synchronization. A remaining and major issue in such a cosimulation, in which simulators of different categories are combined, is the selection and implementation of a proper synchronization mechanism which must ensure the proper progress of the simulation time and a timely data exchange between the domain-specific simulators. This selection is of crucial significance in order to minimize the error propagation in the cosimulation and the synchronization overhead in terms of simulation time. In [1], three main synchronization methods for cosimulation have been specified: time-stepped, global event-driven, and master-slave. There are two different considerations related to the simulation time [12]:

(i) Time resolution: a challenge of the cosimulation is the highly diverse time resolutions of the three simulators. The time steps of power grid simulator reach from milliseconds (electromagnetic processes) to subseconds and above (steady-state and electromechanic processes). The time steps of communication network simulations can even vary from tens of microseconds (e.g., latencies in LANs) to seconds (e.g., latencies in WANs). On the other hand, in energy market simulations, a time step of several minutes can be sufficient as it is the case for Germany's control power market with price calculations on 15-minute basis.

(ii) Time ratio: time ratio describes the relation between simulation time and wall clock time [12]. With appropriate use cases, we want to show how holistic cosimulations with our approach can be used for planning and decision-making. Therefore, it is important to run the scenarios much faster than wall clock time and for time intervals of days as well as of weeks, so that many models with different configurations can be simulated.

The problem is that a very small time step or a high resolution in time impedes short simulation times. Therefore, it is necessary to adjust the time step according to the phenomena that are under investigation. At the same time, it may be feasible to aim at a higher integration of the simulators and sacrifice flexibility and increase the efficiency if both time resolution and time ratio need to be optimized. In Section 5.3, we discuss our design choices regarding the synchronization of the simulators in detail. The approach for an optimization of time resolution and time ratio is further discussed in the Section 5.4.

5. Concept of the Cosimulation Environment

5.1. Data Model for Power System, Communication Network, and Market. As explained in Section 2, one possibility is to extend the cosimulation topology format on CIM, which leads to a superset of CIM. New classes, which are introduced for completing CIM in its representation of smart grids, are linked to the CIM classes using the terminology of the Unified Modeling Language (UML). The proposed format can be structured in four packages:

(i) Original CIM (IEC61970, IEC61968, IEC62325)

(ii) Communication

(iii) Market

(iv) EnergyGrid.

Whenever possible, the CIM classes are used. However, some components might not have an associated class in the standard yet. Then, these components are represented as classes in one of the other three packages. The reason for

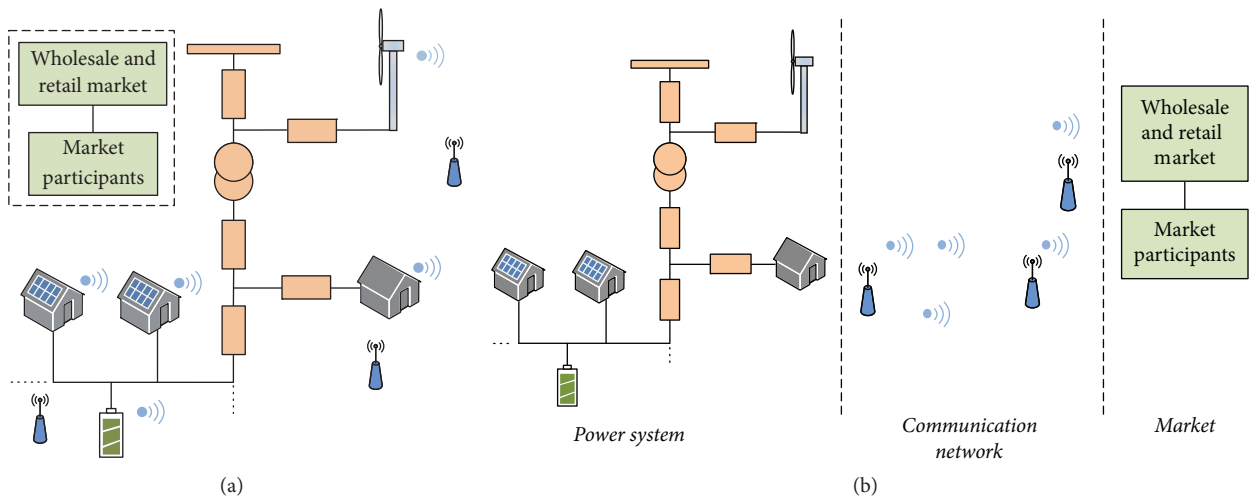

Figure 1: Exemplary topology including components of all domains (a) and domain-specific topologies (b).

this approach is that this way it is easier to update to a new version of CIM without losing the newly added classes and their interconnections.

The most important feature of our model format is the interconnection of domains. In order to accomplish this, we have identified possible interdomain components. Some examples of interdomain components, namely, `BatteryStorage`, `SolarGeneratingUnit`, and `MarketCogeneration`, are shown in Figure 2, which is an excerpt from our data model. According to the UML diagram, the energy market components are associated with the power system components, whereas power system components have an aggregation relationship to communication devices. This means that parameters specific to the market, communication network, and power system which relate to the same device are linked with each other. Therefore, all information on one device is easily accessible but at the same time there is a separation according to the domains. The connections between classes of different domains are defined in a logical and not a topological way. Instead, topological connections exist to connect power system components, for instance.

Coming back to the battery storage device example, the data model is as follows: the device is a part of the grid and has electrical parameters. Furthermore, the battery storage might participate in the market, for example, as part of a virtual power plant (VPP). Market-specific information can be stored in the `MarketBatteryStorage` class which is associated with the electrical representation `BatteryStorage`. The data on the class for a communication modem `ComMod` which could be used to communicate with the VPP is aggregated to the `BatteryStorage` class.

In the following, we briefly mention the domain-specific considerations for the three domains.

(1) Power System Package. The purpose of the EnergyGrid package is to group models for power system components that are not already part of the CIM standard. For the simulation scenario that is presented later, it was necessary to create a new model for electrical energy storages like stationary batteries. A battery storage is a conducting equipment that is able to regulate its energy throughput in both directions. Therefore, the class `BatteryStorage` is a specialization of a CIM `RegulatingConductingEquipment` since it can influence the flow of power at a specific point in the network.

(2) Market Package. The key component of the market package for the scenarios that we would like to investigate is a VPP since the aggregation of small DER units enables their participation at electricity markets. In case the DERs are not owned by the operator of the VPP, they can be seen as customers that offer their energy in exchange for share of the VPP operators profits. Besides, a VPP might support the Distribution System Operator (DSO) in ensuring a safe grid operation which results in an association between the DSO and the VPP.

(3) Communication Package. This package includes all additionally defined classes that are related to the communication network model, such as classes for communication links and technologies, modems, network nodes along with their parameters and their relations with the classes in CIM, power system package, and market package. In this way, the user can model the communication network layer and its specifications in the simulation tool. The communication network topology and its parameters are then used by the communication network simulator for the cosimulation.

Figure 3 shows an excerpt from the communication data model with an aggregation to a `WindGeneratingUnit`. By means of the associated classes for modems, communication requirements, and channels, the model enables a description of network parameters and topology. Furthermore, the communication network data model integrates the flexibility to enable the planning of the communication network under communication and power system requirements even before the beginning of the cosimulation. The topological parameters will be used for an optimal design of the communication network with the desired objective, such as minimum

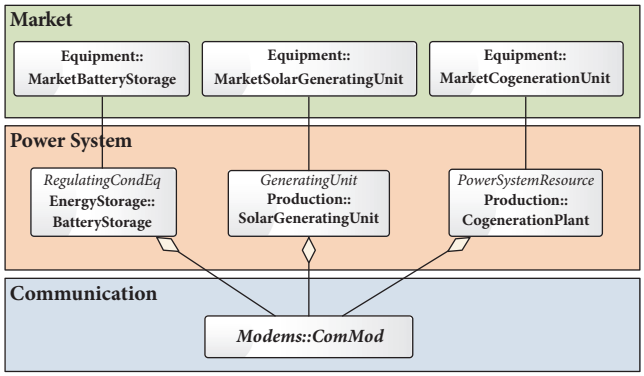

Figure 2: Interdomain connections between classes of power system, communication network, and market.

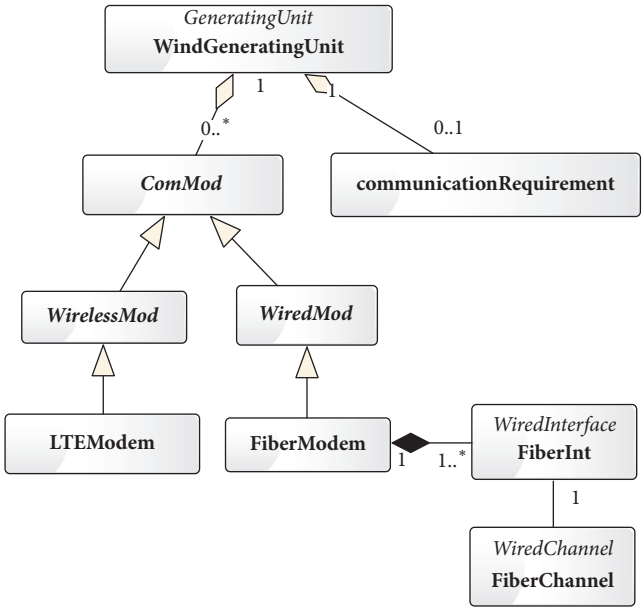

Figure 3: Communication network class association example.

cost, while required conditions are satisfied, such as given reliability metric. An example of this approach is presented in [18] for an integrated design of a wide area measurement system. Eventually, the optimized communication network solution can be evaluated against different scenarios using the cosimulation environment.

5.2. Model Data Processing and Simulation Setup. The overall information flow for the simulation setup is depicted in Figure 4. After the topology is created or modified in a graphical Topology Builder and includes the three domains, the input file, which complies with the common data model of Section 5.1, is sent to the cosimulation interface. The cosimulation interface incorporates a component, based on CIM++ [19], which parses the CIM XML-RDF file and generates a container of C++ objects that contain the topological data. In order to execute a simulation, the Modelica solver requires a Modelica model, whereas

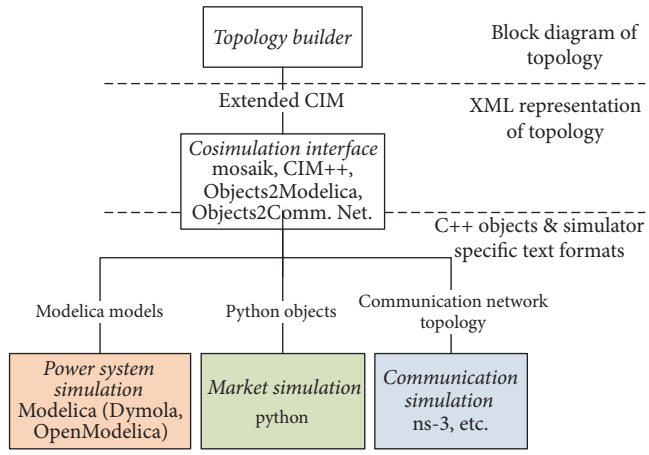

Figure 4: Overall architecture for simulation setup.

the communication network topology can be given to the communication network simulator in JSON or XML format, which includes the components in the network, their connections, and parameters. Since the topology will be available as an XML-RDF file and a container of C++ objects, the relevant information for the power system and communication network is extracted during a deserialization step. In the subsequent transformation step, a component, which we call Objects2Modelica/CommunicationNetwork, generates Modelica and communication network files with the topology and parameters. In contrast, the Python based market simulation relies on a C++/Python interface, which could be realized using one of the common libraries for Python to wrap C++ data types and functions, to retrieve the market relevant information from the C++ objects and store them in Python objects.

The following paragraph explains the translation on the basis of a CIM to Modelica example. The loads are defined in the extended CIM data model described in Section 5.1 as PQ-loads with a characteristic power demand as follows:

```
<cim:SvPowerFlow rdf:ID="PQ1-sv">
<cim:SvPowerFlow.p>1000</cim:
SvPowerFlow.p>
<cim:SvPowerFlow.q>329</cim:
SvPowerFlow.q>
<cim:SvPowerFlow.Terminal

    rdf:resource="#E-1229789360"/>

</cim:SvPowerFlow>
```

The cosimulation interface extracts the corresponding component parameters from the CIM XML-RDF file and introduces them in the Modelica model of the grid. The latter is done by the Objects2Modelica component explained in Section 5.2 which iterates through the list of C++ objects provided by CIM++. Thus, the specification of the parameters P and Q in the CIM model generates two attribute modification equations in the declaration of the PQ-load in Modelica:

```
ModPowerSystems.PhasorSinglePhase.Loads.
PQLoad CIM_PQ1 (Pnom = 1000, Qnom = 329)
```

These values are applied during the quasistationary simulation of the single-phase representation of the grid.

5.3. Synchronization. The synchronization of all three simulators will be performed in fixed time steps. Fixed synchronization time steps have been chosen because of the resulting flexibility to integrate more simulators easily and its comparatively high speed in terms of time steps per simulation time [1]. An event-driven approach as it is implemented in [10] for two simulators requires a deeper integration of the cosimulation framework and the simulators. Apart from that, it was shown in [10] that the cosimulation error can be reduced for fixed time steps by reducing the global time step size.

The synchronization between all simulators for slow phenomena scenarios is performed with mosaik, a well-established cosimulation framework [20] which was developed for stationary simulations with time steps of one second or greater [21]. It allows combining the three simulators in a simple manner as explained in Section 5.4. VILLASnode, a software project for coupling real-time simulations in LANs [22, 23], is a suitable alternative for mosaik in the case of synchronizations with very short intervals.

In Modelica, the synchronization data exchange is achieved by integrating Modelica blocks of the Modelica_DeviceDrivers library, which was originally developed for interfacing device drivers to Modelica models. This conveniently allows the definition of a fixed interval for data exchange. Modelica_DeviceDrivers were chosen instead of the FMI approach shown in [21] because it allows more flexibility in picking the desired simulation variables and choosing the required cosimulation step size independently from the Modelica simulator time step. At synchronization steps between all simulators, the step function of the energy market simulator is called synchronously from the mosaik Python API. After the market simulator has finished the simulation step, the results are retrieved by mosaik.

The simulation time in the DES of the communication network advances with the execution of the generated events, which are stored in an event-list. The execution of events is controlled by a scheduler, which determines the next event and its execution time. Whereas the default scheduler executes the events sequentially without any interruptions, the available simulation environments offer the flexibility to integrate external control inputs to receive external control messages, which can be used to manipulate the simulation flow by changing the module parameters during the simulation. In order to realize this, the event-driven nature of DES tools can be used to generate new events, called flow control events, which stop the communication simulation, exchange data, and use the input data to manipulate the following simulation steps. Furthermore, the execution of events can be controlled and the simulation can be stopped after the execution of the last event before a synchronization point, so that the simulation runs in fixed steps and a data exchange is possible at the end of each step.

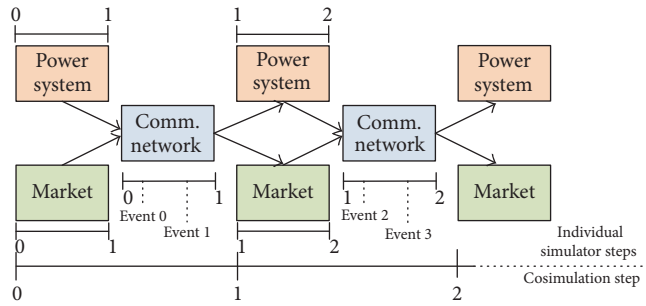

Figure 5: Synchronization scheme of simulators at cosimulation time steps.

Figure 5 depicts the flow of time for the cosimulation and each simulator. It can be seen that the power system and market simulators compute in parallel, whereas the communication network is waiting for their inputs. In a mathematical notation, the interactions between the simulators in each cosimulation step can be defined by

$$\begin{aligned} u_p(n+1) &= F_c\left(F_m\left(u_m(n)\right)\right), \\ u_m(n+1) &= F_c\left(F_p\left(u_p(n)\right)\right), \end{aligned} \tag{1}$$

where u_m and u_p are the corresponding input values of the simulators for the power system, energy market, and communication network for each time step. Therefore, it is required to set initial values, $u_p(0)$, $u_m(0)$, at the beginning of the cosimulation. n denominates the current cosimulation time step. F_c (communication), F_m (market), and F_p (power system) are the functions describing the calculation of the next time step.

5.4. Cosimulation Runtime Interaction. In Figure 6, the coupling of the power system, communication, and market simulator for their cosimulation runtime interaction is shown. In the following, we briefly introduce the individual parts of the cosimulation environment:

(i) Mosaik: as already mentioned, mosaik is used for the coordination during the synchronization steps of several minutes (in simulation time) regarding all simulators [24]. mosaik has two different APIs for simulator coupling. It provides handlers for different simulator types, allows modelling of different simulation scenarios, and schedules the step-wise execution of the connected simulators with the aid of SimPy [25]. The two mosaik APIs are

  (a) the low-level API which uses common TCP/IP network sockets for exchanging messages encapsulated in JSON, an open-source and human-readable data format;

  (b) the high-level API which can be directly used by a simulator and communicate with mosaik through sockets but also handle their creation, events, and message (de)serialization.

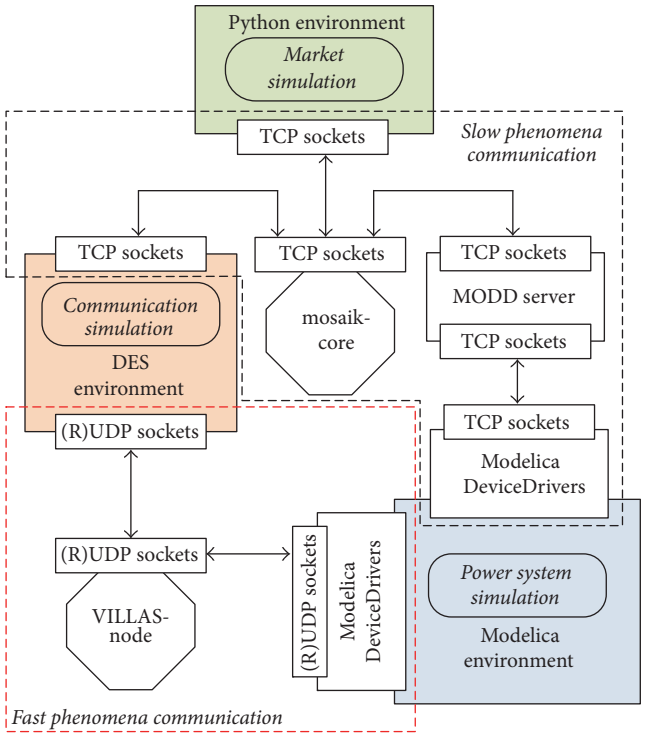

Figure 6: Scheme of runtime interaction between cosimulation components.

(ii) Market simulator: implemented in Python, it can make use of the high-level API as illustrated in Figure 6. The use of the sockets allows the desired flexibility of running all simulators on different computer systems and environments.

(iii) Communication network simulator: based on available DES tools, their network simulation modules are extended with interprocess communication functionalities for JSON message exchange with mosaik.

(iv) Power system simulator: the integration of so-called *TCPIP_Send/Recv_IO blocks* from *Modelica_DeviceDrivers* into the Modelica models, allows the exchange of simulation data via sockets but in the form of Modelica variables as bitvectors instead of JSON messages. Therefore, the MODD Server is implemented.

(v) MODD server: it receives commands from the socket connected with mosaik. Based on these commands it starts, for example, the power system simulator or receives the bitstream from Modelica_DeviceDrivers and encapsulates it into JSON messages before transferring them to mosaik. Besides the synchronization steps controlled by mosaik, there will be also more fine-grained synchronization steps of fractions of seconds between the power system and communication network simulator. That is why a VILLASnode server is included.

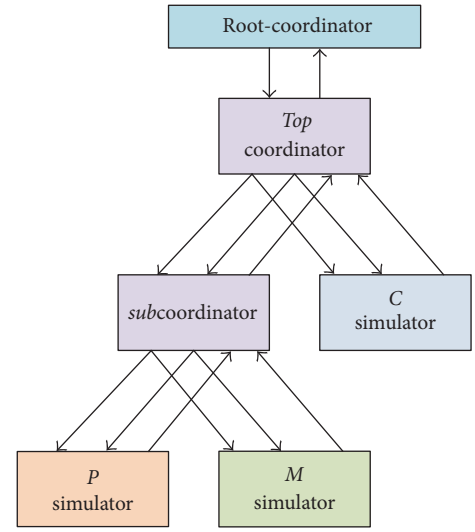

Figure 7: Cosimulation environment as a hierarchical simulator.

(vi) VILLASnode: instead of TCP (Transmission Control Protocol), it makes use of UDP (User Datagram Protocol) sockets for data exchange between real-time simulators, for which it was designed. The use of UDP leads to less overhead and consequently to lower synchronization time steps but with the disadvantage of an unreliable connection. Our solution for avoiding any datagram losses is the usage of Reliable UDP (RUDP) to keep a low overhead in comparison with TCP with the benefit of a reliable connection.

5.5. DEVS Formalization. As explained in Section 5.3, a discrete time base is chosen for the synchronization between the domain-specific simulators. Therefore, the simulators can be formalized by Discrete Time System Specifications (DTSS). Since the time steps are fixed, the DTSS can be simulated by DEVS [17]. The abstraction level of the DEVS has not been considered for the mosaik framework for different reasons [26] and is not needed for the definition of cosimulation scenarios. Therefore, a formal definition of the whole simulation as coupled DEVS is beyond the scope of this paper. However, a so-called *hierarchical* simulator for the three *atomic* simulators P, M, and C (for energy, market, and communication) is shown in Figure 7 as leaves of the hierarchical simulator (i.e., tree) [17] and described in the following. The *root-coordinator* sends an *initialization message* (i, t), which is propagated to all atomic simulators in the tree at simulation start and initiates the simulation steps with *state transition messages* $(*, t)$. The *coordinators* handle the levels of coupled simulators up to the root of the tree. The scheduling of an event is performed by a $(*, t)$ message forwarded by each receiver coordinator to its *imminent child*. The imminent child is the simulator which shall perform its next *internal transition* or the coordinator being the root of the subtree containing the simulator which performs the next internal transition.

In case of our cosimulation architecture, the first $(*, t)$ message is forwarded by the *top* and the *subcoordinator* to the first component in the *event-list* (here. P simulator) computing the new output $y_P = \lambda(s)$ and sending it as *output message* (y_P, t) to the subcoordinator. The subcoordinator then recognizes an *internal coupling* and therefore sends an *x-message* (x_M, t), with $x_M = Z_{P,M}(y_P)$, to the M simulator, whereby $Z_{P,M} : Y_P \rightarrow X_M$ is the *translation function* from the output events of the P simulator to the input events of the M simulator. Although the computations of the M simulator, within the same transition, do not depend on the output of the P simulator, its output message (y_M, t) includes the output of both simulators. This output is translated and forwarded by the subcoordinator to its parent (top coordinator), because of the *external coupling*, as output message (y_N, t) of the belonging Discrete Event Specified Network (DEVN). Afterwards, the top coordinator translates the message to an input message (x_C, t) of the C simulator which computes the output of the whole cosimulation step. This output is transformed by the top coordinator, because of its internal coupling, to an input message for the subcoordinator which translates and sends the message down to the P simulator, because of the *external input coupling*, and the next cosimulation step begins.

An improvement of this formalization based on the hierarchical simulator could be accomplished by a formalization of the P and M simulator as a *conservative parallel discrete event simulation* [17]. Nevertheless, the described communication pattern between the components of the hierarchical simulator shows that the chosen cosimulation synchronization scheme, depicted in Figure 5, is valid, when causality violations between the energy and market simulation within one time step of the cosimulation are avoided which is guaranteed for the considered simulation scenarios.

5.6. Limitations. Due to the communication overhead caused by the cosimulation environment, the simulation time might increase significantly for large network sizes. Currently, real-time simulations are not possible, but the available framework can be extended for real-time and hardware-in-the-loop simulations, for example, by using VILLASnode instead of mosaik.

Furthermore, the synchronization step size cannot be changed during simulation runtime, whereas the domain-specific simulators support variable simulation time steps. To enable a variable step size for an optimized cosimulation through more sophisticated algorithms, modifications of the mosaik framework would be necessary as it allows fixed time steps only. The cosimulation flow managed by mosaik, which allows parallel and sequential progress of simulators, might introduce inaccuracies in the simulation results with respect to the synchronization step size.

Moreover, the simulation of heterogeneous communication networks and standards is possible. However, the abstraction level of the communication protocols influences the simulation time of the communication network simulator and thus the simulation time of the cosimulation.

6. Verification of the Cosimulation Interfaces

In this section, we aim to show that the implemented cosimulation infrastructure does not impair the accuracy of the simulation results. As an exemplary application, we consider a scenario where a VPP operator aims at gaining profits by reducing the VPP's peak power. Thus, a peak-shaving algorithm is employed for an optimal management of distributed battery storage systems. Financial incentives for the peak-shaving behavior might originate from agreements with DSOs regarding the maximum power feed-in of the VPP. Starting from results without the cosimulation framework, we successively include the cosimulation environment and domain-specific simulators to demonstrate that the results do not change under the assumption of an ideal communication network in the same scenario. Eventually, a slightly different scenario is presented where the communication network is supposed to impair the control loop between the power system and the market due to communication device failures, thereby, showing an exemplary use case for the cosimulation architecture presented in this paper.

6.1. Simulation Scenarios and Models. The investigated power system is a part of the IEEE European Low Voltage Test Feeder. The loads in the test feeder are replaced with buildings, each incorporating a PQ-load. Furthermore, several of these buildings feature stationary batteries and solar generation. The battery storages are controlled by a peak-shaving algorithm which is implemented in the market simulator. The peak-shaving algorithm is supposed to represent a VPP operator that utilizes its aggregated storage in a grid supporting way. That is why in a real world application it needs to exchange measurement and control values with the battery storages through the communication network.

In the first simulation scenario, the communication between batteries and the peak-shaving algorithm is ideal and not subject to any communication network failures. This scenario is used to verify the correct exchange of simulation data between the simulators involved in the cosimulation. For this reason, the simulation is first executed without cosimulation framework, connecting the peak-shaving algorithm directly to the power system simulation. Then, the cosimulation environment is introduced and afterwards the communication network simulator. The results of these three simulation cases are presented in Section 6.2.

The second simulation scenario, analyzed in Section 6.3, features a communication network failure in order to show a possible use case of the complete cosimulation environment.

The following equations are implemented in Modelica to simulate the power system components in the buildings. The PQ-loads in the buildings are modelled as ideal constant power loads, which means that the load current is directly dependent on the voltage at the grid connection point.

The implemented Modelica model of the solar generator determines the active power output P_{sg} by

$$\frac{P_{\mathrm{sg}}}{3} = V_{\mathrm{oc}} \cdot I_{\mathrm{sc}} \cdot FF \cdot \frac{P_{\mathrm{sg,inst}}}{P_0}, \tag{2}$$

under the assumption that the plant is operating at its maximum power point and where V_{oc} and I_{sc} are the open-circuit voltage and the short-circuit current, respectively. They vary with temperature and solar radiation, which can be modelled according to [27]. The term $P_{sg,inst}/P_0$ in (3) adapts the magnitude of the output power to the installed power of a specific solar generating unit, given that P_0 represents the installed power of the solar panel used in [27].

The model of the battery storages consists of a simple set of equations describing the derivative of the state of charge (SOC) as

$$\frac{d}{dt}\mathrm{SOC} = \begin{cases} \dfrac{\eta_{\mathrm{ch}} P_B}{C_B}, & P_B \geq 0, \\ \dfrac{P_B}{\eta_{\mathrm{disch}} C_B}, & P_B < 0. \end{cases} \tag{3}$$

In addition, the battery model limits the SOC to be in the range between zero and one. The values specifying the battery capacity C_B, the charging efficiency η_{ch}, and the discharging efficiency η_{disch} are extracted from the extended CIM classes; see Section 5.1.

The VPP algorithm aims at stabilizing the voltage profile by reducing the power exchange between the grid and the buildings using a model predictive control approach. Therefore, the battery charging power P_B is set according to an optimal scheduling which is based on forecasts for solar radiation and load demand. To compensate for inaccuracies in the forecasts, the algorithm receives measurements of actual load demand, generated solar power, and battery state of charge from the power system simulator.

6.2. Comparison of Results with and without Cosimulation Environment. At first, both measurements and set points are neither passed through the communication network simulator nor the cosimulation framework. Instead, the control signals for the battery storages are directly supplied by the peak-shaving algorithm before each power system simulation step. Following this reference case, both simulators are connected through the cosimulation environment as described in Section 5.4. Still, the communication network simulator is not involved. The results depicted in Figure 8 present the voltage profile over time at one node in the test feeder and it can be seen that the results with and without the cosimulation environment are consistent. If the communication network had altered the exchanged data, control values, and measurements, the voltage profile would have changed. Next, we take this one step further and also introduce the communication network simulator. The communication network simulator acts as mediator between the power system and market simulators. Any data that is exchanged between the power system and market has to pass through the former. The communication network simulator is added to the cosimulation as presented in Sections 5.3 and 5.4. To verify that the three simulators are synchronized properly, we include an ideal communication network; that is, all messages are transmitted without any latencies. Evidently, an ideal communication should not affect the information exchange between power system and market, so that the implemented scheduling for battery charging should perform equally.

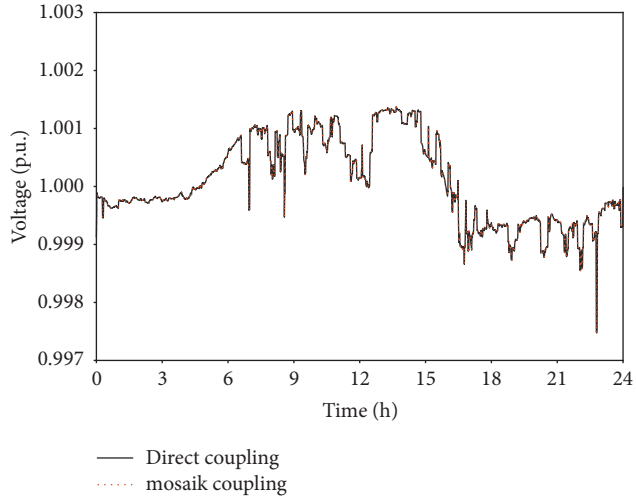

Figure 8: Comparison of simulation results of power system and market with and reference case without cosimulation environment.

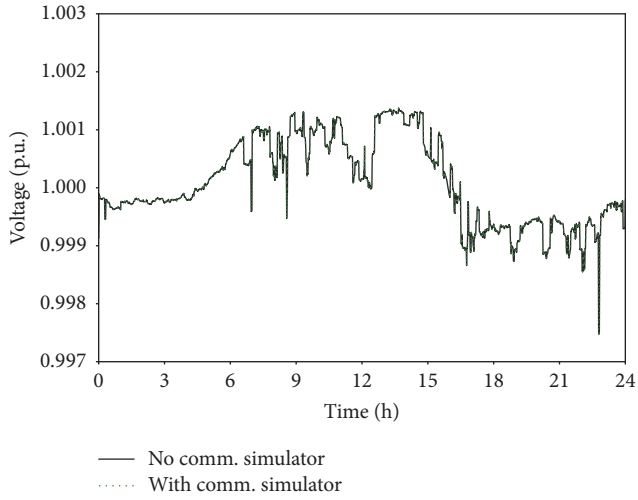

Figure 9: Comparison of simulation results with cosimulation environment and ideal communication network and reference case without cosimulation environment.

In Figure 9, it is visible that the simulation results incorporating the ideal communication network do not deviate from the ones obtained without the communication network even though all messages are now passing through the communication network simulator. Thus, the results confirm a correct synchronization of the three simulators and the consistency of the implemented cosimulation environment.

6.3. Exemplary Cosimulation with Communication Network Failure. In this subsection, the three simulators are exchanging data in the same way as described at the end of Section 6.2. Only this time, the communication network simulator emulates a fault in the communication network which leads to a communication failure of one hour at the site of the

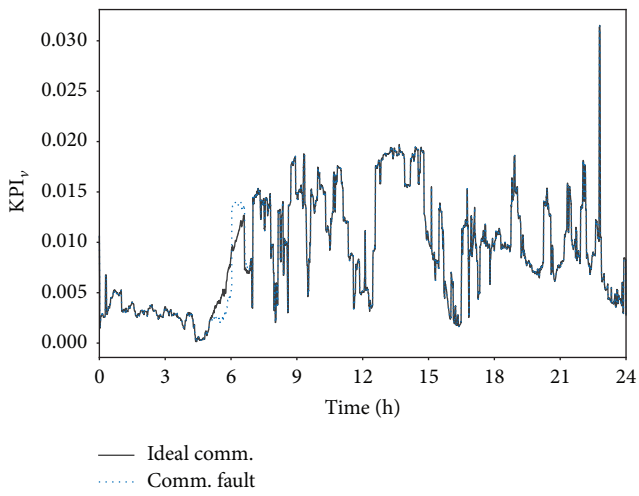

Figure 10: Comparison of voltage KPI for cosimulation with and without communication network fault.

VPP control algorithm. This represents slow phenomena case where the loop between power system and market simulator is affected.

To assess the impact of the communication fault on the whole network section, a voltage key performance indicator (KPI) as defined in (4) is applied to the results:

$$\mathrm{KPI}_v = \frac{1}{N} \cdot \sum_{i \in \mathbb{N}} \left| \frac{v_i - 1}{\Delta v_{\max}} \right|. \quad (4)$$

Here, N is the number of considered voltage nodes, v_i denotes the voltage at one node in per unit, and $\Delta v_{\max}$ is the maximum allowed voltage deviation. Thus, the KPI is representing the average absolute deviation at all network nodes in relation to the maximum allowed deviation. Figure 10 shows that a communication failure between hours five and six clearly affects the voltage profile of the power system. The application of the latest control values during the communication failure results in a charging of the batteries, while after the fault clearance the reactivated control discharges the batteries again. Hence, the entire battery capacity is being made available again for peak-shaving during the midday time. Due to the compensation behavior, the system returns back to a state with completely discharged batteries and consequently the same voltage profile as for ideal communication occurs some time after the fault. By modifying the communication network simulator input, it is also possible to emulate other faults such as faults at single buildings or package loss.

The applied market simulator focuses on the representation of VPP operators which manage as market participants their assets in a peak-shaving manner based on mathematical optimization. The operators scheduling may additionally take into account price trends at wholesale markets, for example, given as historical time series. An enhanced consideration of market dynamics can be obtained by an agent-based simulation of market participants and customers, for example, carried out with the Power TAC platform [11] integrated with the market simulator.

7. Conclusion

The contributions of this paper are a data model that includes three domains, power system, communication network, and market, and the architecture of a software environment to simulate multidomain scenarios for smart grids. The proposed data model facilitates the use of the software environment since the domain-specific smart grid component parameters and their interconnections can be modified and stored in a self-contained topology description. Due to our cosimulation approach we are able to take advantage of established domain-specific simulators for each domain. The proposed cosimulation environment covers use cases which are commonly investigated in literature and relate to power systems in conjunction with communication networks and use cases including the former two domains and the market. Simulation results of our cosimulation environment according to the proposed architecture confirm the consistency of the approach.

Conflicts of Interest

The authors declare that they have no conflicts of interest.

Acknowledgments

The authors gratefully acknowledge the financial support for this project by BMBF (German Federal Ministry of Education and Research) under Promotional Reference 03EK3567B.

References

[1] W. Li, M. Ferdowsi, M. Stevic, A. Monti, and F. Ponci, "Cosimulation for smart grid communications," *IEEE Transactions on Industrial Informatics*, vol. 10, no. 4, pp. 2374–2384, 2014.

[2] Z. Wang and Y. He, "Two-stage optimal demand response with battery energy storage systems," *IET Generation, Transmission & Distribution*, vol. 10, no. 5, pp. 1286–1293, 2016.

[3] L. Exel, F. Felgner, and G. Frey, "Multi-domain modeling of distributed energy systems-The MOCES approach," in *Smart Grid Communications (SmartGridComm), IEEE International Conference*, pp. 774–779, USA, November 2015.

[4] M. Uslar, M. Specht, S. Rohjans, J. Trefke, and J. M. Vasquez González, *The Common Information Model CIM: IEC 61968/61970 and 62325-A practical introduction to the CIM*, Springer Science & Business Media, 2012.

[5] CEN-CENELEC-ETSI Smart Grid Coordination Group, "Smart grid reference architecture," (Accessed on 03.01.02018). [Online]. Available: https://ec.europa.eu/energy/sites/ener/files/documents/xpert_group1_reference_architecture.pdf, Nov. 2012.

[6] E. Haq, D. Haller, K. A. Rahman, and B. Iverson, "Use of Common Information Model (CIM) in electricity market at California ISO," *in Power and Energy Society General Meeting, IEEE*, pp. 1–6, 2011.

[7] J. Fremont, E. Lambert, C. Bouquet, O. Carre, D. Ilhat, and P. Metayer, "CIM extensions for ERDF information system projects," in *Power & Energy Society General Meeting, PES'09. IEEE*, July 2009.

[8] K. Hopkinson, X. Wang, R. Giovanini, J. Thorp, K. Birman, and D. Coury, "EPOCHS: A platform for agent-based electric power and communication simulation built from commercial off-the-shelf components," *IEEE Transactions on Power Systems*, vol. 21, no. 2, pp. 548–558, 2006.

[9] K. Zhu, M. Chenine, and L. Nordstrom, "ICT architecture impact on wide area monitoring and control systems' reliability," *IEEE Transactions on Power Delivery*, vol. 26, no. 4, pp. 2801–2808, 2011.

[10] H. Lin, S. S. Veda, S. S. Shukla, L. Mili, and J. Thorp, "GECO: Global event-driven co-simulation framework for interconnected power system and communication network," *IEEE Transactions on Smart Grid*, vol. 3, no. 3, pp. 1444–1456, 2012.

[11] W. Ketter, J. Collins, and P. Reddy, "Power TAC: A competitive economic simulation of the smart grid," [Online] Available: http://linkinghub.elsevier.com/retrieve/pii/S0140988313000959, vol. 39, pp. 262–270, 2013.

[12] F. Schloegl, S. Rohjans, S. Lehnhoff, J. Velasquez, C. Steinbrink, and P. Palensky, "Towards a classification scheme for co-simulation approaches in energy systems," in *Smart Electric Distribution Systems and Technologies (EDST), International Symposium on IEEE*, pp. 516–521, September 2015.

[13] C. Molitor, S. Gross, J. Zeitz, and A. Monti, "MESCOS-A multienergy system cosimulator for city district energy systems," *IEEE Transactions on Industrial Informatics*, vol. 10, no. 4, pp. 2247–2256, 2014.

[14] M. Mirz, L. Netze, and A. Monti, "A multi-level approach to power system Modelica models," *in Control and Modeling for Power Electronics (COMPEL), 2016 IEEE 17th Workshop on IEEE*, pp. 1–7, 2016.

[15] K. Wehrle, M. Günes, J. Gross, and M. Günes, *Modeling and tools for network simulation*, Springer Science and Business Media, 2010.

[16] W. E. Hart, J.-P. Watson, and D. L. Woodruff, *Pyomo-optimization modeling in python*, vol. 67, Springer, 2012.

[17] B. P. Zeigler, H. Praehofer, and T. G. Kim, *Theory of modeling and simulation: integrating discrete event and continuous complex dynamic systems*, Academic press, 2000.

[18] H. A. Tokel, G. Alirezaei, and R. Mathar, "Integrated network design for measurement and communication infrastructures in smart grids," in *Proceedings of the 26th International Telecommunication Networks and Applications Conference, ITNAC 2016*, pp. 258–264, Dunedin, New Zealand, December 2016.

[19] L. Razik, M. Mirz, D. Knibbe, S. Lankes, and A. Monti, "Automated deserializer generation from CIM ontologies: CIM++an easy-to-use and automated adaptable open-source library for object deserialization in C++ from documents based on user-specified UML models following the Common Information Model (CIM) standards for the energy sector," *Computer Science - Research and Development*, pp. 1–11, 2017.

[20] S. Schütte, S. Scherfke, and M. Tröschel, "Mosaik: A framework for modular simulation of active components in Smart Grids," in *Proceedings of the IEEE 1st International Workshop on Smart Grid Modeling and Simulation, SGMS 2011*, pp. 55–60, October 2011.

[21] S. Rohjans, E. Widl, W. Müller, S. Schütte, and S. Lehnhoff, "Co-Simulation of complex energy systems with mosaik and FMI," *At - Automatisierungstechnik*, vol. 62, no. 5, pp. 325–336, 2014.

[22] S. Vogel, M. Mirz, L. Razik, and A. Monti, "An open solution for next-generation real-time power system simulation," in *Proceedings of the IEEE Conference on Energy Internet and Energy System Integration (EI2)*, pp. 1–6, Nov 2017.

[23] M. Stevic, A. Estebsari, S. Vogel et al., "Multi-site European framework for real-time co-simulation of power systems , IET Generation," *Transmission Distribution*, 2017.

[24] (Accessed 2016-08-18) mosaik documentation –release 2.3.0. [Online]. Available: https://media.readthedocs.org/pdf/mosaik/latest/mosaik.pdf.

[25] (Accessed 2016-08-18) Simpy documentation –release 3.0.9. [Online]. Available: https://media.readthedocs.org/pdf/simpy/latest/simpy.pdf.

[26] S. Schütte, S. Scherfke, and M. Sonnenschein, "Mosaik - Smart grid simulation API: Toward a semantic based standard for interchanging smart grid simulations," in *Proceedings of SMARTGREENS*, pp. 14–24, April 2012.

[27] W. Zhou, H. Yang, and Z. Fang, "A novel model for photovoltaic array performance prediction," *Applied Energy*, vol. 84, no. 12, pp. 1187–1198, 2007.

Hindawi
Complexity
Volume 2018, Article ID 6587493, 14 pages
https://doi.org/10.1155/2018/6587493

Research Article

Minimizing Harmonic Distortion Impact at Distribution System with Considering Large-Scale EV Load Behaviour Using Modified Lightning Search Algorithm and Pareto-Fuzzy Approach

S. N. Syed Nasir, J. J. Jamian, and M. W. Mustafa

Faculty of Electrical Engineering, Universiti Teknologi Malaysia (UTM), 81310 Johor Bahru, Johor, Malaysia

Correspondence should be addressed to J. J. Jamian; jasrul@fke.utm.my

Received 22 October 2017; Accepted 4 January 2018; Published 15 February 2018

Academic Editor: Fernando Lezama

This research is focusing on optimal placement and sizing of multiple variable passive filter (VPF) to mitigate harmonic distortion due to charging station (CS) at 449 bus distribution network. There are 132 units of CS which are scheduled based on user behaviour within 24 hours, with the interval of 15 minutes. By considering the varying of CS patterns and harmonic impact, Modified Lightning Search Algorithm (MLSA) is used to find 22 units of VPF coordination, so that less harmonics will be injected from 415 V bus to the medium voltage network and power loss is also reduced. Power system harmonic flow, VPF, CS, battery, and the analysis will be modelled in MATLAB/m-file platform. High Performance Computing (HPC) is used to make simulation faster. Pareto-Fuzzy technique is used to obtain sizing of VPF from all nondominated solutions. From the result, the optimal placements and sizes of VPF are able to reduce the maximum THD for voltage and current and also the total apparent losses up to 39.14%, 52.5%, and 2.96%, respectively. Therefore, it can be concluded that the MLSA is suitable method to mitigate harmonic and it is beneficial in minimizing the impact of aggressive CS installation at distribution network.

1. Introduction

The vision to have less carbon dioxide (CO2) emissions and less dependency on natural resources has encouraged Electric Vehicle (EV) to become an important option compared to conventional vehicle. Based on report in 2015, around 56.4% global crude oil is used for transportation sector [1]. Furthermore, the unstable price for crude oil has also influenced EV to become suitable alternative. The demand on EV, indirectly, has increased the number of CS installation in the distribution system [2]. However, power losses will increase when a large number of unplanned CS are installed. Furthermore, it will also introduce harmonic distortion due to the power electronic devices that convert alternating current (AC) to direct current (DC) at CS [3, 4]. This harmonic distortion will cause negative impact such as increment heating losses, shorter insulation lifespan, increased temperature and insulation stress, decreased power factor, and lower efficiency [5, 6].

Currently, most of the researchers focus on strategies to reduce loss by coordinating the charging of EVs. Alonso et al. [7] have developed an optimization algorithm to coordinate the charging of EVs using Genetic Algorithm (GA). The charging schedule is based on optimal load pattern for EV charging-based reliability which takes into consideration the thermal line limits, the load on transformers, voltage limits, and parking availability patterns. The proposed method is able to reduce the cost for power system new investment. Furthermore, Bharati and Paudyal [8] have proposed framework to coordinate EVs in the distribution system using bilevel hierarchical vehicle-grid (VG) optimization. This framework requires information exchange among EV aggregators and grid controller and then the EV charging can be scheduled based on the minimum losses to the distribution network. Next, Masoum and Nabavi [9] have also proposed online-overnight PEV coordination using metaheuristic technique which is particle swarm optimization. This method introduces high priority and low priority customer that indicate

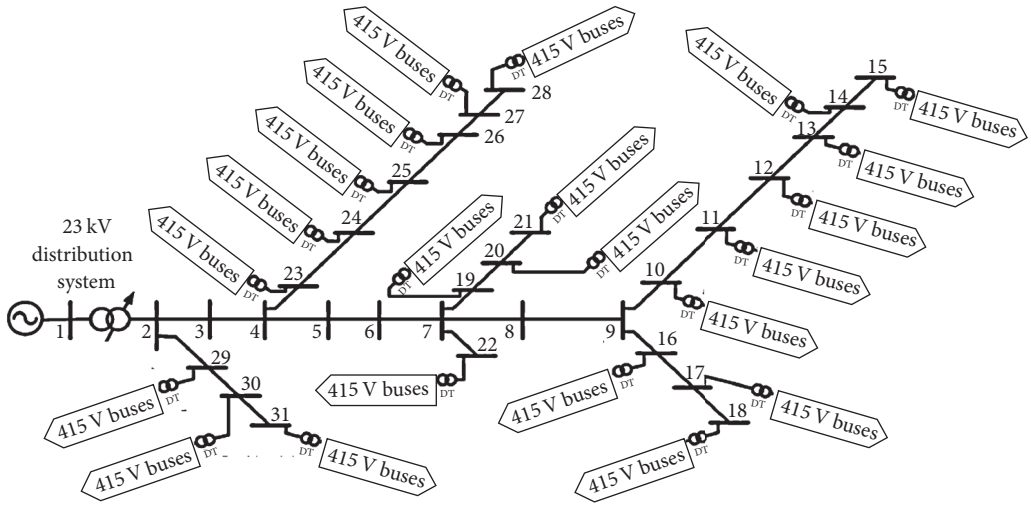

Figure 1: Single-line diagram for 449 bus radial distribution system.

the willingness of customer to be charged. High priority customer will get faster charging services with high tariff and the low priority customer will only charge their vehicle after power loss control in the distribution system is done. Even though many approaches have been introduced to minimize the EV impact, the focus is more towards minimizing the power loss. However, beside power loss, the harmonic injection to the distribution system when many CS are connected must also be taken into consideration in ensuring that the network can operate optimally.

In general, there will be two types of harmonic that will be mitigated in distribution network, which are voltage and current harmonic. Voltage harmonic is measured at the bus, while current harmonic is measured at the lines and cables. Passive filter is the common component used to eliminate these harmonics. Passive filters can provide a low-impedance path to harmonic currents and hence prevent it from flowing into the systems. There are many papers that utilized passive filter to mitigate harmonics in power system using filter devices [10–14] and the most common ones are single tuned filters. Single tuned filters are designed to eliminate or reduce single frequency from the system depending on the design resistance, capacitance, and inductance value [15]. Sakar et al. [16] have suggested a hosting capacity determination for a distorted distribution system due to Photovoltaic connection. In their research, passive filter is used to increase the harmonic-constrained hosting capacity which then improves the voltage, power factor, and filtering the harmonics. Author in [17] proposed an Asymmetric Synchronous Reference Frame Control scheme and harmonic voltage compensator with a Static Var Compensator connected to the grid to mitigate the harmonic. The author used harmonic voltage compensator to reduce voltage THD. Even though many researchers have used passive filter to mitigate the harmonic, very few researchers considered both voltage and current harmonics in their analysis especially for CS.

Therefore, this research proposes a coordination of 22 VPF when 132 unit of CS is adopted in a 449 bus radial distribution system. Section 2 presents the modelling of load profile, CS, battery, passive filter, harmonic, CS scheduling, and radial load flow used in this study. The introduction of MLSA technique will also be covered in this section. The methodology of the proposed coordination will be discussed clearly in Section 3. Result and discussion for 22 units of filter coordination in 449 bus are presented in Section 4. Lastly, conclusion of this research is in Section 5.

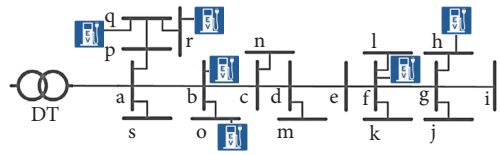

Figure 2: Single-line diagram for 415 V buses.

2. Problem Modelling and Formulation

A typical 449 bus radial distribution system is used in this research to determine the optimal placement and sizing of VPF. Furthermore, forward/backward sweep method is chosen due to the accuracy of this load flow analysis in solving distribution load flow [18–21]. The harmonic pattern for individual EV charger is modelled based on actual single phase charger impact as measured in [22].

2.1. IEEE 31 Bus with 22 Low Voltage 415 V Bus System. Figures 1 and 2 show a single-line diagram for 23 kV IEEE 31 bus radial system with low voltage 415 V buses residential feeder that consist of several CS, respectively. The total number of buses in the network (medium and low voltages) is 449 buses. There are 6 units of CS installed at one residential area which add up to 132 units for overall CS in this distribution system. Line data for low voltage 415 V buses is shown in Table 1.

2.2. Harmonic Load Flow Analysis. Many techniques can be used to perform harmonic analysis such as in [23–25] and the

Table 1: Line data for 415 V buses.

Line		Line resistance R (Ω)	Line reactance X (Ω)
Bus A	Bus B		
a	b	0.0415	0.0145
b	c	0.0424	0.0189
c	d	0.0444	0.0198
d	e	0.0369	0.0165
e	f	0.0520	0.0232
f	g	0.0524	0.0234
g	h	0.0005	0.0002
g	i	0.2002	0.0199
g	j	1.7340	0.1729
f	k	0.2607	0.0260
f	l	1.3605	0.1357
d	m	0.1400	0.0140
c	n	0.7763	0.0774
b	o	0.5977	0.0596
a	p	0.1423	0.0496
p	q	0.0837	0.0292
q	r	0.3123	0.0311
a	s	0.0163	0.0062
DT		0.0000	0.0654

most typical and simplest one is by using current injection analysis method [26]. The electrical parameters that affected the harmonic existence are the line impedances, load variation impedances, and filter impedances values. Equations (1) and (2) represent the line impedance formulation and the impedance for single-tuned filter at harmonic h, respectively, which indirectly caters for resonance impact. Equations (3), (4), and (5) show the impedance formulation for the load used in setting up the harmonic admittance matrix. The harmonic flow is calculated using (6), which consists of harmonic admittance matrix and harmonic current injection as per (7) and (8).

$$Z_{l,h} = R_l + jh\omega L_l, \tag{1}$$

$$Z_{\text{Filter},h} = R_{\text{Filter}} + jh\omega L_{\text{Filter}} - j\frac{1}{h\omega C_{\text{Filter}}}, \tag{2}$$

$$Z_{L,h} = R_L + jX_{L,h}, \tag{3}$$

$$R_L = \frac{V_L^2}{P_L}, \tag{4}$$

$$X_{L,h} = \frac{V_L^2}{hQ_L}, \tag{5}$$

$$\overline{I}_h = \overline{Y}_h \cdot \overline{V}_h, \tag{6}$$

$$\overline{Y}_h = \begin{bmatrix} \overline{y}_{11,h} & \overline{y}_{12,h} & \cdots & \overline{y}_{1N,h} \\ \overline{y}_{21,h} & \overline{y}_{22,h} & \cdots & \vdots \\ \vdots & \vdots & \cdots & \vdots \\ \overline{y}_{N1,h} & \cdots & \cdots & \overline{y}_{NN,h} \end{bmatrix}, \tag{7}$$

$$\overline{I}_h = \begin{bmatrix} \overline{I}_{1,h} \\ \overline{I}_{2,h} \\ \vdots \\ \overline{I}_{N,h} \end{bmatrix}. \tag{8}$$

2.3. Modelling of CS and Battery. CS is typically divided into three categories which are level 1, level 2, and level 3. The level of the CS is based on the power consumed by the charging station. Level 1 takes 6–8 hours, while level 3 requires 30 minutes for fully charging the EV's battery. In this research, level 1 CS is selected since this research focuses on residential area which normally involves single-phase supply. The main different in this work is on CS modelling and its behaviour. The CS modelling in this research has considered the worst harmonic value achievable by individual CS based on the battery characteristic and State of Charge (SOC) state. The initial and final (plug-in and plug-out) battery SOC value depended on customer request, while the current produced by CS to the EV battery is calculated based on that SOC state. SOC state will be updated in every 15 minutes (Δt) and can be calculated using (9), while the current produced by CS can be calculated using (10).

$$\text{SOC}\left(\Delta t_{k+1}, i\right) = \text{SOC}\left(\Delta t_k, i\right) + \left(\frac{\Delta t}{Q_i} I\left(\Delta t_k, i\right)\right) \times 100, \tag{9}$$

$$I\left(\Delta t_k, i\right) = \frac{\sqrt{\left(4 \cdot \Delta t \cdot R_i \cdot P_{\text{CS}}\left(\Delta t_k, i\right) \cdot \eta \cdot \text{CR}_{i(\Delta t_k, i)}\right) + V_{\text{oc},i}^2} - V_{\text{oc},i}}{2R_i \cdot \text{CR}_{i(\Delta t_k, i)}}, \tag{10}$$

where $V_{\text{oc},i}$ is open circuit voltage for th node (V), Q_i is rated battery ampere hour for the ith PEV (Ah), R_i is battery equivalent internal resistance for the ith node (ohm), $\text{CR}_{i(\Delta t_k, i)}$ is maximum charging rate for the ith PEV (A), $\text{SOC}(\Delta t_k, i)$ is state of charge of the ith PEV at kth time slot (%), $\text{SOC}(\Delta t_{k+1}, i)$ is state of charge of the ith PEV at next kth time slot (%), $I(\Delta t_k, i)$ is charging current for the ith PEV at current time slot (A), and $P_{\text{CS}}(\Delta t_k, i)$ is consumed power for the ith PEV (kW).

Figure 3 shows the open circuit voltage (OCV) for lithium iron phosphate (LFP) batteries based on the SOC of battery [27] that can also be presented using (11). Thus, the relation between SOC and V_{OCV} will influence the total current injected during charging process.

$$V_{\text{OCV}} = 3.135 - 0.685\left(-\ln\left(\text{SOC}\right)\right)^{0.478} - \left(1.342 \cdot \text{SOC}\right) + \left(1.734 \cdot e^{0.4(\text{SOC}-1)}\right). \tag{11}$$

Since there is conversion from AC to DC during charging process, the harmonic impact to the network is considered in this study. The harmonic injection is basically based on SOC state, which depended on battery SOC status and is being modelled based on practical data from [18]. Since there are 132 CS units installed within the 22 low voltage residential areas (6 units for every residential area) it might have significant

Table 2: CS and battery data.

Type	Battery capacity (kW)	Charging rate (A)	Power usage (kW)	CS efficiency
1	10	0.052	0.52	0.93
2	15	0.125	1.875	0.93
3	10	0.235	2.35	0.93
4	15	0.15	2.25	0.93
5	10	0.215	2.15	0.93
6	20	0.102	2.04	0.93

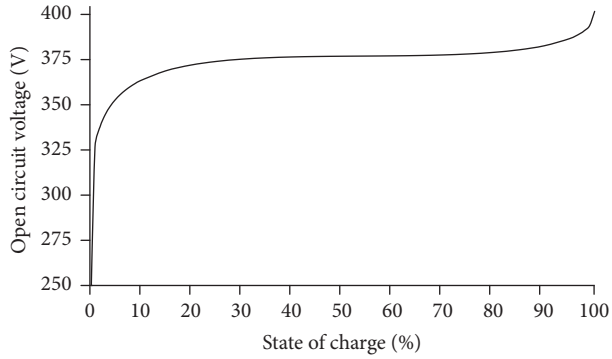

Figure 3: Relationship between open circuit voltage and SOC for LFP battery.

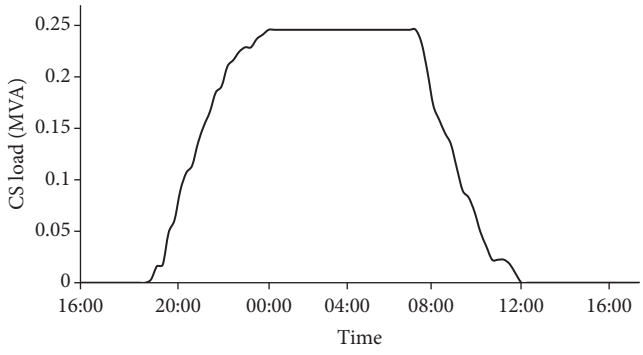

Figure 4: Load produced by CS over time.

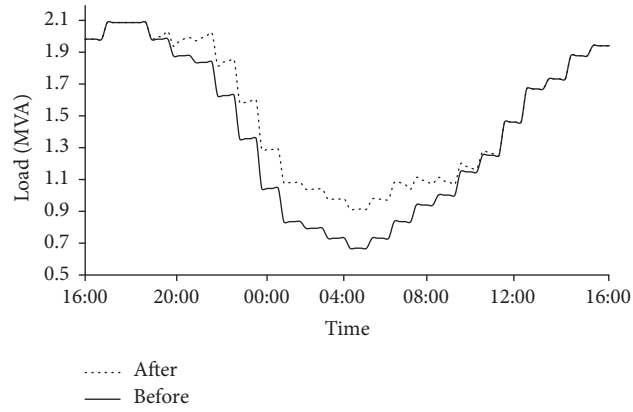

Figure 5: Load profile before and after CS operation.

impact on THD_V and THD_i value when all CS operated simultaneously. All CS and battery data in the residential area are presented as per Table 2.

2.4. Modelling of Load Profile and Charging Station Operation. The load profile for 449 bus system is design based on typical load consumption in residential area during normal day. The peak demand in the system is occurring at the afternoon due to the several usages of electrical appliances, while the lowest demand is at the night when majority of people are asleep. However, the new electrical load CS is normally being charged at the night time. In this study, it is assumed that harmonic produced in the distribution system is coming from CS. Figure 4 shows the loading produced by all CS in the distribution system based on design of CS operation as in Table 3. CS operation is designed based on random behaviour and will penetrate at the night hour. Figure 5 shows the summation of original load profile with CS load. Even though most of the CS is operating during low loaded condition at distribution system, it will cause higher impact on the total harmonic distortion as well as power losses.

2.5. Assumptions and Constraints. There are few assumptions and constraints are considered in this research as shown below:

(i) CS can be plugged in/plugged out at any time according to the customer's request. Customers will input their requested plug-out time and requested final SOCs at the time of plug-in. Once SOC reaches requested SOC, CS will be switched to a standby mode.

(ii) The time slot is 15 min (Δt) or equal to 96 slots for one day.

(iii) The aggregator has access to CS information including their bus locations, harmonic distortion information, charger types, battery sizes, plug-in time, and plug-out time.

(iv) CS are controllable and have variable charging functions. During the charging process, each CS is assumed as a variable active load. The power that is used to charge the battery is based on calculation that is done by the aggregator.

Table 3

Bus	Plug-in	Plug-out	SOC initial	SOC Req	Type
33	18	64	28	58	1
37	21	64	11	80	2
39	23	65	10	82	3
46	21	64	1	78	4
48	19	63	1	69	5
49	22	65	4	85	6
52	15	61	28	58	1
56	18	61	11	80	2
58	20	62	10	82	3
65	18	61	1	78	4
67	16	60	1	69	5
68	19	62	4	85	6
71	23	69	28	58	1
75	26	69	11	80	2
77	28	70	10	82	3
84	26	69	1	78	4
86	24	68	1	69	5
87	27	70	4	85	6
90	13	59	28	58	1
94	16	59	11	80	2
96	18	60	10	82	3
103	16	59	1	78	4
105	14	58	1	69	5
106	17	60	4	85	6
109	17	60	4	85	6
113	14	58	1	69	5
115	16	59	1	78	4
122	18	60	10	82	3
124	16	59	11	80	2
125	13	59	28	58	1
128	26	69	4	85	6
132	23	67	1	69	5
134	25	78	1	78	4
141	27	82	10	82	3
143	25	80	11	80	2
144	22	58	28	58	1
147	33	76	4	85	6
151	30	74	1	69	5
153	32	75	1	78	4
160	34	76	10	82	3
162	32	75	11	80	2
163	29	75	28	58	1
166	18	64	28	58	1
170	21	64	11	80	2
172	23	65	10	82	3
179	21	64	1	78	4
181	19	63	1	69	5
182	22	65	4	85	6

Table 3: Continued.

Bus	Plug-in	Plug-out	SOC initial	SOC Req	Type
185	15	61	28	58	1
189	18	61	11	80	2
191	20	62	10	82	3
198	18	61	1	78	4
200	16	60	1	69	5
201	19	62	4	85	6
204	23	69	28	58	1
208	26	69	11	80	2
210	28	70	10	82	3
217	26	69	1	78	4
219	24	68	1	69	5
220	27	70	4	85	6
223	13	59	28	58	1
227	16	59	11	80	2
229	18	60	10	82	3
236	16	59	1	78	4
238	14	58	1	69	5
239	17	60	4	85	6
242	17	60	4	85	6
246	14	58	1	69	5
248	16	59	1	78	4
255	18	60	10	82	3
257	16	59	11	80	2
258	13	59	28	58	1
261	26	69	4	85	6
265	23	67	1	69	5
267	25	78	1	78	4
274	27	82	10	82	3
276	25	80	11	80	2
277	22	58	28	58	1
280	33	76	4	85	6
284	30	74	1	69	5
286	32	75	1	78	4
293	34	76	10	82	3
295	32	75	11	80	2
296	29	75	28	58	1
299	18	64	28	58	1
303	21	64	11	80	2
305	23	65	10	82	3
312	21	64	1	78	4
314	19	63	1	69	5
315	22	65	4	85	6
318	15	61	28	58	1
322	18	61	11	80	2
324	20	62	10	82	3
331	18	61	1	78	4
333	16	60	1	69	5
334	19	62	4	85	6

Table 3: Continued.

Bus	Plug-in	Plug-out	SOC initial	SOC Req	Type
337	23	69	28	58	1
341	26	69	11	80	2
343	28	70	10	82	3
350	26	69	1	78	4
352	24	68	1	69	5
353	27	70	4	85	6
356	13	59	28	58	1
360	16	59	11	80	2
362	18	60	10	82	3
369	16	59	1	78	4
371	14	58	1	69	5
372	17	60	4	85	6
375	17	60	4	85	6
379	14	58	1	69	5
381	16	59	1	78	4
388	18	60	10	82	3
390	16	59	11	80	2
391	13	59	28	58	1
394	26	69	4	85	6
398	23	67	1	69	5
400	25	78	1	78	4
407	27	82	10	82	3
409	25	80	11	80	2
410	22	58	28	58	1
413	33	76	4	85	6
417	30	74	1	69	5
419	32	75	1	78	4
426	34	76	10	82	3
428	32	75	11	80	2
429	29	75	28	58	1
432	18	64	28	58	1
436	21	64	11	80	2
438	23	65	10	82	3
445	21	64	1	78	4
447	19	63	1	69	5
448	22	65	4	85	6

(v) The requested time for each CS must be greater than the minimum charging time required to charge the battery.

Since 22 variable filters will be placed in the network, the total unknown variables will become 44, which are 22 locations and 22 optimal sizes. All these parameters will have their own constraints that need to be considered. In general, the parameters can be divided into 2 categories which are as follows:

(i) Filter location: the filter will be placed in low voltage bus to avoid any harmonic injection to upper feeder. There are 22 locations in 449 bus radial distribution system. Furthermore, only one VPF will be placed at every low voltage 415 buses system. The constraints are as follows:

$$a_i \leq \text{Filter}_i \leq s_i, \quad i = 1 \ldots 22. \tag{12}$$

(ii) Filter reactive value: each individual variable filter reactive value is limited to

$$0\,\text{kVAr} \leq Q_i \leq 40\,\text{kVAr}, \quad i = 1 \ldots 22. \tag{13}$$

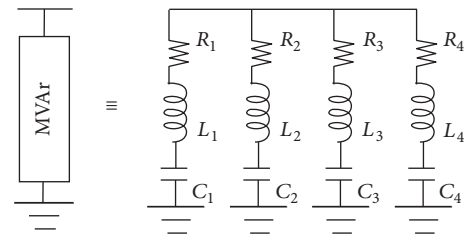

Figure 6: 1 set of filter.

2.6. Modelling of Passive Filter. The main function of a passive filter is to sink the harmonic current that flows in the system based on a selected frequency. The filter impedance will become very low to allow the harmonic to sink. Single tuned filter is the most popular type of filter which is used widely in dealing with harmonic pollution especially in the industrial area [28, 29]. In this research, four units of single tuned filters are considered as one set of filter which can eliminate four frequencies as shown in Figure 6. Equation in [26] is used to calculate capacitor, inductance, and resistance components, respectively, as per (14). Capacitor is calculated based on injected reactive power (Q) and voltage (V) at that bus; meanwhile, inductance and resistance are based on the chosen harmonics (n) that need to be reduced. Four sets of filter will be used to eliminate 3rd, 5th, 7th, and 9th harmonic order in the network.

$$C_{\text{Filter}} = \frac{Q}{2\pi f V^2},$$

$$L_{\text{Filter}} = \frac{V^2}{2n^2 Q^2 \pi f}, \tag{14}$$

$$R_{\text{Filter}} = \frac{V^2}{nQ^2}.$$

2.7. Multiobjective MLSA with Pareto Optimization. In this research, the optimization technique is used to identify optimized locations and sizes for 22 sets of filters in 449 bus radial distribution system. The Lightning Search Algorithm (LSA) is a metaheuristic optimization method inspired by lightning propagation from cloud to ground [30]. The LSA process basically starts with generation of random population before fitness calculation. The worst step leader will be eliminated every 10th iteration before the direction of the step leader is updated. Next, step leader movement is updated based on direction, shape parameter, and scale parameter. Lastly, forking phenomenon is taken place as per (7) for

1% of the better step leader. Since the problem faced in this research is too complicated with many local minima, modification on the existing LSA is needed. In this research, the MLSA is proposed with better convergence for this application compared to existing LSA. MLSA basically is the improvement of LSA method which is proven beneficial for this research.

The placement and sizing of variable filter will be based on five parameters, which are maximum THD_V, maximum THD_i, THD_i summation, average THD_i, and apparent power losses for overall system. The three parameters that involve THD_i are to ensure that the THD_i at all buses is within acceptable range. These parameters are then normalized to get the most accurate solution as defined by (15)–(19). The weight summation with normalized fitness function is shown in (20) after several manual trials are done in order to get the best optimal result. Last but not least, basic equations to calculate THD_i and THD_V are as shown by (21) and (22).

$$\mathrm{fit}_1 = \max\left(\mathrm{THD}_V\right), \quad n = 1 \ldots 449, \tag{15}$$

$$\mathrm{fit}_2 = \max\left(\mathrm{THD}_i\right), \quad n = 1 \ldots 30, \tag{16}$$

$$\mathrm{fit}_3 = \sum_{i=1}^{30} \mathrm{THD}_i, \tag{17}$$

$$\mathrm{fit}_4 = \frac{\sum_{i=1}^{30} \mathrm{THD}_i}{30}, \tag{18}$$

$$\mathrm{fit}_5 = \sum_{i=1}^{449} s_{i-\mathrm{loss}}, \tag{19}$$

$$\mathrm{Fit} = 0.1\mathrm{fit}_1 + 0.2\mathrm{fit}_2 + 0.2\mathrm{fit}_3 + 0.2\mathrm{fit}_4 + 0.3\mathrm{fit}_5, \tag{20}$$

$$\mathrm{THD}_V = \frac{\sqrt{\sum_{h=2}^{9} V_h^2}}{V_1} \times 100\%, \tag{21}$$

$$\mathrm{THD}_i = \frac{\sqrt{\sum_{h=2}^{9} I_h^2}}{I_1} \times 100\%. \tag{22}$$

In order to reduce computational time in this research, bus location is gathered from MLSA with weight summation approach; meanwhile, Pareto optimization is used to determine size of VPF. Normally, Pareto technique will produce a "nondominated" solution which has more than a single solution [31]. Thus, fuzzy satisfying approach is adopted in this research to get the best solution from the "nondominated" solutions. Equation (23) is the weight membership function used in fuzzy approach for all "nondominated" solutions in the fuzzy set. The $\mathrm{fit}_{\max}$ in the formula represents the existing fitness value before implementing the filters, while m represents the number of solutions listed in the "nondominated" list. The highest μ_j value indicates the best solution for this research.

$$\mu_{\mathrm{fit}\_j} = \begin{cases} 1, & \mathrm{fit}_j \le 0 \\ \dfrac{\mathrm{fit}_{\max} - \mathrm{fit}_j}{\mathrm{fit}_{\max}}, & 0 < \mathrm{fit}_j < \mathrm{fit}_{\max} \\ 0, & \mathrm{fit}_j \ge \mathrm{fit}_{\max}, \end{cases}$$

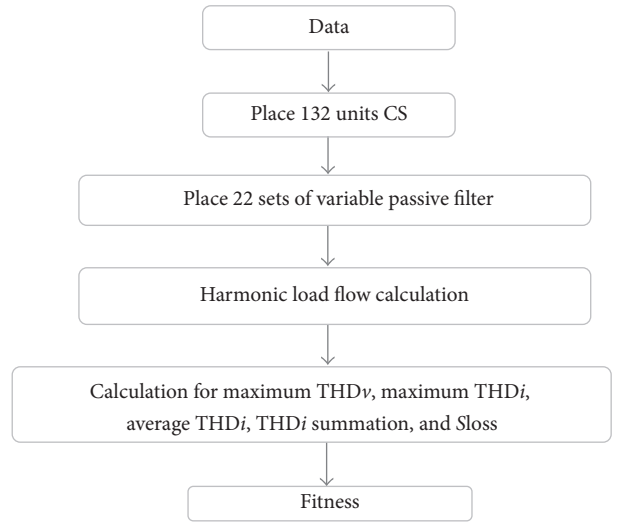

Figure 7: Flowchart to evaluate fitness.

$$\mu_j = \frac{\sum_1^5 \mu_{\mathrm{fit}\_j}}{\sum_1^m \sum_1^5 \mu_{\mathrm{fit}\_j}}. \tag{23}$$

3. Methodology

The variable filter is used to minimize the impact of harmonics due to large-scale deployment of CS in the big distribution system. The numbers of filter are based on how severe the harmonic distortion and power losses on the existing system. By placing 132 CS units (6 units for every low voltage residential area) at specific locations, MLSA will be used to determine optimal placement and size for 22 sets of filters (1 set for every low voltage residential area). The THD_V, THD_i, and S_{loss} will be recorded based on specify CS and filter locations. The overall process to evaluate system performance is as shown in Figure 7.

There are four modifications on MLSA that are made to improve LSA method. The first modification is on channel time; the original channel time is not suitable when dealing with the problems that have many local minima. The second modification is the updating approach; a new updating approach able to check the forward or backward direction is proposed. The third modification is on the scale parameter; in LSA, it is based on exponential distribution, which will cause the step leader movement to be active at 20% of the early iterations as per (24). Thus, in MLSA, the Laplacian distribution equation is used to increase the movement of the step leader during 30% until 70% iterations. Last but not least, the learning factors which make the movement of the step leader more active is implemented in the fourth modification as per (25).

$$P^L{}_{i\_\mathrm{new}} = P^L{}_i \pm \mathrm{normrand}\left(\mu_i, \sigma_i\right), \tag{24}$$

$$\mu_i = R\left(x_i - x_{\mathrm{best}}\right), \tag{25}$$

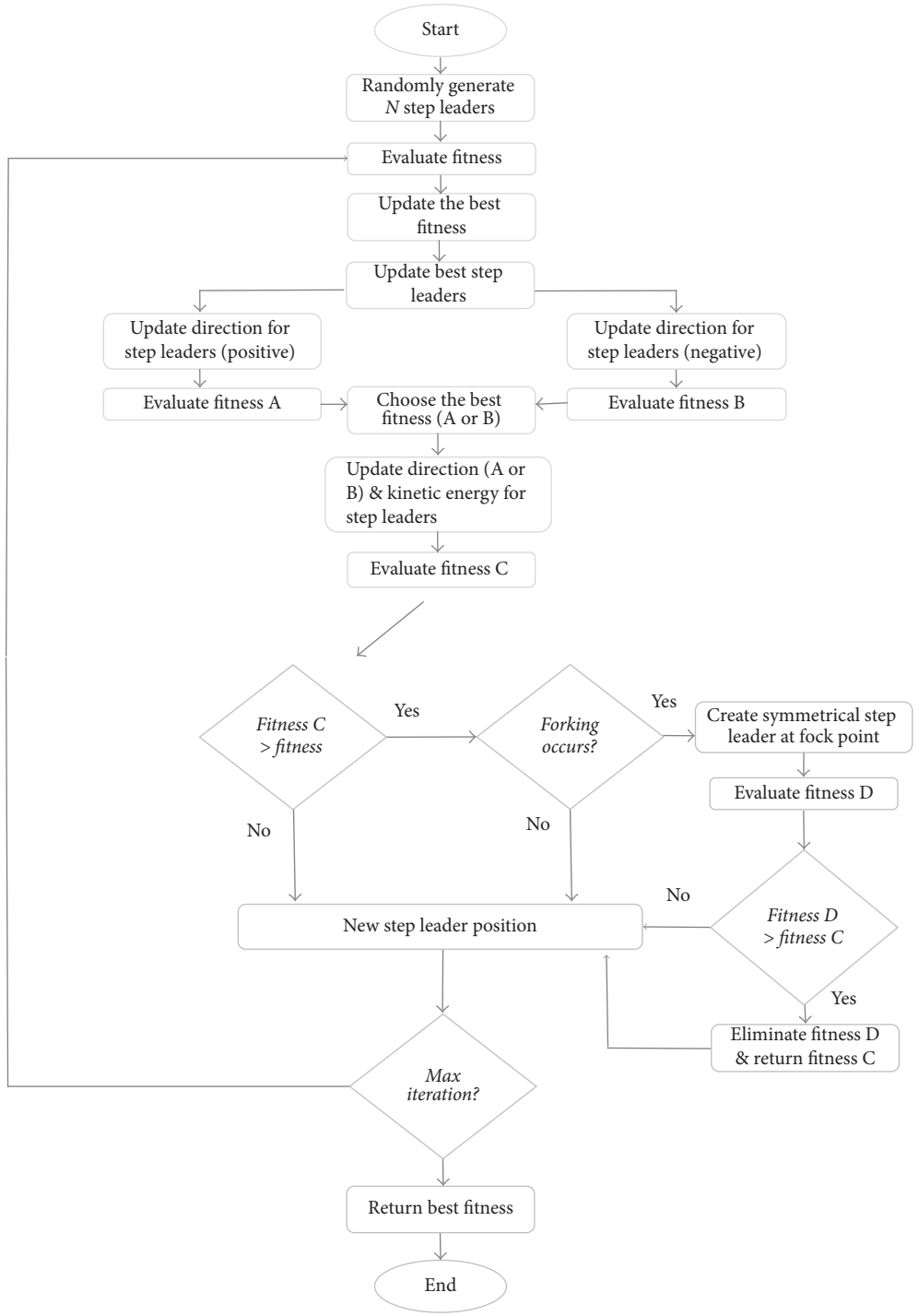

Figure 8: Flowchart for MLSA method to get minimum fitness with weightage summation approach.

where σ_i is the scale parameter at ith iteration $(1/3)e^{-(t-50/15)}$, R is learning factor (2.0 in this research), $P^L{}_{i\_\text{new}}$ is new position in lead projectile at ith iteration, $P^L{}_i$ is position in lead projectile at ith iteration, μ_i is shape parameter at ith iteration, x_i is the position at ith iteration, and x_{best} is the best individual during minimum.

Figure 8 shows the flowchart for MLSA optimization process using weightage summation approach for this research. In this process, simulation involves 500 iterations and 50 populations. Next, the bus location results will be used in the next stage by the MLSA-Pareto-Fuzzy combination technique. Figure 9 shows the flowchart for MLSA optimization process with Pareto-Fuzzy technique. In this stage, Pareto technique will be adopted in finding the best solution, while fuzzy approach will be used at the end of process to find the best solution among nondominated solutions.

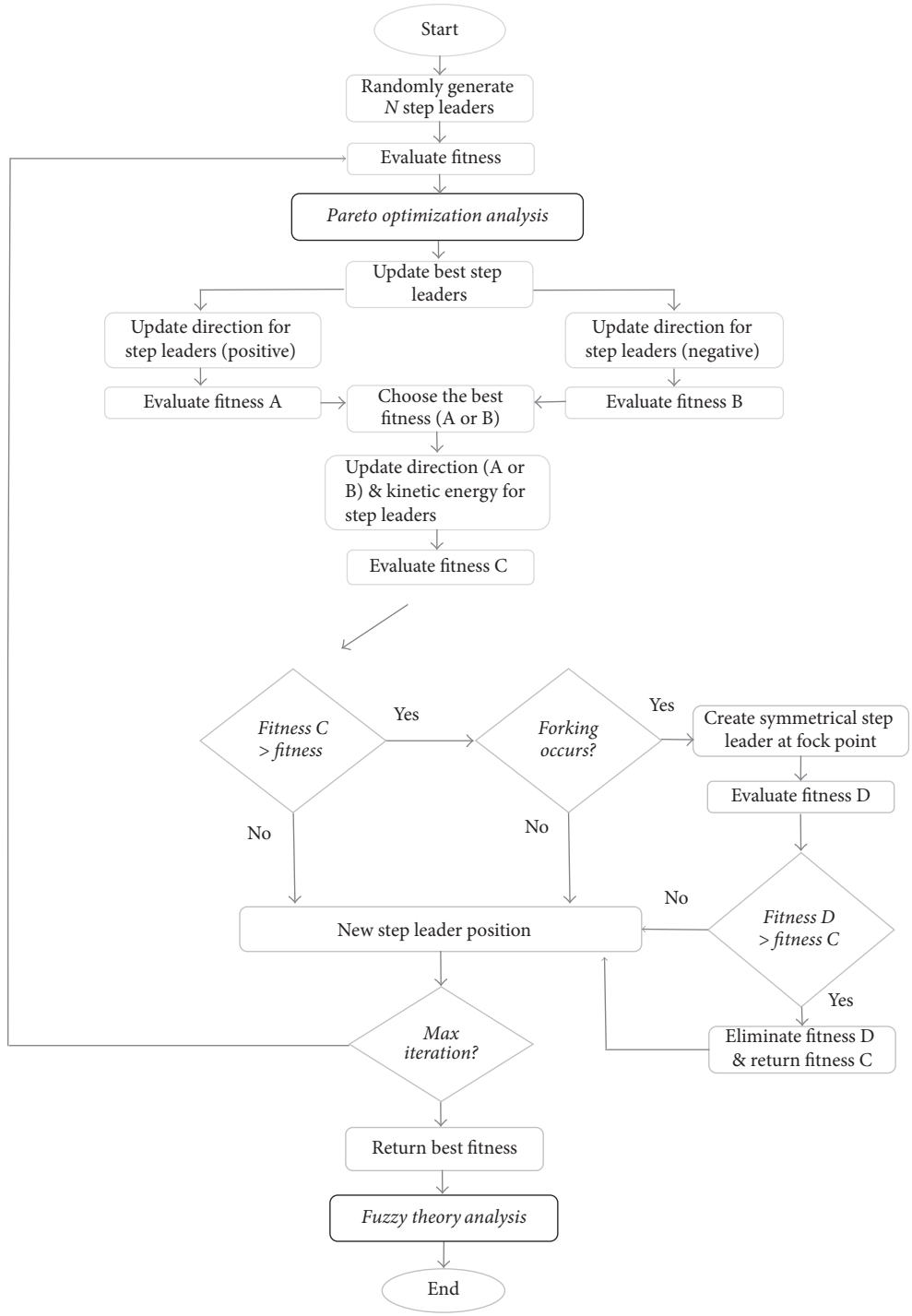

Figure 9: Flowchart for MLSA method to get minimum fitness with Pareto-Fuzzy technique.

4. Result and Discussion

The simulation on this research was done based on the scenario where 132 CS units are installed in low voltage 415 V buses for 24 hours (96 states, 1 state = 15 minutes). The schedule for CS operation can be referred to in Table 3. The THD_V and THD_i for all medium voltage buses and lines are shown in Figures 11 and 12, respectively, for sampling time at 30 and 63. Sampling time 63 is chosen due to the worst harmonic recorded in 24 hours, while sampling time 30 is chosen due to the lowest harmonic injection. From the result, without VPF, maximum THD_V for sampling time 30 is recorded at bus 15 with 0.8750% and maximum THD_i is recorded at lines between buses 26 and 27 (line number 27) with the value 0.6780%. For sampling time 63, maximum THD_V is 0.9032% at bus 15, while maximum THD_i

Table 4: Bus location and filter size after 500 iterations.

Number	Bus location	Filter size (kVAr)
(1)	42	28.007
(2)	56	16.494
(3)	85	22.724
(4)	105	1.018
(5)	119	1.777
(6)	145	24.54
(7)	161	28.731
(8)	168	27.679
(9)	193	29.999
(10)	217	8.927
(11)	222	2.109
(12)	254	1.024
(13)	275	27.391
(14)	282	17.989
(15)	305	14.646
(16)	322	24.733
(17)	337	26.043
(18)	367	24.758
(19)	387	29.863
(20)	407	21.946
(21)	424	26.069
(22)	447	28.156

Table 5: Result using MLSA with multiobjective function.

Function	Existing	After multiobjective function
Max THD_V	1.258004	0.74478
Max THD_i	2.019816	1.16256
THD_i average	0.474635	0.322456
THD_i sum	14.71369	9.996144
S_{loss}	0.04175	0.043149
Fitness	1	0.75612

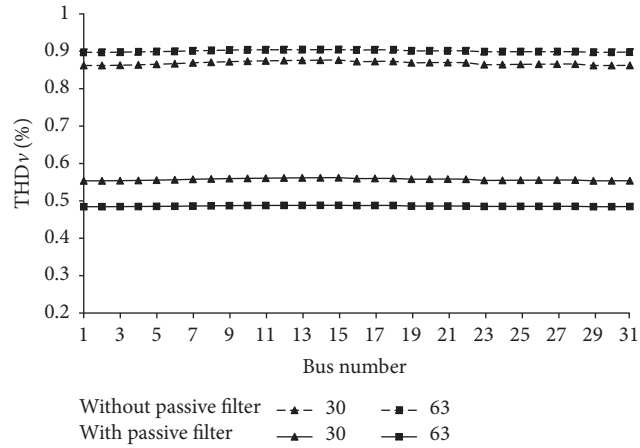

Figure 10: THD_V at medium voltage for times 30 and 63 with and without passive filter.

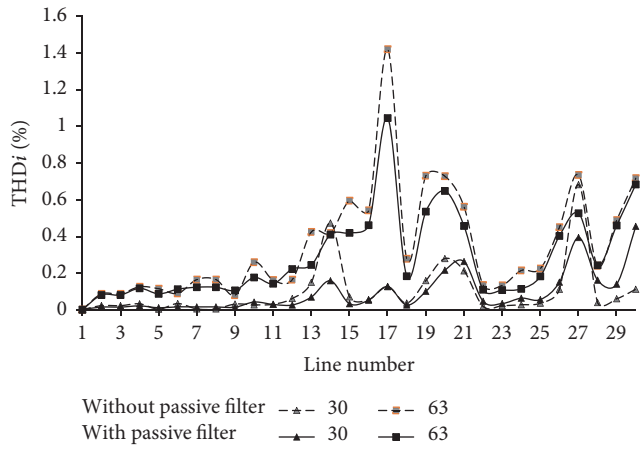

Figure 11: THD_i at medium voltage for times 30 and 63 with and without passive filter.

is recorded at lines between buses 12 and 13 (line number 17) with the value 1.4166%. Apparent losses for both sampling times are 90.3 kVA and 40.4 kVA, respectively.

Next, 22 sets of VPFs are placed at low voltage 415 V buses using MLSA optimization with multiobjective function. The optimal location and size for all filters are tabulated in Table 4, while the parameter value is shown at Table 5. From the results in Table 5, there is a significant reduction for maximum THD_V from 1.258004% to 0.74478% and maximum THD_i from 2.019816% to 1.16256% after MLSA get the optimal placement for VPF. However, the total apparent losses in the network are increased. Thus, a Pareto-Fuzzy approach is used to cater this issue at the next step.

The results from Pareto consist of multiple set solutions where the possible solution is the best solution as long as one of their objectives functions is dominant compared to other solutions. Fuzzy approach will be used to find the best among solutions in Pareto set. In this study, the solution consists of THD_V, THD_i (minimum, average, and summation), and power loss. From the analysis, the total Pareto result for sampling time at 63 in MLSA is 137 sets. The fuzzy approach is used in order to get the best single solution. The highest value of weight membership function in fuzzy approach will be chosen as the best solution in this research. Tables 6 and 7 show the five best solutions with the highest μ_j for sampling times 63 and 30. From the result, the best sizing for all filters is shown in Table 8 at sampling time 63. The size of filter to cater harmonic is different between times 30 and 63 which indicates that the size of passive filter is very crucial in this study. The THD_V and THD_i for buses and lines, after the filter implementation as per MLSA with Pareto-Fuzzy best solution, are shown in Figures 10 and 11. From the results, it shows significant reduction of THD_V at all medium voltage buses, while majority of THD_i also shows reduction. From the best solution, the THD_i and THD_v for the 449 bus distribution system have been reduced effectively after filter installations. The results for all 96 slots are shown in Figures 12–16. Based on Figures 12 and 13, maximum THD_V and THD_i show reduction for all states which indicate that the system is better compared to previous

Table 6: The five best solutions based on the highest μ_j using fuzzy approach for 137 sets of solutions (sampling time = 63).

Number	Fitness parameter					μ_{fit}^1	μ_{fit}^2	μ_{fit}^3	μ_{fit}^4	μ_{fit}^5	μ_j
	fit_1	fit_2	fit_3	fit_4	fit_5						
(1)	*0.731905*	*1.042406*	*0.308344*	*9.558658*	*0.040295*	*0.350982*	*0.26416*	*0.196401*	*0.196401*	*0.004568*	*0.009541*
(2)	0.715371	1.087904	0.308852	9.574414	0.040469	0.365644	0.232043	0.195076	0.195076	0.000013	0.009308
(3)	0.691356	1.213682	0.299624	9.288355	0.040021	0.386939	0.143255	0.219125	0.219125	0.011102	0.00923
(4)	0.691356	1.213682	0.299624	9.288355	0.040021	0.386939	0.143255	0.219125	0.219125	0.011102	0.00923
(5)	0.691356	1.213682	0.299624	9.288355	0.040021	0.386939	0.143255	0.219125	0.219125	0.011102	0.00923

Table 7: The five best solutions based on the highest μ_j using fuzzy approach for 10 sets of solutions (sampling time = 30).

Number	Fitness parameter					μ_{fit}^1	μ_{fit}^2	μ_{fit}^3	μ_{fit}^4	μ_{fit}^5	μ_j
	fit_1	fit_2	fit_3	fit_4	fit_5						
(1)	*0.62029*	*0.452838*	*0.093176*	*2.888464*	*0.089405*	*0.34565*	*0.334048*	*0.081789*	*0.081789*	*0.009764*	*0.124558*
(2)	0.647588	0.41204	0.095228	2.952076	0.089555	0.316852	0.394046	0.061568	0.061568	0.0081	0.122965
(3)	0.639053	0.421681	0.097018	3.007568	0.089525	0.325856	0.379868	0.043927	0.043927	0.00843	0.117106
(4)	0.639053	0.421681	0.097018	3.007568	0.089525	0.325856	0.379868	0.043927	0.043927	0.00843	0.117106
(5)	0.652162	0.410311	0.10102	3.131623	0.089686	0.312028	0.396589	0.004492	0.004492	0.006651	0.105752

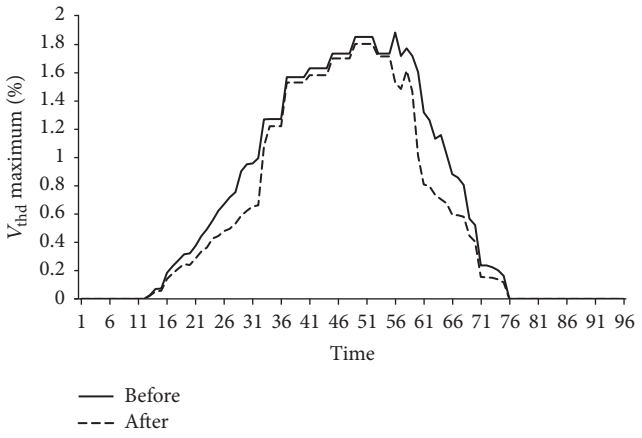

Figure 12: THD_v maximum for 24 hours with and without passive filter.

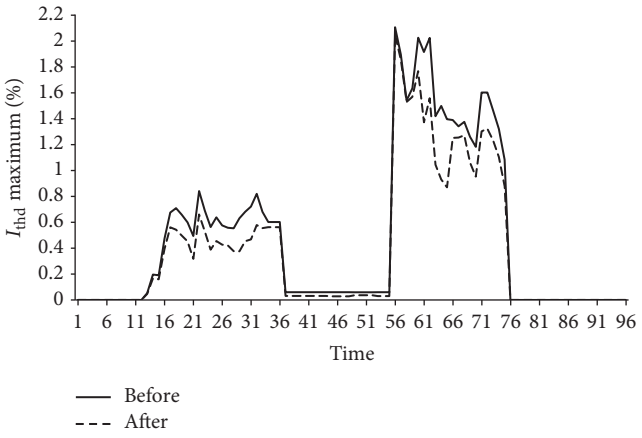

Figure 13: THD_i maximum for 24 hours with and without passive filter.

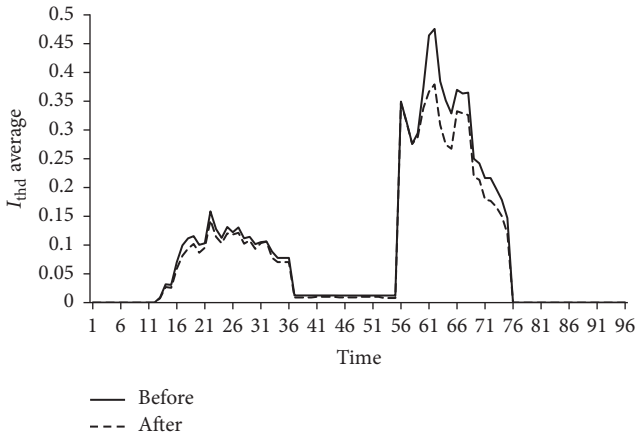

Figure 14: THD_i average for 24 hours with and without passive filter.

value, while apparent losses at Figure 16 show the capability of this method to also reduce losses together with harmonic. Next, Figures 14 and 15 also show reduction which assist THD_i improvement in overall system indirectly. From the result, implementation of VPF with changes every 15 minutes is able to reduce harmonic for 24 hours. Other than that, it is obvious that the implementation of MLSA with Pareto-Fuzzy is able to identify the best solution that provides the greatest improvement to the overall system.

Based on the collective result gathered from all 96 simulations that represent 24 hours, minimum and maximum values of VPF at dedicated bus are acquired. Table 9 shows the minimum and maximum VPF required to solve harmonic problem after EV is installed.

5. Conclusion

Optimal placement and sizing of VPF in the distribution system can avoid harmonic injection to the medium voltage

Table 8: Filter size based on the best solution after fuzzy at sampling times 30 and 63.

Number	Bus location	Filter size (MVAr)	
		(Time = 30)	(Time = 63)
(1)	42	0.017278	0.025038
(2)	56	0.02187	0.005959
(3)	85	0.010198	0.019481
(4)	105	0.029332	0.011044
(5)	119	0.014816	0.001792
(6)	145	0.019336	0.02311
(7)	161	0.002469	0.026056
(8)	168	0.023573	0.022019
(9)	193	0.003353	0.018806
(10)	217	0.018943	0.008713
(11)	222	0.019898	0.016408
(12)	254	0.024081	0.002977
(13)	275	0.0176	0.018999
(14)	282	0.020249	0.029898
(15)	305	0.01956	0.022548
(16)	322	0.016437	0.015687
(17)	337	0.014686	0.01437
(18)	367	0.026797	0.016679
(19)	387	0.022292	0.012124
(20)	407	0.011888	0.016332
(21)	424	0.001049	0.011097
(22)	447	0.020735	0.028984

Table 9: Minimum and maximum VPF size based on 96 simulations.

Number	Bus location	Filter size (kVAr)	
		Minimum	Maximum
(1)	42	1.021	28.916
(2)	56	1.282	28.659
(3)	85	0.619	28.838
(4)	105	0.637	29.498
(5)	119	0.692	20.457
(6)	145	0.855	29.559
(7)	161	0.204	29.944
(8)	168	0.5	29.769
(9)	193	0.725	18.806
(10)	217	0.724	29.936
(11)	222	0.228	29.927
(12)	254	0.319	29.996
(13)	275	0.171	28.969
(14)	282	0.409	29.898
(15)	305	0.654	29.805
(16)	322	0.318	29.859
(17)	337	0.84	29.565
(18)	367	0.176	29.56
(19)	387	1.385	29.576
(20)	407	0.235	26.327
(21)	424	1.049	28.326
(22)	447	0.244	29.922

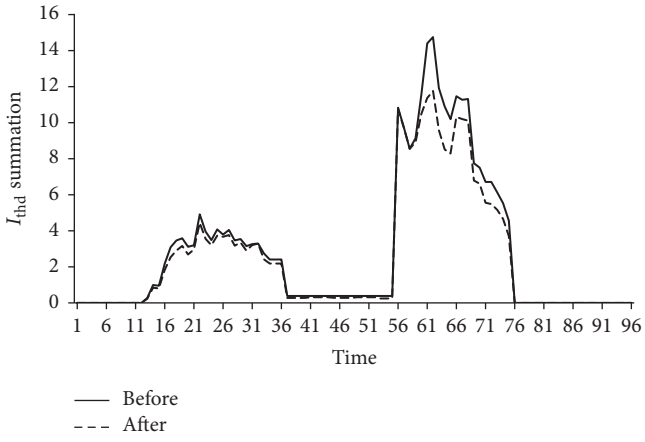

Figure 15: THD_i summation for 24 hours with and without passive filter.

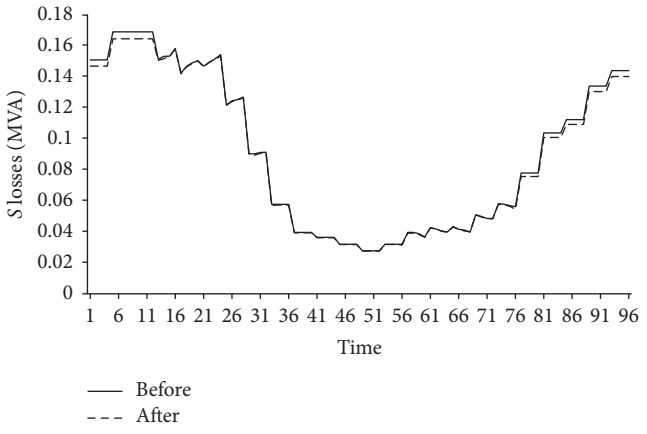

Figure 16: Apparent power losses for 24 hours with and without passive filter.

network as well as reducing apparent power losses. This research has shown that MLSA with multiobjective function and Pareto-Fuzzy are able to determine appropriate filter location and size to reduce harmonic distortion and apparent losses in 449 bus system with 132 units of CS. Furthermore, the placement of twenty-two sets of four unit single-tuned filters is able to reduce the four harmonic orders. Based on simulation run for every 15 minutes, the proposed technique is able to improve maximum THD_V, maximum THD_i, and S_{loss} up to 39.14%, 52.5%, and 2.96%, respectively. The study is very important for future distribution grid that might have many CS in the network. For future work, the study can be expanded to other types of passive filter able to have better impact on the system such as C-type filter and others.

Conflicts of Interest

The authors declare that they have no conflicts of interest.

Acknowledgments

The researchers would like to express their appreciation to the Universiti Teknologi Malaysia (UTM) for supporting this work through GUP Grant (15H89).

References

[1] World Balance, https://www.iea.org/Sankey/#?c=World&s=Finalconsumption.

[2] A. Lucas, F. Bonavitacola, E. Kotsakis, and G. Fulli, "Grid harmonic impact of multiple electric vehicle fast charging," *Electric Power Systems Research*, vol. 127, pp. 13–21, 2015.

[3] J. Niitsoo, J. Kilter, I. Palu, P. Taklaja, and L. Kütt, "Harmonic levels of domestic and electrical vehicle loads in residential distribution networks," in *Proceedings of the IEEE (AFRICON '13)*, pp. 184–188, Mauritius, September 2013.

[4] S. Pazouki, A. Mohsenzadeh, M.-R. Haghifam, and S. Ardalan, "Simultaneous allocation of charging stations and capacitors in distribution networks improving voltage and power loss," *Canadian Journal of Electrical and Computer Engineering*, vol. 38, no. 2, Article ID 7097124, pp. 100–105, 2015.

[5] M. S. Taci, M. H. Sarul, and G. Yildirmaz, "Effects of the harmonic components upon transformer active losses in case of (non) sinusoidal sources and (non) linear loads," in *Proceedings of the IEEE International Conference on Industrial Technology 2000*, vol. 1, pp. 741–746, IEEE, January 2000.

[6] N. Zhou, J. Wang, Q. Wang, N. Wei, and X. Lou, "Capacity calculation of shunt active power filters for electric vehicle charging stations based on harmonic parameter estimation and analytical modeling," *Energies*, vol. 7, no. 8, pp. 5425–5443, 2014.

[7] M. Alonso, H. Amaris, J. G. Germain, and J. M. Galan, "Optimal charging scheduling of electric vehicles in smart grids by heuristic algorithms," *Energies*, vol. 7, no. 4, pp. 2449–2475, 2014.

[8] G. R. Bharati and S. Paudyal, "Coordinated control of distribution grid and electric vehicle loads," *Electric Power Systems Research*, vol. 140, pp. 761–768, 2016.

[9] M. A. S. Masoum and S. M. H. Nabavi, "Hybrid optimal online-overnight charging coordination of plug-in electric vehicles in smart grid," *Journal of Power Sources*, vol. 330, pp. 7–17, 2016.

[10] B. P. De Campos, L. A. R. De Sousa, and P. F. Ribeiro, "Mitigation of harmonic distortion with passive filters," in *Proceedings of the 17th International Conference on Harmonics and Quality of Power, (ICHQP '16)*, pp. 646–651, IEEE, Brazil, October 2016.

[11] K. H. Shafad, J. J. Jamian, and S. A. S. Nasir, "Harmonic distortion mitigation for multiple modes charging station via optimum passive filter design," in *Proceedings of the 2016 IEEE Conference on Systems, Process and Control, (ICSPC '16)*, pp. 219–223, Malaysia, December 2016.

[12] V.-L. Nguyen, T. Tran-Quoc, and S. Bacha, "Harmonic distortion mitigation for electric vehicle fast charging systems," in *Proceedings of the 2013 IEEE Grenoble Conference PowerTech, (POWERTECH '13)*, pp. 1–6, IEEE, Grenoble, France, June 2013.

[13] C. C. Hao, Y. J. Tang, and J. Shi, "Study on the harmonic impact of large scale electric vehicles to grid," *AMM Applied Mechanics and Materials*, vol. 443, pp. 273–278, 2013.

[14] S. Pirouzi, M. A. Latify, and G. R. Yousefi, "Investigation on reactive power support capability of PEVS in distribution network operation," in *Proceedings of the 23rd Iranian Conference on Electrical Engineering, (ICEE '15)*, pp. 1591–1596, IEEE, Tehran, Iran, May 2015.

[15] Y. Cho and H. Cha, "Single-tuned passive harmonic filter design considering variances of tuning and quality factor," *Journal of International Council on Electrical Engineering*, vol. 1, pp. 7–13, 2011.

[16] S. Sakar, M. E. Balci, S. H. E. Abdel Aleem, and A. F. Zobaa, "Increasing PV hosting capacity in distorted distribution systems using passive harmonic filtering," *Electric Power Systems Research*, vol. 148, pp. 74–86, 2017.

[17] S. Farkoush, C. Kim, and S. Rhee, "THD reduction of distribution system based on ASRFC and HVC method for SVC under EV charger condition for power factor improvement," *Symmetry*, vol. 8, no. 12, p. 156, 2016.

[18] G. Chang, S. Chu, and H. Wang, "A simplified forward and backward sweep approach for distribution system load flow analysis," in *Proceedings of the International Conference on Power System Technology*, pp. 1–5, 2006.

[19] M. Abdel-Akher, "Voltage stability analysis of unbalanced distribution systems using backward/forward sweep load-flow analysis method with secant predictor," *IET Generation, Transmission & Distribution*, vol. 7, no. 3, pp. 309–317, 2013.

[20] P. Samal and S. Ganguly, "A modified forward backward sweep load flow algorithm for unbalanced radial distribution systems," in *Proceedings of the IEEE Power and Energy Society General Meeting, (PESGM '15)*, pp. 1–5, IEEE, Denver, CO, USA, July 2015.

[21] C. S. Gupta, "Review of forward & backward sweep method for load flow analysis of radial distribution system," *IJAREEIE International Journal of Advanced Research in Electrical, Electronics and Instrumentation Engineering*, vol. 04, pp. 5595–5599, 2015.

[22] R. Bass and N. Zimmerman, "Impacts of electric vehicle charging on electric power distribution systems," *OTREC-SS-731. Portland, OR: Transportation Research and Education Center (TREC)*, 2013.

[23] S. A. Kumar and K. R. Reddy, "Computation of the power flow solution of a radial distribution system for harmonic components," *International Journal of Energy*, 2013.

[24] J.-H. Teng, S.-H. Liao, and R.-C. Leou, "Three-phase harmonic analysis method for unbalanced distribution systems," *Energies*, vol. 7, no. 1, pp. 365–384, 2014.

[25] J.-H. Teng and C.-Y. Chang, "Backward/forward sweep-based harmonic analysis method for distribution systems," *IEEE Transactions on Power Delivery*, vol. 22, no. 3, pp. 1665–1672, 2007.

[26] S. M. Halpin, P. F. Ribeiro, and J. J. Dai, "Frequency-domain harmonic analysis methods," *IEEE Power Engineering Society: Tutorial in Harmonics Modeling and Simulation*, pp. 49–54, 1998.

[27] C. Zhang, J. Jiang, L. Zhang, S. Liu, L. Wang, and P. C. Loh, "A generalized SOC-OCV model for lithium-ion batteries and the SOC estimation for LNMCO battery," *Energies*, vol. 9, no. 11, article no. 900, 2016.

[28] M. Awadalla, M. Omer, and A. Mohamed, "Single-tuned filter design for harmonic mitigation and optimization with capacitor banks," in *Proceedings of the 1st International Conference on Computing, Control, Networking, Electronics and Embedded Systems Engineering, (ICCNEEE '15)*, pp. 242–247, IEEE, Khartoum, Sudan, September 2015.

[29] D. M. Soomro and M. M. Almelian, "Optimal design of a single tuned passive filter to mitigate harmonics in power frequency," *ARPN Journal of Engineering and Applied Sciences*, vol. 10, no. 19, pp. 9009–9014, 2015.

[30] H. Shareef, A. A. Ibrahim, and A. H. Mutlag, "Lightning search algorithm," *Applied Soft Computing*, vol. 36, pp. 315–333, 2015.

[31] R. N. S. R. Mukhtaruddin, H. A. Rahman, M. Y. Hassan, and J. J. Jamian, "Optimal hybrid renewable energy design in autonomous system using Iterative-Pareto-Fuzzy technique," *International Journal of Electrical Power & Energy Systems*, vol. 64, pp. 242–249, 2015.